Mineralogical Association of Canada

Recent and not-so-recent developments in uranium deposits and implications for exploration

Michel Cuney &
Kurt Kyser

Short Course Series
Volume

39

QUEBEC CITY, QUEBEC, 2008
Series Editor
Robert Raeside

SOCIETY for GEOLOGY APPLIED to MINERAL DEPOSITS

Mineralogical Association of Canada

Recent and not-so-recent developments in uranium deposits and implications for exploration

Michel Cuney &
Kurt Kyser

Short Course Series
Volume

39

QUEBEC CITY, QUEBEC, 2008
Series Editor
Robert Raeside

Mineralogical Association of Canada

Recent and not-so-recent developments in uranium deposits and implications for exploration

Michel Cuney &
Kurt Kyser

Short Course Series
Volume

39

QUEBEC CITY, QUEBEC, 2008
Series Editor
Robert Raeside

SOCIETY for GEOLOGY APPLIED to MINERAL DEPOSITS

CHAPTER 1: INTRODUCTION

Kurt Kyser
Department of Geological Sciences and Geological Engineering,
Queen's University,
Kingston, Ontario, K7L 3N6, Canada
kyser@geol.queensu.ca

and

Michel Cuney
G2R, Nancy-Université, CNRS, CREGU,
B.P. 239,
F-54506 Vandoeuvre lés Nancy, France
michel.cuney@g2r.uhp-nancy.fr

Uranium is one of the most important energy-related materials, with current use almost entirely for generating electricity and a small proportion for producing medical isotopes. About 17% of the world's electricity is generated from 440 nuclear reactors spread across 30 countries, and 8% of the total energy consumed globally comes from nuclear power (EIA 2007). Energy generated from U has a minimal "carbon footprint" and substitution of nuclear generated electricity for coal has been proposed to offset the additional emissions expected from the increase in energy anticipated in the future (Pacala & Socolow 2004). To meet the current and projected needs of the uranium industry, discovery of new deposits and development of new technologies for both exploration and processing are critical.

The discovery of uranium is attributed to Klaproth, a German chemist who, in 1789, precipitated a yellow compound by dissolving pitchblende in nitric acid and neutralizing the solution with sodium hydroxide. He heated it with charcoal to obtain a black powder, which was a uranium oxide. He named the newly discovered element after the planet Uranus, which had been discovered eight years earlier by William Herschel. In 1841, Péligot, a French chemist working at the Baccarat crystal factory in Lorraine, isolated the first sample of U metal by heating U tetrachloride with K. Uranium was not seen as being particularly dangerous during much of the 19th century, leading to use of the element in coloring pottery and glass.

Radioactivity was discovered by Becquerel in 1896 when he accidentally exposed a photographic plate to U (Becquerel 1896). Realization that U isolated from pitchblende was less radioactive than the pitchblende led to the discovery of Po and Ra shortly thereafter by the Curies (Curie & Curie 1898). Much later, a team led by Enrico Fermi in 1934 observed that bombarding U with neutrons produces the emission of beta rays, and lead to the discovery of fission of U. On December 2, 1942, a team led by Enrico Fermi initiated a controlled nuclear chain reaction.

Uranium is a ubiquitous element that occurs everywhere; the concentration of U is normally low, averaging only 3 ppm in the upper continental crust (1.7 ppm in the entire crust) and 0.0032 mg/L in seawater (Clark *et al.* 1966). Uranium is a member of the actinide series of elements, as are thorium and plutonium. Uranium has an atomic number of 92 and has 3 naturally occurring radioactive isotopes, ^{234}U, ^{235}U and ^{238}U. The most abundant isotopes of U, ^{235}U and ^{238}U, along with ^{232}Th are commonly used in geological sciences as geochronometers because of their long half-lives (the time required for half the number of atoms of an isotope to decay) and because they each decay to an isotope of Pb (Table 1-1). The isotope ^{234}U, which occurs as the decay product of ^{238}U and is used as a geochronometer as well, makes up only 0.0055% of natural U because its half-life of 246,000 years is only about 0.000055 as long as the half-life of ^{238}U.

The decays of ^{235}U and ^{238}U are complex, with many intermediate daughter products. These products decay to daughters along the chain until ^{207}Pb is reached in the ^{235}U chain or ^{206}Pb is produced in the ^{238}U decay scheme (Fig. 1-1). Because of differences in the geochemical properties of the daughter elements produced, these can be differentially dispersed into the environment resulting in disequilibrium in the radioactivity of

Short course co-sponsored by the the SGA and MAC, Québec City, May 2008, p. 1–14

TABLE 1-1. FINAL DECAY PRODUCTS OF U AND TH ISOTOPES

^{238}U	$\rightarrow {}^{206}Pb$	$t_{½} = 4.469 \times 10^9$
^{235}U	$\rightarrow {}^{207}Pb$	$t_{½} = 0.7038 \times 10^9$
^{232}Th	$\rightarrow {}^{208}Pb$	$t_{½} = 14.01 \times 10^9$

$(^{238}U/^{235}U)_{now}$ is 137.88

^{204}Pb is the only non-radiogenic isotope of Pb

Final decay products of naturally occurring U and Th isotopes to isotopes of Pb along with their half-lives ($t_{½}$) that are used for geochronometers in the earth sciences. Also indicated are the normal $^{238}U/^{235}U$ ratio and the only non-radiogenic isotope of Pb.

isotopes in the decay schemes. Disequilibria in the radioactivity of isotopes in the decay schemes are used to determine the timing at which recent events have produced open systems in U ores. In deposit studies, the decay schemes of ^{235}U and ^{238}U along with the isotopes of Pb are used to determine the age of U minerals, as discussed in Chapter 3.

NUCLEAR POWER

The current major use of U is the generation of electricity. Globally, there are 440 nuclear power reactors in 30 countries and 270 research reactors that required nearly 70,000 t (181 million pounds U_3O_8) of U in 2007 (OECD 2008). About 25% of these reactors are in North America and 37% are in Europe (Fig. 1-2). Given all of the existing reactors and the 27 reactors currently under construction and those anticipated, the need for U will increase by about 30% to 82,000 to 100,000 t U (212 to 259 million lbs U_3O_8) by the year 2025 (EIA 2007). The balance of need and supply is discussed more in detail in Chapter 2.

The Nuclear Fuel Cycle

The isotope ^{235}U is important for both nuclear reactors and nuclear weapons because it is the only isotope existing in nature to any appreciable extent that is fissile. There are two types of reactors currently in use, those that use U enriched in ^{235}U and normal water around the fuel rods (light water reactors) and those that use U without any enrichment and heavy water to moderate the fission reactions (heavy water reactors). Enrichment of natural, mined U through isotope separation to concentrate the fissionable ^{235}U is needed for use in nuclear weapons and light water reactors as shown by the U cycle in Figure 1-3.

Only 0.7204% of natural U is ^{235}U. This is too low a concentration to sustain a nuclear chain reaction without the help of a moderator that can

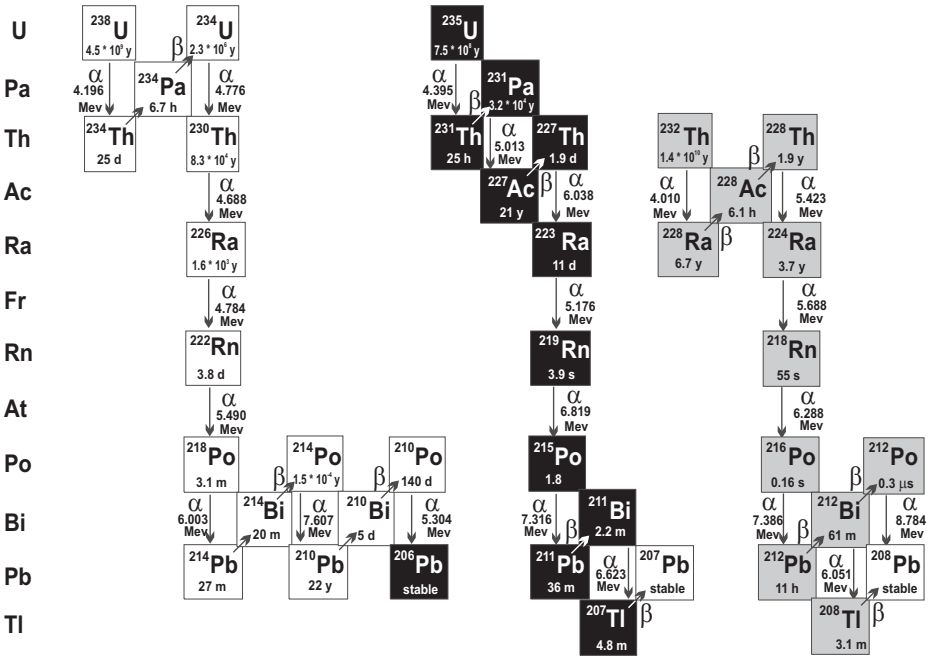

FIG. 1-1. Decay schemes of ^{235}U, ^{238}U and ^{232}Th showing the position of ^{234}U in the decay chain of ^{238}U. The geochemical properties of the decay products are quite distinct, including production of radon gas, and these will tend to separate from the ores in open systems.

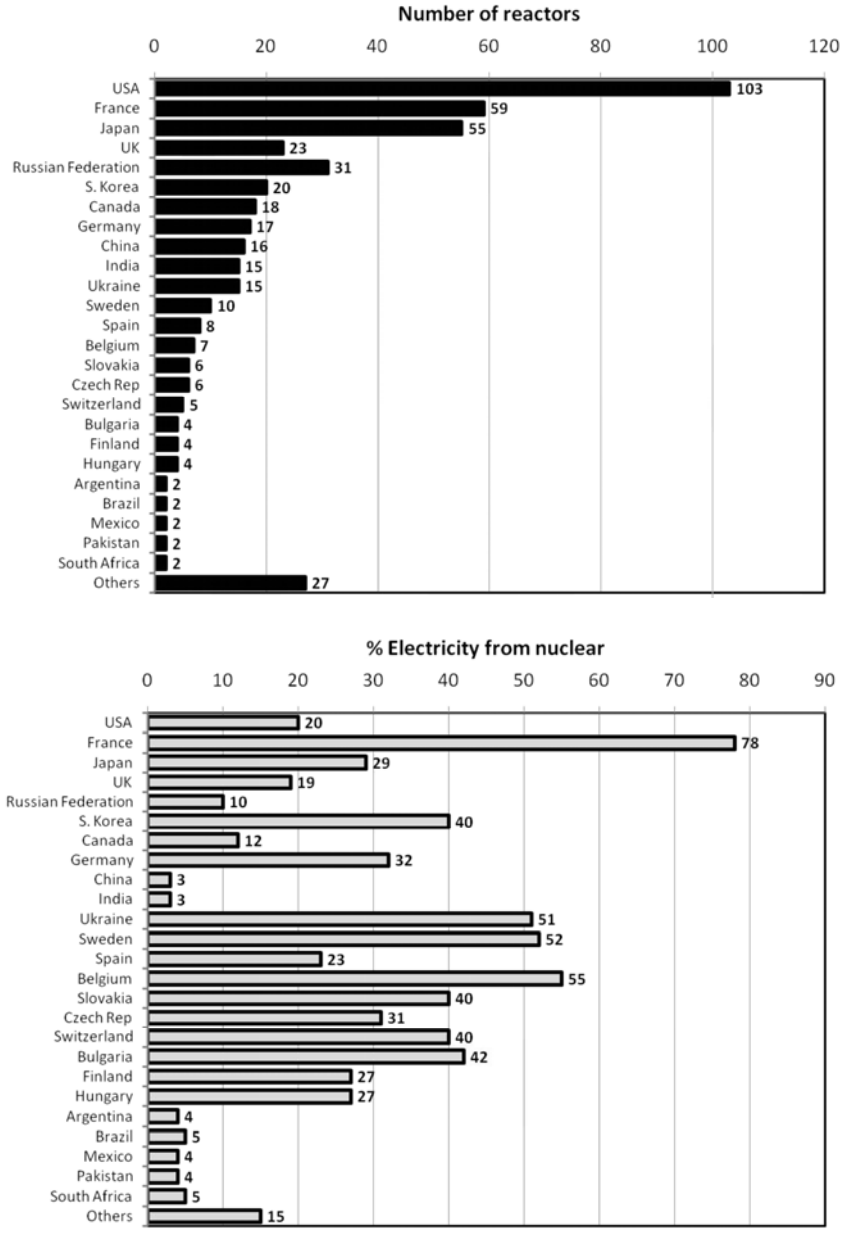

FIG. 1-2. Number of reactors (top) and % electricity generated by nuclear power (bottom) as a function of country. Data from OECD (2006) and OECD (2008).

slow down a neutron without absorbing it. Reactors using natural U can be made using graphite or heavy water as a moderator whereas normal water can be used as a moderator in reactors that use enriched U with greater than 3% ^{235}U. This enriched U typically has a ^{235}U concentration of between 3 and 5%. The process produces huge quantities of depleted U with 0.2% to 0.3% ^{235}U (Fig. 1-3). Enriched U contains more ^{234}U than natural U, and depleted U contains much less ^{234}U (around 0.001%) which makes its radioactivity slightly more than half that of natural U.

The most abundant isotope of U, ^{238}U, can be converted by irradiation with neutrons into ^{239}Pu, a fissionable material that can also be used as a fuel in nuclear reactors as MOX, mixed oxides of U and Pu (Fig. 1-3). Although it does not occur naturally, ^{233}U is also a fissionable material that can be used as a fuel in nuclear reactors. Thorium, which naturally is 100% ^{232}Th, is exposed to neutrons to

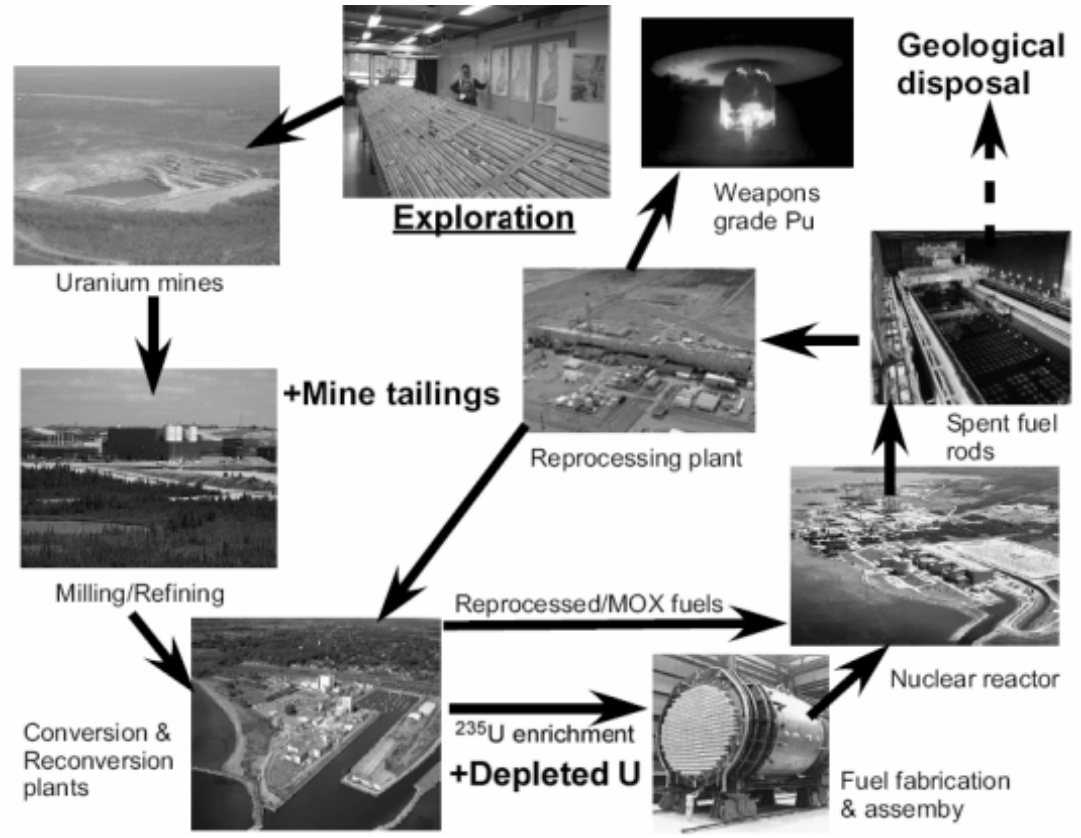

FIG. 1-3. Condensed version of the U fuel cycle, of which exploration and finding deposits is the first and most critical step. Modified from World Nuclear Association (2008).

produce ^{233}U, an isotope that produces more neutrons per captured neutron at thermal energies than either ^{235}U or ^{239}Pu. Thus, thorium can be partially substituted for U in reactors with the advantage of reducing the amount of long-lived isotopes of Np, Am, Cu and Pu in the spent fuel and producing high-level nuclear waste that is "safer" (MacFarlane & Miller 2007). If completely fissioned, one pound (0.45 kg) of ^{233}U will provide the same amount of energy as burning 1,350 tonnes of coal.

The U cycle shown in Figure 1-3 is often referred to by others as the nuclear fuel cycle. In most renditions of the nuclear fuel cycle, the very first step involving exploration is overlooked. This is the first critical step and probably the least trivial in the nuclear fuel cycle as it cannot be engineered. Once an ore deposit is discovered, a mine is developed and U extracted by a variety of mining techniques, depending on the type of deposit. The resulting ore is treated to extract the U, which is normally converted to ammonium diuranate, which is yellow in color, and tailings are produced (Fig 1-3). The "yellow cake" is sent to a processing plant and either converted to UO_2 for use in heavy water reactors, or to UF_6 and then enriched in ^{235}U and fabricated into UO_2 fuel rods for use in light water reactors. These are used by the reactors, resulting in spent fuel rods that are reprocessed and converted into additional fuel (or Pu for weapons), or stored (Fig. 1-3).

Concerns about nuclear power

The use of U as a fuel for nuclear reactors is not without its caveats. Constraints on the use of nuclear energy include the cost, the waste produced, safety and resources (MacFarlane & Miller 2007). Although the focus of this volume is the latter, those working in U exploration must be aware of the strongest and weakest links in the industry and the complexities that affect the need for U, both perceived and real.

The operational, maintenance and fuel costs for nuclear power are only half of that for fossil fuels, but nuclear power plants cost 4 times as much and require much longer times to build than

plants that use fossil fuels (Ansolabehere *et al.* 2003). Securing licenses for nuclear power plants is an arduous and expensive task, as is getting acceptance by the local community. Some of these higher costs for nuclear power plants may be offset by carbon taxes in the future, but the lead time for building a nuclear power plant is lengthy, at least 10 years (Ansolabehere *et al.* 2003). The amount of spent fuel produced each year is about 12,000 tonnes (World Nuclear Association 2008). The composition of spent enriched fuel is 95% ^{238}U, 1% ^{235}U and 1% ^{239}Pu, so that most of the potential energy in the fuel is not used. However, the spent fuel also contains fission products such as bioactive ^{131}I, ^{90}Sr and ^{137}Cs with relatively short half-lives, and many longer lived, intensely radioactive isotopes such as ^{99}Tc, ^{140}Ce and ^{239}Pu that render it dangerous, thus requiring reprocessing, disposal or storage for hundreds to thousands of years.

Spent fuel is currently stored in cooling pools at reactor sites or centralized facilities as no country has established a permanent solution to disposing of high-level waste, although most are examining sites based on knowledge of the geochemical behavior of U in natural geological environments. The method of disposal has been debated, not only on the grounds of whether it should be permanent or temporary so that the unused portion of the fuel can be reclaimed with technological advances, but also whether the current practice of storing the fuel in densely packed configurations in cooling pools proximal to reactors is a target for terrorists. The disposal issue is charged with political and social concerns that are unlikely to be solved, or to remain static, in the near future.

Uranium used in nuclear reactors has a significant risk in the proliferation of nuclear weapons. Plants constructed to enrich natural U with a centrifuge process to produce fuels for light water reactors also can be converted to produce weapons-grade U which has > 90% ^{233}U. In addition, spent fuel can be reprocessed using a closed fuel cycle to extract the Pu, which is used by France, UK, Russia, India and Japan to reuse Pu in mixed oxide fuels. In the past, this Pu was diverted to make nuclear weapons, and the fear is that this could be done again, even under the auspices of strict regulations. Regardless of how secure the process is by which fuels are made and reused, the legacy of U as the world's most dangerous waste and its use in weapons will always persist. Projections by the Energy Information Agency (EIA 2007) indicate that all forms of energy will increase by 32% over the next 20 years (Fig. 1-4), primarily in response to demand from India and China. Nuclear energy and renewable sources of energy will remain equal, but both pale in proportion to the energy supplied by fossil fuels. The current known reserves of U might be sufficient to supply the increased demand for nuclear reactors for the next century, but this depends greatly on the economic landscape that develops. The development of the fourth generation of nuclear reactors in the foreseeable future could theoretically increase the usefulness of U resources by a factor of a hundred.

MAJOR DEPOSIT TYPES

There are many different ways of classifying U deposits depending on the tendency of the classifier to put deposits into more generic classes, or divide deposits according to their style of occurrence. Most classifications by the IAEA and major U mining companies are similar and involve between 12 and 18 deposit types. One of the problems with subdividing deposits is that a genetic connotation can be implied, but one of the advantages is that the model of formation or location that is implied can be used to refine exploration strategies. This can lead to the discovery of new deposits if the model is sophisticated enough to identify prospective areas from barren areas. One widely used classification (OECD 2000, IAEA 2004, 2006) groups deposits into 15 categories based on their geologic setting, with the 11 major types shown in Table 1-2. The following is a brief description of each, outlining the salient features as summarized in Table 1-2 and Figure 1-5.

(1) Unconformity-related deposits occur close to major unconformities between Archean–Paleoproterozoic metasedimentary rocks and overlying Paleo–Mesoproterozoic sandstone units in large marginal or intracratonic basins (Fig. 1-5). The deposits occur within the basement or sandstone, but within a few hundred metres of the unconformity. The deposits are hosted by faults and are commonly associated with brecciation. They involve formation from brines at 150–250°C. Those discovered so far are restricted to the Proterozoic and most formed shortly after the assembly of large continents (Table 1-2).

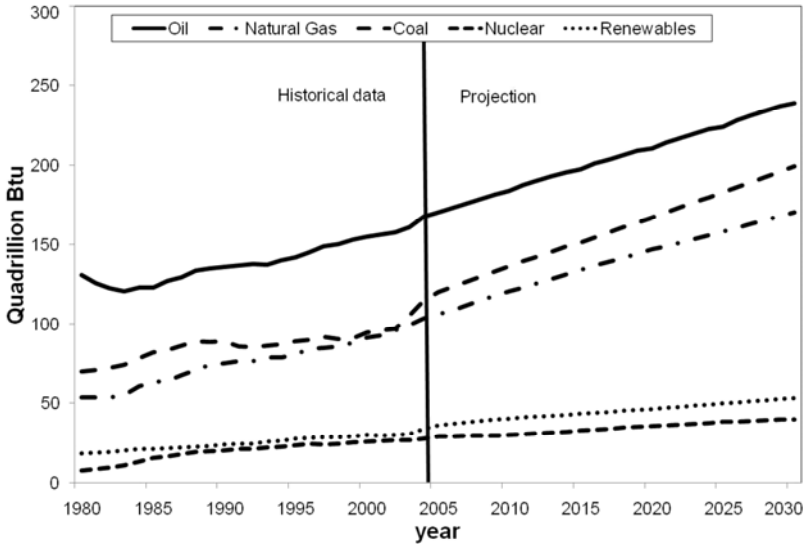

FIG. 1-4. World Marketed Energy Use by Fuel Type for 1980-2030. Historical data from before 2005 and other data from projections by EIA (2007).

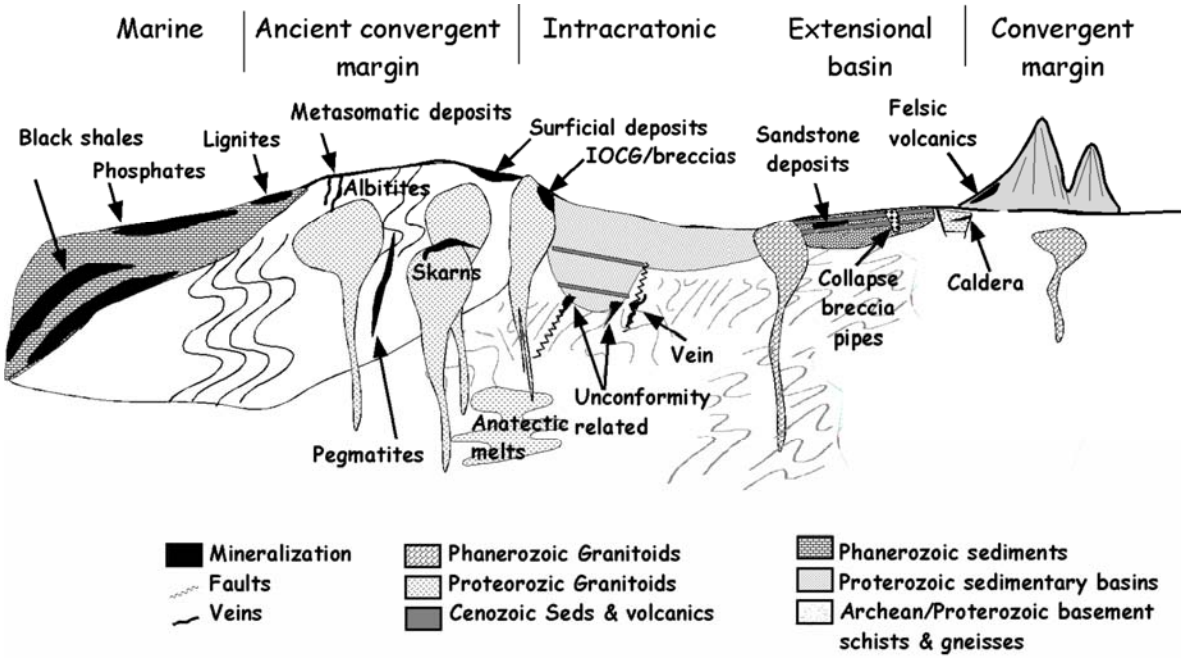

FIG. 1-5. Schematic representation of the location of various types of U deposits. See Table 1-2 and text for explanation.

Unconformity-related deposits constitute about 12% of the total U resources globally, but 33% of the current global production and include some of the largest and richest U deposits (*e.g.* McMurray 2006). Uraninite is the major mineral in these deposits, although many of them have been affected by later fluid events that have altered the uraninite. Major deposits occur in the Athabasca Basin in Canada and the Alligator River region of Australia and these deposits average 0.8% U, with the largest deposits up to 23% U (Jefferson *et al.* 2007). Recent discoveries have indicated unconformity-related deposits occur in the Karelia region of Russia and Finland (Velichkin *et al.* 2005), the Paterson Basin in Western Australia (McKay & Miezitis 2001) and the Thelon Basin in

TABLE 1-2. GENERAL CHARACTERISTICS OF URANIUM DEPOSITS LISTED IN ORDER OF ECONOMIC SIGNIFICANCE.

DEPOSIT TYPE	GEOLOGY	GRADE (% U)	GLOBAL RESOURCE 2007 (tU)	GLOBAL PRODUCTION 2007 (tU)	TEMP. FORMED (°C)	TYPES OF FLUIDS	MAIN AGE	EXAMPLES
Unconform-ity-related	Intracratonic/ marginal basins	1.0 - 25.0	649700	15600	200-300	Basinal & basement brines	1500-1900 Ma	Rabbit Lake, McArthur River (Athabasca Basin); Narbarlek, Ranger (NT, Australia); Karku (Russia)
Sandstone hosted	Extensional rift basins	0.05 - 0.5	1524000	10000	25-100	Groundwater	Phanerozoic to Tertiary	Mokum, Inkay (Kazakhstan), Colorado Plateau (USA), Beverley (Australia), Akouta (Niger)
Vein deposits	Post orogenic extensional basins	0.1 - 2.0	324500	4220	200-500	Metamorphic & hydrothermal	Proterozoic to Mesozoic	Pribram , Jachymov (Czech Republic), Shinkolobwe (DR Congo), Massif Central (France), Iberia (Spain/Portugal), Dhada (Congo), Schwartzwalder (USA)
Metasomatic	Rift/back arc basins	0.05 - 0.2	673700	3800	300-700	Metamorphic & magmatic	Proterozoic	Pervomayskoye (Ukraine), Lagoa Real (Brazil), Valhalla (Australia)
IOCG/ breccia	Arc/Marginal Basin	0.03 - 0.05	901000	2000	200-500	Magmatic & later hydrothermal	Proterozoic	Olympic Dam (Australia)
Intrusive	Alkaline complexes	0.01 - 0.5	287900	1000	300-700	Magmatic & hydrothermal	All	Rössing (Namibia), Ilimaussaq (Greenland), Palabora (S. Africa)
Volcanic associated	Rift/back arc basins	0.03 - 0.3	211300	1000	200-500	Basinal brines & magmatic fluids	All	Streltsovsk caldera (Russia), Dornot (Mongolia), Nopal (Mexico), McDermitt (USA), Xiangshan (China)
Quartz-pebble con-glomerate	Intracratonic & marginal basins		300000	600	50-300	Groundwater & later hydrothermal	2200-2700 Ma	Witswatersrand (S. Africa), Blind River/ Elliot Lake (Canada)
Surficial	Drainage basin	0.03 - 0.1	100000	0	25-50	Groundwater	Tertiary	Yeelirrie (Australia), Langer Heinrich (Namibia)
Collapse breccia pipes	Intracratonic & extensional basins	0.4 - 1.5	50000	0	200-300	Basinal brines	Tertiary	Arizona Strip (USA)
Phosphorite	Continental shelf/marine	0.005 - 0.05	447000	0	20-50	Marine & brackish fluids	Phanerozoic	Uncle Sam (USA), Gantour, (Morocco), Al-Abiad (Jordan), Randstat (Sweden)

Data sources: Dahlkamp (1993), Plant *et al.* (1999), OCED (2008), McMurray (2006), Shatalov *et al.* (2006). Resources are for <US$ 130/kg. and total 5,469,000.

the Northwest Territories of Canada (Davidson & Gandhi 1989). All of Canada's U production is from unconformity-related deposits, which occur in either the basement rocks or overlying sandstones. In contrast, unconformity-related deposits in Australia are hosted by metamorphic basement rocks beneath the unconformity. Many, but not all, unconformity-related deposits are associated with graphitic sedimentary units in the basement.

A few deposits occur in the Paleoproterozoic Hornby Bay Basin in Canada and the Franceville Basin in Gabon, but at the boundary between sandstone and grey or black shale (*e.g.*, Dahlkamp 1993). Although these are normally classified as sandstone U deposits, they have characteristics that are transitional between unconformity-related deposits and sandstone deposits.

The total age spectrum of unconformity-related U mineralization is between 1000 and 2000 Ma, with the oldest deposits from the Franceville Basin in Gabon. Some of these latter deposits preserve the effects of natural reactors gone critical due to the higher ^{235}U contents (3.7% ^{235}U at 3 Ga) they had relative to younger deposits.

(2) Sandstone uranium deposits occur in medium to coarse-grained arkosic sandstone units deposited in continental fluvial or marginal marine sedimentary environments (*e.g.*, Sanford 1994). Impermeable mudstone, which is interbedded in the sedimentary sequence, commonly occurs above and below the mineralized sandstone (Fig. 1-5). Uranium is precipitated as UO_2 or $USiO_4$ (coffinite) by reduction of U^{6+} (see Chapter 3) by fluids that interact with reductants such as carbonaceous materials, sulfides, hydrocarbons and interbedded mafic volcanic rocks with abundant Fe-bearing minerals like chlorite (IAEA 1985). Most deposits are younger than 440 Ma, after the point in Earth history when organisms began to invade the continents. Most form at low temperatures and from slightly modified basinal brines. Sandstone deposits constitute about 28% of world U resources, 32% of the global production, have grades of 0.05 to 0.5% U, and have a maximum size of about 15,000 t U (Table 1-2). Most current mining operations involve *in situ* leach methods.

Three main types of sandstone deposits are found:

1. Roll front deposits are arcuate bodies of U mineralization that cross-cut sandstone bedding. They form in intracratonic basins, and tend to be overlain by volcanic ashes, which may be a source of the U.
2. Tabular deposits form sub-parallel to bedding and parallel to the paleo-drainage direction and tend to be underlain by evaporite deposits and overlain by mudstone (Young 1984, Sanford 1994). These deposits represent the largest U resource in the U.S.A.
3. Tectonic/lithologic deposits occur in sandstone adjacent to permeable fault zones. Most have limited volumes and all have variable grades.

Large resources of sandstone U deposits occur in sandstone deposits in Niger, Kazakhstan, Uzbekistan and the Karoo of South Africa.

(3) Vein deposits occur as veins in metamorphic (and other) rocks and commonly contain deposits that do not fit into other types, and have origins that are complex (Ruzicka 1982, IAEA 1986, Martin-Izard *et al.* 2002). Vein deposits constitute 7% of the global reserves and about 10% of world U production. Major deposits include Jachymov (Czech Republic) and Shinkolobwe (Democratic Republic of the Congo).

(4) Metasomatic deposits occur in structurally deformed rocks mainly altered by sodium or calcium metasomatism and hematization (Dahlkamp 1993, Plant *et al.* 1999). Major examples of this deposit type are Lagoa Real in Brazil, Zheltye Vody deposit in Ukraine and Valhalla in Australia. The grades tend to be low, less than 0.17% U and these deposits currently constitute 9% of the global reserves and, together with breccia-hosted deposits, constitute about 10% of the global U production.

(5) Breccia complex deposits of U are dominated by the Mesoproterozoic (1590 Ma) Olympic Dam iron oxide–copper–gold (IOCG) deposit, the world's largest deposit at about 2,200,000 t U , and which occurs in a hematite-rich granite breccia complex in the Gawler Craton (Reeve *et al.* 1990). The central core of the complex is barren hematite–quartz breccia, flanked to the east and west by zones of hematite-rich breccia and granitic breccia approximately one kilometre wide and extending almost 5 km in a northwest–southeast direction. Copper–uranium mineralization is hosted by this hematite-rich breccia. Granitic breccia, extending up to 3 km beyond the outer limits of the hematite-rich breccia, contains Fe, Cu, U, Au, Ag, REE and F. Only Cu, U, Au, and Ag are recovered and U

grades average about 0.04% U (Table 1-2). Principal mechanisms which formed the breccia complex are considered to have been hydraulic fracturing, tectonic faulting, chemical corrosion, and gravity collapse in the near-surface eruptive environment of a crater complex during eruptions caused by boiling and explosive interaction of groundwater or brines with magma. The few other IOCG-related deposits that contain U, such as Ernest Henry in Australia, are of much lower grades and size (Table 1-2). As a group, these deposits constitute 15% of the global reserves and 10% of the global production of U (along with vein-type deposits). They have the lowest grades and normally would not be considered as U deposits were they not polymetallic.

(6) Intrusive deposits are associated with high temperature concentrations of U in intrusive rocks including alaskite, granite, pegmatite, carbonatite, and monzonite. Major world deposits include Rössing (Namibia), Ilimaussaq (Greenland) and Palabora (South Africa). They tend to have low grades and comprise 5% of the global reserves and 3% of the current global production.

(7) Volcanic associated deposits occur with felsic volcanic rocks, mainly in continental extensional settings, and in some cases in caldera complexes (Leroy & George-Aniel 1992). The deposits are related to faults and shears within the volcanic units and U is commonly associated with Mo, F, Th, and REEs (Plant *et al.* 1999). They comprise 3% of the global U production and typically have grades of 0.04–4% U. These form from U-enriched felsic magmas that are subsequently enriched by hydrothermal fluids. They range in age from Proterozoic to Tertiary. The best known deposits are those at Streltsovsk caldera in Russia, the McDermitt caldera in Basin and Range in the USA, Peña Blanca in Mexico and Xiangshan in China.

(8) Quartz-pebble conglomerate deposits constitute about 6% of the global U reserves and only 2% of the global production. The deposits occur as uraninite, brannerite, monazite and thoro-uraninite in basal Paleoproterozoic conglomerate units that overlie Archean basement (IAEA 1987). The U occurs in seams rich in pyrite and organic matter. The grade may be as low as 0.008% U when produced as a by-product of gold mining at the Witwatersrand Au–U deposits in South Africa, and as high as 0.14% U in deposits mined exclusively for U, such as the Elliot Lake deposits in Canada. Each of these deposits contains about 170,000 t U, although the total resources are much larger. Although the mining operations in the Elliot Lake area have closed, these deposits may become economic under current U market conditions. The origin of the U in these deposits remains contentious, with most models favoring a detrital origin for some of the U and a later hydrothermal remobilization and introduction of additional U that reacted with carbonaceous material.

(9) Surficial uranium deposits are Tertiary to Recent U concentrations in sediment or soil (IAEA 1984). These deposits have abundant secondary cements and those in calcretes are the largest of the surficial deposits. The main mineral in these deposits is carnotite, a potassium uranium vanadate. Surficial deposits comprise about 2% of global resources of U but are approaching 5% of the global production. These deposits form from low temperature groundwater in arid environments to produce calcretes, under cool wet conditions in peat bogs and in limestone caverns. The typical ore grades of these deposits are 0.2% U for Yeleeree in Australia and 0.06% U for Langer Heinrich in Namibia. Because these deposits form at the surface, they most likely reflect specific environmental conditions in earth history, such as periods transitional from wet to dry climates.

(10) Collapse breccia pipe deposits occur uniquely in Arizona and are hosted in a sequence of limestone, sandstone and shale (*e.g.*, Wenrich *et al.* 1995). These deposits average about 0.5% U, but are second to unconformity-related deposits in terms of highest grades. They have properties that are somewhat akin to sandstone deposits, but also to unconformity-related systems.

(11) Phosphorite deposits form from upwelling of nutrient-rich marine waters onto a shallow continental shelf with restricted circulation. Although the grades can reach 0.065% U and the resource is substantial, the U is also associated with other elements such as Se and As and the waste would be an environmental problem. Up to 900 t/yr were mined from the Florida phosphates, mainly during the 1980s. Currently no phosphates are mined for U, but U is recovered unofficially from phosphates used for the production of fertilizers by several countries and most countries do not report U from phosphorite as a resource.

Reserves of U from phosphorite deposits are dominated by those from Morocco. The estimates shown in Table 1-2 are extremely conservative, and recent estimates reach 22 million tU globally (OECD 2008). Notwithstanding the problems associated with extracting the U and other elements from phosphorite, these deposits represent a significant reservoir of U that may be more strategic in the near future.

(12) Black shale and seawater also represent significant reserves of U, although economic extraction of U from each is a challenge. Uranium in shale resides with organic matter. The U contents of black shale are variable but can reach 400 ppm, such as in the Ranstad deposit in Sweden. Exploration for black shale deposits is currently in progress in several countries, with consideration for a mix of metals in addition to U. Significant reserves of U have been reported from the Chattanooga (USA) and Ronneburg (Germany) black shale, totaling nearly 4.2 million tU (OECD 2008).

The U concentration of sea water is only 3.2 ppb but the quantity of U is substantial, about 4 billion tonnes. Research on an extraction process being developed in Japan suggests that it might be feasible to recover U from seawater at a cost of US $300/kg of U (Nobukawa 1994; OECD 2008).

THORIUM

Thorium is becoming a much more strategic element for energy production because ^{232}Th produces ^{233}U, an effective fuel when exposed to neutrons. Although this requires U to supply the flux of neutrons, fourth generation reactors should have the capability to burn more of the fuel available and produce waste that is less hazardous.

Most of the currently known global resources of Th resulted from exploration for U, rare earth elements, Nb and Ti in alkaline igneous complexes. Global reserves for Th total about 6,100,000 tonnes at <US$ 130/kg Th, with carbonatites, placer deposits, vein-type mineralization and alkaline complexes as the major sources (OECD 2008). Currently, Th is recovered mainly from the mineral monazite as a by-product of heavy mineral mining. Those countries that report reserves of Th include Australia, USA, Turkey, India and Brazil, although most countries have not been diligent in reporting Th occurrences because currently there is no market.

DISTRIBUTION OF MINES AND RESOURCES

Uranium mines operate in 20 countries globally, though more than two-thirds of world production comes from just ten mines that have average grades in excess of 0.10% U, with some Canadian mines such as McArthur River and Cigar Lake having average grades up to 25% U (Fig. 1-6). Some U is recovered as a by-product with copper, such as at Olympic Dam in Australia, or as by-product from the treatment of gold, such as the gold-bearing ores of South Africa.

Australia has the largest recoverable reserves of U at 23% of the global total, in large part because of the Olympic Dam IOCG deposit and unconformity-related deposits (Table 1-3). Kazakhstan has 15% of the global reserves, which are mainly sandstone-type deposits mined using *in situ* leach (ISL) methods, and Canada has the next most plentiful reserves at 8%, entirely from unconformity-related ore deposits (Table 1-3).

Australia emerged as a major source of U in the 1970s with important discoveries of unconformity-related deposits at Ranger, Jabiluka and Nabarlek, and IOGC-related deposits at Olympic Dam.

Kazakhstan has been a source of U for more than fifty years, with U historically mined in vein and volcanic-hosted deposits, but almost all production is currently from ISL mines in sedimentary basins. Uranium production in South Africa was primarily a by-product of gold mining. In Namibia, the large Rössing open cut mine has been in operation since 1976, and currently produces about 7.5% of world supply, and Langer Heinrich, a calcrete deposit, will open in the near future. Niger produces 5% of the global production through the Akouta underground mine and Arlit open pit mine. China had U mines fully operational beginning in 1962 and currently has 26 major U mines. China is focusing on *in situ* and heap leach technologies.

The first phase of Canadian U production peaked in 1959 when more than 12,000 tonnes of U were produced. However, U exploration in Canada began in earnest with the discovery of unconformity-related U deposits in the Athabasca Basin. The Rabbit Lake, Cluff Lake and Key Lake mines began operation in 1975 to 1983 and exploration resulted in the discovery of Midwest, McClean Lake and Cigar Lake deposits. In 1988, Cameco Corporation discovered the McArthur River deposit at a depth of over 500 metres and a

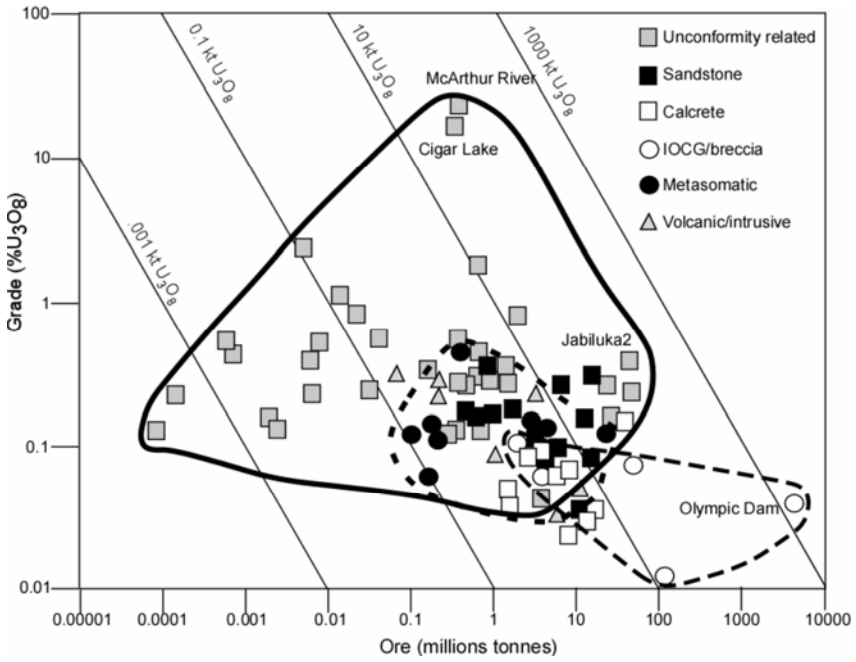

FIG. 1-6. Grade *vs*. tonnage for major types of U ore deposits. Unconformity-related deposits, encompassed by the solid line, have the highest grade and large reserves. Particularly high grades and reserves characterize the deposits at Cigar Lake and McArthur River in the Athabasca Basin, and large reserves also occur in the Jabiluka2 deposit in Australia. Volcanic/intrusive, metasomatic, sandstone and calcrete U deposits, indicated by the group surrounded by the short dashed line, have much lower grades and are smaller, as are IOCG/breccia related deposits, shown by group indicated by the long dashed line, except for Olympic Dam where U is a by-product.

TABLE 1-3. KNOWN RECOVERABLE RESOURCES OF URANIUM TO US$ 130/KG U

Country	tonnes U	% of world
Australia	1,243,000	23%
Kazakhstan	817,300	15%
Russian Fed.	545,600	10%
South Africa	435,100	8%
Canada	423,200	8%
USA	339,000	6%
Brazil	278,400	5%
Namibia	275,000	5%
Niger	274,000	5%
Ukraine	199,500	4%
Jordan	111,800	2%
Uzbekistan	111,000	2%
India	72,900	1%
China	67,900	1%
Other	287,000	5%
World total	5,469,000	

Source: (OECD 2008).

grade of 21% U, currently supplying 17% of the total global U production. Canada produces about one third of the global primary U production.

The largest single source of U ore in the United States was the Colorado Plateau located in Colorado, Utah, New Mexico, and Arizona. The U.S. federal government paid discovery bonuses and guaranteed purchase prices to anyone who found and delivered U ore, and was the sole legal purchaser of the U. The economic incentives resulted in a frenzy of exploration and mining activity throughout the Colorado Plateau from 1947 through 1959.

MINING AND PROCESSING METHODS FOR URANIUM

There are three main methods by which U ore is mined, depending on the type of deposit (World Nuclear Assoc – www.world-nuclear.org/education/mining.htm).

Open pit. Where ore bodies lie close to the surface, they are usually accessed by open cut mining, involving a large pit and the removal of much overburden as well as a lot of waste rock. About

30% of all U ore mined in 2007 was from open pits less than 200 m depth. This extraction method is similar to any other surface mine or quarry and involves drilling, blasting and transport to the crushing and milling plant. Some of the world's largest U deposits (Ranger, Australia; Rössing, Namibia; McClean Lake, Canada) are mined by open pit methods.

Underground. Where ore bodies are deeper, underground mining is usually employed, involving construction of access tunnels and shafts but with less waste rock removed and less environmental impact. About 50% of U ore is mined from underground. This method has hazards associated with radon gas and radioactivity from high-grade ores, so that remote controlled methods have been developed to minimize the risk of exposure to operators. The world's largest U mine at McArthur River in Canada, Rabbit Lake in Canada and Akouta in Niger are mined in this way.

In situ leaching. Some ore bodies lie in porous unconsolidated material and may be accessed by leaching with oxygenated groundwater or various acids. About 20% of U mining is done by *in situ* leaching. This technology is only suitable for permeable ore bodies such as sandstone-hosted deposits lying between two impervious clay-rich layers. The host rock is relatively undisturbed, minimizing disturbance to the surface with very little waste tailings. In this method either an alkaline or acid solution is injected into the ore body from a grid of wells along with an oxidant. The U is dissolved into the solution and the fluid pumped to the surface. Uranium from the leachate is removed using either an ion exchange system or solvent extraction depending on the salinity of the fluid. With the ion exchange system the U slurry is dewatered and dried to give hydrated U peroxide. After the U has been removed from the solution, the fluid is re-injected into a closed circuit. A small amount of the fluid is removed to avoid any contamination of surrounding aquifers.

Ore extracted by open pit or underground mining is first crushed and ground to a fine powder and then mixed with water into a slurry. The slurry is pumped into leaching tanks where acid is used to dissolve the U minerals from the ore. The U in solution is then separated from the tailings and the U is separated with a solvent extraction process. The dissolved U is precipitated as ammonium diuranate, commonly referred to as "yellowcake" because of its bright yellow color.

About 10% of U mined is recovered as a by-product of copper or gold mining operations, primarily from the Olympic Dam mine in South Australia. The ore at Olympic Dam is extracted and crushed underground before being transported to the surface for milling. It is then treated in a copper sulfide flotation plant to remove Cu. Approximately 80% of the U remains in the tailings and is recovered by acid leaching. The copper concentrate is also processed through an acid leach to remove any remaining U.

SYNOPSIS

Knowledge of the general properties of U, the nuclear power cycle, deposit types and mining methods are all important to the U industry, but to exploration in particular because discovery of deposits is now, and always has been, the overall rate-limiting step to success of the industry. To have a mine, discovery of ore bodies is necessary, which requires a knowledge base that must be constructed, expanded and always refined. Most of the largest and most profitable mines are associated with sedimentary basins, particularly those mined using open pit methods. Finding these and other types of U deposits requires knowledge of how economics in the U industry and research results might affect exploration strategies. This is the subject of Chapter 2.

REFERENCES

ANSOLABEHERE, S., DEUTCH, J., DRISCOLL, M., GRAY, P.E., HOLDREN, J.P., JOSKOW, P.L., LESTER, R.K., MONIZ, E.J. & TODREAS, N.E. (2003): The Future of Nuclear Power. *Mass. Inst. Technology*, Cambridge, MA, 180 pp, http://web.mit.edu/ nuclearpower/.

BECQUEREL, A.H. (1896): On the invisible rays emitted by phosphorescent bodies. *Comptes Rendus de Séances de l'Académie de Sciences*, **122**, 501-503.

CLARK, S.P., JR., PETERMAN, Z.E. & HEIER, K.S. (1966): Abundances of uranium, thorium, and potassium. In: S.P. Clark Jr. (Ed.), *Handbook of Physical Constants, revised edition*. Geol. Soc. Am., Memoir **97**, 521-541.

CURIE, P. & CURIE, M. (1898): Sur une nouvelle substance radioactive, contenue dans la pechblende. *Comptes Rendus de Séances de l'Académie de Sciences* **127**, 175-178.

DAHLKAMP, F.J. (1993): *Uranium Ore Deposits*.

Springer-Verlag, Berlin, 460 pp.

DAVIDSON, G.I. & GANDHI, S.S. (1989): Unconformity-related U-Au mineralization in the middle Proterozoic Thelon Sandstone, Boomerang Lake Prospect, Northwest Territories, Canada. *Econ. Geol.* **84**, 143-157.

ENERGY INFORMATION ADMINISTRATION (2007): *International Energy Outlook 2007*. Department of Energy, Washington, D.C., www.eia.doe.gov/oiaf/ieo/index.html.

IAEA (1984): *Surficial Uranium Deposits*. IAEA-TECDOC-322, Austria, 252 pp.

IAEA (1985): *Geological Environments of Sandstone-Type Uranium Deposits*. IAEA-TECDOC-328, 408 pp.

IAEA (1986): *Vein Type Uranium Deposits*. IAEA-TECDOC-361, 423 pp.

IAEA (1987): Uranium deposits in Proterozoic quartz-pebble conglomerates. IAEA-TECDOC-427, 459 pp.

JEFFERSON, C.W., THOMAS, D.J., GANDHI, S.S., RAMAEKERS, P., DELANEY, G., BRISBAN, D., CUTTS, C., PORTELLA, P. & OLSON, R.A. (2007): Unconformity associated uranium deposits. *In*: Goodfellow W.D. (ed) Mineral Resources of Canada: A Synthesis of Major Deposit-types, District Metallogeny, the Evolution of Geological Provinces, and Exploration Methods, 273-306. Mineral Deposits Division of the Geological Association of Canada.

LEROY, J.L. & GEORGE-ANIEL, B, (1992): Volcanism and uranium mineralization: the concept of source rock and concentration mechanism. *J. Volcan. Geotherm. Res.* **50**, 247-272.

MACFARLANE, A.M. & MILLER, M. (2007): Nuclear energy and uranium resources. *Elements* **3**, 185-192.

MARTIN-IZARD, A., ARRIBAS, A., SR, ARIAS, D., RUIZ, J. & FERNANDEZ, F.J. (2002): The Fe deposit, West-Central Spain; tectonic-hydrothermal uranium mineralization associated with transpressional faulting of Alpine age. *Can. Mineral.* **40,** 1505-1520.

MCKAY, A.D. & MIEZITIS, Y. (2001): Australia's uranium resources, geology and development of deposits. *AGSO-Geoscience Australia, Mineral Resource Report* **1**, 115 pp.

MCMURRAY, J.M. (2006): Worldwide uranium resources and production capacity – the future of the industry. *In:* Uranium production and raw materials for the nuclear fuel cycle – Supply and demand, economics, the environment and energy security. IAEA-CN-128, IAEA, Vienna, 27-35.

NOBUKAWA, H. (1994): Development of a floating type system for uranium extraction from sea water using sea current and wave power. In Proceedings of the 4th International Offshore and Polar Engineering Conference (Osaka, Japan), 294-300.

OECD/NEA-IAEA (2000): *Uranium 1999: Resources, Production and Demand, 1999 Red Book*. OECD, Paris, France.

OECD/NEA-IAEA (2006): *Uranium 2005: Resources, Production and Demand, 2005 Red Book*. OECD, Paris, France.

OECD/NEA-IAEA (2008): *Uranium 2007: Resources, Production and Demand, 2007 Red Book*. OECD, Paris, France.

PACALA, S. & SOCOLOW, R. (2004): Stabilization wedges: Solving the climate problem for the next 50 years with current technologies. *Science* **305**, 968-972.

PLANT, J.A., SIMPSON, P.R., SMITH, B. & WINDLEY, B. (1999): Uranium ore deposits – products of the radioactive Earth. *In*: Burns, P.C., Finch, R. (eds) Uranium: Mineralogy, Geochemistry and the Environment. *Mineral. Soc. Am., Rev. in Mineral.* **38**, 255-319.

REEVE, J.S., CROSS, K.C., SMITH, R.N. & ORESKES, N. (1990): Olympic Dam copper-uranium-gold-silver deposit, Melbourne. *Australasian Inst. Mining Metallurgy Monograph* **14**, 1009–1035.

RUZICKA, V. (1982): Notes on mineralogy of various types of uranium deposits and genetic implications. *Geol. Survey Can. Paper* **82,** 341 p.

SANFORD, R. (1994): Hydrogeology of Jurassic and Triassic wetlands in the Colorado Plateau and the origin of tabular sandstone uranium deposits. *U.S. Geol. Surv. Prof. Paper* **1548**.

SHATALOV, V.V., TAKHANOV, A.V., BOLDYREV, V.A. & KNYAZEV, O.I. (2006): Analysis of uranium world resources and ways of their extension. *In:* Uranium production and raw materials for the nuclear fuel cycle–Supply and demand, economics, the environment and energy security. *IAEA-CN-128*, IAEA, Vienna, 103-110.

VELICHKIN, V.I., KUSHNERENKO, V.K., TARASOV, N.N., ANDREEVA, O.V., KISELEVA, G.D., KRYLOVA, T.L., DONIKOVA, O.A., GOLUBEV,

V.N. & GOLOVIN, V.A. (2005): Geology and formation conditions of the Karku unconformity-type deposit in the Northern Ladoga region (Russia). *Geology of Ore Deposits* **47**, 87-112.

WENRICH K. J., VAN GOSEN B. S. & FINCH W. I. (1995): Solution-collapse breccia pipe U deposits; Preliminary compilation of descriptive geoenvironmental mineral deposit models. *USGS Open File Report* **95-0831,** 244-251.

WORLD NUCLEAR ASSOCIATION (2008): The nuclear fuel cycle. http://www.world-nuclear.org/info/inf03.html

YOUNG, R. (1984): Uranium deposits of the world, excluding Europe. *In*: Vivo, B.D., Ippolito, F., Capaldi, G. & Simpson, P.R. (*eds*.) Uranium Geochemistry, Mineralogy, Geology, Exploration and Resources. Inst. Min. & Metallurgy, London, pp 117-139.

CHAPTER 2: THE EFFECT OF ECONOMIC AND RESEARCH FACTORS IN UNDERSTANDING URANIUM EXPLORATION AND DISCOVERY OF DEPOSITS

Kurt Kyser
Department of Geological Sciences and Geological Engineering,
Queen's University,
Kingston, Ontario, K7L 3N6, Canada
kyser@geol.queensu.ca

and

Michel Cuney
G2R, Nancy-Université, CNRS, CREGU,
B.P. 239,
F-54506 Vandoeuvre lés Nancy, France
michel.cuney@g2r.uhp-nancy.fr

Two factors figure greatly in the exploration and exploitation of ore deposits, namely economic factors and the role of research. Although awareness of economics has become more acute by most geologists because profit is the bottom line, the effective analysis of economic factors and the role of research in understanding U exploration are sometimes overlooked. The purpose of this chapter is to review some of the financial realities of the U industry and to discuss research strategies during the past 30 years that affect exploration.

ECONOMIC FACTORS

As a metal commodity, U is distinguished by its use in energy generation, but also by the historical use as a military weapon. As a consequence, the past 30 years have seen unrivalled global efforts to collect data on the state of the U industry, in part to aid in more effective regulation. Until 20 years ago, this effort was largely a Western world one, with only estimates of resources for China and the USSR. The breakup of the former Soviet Union and changes in global politics afforded more reliable data from the East, and the release of research results on U deposits that were formerly unavailable to the West. Globally, the U industry, which currently comprises about 56,000 man-years of employment, thinks of itself as transparent and current, with databases and regulations that far exceed those for most other commodities.

The Organization for Economic Co-operation and Development (OECD) and the International Atomic Energy Association (IAEA) host the U Group, a data collection and analysis organization that focuses on establishing a global U resource base. Reports by the Uranium Group on the status of the U industry, which have been published biennially since 1965, are entitled ***Uranium: Resources, Production and Demand***, commonly known as the "Red Book". These publications are an excellent source of where U is mined, how much is mined, the value of the reserves, the environmental issues and the financial state of the industry. In addition to the "Red Book" as a source of data on the U industry, ***The Red Book Prospective*** is a publication by the OECD that summarizes, analyzes and complements data from the "Red Book", providing information on nuclear capacity, inventories of U and Th, mine histories and environmental aspects related to the U industry (Price *et al.* 2006).

The Uranium Group classifies U resources into three main categories:

1. Reasonably assured resources (RAR).
2. Inferred resources (IR).
3. Speculative resources (SR).

The first two categories are often combined into Identified Resources to reflect the realistic resources recoverable (Table 2-1). However, the true "resource" of a commodity is a function of the resources that can be recovered within a given price range. Consequently, estimates of resources are based on the price of U, which also is divided into three categories: <US $40/kg U (US $15/ pound U_3O_8), <US $80/kg U (US $33/pound U_3O_8), <US $130/kg U (US $50/pound U_3O_8). For example, the global resources in 2007 were 4.456 million tonnes of U (t U) at <US $80/kg and 5.469 million t U at <US $130/kg (Table 2-1). Recently, these estimates

Short course co-sponsored by the the SGA and MAC, Québec City, May 2008, p. 15–22

TABLE 2.1. IDENTIFIED (REASONABLY ASSURED + INFERRED) RESOURCES OF URANIUM (IN 1000 T U) AS OF 2007.

	<US $40 / kg U	<US $80 kg U	<US $130 / kg U
World	2970	4456	5469
Australia	709 + 487	714 + 502	725 + 518
Canada	270 + 82	329 + 94	329 + 94
Kazakhstan	235 + 282	344 + 407	378 + 439
Niger	21 + 13	44 + 31	243 + 31
Brazil	140 + 0	158 + 74	158 + 121
South Africa	115 + 120	206 + 137	284 + 151
Namibia	56 + 61	145 + 86	176 + 99
USA	NA	99	339
Uzbekistan	55 + 31	55 + 31	72 + 39
Russia	48 + 36	172 + 323	172 + 373

have changed significantly because of re-evaluations and the upgrade of the total resources of the Olympic Dam deposit from 1.27 million t U at the end of 2004, to 2.25 million t U at the beginning of 2008. About 85% of highly confident resources (RAR) and inferred resources are recoverable at <US $80/kg, although there is a distinct lack of geographic diversity with 75% of these resources located in just 4 countries (Table 2-1). These resources were to feed the 440 nuclear power reactors and the 270 research reactors that required nearly 70,000 t U (132 million pounds U_3O_8) in 2007 (OECD 2008). Given these and the reactors under construction and anticipated, the need will be 82,000 to 100,000 t U (155 to 189 million pounds U_3O_8) by the year 2025.

Uranium supply is divided into two categories, primary supply and secondary supply. Primary supply includes newly mined and processed U whereas secondary supply includes highly enriched U (HEU) from dismantling of nuclear weapons, reprocessed U from tailings and other sources, mixed oxide fuels and U from stockpiles (McMurray 2006).

Using data from **2007: *Uranium: Resources, Production and Demand***, published by OECD-IAEA, as summarized in Table 2-1, Australia has the largest Identified Resources, followed by Kazakhstan and then the Russian Federation, Canada, South Africa and the USA. Australia, Kazakhstan, the Russian Federation and Canada combined have 56% of the global Inferred Resources (Fig. 2-1). The major source of this U in each country is different, with the iron oxide–copper–gold (IOCG) deposit at Olympic Dam and unconformity-related deposits being the major U resources in Australia, sandstone-hosted deposits that are amenable to *in situ* leach as the major U resource in Kazakhstan and the USA, volcanic-hosted and a mix of other deposit types in the Russian Federation, unconformity- related deposits as the exclusive resource of U in Canada and U in conglomerate as the major resource in South Africa. Note that most of these resources are related to sedimentary basins.

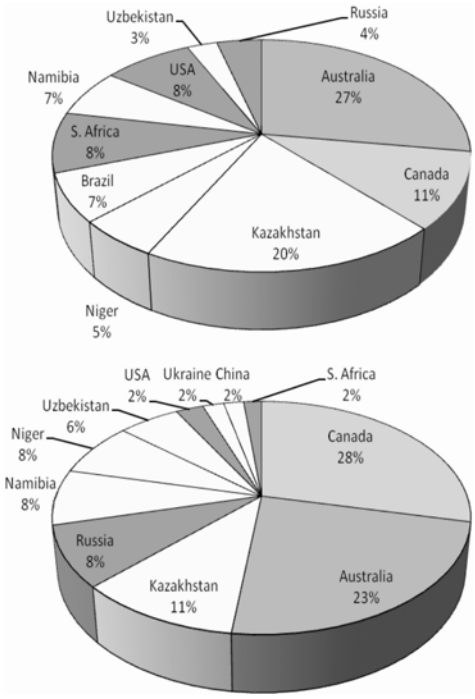

Fig. 2-1. Top panel shows the percentage of global Identified Resources (at < US $130/kg) whereas bottom shows the percentage of U produced in 2006-7 (OECD 2008).

Although Identified Resources at <US $130/ kg are a measure of the spatial distribution of possible global reserves, global annual production has a slightly different distribution (Fig. 2-1). Canada is currently the most significant producer of U globally, followed by Australia and Kazakhstan. Together, these countries account for more than half of the current global primary production of U. However, the USSR, USA and Canada have each accounted for about 17% of the cumulative historical production of U, with the contribution from Canada reflecting the new class of unconformity-related deposits that led to a change in the production profile. The USSR controlled nearly half of the world U production until its collapse in 1991.

Peak global U production occurred during 1980-1990, when annual production was nearly 60,000 t U, well above the civilian annual consumption (Fig. 2-2). Production remained high until 1990 and then declined to about 60% of the annual consumption. The over-production until 1990 resulted in significant stockpiles and low prices, which in turn resulted in low annual production of about 40,000 t U (88 million pounds), much less than the 70,000 t U (154 million pounds) consumed annually since 2003 (Vance *et al.* 2006), and also further reduction in exploration activity.

Primary production of U has been less than reactor requirements since 1990 and secondary sources have made up the difference. Global U primary production currently provides only about 60 percent of reactor requirements (Fig. 2-2). Current production from primary sources (at <US $80/kg) and known secondary sources could nearly supply demand for existing and anticipated reactors until 2010 if all mines that should come into production do so, and no disasters occur (Fig. 2-2). As has been the case for some time, secondary sources are required to ensure that the demands for U are met, but secondary sources are projected to decline significantly after 2015 (Vance *et al.* 2006) and primary sources typically require in excess of ten years from discovery to production. Consequently, after about the year 2020, needs by commercial reactors will have to be met by additional primary U supplies, new technologies for more efficient exploitation of secondary sources, or both of these.

The market price for U reached a peak in the late 1970s as a result of the construction of civilian reactors and the perception that nuclear power would be important in the future (Fig. 2-3). Several factors conspired to decrease and maintain a price near US $20/kg, including a slower growth than anticipated in nuclear power, low oil prices, the accidents at Chernobyl and Three Mile Island and excess supplies. After 2000, the price began to rebound smoothly until 2003 because of supply shortfalls, and then to jump abruptly up to US $350/kg U in July 2007 because of the increase in oil prices (Fig. 2-3). It should be noted that the spot or market price of U is only one reflection of the health of the industry because 90% of the U used globally is not sold at spot market prices. Nevertheless, as stockpiles have decreased, the spot price increases along with an increased exploration effort.

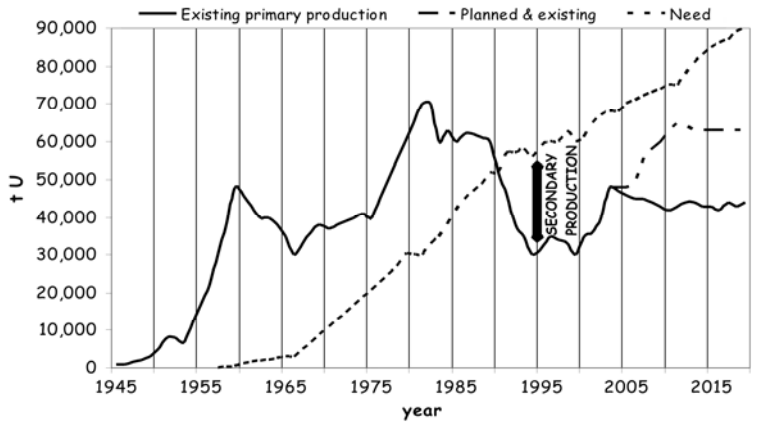

Fig. 2-2. Primary U production (in tonnes of U), production +planned primary sources at < US$80/kg and U needed for civilian use as a function of year, including estimates of these until 2020. Global primary production exceeded use of U until 1990. The difference between primary production and U needed represents the inventory buildup prior to 1990 or U derived from secondary sources since 1990 (as indicated). Data from Vance *et al.* (2006), Cornell (2006), Shatalov *et al*. (2006), OECD (2006, 2008).

During the 1990s, injection of U from secondary supplies, such as former-USSR stockpiles and nuclear warheads, and then from the U.S. Department of Energy, was partly responsible for a low market price of U (Fig. 2-3). Postponement of developing new mines and the demise of primary production from marginal sources such as USA, western Europe (mainly France) and Gabon, and the drop in production from Australia, South Africa and Namibia (McMurray 2006) also resulted in a low market price. This also led to an aborted surge in exploration activity in the late 1990s, further delaying the search for new deposits, and severely impacting the capacity of the industry to do so, as many U geologists shifted careers or became involved in the search for other commodities. A new exploration cycle was never realized.

The market price of U was subsequently affected by a variety of events (Cornell 2006). For example, in 2001 there was a fire at the mill at Olympic Dam which stopped production from there. In 2003, flooding at the MacArthur River deposit in Canada temporarily stopped production from the largest single supplier of U globally. In 2004, one of the last converters was shut down in USA, there was a strike at Port Hope, one of the few major processing plants, and there was a contract dispute involving the Russian highly enriched U agreement. In 2006, the Cigar Lake mine, a major new U production site with a planned annual production capacity of about 7,000 t U beginning in 2007, was flooded and will not be able to start production before 2011. All of these along with the tremendous growth in energy demand from China and India, which have limited U resources but plans for building new nuclear power stations, and the dwindling stockpiles conspired to increase the price of U after 2003 (Fig. 2-3) and helped foster the current boom in U exploration.

Most of the U in the world is supplied from deposits associated with sandstone-related environments (Fig. 2-4). For example, in 2006-7, about 42% of U production was from unconformity-related deposits (ca. 14,000 t U/yr), 20% was from *in situ* leach extraction from sandstone-related deposits (*ca*. 9,500 t U/yr) and 10% was from conventional mining of sandstone-related deposits (*ca*. 4,000 t U/yr). The largest unconformity-related deposit, McArthur River in Canada, has an annual capacity near 8,000 t U and most of the capacity from these deposits comes from only 4 mines averaging about 5,000 t U/yr. In contrast, 14 ISL-amenable sandstone deposits have average capacities of only about 600 t U/yr. Therefore, the most lucrative targets for U exploration are those associated with sedimentary rocks, specifically those associated with unconformities.

In terms of mine types that have the greatest capacity potential, open pit mines generally have greater capacity than do underground mines, and underground mines have greater capacity than mines where U is extracted from *in situ* leach technology. However, underground mines supply about 40% of the global U production, open-pit mining methods supply about 30% and *in situ* leach technology about 20% of the U produced. The higher proportional contribution from underground mines is primarily due to the high grades of *ca*. 15% U from unconformity-related deposits in Canada, most of which are mined

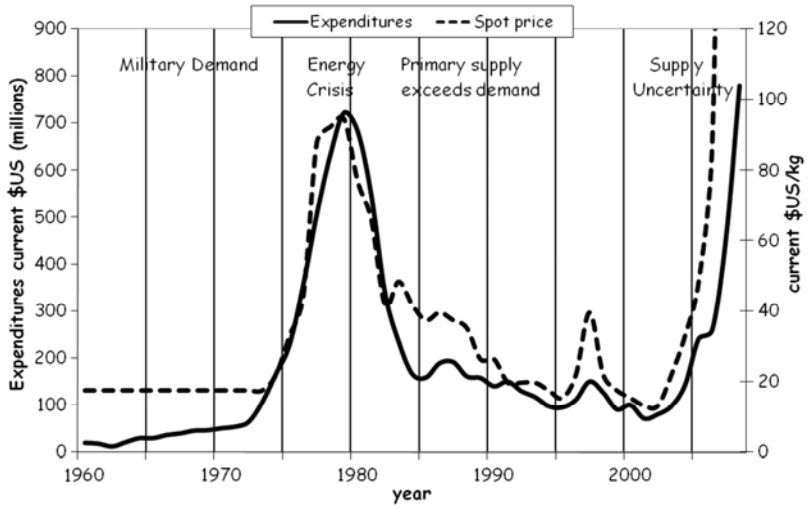

Fig. 2-3. Spot market price of U in $US/kg for each year and expenditures in millions of $US for exploration of U deposits as a function of year since 1960. Data from OECD (2006, 2008) and Price (2006).

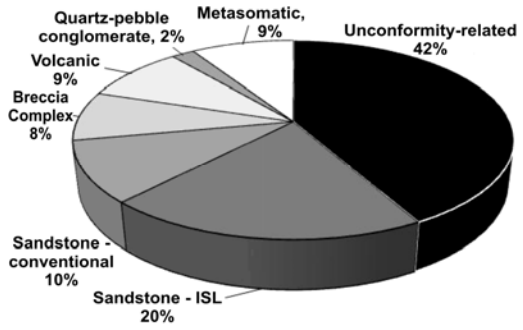

Fig. 2-4. Percentage of the total production of U as a function of deposit type for 2006-7. Data from McMurray (2005) and OECD (2006, 2008).

using underground methods. However, deposits near the surface, even at low grades such as the Rössing deposit in Namibia with a grade of 0.03% U, can be significant sources of U.

Exploration expenditures (especially in constant dollars) have an excellent correlation with U price, with the influence of a price increase on expenditures occurring 1-2 years after the price change (Fig. 2-3). Beginning in 1975, expenditures for exploration rose rapidly to a peak of US $756M in 1979 and then plummeted rapidly along with the spot price of U (Vance *et al.* 2006). This rise in expenditures and price resulted first from a combination of growth in military needs until the early sixties, a period of time during which the cost of U extraction was not controlled by economic parameters, and then to feed the reactors since 1973. Since 1945, the total spent on U exploration has been about US $15 billion, with the former USSR accounting for about 20% of this and Canada only 10% (Price *et al.* 2006). Estimates of the average historical expenditures aggregated across the exploration industry required to find unconformity-related deposits in the Athabasca Basin of Canada vary from US $60–90 million (Marlatt, pers. comm.). Future discoveries will come at significantly higher costs as the impact of resource depletion and current exploration technology limitations are realized.

Uranium is a global commodity because it is related to energy. The geographic disparity in the distribution of U resources relative to the nations that rely heavily on nuclear power is extreme. For example, the largest consumers of U are European countries (France, Belgium, Germany, Sweden), Japan and USA, but they mine virtually no U. Of the global producers (Canada, Australia, Kazakhstan and the Russian Federation), only Canada and the Russian Federation have any significant nuclear power generation, and this is about 11% of the total energy needs of these countries (Fig. 1-2). In effect, almost all of the nations that produce U shown in Table 2-1 except Canada, USA and Russia, do not rely on nuclear energy and are not consumers of U.

Although U is among the most efficient energy-related commodities, its economic value is pale relative to other energy-related commodities. The global monetary value of oil, based on the price and amount when delivered to utilities, is nearly 1000 times the value of U, natural gas is 500 times and coal is 10 times (Cornell 2006). As is the case for U, the reserves for these other energy-related commodities are also uncertain, so their value and market price will certainly increase in the future as well.

RESEARCH IN EXPORATION AND DEPOSIT STUDIES OF URANIUM

The role that research plays in deposit studies is to provide data and models that characterize the processes involved in the formation of the deposit. Although research normally leads to discovery of the geological, physical and chemical processes that were operating when the deposit formed, rarely are these processes predictive because similar environments nearby that have similar characteristics as the deposits and should harbor mineralization, don't. For research results to lead to prediction of deposit locations, the processes that are critical to deposit formation must be discovered, including those associated with both space and time. In addition, areas that should host mineralization but don't must be understood equally as well as those where the deposits are. For research to aid in exploration, the exploration process must be defined. The exploration process can be defined by distinct phases that occur in both the mineral and petroleum industries in response to the number of discoveries in relation to exploration expenditures. An example of the exploration discovery cycle that typifies U is revealed in the history of the search for unconformity-related deposits in the Athabasca Basin of Canada (Fig. 2-5). The discovery cycle in the Athabasca Basin can be divided into three learning curves (Marlatt 2006). These are the same curves that characterize the cycles for most metal and petroleum deposits, although the relationship between discoveries and expenditures varies.

The first stage, or learning curve, is *prospector-driven exploration* where deposits near the surface are discovered and no real model is

integrated in the exploration strategy. Initial discoveries involve minimal expenditures, but the frequency of discoveries quickly declines as prospecting proceeds. Large deposits are typically discovered early and subsequent deposits are typically smaller, and take longer and cost more to find. In the case of the Athabasca, the prospector driven exploration of the discovery cycle lasted for about 20 years. Companies who move to the next stage or learning curve through research and development encounter the probability of winning a bigger prize.

Research plays a critical role in the next phase of the exploration cycle by providing data that allows genetic models of the deposits to be formulated. *Model-driven exploration* (Fig. 2-5) incorporates research results on the geological and geochemical aspects of the deposits in combination with data gathered as the deposits are exploited. This approach eventually led to the discovery of the world's largest and highest grade U deposit at McArthur River. This deposit sits at a depth of over 500m below the surface, and discovery was driven in large part by drilling favorable geological locations associated with an EM conductor. Many other similar locations have been explored using this model, and thousands of holes drilled chasing conductors, but only a few deposits have been discovered. This stage in the discovery cycle of the Athabasca Basin has lasted for the past 27 years.

Research/technology-driven exploration relies significantly on exploration experience and results from research to refine exploration strategies (Fig. 2-5). Provided there are deposits remaining to be discovered, research that leads to more efficient exploration, including refined models and new technologies, plays a major role, ensuring that significant discoveries are found as expenditures increase. The research that is required to find large, high-grade deposits must enhance the knowledge base in both the critical controls on deposit formation and in developing new technologies. These will be revisited in the last chapter on exploration strategies.

During "boom" periods when the market price of a commodity rises, the tendency of exploration is to regress down the discovery curve toward prospector-driven exploration. This may characterize much of the current U industry, with few companies investing in the long-term knowledge base because much of the exploration mentality is largely prospector, or at best model-driven. However, most of the current global exploration involves some type of "a model", so in reality, much of the current activity is really on the move to the third learning curve for the discovery of the next generation of deposits, regardless of what type of deposit is being sought. However, the current "models" are not resulting in new discoveries.

Successful exploration realizes that there is no "silver bullet", but many researchers often view their results as definitive indicators of discovery even though they represent only marginal advances.

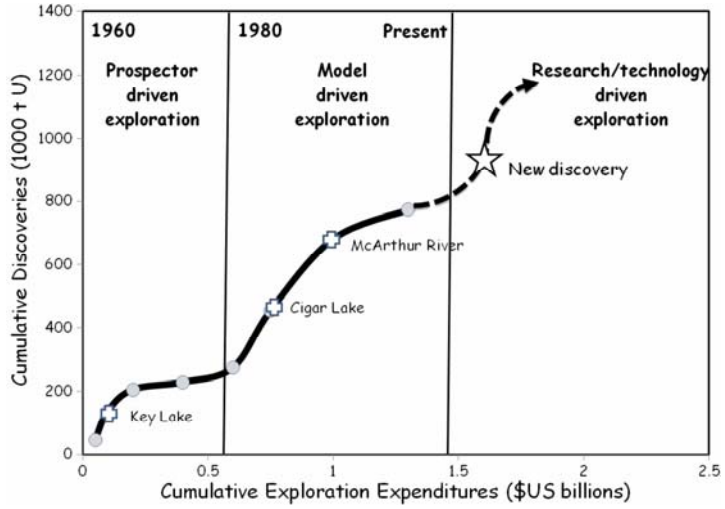

Fig. 2-5. Relationship between discoveries and exploration expenditures for the Athabasca Basin since 1960. The first stage is prospector-driven exploration, which occurred from 1960 to 1980. The second stage is model-driven exploration from 1981 to the present and the future stage will be research and technology-driven exploration, which will require collaboration between researchers and explorationists. Diagram courtesy of J. Marlatt (2006).

On the other hand, those in industry are disappointed when the research does not lead to a "silver bullet", and thus are reluctant to integrate the research results into their exploration strategies because their impact has been less than expected or integration is too onerous. Technology and knowledge must be transferred efficiently, and this can only be done through collaboration. The cost of collaboration is significant in terms of the normal activities of both the researchers and the explorationists because collaboration requires time and effort on the part of all parties involved. As a consequence, collaboration, and therefore where a company is on the exploration cycle, is controlled largely by human factors, namely whether the researchers and the explorationists share similar goals and mutual respect for each other.

Does research figure into U deposit studies and exploration and facilitate moving beyond the prospector learning cycle? One historical measure of whether this happens is how the number of publications on U deposits relates to the boom/bust periods in the U industry as reflected by the market price of U (Fig. 2-6). Perhaps a better reflection of the impact of research on the industry overall is the number of publications on U deposits and geology in peer-reviewed journals, which should be scrutinized more for their scientific validity and significance than non-refereed publications that typify many organizations or conference proceedings. Because exploration expenditures and the market price track each other almost perfectly (Fig. 2-3), the relationship between publication numbers and spot price should be a measure of the potential investment by industry in research. Most deposit studies and models are disseminated in the literature by researchers in academia, government and industry, with the most significant refereed publications involving collaboration among two or all of these.

The development of ore deposit models from research is, in some cases, limited by the restricted access to some deposits by the researchers. For example, all the deposits controlled by the former USSR were virtually inaccessible to western scientists. Prior to this, volcanic-related deposits were considered by most western researchers as minor resources. The realization by western geologists of significant U resources in Transbaikalia, Mongolia and Kazakhstan has led to reconsideration of deposit models related to volcanism and their resource potential. The same is true for some other deposit types, such as those associated with alkali metasomatism in China and India. Closer to home, research is very limited on U in IOCG deposits, particularly on the huge Olympic Dam deposit in Southern Australia, in part because of limited access.

The relationship between the annual spot price of U and number of total publications on U deposits and geology shows that research began to increase with the boom in 1975 but peaked after the boom and remained high until 1990. The same is true for the number of refereed publications, which peaked in 1990 and also rapidly declined thereafter. Overall, the number of publications is slightly higher after the boom than prior to it. This slight increase reflects the research that continued on U deposits, and the delay by several years between the time when the research is being done and the time

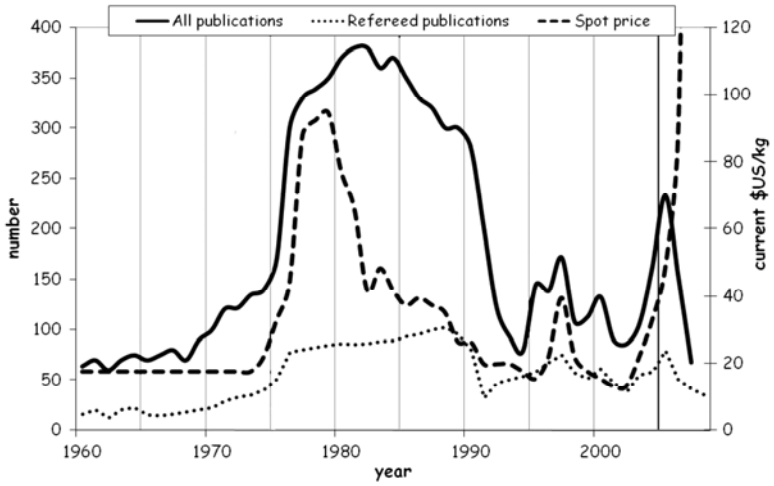

Fig. 2-6. Number of all publications (conference proceedings, abstracts and papers) and refereed publications in U deposits and geology as a function of year. Also shown is the spot price of U.

necessary to complete the research, to reach sufficient scientific maturity to write the paper, to go through the peer-review process and finally reach publication. In addition, the peaks after 1990 reflect exploration results released from the former Soviet Union and an increasing number of publications on U deposits geology from researchers in Asia. The abrupt end of the last U boom occurred in 1985, but the number of publications in U plummeted later in 1990 (Fig. 2-6). One implication of this is that many of the geologists and researchers who were once involved in the U industry pursued other interests and those who continued in exploration or research are now 15 to 20 years older.

One interpretation of these results is that much of the research in U deposits, and therefore the ideas needed to move up the discovery cycle, takes several years to develop. In other words, research responds to the interest and investment by industry, but it takes about ten years to develop a healthy knowledge base. A small portion of this, about two years, is normally the time required to publish results in refereed journals, but most of the publications in Fig 2-6 are from organizations or conferences where peer review was minimal. If this is a valid interpretation, the current boom in the U industry, which has yet to realize any significant new research, must rely on the research that occurred after the boom to move up the discovery cycle. Moreover, to move from prospector-driven exploration mentality that characterizes the current boom, to the third learning cycle shown in Fig. 2-5, requires that explorationists understand and integrate the research that has occurred during the past 20 years and also invest in research in a timely way to continue the knowledge base.

REFERENCES

CORNELL, J.C. (2006): Changing role of secondary supply in the global uranium market. *In:* Uranium production and raw materials for the nuclear fuel cycle–Supply and demand, economics, the environment and energy security. *IAEA-CN-128*, IAEA, Vienna, 63-69.

MARLATT, J. (2006): The Role of Uranium Exploration in Future Supply. In: Giant uranium deposits: Exploration guidelines, models, and discovery techniques (T.K. Kyser, ed.), *SEG-PDAC Uranium Short Course 2006*.

MCMURRAY, J.M. (2005): The relationship between the uranium market price and supply-demand relationships, Recent developments in uranium exploration, production and environmental issues. *IAEA-TECDOC-1463*, 63-72.

MCMURRAY, J.M. (2006): Worldwide uranium resources and production capacity — the future of the industry. *In:* Uranium production and raw materials for the nuclear fuel cycle–Supply and demand, economics, the environment and energy security. *IAEA-CN-128*, IAEA, Vienna, 27-35.

OECD/NEA-IAEA (2006): *Uranium 2005: Resources, Production and Demand, 2005 Red Book*. OECD, Paris, France.

OECD/NEA-IAEA (2008): *Uranium 2007: Resources, Production and Demand, 2007 Red Book*. OECD, Paris, France.

PRICE, R.R. (2006): An Analysis of Historical Data on Uranium Exploration Expenditures and Price. *In:* Uranium production and raw materials for the nuclear fuel cycle–Supply and demand, economics, the environment and energy security. *IAEA-CN-128/1P*, IAEA, Vienna.

PRICE, R., BARTHEL, F. & BLAISE, J.-R. (2006): Forty years of uranium resources, production and demand in perspective. In: Facts and opinions, *NEA News*, **24.1**, 4-6.

SHATALOV, V.V., TAKHANOV, A.V., BOLDYREV, V.A. & KNYAZEV, O.I. (2006): Analysis of uranium world resources and ways of their extension. *In:* Uranium production and raw materials for the nuclear fuel cycle–Supply and demand, economics, the environment and energy security. *IAEA-CN-128*, IAEA, Vienna, 103-110.

VANCE, R.E., PRICE, R.R. & BARTHEL, F. (2006): Recent activities of the joint Nuclear Energy Agency (NEA)/International Atomic Energy Agency (IAEA) Uranium Group. *In:* Uranium production and raw materials for the nuclear fuel cycle–Supply and demand, economics, the environment and energy security. *IAEA-CN-128*, IAEA, Vienna, 40-46.

CHAPTER 3: GEOCHEMICAL CHARACTERISTICS OF URANIUM AND ANALYTICAL METHODOLOGIES

Kurt Kyser
Department of Geological Sciences and Geological Engineering,
Queen's University,
Kingston, Ontario, K7L 3N6, Canada
kyser@geol.queensu.ca

and

Michel Cuney
G2R, Nancy-Université, CNRS, CREGU,
B.P. 239,
F-54506 Vandoeuvre lés Nancy, France
michel.cuney@g2r.uhp-nancy.fr

URANIUM IN ROCKS AND MINERALS

Uranium is an actinide element like Th, has an atomic number of 92, an atomic mass of 238.05079 and three main naturally occurring isotopes (^{234}U, ^{235}U and ^{238}U), of which ^{238}U is the most abundant at 99.3%. Like Th, it is a radioactive element, and its most stable isotope, ^{238}U, has a long half-life of 4.46 x 10^9 years, similar to the age of the earth.

Uranium occurs in natural systems in three oxidation states, U^{4+}, U^{5+} and U^{6+}, in contrast to Th which occurs exclusively as Th^{4+}. In primary crustal processes, U behaves as an incompatible element because of its high charge density so that U is concentrated in the upper continental crust relative to all other earth reservoirs. In magmas, the highly charged U^{4+} ion (ionic radius 1 Å), behaves incompatibly, becoming concentrated in late-stage differentiates in a variety of accessory minerals such as zircon, apatite, monazite, titanite, allanite and uraninite. Granite and pegmatites produced from evolved magmas are richer in U than mafic igneous rocks (Table 3-1). Uranium is progressively enriched in a silicate melt during differentiation and is generally highest in felsic rocks. Uranium is always enriched in peralkaline rocks over calc-alkalic and peraluminous equivalents. Secondary concentration of U may occur as a result of hydrothermal activity associated with the emplacement of felsic volcanic and intrusive rocks.

In igneous rocks, U is associated with Th, Zr, Ti, Nb, Ta and rare earth elements, particularly in peralkaline rocks, but less so for metaluminous rocks and not at all for peraluminous rocks. In other lithologic environments, U is most closely associated with redox active elements such as Mo, V, Se, As and Cu.

Levels of U in sedimentary rocks are closely related to their redox conditions, with the highest concentrations found in organic-rich facies (6–1000 ppm) associated with anoxic environments and phosphatic sediments (50–300 ppm). Lower values are recorded in coarse-grained inorganic rocks, with clay-rich sediments having generally higher levels. The average value cited for shale is 3.7 ppm and carbonate rocks have 2.2 ppm (Table 3-1). Average U contents for loess and river particulates are 2.5–3 ppm and soils typically have 0.8 to 11 ppm U.

Uranium occurs in rocks as its own minerals, as a substitute element in rock-forming and

TABLE 3-1. URANIUM CONCENTRATIONS IN GEOLOGIC MATERIALS.

Reservoir	ppm
Average Crust	1.7
Oceanic Crust	0.5
Upper Continental Crust	2.7
Peridotite	0.003–0.05
Eclogite	0.013–0.8
Average Basalt	0.3
MORB basalt	0.07–0.1
Continental Andesite	0.5–1.0
Island Arc Andesite	0.2–0.4
Average Granodiorite	2.0
Average Granite	3.8
Nepheline Syenite	200–600
Common Shale	3.7
Black Shale	3–1250
Sandstone	0.45–3.2
Average Carbonate rock	2.2
Marine Phosphate rocks	50–300
Evaporite rocks	0.01–0.43
Seawater	0.003

Short course co-sponsored by the the SGA and MAC, Québec City, May 2008, p. 23–55

accessory minerals, in exchangeable positions in zeolite and clay minerals, adsorbed on crystal faces and dissolved in intergranular fluids and fluid inclusions. Approximately 5% of all known minerals contain U as an essential structural constituent, which reflects the diversity of U minerals (Burns 1999). The mineralogy of U is controlled by its high charge density, and the two principal minerals are uraninite (written as UO_2 but chemically UO_{2+x} (Janeczek & Ewing 1992)) and coffinite $USiO_4$ (Table 3-2). Pitchblende is a general term given to the fine grained, massive colloform variety of uraninite. Uranium also occurs as ningyoite $(U,Ca,Ce)_2(PO_4)_2,1.5H_2O$), brannerite $(U,Ca,Ce)(Ti,Fe)_2O_6$, uranothorite $(Th,U)SiO_4$, uranmicrolite $(U,Ca,Ce)_2(Nb,Ta)_2O_6(OH,F)$, uran-pyrochlore $(U,Ca,Ce)_2(Ta,Nb)_2O_6(OH,F)$ and euxenite (Y, Er, Ce, La, U)$(Nb, Ti, Ta)_2(O,OH)_6$ as well as a variety of highly colored U^{6+} minerals which can be deposited either as primary ore minerals such as carnotite $K_2(UO_2)_2(VO_4)_2,3H_2O$, tyuyamunite $Ca(UO_2)_2(VO_4)_2,3H_2O$, or more commonly after the alteration of uraninite (Finch & Murakami 1999) such as autunite $Ca(UO_2)_2(PO_4)_2.10H_2O$ or uranophane $Ca(UO_2)_2Si0_3(OH)_2.5H_2O$. In reducing environments, U occurs as pitchblende, coffinite, phosphate minerals, and in organic compounds such as thucolite.

The degree of substitution of U into accessory minerals is controlled by its effective ionic radius in octahedral coordination, the most common for U bearing minerals (1.00Å for U^{4+}; Shannon 1976). Complete substitution occurs with Th^{4+} (1.05Å) in uranothorianite and up to 30% UO_2 in uranothorite Cuney & Friedrich 1987). Limited substitution occurs for Ca^{2+} (1.12Å) in rock-forming minerals and for Zr^{4+} (0.84Å), Nb^{5+} (0.74Å) and Ta^{5+} (0.74Å) in accessory minerals. Extensive substitution of uranous ion occurs for Th^{4+} (1.05Å) and REEs (*i.e.*, La^{3+} (1.143Å) to Lu^{3+} (0.977Å)) in rare earth fluorocarbonates such as bastnaesite $((LREE)CO_3F,)$ and phosphates such as monazite, $((LREE,Th,U)PO_4)$ and xenotime ((Y, HREE,U) PO_4). For a comprehensive list of the structure and chemical formulas of U minerals, the reader is referred to Burns (1999), Finch & Murakami (1999), and Krivovichev *et al.* (2006).

URANIUM SOLUBILITY IN AQUEOUS FLUIDS

Understanding the aqueous geochemical characteristics of U is necessary to understand U ore deposits because deposits are, in reality, uniquely geochemical anomalies. Most deposits require that U is solubilized from a source, transported to the site of deposition by a melt or a fluid, effectively trapped and concentrated, all of which are geochemical processes. However, they also depend on geology in terms of characteristics of the magmas and fluids, permeability of the rocks and nature of fluid–rock interactions. From an exploration perspective, understanding what controls the U or associated element concentration in magmas and waters is prerequisite for effectively evaluating stream, soil and sediment data. Perhaps U deposits do not produce anomalies in these media except under particular conditions.

Much of our understanding of the

TABLE 3-2. MOST COMMON URANIUM ORE MINERALS

Mineral	Type of mineral	Most common depositional environment
Uraninite	Uranium oxide UO_{2+x}	Magmatic, hydrothermal or sedimentary-hosted deposits
Pitchblende	Uranium oxide (a botryoidal variety of uraninite)	Hydrothermal or sedimentary-hosted deposits
Coffinite	Uranium silicate $USiO_4$	Hydrothermal or sedimentary-hosted deposits
Brannerite	Uranium titanate $(U,Ca,Ce)(Ti,Fe)_2O_6$	Hydrothermal or sedimentary-hosted deposits
Carnotite	Uranyl vanadate $K_2(UO_2)_2(VO_4)_2•3H_2O$	Sandstone-hosted deposits, calcretes
Tyuyamunite	Uranyl vanadate $Ca(UO_2)_2(V_2O_8)•8H_2O$	Sandstone-hosted deposits
Uranophane	Uranyl silicate $Ca(UO_2)_2(SiO_3OH)_2•5H_2O$	Sandstone-hosted deposits Alteration of U oxide

geochemistry of U comes from research done in the 1960s and 1970s in the drive to understand how deposits form and then subsequently as the need to dispose of high-level waste prompted research on the behavior of the actinides in disposal environments. The approach taken to understand the geochemical characteristics of U was three-fold, involving (1) experimental, measuring directly the solubility of U minerals, (2) theoretical, using measured and estimated thermodynamic data and, to a lesser extent, kinetic data to calculate what should happen and how fast, and (3) data from the deposits themselves, particularly mineral associations and fluid characteristics from isotopes and fluid inclusions.

It is convenient to separate the geochemical characteristics of U into those at low (<100ºC) and high temperatures (>100ºC) because the data for low temperature characteristics are more extensive than those for high temperatures. Although there have been successful efforts to refine the data devised or estimated from 30–40 years ago, deductions about the geochemistry of U from them have not changed much, we are just more sure of how U behaves in certain environments.

Low temperature uranium geochemistry

Uraninite and most other common U minerals are only sparingly soluble in water at neutral pH and low temperatures (Fig. 3-1), depending on the oxidation potential of the water. The solubility of uraninite in dilute water is controlled primarily by complexes of the cation UO_2^{2+}. However, the solubility increases markedly in the presence of strong anions such as F^-, Cl^-, CO_3^{2-} SO_4^{2-} and PO_4^{3-} (*e.g.*, Langmuir 1978), depending on the oxidation potential of the fluid. These complexes normally increase the solubility of U minerals and the mobility of U in ground waters. The fate of other components in the uraninite is less certain, as is their effects on the solubility of uraninite (Janeczek & Ewing 1992).

The aqueous geochemistry of U is unusual in that U is generally more soluble in oxidizing, alkaline and carbonate-rich water than in acidic, reducing water (Fig. 3-1). This is due primarily to the tendency of U^{6+} to form strong complexes in oxidizing fluids, regardless of the temperature.

Uranium is readily soluble in the strongly acid, oxidizing water commonly associated with acid mine drainage because the hydrated cation UO_2^{2+}

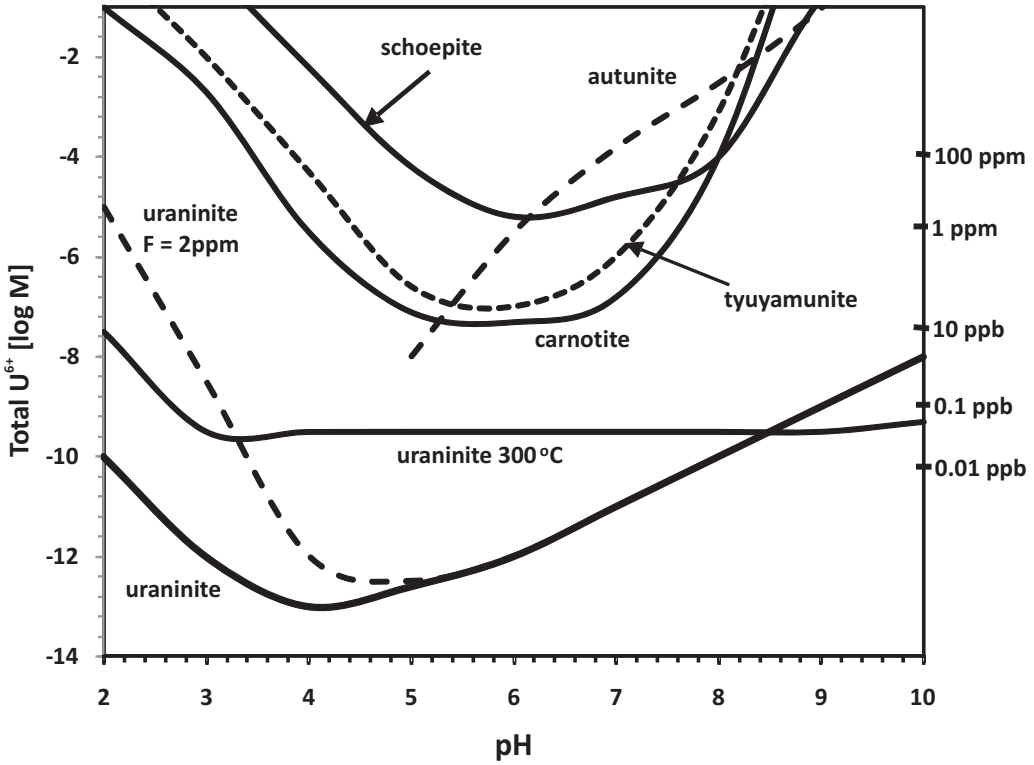

FIG. 3-1. Solubility of U minerals as a function of pH at 25ºC (as well as 300ºC for uraninite). All solubilities are in water except for the fluid with 2 ppm fluoride and different oxygen fugacities to stabilize minerals being studied. Data from Langmuir (1978), Shock *et al.* (1997), Casas *et al.* (1998) and Suzuki & Banfield (1999).

and fluoro-complexes of U are stable below pH 4, so that acidic fluids with F can transport a significant amount of U (Fig. 3-2). In oxidized fluids between pH 4 and 7.5, uranyl phosphate complexes are the important species and at higher pH, uranyl carbonate complexes are dominant (Fig. 3-2). In groundwater with normal sulfate concentrations of 100 ppm, uranyl sulfate complexes can be a significant species at pH < 7 (Fig. 3-2). However, the uranyl phosphate complex is so stable that, for oxidizing groundwaters with typical concentrations of 0.1 ppm PO_4, this complex predominates over all others from pH 4 to 10 (Fig. 3-2).

Uraninite is sparingly soluble at normal pH in dilute, reducing groundwaters (Langmuir 1978, Parks & Pohl 1988). Reported UO_2 solubilities vary from $10^{-7.1\pm0.2}$ (Bruno *et al.* 1991) to $10^{-14.86\pm0.44}$ mol/L (Guillaumont *et al.* 2003) for pH above 5, which is seven orders of magnitude. The values depend on the degree of crystallinity of the uraninite, the oxidation state of the U and level of impurities. The solubility of uraninite increases with temperature and dissolved F, Cl and CO_2 contents such that dissolved U^{4+} concentrations in brines are an order of magnitude higher than fresh water (Giblin & Appleyard 1987). In reduced ground waters, only fluoride complexes of U^{4+} are significant and then only at very low pH (Langmuir 1978). At very high pH in reduced ground water, uranyl hydroxide complexes are the dominant species. The insolubility of the most common U minerals, uraninite and coffinite, in reducing groundwater with pH between 4 and 8 and at low Eh values indicates U is immobile in these environments unless fluoride is present (Fig. 3-1). In environments with higher Eh values (*i.e.* >–2 volts), however, oxidation of uraninite and coffinite ($USiO_4$) can render greater solubilities by several orders of magnitude, particularly when phosphate and carbonate are present. As a result, sulfuric acid with pH of about 1 is used for *in situ* leaching in Kazakhstan and phosphate-bearing fluids and ammonium carbonate solutions with an oxidant have been used for *in situ* leaching of U in sandstone deposits elsewhere.

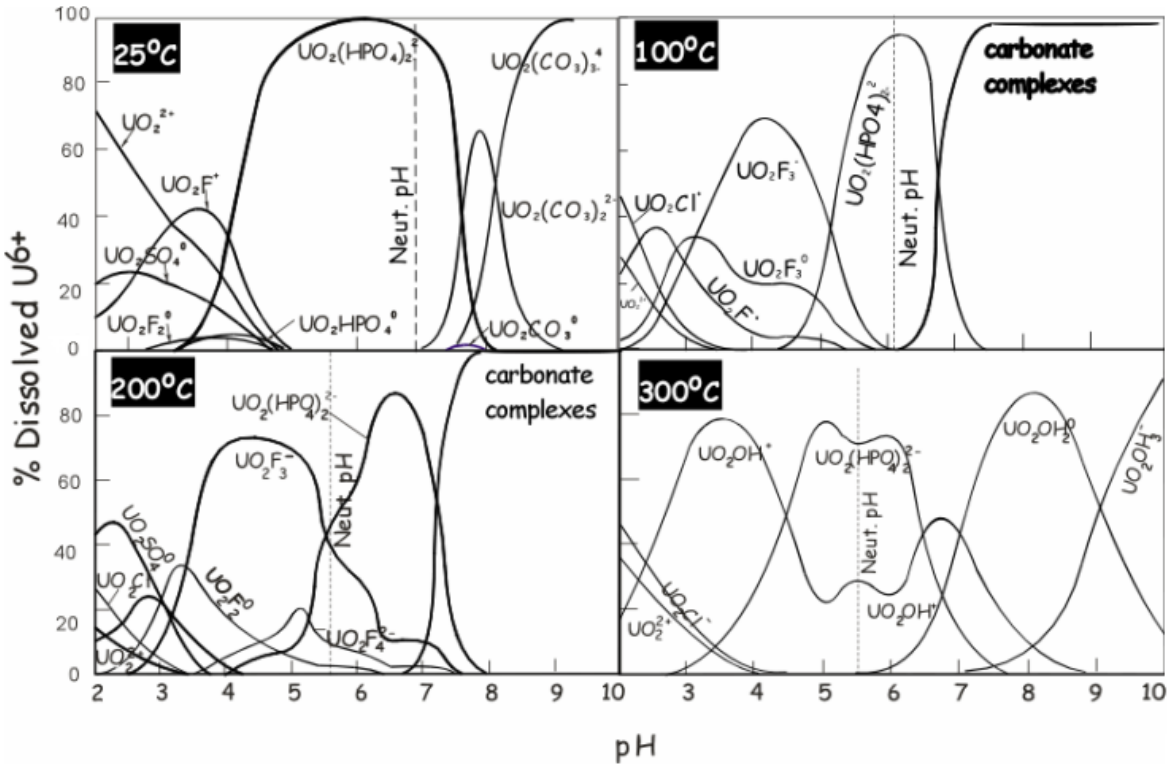

FIG. 3-2. Relative concentration of uranyl complexes as a function of pH and temperature for a fluid with $\Sigma U^{6+} = 10^{-8}$ M, ΣF = 0.3 ppm, ΣCI = 10 ppm, ΣSO_4 = 100 ppm, ΣPO_4 = 0.1 ppm, $\Sigma Si0_2$ = 30 ppm and $P_{CO2} = 10^{-2.5}$ atm.; at 100°C for a fluid with ΣF = 10 ppm, NaCl = 1M, ΣSO_4 = 1000 ppm, ΣPO_4 = 0.1 ppm, and P_{CO2} = 1 atm; at 200°C for a fluid with ΣF = 100 ppm, NaCl = 1m, ΣSO_4 = 1000 ppm, ΣPO_4 = 1 ppm and P_{CO2} = 1 atm; at 300°C for a fluid with ΣF =10 ppm, NaCl = 1m, ΣSO_4 = 1000 ppm, ΣPO_4 =10 ppm and P_{CO2} = 10 atm. After Romberger (1984), Langmuir (1978), Tripathi (1979) and Kojima *et al.* (1994).

High temperature uranium geochemistry

At high temperature, solubility data are extremely rare and available values are from extrapolation of low temperature thermodynamic data to higher temperatures (*e.g.* Shock *et al.* 1997). Uncertainties in these data result from the existence of different types of complexes at low relative to high temperatures for which thermodynamic data are unavailable, or complexes that are not considered in the models but are present in experimental results. Keeping in mind these uncertainties, the extrapolated solubility of UO_2 in fluids appears to be independent of pH in the range $4 < pH < 10$ (Fig. 3-1) and has minimal temperature dependence from 100 to 300°C (Parks & Pohl 1988, Shock *et al.* 1997). The solubility of uraninite (UO_2) in aqueous solutions in basinal brines indicates that uranyl carbonate complexes $UO_2(CO_3)^{2-}$ are dominant under relatively oxidizing and near-neutral pH conditions and that UO_2C1^- is dominant (Fig. 3-2) in fluids under acidic conditions at temperatures up to 200°C (Romberger 1984, Kojima *et al.* 1994) As the temperature increases, carbonate complexes become less important and hydroxide complexes become dominant (Romberger 1984).

Both oxygen activity and pH are the most important factors controlling uraninite solubility at low temperatures, but oxygen activity is the major control at high temperatures. As with low temperatures, theoretical calculations indicate that U at 100°C in relatively oxidizing brines is dominantly carbonate complexes of U^{6+} at high pH, phosphate complexes at neutral pH and fluoride and chloride complexes at less than neutral pH (Fig. 3-2). At higher temperatures than 200°C, the results are similar except that sulfate complexes become stable at very low pH (Fig. 3-2). As the temperature increases, hydroxyl complexes become dominant, particularly at low and high pH, but phosphate complexes remain dominant at neutral pH despite the emergence of important hydroxyl complexes (Fig. 3-2).

Most calculations indicate that the solubility of uraninite is both pH and temperature-independent under reducing conditions, and that above pH 4, uraninite may have slight retrograde solubility (Romberger 1984, Shock *et al.* 1997). Thus, even moderate temperature changes in the fluid will not result in precipitation of uraninite (Romberger 1984). Instead, Romberger (1984), who modeled the phase relations in brines at 200ºC (Fig. 3-3), suggested that only an increase in pH or decrease in the activity of oxygen could facilitate precipitation of uraninite. At 200ºC and high oxygen activities, hematite, a mineral commonly associated with hydrothermal U deposits, would also form, whereas at low activities, pyrite would be coeval with uraninite (Fig. 3-3). The models obtained by Romberger (1984) and others (*e.g.*, Komninou & Sverjensky 1996) indicate that uraninite can form from the same fluids as their associated alteration minerals in hydrothermal U ore deposits (*e.g.*, Hoeve & Sibbald 1978). In addition, U^{6+} reduction by reaction with Fe^{2+} or C species (graphite does not seem to be reactive below 400°C) are the most likely mechanisms by which uraninite precipitates.

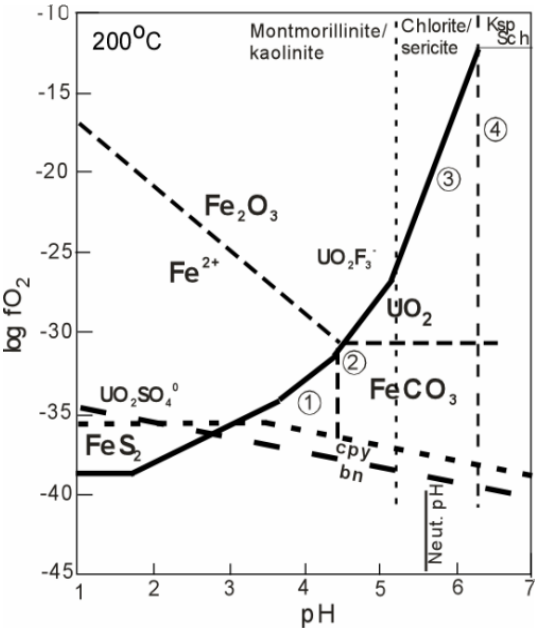

FIG. 3-3. Phases stable under various fO_2 and pH conditions for the system U–O–S–Fe–C–H with 10 ppm Fe, 100 ppm F, 1000 ppm S, 1000 ppm K, 1m NaCl and P_{CO2} = 10 atm. (after Romberger 1984). Bold line is the boundary between uraninite (UO_2) and U^{6+} complexes, below which uraninite is stable. Also shown are the stability fields for pyrite–Fe^{+2}, hematite–Fe^{+2}–siderite and chalcopyrite (cpy)–bornite (bn). Superimposed are the stability fields of kaolinite–sericite or Mg-montmorillonite–Mg-chlorite (if 100 ppm Mg is in the fluid), and the fields of K-feldspar (Ksp) and schoepite (sch). A fluid at 1 would have uraninite + kaolinite/Mg-montmorillonite, fluid 2 would be uraninite + siderite + kaolinite/Mg-montmorillonite, fluid 3 would have uraninite + Mg-chlorite/sericite and fluid at 4 would be uraninite + feldspar.

URANIUM SOLUBILITY IN SILICATE MELTS AND MAGMATIC FLUIDS

Solubility experiments on Zr (Watson and Harrison, 1983), REEs (Montel 1993) and U (Peiffert *et al.,* 1994, 1996) in silicate liquids indicate that large, highly charged ions dissolve depending on the degree of depolymerization of the melts (Farges *et al.* 1992). Depolymerization of the melts depends on the excess of alkali elements + Ca relative to Al and the temperature. Increasing either one results in breaking of the Si–Al tetrahedron chains in the silicate melt, thereby enhancing depolymerization and the solubility of large, highly charged ions.

The solubility of U has been examined experimentally in simplified granitic melts at 770°C, 2 kbar pressure, variable fO_2 conditions and different aqueous fluids in equilibrium with the melts (Peiffert 1993, Peiffert *et al.* 1994, 1996). The extreme chemical compositions of the melts in the experiments correspond to peraluminous melts (Na + K/Al = 0.7), similar to the two-mica granites that host U deposits at Saint Sylvestre, Limousin, or the peraluminous acidic volcanic rocks of Macusani, Peru, and to peralkaline melts (Na + K/Al = 1.6), that host deposits at Ilímaussaq, Greenland (Table 1-2). These experiments were designed to examine the effects of various parameters on the solubility of U in silicate melts.

Melt composition is a significant factor controlling U solubility in silicate melt. The solubility increases from 10 ppm to percent levels with increasing (Na + K)/Al ratios from 0.7 to 1.6, respectively (Fig. 3-4). Similar experiments by Zharikov *et al.* (1987) showed no compositional effect on U solubility, but these were of much shorter duration and did not reach equilibrium.

Increasing the oxygen fugacity from the Ni–NiO to the Cu_2O–CuO buffer increases U solubility only by a factor of 3 and decreases the dependence of solubility on the (Na + K)/Al ratio (Fig. 3-4). Uranium in a silicate melt at the lower oxygen fugacity is in the U^{4+} form, whereas U^{6+} dominates in the most oxidized conditions, with variable proportions of U^{5+} (Calas 1979). Hence, more oxidized forms of U are more soluble in silicate liquids.

Carbon dioxide or C in the aqueous fluid in equilibrium with the silicate melt has minimal effect on the solubility of U in the melt (Fig. 3-4). Both anions have limited solubility in acidic silicate melts at low pressure, but the solubility of U in melts tends to be slightly higher in chloride systems (Peiffert *et al.* 1994). This is likely due to the lower K/Na ratio of the silicate melt resulting from the strong partitioning of K into the chloride-rich aqueous solution. In support of this is the enhanced solubility of U in Na-bearing melts compared to K-bearing ones (Dominé & Velde 1985).

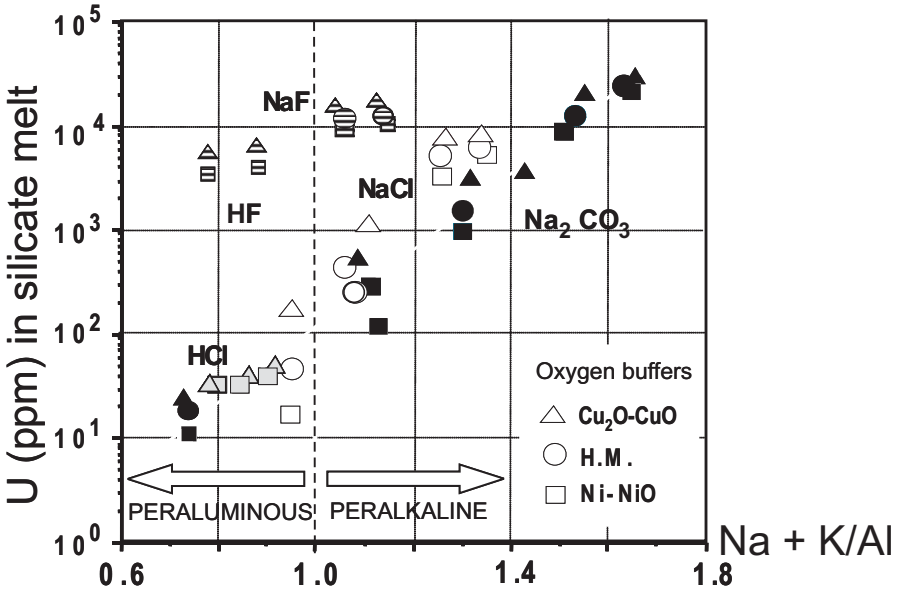

FIG. 3-4. Uranium solubility in silicate melt as a function of [K + Na]/Al ratio of the melt, oxygen fugacity (Ni–NiO, Hematite–Magnetite (HM) and Cu_2O–CuO) and different aqueous fluid compositions. Data from Peiffert (1993) and Peiffert *et al.* (1994, 1996). Black symbols: experiments with Na_2CO_3 in the fluid phase at equilibrium with the melt; unfilled symbols are experiments with NaCl; grey symbols with HCl; hatched symbols with HF and NaF.

In contrast to carbon dioxide and Cl, F is strongly partitioned into silicate melts, reaching levels of 10 000 ppm, because it reacts with Al to form AlF_6^{3-}, thereby depolymerizing the tetrahedral aluminosilicate framework (Manning 1981, Kohn *et al.* 1991, Schaller *et al.* 1992). The concomitant production of additional non-bridging O atoms enhances the U solubility in the melt (Fig. 3-4). The effect of increasing alkalinity on U solubility is negligible in an F-rich silicate melt, as is the effect of increasing the O fugacity. Thus, fluoride is the main parameter controlling U solubility in the melt in F-bearing systems. This is due to its effect on the structure of the melt as no evidence for U fluoride complexes in silicate glasses has been found (Farges *et al.* 1992).

Uranium in fluids from granites

Chloride and fluoride constitute two major anions in natural aqueous fluid phases and both form complexes with metals at most temperatures. These complexes are responsible for the transport of metals in hydrothermal solutions and could play a critical role in the genesis of U deposits originating from magmatic-metasomatic processes like the Tranomaro uranothorianite-bearing pyroxenite in Madagascar.

Experimental results indicate that the solubility of U in an aqueous fluid in equilibrium with a silicate melt increases with increasing O fugacity and chloride concentrations (Peiffert *et al.* 1994, 1996). Under oxidizing conditions (Cu_2O–CuO buffer) and for relatively low chloride concentrations (0.085 to 0.45m), high solubilities of U in the fluid of up to 170 ppm result from formation of U^{6+} chloride or hydroxyl–chloride complexes.

Under oxidizing conditions, U solubilities are 10 times higher in chloride solutions than in carbonate solutions and eight times higher than in fluoride solutions. However, the solubility of U in reducing fluids with fluoride is 10 times higher relative to chloride fluids at slightly acidic pH. In near neutral pH and oxidizing solutions, the U^{6+} ion forms weak and mixed complexes with OH^- and Cl^- (Nguyen-Trung *et al.* 1991):

Using the experimental results from Peiffert *et al.* (1994, 1996) and Peiffert (1993), the partition coefficients between fluid and melt at 770°C and 2 kbar vary over six orders of magnitude (Fig. 3-5). The lowest partition coefficients are for peralkaline melt compositions with carbon dioxide as a major component. Such low partition coefficients indicate that U is highly soluble in peralkaline melts, and thus is strongly retained by the silicate melt structure. Carbon dioxide is a weak complexing agent for U in an aqueous fluid at high temperature. The highest partition coefficients are for the most peraluminous melts in equilibrium with an acidic chlorine-rich fluid phase (Fig. 3-5), indicating that U solubility in peraluminous melts is low, but high in acidic fluids in the presence of Cl complexes.

Application to natural examples

Peralkaline melts rarely contain more than a few hundred ppm U (Böhse *et al.* 1974) and thus never reach uraninite saturation. During fractional crystallization of peralkaline magmas, U will be continuously enriched in the fractionated melts. This is why U mineralization is associated with the most fractionated phases of peralkaline suites. In contrast, the low U solubilities of less than 35 ppm for highly peraluminous melts explain why uraninite is a magmatic phase in melts containing only a few tens of ppm of U (Friedrich *et al.* 1987, Cuney and Friedrich 1987).

In fluoride-rich melts, the solubility of U in the fluid is lower compared to Cl-bearing melts even for peraluminous compositions. Uranium will be strongly partitioned into chloride-bearing magmatic fluids that are exsolved from peraluminous granite. Hence, the U content of the granite will no longer be representative of the initial melt and significant amounts of U will be transferred into the country rocks, increasing background U concentrations, as observed in the Saint-Sylvestre peraluminous leucogranite bodies (Friedrich *et al.* 1987, Cuney *et al.* 1989). At the Rössing deposit in Namibia, high U contents are observed in the alaskite (several hundreds of ppm up to 1000 ppm) because the magma was weakly peraluminous, relatively rich in fluorine, and part of the U precipitated from the magmatic fluids (Cuney 1980).

ALTERATION OF URANIUM MINERALS

Uraninite contains "impurities" such as Pb, Ca, Si, U^{6+}, Th, Zr, Fe and REEs that affect its thermodynamic properties, the rate of alteration, and the nature of the alteration products (Janeczek & Ewing 1992). The fate of uraninite is controlled primarily by the activity of O in the fluid (*i.e.* the oxidation of U^{4+} to U^{6+}), the openness of the fluid–ore system (*i.e.* how fast does water flush through the system) and the chemistry of the uraninite itself. A simplified model of the alteration products of

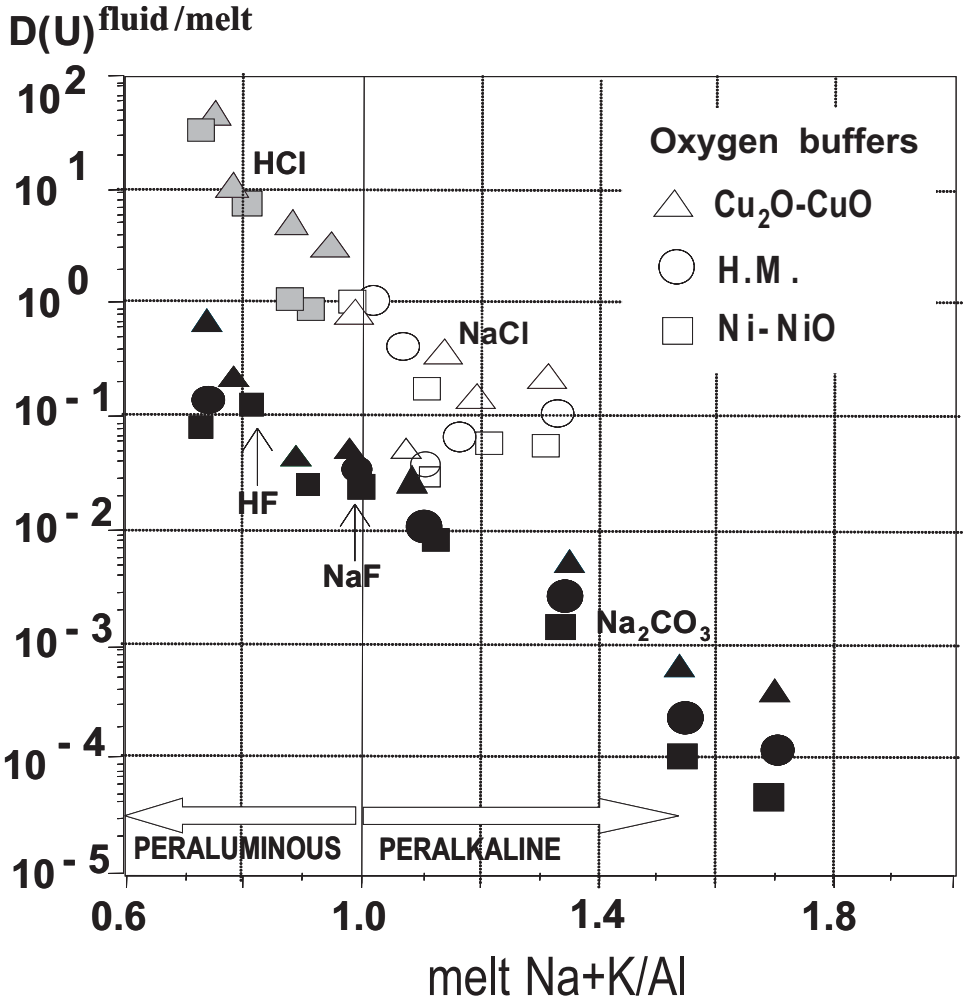

FIG. 3-5. Uranium partition coefficient between a granitic melt and a fluid phase having different compositions as indicated at equilibrium as a function of (Na + K/Al) ratio in the melt and three oxygen fugacities : Ni–NiO, Hematite–magnetite (HM) and Cu_2O–CuO. Data from Peiffert (1993) and Peiffert *et al.* (1994, 1996). Black symbols: experiments with Na_2CO_3 in the fluid phase at equilibrium with the melt; white symbols are experiments with NaCl; grey symbols with HCl; HF and NaF are labeled.

uraninite at low temperatures is shown in Fig. 3-6 along with the general reactions that occur. These alteration products, in turn, control the level of U and associated elements that may migrate away from the deposit as it alters (Allard *et al.* 2007, Kikuchi *et al.* 2007).

As U deposits are altered by oxidizing ground waters, there are regular changes that have been observed in their mineralogy (*e.g.* Patrier *et al.* 1997). The alteration of uraninite by oxidizing fluids results in the oxidation of U^{4+} to U^{6+}, a change in the color of uraninite from black to brown and a loss of luster. As alteration progresses, hydration begins and U is mobilized (Frondel 1958). Further alteration results in complete conversion of uraninite into secondary uranyl minerals, the mineral formed depending on the chemical composition of the altering fluids. In most cases, uraninite begins to dissolve and uranyl oxyhydroxides, such as becquerelite, schoepite and vandendriesscheite, precipitate within voids and fractures of the uraninite. As alteration proceeds, these uranyl oxyhydroxides are replaced by uranyl silicates and Pb-poor minerals and Pb-rich U minerals. Some U is transported short distances and precipitates on surfaces of corroding uraninite as uranyl oxyhydroxides or is absorbed onto Fe oxyhydroxides. Uranyl phosphates, when present, form relatively late.

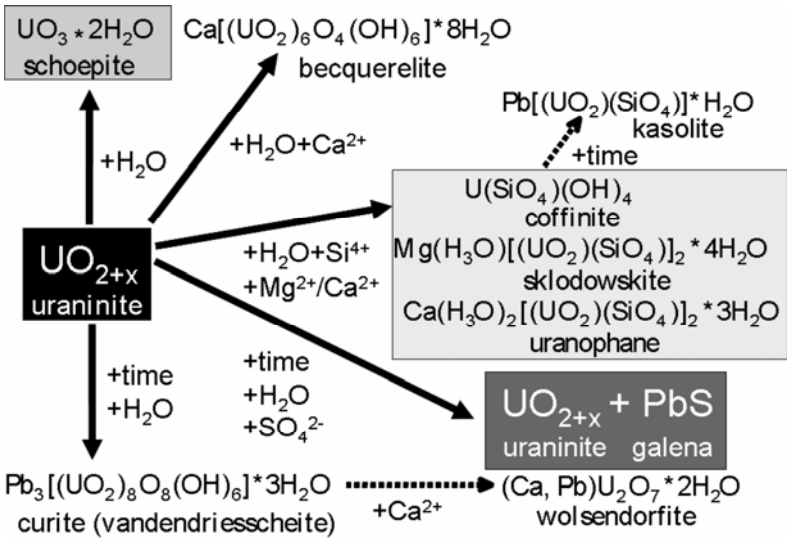

FIG. 3-6. Minerals that result from alteration of uraninite by ground waters and hydrothermal fluids. Based on results from Finch & Ewing (1992), Isobe *et al.* (1992), Fayek *et al.* (1997) and Finch & Murakami (1999).

In the presence of water, Fayek *et al.* (1997) found that Proterozoic uraninite alters rapidly to curite with the release of U and Ca into solution and the precipitation of becquerelite (Fig. 3-6). In the presence of silica-saturated fluids, U silicates such as soddyite and kasolite are precipitated along with curite and schoepite. This mineral paragenesis is similar to that observed in oxidized zones in U deposits and in UO_2–water interaction experiments.

The nature of hexavalent U minerals depends mainly on the nature of the available cations in the enclosing rocks. In chalcopyrite-bearing deposits, torbernite occurs whereas, in Ca-rich environments, autunite will form. However, Cathelineau *et al.* (1979) have shown that U oxides may have oxidation states up to $UO_{2.6}$ with preservation of the cubic structure of the mineral.

Under reducing conditions, uraninite in the presence of hydrothermal solutions may be altered through dissolution and coffinitization, with preferential loss of radiogenic Pb and Y + HREE, (Janeczek & Ewing 1992). Loss of radiogenic Pb is not associated with U mobilization. In addition to uraninite dissolution, coffinitization can result in U, Pb, and REE release.

Mobility of uranium in groundwaters

In most natural waters, U is present at concentrations between 0.1 and 10 ppb (*e.g.* Hem *et al.* 1993), although concentrations of 2 ppm correspond to water in equilibrium with U oxides in oxidizing conditions (Langmuir & Chatham 1980). The complex solution chemistry and disparity in the geochemical behavior between the two most common oxidation states of uranium, U^{4+} and U^{6+}, ensure that high levels in both water and anoxic stream sediments rarely occur together on regional geochemical maps.

Uranium is fixed in the sedimentary environment by a variety of processes including reduction of uranyl to uranous ion and precipitation as an oxide, as well as adsorption on organic matter (*e.g.* Artinger *et al.* 2002), oxides and fine clays. Precipitation of insoluble uranyl compounds such as carnotite also fixes U in sediments (Duff *et al.* 1997). Dissolved U tends to form strong associations with organic matter such as humic and fulvic acids, Fe and Ti oxides and with dissolved phosphates, the latter inducing co-precipitation with Ca or Pb, or with secondary Fe oxides. Where dissolved silica is present, U may precipitate as coffinite, $USiO_4$.

Langmuir (1978), in his analysis of U speciation in fluids at low temperatures, discussed the role of sorption of U on Fe oxyhydroxides as a mechanism to retard U mobility. Sorption of U^{6+} on Fe-oxide minerals such as hematite (Fe_2O_3) and goethite (FeOOH) and by Fe-oxide coatings can retard U mobility (Bruno *et al.* 1995, Moyes *et al.* 2000), eventually precipitating U^{6+} as crystalline uranyl phases similar to schoepite ($UO_2(OH)_2 \cdot 2H_2O$, Duff *et al.* 1999). Use of both the sorption properties of U and reduction and precipitation of actinides by microbes has been proposed as a strategy for fixing high-level nuclear waste and for remediation of U mines. However, interaction of mobilized U with Fe-oxides and microbes may reduce U contents in waters collected for exploration purposes.

The relation between coffinite ($USiO_4$) and

uraninite (UO_2) at low temperatures can be expressed as:

$$UO_2 + SiO_{2(aq)} = USiO_4$$

Theoretically, if both phases are present, the dissolved silica contents should be about 8 ppm (Langmuir 1978). Silica concentrations in ground waters are normally much higher, averaging about 17 ppm, and where coffinite is found in natural systems, it is stable relative to uraninite only when dissolved silica in groundwater exceeds 60 ppm. The conversion of uraninite to coffinite, therefore, is probably kinetically controlled. Regardless, both uraninite and coffinite are extremely insoluble at groundwater pH between 4 and 8 in low Eh environments indicating that U is immobile in these conditions. At higher Eh, however, oxidation of uraninite and coffinite render much greater solubilities by several orders of magnitude.

Natural examples of the complexities of U mobility at low temperatures are evident from numerous studies of ground waters near U deposits. On the Colorado Plateau where sandstone deposits are dominant, weakly alkaline, moderately reducing ground water with above average concentrations of dissolved carbonate species transport U in the form of uranyl bicarbonate and tricarbonate complexes. Precipitation results either from reduction of aqueous U^{6+} species to form uraninite in reducing conditions or fixation of uranyl ions with K ions and V^{5+} to form carnotite in oxidizing conditions (Hostetler & Garrels 1962).

In another example, the U distribution in the groundwater of five boreholes in granite near a restored vein-type U mine in Spain showed U contents varied from <1 ppb in reduced water far from the area of influence of the U ore-containing dyke, to 104 ppb in a borehole hydraulically connected to the mine (Gomez *et al.* 2006). Percolation of oxidized waters through the fractured granite led to dissolution of pitchblende and release of U^{6+} species to the groundwater, but also to oxidation of pyrite and arsenopyrite and the precipitation of Fe oxyhydroxides. The U^{6+} species were then retained by Fe hydroxides, and secondary U species eventually formed as reducing conditions were re-established due to water–rock interactions. Adsorption of U on Fe oxides and formation of secondary U minerals, which are ubiquitous in most U deposits, commonly limit the mobility of U away from the deposit, thereby complicating the use of hydrogeochemistry based on U contents for exploration.

BIOGEOCHEMISTRY OF URANIUM

Micro-organisms are ubiquitous in the surface of the Earth, with estimates of 100,000,000 micro-organisms in 1 gram of soil. Micro-organisms affect reactions at mineral surfaces and in solutions because the cells comprise a significant fraction of reactive surface area in the system. They thrive at temperatures in excess of 100°C, occur in the oldest Antarctic ice, are concentrated in acidic fluids and inhabit aquifers several kilometres below the surface.

Uranium accumulation by micro-organisms has been extensively studied. Several micro-organisms are known to interact with U, and the biological behavior of U resembles that of Fe (Figueroa *et al.* 2006). Enzymatic reduction of U^{6+} by microbes results in U precipitation. In most instances, these microbes precipitate U on the outside of their cells, although some incorporate U inside. The fixation of U is a complex process that is affected by other redox-sensitive elements in the system, as well as by the type of micro-organism. As these organisms die and decompose with time, the U can be released in the form of gases and organic complexes, which may migrate into the near surface environment above the original deposits.

Reduction of U^{6+} has generally been regarded as an abiological reaction in which sulfide, molecular hydrogen or organic compounds function as the reductant (Hostetler & Garrels 1962, Langmuir 1978). Although microbial involvement can involve indirect effects, such as reduced compounds from microbes for abiological U^{6+} reduction, dissimilatory Fe^{3+}-reducing micro-organisms can directly reduce U^{6+}, which can be much faster than abiological mechanisms for U^{6+} reduction (Lovley *et al.* 1991). Sulfate- and Fe-reducing microbes are known to reduce $U^{6+}$to U^{4+}, thereby immobilizing U, particularly in microbial havens such as anoxic sediments (*e.g.* Duff *et al.* 1999, Petrie *et al.* 2003) or in some sandstone-hosted U deposits (Min *et al.* 2005). Given that some microbial consortia probably can use the redox sensitive U in their metabolism, mobilization of U and other constituents from the ores themselves by gaseous and aqueous compounds might be used in exploring for deposits at depth, provided the U is not fixed by the reducing environment associated with some microbes or sorbed on mineral surfaces within the deposit.

Some organisms, such as the lichen *Trapelia involuta* or micro-organisms such as the bacterium *Citrobacter*, can absorb concentrations of U that are

up to 300 times higher than in their environment. *Citrobacter* species absorb uranyl ions when given organic phosphates (Macaskie *et al.* 1992). One gram of bacteria will encrust themselves with nine grams of uranyl phosphate crystals in just one day, suggesting that these organisms could be used in bioremediation to decontaminate U-polluted water (Simonoff *et al.* 2007).

Microbially mediated reduction of soluble to insoluble UO_2 to inhibit the migration of radionuclides in groundwater is negated by the oxidative resolubilization of U. Manipulation of the rate at which bioreduction occurs by varying the density of *Shewanella putrefaciens* CN32 added to solutions with U^{6+} showed that UO_2 nanoparticles formed by relatively slow rates of U^{6+} reduction were larger and more highly aggregated than those formed by relatively rapid reduction (Senko *et al.* 2007). Moreover, larger nanoparticles were oxidized at a slower rate suggesting the enhanced stability of more slowly precipitated UO_2.

Microbes may play a critical role in the formation of some sandstone-hosted deposits where extreme redox conditions are proximal, such as at a roll-front. Moreover, they are probably involved in tabular deposits in sandstones where redox reactions continually modify both the U mineralization and the organic matter. They actually may facilitate the mobilization of U from all U deposits at depth as they use the U in redox-reactions, the structures provide access for water and phosphates and other minerals supply nutrients.

Uranium and human health

Almost all U that is ingested is excreted during digestion, but up to 5% is absorbed by the body if the soluble uranyl ion is ingested. Soluble U compounds tend to pass through the body quickly whereas insoluble U compounds, especially when ingested via dust into the lungs, pose a more serious exposure hazard (Craft *et al.* 2004). After entering the bloodstream, the absorbed U tends to bioaccumulate for many years in bone tissue because of affinity of U for phosphates. Uranium does not absorb through the skin, and alpha particles released by the decay of U cannot penetrate the skin (ATSDR 1999).

The greatest health risk from U ingestion is toxic damage to the kidneys, because, in addition to being weakly radioactive, U is a toxic metal (Arfsten *et al.* 2001). No human cancer has been seen as a result of exposure to natural or depleted U, but exposure to some of its decay products, especially Rn, does pose a significant health threat.

The main anthropogenic sources of U and its by-products include nuclear testing, U mining and milling, nuclear effluents, phosphate fertilizers and coal combustion (Reimann & de Caritat 1998).

ANALYTICAL METHODOLOGIES

Radiogenic isotopes and uranium ore deposits

A critical aspect of ore deposits that is often overlooked is the age of the deposit and the timing of subsequent events that affected the ores. Uranium deposits are entities in both space and time, the former related to geology and geochemistry and the latter related to the timing of the initial formation of the ores and events that have affected them. The property that makes U a valuable commodity, namely its nuclear instability, also renders it a useful geochronometer, as do other elements incorporated into U minerals (Table 3-3). The age of U mineralization is useful for exploration because the geological architecture at the time the deposit formed can be realized. In addition, subsequent events can mobilize components in the ores into the environment where they can be used as vectors to mineralization.

Uranium minerals can have complex radiogenic isotope systematics for a multitude of reasons. The crystal structures of common U minerals are such that each may accommodate different ratios of radioactive parents and radiogenic daughters. For example, U and Sm are readily incorporated into the structure of uraninite, thereby rendering the ^{238}U–^{206}Pb, ^{235}U–^{207}Pb and ^{147}Sm–^{143}Nd systems useful geochronometers (Fig. 3-7). However, uraninite also incorporates some Nd but no Pb in its structure, so that the Pb in uraninite is generally produced *in situ* from decay of U parents whereas the Nd originates from both the Nd originally incorporated into uraninite as well as from decay of ^{147}Sm. In contrast, Rb is not compatible with the uraninite structure but Sr is. Consequently, the ^{87}Rb–^{87}Sr system cannot be used as a geochronometer in uraninite, but the isotopic composition of Sr can be used to infer the origin of the fluid that formed the uraninite. Associated gangue minerals in U ores such as feldspar, biotite, and muscovite have high contents of K and Rb (Fig. 3-7), and can be used to infer the age of U mineral formation **only if** these gangue minerals are coeval with the U minerals.

The principles of radiogenic isotope geochemistry and their applications have been reviewed in several classic publications (*e.g.* Faure

TABLE 3-3. RADIOACTIVE ISOTOPE AND RADIOGENIC PAIRS.

Parent-Daughter	Decay type	Half Life (m.y.)	Decay Constant $\lambda = 10^{-11}yr^{-1}$
$^{235}_{92}U \rightarrow {}^{207}_{82}Pb$	7α	704	98.485
$^{40}_{19}K \rightarrow {}^{40}_{20}Pb$	EC	1 250	55.43
$^{238}_{92}U \rightarrow {}^{206}_{82}Pb$	8α	4 468	15.5125
$^{232}_{90}Th \rightarrow {}^{208}_{82}Pb$	6α	14 010	4.9475
$^{176}_{71}Lu \rightarrow {}^{176}_{72}Hf$	β–	35 700	1.94
$^{187}_{75}Re \rightarrow {}^{187}_{76}Os$	β–	45 600	1.52
$^{87}_{37}Rb \rightarrow {}^{87}_{38}Sr$	β–	48 800	1.42
$^{147}_{62}Sm \rightarrow {}^{143}_{60}Nd$	α	106 300	0.654

Radioactive isotope and radiogenic pairs, their type of decay, half-lives and decay constants for systems that may be applicable to minerals in U deposits.

1986, McDougall & Harrison 1999, Heaman & Ludden 1991), to which the reader is referred for more rigour and detail. The purpose here is to review enough of the principles to permit an understanding of how radiogenic isotope systems should work in U minerals, and to discuss applications in the study of the age and origin of fluid events associated with the formation and alteration of U minerals. This is because estimation of an age or initial isotopic composition using radiogenic isotope geochemistry is only an interpretation of a set of data, and not an absolute.

Decay schemes

Nuclei of unstable atoms undergo radioactive decay during which they transform to stable nuclides with the emission of particles and energy. Alpha decay involves the expulsion of relatively large particles equivalent to He nuclei (*i.e.* 2 protons and 2 neutrons) along with radiant energy. The most relevant examples are the decays of ^{235}U and ^{238}U to ^{207}Pb and ^{206}Pb, respectively, and ^{232}Th to ^{208}Pb, which occur through a series of decay schemes (see Fig. 1.1 in Chapter 1). The intermediate products of the decay scheme are normally used to estimate relatively short-term processes (*e.g.* monitoring element migration around areas of U mineralization) whereas the radiogenic Pb isotopes are used for much longer term processes such as the age of U mineralization in natural systems.

The instability of U isotopes can result in spontaneous fission, particularly of ^{235}U, during which both fission products and thermal neutrons are released. A myriad of fission-induced products can be produced having a spectrum of decay rates themselves. These radioactive products and their daughters are used to determine the age of some U minerals, evaluate if high-grade U deposits were natural reactors and to estimate rates at which U minerals react with fluids.

Another alpha-decay system of use in U geochemistry is the rare-earth element (REE) isotope ^{147}Sm, which decays to the REE isotope ^{143}Nd (Table 3-3). REEs normally proxy for Ca, and thus can be incorporated into the structure of common U minerals (Table 3-4). However, REEs are more compatible with the structures of minerals such as carbonates and phosphates, which is advantageous if these phases are cogenetic with the U minerals, but problematic if they are not. As with the decay ^{235}U and ^{238}U to ^{207}Pb and ^{206}Pb, respectively (Table 3-3), the decay rate for ^{147}Sm is slow, thus requiring hundreds of millions of years before it is useful as a geochronometer.

Beta decay involves the transformation of a neutron to a proton and an electron, the latter of which is expelled from the nucleus as a negative beta particle. The systems most applicable to U ores involve the decay of alkali metal nuclides, ^{40}K and ^{87}Rb (Table 3-3), which are concentrated in associated minerals in the deposits such as feldspars or illite (Table 3-4). These nuclides are particularly useful in determining the age and origin of cogenetic illite commonly associated with U ores because they are readily incorporated into its structure.

Electron capture decay can be viewed as the capture of an extranuclear electron by the nucleus and transformation of a proton and the electron to a neutron. The nuclide ^{40}K decays by electron capture as well as beta decay (Fig. 3-7). The former is

TABLE 3-4. URANIUM AND ASSOCIATED MINERALS USED FOR RADIOGENIC ISOTOPE GEOCHEMISTRY OF URANIUM DEPOSITS.

Minerals	Compositions	Radiogenic methods
Uraninite	$UO_{(2+x)}$	U/Pb, Sm/Nd, U/Th
Schoepite	UO_3*2H_2O	U/Pb, U/Th
Becquerelite	$Ca[(UO_2)_6O_4(OH)_6]*8H_2O$	U/Pb, Sm/Nd, U/Th
Coffinite	$USiO_4$	Pb/Pb, U/Pb
Illite	$(K,Na)_{1.8}(Al,Mg,Fe)_4[(Si,Al)_8O_{20}](OH)_4$	K/Ar, Ar/Ar, Rb/Sr
K-feldspar	$KAlSi_3O_8$	K/Ar, Ar/Ar, K/Ca, Rb/Sr
Goyazite	$(Sr\ Al_3\ P_2O_7\ (OH)_7)$	U/Pb, Pb/Pb, Rb/Sr
Apatite	$Ca_5(PO_4)_3(OH,F,Cl)$	U/Pb, Pb/Pb, Sm/Nd, Rb/Sr
Zircon	$Zr(SiO_4)$	U/Pb, Pb/Pb, Sm/Nd, Rb/Sr
Gypsum/Anhydrite	$CaSO_4\ (H_2O)_x$	Rb/Sr
Carbonates	(Ca, Mg, Fe, Mn)) (CO_3)	Sm/Nd, Rb/Sr
Monazite	(Ce, Y, Th, REE) PO_4	U/Pb, Pb/Pb, Th/Pb, Rb/Sr

useful in determining the age of associated K-feldspar or clay minerals such as illite. Only 11% of ^{40}K decays by electron capture to ^{40}Ar, the remainder 89% via beta decay to ^{40}Ca. The beta decay scheme for ^{40}K to ^{40}Ca has yet to be used in the study of clay minerals, primarily because it is easier and more precise to measure the quantity of ^{40}Ar rather than ^{40}Ca in a sample. In addition, most minerals do not incorporate Ar in their structures initially, but do incorporate some Ca, thereby diluting the ^{40}Ca produced by the *in situ* decay of ^{40}K in the clay mineral and complicating any age determination. In effect, cogenetic minerals with different K/Ca ratios are required to measure the initial isotopic composition of Ca and K–Ca ages whereas only the amount of K and ^{40}Ar in the mineral are required for estimating its age. Not surprisingly, the rates at which ^{40}K undergoes beta decay and electron capture are quite different, the latter being 8.4 times slower than the beta decay.

Two other decay systems that have yet to be used in the study of U minerals are ^{176}Lu, which decays to ^{176}Hf by beta decay and to ^{176}Yb by electron capture, and ^{187}Re, which decays to ^{187}Os (Table 3-3). The low contents of these nuclides in U minerals and associated phases and the difficulty in analyzing their isotopic compositions routinely render the analyses difficult. However, there are phases such as phosphates, oxides and some sulfides with much higher contents that may be useful provided these phases are cogenetic with the U minerals.

The age equation

The rate of radioactive decay can be described as first order, which means that the disappearance of the radioactive parent isotope depends on both time and the amount of parent remaining. As a consequence, the amount of radioactive parent remaining, and radiogenic daughter produced, are not linear with time. The half-life of a nuclide is the time required for 50% of the nuclide to decay. For example, ^{235}U is a radioactive nuclide that decays to ^{207}Pb (Table 3-3). The change in the number of ^{235}U atoms in a sample with time can be described as:

$$-d[^{235}U]/dt = \lambda[^{235}U] \qquad (1)$$

where the brackets signify concentration, t is time, and λ is the decay (or rate) constant. To describe what happens after a length of time t has passed to the concentration of ^{235}U starting with an initial number of ^{235}U atoms, N_o, at time = 0, equation (1) is rearranged:

$$-\int_{No}^{N} d[^{235}U]/[^{235}U] = \lambda \int_{0}^{t} dt \qquad (2)$$

and the change in the number of ^{235}U atoms with time is integrated between the initial conditions (N_o atoms of ^{235}U and time = 0) and the final conditions (N atoms of ^{235}U remaining after time = t) to give:

$$\ln ([^{235}U]_{now}/[^{235}U]_{original}) = -\lambda t \qquad (3)$$

where $[^{235}U]_{now}$ signifies the amount of ^{235}U remaining in the sample at present. Therefore, the amount of ^{235}U in the sample remaining today is related to the original amount of ^{235}U in the sample and the amount of time that has passed by:

$$[^{235}U]_{now} = [^{235}U]_{original}\, e^{-\lambda t} \quad (4)$$

The amount of ^{207}Pb in the sample resulting from the decay of ^{235}U is simply the difference between the original amount of ^{235}U and the present amount of ^{235}U

$$[^{207}Pb]_{radiogenic} = [^{235}U]_{original} - [^{235}U]_{now} \quad (5)$$

which reduces to the following when equation (4) is substituted into (5):

$$[^{207}Pb]_{radiogenic} = [^{235}U]_{original}\,(1 - e^{-\lambda t}) \quad (6)$$

This expression relates the amount of radiogenic ^{207}Pb in a sample produced after a time t to the initial amount of the parent isotope ^{235}U. A similar expression will relate the amount of the daughter isotope after a time t to the present amount of the parent isotope, which is more useful because the present amounts can be measured directly.

The half-life ($t_{½}$) is defined as the time it takes to reduce an initial amount of a radioactive isotope by 50%. In the case of ^{235}U, the number of parent atoms in a sample after this time is related to the initial amount by:

$$[^{235}U] = ½[^{235}U]_{original} \quad (7)$$

so that,

$$½\,[^{235}U]_{original} = [^{235}U]_{original}\, e^{-\lambda t_{½}} \quad (8)$$

The half-life can then be related to the decay constant by:

$$t_{½} = 0.693/\lambda \quad (9)$$

Selected decay constants and half-life values for isotope systems that can be applied to U minerals are shown in Table 3-3.

In any U mineral, only the amount of radioactive parent (*i.e.* ^{235}U) remaining and the total amount of daughter isotope (*i.e.* $[^{207}Pb]_{now} + [^{207}Pb]_{original}$) can be measured. The amount of the daughter isotope in a sample produced by the decay of the radioactive parent can be related to the amount of the parent presently in the sample and the amount of time that has passed as:

$$[^{207}Pb]_{radiogenic} = [^{235}U]_{now}\,(e^{\lambda t} - 1) \quad (10)$$

Except for the K–Ar system wherein there are few sites in the lattice of most minerals for the incorporation of any Ar during initial formation, most minerals can accommodate daughter isotopes in their structure when they initially form. This means that there may be an initial amount of the daughter isotope ^{207}Pb in the U mineral prior to any production from the radioactive parent in that mineral. In the case of the U–Pb system, the total amount of the daughter isotope ^{207}Pb present in any mineral is really from two components, the initial amount incorporated when the mineral formed and the amount resulting from the decay of ^{235}U in the mineral,

$$[^{207}Pb]_{total} = [^{207}Pb]_{original} + [^{207}Pb]_{radiogenic} \quad (11)$$

which can be related to the amount of ^{235}U in the sample and the amount of time that has passed from combination of equations (6) and (11)

$$[^{207}Pb]_{total} = [^{207}Pb]_{original} + [^{235}U]_{now}\,(e^{\lambda t} - 1) \quad (12)$$

This is the basic age equation for the ^{235}U–^{207}Pb system for which the time, t, since the system closed to any loss of U or Pb can be determined. One simply has to measure the amount of ^{235}U and ^{207}Pb in the sample and somehow determine the amount of ^{207}Pb that was initially incorporated into the sample. In an ideal case, such as with uraninite, the initial amount of ^{207}Pb will be negligible, but in most cases some initial "common Pb" was incorporated into the sample, and this must be determined.

There are two techniques that can be used to determine how much of the daughter isotope was initially incorporated into the sample. The simplest, but less sure, method uses the amount of the non-radiogenic isotope ^{204}Pb to reflect the initial ^{207}Pb. This technique requires that the $^{207}Pb/^{204}Pb$ ratio of the initial "common" Pb is known. Normally, this is estimated using the average change in the $^{207}Pb/^{204}Pb$ ratio that has occurred as the crust has evolved (*e.g.*, Faure 1986). Complicating this estimate are different models for this evolution, potential heterogeneities in the U/Pb ratio in some areas of the crust and the time at which the common Pb was incorporated since the $^{207}Pb/^{204}Pb$ ratio depends on the age of the crust. For U minerals with structures in which Pb is not compatible, common Pb is not usually an issue. Instead, the problem is whether all the radiogenic Pb that was produced by the decay of U is still resident in the mineral.

An alternative technique uses several minerals that formed simultaneously but with different initial U/Pb ratios to determine precisely the initial amount of ^{207}Pb and $^{207}Pb/^{204}Pb$ ratio in each mineral. Each mineral incorporates different amounts of the parent and daughter isotope when it forms that depends on mineral structure. Three cogenetic minerals, such as two forms of uraninite and apatite, will have different U and Pb contents, and U/Pb ratios. During their initial crystallization, each mineral incorporates different amounts of common Pb, but

the isotopic composition of this Pb in each is the same. Therefore, the ratio of the radiogenic isotope of Pb (^{207}Pb) to the stable isotope of Pb (*i.e.*, ^{207}Pb/^{204}Pb ratio) was the same for the two forms of uraninite and apatite just after crystallization. This ratio changes differentially in each with the passage of time because each mineral has a different U/Pb ratio, which is reflected by the ^{235}U/^{204}Pb ratio. Consequently, the ^{207}Pb/^{204}Pb and ^{235}U/^{204}Pb ratios presently in each mineral are distinct. This is illustrated in Figure 3-7, in which the isotopic composition of Pb (*i.e.* ^{207}Pb/^{204}Pb) changes as a function of the ratio of the radioactive isotope ^{235}U to the non-radiogenic isotope of Pb (^{235}U/^{204}Pb) in the uraninite grains and apatite after times t_1 and t_2. Essentially by "normalizing" the isotopic concentrations expressed in equation (12) to a non-radiogenic isotope of the daughter element, (*i.e.*, ^{204}Pb), the age and initial isotopic composition of Pb in the cogenetic uraninite and apatite can be calculated from the slope and intercept, respectively, of the line defined by:

$$[^{207}Pb/^{204}Pb]_{now} = [^{207}Pb/^{204}Pb]_{original} + [^{235}U/^{204}Pb]_{now} (e^{\lambda t} - 1) \quad (13)$$

This is the basic age equation for the ^{235}U–^{207}Pb system, but is similar for all the other systems. Each system has a non-radiogenic reference isotope of the radiogenic element that is used to normalize the isotopic concentrations.

The slope of the line defines the age of our isochronous minerals uraninite and apatite (they lie on an "isochron"), and the intercept defines the initial isotopic composition of Pb from which the minerals crystallised. For the ^{235}U–^{207}Pb system, the $[^{207}Pb]_{now}$, $[^{204}Pb]_{now}$ and $[^{235}U]_{now}$ can be measured in the laboratory for a series of cogenetic minerals. Knowing the decay constant, λ, the only unknowns are t and $[^{207}Pb/^{204}Pb]_{original}$. Ages and initial ratios can be determined only if there is enough disparity in the parent/daughter ratios of similar minerals or there are at least two cogenetic phases with distinct parent/daughter ratios so that the isotopic compositions of the daughter element will change differentially with time. Otherwise, an initial isotopic composition of Pb must be assumed if only one, or similar, phases are available. These requirements are also applicable to all of the systems listed in Table 3-3.

Ages and initial ratios are obtained from regression of the data, and most uncertainties are cited at the 95% confidence level. Errors in the ages are enhanced by analysis of only a few samples or by analysis of samples having a restricted range in parent/daughter ratios. Some researchers report the MSWD (mean square of weighted deviates) values for their isochrons, which should be near unity if the errors are primarily analytical. MSWD values in excess of unity normally signify non-analytical scatter. Difficulties in isolating unaltered U minerals and associated minerals representative of single events make estimation of the errors of ages and initial isotopic composition difficult, resulting in MSWD values that can be much greater than 1.

Mixing between two or more phases that are not genetically related, such as detrital phosphate or illite with authigenic uraninite, can produce apparent isochrons that are really "mixingchrons". The ages and initial isotopic compositions obtained normally have no significance. Characterization of the paragenesis of all phases and use of pure separates are prerequisite for meaningful isochrons.

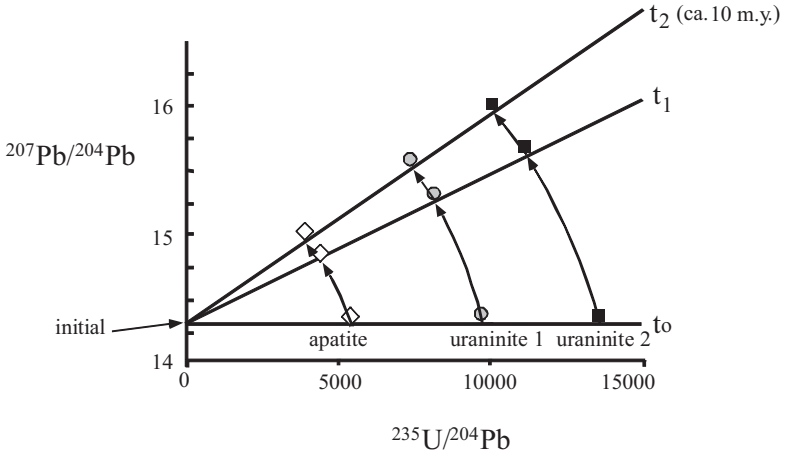

FIG. 3-7. ^{235}U-^{207}Pb isochron showing the evolution of ^{207}Pb/^{204}Pb and ^{235}U/^{204}Pb ratios in coexisting apatite and two different uraninite forms from initial crystallization (t_0) to a later time (t_1) and to t_2, 10 million years after the system closed for this decay system.

In addition to difficulties in separating and adequately characterizing minerals for isotope geochemistry, the age and initial isotopic composition of a sample really records the time that the radiogenic daughter is effectively retained as a closed system by a crystal. Prior to this being achieved, the daughter diffuses out of the crystal until the rate of diffusion slows enough so that those daughters farthest from the edge are retained. Dodson (1973) formulated this process primarily for metamorphic systems, and showed that the diffusion rate is a function of diffusion parameters (*e.g.*, activation energy for diffusion), cooling rate, and effective ionic radius of the element in the host crystal. He developed the concept of closure, which is the condition at which diffusion of a daughter isotope slows enough in a crystal to be retained, and the "age" begins. Faster cooling rates and larger grains lead to more robust closure conditions. Thus, thermal effects associated with intrusions, faulting or tectonics can partially reset a chronometer in a mineral, with the degree of resetting dependent on the duration of the event. Most commonly these thermal effects are associated with fluid circulation and alteration of the minerals. Similarly, interactions between minerals and fluids during which the crystal structure is altered will equally affect most chronometers.

U–Pb systems

Measurement of the isotopic composition of Pb necessitates determining the ^{204}Pb, ^{206}Pb, ^{207}Pb and ^{208}Pb contents. As a consequence, information about the ^{235}U–^{207}Pb, ^{238}U–^{206}Pb and ^{232}Th–^{208}Pb systems in U minerals can be determined simultaneously. In minerals like uraninite, where most of the Pb is radiogenic because little Pb is incorporated originally, the initial isotopic composition of Pb and the need to normalize to the non-radiogenic isotope ^{204}Pb in the general age equation become insignificant. The U and Pb contents and isotopic compositions should be directly related to the time that has passed since the minerals closed with respect to diffusive loss of U or Pb. Given the general age equation for both isotopes of U (*i.e.*, equation 12), both can be solved for t and equated such that:

$$1/\lambda_{235}[\ln [(^{207}Pb_{now} - {}^{207}Pb_{original})/^{235}U)_{now} + 1] = 1/\lambda_{238}[\ln [(^{206}Pb - {}^{206}Pb_{original})/^{238}U)_{now} + 1] \quad (14)$$

The amount of $^{207}Pb_{original}$ and $^{206}Pb_{original}$ can be estimated from the amount of common Pb in the sample. The ratios ^{206}Pb*/^{238}U and ^{207}Pb*/^{235}U (* indicates radiogenic Pb after the common Pb has been subtracted) can be calculated for each time t, the time the mineral closed with respect to the U–Pb system. Because ^{235}U decays much faster than ^{238}U (Table 3-3), a plot of ^{206}Pb*/^{238}U versus ^{207}Pb*/^{235}U will be curved along a line as shown in Figure 3-8. For example, when a uraninite first precipitates and has no ^{207}Pb or ^{206}Pb, it would plot at the ordinate on the U–Pb isochron plot (Fig. 3-8) and move along the curve (referred to as concordia because both the U–Pb ages are concordant) as time progresses. If undisturbed, this uraninite would plot on concordia at 1650 Ma. If total loss of Pb occurs later, for example at 900 Ma, the system is restarted and the neoformed uraninite would now plot on concordia at 900 Ma. If partial loss of Pb occurs in some samples at 900 Ma or some of the Pb migrates to older parts of the uraninite, these will plot on a discordia line defined by the initial age of 1650 Ma and the rest age of 900 Ma. If any of these uraninite grains are then affected by recent weathering, they will be displaced towards the ordinate and fall within the shaded area shown in Figure 3-8. Because Pb is not compatible within the uraninite structure as it has an effective ionic radius of 1.28Å instead of 1Å for U^{4+} in hexavalent coordination, and because the crystallinity of the uraninite is degraded by the effects of radioactive decay, loss of Pb from uraninite is generally the rule, rather than the exception. Large amounts of radiogenic lead can be lost from the U minerals at the scale of a deposit (Holk *et al.* 2003, Kister *et al.* 2004) and radiogenic galena can form within and in the vicinity of the U minerals, implying later percolation of sulfur-bearing fluids within the crystals. In addition, most U deposits are structurally hosted and are therefore susceptible to later fluid circulation events related to reactivation of the tectonic structures that facilitate recrystallization of uraninite. These render determining the age of the originally formed uraninite extremely difficult.

Ages of uraninite grains can be obtained using three different methods. The least precise and accurate method does not use isotopic compositions, but has the greatest spatial resolution of a few micrometres. Instead, the concentrations of U and Pb are used, as determined from electron microprobe data (Bowles 1990). Although the spatial resolution is on the micrometre scale, this method requires the assumption that all of the Pb measured is from the decay of U and none has been lost, thus permitting estimates of how much time has passed. This method is suited for uraninite

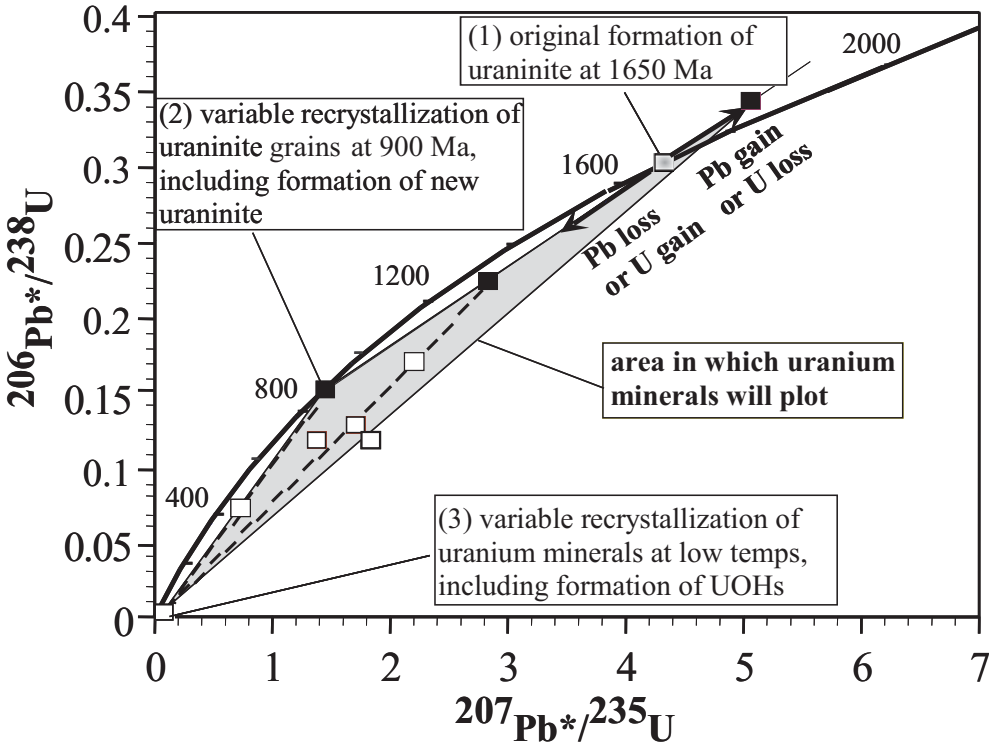

FIG. 3-8. U-Pb isotope systematics of uraninite grains that (1) initially formed at 1650 Ma and presently plot on concordia (shaded square), (2) were variably recrystallized by an event at 900 Ma and then (3) were variably affected by recent weathering. During the subsequent alteration events, neoformed uraninite will plot on concordia at 900 Ma and 0 Ma, but uraninite grains variably reset by the event at 900 Ma (solid squares) will fall along a discordia line determined by the initial age of 1650 Ma and the reset age of 900 Ma. Pb can migrate into other parts of the uraninite, resulting in Pb gain, but these samples will also plot on the Discordia line. If these are affected by recent weathering, they will be displaced towards the ordinate (open squares).

grains, or domains within uraninite grains, that have escaped resetting by later fluids. Such a study is also a prerequisite to evaluate the degree of homogeneity of U and Pb distributions within the minerals selected for isotopic studies.

Another method uses only the $^{207}Pb/^{206}Pb$ ratios to reflect the age (*e.g.*, Kotzer & Kyser 1993). This method requires the assumption that, although the uraninite may have lost radiogenic Pb since it formed, the loss is recent (within the past few million years), most likely due to weathering. Thus, the $^{206}Pb^*/^{238}U$ and $^{207}Pb^*/^{235}U$ are lowered because of the loss of radiogenic Pb, but the $^{207}Pb/^{206}Pb$ ratios are not changed. For many U deposits, this method can be robust, particularly since the $^{207}Pb/^{206}Pb$ ratios can be determined more accurately and precisely than $^{206}Pb/^{238}U$ and $^{207}Pb/^{235}U$ ratios.

The third method is the most meaningful because it uses the relationship between the $^{206}Pb^*/^{238}U$ and $^{207}Pb^*/^{235}U$ ratios as described previously. Because $^{207}Pb/^{206}Pb$ ratios are also determined at the same time, the Pb–Pb methods can also be used.

There are four isotopic techniques that are currently used for precise U–Pb geochronology of U ores:

1. thermal ionization mass spectrometry (TIMS) of U and Pb after dissolution of several milligrams of sample and separation of both U and Pb from the resulting solution (*e.g.*, Hills & Richards 1976, Ludwig 1978, Baadsgaard *et al.* 1984, Ludwig *et al.* 1987);
2. secondary ion mass spectrometry (SIMS), which uses an ion beam to sample >10 μm spots *in situ* (*e.g.*, Fayek *et al.* 2000, 2002a, 2002b).
3. solution ICPMS, using dissolution of a few milligrams of the sample, without the need for separation of U or Pb (*e.g.*, Longerich *et al.* 1992);
4. laser ablation (LA) ICP–MS, which uses a laser to sample specific areas *in situ* of a few micrograms from 20–50 micrometre spots on the sample (Chipley *et al.* 2007);

Both the TIMS and solution ICPMS techniques require that the sample be dissolved, so that powdered bulk samples or areas drilled from chips of the sample must be used. The LA–ICP–MS and SIMS are both microbeam, *in situ* sampling techniques, with sampling spatial resolutions on the micrometre scale. They require minimal sample preparation and are well suited for samples that are heterogeneous, such as uraninite from U deposits. An example of how new technologies have affected our concept of when U deposits form and evolve is evident from the history of published ages for unconformity-related U deposits in the Athabasca Basin (Fig. 3-9). TIMS analyses on whole rock samples and subsequently on separated uraninite returned ages near 1300 Ma. More recent publications, in which LA–ICP–MS or SIMS were used to evaluate the age of mineralization, return ages of in excess of 1500 Ma, and the ages are similar for either technique. The disparity in ages obtained with TIMS relative to the microbeam techniques reflects the extreme heterogeneity of older uraninite due to partial resetting by later fluid events (*e.g.* Alexandre & Kyser 2003). On the micrometre scale, domains from the original precipitation event are still present, although rare, and can be detected with microbeam techniques whereas much of the uraninite has been altered, thereby giving younger apparent ages (Alexandre & Kyser 2005, Polito *et al.* 2004). In effect, the incompatibility of Pb in the uraninite structure renders uraninite a potentially superb record of major fluid events in an area, but also makes the interpretation of the age of initial deposition challenging.

Sm–Nd systems

The REEs are compatible with the uraninite structure and are relatively immobile in most fluids that alter uraninite (*e.g.*, Fayek & Kyser 1997). As a consequence, the ^{147}Sm–^{143}Nd decay system has been used to reflect the time at which uraninite formed. The technique was pioneered by Fryer & Taylor (1984), who used the Sm–Nd system to differentiate ages of petrographically distinct uraninite from the Collins Bay unconformity-related deposit (Fig. 3-10), and then by Maas (1989) for unconformity-related deposits in Australia. As with the U–Pb results from these deposits, this uraninite is heterogeneous because it has been variably reset, but maybe less so for the Sm–Nd system. To date, there are no results for the Sm–Nd system using a microbeam technique. However, the Sm–Nd isochron ages reported by Maas (1989) are similar to the oldest U–Pb ages obtained using microbeam techniques for most deposits.

One advantage of Sm–Nd isochrons is the initial $^{143}Nd/^{144}Nd$ ratios that are obtained (Fig. 3-10). These have been used to trace the origin of the Nd in uraninite, thereby tracing where the fluids obtained their Nd. The isotopic composition of Sm and Nd has also been used to verify that some of the U deposits in the Paleoproterozoic Franceville Basin were natural reactors (Gauthier-Lafaye *et al.* 1989, Hidaka & Holliger 1998) and that others in Paleoproterozoic basins in Australia were not (Maas & McCulloch 1990).

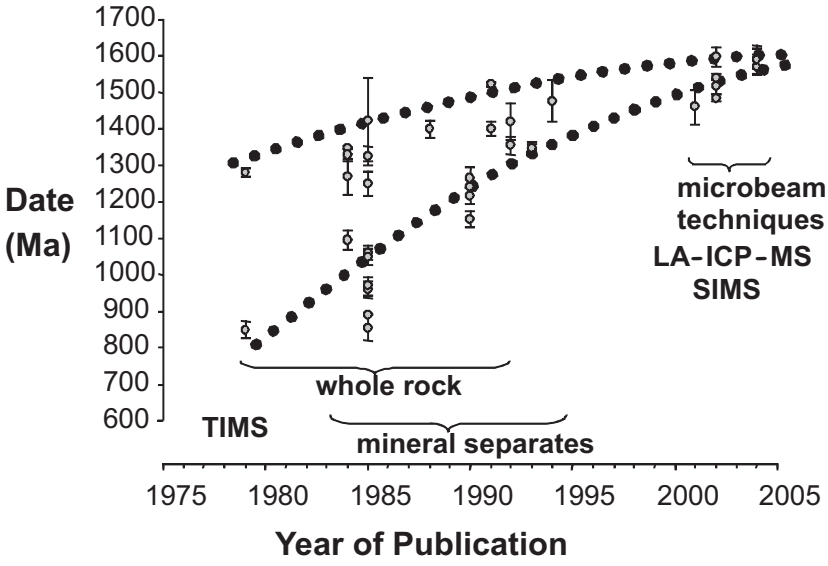

FIG. 3-9. Published dates of uraninite using the U-Pb system for unconformity-related deposits in the Athabasca Basin as a function of the year the data was published. Prior to 2000, only TIMS data are reported and these are on whole-rock samples or mineral separates. The advent of microbeam techniques gives the oldest and most consistent ages. Figure from P. Alexandre (pers. comm.).

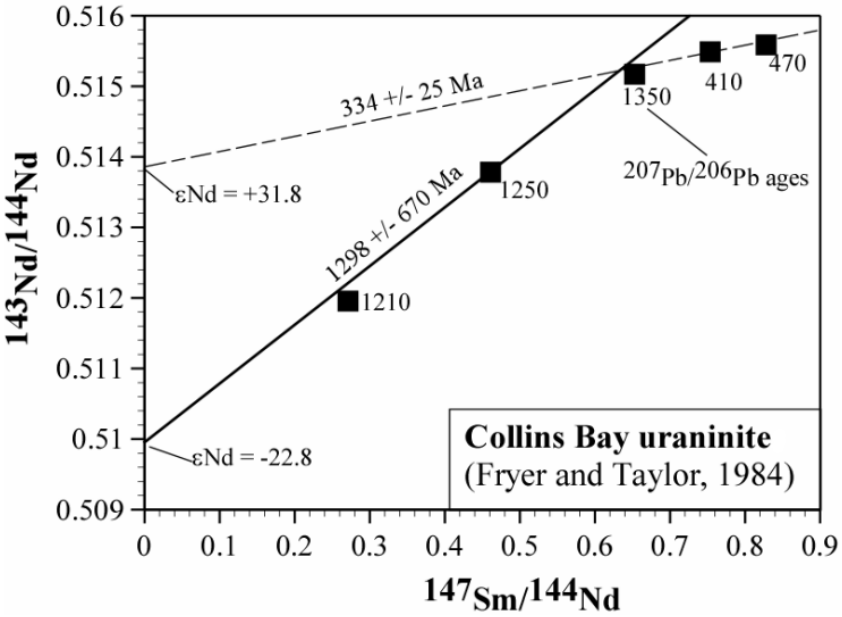

FIG. 3-10. Sm-Nd isochron for uraninite from the Collins Bay deposit in the Athabasca Basin. The data are interpreted to reflect two "crystallization" events, one at 1298 Ma and the other at 334 Ma. Also shown are the $^{207}Pb/^{206}Pb$ ages. The two groups define different initial Nd isotopic compositions (εNd) as indicated. Data from Fryer & Taylor (1984).

K–Ar and Ar–Ar systems

The decay of ^{40}K to ^{40}Ar is exploited in geochronology because K-rich phases such as illite, muscovite, biotite, and feldspars are commonly associated with U minerals and because isochrons are not always necessary to estimate ages due to the lack of incorporation of initial Ar into these minerals. Two techniques are used, K–Ar and ^{40}Ar–^{39}Ar, which differ primarily in the way the amount of ^{40}K that produced the ^{40}Ar in the sample is measured. The conventional K–Ar method requires that the K and ^{40}Ar contents be measured on separate fractions of the sample whereas, in the ^{40}Ar–^{39}Ar method, part of the K in the sample is first converted to ^{39}Ar via irradiation with neutrons and measured simultaneously with the ^{40}Ar.

The ^{40}Ar–^{39}Ar method uses fast neutrons to convert some of the ^{39}K in the sample to ^{39}Ar ($t_{½}$ = 269 years) The $^{40}Ar/^{39}Ar$ ratio in the sample is proportional to the $^{40}Ar/^{40}K$ ratio so that this technique is potentially more precise (*ca*. 0.6%) than the K–Ar method because K and Ar isotopic compositions and contents are measured at the same time. Any Ca, K, Ar and Cl can also produce Ar isotopes when irradiated, and the conversion of ^{40}Ca to ^{37}Ar can be used to estimate the Ca/K ratio in a sample.

Although the total amount of ^{40}Ar and ^{39}Ar released from a sample can be used to estimate an age, extraction with incremental heating permits Ar loss, contamination, or inheritance to be better studied. Essentially, the sample is heated in incremental temperature steps, and the $^{40}Ar/^{39}Ar$ ratios for each step are used to calculate an age. The apparent ages are plotted as a function of the fraction of ^{39}Ar released, resulting in an age spectrum. In an ideal mineral, the K and ^{40}Ar are evenly distributed throughout, as are the ^{39}Ar and ^{40}Ar after irradiation. Heating the mineral in increasing steps should first release the Ar closest to the edge of the grain, with sequential temperatures releasing Ar from the sites having higher retentivity. The $^{40}Ar/^{39}Ar$ ratios, which are related to the apparent ages, for each temperature should be similar. If a portion of the grains have been altered or recrystallized with loss of ^{40}Ar, the low-temperature steps will have low $^{40}Ar/^{39}Ar$ ratios relative to the remainder of the grain, resulting in a disturbed age spectrum. The spectrum can also be disturbed if there are other phases, such as inherited detrital phases or domains, that release their ^{40}Ar or ^{39}Ar at a given temperature, or if there is loss of ^{39}Ar from an area after irradiation. These spectra are often complex, and can have little to no age significance.

Loss of ^{39}Ar is problematic with clay minerals because such fine grains are used (*e.g.* Foland *et al.* 1992). Loss of ^{39}Ar as a result of recoil appears not to be simply a function of the grain size of the clay mineral, but also of crystallinity and morphology. Plate-like minerals such as illite of <2 μm can lose significant amounts of ^{39}Ar as a result of recoil, thus resulting in ^{40}Ar–^{39}Ar ages that are much older than the mineral because the $^{40}Ar/^{39}K$ ratios are too high (*e.g.*, Hess *et al.* 1986). Loss due to recoil is most pronounced at the edges of the grains so that

extraction of Ar from various portions of the grains are attempted using differential heating, the ideal being that high extraction temperatures remove Ar from the more central portions of the grains. Alternatively, the ^{39}Ar lost during recoil can be collected if the sample is sealed in a quartz tube prior to irradiation.

The ^{40}Ar and ^{39}Ar can be extracted from a sample with a laser as a point heat source to release the Ar from a small portion of the sample, *ca*. >50 μm (*e.g.* Bray *et al.* 1987). The beam size of the laser normally exceeds that of the clay minerals, so that large grains, or masses of grains must be available. Bray *et al.* (1987) reported that the K–Ar ages for illite separates were comparable to the laser-extracted Ar–Ar ages for 2M illite from the Proterozoic Athabasca Basin in Canada, although aberrantly low ^{40}Ar/^{39}Ar ratios released at low temperatures indicated there had been loss of ^{40}Ar. They used only the ^{40}Ar/^{39}Ar ratios from the higher temperature releases with the laser, and suggested that recoil of ^{39}Ar had a minimal effect.

As with K–Ar ages, the validity of ^{40}Ar–^{39}Ar ages requires intimate knowledge of the character of the mineral and independent constraints on the geologic and temporal evolution of an area. Loss of ^{39}Ar due to recoil can be extreme for some samples. The use of lasers as point heat sources shows great promise for *in situ* analysis of illite (and feldspar), but this technique, like all others, is limited by the grain size, crystallinity, and paragenic relations of the clay minerals.

Radiogenic isotopes as tracers

The initial Sr, Nd, and Pb isotopic compositions of a mineral theoretically can be used to trace the composition of the fluid from which the mineral formed. The relatively long half-life of ^{147}Sm and the similarity in the chemical characteristics of Sm and Nd result in total variations in the Nd isotopic compositions of most natural reservoirs of *ca*. 0.2%. A convenient way of expressing the Nd isotopic composition in light of these limited variations is using εNd values (Fig. 3-12) which are defined as

$$\varepsilon Nd = [(^{143}Nd/^{144}Nd)_{sample(t)}/(^{143}Nd/^{144}Nd)_{CHUR(t)}-1]*10{,}000 \quad (15)$$

where (t) is the age of interest and CHUR is the composition at time = t of a CHondritic Uniform Reservoir, comparable to the primitive earth. As shown in Figure 3-11, partial melting of the earth in the past resulted in melts with lower Sm/Nd ratios than the primitive earth, and a slower change in their ^{143}Nd/^{144}Nd ratio. The residues have higher Sm/Nd ratios because Sm is more compatible with the mineralogy of the residue than is Nd, and correspondingly more rapid rise in their ^{143}Nd/^{144}Nd ratios. Similar values can be calculated for Sr (εSr), although positive εSr values, but negative εNd values, correspond to crustal sources (Fig. 3-11). Given the age of a mineral, the εSr and εNd values, like the initial isotopic compositions, can be used as measure of the relative contributions of various sources.

Despite the potential of radiogenic isotope systems to reveal the timing and source of mineralizing events related to U deposits, all of the difficulties discussed here require a significant effort to overcome. The number of studies is limited that integrate initial isotopic compositions of Sr and

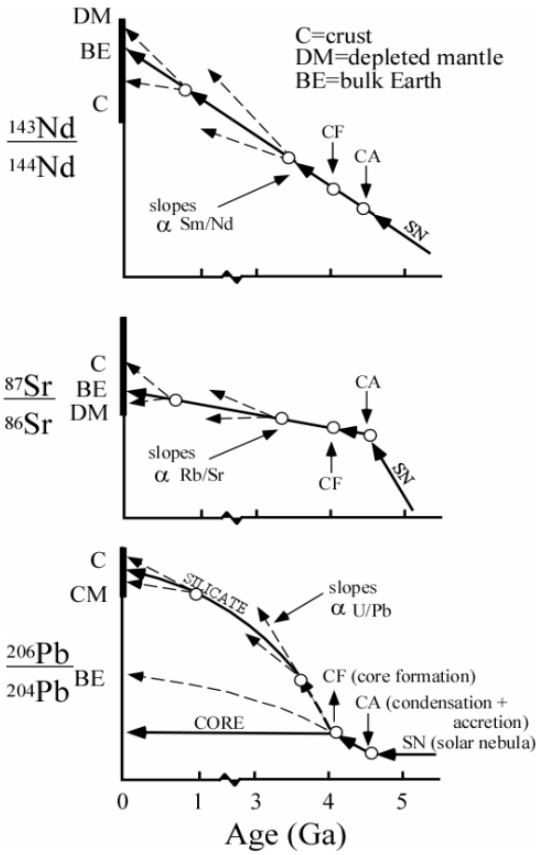

FIG. 3-11. Evolution of Nd, Sr and Pb isotopic compositions as a function of age of the Earth. Each of these ratios increases because the denominator is a radiogenic isotope whereas the numerator is a non-radiogenic isotope of these elements. Also shown are the ratios for depleted mantle (DM), bulk earth (BE) and crust (C).

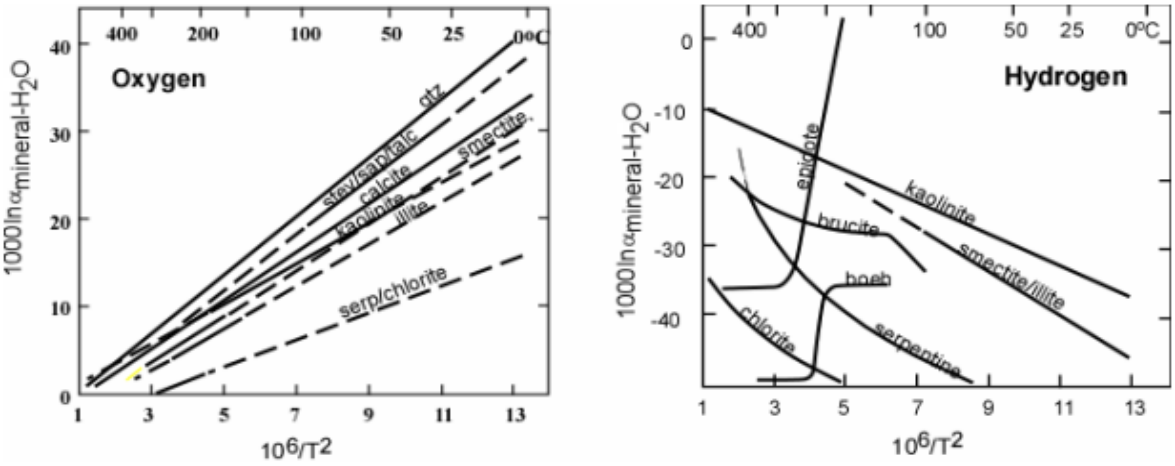

FIG. 3-12. Fractionation factors ($1000\ln a = \delta_{mineral}-\delta_{H2O}$) for oxygen and hydrogen isotopes between minerals and water. After Kyser (1987).

Nd in conjunction with the dates obtained to constrain the components within a system that are reacting to produce U minerals. Pagel *et al.* (1992) and Kotzer & Kyser (1995) used initial Sr and Nd isotopic compositions of alteration minerals to trace the relative contributions of basement and basinal fluids in the formation of unconformity U deposits in Canada. Turpin *et al.* (1990) compared Sr and Nd initial isotopic compositions in intrusive hosted U deposits and barren areas in France and Turpin *et al.* (1991) examined the systematic of U–Pb, Sm–Nd and K–Ar in the sandstone-hosted Akouta U deposit, Niger. These studies have variable success that is more limited by understanding of the mineral paragenesis and mineral reactivity with later fluids than by the technology.

Stable isotope geochemistry

Stable isotopic studies of U ore deposits have been applied largely in the context of tracing fluid sources, geothermometry, to test for equilibrium *versus* disequilibrium and for open *versus* closed system conditions. Modern stable isotope geochemistry primarily involves accounting for variations in the isotopic composition of H, C, N, O and S in a variety of natural substances. These elements are comprised of one very abundant isotope and one or more minor isotopes. The stable isotopic ratios of these elements are particularly useful in U exploration for the following reasons:

1. unlike radiogenic isotopes, the isotopic composition of these elements in natural substances is not a function of time or the chemical disparity between the parent and daughter elements;
2. these elements are the main components of most rocks, minerals, and fluids, so that if you want to trace the source of an aqueous fluid, the major components of the fluid are H and O, and their isotopes are the most definitive indicators of the fluid source;
3. the distribution of the isotopes of these elements among different phases varies primarily as a function of redox conditions and temperature;
4. occurrence of more than one oxidation state as with C, N, and S or of very different types of bonds as in H–O, C–O, or S–O enhances the mass-dependent fractionation of isotopes;
5. the great abundance of these elements in most substances coupled with the ability to determine precise relative isotope ratios using isotope ratio mass spectroscopy (IRMS) allows determination of the isotopic composition of many geologically relevant materials.

The isotopic composition of an element such as oxygen in coexisting phases may be different because of small differences in the thermodynamic properties of the isotopes in these phases. In theory, the $^{18}O/^{16}O$ ratio of an ancient fluid could be determined from analyses of the $^{18}O/^{16}O$ ratios in solid phases which were in equilibrium with the fluid provided the variables that affect isotopic fractionations are known. Inasmuch as temperature is a major variable for isotopic fractionations, it is necessary to know the fractionation of isotopes among various phases as a function of temperature. Such fractionations are determined from theoretical calculations, laboratory experiments, or empirical methods using natural samples.

The isotope fractionation factor between two substances, A and B, is defined as:

$$\alpha_{A-B} = R_a/R_b \quad (16)$$

where R_a is the ratio of the heavy (minor) isotope to the light (abundant) stable isotope in phase A, such as D/H, $^{18}O/^{16}O$, or $^{13}C/^{12}C$. Rather than determining the absolute ratios (*i.e.*, $^{18}O/^{16}O$), in every phase, it is easier and more precise to measure the differences in ratios between two substances. As such, stable isotopic abundances are normally reported as delta (δ) values in units of permil (indicated by the symbol, ‰) relative to a standard such that:

$$\delta_A = [(R_A/R_{stnd.}) - 1] \times 1000 \quad (17)$$

where R_A is the ratio in the sample and $R_{stnd.}$ is the ratio in the standard. The standards are Vienna Standard Mean Ocean Water (VSMOW) for both hydrogen and oxygen, a belemnite from the Cretaceous Pee Dee Formation, South Carolina (VPDB) for carbon (and, in some cases, for oxygen in carbonates), and troilite from the Canyon Diablo iron meteorite (CDT) for sulfur. Thus, a $\delta^{18}O$ value of +10 permil for a quartz sample has an absolute $^{18}O/^{16}O$ ratio that is 1% (or 10 permil) greater than that of Vienna Standard Mean Ocean Water (VSMOW). Similarly, a δD value of –70 for a biotite has an absolute D/H ratio 7% (or 70 permil) lower than VSMOW.

The relation between δ values, which are the isotope ratios of samples relative to the standards, to fractionation factors, which are equilibrium constants that describe how the isotopes are partitioned between two phases, is:

$$\alpha_{A-B} = \frac{1+\delta_A/1000}{1+\delta_B/1000} = \frac{1000+\delta_A}{1000+\delta_B} \quad (18)$$

Values of α are usually close to unity, so that isotopic fractionations are expressed as permil fractionations. For example, α for oxygen isotopes between quartz and water at 200°C is 1.0110 so that the fractionation of oxygen isotopes between quartz and H_2O is +11 permil; that is, quartz is enriched in ^{18}O by 11 permil relative to water. Similarly, α for oxygen isotopes between water and quartz at 200°C is 0.9890 so that water is depleted in ^{18}O by 11 permil relative to quartz.

As with any equilibrium constant, α is related to the energy of any exchange reaction as ln α. The energies involved in any reaction having an equilibrium constant close to unity are small, *i.e.*, ln α(quartz–water) = 0.011 at 200°C. For α = 1.0X, 1000 ln α is approximately equal to X so that for the quartz–water exchange reaction at 200°C, 1000 ln α = +11. Thus, 1000 ln α is approximately the permil fractionation. From equation (17), and defining Δ_{A-B} as $\delta_A - \delta_B$:

$$1000\ln\alpha_{A-B} \approx \delta_A - \delta_B = \Delta_{A-B} \quad (19)$$

provided α_{A-B} is within about 2 percent of unity. Therefore, the difference between the δ values of two coexisting phases is approximately equal to the permil fractionation. Most anhydrous silicates at room temperatures are described by fractionations that vary as $1/T^2$ (Bigeleisen & Mayer 1947, Bottinga & Javoy 1973). Phases containing hydroxyl groups may be more a function of 1/T or $1/T + 1/T^2$. At infinite temperature, $\ln \alpha_{A-B}$ must become zero (*i.e.*, the energy levels for isotopic compounds are equal).

Isotope fractionations for several minerals of interest are shown in Figure 3-12. Fractionation factors for oxygen isotopes indicate that $^{18}O/^{16}O$ ratios at equilibrium increase in the order; H_2O << serpentine = chlorite < illite < smectite = kaolinite < calcite < quartz. With few exceptions, hydroxyl minerals are depleted in deuterium relative to water and the degree of depletion increases with decreasing temperature. Hydrogen isotope fractionations vary as a function of the type of cation in the octahedral sites. Exchange experiments for hydrogen isotopes between silicates and water indicate very slow rates of isotope exchange, suggesting that most hydrous minerals are resistant to simple hydrogen isotope exchange with water, unless there is concomitant elemental exchange. Clay–water systems for which the hydrogen isotope fractionation factors are reasonably known, have temperature dependencies that are similar below 150°C regardless of whether there is hydrogen bonding in the mineral.

An important secondary effect on isotopic fractionations in mineral–water systems is the chemical composition of the fluid (*e.g.*, Horita *et al.* 1993). Those anions and cations that modify hydrogen bonding in water to the greatest extent should have the greatest effect on mineral–H_2O fractionation factors. The effect is most pronounced in solutions in which the solutes have the highest ionic charge, smallest ionic radii and greatest concentrations.

Reference is often made in the literature to various types of waters, and some of these have genetic connotations whereas others do not. Formation water refers simply to the fluid resident in

rocks, and has no significance to origin or age. Connate water is the fluid deposited with the sediments or rocks and can be modified via reactions with the reservoir rocks. Meteoric water originates from rain or snow and can be modified via interaction with rocks at elevated temperatures to become a hydrothermal fluid. Marine or ocean water is a fluid derived primarily from seawater, including those that have been modified through evaporation or interaction with rocks in ocean ridge or basin settings. Metamorphic water is that associated with metamorphism although sometimes the ultimate origin of this fluid (*i.e.*, meteoric water, connate water, seawater, or water from dehydration reactions) can be determined with hydrogen and oxygen isotopes. Magmatic water is that hydrous fluid usually released from a crystallizing magma. Other than formation waters, these "categories" of water are applicable to describing the origin of only some fluids because the extensive interactions between most fluids and rocks obscure their origin. The observed ranges in the isotopic composition of fluids that may be involved in the formation or alteration of U deposits are shown in Figure 3-13. Seawater has δD and $\delta^{18}O$ values near 0 ‰ by definition. Most meteoric waters have regular variations in their isotopic compositions such that they plot along the meteoric water line (MWL) at a position that varies primarily with latitude and altitude. The global meteoric water line is defined by the relation:

$$\delta D = 8(\delta^{18}O) + 10 \qquad (20)$$

At high latitudes, meteoric water is ^{18}O- and D-depleted relative to precipitation at low latitudes which has isotopic compositions near those of seawater. Most meteoric waters are from condensation of water vapor originating from evaporation of seawater, although their trend is displaced from seawater because of a kinetic effect associated with evaporation. The regular variation in δD and $\delta^{18}O$ values of meteoric water results from consistency in the difference between the fractionation factors of hydrogen and oxygen with temperature for the system H_2O(liquid)–H_2O(vapor). The effects of both temperature and solute composition on fractionation factors between liquid water and other substances have important implications for several low-temperature processes. When seawater evaporates the δD and $\delta^{18}O$ values of residual brines first increase as evaporation proceeds, and then decrease when the solute concentration becomes high enough to reverse the fractionation factor between water liquid and water vapor (Sofer & Gat 1975). As a consequence of this reversal, highly evaporated seawater, such as that trapped in fluid inclusions of marine evaporites, can obtain lower δD and $\delta^{18}O$ values than starting compositions (Fig. 3-13). The stable isotope

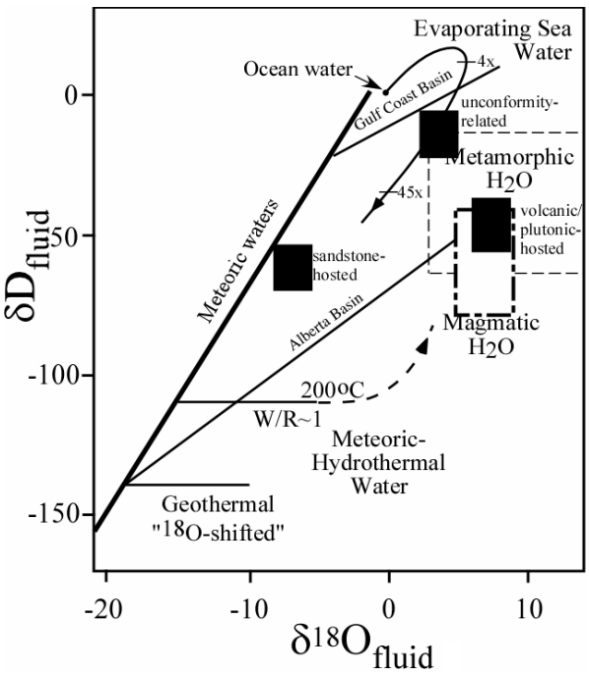

FIG. 3-13. Isotopic composition of hydrogen and oxygen, expressed in units of permil as δD and $\delta^{18}O$ values, respectively, for fluids associated with U ore deposits. Shown are the fields for magmatic and metamorphic fluids, basinal brines for the Gulf Coast Basin (low latitude) and the Alberta Basin (high latitude), the meteoric water line, ocean water and the effect of evaporation on seawater (4x and 45x evaporated) and changes that occur in the values of meteoric waters reacting with rocks during hydrothermal alteration (geothermal shifted and meteoric-hydrothermal) for water/rock ratios (W/R) near 1. After Kyser (1987). Also shown are the fields for unconformity-related, volcanic/ plutonic-hosted and sandstone-hosted U deposits.

systematics of basinal brines (Fig. 3-13) indicate they reflect modification of meteoric waters (Clayton *et al* 1966), mixing between relatively modern meteoric water and diagenetically modified or evaporated seawater (Hitchon & Friedman 1969, Knauth & Beeunas 1986).

As meteoric water is heated and reacts with rocks, the water exchanges oxygen with the vast reservoir of oxygen in the rocks and generally becomes more ^{18}O-rich. Only when the water/rock ratio decreases significantly is the hydrogen isotopic composition of fluid affected depending on the D/H ratio and quantity of hydrogen in the rock. Fluids in basins have isotopic compositions that resemble mixing between modern meteoric water in the basin and a ^{18}O-rich brine.

Inasmuch as water is composed only of hydrogen and oxygen, δD and δ^{18}O values should be valuable tools for tracing the origin and evolution of a fluid. Chemical compositions such as chlorine/bromine ratios (Sonnenfeld 1984) and ^{37}Cl/^{35}Cl ratios (Eggenkamp *et al.* 1995) may also be used to trace the evolution of a fluid, but hydrogen isotopes behave most frequently as the best conservative elements that can be used to trace the origin of a fluid.

Application of stable isotope geochemistry to uranium

Results from several stable isotope studies on U deposits have been summarized by Fayek & Kyser (1999). As an example of the application of stable isotope geochemistry to U deposits, unconformity-related deposits have been well studied. Basinal fluids obtain their chemical and isotopic compositions in part because of reactions with sedimentary minerals in the basin. Evidence of reactions between fluids and sedimentary rocks can not only be found in the compositions of the fluids, but also in minerals in the sediments that were produced or greatly affected by the fluids. For example, the fluid history of the Proterozoic Athabasca Basin in northern Saskatchewan, Canada, can be constrained using a combination of petrography to reveal the paragenesis of the minerals, measurements of the temperatures and compositions of fluid inclusions in the diagenetic quartz, hydrogen and oxygen isotopic compositions of water in inclusions and of hydrous minerals to constrain the origin of the fluids, and radiogenic isotope systematics to determine the timing of the fluid events.

The Athabasca Basin has had a complex fluid history primarily because it is made of mature sandstone and conglomerate that initially facilitated fluid flow and formation of brines, and because there are major faults and structural elements some of which contain unconformity-type U deposits, that have periodically been activated throughout the history of the basin and served as areas of enhanced permeability. Stable isotopic compositions of authigenic minerals in the basin, alteration minerals in the deposits and the uraninite itself indicate that both early brines and later meteoric waters have affected the basin and the deposits. Three distinct fluids are associated with the U deposits in the Athabasca Basin, based on stable isotopic compositions and fluid inclusion results (Kotzer & Kyser 1995, Derome *et al.* 2005). A fluid with characteristics of basinal brines appears to have mixed with a fluid in isotopic and chemical equilibrium with the basement rocks. The compositions of these fluids are NaCl for the former and Ca–Mg–Cl for the latter. There is also isotopic evidence for late low-temperature meteoric waters that have affected the uraninite in the deposits and clay minerals in fracture systems.

Integrated water/rock ratios can be calculated from the oxygen and hydrogen isotopic compositions in rocks and minerals. For example, at low water/rock ratios, the isotopic composition of the rock changes very little and the fluid will be substantially affected. Quantitative estimates of water/rock ratios can be calculated assuming open system conditions. Water/rock ratios ranging from 0.2 to 0.8 were calculated using this technique for unconformity-related U deposits in the Athabasca Basin, and much higher water/rock ratios in excess of 10 were calculated for reactivated fault zones (Kotzer and Kyser 1995) and from mass balance calculations to explain quartz dissolution in the sandstone units (Lorilleux *et al.* 2002).

Carbon and sulfur isotopic compositions have been used in studies of U deposits to characterize the redox reactions and trace the source of these elements in various U deposits. For example, carbon isotopic compositions indicate the participation of graphite (Kyser *et al.* 1989), organic matter (Ewers *et al.* 1983) or carbon from an abiogenic origin (Sangély *et al.* 2007) in unconformity-related deposits, magmatic sources in vein type deposits in Colorado (Wallace & Whelan 1986), and microbial interactions in sandstone-hosted deposits in Texas (Reynolds *et al.* 1982).

Fluid inclusion studies

Fluid inclusions can occur in any mineral that has interacted with a fluid medium. Recorded in the inclusion are the temperature, pressure and composition of the fluid present when the host mineral was formed for primary inclusions, or some later hydrothermal event for secondary trapped inclusions along microfractures (Shepherd *et al.* 1985). The temperatures at which there are phase changes in the inclusion can be linked to the chemical composition of the fluid. In addition, the chemical composition of the fluid in the inclusion can be extracted and measured directly (*e.g.* Nex *et al.* 2001, Polito *et al.* 2006, Derome *et al.* 2007). Relative to the value of the information revealed by analyses of fluid inclusions, the cost is minimal.

A substantial amount of fluid inclusion data exists on hydrothermal U deposits. However, some of these data are of limited value because homogenization temperatures are reported without estimates of fluid compositions, pressure corrections and the minerals that contain the fluid inclusions are not paragenetically constrained. Fluid inclusion populations, like minerals in deposits, must be put into a temporal context to be meaningful. This requires great care in classifying the types of inclusions, their associations and their cross-cutting relationships. Because fluid inclusions are within minerals, the paragenesis of the minerals must be known prior to expending the effort on analyzing fluid inclusions. Because this is rarely done, a lot of fluid inclusion results have met with skepticism, and justifiably so. However, when constrained by detailed mineral and inclusion paragenesis, they can faithfully record both the physical and chemical characteristics of the fluids that precipitated the minerals in which they are hosted.

Fluid inclusions are commonly hosted in minerals such as quartz, fluorite, halite, apatite and carbonate minerals, but also in opaque minerals such as sulfides and oxides (*e.g.* Oreskes & Einaudi 1992, Min *et al.* 1997). They tend to be small, ranging from a few to 100 micrometres in size, although they can reach a few centimetres long, and have highly variable morphologies. Inclusions are classified according to what phases are observed at room temperatures and the specific daughter minerals and gases and the proportions of phases present. The underlying assumption in measuring the properties of fluid inclusions is that there have been no changes in the density (volume) or composition of the inclusion since the time of entrapment. When these changes have occurred, necking of the inclusion or leaking may be evident.

Once the properties of the inclusions, such as cross-cutting relationships, and the properties of the phases are determined at room temperature, the inclusion is cooled below –100°C. Upon heating, the resulting phases will undergo changes at specific temperatures depending on their compositions. For example, a frozen 2-phase fluid that melts at 0°C is pure water whereas an inclusion that melts at –56.6°C is pure CO_2.

Once the inclusion has been frozen, it is slowly heated and any changes, particularly the temperature of first melting, are measured. If the inclusion is a mix of an aqueous fluid and gases, the temperature of first melting reflects the composition of gases that may be present. For example, CO_2 with CH_4 and N_2 will melt at temperatures –56.6°C whereas pure CO_2 will melt at –56.6°C.

The temperature of first melting of the former aqueous phase will reflect the eutectic temperature, which depends on the composition of salts dissolved in the liquid. This is exemplified in Figure 3-14, wherein the depression of the freezing point, which is the eutectic, changes as a function of the content of the dissolved species. For example, first melting temperatures less than –21°C indicate the presence of Mg, Ca, Na and K chlorides whereas first melting at –21°C indicates a NaCl brine. In addition, some of these salt species melt incongruently, which further aids in their identification and quantification. As the inclusion is heated further, the temperature at which the ice or the gas–water clathrate melts, provides information on the salinity of the fluid and the nature of the cations.

As heating continues, the coexisting liquid and vapor phases in the inclusion move along the phase boundary between them, such as is shown in Figure 3-15. Once the inclusion reaches the temperature near that of the trapping temperature, it moves off the two-phase boundary because most fluids are trapped as a single phase and into the one-phase region along a line of isodensity, commonly referred to as the isochore. Once in the liquid or vapor field, continued heating produces no visible changes unless a solid is present because the inclusion has been homogenized. Consequently, most homogenization temperatures represent

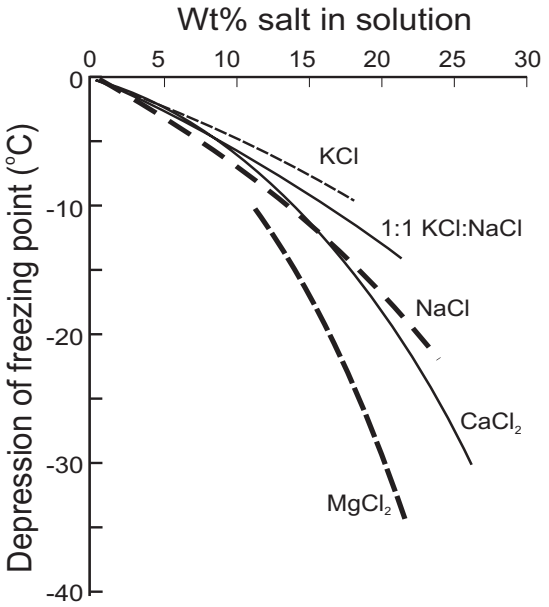

FIG. 3-14. Effect of different salts on the freezing point of water. During heating of a supercooled inclusion, the first melting temperature will correspond to which salts are present in the inclusion, and the melting temperature of the ice will reflect the quantity of solutes in an inclusion.

minimum trapping temperatures because the inclusion was trapped at a higher pressure than that along the two-phase boundary, except if the fluid was boiling at the time of trapping as shown by the coexistence of vapor-rich and liquid-rich inclusions homogenizing at the same temperature.

A variety of techniques has been developed to determine the pressure of trapping, which allows the true trapping temperature to be ascertained (*e.g.* Robinson & Ohmoto 1973, Derome *et al.* 2003). Fluid inclusion and stable isotopic studies of intrusion-related U deposits of the Massif Central indicate that uraninite precipitated from low salinity fluids at temperatures of 160°–180°C (Cathelineau *et al.* 1990, Lespinasse & Cathelineau 1990) and pressures of some hundreds of bars, whereas unconformity-related U deposits from the Athabasca Basin formed from high-salinity, CO_2-poor fluids at temperatures of 150–200°C and pressures of about 1 kbar (Pagel *et al.* 1980, Kotzer & Kyser 1995, Derome *et al.* 2005).

Data from fluid inclusions are normally presented as histograms of homogenization temperatures or homogenization temperatures *vs.* salinity plots. Homogenization temperatures alone are misleading in terms of identification of various fluids and compositional data are needed. In addition to providing information on the trapping conditions of the fluid and the major element chemistry, fluid inclusions contain the minor and trace element compositions of the fluid. These are revealed using a variety of analytical techniques. Laser Raman spectroscopy is a technique that allows various gases such as CO_2, CH_4 and H_2S, anion complexes and minerals to be measured in micrometre-sized inclusions (Derome *et al.* 2003). Laser ablation emission spectroscopy (LIBS) allows

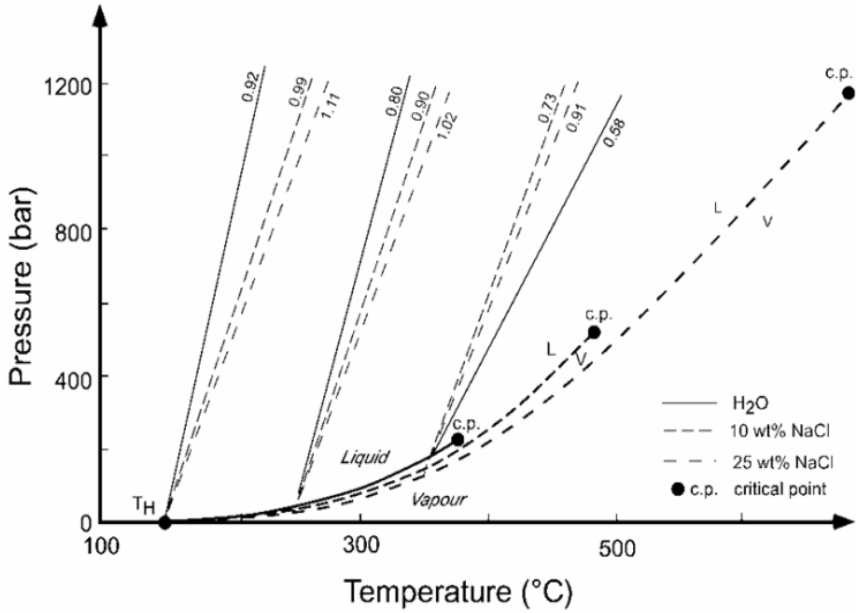

FIG. 3-15. Phase diagram for the system H_2O-NaCl showing the fields of liquid and vapour and the critical points for pure water, brine with 10 wt% NaCl and brine with 25 wt% NaCl as a function of temperature and pressure. The lines indicate the densities (isochores) of these fluids. Intersection of the isochore with the 2-phase field is the homogenization temperature, but the trapping temperature can be higher depending where on the isochore line the fluid was trapped.

the determination of the ratios between major and some minor cations. More recently, laser ablation inductively coupled mass spectrometry (LA–ICP–MS) has been used to analyze fluid inclusions, usually as groups of fluid inclusions. The problem with individual inclusion analysis is that the volume of the inclusions is small so that the signal is low. Nevertheless, LA–ICP–MS has been applied to the analysis of single fluid inclusions in selected deposits with great success, quantifying their metal content including U (Richard *et al.* 2008). Uranium has also been detected in fluid inclusions associated with U mineralization using synchrotron X-ray microfluorescence (Philippot *et al.* 2000, McCready *et al.* 2005). *In situ* determination of metal speciation in inclusions should soon be possible using X-ray absorption spectrometry (XAS) with a synchrotron source.

REFERENCES

ALEXANDRE, P. & KYSER, T.K. (2003), Geochronology of the Paleoproterozoic basement-hosted unconformity-type uranium deposits in northern Saskatchewan, Canada. *Proc. Uranium Geochemistry Conference*, Nancy, France, 37–40.

ALEXANDRE, P. & KYSER, K. (2005): Effect of cation substitutions and alteration of uraninite: *Can. Mineral.* **45**, 1005-1017.

ALLARD, T., CALAS, G. AND ILDEFONSE, P. (2007): Reconstruction of past U migration in a sedimentary deposit (Coutras, France): Implications for a radwaste repository. *Chem. Geol.* **239**, 50-63.

ARFSTEN, D.P., STILL, K.R. & RITCHIE, G.D. (2001): A review of the effects of uranium and depleted uranium exposure on reproduction and fetal development. *Toxicology & Industrial Health* **17**, 180–191.

ARTINGER, R., RABUNG, T., KIM, J.I., SACHS, S., SCHMEIDE, K., HEISE, K.H., BERNHARD, G. & NITSCHE, H. (2002): Humic colloid-borne migration of uranium in sand columns. *J. Contaminant Hydrology* **58**, 1-12.

ATSDR (AGENCY FOR TOXIC SUBSTANCES AND DISEASE REGISTRY) (1999): Toxicological profile for uranium. Atlanta, GA: U.S. Dept. Health & Human Services, Public Health Service.

BAADSGAARD, H., CUMMING, G.L. & WORDEN, J.M. (1984): U-Pb geochronology of minerals from the Midwest uranium deposit, northern Saskatchewan. *Can. J. Earth Sci.* **21**, 642-648.

BIGELEISEN, J. & MAYER, M.G. (1947): Calculation of equilibrium constants for isotopic exchange reactions. *J. Chem. Phys*. **15**, 261-267.

BÖHSE, H., ROSE, H.J., SORENSEN, H., STEENFELT, A., LOVBORG, L. & KUNZENDORF, H. (1974): On the behaviour of uranium during crystallization of magmas with special emphasis on alkaline magmas. *IAEA Proc. Ser. Form. Uranium Ore Deposits* 49-60.

BOTTINGA, Y. & JAVOY, M. (1973): Comments on oxygen isotope geothermometry. *Earth Planet. Sci. Lett.* **20**, 250-265.

BOWLES, J.F.W. (1990): Age dating of individual grains of uraninite in rocks from electron microprobe analyses. *Chem. Geol.* **83**, 47-53.

BRAY, C.J., SPOONER, E.T.C., HALL, C.M., YORK, D., BILLS, T.M. & KRUEGER, H.W. (1987): Laser probe ^{40}Ar-^{39}Ar and conventional K/Ar dating of illites associated with the McClean unconformity related uranium deposits, N. Saskatchewan. Canada, *Can. J. Earth Sci*. **24**, 10-23.

BRUNO, J., CASAS, I. & PUIGDOMENECH, I. (1991): The kinetics of dissolution of UO_2(s) under reducing conditions and the influence of an oxidized layer UO_2(s). Application of flow through a reactor. *Geochim. Cosmochim. Acta* **55**, 647-658.

BRUNO, J., DE PABLO, J., DURO, L. & FIGUEROLA, E. (1995): Experimental study and modeling of the U(VI)-Fe$(OH)_3$ surface precipitation/coprecipitation equilibria. *Geochim. Cosmochim. Acta* **59,** 4113-4123.

BURNS, P. (1999): The crystal chemistry of uranium. In: Burns, P.C., Finch, R. (eds) Uranium: Mineralogy, Geochemistry and the Environment. *Mineral. Soc. Am. Reviews in Mineralogy* **38**, 23-90.

CALAS, G. (1979): Etude expérimentale du comportement de l'uranium dans les magmas, Etats d'oxydation et de coordinance. *Geochim. Cosmochim. Acta* **43**, 1521-1531.

CASAS, I., DE PABLO, J., GIMÉNEZ, J., TORRERO, M. E., BRUNO, J., CERA, E. FINCH, R.J. & EWING, R.C. (1998): The role of pe, pH, and carbonate on the solubility of UO_2 and uraninite under nominally reducing conditions. *Geochim. Cosmochim. Acta* **62,** 2223-2231.

CATHELINEAU, M., CUNEY, M., LEROY, L. LHOTE, F., NGUYEN-TRUNG, C., PAGEL, M. & POTY, B. (1979): Caractères minéralogiques des pechblendes de la province hercynienne d'Europe. Comparaison avec les oxydes d'uranium du protérozoïque de différents gisements d'Amérique du Nord, d'Afrique et d'Australie. *In* Vein-type and similar uranium deposits in rocks younger than Proterozoic. *IAEA, Vienna, Proc. Symp. Lisbon*, 159-177.

CATHELINEAU, M., BOIRON, M.C., HOLLIGER, P. & POTY, B. (1990): Metallogenesis of the French part of the Variscan orogen. Part II: time-space relationships between U, Au, Sn-W ore deposition and geodynamic events: mineralogical and U-Pb data. *Tectonophysics* **177**, 59-79.

CHIPLEY, D., POLITO, P.A. & KYSER, T.K. (2007). Measurement of U-Pb ages of uraninite and davidite by Laser Ablation-HR-ICP-MS. *Am. Minera.* **92**, 1925-1935.

CLAYTON, R.N., FRIEDMAN, I., GRAF, D.L., MAYEDA, T.K., MEENTS, W.F. & SHIMP, N.F. (1966): The origin of saline formation waters. *J. Geophys. Res.* **71**, 3869-3882.

CRAFT, E.S., ABU-QARE, A.W., FLAHERTY, M.M., GAROFOLO, M.C., RINCAVAGE, H.L. & ABOU-DONIA, M.B. (2004): Depleted and natural uranium: chemistry and toxicological effects. *J. Toxicology & Environmental Health* **7**, 297-317.

CUNEY, M. (1980): Preliminary results on the petrology and fluid inclusions of the Rössing uraniferous alaskites. *Trans. Geol. Soc. South. Africa* **83**, 39-45.

CUNEY, M. & FRIEDRICH, M. (1987): Physico-chemical and crystal chemical controls on accessory mineral paragenesis in granitoids. Implications for uranium metallogenesis. *Bull. de Minéralogie* **110**, 235- 247.

CUNEY, M., FRIEDRICH, M., BLUMENFELD, P., BOURGUIGNON, A., BOIRON, M.C., VIGNERESSE, J.L. & POTY, B. (1989): Metallogenesis in the French part of the Variscan orogen. Part I. U-preconcentrations in the pre-Variscan and Variscan formations - a comparison with Sn, W and Au. *Tectonophysics* **177**, 39-57.

DEROME, D., CUNEY, M., CATHELINEAU, M., FABRE, C., DUBESSY, J., BRUNETON, P. & HUBERT, A. (2003): A detailed fluid inclusion study in silicified breccias from the Kombolgie sandstones (Northern Territory, Australia): inferences for the genesis of middle-Proterozoic unconformity-type uranium deposits. *J. Geochem. Explor.* **80,** 259-275.

DEROME, D., CATHELINEAU, M., CUNEY, M., FABRE, C. AND LHOMME, T. (2005): Mixing of sodic and calcic brines and uranium deposition at McArthur River, Saskatchewan, Canada: A Raman and laser-induced breakdown spectroscopic study of fluid inclusions. *Econ. Geol.* **100**, 1529-1545.

DEROME, D., CATHELINEAU, M., FABRE, C., BOIRON, M., BANKS, D. A., LHOMME, T. & CUNEY, M. (2007): Paleo-fluid composition determined from individual fluid inclusions by Raman and LIBS; application to mid-Proterozoic evaporitic Na-Ca brines (Alligator Rivers uranium field, Northern Territories, Australia); New results in fluid and melt inclusion research. *Chem. Geol.* **237,** 240-254.

DODSON, M.H. (1973): Closure temperature in cooling geochronological and petrological systems. *Contrib. Mineral. Petrol.* **40**, 259-274.

DOMINÉ, F. & VELDE, B. (1985): Preliminary investigation of the processes governing the solubility of uranium in the silicate melts. *Bull. de Minéralogie* **108**, 755-765.

DUFF, M. C., AMRHEIN, C., BERTSCH, P. M. & HUNTER, D. B. (1997): The chemistry of uranium in evaporation pond sediment in the San Joaquin valley, California, USA, using X-ray fluorescence and XANES techniques. *Geochim. Cosmochim. Acta* **61,** 73-81.

DUFF, M.C., HUNTER, D.B., BERTSCH, P.M. & AMRHEIN, C. (1999): Factors influencing uranium reduction and solubility in evaporation pond sediments. *Biogeochemistry* **45**, 95–114.

EGGENKAMP, H.G.M., KREULEN, R. & KOSTER VAN GROOS, A. F. (1995): Chlorine stable isotope fractionation in evaporates. *Geochim. Cosmochim. Acta* **59**, 5169-5175.

EWERS, G.R., FERGUSON, J. AND DONNELLY, T.H. (1983): The Nabarlek uranium deposit, Northern Territory, Australia: Some petrologic and geochemical constraints on the genesis. *Econ. Geol.* **78**, 823-837.

FARGES, F., PONADER, C.W., CALAS, G. & BROWN, G.E. Jr. (1992): Structural environments of incompatible elements in silicate glass/ melt systems. II. U(IV), U(V), and U(VI). *Geochim. Cosmochim. Acta* 56, 4205-4220.

FAURE, F. (1986): *Principles of Isotope Geology* (second edition). John Wiley & sons. 589 p.

FAYEK, M. & KYSER, K (1997): Characterization of multiple fluid-flow events and rare-earth elements mobility associated with formation of unconformity uranium deposits in the Athabasca Basin, Saskatchewan. *Can. Mineral.* **35,** 627-658.

FAYEK, M. & KYSER, T. K. (1999): Stable isotope geochemistry of uranium deposits. In: Burns, P.C., Finch, R. (eds) Uranium: Mineralogy, Geochemistry and the Environment. *Mineral. Soc. Am. Reviews in Mineralogy* **38,** 181-220.

FAYEK, M., JANECZEK, J.& EWING, R.C. (1997): Mineral chemistry and oxygen isotopic analyses of uraninite, pitchblende and uranium alteration minerals from the Cigar Lake Deposit, Saskatchewan, Canada. *Appl. Geochem.* **12,** 549-565.

FAYEK, M., HARRISON, T.M., GROVE, M. & COATH, C.D. (2000): A rapid *in situ* method for determining the ages of uranium oxide minerals. *Intl. Geol. Rev.* **42**, 163-171.

FAYEK, M., KYSER ,T. K. & RICIPUTI, L. R. (2002a): U and Pb isotope analysis of uranium minerals by ion microprobe and the geochronology of the McArthur River and Sue Zone uranium deposits, Saskatchewan, Canada. *Can. Mineral.* **40,** 1553-1569.

FAYEK, M., RICIPUTI, L. R. & KYSER, T. K. (2002b): A new method for U-Pb isotopic analyses of uranium oxide minerals by SIMS. *Geochim. Cosmochim. Acta* **66,** 226.

FIGUEROA L., HONEYMAN B & RANVILLE J. (2006): Coupled Microbial and Chemical Reactions in Uranium Bioremediation. *Proceedings of the 4th International Conference on Uranium and Hydrogeology,* Sept 11-16, 2005, Freiberg, Germany, 183-190.

FINCH, R.J. & EWING, R.C. (1992): The corrosion of uraninite under oxidizing conditions. *J. Nuclear Materials* **190,** 133-156.

FINCH, R. & MURAKAMI, T. (1999): Systematics and paragenesis of uranium minerals. *In*: Burns, P.C., Finch, R. (*eds.*) Uranium: Mineralogy, Geochemistry and the Environment. *Mineral. Soc. Am., Rev. in Mineralogy* **38**, 91-180.

FOLAND, K. A., HUBACHER, F. A. & AREHART, G. B. (1992): $^{40}Ar/^{39}Ar$ dating of very fine-grained samples; an encapsulated-vial procedure to overcome the problem of ^{39}Ar recoil loss. *Chem. Geol.* **102,** 269-276.

FRIEDRICH, M., CUNEY, M. & POTY, B. (1987): Uranium geochemistry in peraluminous leucogranites. *Uranium* **3**, 353-385.

FRONDEL, C. (1958): Systematic mineralogy of uranium and thorium. *U.S. Geol. Surv. Bull.* **1064**, 400 p.

FRYER, B.J. & TAYLOR, R.P. (1984): Sm-Nd direct dating of the Collins Bay hydrothermal uranium deposit, Saskatchewan. *Geology* **12**, 479-482.

GAUTHIER-LAFAYE, F., WEBER, F. & OHMOTO, H. (1989): Natural fission reactors of Oklo, *Econ. Geol.* **84**, 2286-2295.

GIBLIN, A.M. & APPLEYARD, E.C. (1987): Uranium mobility in non-oxidizing brines; field and experimental evidence. *Appl. Geochem* **2,** 285-295.

GOMEZ, P., GARRALON, A., BUIL, B., TURRERO, M.J., SANCHEZ, L. & DE LA CRUZ, B. (2006): Modeling of geochemical processes related to uranium mobilization in the groundwater of a uranium mine. *Science of the Total Environment* **366**, 295–309.

GUILLAUMONT, R., FANGHÄNEL, T., FUGER J., GRENTHE, I., NECK, V, PALMER, D.A. & RAND, M.H. (2003): Update on the chemical thermodynamics of Uranium, Neptunium, Plutonium, Americium, and Technecium. *NEA-OECD*, **5**.

HEAMAN, L. & LUDDEN, J.N., eds. (1991): *Applications of Radiogenic Isotope Systems to Problems in Geology*. Mineral. Assoc. Can., Short Course **19**, 498 p.

HEM, J. D., PAULSON, R. W., CHASE, E. B., WILLIAMS, J. S. & MOODY, D. W. (1993): Factors affecting stream water quality, and water-quality trends in four drainage basins in the conterminous United States, 1905-90. National water summary 1990-91; hydrologic events and stream water quality, U.S. Geol. Surv. **W 2400,** 67-92.

HESS, J.C., LIPPOLT, H.J. & BORSUK, A.M. (1986): The Neogene volcanism of the northern Great Caucasus; isotope and age studies on rift-related alkali rhyolites. *Neues Jahrb. Mineral.. Abh.* **156,** 63-80.

HIDAKA, H. & HOLLIGER, P. (1998): Geochemical and neutronic characteristics of the natural fossil fission reactors at Oklo and Bangombé, Gabon. *Geochim. Cosmochim. Acta* **62**, 89-108.

HILLS, J.H., & RICHARDS, J.R. (1976): Pitchblende and Galena Ages in the Alligator Rivers Region, Northern Territory, Australia, *Mineral. Deposita* **11**, 133-154.

HITCHON, B. & FRIEDMAN, I. (1969): Geochemistry and origin of formation waters in the western Canada sedimentary basin: I. Stable isotopes of hydrogen and oxygen. *Geochim. Cosmochim. Acta* **33**, 1321-1349.

HOEVE J. & SIBBALD T.I.I. (1978): On the genesis of Rabbit Lake and other unconformity-type uranium deposits in northern Saskatchewan, Canada. *Econ. Geol.* **73**, 1450-1473.

HOLK, G.J., KYSER, T.K., CHIPLEY, D., HIATT, E.E. & MARLATT, J. (2003): Mobile Pb-isotopes in Proterozoic sedimentary basins as guides for exploration of uranium deposits, *J. Geochem. Explor.* **80**, 297–320.

HORITA, J., COLE, D.R. & WESOLOWSKI, D.J. (1993): The activity-composition relationship of oxygen and hydrogen isotopes in aqueous salt solutions; II, Vapor-liquid water equilibration of mixed salt solutions from 50 to 100 degrees C and geochemical implications. *Geochim. Cosmochim. Acta* **57,** 4703-4711.

HOSTETLER, P.B. & GARRELS, R.M. (1962): Transportation and precipitation of uranium and vanadium at low temperatures, with special reference to sandstone-type uranium deposits. *Econ. Geol.* **57**, 137−167.

ISOBE, H., MURAKAMI, T. & EWING, R.C. (1992): Alteration of uranium minerals in the Koongarra Deposit, Australia; unweathered zone. *J. Nuclear Materials* **190,** 174-187.

JANECZEK, J. & EWING, R.C. (1992): Structural formula of uraninite. *J. Nuclear Materials* **190,** 128-132.

KIKUCHI, M., HIDAKA, H., HORIE, K. AND GAUTHIER-LAFAYE, F. (2007): Redistribution of REE, Pb and U by supergene weathering studied from *in-situ* isotopic analyses of the Bangombé natural reactor, Gabon. *Geochim. Cosmochim. Acta* **71**, 4716-4726.

KISTER, P., CUNEY, M., GOLUBEV, V.N., ROYER, J.J., LE CARLIER DE VESULD, CH. & RIPPERT J.C. (2004): Radiogenic lead mobility in the Shea Creek unconformity-related uranium deposit (Saskatchewan, Canada): migration pathways and Pb loss quantification. *Comptes Rendus Geosciences* **336**, 205-215.

KNAUTH, L.P. & BEEUNAS, M.A. (1986): Isotope geochemistry of fluid inclusions in Permian halite with implications for the isotopic history of ocean water and the origin of saline formation waters. *Geochim. Cosmochim. Acta* **50**, 419-433.

KOHN, S.C., DUPREE, R., MORTUZA, M.G. & HENDERSON, C.M.B. (1991): NMR evidence of five- and six-coordinated aluminium fluoride complexes in F-bearing alumino-silicate glasses. *Am. Mineral*. **76**, 309-312.

KOJIMA, S., TAKEDA, S. & KOGITA, S. (1994): Chemical factors controlling the solubility of uraninite and their significance in the genesis of unconformity-related uranium deposits. *Mineral. Deposita* **29**, 353-360.

KOMNINOU, A. & SVERJENSKY, D. A. (1996): Geochemical modeling of the formation of an unconformity-type uranium deposit. *Econ. Geol. Bull. Soc. Econ. Geol.* **91,** 590-606.

KOTZER, T.G. & KYSER, T.K. (1993): O, U, and Pb isotopic and chemical variations in uraninite: Implications for determining the temporal and fluid history of ancient terrains. *Am. Mineral.* **78**, 1262-1274.

KOTZER, T.G. & KYSER, T.K. (1995): Petrogenesis of the Proterozoic Athabasca Basin, northern Saskatchewan, Canada, and its relation to diagenesis, hydrothermal uranium mineralization and paleohydrogeology. *Chem. Geol.* **120**, 45-89.

KRIVOVICHEV, S., BURNS, P. & TANANAEV, I. (2006): *Chemistry Of Inorganic Actinide Compounds.* St Petersburg, Notre Dame, Moscow, Elsevier. 494 p.

KYSER, T.K. (1987): Equilibrium fractionation factors for stable isotopes. In *Stable Isotope Geochemistry of Low Temperature Fluids*, Kyser, T.K. (ed), Mineral. Assoc. Can. Short Course **13**, 1-84.

KYSER, T. K., WILSON, M. R. & RUHRMANN G. (1989): Stable isotope constraints on the role of graphite in the genesis of unconformity-type uranium deposits. *Can. J. Earth Sci.* **26,** 490-498.

LANGMUIR, D. (1978): Uranium solution-mineral equilibria at low temperatures with applications to sedimentary ore deposits. *Geochim. Cosmochim. Acta* **42**, 547-569.

LANGMUIR, D., & CHATHAM, J.R. (1980): Ground-water prospecting for sandstone-type uranium deposits: a preliminary comparison of the merits of mineral-solution equilibria, and single-element tracer methods. *J. Geochem. Explor.* **13, 2**01-219.

LESPINASSE, M. & CATHELINEAU, M. (1990): Fluid percolations in a fault zone: a study of fluid inclusion planes in the St-Sylvestre granite, northwest Massif Central, France. *Tectonophysics* **184**, 173-187.

LONGERICH, H.P., WILTON, D.H.C. & FRYER, B.J. (1992) Isotopic and elemental analysis of uraninite concentrates using inductively coupled plasma-mass spectrometry (ICP-MS). *J. Geochem. Explor.* **43**, 111-125.

LORILLEUX, G., JEBRAK, M., CUNEY, M. & BAUDEMONT, D. (2002): Polyphased hydrothermal breccias associated with unconformity uranium mineralization (Northern Saskatchewan, Canada. *J. Struct. Geol.* **24**, 323-338

LOVLEY, D.R., PHILLIPS, E.J.P., GORBY, Y.A. & LANDA, E.R. (1991): Microbial uranium reduction. *Nature*, **350** 413–416.

LUDWIG, K.R. (1978): Uranium-daughter migration and U/Pb isotope apparent ages of uranium ores, Shirley basin, Wyoming. *Econ. Geol.* **73**, 29-49.

LUDWIG, K.R., GRAUCH, R.I., NUTT, C.J., NASH, J.T., FRISHMAN, D. & SIMMONS, K.R. (1987): Age of uranium mineralization at the Jabiluka and Ranger deposits, Northern Territory, Australia: new U-Pb isotope evidence. *Econ. Geol.* **82**, 857-874.

MAAS, R. (1989): Nd-Sr isotope constraints on the age and origin of unconformity-type uranium deposits in the Alligator Rivers Uranium Field, Northern Territory, Australia. *Econ. Geol.* **84**, 64-90.

MAAS, R. & MCCULLOCH, M.T. (1990): A search for fossil nuclear reactors in the Alligator River Uranium Field, Australia: Constraints from Sm, Gd and Nd isotopic studies. *Chem. Geol.* **88**, 301-315.

MACASKIE, L.E., EMPERSON, R.M., CHEETHAM, A.K., GREY, C.P. & SKARNULIS, A.J. (1992): Uranium bioaccumulation by a *Citrobacter sp*.as a result of enzymatically medicated growth of polycrystalline HUO_2PO_4. *Science* **257,** 782–4.

MANNING, D.A.C. (1981): The effect of fluorine on liquidus phase relationships in the system Qz-Ab-Or with excess water at 1 kbar. *Contrib. Mineral. Petrol*. **76**, 257-262.

MCCREADY, A.J., DEROME, D., ANNESLEY, I.R., CUNEY, M., CAVELL, R.G., RICKERS, K., BAKKER, R.J. & WEBB, M. A. (2005): Paleofluid chemistry from the McArthur River uranium deposit, Athabasca Basin, Canada: results and implications from Synchrotron X-Ray Fluorescence (SXRF), *Program with Abstracts, Joint Annual Meeting Geol. Assoc. Can. – Mineral. Assoc. Can.*

MCDOUGALL I. & HARRISON, T.M. (1999): *Geochronology and Thermochronology by the $^{40}Ar/^{39}Ar$ method*. Oxford University Press, New York, 269 p.

MIN, M., ZHENG, D., SHEN B., WEN, G., WANG, X & GANDHI, S. S. (1997): Genesis of the Sanbaqi deposit: a paleokarst-hosted uranium deposit in China. *Miner. Deposita* **32,** 505-519.

MIN, M., CHEN, J., WANG, J., WEI, G. & FAYEK, M. (2005): Mineral paragenesis and textures associated with sandstone-hosted roll-front uranium deposits, NW China. *Ore Geol. Reviews* **26,** 51-69.

MONTEL, J.M. (1993): A model for monazite/melt equilibrium and application to the generation of granitic magmas: *Chem. Geol.* **110**, 127-146.

MOYES, L.N., PARKMAN, R.H., CHARNOCK, D.J., LIVENS, F.T., HUGHES, C.R. & BRAITHWAITE A. (2000): Uranium uptake from aqueous solution by interaction with goethite, lepidocrocite, muscovite and mackinawite: An x-ray absorption spectroscopy study. *Environ. Sci. Technol.* **34,** 1062–1068.

NEX, P., HERD, D. & KINNAIRD, J. A. (2001): Fluid extraction from quartz in sheeted leucogranites as a monitor to styles of uranium mineralization; an example from the Roessing area, Namibia. *Geochemistry - Exploration Environment Analysis* **2,** 83-96.

NGUYEN-TRUNG, C., PALMER, D.A., MESMER, R.E. & BEGUN, G.M. (1991): Raman, UV-visible absorption spectral and potentiometric studies of complexation of uranyl (VI) ion in aqueous solutions at 25°C, 1 bar. In *Proceedings Source Transport and Deposition of Metals*. M. Pagel and J. Leroy (*eds.*). Balkema (Rotterdam), 99-101.

ORESKES, N. & EINAUDI, M.T. (1992): Origin of hydrothermal fluids at Olympic Dam; preliminary results from fluid inclusions and stable isotopes. *Econ.Geol.* **87,** 64-90.

PAGEL, M., POTY, B. & SHEPPARD, S.M.F. (1980): Contribution to some Saskatchewan uranium deposits mainly from fluid inclusion and isotopic data; Uranium in the Pine Creek Geosyncline. *Proceedings Series - International Atomic Energy Agency* 639-654.

PAGEL, M., MICHARD, A., JUTEAU, M. & TURPIN, M. (1992): Sm-Nd, Pb-Pb, and Rb-Sr systematics of the basement in the Cigar Lake area,

Saskatchewan, Canada. *Can. J. Earth Sci.* **30**, 731-742.

PARKS, G.A. & POHL, D.C. (1988): Hydrothermal solubility of uraninite. *Geochim. Cosmochim. Acta* **52**, 863-875.

PATRIER, P., BEAUFORT, D., BRIL, H., BONHOMME, M., FOUILLAC, A.M., AUMÂITRE, R. (1997): Alteration-mineralization at the Bernardan U deposit (Western Marche, France): The contribution of alteration petrology and crystal chemistry of secondary phases to a new genetic model. *Econ. Geol.* **92**, 448-467.

PEIFFERT, C. (1993): *Détermination du coefficient de partage d'un métal entre un fluide et un liquide silicaté de composition granitique à haute T et P.* Unpub. PhD thesis, Nancy University, France.

PEIFFERT, C., CUNEY, M. & NGUYEN-TRUNG, C. (1994): Uranium in granitic magmas. Part I: Experimental determination of uranium solubility and fluid-melt partition coefficients in the uranium oxide-haplogranite-H_2O-$NaCO_3$ system at 770°C, 2 kbar. *Geochim. Cosmochim. Acta* 58, 2495-2507.

PEIFFERT, C., NGUYEN-TRUNG C. & CUNEY M. (1996): Uranium in granitic magmas. Part II: Experimental determination of uranium solubility and fluid-melt partition coefficients in the UO_2 - haplogranite - H_2O-halides system at 720-770°C, 200 MPa. *Geochim. Cosmochim. Acta* **60**, 1515-1529

PETRIE, L., NORTH, N.N., DOLLHOPF, S.L., BALKWILL, D.L. & KOSTKA J.E. (2003): Enumeration and characterization of Iiron(III)-reducing microbial communities from acidic subsurface sediments contaminated with uranium(VI). *Appl. Environ. Microbiol.* **69**, 7467-7479.

PHILIPPOT, P., MENEZ, B., SIMIONOVICI, A., CHABIRON, A., CUNEY, M., SNIGIREV, A. & SNIGIREVA, I. (2000): X-ray imaging of uranium in individual fluid inclusions. *Terra Nova* **12,** 84-89.

POLITO, P., KYSER, T.K., MARLATT, J., ALEXANDRE, P., BAJWAH, Z. & DREVER, G. (2004): Significance of alteration assemblages for the origin and evolution of the Proterozoic Nabarlek unconformity-related uranium deposit, Northern Territory, Australia. *Econ. Geol.* **99**, 113–139.

POLITO, P.A., KYSER, T.K. & JACKSON, M.J. (2006): The role of sandstone diagenesis and aquifer evolution in the formation of uranium and zinc-lead deposits, southern McArthur Basin, Northern Territory, Australia. *Econ. Geol.* **101,** 1189-1209.

REIMANN, C. & DE CARITAT, P. (1998): *Chemical Elements in the Environment; Fact Sheets for The Geochemist and Environmental Scientist.* Springer-Verlag Berlin, Heidelberg, 398 p.

REYNOLDS, R.L., GOLDHABER, M.B. & CARPENTER, D.J. (1982): Biogenic and nonbiogenic ore-forming processes in the south Texas uranium district; evidence from the Panna Maria deposit. *Econ. Geol. Bull. Soc. Econ. Geol.***77,** 541-556.

RICHARD, A., BOIRON, M.-C., CATHELINEAU, M., DEROME, D., PETTKE, T., BANKS, D., MERCADIER, J. & CUNEY, M. (2008): U concentrations in ore fluids: a LA-ICP-MS investigation of fluids associated with unconformity-related uranium deposits. Abstract in *Proceeding of the GAC-MAC Conference*, May 2008, Québec, Canada.

ROBINSON, B.W. & OHMOTO, H. (1973): Mineralogy, fluid inclusions, and stable isotopes of the Echo Bay U-Ni-Ag-Cu Deposits, Northwest Territories, Canada. *Econ. Geol. Bull. Soc. Econ. Geol.* **68,** 635-656.

ROMBERGER, S. B. (1984): Transport and deposition of uranium in hydrothermal systems at temperatures up to 300°C, with genetic implications; Geology of uranium deposits. *Special Volume, Can. Inst. Mining Metall.* **32,** 12-17.

SANGÉLY, L., CHAUSSIDON, M., MICHELS, R., BROUAND, M., CUNEY, M., HUAULT, V., & LANDAIS, P. (2007): Micrometer scale carbon isotopic study of bitumen associated with Athabasca uranium deposits: Constraints on the genetic relationship with petroleum source-rocks and the abiogenic origin hypothesis. *Earth Planet. Sci. Lett.* **258**, 378-396.

SCHALLER, T., DINGWELL, D.B., KEPPLER, H., KNOLLER, W., MERWIN, L. & SEBALD, A. (1992): Fluorine in silicate glasses: a multinuclear nuclear magnetic resonance study. *Geochim. Cosmochim. Acta* 56, 701-707.

SENKO, J.M., KELLY, S.D., DOHNALKOVA, A.C., MCDONOUGH, J.T., KEMNER, K.M. & BURGOS,W.D (2007): The effect of U(VI) bioreduction kinetics on subsequent reoxidation of biogenic U(IV). *Geochim. Cosmochim. Acta* **71**, 4644-4654.

SHANNON, R.D. (1976): Systematic studies of interatomic distances in oxides. In *The physics and chemistry of minerals and rocks.* R.G.J. Strens (*ed.*). John Wiley & Sons, London, United Kingdom, 403-431.

SHEPHERD, T. J., RANKIN, A. H., & ALDERTON, D. H. M. (1985): *A Practical Guide to Fluid Inclusion Studies*. New York, Blackie and Sons, 232 p.

SHOCK ,E.L., SASSANI, D.C. & BETZ, H. (1997): Uranium in geologic fluids; estimates of standard partial molal properties, oxidation potentials, and hydrolysis constants at high temperatures and pressures. *Geochim. Cosmochim. Acta* **61,** 4245-4266.

SIMONOFF, M., SERGEANT, C., POULAIN, S. & PRAVIKOFF (2007): Microorganisms and migration of radionuclides in environment. *Comptes Rendues Chimie* **10**, 1092-1107.

SOFER, Z. & GAT, J. R. (1975): The isotope composition of evaporating brines; effect of the isotopic activity ratio in saline solutions. *Earth Planet. Sci. Lett.* **26,** 179-186.

SONNENFELD, P. (1984): *Brines and Evaporites*. Academic Press, Orlando, 613pp.

SUZUKI, Y. & BANFIELD, J.F. (1999): Geomicrobiology of uranium; Uranium; mineralogy, geochemistry and the environment. *Rev. Mineral.* **38,** 393-432.

TRIPATHI, V.S. (1979): Comments on "Uranium solution-mineral equilibria at low temperatures with applications to sedimentary ore deposits." *Geochim. Cosmochim. Acta* **43**, 1989-1990.

TURPIN, L., LEROY, J.L. & SHEPPARD, S.M.F. (1990): Isotopic systematics (O, H, C, Sr, Nd) of superimposed barren and U-bearing hydrothermal systems in a Hercynian granite, Massif Central, France. *Chem. Geol.* **88**, 85-98.

TURPIN, L., CLAUER, N., FORBES, P. & PAGEL, M. (1991): U-Pb, Sm-Nd and K-Ar systematics of the Akouta uranium deposit, Niger. *Chem. Geol.* **87**, 217-230.

WALLACE, A.R. & WHELAN, J.F. (1986): The Schwartzwalder uranium deposit; III, Alteration, vein mineralization, light stable isotopes, and genesis of the deposit. *Economic Geology* **81,** 872-888.

WATSON, E.B. & HARRISON, T.M., (1983): Zircon saturation revisited: temperature and composition effects in a variety of crustal magma types: *Earth Planet. Sci. Lett.* **64**, p. 295–304.

ZHARIKOV, V.A., IVANOV, I.P., OMEL'YANENKO, B.I., RED'KIN, A.F. & YUDINTSEV, S.V. (1987): Experimental study of the solubility of uraninite in granitic melts and fluid solutions at high pressures and temperatures. *Int. Geol. Rev.* **29**, 997-1004.

CHAPTER 4: DEPOSITS RELATED TO MAGMATIC DIFFERENTIATION

Michel Cuney
G2R, Nancy-Université, CNRS, CREGU,
B.P. 239,
F-54506 Vandoeuvre lés Nancy, France
michel.cuney@g2r.uhp-nancy.fr

and

Kurt Kyser
Department of Geological Sciences and Geological Engineering,
Queen's University,
Kingston, Ontario, K7L 3N6, Canada
kyser@geol.queensu.ca

MAGMATIC DIFFERENTIATION

Extreme fractional crystallization of peralkaline magmas may lead to the formation of very large, low-grade U and Th resources, such as the Kvanefjeld deposit at Ilímaussaq, Greenland (Sørensen 2001, Bohse *et al.* 1974). Other major occurrences of this type are: Pocos de Caldas, Brazil (Fraenkel *et al.* 1985), Bokan Mountain, Alaska (MacKevett 1963), Lovozero Massif, Kola Peninsula, Russia (Balashov 1968), and the Kaffo Valley, Nigeria (Bowden & Turner 1974). Such an association can be also extended to the ultimate fractionation products of peralkaline complexes, namely carbonatite intrusions such as Palabora, South Africa (Verwoerd 1986). The association of peralkaline complexes with U and Th enrichments reflects the high solubility of U and Th in high temperature peralkaline silicate melts (see Chapter 3). Peralkaline granite and syenite bodies are always enriched in U, Th, and other high field strength (HFS) elements such as Zr and REEs, as a result of the high solubility of these elements in highly depolymerized magmas and the low degrees of partial melting that produce peralkaline liquids. Their high solubility leads to their continuous enrichment during magmatic fractionation. However, simultaneous enrichment of U, Th, Zr, REE, Th, Nb, and Ta can led to crystallization of complex Zr, REE, Th, Nb, and Ta minerals that can incorporate U. Uranium will not be able to crystallize independently as uraninite, or only in very small amounts. Therefore, even if the U content of some deposits related to peralkaline melts may be relatively high, they have not generally been mined because of the high cost of uranium extraction from highly refractory minerals. The Kvanefjeld deposit in the Ilímaussaq peralkaline complex (Sørensen *et al.* 1974) represents one of the best examples of such a uranium deposit, where U is mainly hosted by steenstrupine, a complex silico-phosphate of U, Th, and REE.

Another consequence of the strongly incompatible behavior of U together with Zr, REE, Th, Nb, and Ta in peralkaline magmas is the association of uranium mineralization with the most fractionated part of peralkaline complexes. These rocks are also generally located in the more apical part of the complex or at its margin, where low-viscosity residual melts and exsolved fluids are emplaced. Although the fluid/melt partition coefficients are extremely low in peralkaline systems, in some occurrences, U, Th, and the REE may be transported a few hundreds of metres (*e.g.*, Bokan Mountain) or over several kilometres (*e.g.*, Ilímaussaq and Th veins of the Front Range) from the intrusion. None of these veins has sufficient grade or tonnage to be mined.

From a geodynamic point of view, peralkaline intrusions are emplaced in post-orogenic to anorogenic environments. They tend to form circular intrusions, generally concentric and associated with ring dykes, because of their emplacement by cauldron subsidence in a consolidated basement without important shear tectonics. They form very large to small plutonic complexes. They may represent a wide range of intrusions from gabbro to highly fractionated granite, are always emplaced at a very high structural level and are commonly associated with contemporaneous volcanism.

Short course co-sponsored by the the SGA and MAC, Québec City, May 2008, p. 57-77

Ilímaussaq (South Greenland)

Regional geology. The Ilímaussaq intrusion is a peralkaline, silica-undersaturated plutonic complex situated in the eastern part of the 1.1–1.3 Ga Gardar intracratonic rifting province of South Greenland (Fig. 4-1). Magmatism in the Gardar Province is related to two main rifting events at 1280 Ma and 1180 to 1140 Ma. A series of 10 major plutonic complexes of gabbroic and nepheline-bearing to quartz-saturated granitoid rocks intrude a basement consisting of Paleoproterozoic granite and gneiss, which were unconformably overlain by Meso-proterozoic Gardar basalt and sandstone of the Eriksfjord Formation (Fig. 4-1). Two of the intrusive complexes contain carbonatite, and many alkali gabbroic dikes throughout the Gardar province contain anorthosite xenoliths (Bridgwater & Harry 1968). The association of alkali gabbro intrusions, anorthosite xenoliths, and carbonatite with granitoid intrusions has been interpreted to reflect large-scale melting processes of asthenospheric mantle. The alkali basaltic melts were ponded at the crust–mantle boundary and would have given rise, by fractionation, to massif-type anorthosite and later to alkaline or peralkaline melts in the roof region of these magma chambers (Larsen & Sørensen 1987). A U–Pb age of 1160±5 Ma on baddeleyite from the first magma batch

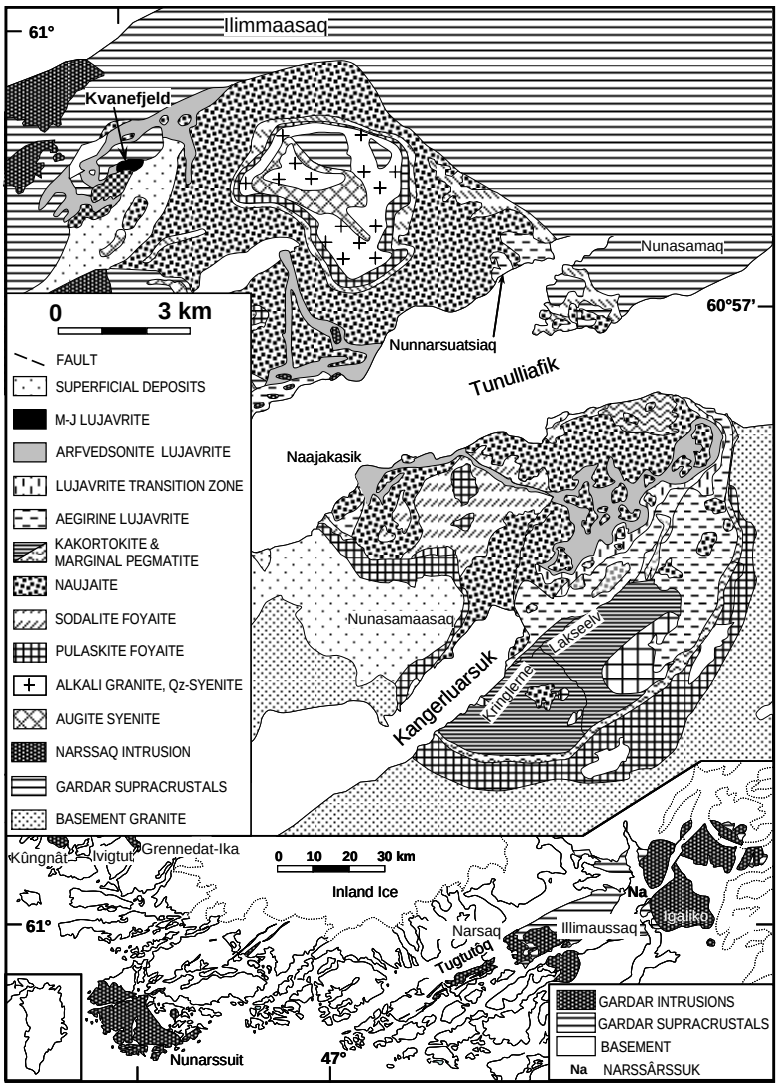

FIG. 4-1. Geologic map of the Ilímaussaq peralkaline complex (South Greenland), with the location of the Kvanefjeld deposit, modified from Sørensen & Larsen (2001). Inserted is the simplified geologic map of the Gardar alkaline province with the location of the Ilímaussaq intrusion.

(Krumrei 2006) indicates that the intrusion belongs to the second period of rifting and is the youngest of the province. The igneous complex covers about 156 km^2, and comprises an extraordinary diversity of granitic and syenitic rock types, emplaced as three successive melt batches, which intruded and fractionated at a depth of 3 to 4 km (Larsen et Sørensen 1987):

- Stage I corresponds to a mildly alkaline augite syenite which occurs both as a few hundred metres thick shell along the W, S, and SE margins of the intrusion, and as a 150 m thick layer on top of the intrusion (Fig. 4-1). The contacts between augite syenite and the nepheline–sodalite syenite (phase III) may locally appear gradational, but the sharp cross-cutting relationships occurring at other places demonstrate that the augite syenite is older.
- Stage II corresponds to a small unit of quartz syenite and alkali granite, which represent a break in the magmatic evolution of the complex. This unit occurs at the top of the intrusion.
- Stage III corresponds to the intrusion of nepheline- and sodalite-bearing syenite, presumed to be derived from the same deep magma chamber as the stage I intrusion. Stage III starts with Si-undersaturated slightly peralkaline rocks, evolving toward nepheline syenite. Within these syenite rocks, minor volumes of pulaskite, foyaite and sodalite have crystallized *in situ* from the roof downwards. The sodalite-rich syenite represents a 600 m thick flotation cumulate of sodalite (Ferguson 1964). Chemically and texturally distinct varieties of nepheline syenite formed below these roof rocks. Small bodies of medium- to coarse-grained lujavrite (hereafter indicated as m-c lujavrite), the most U-mineralized rocks, intrude arfvedsonite lujavrite, but are thought to represent a more primitive stage of the lujavrite magmas (Andersen *et al.* 1981). The m-c lujavrite occurs in the uppermost structural level of the peralkaline complex, just below the Gardar supracrustal rocks (Fig. 4-1).

The mineral assemblages of these rocks are given by Ferguson (1964, 1970), and Sørensen (2001). The early magmatic and intercumulus assemblage may partially be overprinted by later magmatic minerals and, in most places, by a post-magmatic or hydrothermal assemblage. The mineralized lujavrite typically contains nepheline, eudialyte, sodalite, and clinopyroxene crystals enclosed in a mixture of albite and microcline, whereas aegirine and amphibole appear texturally late. Black lujavrite is rich in arfvedsonite and green lujavrite is rich in aegirine. Ussingite $NaAlSi_3O_8$. NaOH, naujakasite $Na_6(Fe,Mn)Al_4Si_8O_{26}$, steenstrupine $Na_{14}Ce_6Mn_2Fe_2(Zr,Th,U)(Si_6O_{18})_2(PO_4)_7,3H_2O$ and villiaumite (NaF) may represent major constituents.

Geochemistry. The lujavrite bodies represent the most fractionated melts and therefore are the most enriched in incompatible elements. Most lujavrite is cumulate and its geochemistry is not always representative of melt compositions.

In an Q–P diagram (Fig. 4-2), the first unit (augite syenite) is close to quartz saturation, the rocks from the second unit (quartz syenite and granite) are quartz-saturated and the richest in potassium, and the third unit (various types of nepheline syenite) is strongly quartz-undersaturated and variable in composition. The most sodic members tend to be the most silica-undersaturated, the naujaite being the most extreme because of its strong enrichment in sodalite. In an A–B diagram (Fig. 4-3), the first unit is moderately meta-aluminous and is the only one to have an agpaitic ratio lower than one (Table 4-1).

The second unit is peralkaline (Na+K)/Al = 1.1 to 1.2). The third unit is strongly peralkaline

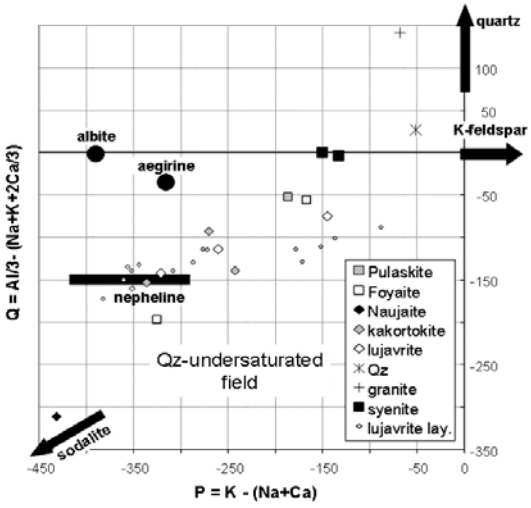

FIG. 4-2: Variation of P *versus* Q parameters for units from the Ilímaussaq peralkaline complex. Q–P mineralogical–chemical diagram from Debon & Lefort (1988), parameters in thousands of cations. The values for the main rock-forming minerals are also indicated in the diagram (large symbols are average data from Sørensen *et al*. 1974; intermediate size symbols are from Bailey 2006; smallest symbols are layered lujavrite from Bailey *et al.* 2006).

TABLE 4-1: AVERAGE CHEMICAL COMPOSITION OF THE MAJOR ROCK TYPES IN THE ILÍMAUSSAQ COMPLEX.

Sample	1	2	3	4	5	6	7	8	9	10	11	12	13	14
n	6	5	5	8	11	5	9	13	11	5	11	10	8	3
SiO_2 wt%	55.82	56.14	63.59	72.01	60.34	58.5	49.98	46.32	48.6	52.22	52.57	54.09	52.63	53.68
TiO_2	2.29	1.64	0.32	0.28	0.19	0.32	0.3	0.4	0.44	0.35	0.2	0.18	0.2	0.37
Al_2O_3	14.94	16.15	14.53	10.52	16.53	16.16	17.96	20.2	8.47	10.93	15.76	15.93	13.71	13.22
Fe_2O_3	2.03	1.47	3.03	2.65	3.38	3.07	4.77	3.39	8.26	5.61	5.82	8.29	4.55	3.48
FeO	8.82	7.64	4.07	3.18	2.42	4.38	4.57	4.11	14.84	5.72	4.36	0.92	7.36	8.23
MnO	0.24	0.22	0.18	0.14	0.18	0.21	0.25	0.19	0.47	0.4	0.26	0.22	0.55	0.61
MgO	1.01	1.35	0.15	0.14	0.14	0.16	0.13	0.13	0.48	0.28	0.21	0.11	0.12	0.16
CaO	3.47	3.88	0.96	0.4	1.53	2.02	1.83	1.89	2.48	3.58	1.92	0.69	0.34	0.25
Na_2O	5.53	5.16	5.41	4.88	8.19	7.56	11.55	14.63	8.67	10.43	9.55	11.52	10.18	7.91
K_2O	4.25	4.83	6.6	4.52	4.94	5.31	3.76	3.48	2.51	3.02	4.69	2.95	3.47	5.4
P_2O_5	0.74	0.52	0.02	0.02	0.05	0.05	0.05	0.03	0.02	0.04	0.03	0.03	0.44	0.47
I,L,	0.67	0.62	0.5	0.45	1.26	1.47	3.06	1.73	2.47	2.7	2.47	2.88	4.29	3.48
Total	99.81	99.62	99.36	99.19	99.15	99.21	98.21	96.5	97.71	95.28	97.84	97.81	97.84	97.26
P	-150	-133	-51	-68	-186	-167	-325	-432	-271	-336	-243	-321	-261	-145
B	0	-4	27	142	-52	-56	-197	-311	-93	-153	-139	-142	-114	-75
Q	202	179	102	84	82	107	130	108	327	161	141	121	165	167
A	-100	-91	-64	-61	-100	-112	-166	-217	-255	-314	-167	-146	-145	-120
Na+K/Al	0.92	0.85	1.10	1.23	1.14	1.13	1.28	1.38	2.00	1.87	1.32	1.39	1.50	1.43
Rb (ppm)	69	97	438	481	323	301	395	332	193	314	525	662	685	1280
La	71	74	252	325	223	236	540	409	393	1330	555	1410	3300	2830
Th	**4.1**	**5.7**	**53**	**79**	**38**	**26**	**54**	**33**	**15**	**46**	**43**	**55**	**89**	**466**
U	**1.3**	**1.7**	**16**	**27**	**9.4**	**7.5**	**15**	**9.6**	**6**	**21**	**17**	**58**	**178**	**490**
Zr	288	431	1950	2035	2230	1870	3200	3610	5830	20100	7610	7250	4130	724
Nb	55	92	312	291	327	250	546	580	495	1890	779	648	445	484
Be	3.5	3.2	28	22	16	14	31	21	15	28	26	32	46	104
F	990	1340	3310	3850	2270	2170	3090	4740	10200	6160	7070	502	1310	1140
Th/U	3.15	3.35	3.31	2.93	4.04	3.47	3.60	3.43	2.50	2.19	2.53	0.95	0.50	0.95

From Bailey (2006). Unit I: 1) fine grained augite syenite, 2) coarse grained augite syenite; Unit II : 3) quartz syenite, 4) alkali granite; Unit III: 5) pulaskite, 6) foyaite, 7) sodalite foyaite, 8) naujaite, 9) black kakortokite, 10) red kakortokite, 11) white kakortokite, 12) aegirine lujavrite, 13) arfvedsonite lujavrite, 14) medium to coarse grained lujavrite.

(Na+K)/Al up to 2.0). The abundance of Fe–Ti-minerals tends to decrease with increasing peralkalinity, especially in layered lujavrite.

The K/Rb ratios continually decrease during fractionation from 500 in the augite syenite to 35 in the most evolved lujavrite, whereas Zr/Hf ratios continually increase, from 45 to 97. Total REE contents and LREE/HREE ratios increase during fractionation (Bailey *et al.* 2001) whereas elements such as Zr, Cl, F, Zn, and W show irregularities or maximums in some rock types that are related to cumulus processes (Bailey *et al.* 2001). Th and U contents increase, from the augite syenite to the m-c lujavrite, with a Th/U ratio close to 3 (Fig. 4-4). However, the other types of lujavrite have the lowest Th/U ratios of less than 1.

Larsen & Sørensen (1987) proposed fractionation at depth, possibly at the crust–mantle boundary, of the melts parental to the Ilímaussaq rocks. Successive 'leaking' of this deep-level magma chamber was responsible for the three magma batches rising to the high-level chamber, where further low-pressure closed-system crystal fractionation continued.

Fluid inclusion studies have shown that water and methane are important fluid phases in equilibrium with the peralkaline melts (Konnerup-Madsen *et al.* 1985, 1988). Higher hydrocarbons also occur in small percentages, whereas highly saline fluid inclusions are abundant in the alkali granite. Pressures of 1 kbar have been obtained from fluid inclusion data for the alkali granite (Konnerup-Madsen & Rose-Hansen 1984) and from the estimated 3–4 km thickness of the overlying Eriksfjord Formation. Primary fluid inclusions in sodalite crystals from naujaite give temperatures between 700 and 900°C and pressures between 1.5 and 3.5 kbar, reflecting their crystallization during

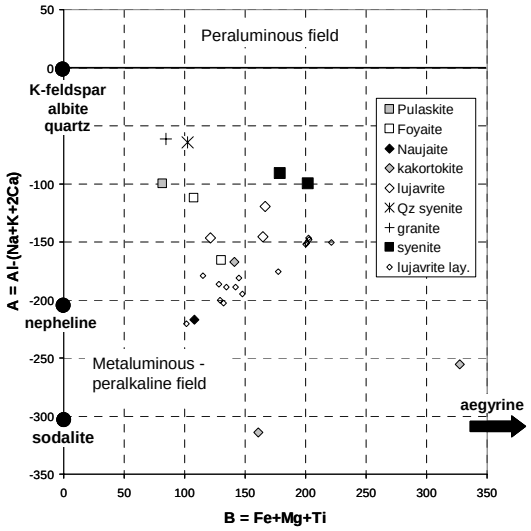

FIG 4-3. Variation in the peraluminous index A with fractionation parameter B for the Ilímaussaq peralkaline complex igneous units. A–B mineralogical–chemical diagram from Debon & LeFort (1988), parameters in thousands of cations (same symbols as Figure 4.2).

the ascent of the magma. Temperatures of crystallization from 450–500 to 1000°C have been reported for nepheline and pyroxenes (Markl *et al.* 2001).

Mineral compositions (Markl *et al.* 2001) show that the earliest augite syenite melt at Ilímaussaq was reduced, with fO_2 almost two orders of magnitude below the FMQ (Fayalite–Magnetite–Quartz) buffer, and methane as a stable fluid phase, very low water activities (<0.2), relatively low silica activities of 0.8, and relatively high alkali/Al ratios. Subsequently, high-level fractionation of augite syenitic melts led to a drastic reduction of silica activities to 0.4 and a strong decrease of fO_2, down to four orders of magnitude less than the FMQ buffer. Further deep-level fractionation also leads to decreasing silica activities and increasing (Na+K)/Al ratios, thus generating the peralkaline rocks of the syenitic magma batch. The anorthosite xenoliths found throughout the Gardar province may reflect these deep-seated processes. Subsequently, when the melt (Na+K)/Al ratio became greater than 1, crystallization of alkali feldspar and nepheline, with a (Na+K)/Al ratio of 1, further increased the ratio of the melt. At this stage, fluid inclusions show that methane is still the stable fluid phase, but fO_2 increases significantly, to two orders of magnitude above FMQ, whereas silica activity drops to 0.3 in the late stages of the last

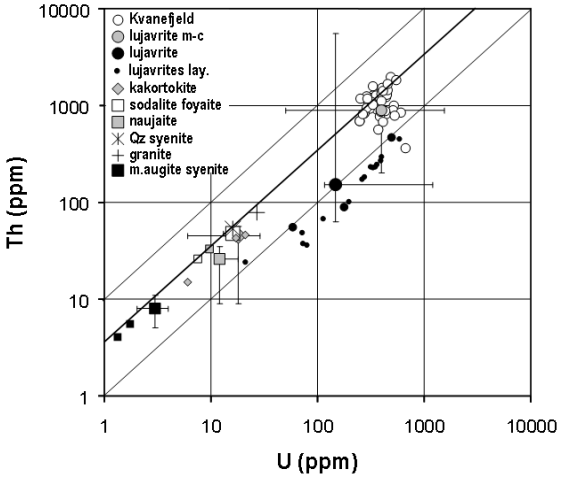

FIG. 4-4: Th–U variations in the plutonic units of the Ilímaussaq intrusion (same symbols as Fig. 4-2), and in the Kvanefjeld deposit (Clausen 1982).

peralkaline magma batch. When these rocks are intruded into the red Mesoproterozoic sandstones, the latter turn green as a result of the reduction of hematite.

In lujavrite, oxygen fugacity is no longer controlled by a solid–solid buffer reaction and fO_2 can vary. The transition from a methane-dominated to a very low salinity aqueous fluid in the late lujavrite crystallization stages appears to occur at fO_2 close to the magnetite–hematite buffer and silica activity drops to values lower than 0.2. This explains why most Fe in the final lujavrite is trivalent, and uranium reaches its highest concentration. Karup-Møller (1978) used ore minerals from the Ilímaussaq lujavrite and pegmatite to suggest that fO_2 was between 10^{-16} and 10^{-21} at 500°C. These oxygen fugacity values are 1 to 4 orders of magnitude above the magnetite–hematite buffer. By changing solid-phase buffers from FMQ to arfvedsonite–aegirine, alkaline and peralkaline melts are intensely reduced in the early stages of crystallization, but highly oxidized in the late stages. These calculations also support a model of successive magma batches derived from one continuously fractionating magma at depth.

Uranium mineralization. The Kvanefjeld uranium deposit was discovered in 1956, one year after the initiation of a regional uranium exploration program. It is situated at the northwestern edge of the intrusion (Fig. 4-1). The deposit is magmatic mineralization formed during the latest emplacement stages of the intrusion. The uranium mineralization is associated with the youngest

nepheline syenite, and the medium-coarse lujavrite, which is generally dark, shows a pronounced magmatic layering, and is enriched both in U and Th, as well as in Nb, Zr, Be, Li, F, and REE. In the Kvanefjeld area, under a roof of gabbro and basic volcanic rocks, a mega-breccia of volcanic and sedimentary rocks, together with rocks from the early phases of the intrusion are cemented by lujavrite. Three main types of lujavrite occur: the first was a fine-grained arfvedsonite lujavrite, followed by a naujakasite lujavrite and by the medium-coarse lujavrite. The U content of the arfvedsonite lujavrite and the medium-coarse lujavrite is about 150–200 ppm. In contrast, the naujakasite lujavrite contains several zones with 300–500 ppm U. The highest U and Th values are generally observed in the upper part and at the contact of the medium-coarse lujavrite with enclosing altered volcanic rocks intruded by fine-grained lujavrite. The thickness of the mineralized zones vary from a few metres up to about 50 m. Analcime–steenstrupine veins also intersect altered volcanic rocks. High-grade veins and pegmatites are not of economic importance because of their small volume, but their U and Th contents vary widely (117–1200 ppm U and 63–5500 ppm Th).

Two U enrichment trends can be observed in the Kvanefjeld mineralization (Fig 4-5): a magmatic trend with an average Th/U ratio of about 3.5, similar to the main fractionation trend defined by the less fractionated units of the complex and a fluid fractionation trend with a U enrichment at constant Th content, and a Th/U ratio decreasing to less than 2. These two trends and the large variations in U and Th contents observed in the different types of

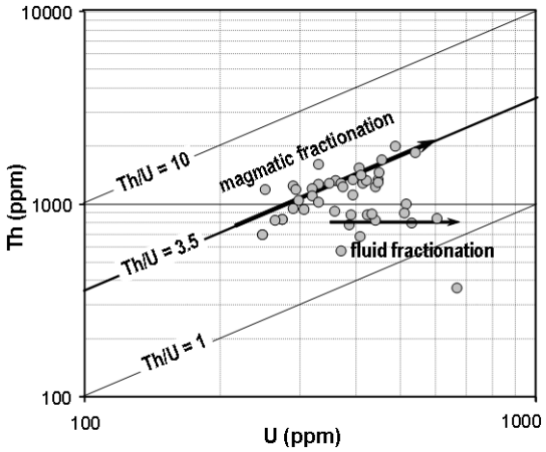

FIG. 4.5. Relations between Th and U in the Kvanefjeld mineralization (data from Clausen, 1982) indicating two types of fractionation.

lujavrite reflect the effects of magmatic and late- to post-magmatic processes related to exsolution of a fluid phase.

Numerous mineralized veins, up to several kilometres long, striking NE–SW, perpendicular to the main axis of the Ilímaussaq peralkaline complex, and predominantly vertical, transect all rock types to the east of the Ilímaussaq intrusion (Hansen 1968). Three main types of veins are mineralized:

- brown albitic veins, composed of albite, hematite, quartz, and small amounts of chlorite, calcite, apatite, monazite, eudialyte, and thorite;
- green veins composed of albite and aegirine, occasionally with microcline, hematite, and some accessories, such as mica, apatite, chlorite, quartz, sphalerite, monazite, bastnaesite $CeCO_3(OH,F)$, neptunite $KNa_2Li(Fe,Mn)_2Ti_2Si_8O_{24}$, and thorite;
- composite veins with the components from the two other types, with accessory eudialyte ($Na_{12}Ca_6Fe_3Zr_3[(Si_3O_9)_2(OH,Cl)_2]$) and thorite.

Nearly all veins have elevated and highly variable Th/U ratios (1–57), Th (60–4500 ppm) and U (17–1500 ppm) contents, indicating that Th has been mobilized by a fluid and deposited in the veins along a distance of several kilometres. However, U has migrated further, as reflected by low Th/U ratios of the veins, because of the highly oxidizing conditions recorded by the presence of hematite in the veins. The source of these veins is certainly the Ilímaussaq peralkaline complex, because they have been traced to the contact with the complex and similar veins have been observed within the complex.

Steenstrupine, is an important rock-forming mineral in lujavrite and the main U mineral in the medium coarse lujavrite of the Kvanefjeld uranium deposit. Steenstrupine occurs instead of eudialyte, the main U- and Th-bearing mineral in the other rocks of the complex (Table 4-2 and 4-3). Steenstrupine is also common in the sodic pegmatite bodies and hydrothermal mineralization and in the fenitized volcanic rocks of the roof of the Kvanefjeld plateau. In the Lovozero complex of the Kola Peninsula, Russia, steenstrupine is also common in the zeolite-rich cores of pegmatite and in hydrothermal veinlets (Khomyakov 1995, Semenov 1997). U and Th contents of steenstrupine vary from 0.1–1.4 wt.% U and 0.2–7.4 wt% Th (Hansen 1968, Makovicky *et al.* 1980) (Table 4-3). The central part of these crystals is metamict and richer in U, Th, and Y than the non-metamict

TABLE 4-2. U AND TH CONTENTS OF THE MAJOR ROCK TYPES IN THE ILÍMAUSSAQ PERALKALINE COMPLEX AND MAIN U-BEARING MINERALS

	U minerals	U	Th	Th/U
augite syenite		3 (2–4)	8 (5–11)	2.7
foyaite	eudialyte	16 (13–19)	48 (43–53)	3.0
naujaite	eudialyte	12 (6–27)	26 (9–35)	2.5
kakortokite	eudialyte rinkite	18 (6–29)	45 (9–57)	2.5
lujavrite	eudialyte monazite lovozerite steenstrupine	146 (117–1200)	154 (63–5500)	1
lujavrite m-c	steenstrupine monazite	400 (50–1550)	890 (200–1100)	2.2

From Sørensen *et al.* (1974)

margins, whereas ZrO_2, MnO, Na_2O, and P_2O_5 are higher in the margins (Table 4-4). The decrease of U and Th contents in the marginal parts reflects the progressive fractionation of U and Th into the exsolving fluid phase to produce the U–Th mineralization in the fenitized volcanic rocks of the roof of the complex (Sørensen *et al.* 1974).

The high fO_2 developed in the latest intrusion should cause a preferential loss of U as $(UO_2)^{2+}$, as indicated by the high Th/U observed in the upper part of drill holes (Fig. 4-5). Deposition of U elsewhere is indicated by the fluid fractionation trend, with U enrichment at nearly constant Th content in the whole rock geochemical data of the Kvanefjeld tunnel (Fig. 4-4). In steenstrupine, the reverse evolution is observed (Table 4-4), but the higher Th/U ratio in the centre of the crystal relative to its rim results from the central part of the mineral, which is the richest in U and Th, is metamict and therefore has lost a large part of its initial U.

TABLE 4-3. U AND TH CONTENTS OF THE MAIN RADIOACTIVE MINERALS OF THE ILÍMAUSSAQ PERALKALINE COMPLEX

	U (ppm)	Th (ppm)
Steenstrupine $Na_{14}Ce_6Mn_2Fe_2(Zr,Th,U)(Si_6O_{18})_2(PO_4)_7,3H_2O$	2,000–15,000	2,000–74,000
Monazite $(LREE,Th,U)PO_4$	138–12,800	300–57,300
Thorite $(Th,U)SiO_4$	31,000	405,000
Britholite $(Na,LREE,Ca,Y)_5[(Si,P)O_4]_3(OH,F)$		6,900
Eudialyte $(Na,LREE,Ca,K)_{15}(Ca,Mn)_6(Mn,Fe)_3(Zr,Nb,Hf)_3(Nb,Ta,Si)Si_{26}O_{74}(OH,Cl,F)_2,2H_2O$	55–600	30–340
Pyrochlore $(Ca, Na)_2(Nb,Ta)_2O_6(OH,F)$	2,000	7,000
Rinkite $(Ca,LREE)_4Na(Na,Ca)_2(Ti,Nb,Zr)(Si_2O_7)_2F_2(O,F)_2$	3,000–12,000	

From Sørensen *et al.* (1974). Eudialyte formula from Plivo & William-Jones (1999).

TABLE 4-4. MICROPROBE ANALYSES OF STEENSTRUPINE CRYSTALS.

Sample wt %	50-149.7 centre (5)	50·149.7 rim (6)	50-150.6 centre (2)	50-150.6 rim (1)	199104 centre (4)	199104 rim (1)
SiO_2	26.94	27.75	27.54	25.98	27.40	27.06
TiO_2	0.16	0.07	0.28	0.18	0.25	0.20
ZrO_2	n.a.	n.a.	n.a.	n.a.	1.41	2.33
ThO_2	3.95	0.42	4.13	1.40	5.04	1.83
Al_2O_3	n.a.	n.a.	n.a.	n.a.	0.28	0.04
La_2O_3	8.78	12.85	8.94	14.22	11.49	11.79
Ce_2O_3	14.57	15.53	13.80	13.76	15.74	16.49
Pr_2O_3	1.29	1.04	1.28	1.54	2.39	2.08
Nd_2O_3	3.72	2.80	3.50	2.78	4.01	4.22
Sm_2O_3	0.31	0.19	0.19	0.15	n.a.	n.a.
Y_2O_3	1.47	1.05	1.56	0.31	1.05	0.10
FeO	4.34	2.50	3.96	1.85	3.87	3.42
MnO	3.61	6.22	3.42	5.69	4.42	5.00
CaO	2.18	1.58	2.00	1.65	1.88	1.95
SrO	0.10	0.14	0.07	0.11	n.a.	n.a.
Na_2O	8.41	12.98	7.88	13.65	2.75	6.59
K_2O	0.05	0.02	0.20	0.31	n.a.	n.a.
P_2O_5	9.36	11.26	8.50	9.35	11.31	12.30
Nb_2O_5	0.10	0.24	0.13	0.67	n.a.	n.a.
U_30_8	n.a	n.a.	n.a	n.a	0.70	0.35
Total	89.34	96.64	87.38	93.60	93.89	95.75
ΣRE_2O_3	28.67	32.41	27.71	32.45	33.63	34.58
La_2O_3/Nd_2O_3	2.36	4.59	2.55	5.12	2.86	2.79
Th/U	-	-	-	-	7.46	5.42

Analyses from a vein with 350 ppm U and 2,000 ppm Th sampled in drill core 50 from the Kvanefjeld deposit (from Khomyakov & Sørensen, 2001). OH and F have not been analyzed. n.a. = not analyzed.

The preferential loss of U during fluid oversaturation of the lujavrite melts may also explain the occurrence of pitchblende veins in the Proterozoic granite close to Narssaq, Narssarssuaq, and Julianehåb in South Greenland (Armour-Brown *et al.* 1982). The 1180 Ma age for the pitchblende compared to 1160 Ma for the Ilímaussaq intrusion suggests that this mineralization is derived from hydrothermal activity associated with the emplacement of the Gardar alkaline complex.

Resource estimations. In the 1970s, detailed exploration at Kvanefjeld, with 11852 m of core from 76 drill holes, led to a total estimated resource of 43,000 t U at 340g/t U for a 250g/t U cut-off, with 27,000 t U of reasonably assured resources and 16,000 t U of estimated additional resources. Further exploration from 1979 to 1986 resulted in the identification of 60,000 t U of speculative resources. According to the International Nuclear Energy Agency, untested mineralized host rocks could add significantly to these estimates. In addition to U, other mineralization includes Be (180,000 t at 0.1% Be) and Li (235,000 t at 600–1900 ppm). Estimates of U potential considering an average U concentration of 100 to 200 ppm over 12 km^2 and a thickness of 600 m, would correspond to 3 Mt U (Bondam & Sørensen 1959).

The recovery cost of U by sulfatizing roast was $40 to $70 /kg of U, depending of the type of ore (Gamborg-Hansen 1977). For the Carbonate Pressure Leaching process, the recovery cost was $70 to $90 per kg of U. About 5000 tons of ore were extracted from the Kvanefjeld tunnel driven through the ore body in 1980–81.

Bokan Mountain (USA)

Regional geology. The Bokan Mountain U–Th deposit at Kendrick Bay, southeastern Alaska, is associated with a Late Jurassic peralkaline granite.

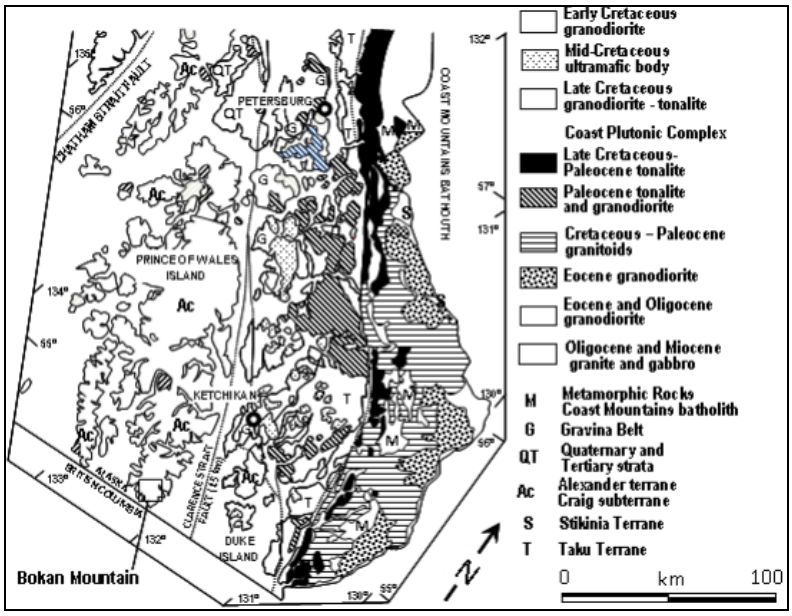

FIG. 4-6. Geologic map of SE Alaska with the location of the Bokan Mountain granite and of the major terranes (from Churkin & Eberlein 1977).

The pluton is post-tectonic and intrudes Paleozoic metasedimentary and metavolcanic rocks, quartz diorite and quartz monzonite, at the western side of the Chatham Strait fault (Fig. 4-6). The area is part of the Alexander terrane located at the western margin of the Canadian Cordillera (Churkin & Eberlein 1977). A U–Pb age on zircon of 171 ±5 Ma has been obtained for the Bokan Mountain granite (De Saint André *et al.* 1983), corresponding to a major episode of thrust tectonics in the North American Cordillera. However, as peralkaline magmatism is typically emplaced in stable continental crust in anorogenic settings, the Alexander terrane was probably accreted to the North American continent more recently (Collot 1981).

Geology of the pluton. The pluton is circular, multiphased, zoned, and forms a topographic high of 670 m. It outcrops over 3.2 km^2, but a much larger complex is presumed at depth, as is usually the case in such granite bodies. The ring structure is defined by a core of riebeckite–aegirine granite forming the main part of the pluton, surrounded by an aegirine-only granite and a border zone pegmatite (Fig. 4-7). Fine-grained aegirine granite xenoliths, preserved in the central upper part of the pluton, probably represent the roof of the pluton, as attested by the occurrence of enclaves of host metamorphic rocks. However, no magmatic contacts have been observed between the various units and the petrologic variations seem to result from an internal evolution related to differences in crystallization conditions. This interpretation is confirmed by the lack of geochemical differences between various units (see below). Felsic dikes in the host rocks are enriched in Ta, Nb, U, Th, REE, and Zr, and are therefore probably related to the Bokan Mountain intrusion.

The main rock forming minerals are euhedral quartz, microcline with abundant perthite, nearly pure albite, aegirine, and arfvedsonite. Albite occurs as individual crystals, perthite along the growth zones of quartz, coronas around microcline crystals, and along microfractures in microcline. There is a progressive transition between purely magmatic crystallization of albite and late- to post-magmatic growth from a fluid phase. Arfvedsonite and aegirine crystals are poikilitic, enclosing quartz, albite and microcline crystals. Zircon is ubiquitous, abundant, and generally xenomorphic suggesting a late crystallization stage. Fluorite is very common. Astrophyllite, $(K,Na)_3(Fe^{2+},Mn)_7Ti_2Si_8O_{24}(O,OH)_7$, a typical mica of peralkaline intrusions, only occurs in the fine-grained unit. Magnetite and hematite are related to alteration. An early stage of micro-fracturing, occurring at a sub-magmatic stage ("protoclasis" of Collot 1981) typically affects the granite and results from an overpressure produced during the exsolution of the vapor phase from the granitic magma during its late crystallization stages.

Geochemistry. The Bokan Mountain granitic pluton is typically peralkaline with a negative

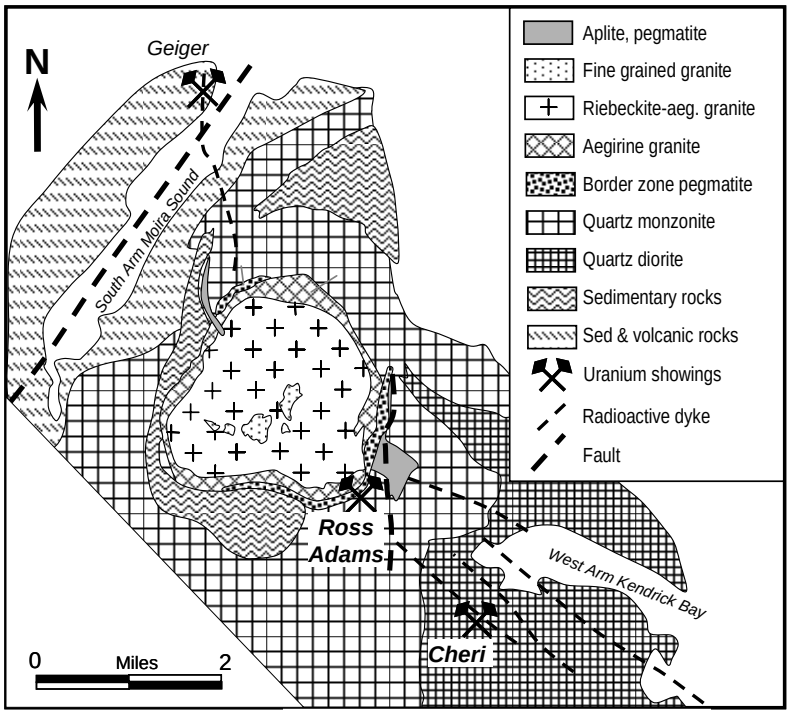

FIG. 4-7. Geology of the Bokan Mountain peralkaline complex area and location of the main U showings (from MacKevett 1963, modified).

peraluminous index (Table 4-5, Fig. 4-8). The granites are also rich in iron (4.6 wt % F_2O_3 on average), poor in calcium (0.09 wt % CaO on average, essentially hosted by fluorite), and extremely poor in magnesium (0.01 wt% on average). The main chemical variations correspond to the relative abundance of albite and K-feldspar with a tendency for larger amounts of quartz in the most potassic samples (Fig. 4-9). Mafic mineral content is relatively high and variable especially in the aegyrine–arfvedsonite albitic granite. No variation of chemical composition is evident from the major element contents that can be attributed to magmatic fractionation trends.

The granites are moderately rich in Th and U (24 and 12 ppm respectively). Th is well correlated with U (Fig. 4-10), with a slight decrease of Th/U ratios from about 4 to 2 with increasing Th and U concentrations, but without any correlation with petrographic units. Zr contents are typically elevated, averaging 1040 ppm (150 to 2200 ppm), but Zr content variations in non-altered granite are not correlated with Th (Fig. 4-11). F contents are elevated and extremely variable (200– 3200 ppm).

Uranium mineralization. The Ross Adams U deposit was discovered by D. Ross in 1956. It was mined from 1957 to 1971, first from open pit and later as underground working by a series of companies (Climax Molybdenum, Bay West Inc.,

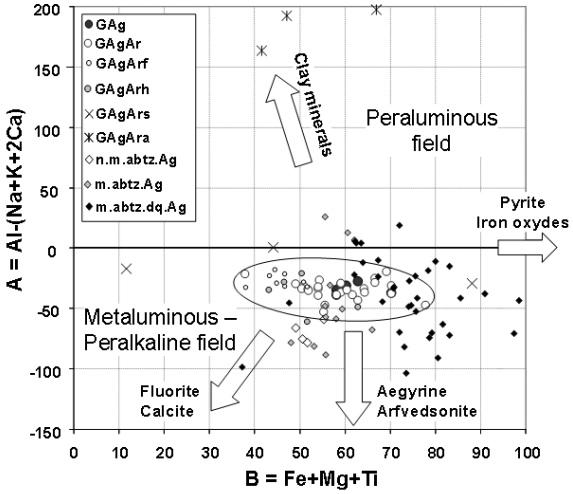

FIG. 4-8. Variation of the peraluminous index (A) with fractionation (parameter B) for the Bokan Mountain complex igneous units and altered zones. The field of unaltered granite is circled. A–B mineralogical–chemical diagram from Debon & LeFort (1988), parameters in thousands of cations. (GAg: aegirine granite, GAgAr: aegirine–arfvedsonite granite, GAgArf: fine grained aegirine–arfvedsonite granite, GAgArh: heterogeneous, GAgArs: silicified, GAgAra: argillized and for the altered and mineralized bodies (n.m.abtz.Ag: non-mineralized albitized aegirine granite, m.abtz.Ag: mineralized albitized aegirine granite, m.abtz.dq.Ag: non-mineralized albitized and dequartzified aegirine granite).

TABLE 4-5. SELECTED GEOCHEMICAL ANALYSES OF THE BOKAN MOUNTAIN GRANITE AND MINERALIZATION.

wt%	293	430	494	275	290	549	276	411	464	473	541	550	554	578	524	534	538	567
SiO_2	73.7	73.6	74.6	73.5	74.9	72.4	72.6	73.2	74.5	73.8	74.3	73	72.9	70.4	66.4	61.9	67.3	65.4
TiO_2	0.01	0.01	0.01	0.02	0.01	0.01	0.01	0.01	0.01	0.01	0.01	0.02	0.01	0.03	0.01	0.02	0.02	0.03
Al_20_3	11	10.7	11	11.3	10.3	12.2	12.6	12.3	11.6	11	11.6	11.6	11.3	13	14	12.4	11.3	14.4
Fe_20_3	5	5.6	4.6	4.7	4.8	4.1	3.4	3.5	3.7	5.2	4.4	4.7	4.4	4.9	2.7	6	6.1	5.8
MnO	0.01	0.01	0.01	0.01	0.01	0.01	0.01	0.01	0.01	0.01	0.01	0.01	0.01	0.01	0.05	0.04	0.03	0.02
MgO	0.017	0.015	0.028	0.017	0.017	0.03	0.033	0.033	0.017	0.015	0.015	0.025	0.03	0.032	0.139	0.221	0.086	0.028
CaO	0.035	0.105	0.133	0.07	0.056	0.364	0.07	0.056	0.024	0.032	0.02	0.136	0.137	0.155	2.2	0.532	0.161	0.057
Na_2O	4.6	4.9	5.7	5.3	4.5	5	4.8	5.2	5.1	6.5	8.8	8.4	9.4	7.4	8.8	9.5	7.2	11.1
K_2O	4.4	4	3.1	4	4.2	4.7	5.3	4.2	4.4	2.4	0.1	0.1	0.1	0.2	0.5	0.4	0.1	0.2
P_2O_5	0.05	0.02	0.04	0.02	0.01	0.05	0.02	0.03	0.01	0	0.02	0.04	0.01	0.15	0.15	0.18	0.15	0.04
Total	98.82	98.96	99.22	98.94	98.80	98.86	98.84	98.54	99.37	98.97	99.28	98.03	98.30	96.28	94.95	91.19	92.45	97.08
P	-56	-77	-123	-88	-58	-74	-45	-80	-72	-160	-282	-274	-306	-240	-352	-317	-236	-356
Q	167	164	163	151	181	136	135	149	155	149	126	131	98	146	48	22	137	0
B	63	70	58	59	60	52	43	45	47	65	55	59	56	62	37	81	78	73
A	-27	-37	-39	-37	-34	-35	-23	-18	-31	-46	-59	-50	-89	7	-98	-91	-18	-82
ppm																		
F	320	820	1020	1320	980	3300	810	1140	1130	1140	140	1140	1050	1040	10200	1800	530	420
U	5.6	2.2	17	14	6	17.5	7.6	26	14.5	10.5	24	81	91	1300	6900	17400	6100	820
Th	9	15	40	37	11	56	13	34	27	18	32	4590	3710	2150	3240	19400	27000	1180
Zr	1086	1370	1125	578	2221	642	722	1185	946	1076	134	772	1300	5129	762	2714	2072	8466

From Collot (1981, unpub. data). Analyses 293, 430, 494: albite–aegirine granite; 275, 290, 549: albite–aegirine–arfvedsonite granite; 276, 411, 464: fine grained albite–aegirine–arfvedsonite granite; 473, 54: non mineralized albitized albite–aegirine granite; 550, 554, 578: mineralized albitized albite–aegirine granite; 524, 534, 538, 567: mineralized albitized and dequartzified albite–aegirine granite. P, Q, A, B: chemical–mineralogical parameter (in thousands of cations) used and defined in the diagrams.

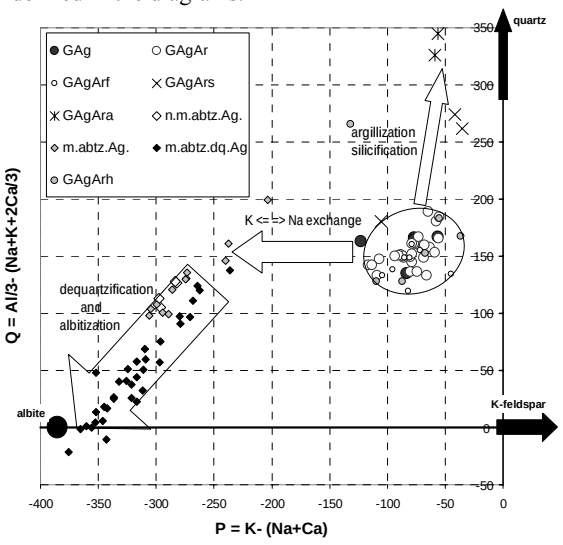

FIG. 4-9. Variation of the K-feldspar/albite (P parameter) *versus* quartz contents (Q parameter) for the Bokan Mountain igneous units and altered zones. The field of unaltered granites is circled. Q–P mineralogical–chemical diagram from Debon & LeFort (1988), parameters in thousands of cations. Same legend for the symbols as in Fig. 4-8.

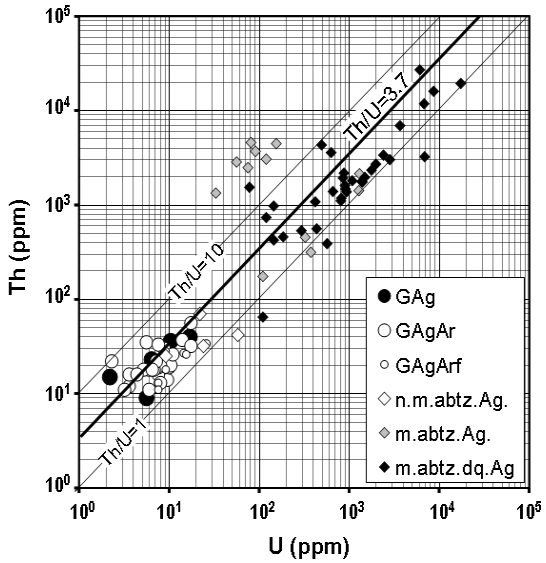

FIG. 4-10. Relation between Th and U in different plutonic units of the Bokan Mountain peralkaline Complex. Same legend for the symbols as Figure 4-8.

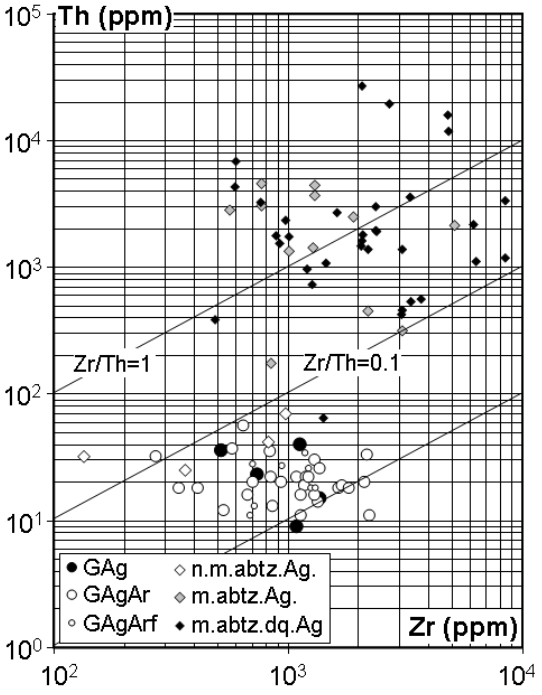

FIG. 4-11. Relation between Th and Zr in the different plutonic units of the Bokan Mountain peralkaline complex (same legend as Fig 4.8)

Standard Metals, and Newmont Exploration, Ltd.) during the 1950s and the 1960s. Standard Metals and a prospector R. Dotson discovered a NW trending U vein and shear system SE of the Ross Adams deposit – the Dotson Shear – extending over 2.5 km to the shoreline. A U vein and shear system, named the I and L deposit, was discovered adjacent to the Ross Adams area in the early 1970s, and represents the fault-displaced NW extension of the Dotson shear–vein system. Although significant U grades were defined at the I and L deposit, it remains unmined. High contents of REE, Nb, and Zr are associated with some of the U zones (MacKevett 1963, Thompson 1998, Staatz *et al.* 1979).

Several types of U mineralization have been recognized by MacKevett (1963) in the area:

1) the main type of U–Th mineralization, the Ross Adams deposit, is associated with a desilicified and albitized part of the pluton forming plunging pipe-like bodies along the contact with the aegirine granite or occurring as pods in *en echelon* NW-striking shear zones. The ore minerals are uranothorite, uraninite, with generally less than 2% of sulfides disseminated in nearly pure albite;
2) some disseminated U mineralization also occurs in NW-oriented, steeply dipping albite–quartz dike systems and associated shear zones peripheral to the complex;
3) mineralized pegmatite veins within a marginal phase of the complex;
4) U vein-type mineralization;
5) matrix replacement phases in hornfelsed and hydrothermally altered sandstone adjacent to or overlying the intrusion.

Nearly all U occurrences are in or near the granite stock. A total of 89,000 t of ore have been mined at a grade of about 0.85% U and 2.5% Th with an average Th/U close to 3, mainly from the Ross Adams deposit.

The Ross Adams ore body is situated at the SE margin of the aegirine granite. It is up to 24 m wide and was mined along strike for over 300 m. The pod-like ore zones have dense microfracturing, produced during late magmatic devolatilization of the magma chamber.

Geochemical data indicate that alteration of the host aegirine granite proceeded in two main steps (Fig. 4-9). First, albitization of K-feldspar produced typical chessboard structure in the crystals, at nearly constant quartz content. The rocks affected by this type of alteration are only weakly or not mineralized. This was followed by progressive dissolution of quartz with simultaneous precipitation of albite, resulting in albitite. During alteration, Al and Fe mineral contents (B parameter) did not change significantly in the rocks (Fig. 4-8). Variation in the peraluminous index is due to the combined effect of incipient clay alteration in some of the samples, increasing the peraluminosity of the rock because of Na or Ca leaching, and to formation of a minor amount of Ca-bearing, Al-free minerals such as fluorite and carbonates, which decreases the peraluminous index value. The mafic mineral content of the syenite tends to be higher, because the volume loss from quartz dissolution was not totally compensated by albite formation and there was formation of secondary pyrite and iron oxides. The U–Th mineralization is essentially hosted in these desilicified and albitized parts of the granite predominantly as uranothorite, forming 30 to 500 μm long crystals disseminated in chessboard albite. Zr was not significantly enriched during the mineralization process; its concentration only doubled. The fluorine content of the mineralized rocks is slightly higher than that of the granite, but a large part may have been lost with the fluids.

Veins represent the second most important U mineralization at the Ross Adams deposit. The

largest ones extend to more than 2.5 km away from the Bokan Mountain pluton and strike WNW. The most important veins are 25–250 long and form a cluster up to 130 m thick in the vicinity of the pluton where aplite is abundant. Pegmatite dikes of aegirine granite occur within these veins. Compared to the intragranitic Ross Adams mineralization, the exogranitic mineralization is characterized by the association of large amounts of REE and Nb together with Th, U, and Zr. The main REE-bearing mineral is bastnaesite ([LREE]FCO_3). In the veins, the quartz–aegirine ore lenses are up to 3 m thick and 30 m long. U grades defined by drilling vary from 0.14 to 1.92% U. Wall-rock alteration within and adjacent to the ore bodies consists of pervasive albitization with lesser amounts of chlorite, fluorite, calcite, quartz, sericite, and tourmaline. Hematite is present as an envelope around the ore zones. Chlorite is heavily developed within higher-grade (>0.43% U) zones whereas pervasive hematite alteration is more commonly associated with areas of lower grade (<0.43% U) (Thompson 1988).

Genetic model. By comparison with other world occurrences of peralkaline plutonic complexes, the Bokan Mountain granite represents the most fractionated and most apical part of a larger magmatic complex existing at a relatively shallow depth. Similar albite–aegirine–arfvedsonite granite bodies are known in many part of the world, some of the best known being those from Nigeria (Bowden & Turner 1974). U mineralization associated with this type of granite is most likely derived directly from the mantle. Although no Sr–Nd–O isotopic data are available on the Bokan Mountain granites, peralkaline magmas are considered to reflect low degrees of partial melting of the mantle with subsequent fractionation during ascent of the melts. They have $^{87}Sr/^{86}Sr$ ratios lower than 0.705 and $^{18}O/^{16}O$ ratios lower than 7 to 8 (Javoy & Weiss 1987). The initial enrichment of the mantle in incompatible elements, and especially in U and Th, through the subduction of an oceanic slab with variable amounts of sedimentary rocks derived from alteration of the continental crust, may considerably enhance the final U and Th concentrations in the melts that are generated. It is not possible to generate peralkaline melts from crustal material, which is generally peraluminous, except if evaporite rocks can be incorporated. Contrary to most disseminated U mineralization associated with pegmatoid rocks in anatectic domains, the Th/U ratios remain close to the chondritic ratio of 3.5 during magmatic fractionation, even in the mineralized albitite.

The peralkaline nature of the melts and their high temperatures have allowed continuous and simultaneous fractionation of U and Th during magmatic fractionation. However, the unaltered granite only has moderate U (12 ppm on average) and Th (24 ppm on average) enrichment, despite the association with late-magmatic U mineralization. Such inconsistency can be resolved if the outer part of the pluton crystallized rapidly and magmatic fractionation had to proceed inwards. Therefore, the most fractionated melts, richer in U, Th, and fluids, occur in the deep central part of the pluton.

At a certain stage of fractional crystallization, fluid saturation of the melts occurred leading to the deposition of a major part of the U and Th mineralization. Expulsion of fluids was focused in a zone of weakness, principally at the southeastern margin of the pluton, producing intense microfracturing and alteration of the granite. The alteration started with albitization of K-feldspar and with increased fluid percolation, simultaneous quartz dissolution, and new albite growth occurred leading to the formation of albitic episyenite. At a pressure lower than 1 kbar, dissolution of quartz may have occurred when a fluid cooled from magmatic temperatures of 700–600°C down to about 350°C, because the quartz solubility curve passes through a maximum at about 350°C under low pressure conditions. According to the inward fractionation hypothesis proposed above, the fluids are exsolved from a hotter and deeper-seated part of the pluton and migrated towards the marginal and cooler part of the pluton, the cooling of the magmatic fluid allowing the dissolution of quartz. Similar mineralization may also have existed at the level of the roof of the pluton, but was eroded away.

Part of the fluids enriched in F, U, Th, Nb, and REE escaped into the host rocks along veins, some of them extending several kilometres from the pluton. The filling of these veins started at the magmatic stage as indicated by the occurrence of aplitic–pegmatitic veins of aegirine granite within them.

Thompson (1988) reported only aqueous fluids in the mineralized zones with homogenization temperatures between 320 and 331°C, corresponding to temperatures of at least 420°C when pressure corrections are taken into account. These inclusions probably represent relatively late fluids.

Unpublished observations of the first author indicate three-phase inclusions containing a solid and variable proportions of water and carbon dioxide (5−70 vol%) in the residual quartz of mineralized albitite. The variable proportions of the latter two phases may be an indication of a fluid unmixing. Some of the fluid inclusions in fluorite also contain several birefringent solids. In contrast to Ilímaussaq (Konnerup-Madsen *et al.* 1985), the carbon dioxide phase is devoid of methane or higher hydrocarbons. Unmixing of water and carbon dioxide fluid may have enhanced the overpressurization of the fluids responsible for the microfracturing the granite in the ore zone.

Oxygen ($\delta^{18}O_{H2O}$ 6.8−8.1‰) and carbon ($\delta^{13}C$ −4.3 to −7.0‰) isotope data support a magmatic origin for the calcite associated with the Th–U deposits (Thompson 1988). Sulfur isotope analyses on pyrite, galena, sphalerite, and pyrrhotite indicate disequilibrium, but $\delta^{34}S_{H2S}$ is estimated at 7.6‰ (Thompson 1988).

Other occurrences of albitic episyenite. Numerous occurrences of mineralized or barren albitic episyenite have been reported all over the world, mainly in highly potassic calcalkaline granite suites (A2 type granite) and more rarely in peraluminous granite (S-type granite), where the episyenite generally corresponds to simple quartz dissolution. Unlike at Bokan Mountain, most of these occurrences result from hydrothermal fluid circulation disconnected from magmatic crystallization of the granite. Examples include the U-mineralized episyenite of the high-K calcalkalic Kab Amiri Granite, Central Eastern Desert, Egypt (Abdel-Monem *et al.* 1994), the barren episyenite from amphibole-bearing and biotite high-K calcalkalic granodiorite and monzogranite from the Central Iberian Massif, Spain (Recio *et al.* 1997), the Sn mineralized episyenite from the peraluminous topaz highly potassic calcalkalic granite of Agua Boa, Amazonas, northern Brazil, (Costi *et al.* 2002), the U–Zr mineralized episyenite related to the highly potassic calcalkalic Kurupung granite of Guyana (Cinelu & Cuney 2006), the barren episyenite from the high-K calcalkalic Bohus Granite of Sweden (Gerasimovsky *et al.* 1997), the slightly U–Th–REE mineralized episyenite of Les Bombes, southeast French Massif Central, in the high-K calcalkalic granite of La Borne (Cathelineau 1987), and the barren episyenite of the Salvezines peraluminous granite, French Pyrénées, (Boulvais *et al.* 2007).

Other world occurrences of mineralized peralkaline granite

The albite–riebeckite granites of Kaffo Valley, Nigeria, have many similarities with Bokan Mountain (Orajaka 1986). They are post-tectonic intrusions of peralkaline character with vein and disseminated uranium deposits.

Poços de Caldas U–Mo–Zr mineralization (Brazil). Poços de Caldas (São Paulo and Minas Gerais states) is one of the largest peralkaline complexes in the world, extending over some 800 km² (Schorscher & Shea 1992). Similar to Ilimaussaq, it is composed of a silica-undersaturated igneous suite. The igneous complex forms a nearly perfect circular ring structure of caldera type, about 28 km in diameter (Fig. 4-12). It is emplaced in the Guaxupé block, between the Paraná basin and São Francisco craton. Widespread alkaline-carbonatite and alkaline magmatism with both potassic-ultrapotassic and sodic affinities occurred in the area from 90 to 54 Ma. Ulbrich *et al.* (2002) proposed a date of 79 Ma as the age for the emplacement of the main nepheline syenite and phonolite of the Poços de Caldas complex with a duration of about 1–2 m.y. for the entire felsic magmatism. Two $^{40}Ar/^{39}Ar$ ages (75.7 ±0.3 and 76.2 ±0.8 Ma) for phlogopite from a fresh lamprophyric dike cross-cutting hydro-thermally altered nepheline syenite and phonolite from the Osamu Utsumi open pit U mine (Shea 1992) show that the duration for the entire magmatism may be well in excess of 5 m.y. (Vlach *et al.* 2002).

The Poços de Caldas massif was formed by multiple magmatic intrusions of phonolite–nepheline-syenite compositions, and by basanite–tephrite–ankaramite volcanic rocks successively intruded by phonolitic and lamprophyric dykes (Lustrino *et al.* 2003). The rocks are mainly phonolite (~80% of the outcrops) and nepheline syenite (~14%), generally very potassic. Sodic breccia, agglomerate, tuff made of tephrite with subordinate ankaramite, nephelinite, and phonotephrite are all sodic and occur at the western margin of the massif. Dikes of tephrite, trachybasalt, and basaltic trachyandesite occur to the northwest. Mafic-ultramafic dikes of lamprophyric to carbonatitic affinity occur within the Osamu Utsumi pit. Ultramafic lamprophyric with alnöitic affinity and siliceous carbonatite dikes intrude the Neoproterozoic quartz mangerite near the northern borders of the complex.

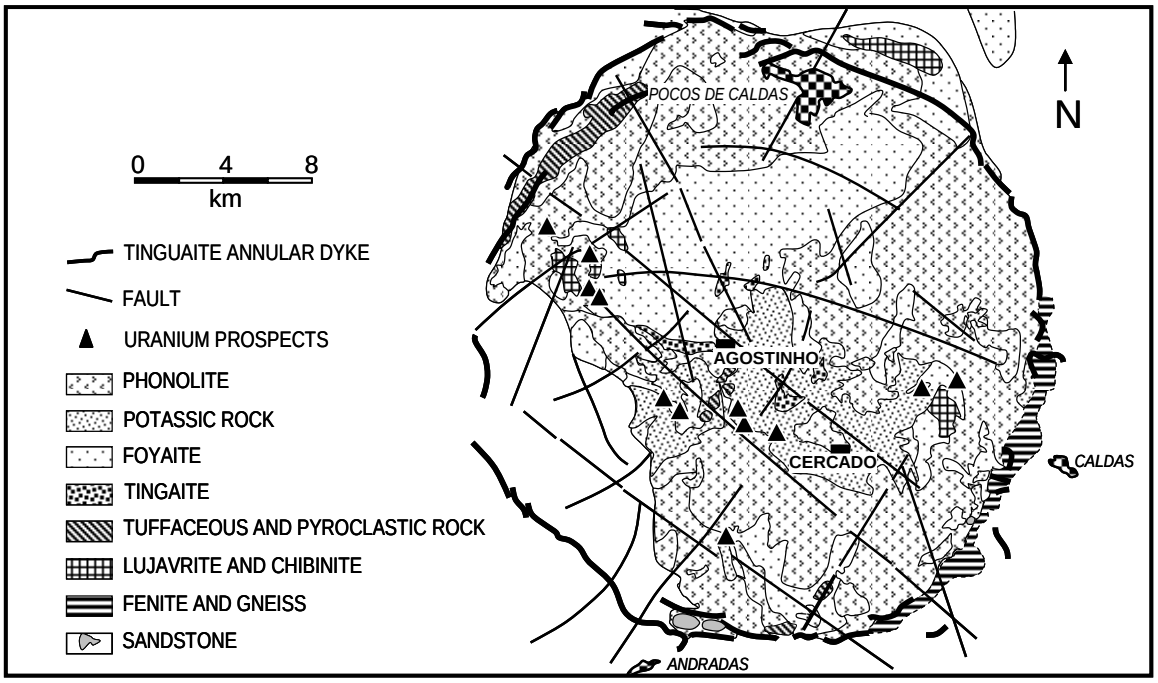

FIG. 4-12. Geologic map of the Poços de Caldas peralkaline complex with the location of the main uranium ore deposits and showings (modified from Fraenkel *et al.* 1985).

Phonolite is very fine grained and composed of K-feldspar, nepheline, clinopyroxene with diopside cores to hedenbergite and aegirine–augite rims, titanite, and rare Ti-magnetite. Peralkaline phonolite is characterized by astrophyllite $(K,Na)_3(Fe,Mn)_7Ti_2(SiO_3)_8(O,OH)_7$, eudialyte–hainite $Na_4Ca_8(Ti,Zr,Mn,Fe)_3(SiO_2)8F_8$, arfvedsonite, aenigmatite $(Na_2Fe^{2+}{}_5TiSi_6O_{20})$, sodalite, and fluorite. Nepheline syenite has approximately the same mineralogy as the phonolite, but contain less than 20 vol.% of mafic minerals, with occasional sodalite, arfvedsonite, and biotite. The occurrence of eudialyte-rich variants (lujavrite) is rare. Zircon is ubiquitous.

Most of the rocks are very poor in SiO_2 and Mg and rich in Fe, as are classical peralkaline rocks, but these rocks are also characterized by very low Na content and strong enrichment in K, which results at least partially from late stage K-metasomatism (Table 4-6). High-K compositions with strong U, Y, and REE enrichments also characterize the mafic-ultramafic lamprophyre dikes. Several late carbonatitic veins (5–20 cm wide) cross-cut all the above rocks. Some of them are made up of almost pure calcite, others contain calcite + fluorite, calcite + phlogopite + fluorite, calcite + phlogopite + magnetite + apatite, calcite + phlogopite + fluorite ± albite. Occasionally they contain thorite, REE fluorcarbonates, and accessory minerals.

Six stages have been recognized in the complex formation:

(i) volcanic activity;
(ii) caldera formation;
(iii) alkaline magmatic activity;
(iv) annular dike formation;
(v) foidite, chibinite, and lujavrite intrusions,
(vi) ultramafic dyke emplacement.

Two large fault systems with predominant directions of N60W and N40E occur in the alkaline complex. The former is correlated with the regional tectonic and the latter with the caldera formation processes (Fraenkel *et al.* 1985).

In the Poços de Caldas peralkaline complex, the 48 radioactive showings can be grouped into three associations: U–Zr, Th–REE, and U–Mo (Oliveira 1974, Fraenkel *et al.* 1985, Waber *et al.* 1992). The U–Zr association is the most common one in alluvial and eluvial type deposits. The Th–REE association is the second most common one, especially in the Morro do Ferro deposit. The U–Mo association occurs in lodes and lenticular bodies and forms the mined deposits. Using from satellite image analysis Almeida & Paradella (1976) proposed the existence of 7 secondary circular structures and showed that all the radioactive anomalies are located along the borders of these structures.

TABLE 4-6. COMPOSITIONS OF SELECTED UNMINERALIZED AND MINERALIZED ROCKS OF THE POÇOS DE CALDAS PERALKALINE COMPLEX, BRAZIL

wt%	84-56	84-57	84-45	84-46	84-58	84-44	84-47
SiO_2	56.81	55.06	58.65	59.93	54.98	55.09	56.6
Al_2O_3	22.89	23.78	24.14	22.49	21.43	20.92	21.29
Fe_2O_3t	3.11	3.29	1.46	1.23	3.88	3.73	4.2
MnO	0.24	0.25	0.02	0.01	0.58	0.52	0.02
MgO	bdl	bdl	0.03	0.2	bdl	0.27	0.15
CaO	bdl	bdl	bdl	bdl	0.91	1.22	bdl
Na_2O	0.09	0.22	0.19	0.06	0.3	1.79	0.13
K_2O	12.95	12.63	13.26	13.77	12.75	10	13.42
TiO_2	0.53	0.65	0.51	0.37	0.63	0.45	0.4
P_2O_5	0.12	bdl	0.15	0.17	bdl	0.11	0.16
IL	3.63	3.74	3.25	2.01	3.33	5.61	3.62
Total	100.37	99.62	99.86	100.24	98.79	99.71	99.99
F ppm	1100	1100	900	600	700	900	700
CO_2 %	0.27	0.27	0.05	0.05	1	1.61	0.07
P	273	262	276	291	245	133	281
Q	37	30	37	38	13	21	25
B	46	49	25	25	56	59	61
A	171	191	185	146	107	96	128
Ba ppm	634	1845	409	459	1088	1142	473
Co	<10	<10	<10	<10	<10	<10	<10
Cr	56	<10	<10	<10	<10	11	<10
Cu	<10	<10	<10	<10	<10	<10	<10
Ni	<10	<10	<10	<10	<10	<10	<10
Sr	468	235	132	255	331	335	561
V	312	177	398	179	128	186	238
Rb	346	532	463	432	501	520	500
U	15.6	14.5	62	78.5	29	345	963
Th	51	41	30	91	38	35	47
Th/U	3.27	2.84	0.48	1.15	1.28	0.10	0.05

84-56: massive foyaite, CDSC262–596m; 84-57: foyaite, CDSC262–622 m ; 84-45: sulfide foyaite, open pit; 84-46: ocellar foyaite, open pit; 84-58: tingaite, CDSC262–602 m ; 84-44: tinguaite breccia, open pit; 84-47: mineralized tinguaite contact ore E – B; bdl: below detection limit (M. Cuney, unp. data).

The Osamu Utsumi U mine (also named Cercado), which comprises the ore bodies A, B, and E, covers an area of about 2.5 km^2 at the southern margin of a major secondary circular structure called Planalto (Fig. 4-12). The Agostinho deposit is located at the northeastern margin of the Planalto structure (Fig. 4-12). Ore bodies A and B are hosted by tinguaite and phonolite of the internal part of the Planalto structure, whereas the ore body B is hosted by pyroclastic rocks, including various types of phonolite, tuff, and breccia cross-cut by dikes of ultrabasic rocks and overlying a foyaite along the circular structure. Several breccia pipes cut these formations. Ore body A has an extension of 900 by 500 m. It comprises near-vertical breccia veins in which U has been leached out from the upper part, with redeposition at a subhorizontal redox front at a depth of –100 m (Lichtner & Waber 1992). Ore body E has an extension of 1100 m by 500 m and the mineralization occurs at a depth of –150 m. The mineralization here is totally epigenetic and only located along a subhorizontal redox front. Ore body B has an extension of 1400 m by 400 m. The lower part of the mineralization corresponds to hydrothermal deposition of U in lenticular bodies developed in the porous pyroclastic rocks and intersected by mineralized breccia pipes rich in fluorite. Secondary U mineralization is also developed at the redox interface. In the Agostinho deposit, the U mineralization is restricted to a near-vertical breccia body. The U mineralization seems to result from the combination of magmatic and late magmatic–hydrothermal fractionation as in all other world occurrences, but part of the economic mineralization results from an overprinting by supergene alteration (lateritization). The U–Zr–REE mineralization is concentrated in the matrix of the breccias. Unlike at Ilímaussaq and Bokan Mountain, Th is not significantly enriched during the mineralization process at Poços de Caldas, despite the occurrence of fluorine in the system (Table 4-6). Hydrothermal alteration following the formation of the breccia has resulted in the potassic alteration and pyritization of the hosting phonolite and syenite. Small fluorite and pyrite veins are also common. All feldspars of the initial rocks are transformed into pure potassic feldspars, nepheline into illite and kaolinite, and clinopyroxenes into a mixture of TiO_2-rich minerals, clay minerals, and pyrite. In this alteration zone K, S, U, Pb, Rb, Ba, and Mo are strongly enriched, whereas Ca, Na, Mg, and Sr are depleted. Fluid inclusion data indicate relatively low temperatures for the alteration process, around 250°C, and aqueous fluid compositions with approximately 7 wt.% KCl. In the breccia pipes where Zr, Hf, F, and minor REE are enriched, fluid inclusion data indicate boiling of a brine with a temperature of 210°C and 40–45 wt.% KCl–NaCl together with $FeSO_4$ and KF. Higher temperature fluids of magmatic origin should have been involved in these processes to explain the formation of the breccia pipes, the Zr, Hf, F, and REE enrichment, the occurrence of uraninite, and the $\delta^{34}S$ values of the hydrothermal pyrites near 0‰, but such fluids have not been observed.

The main U minerals are uraninite with 2 wt.%

Th, coffinite, and brannerite. The major REE mineral is monazite and the main Zr minerals are zircon and baddeleyite associated with jordisite (MoS_2), pyrite, galena, sphalerite, and fluorite in the high-grade mineralization of the breccia. Low-grade pitchblende mineralization occurs in the altered host rocks. The ultramafic dikes of the open pit are dated at 76 Ma, putting a lower age limit to this early mineralization event.

Subsequently, lateritic weathering led to the oxidation of the sulfides to iron hydroxides–oxides and alunite–jarosite to depths of 80 to 140 m below surface and to greater depths along fractures. The resulting redox front is typically marked by a change from reddish-brown oxidized to bluish-grey reduced rocks. A secondary mineralization of pitchblende, partly occurring as nodules associated with secondary pyrite, has been developed at this redox front. This secondary pyrite has low $\delta^{34}S$ (−13‰) attributed to microbial activity.

In the immediate vicinity of the redox front, K-feldspar is altered to kaolinite. Gibbsite is present at the saprolite–laterite contact. Part of the U is adsorbed on poorly crystalline phases. Only a slight loss of REEs, mainly the LREEs, is observed between oxidized and reduced rock. REEs are mainly trapped as clay-sized crandallite group minerals. Selective fractionation of Ce, typical of lateritic weathering, is observed. Zr occurs in caldasite, a U- and Th-bearing mixture of fibrous baddeleyite (ZrO_2) and in metamict zircon (Tolbert 1966). Caldasite forms a significant part of the ore.

Weathering of Poços de Caldas has required up to 2 m.y. in the absence of pyrite, and up to 0.5 m.y. when pyrite was present at the Osamu Utsumi U mine. A large proportion of the U mined at Poços comes from these weathering redox fronts. The resources estimated in 1985 were 22,780 t U, 25,000 t Mo_2O_3 and 172,400 t ZrO_2 (Fraenkel *et al.* 1985). Between 1982 and 1995 the cumulative U production was 1,030 t U from Poços de Caldas.

Thor Lake (Canada). The Thor Lake deposits in the Great Slave Lake district are related to a nearly circular (16 by 33 km), high level peralkaline complex, the Blatchford Lake Intrusive Suite. They consist mainly of Be, Y, REE, Nb, Ta, Zr, and Ga deposits (Davidson 1982), but Th and U mineralization are also known in the area. The Thor Lake area has peralkaline intrusions in association with less fractionated plutonic units. The Blatchford Lake complex consists of an earlier suite of gabbro, quartz syenite and granite, and the later intrusion of the large Grace Lake Granite, intruded itself in its core by the Thor Lake Syenite. The two members of the late suite are peralkaline and classically show a noticeable enrichment in Fe, Mn, Na, Nb, REE, F, and partially in Be and Li. The granite and syenite are characterized by moderately high K_2O (4.6% on average), average U (3 ppm) and Th (18 ppm) contents and a Th/U ratio of 6. Principal radioactive minerals in these rocks are zircon and bastnaesite with minor REE-rich apatite and monazite. Felsic dikes within the Grace Lake Granite and Thor Lake Syenite are one order of magnitude richer in U and Th than host rocks and are also enriched in elements occurring in the Thor Lake deposits.

The suite intrudes Archean metasedimentary rocks and calc-alkalic granitoid intrusions of the Slave Province to the north and is proximal to Paleoproterozoic metasedimentary rocks, metavolcanic rocks, and intrusions of the Athapuscow aulacogen of Great Slave Lake on the south. The Hearne Channel Granite and the Thor Lake Syenite have been dated by U–Pb in zircon at 2175 ±10 and 2094 ±10 Ma, respectively (Bowring *et al.* 1984). The Grace Lake granite is reddish pink to buff to pale gray, coarse-grained, equigranular rock. It is a hypersolvus granite with mesoperthitic alkali feldspar, quartz and riebeckite. Accessory minerals include fluorite, magnetite, zircon, carbonates and phenacite. The Thor Lake Syenite is medium- to coarse-grained, hypersolvus with perthitic alkali feldspar, riebeckite, and minor quartz. Accessory minerals include magnetite, zircon and ferromagnesian mica. A pyroxene–olivine-bearing syenite forms a thin rim along the margins of the syenite body and subhorizontal pods and sheets of syenite pegmatite occur within it. Contact between granite and syenite is transitional in the western part. In the north and east, the granite dips under the syenite and the contact is sharp.

Most mineralized zones occur within the western part of the Thor Lake syenite. The deposits are related to albitite or greisen. For example, the core is occupied by breccia composed of syenite pegmatite clasts cemented by a fine- to coarse-grained matrix of albite and ferromagnesian mica. Accessory minerals include zircon, uranothorite, allanite, magnetite, hematite, columbite, pyrochlore, carbonates, bastnaesite, and lanthanite. Quest Uranium Corporation in the Thor Lake area has reported average assays of 535 ppm U from 196 channeled samples. U occurs in an east–west trending pegmatite dike complex that can be traced over a strike length of 2.5 km and widths of up to 400 m.

Palabora carbonatite (South Africa). The peralkaline Palabora intrusive complex was emplaced at about 2030 ±18 Ma in Archean formations in north-eastern Transvaal (Eriksson 1984). The successive intrusions comprise a kidney-shaped pyroxenite followed by a syenite and ultrabasic pegmatoid units. The apatite–phlogopite-rich pyroxenite extends over 6 by 2.5 km and forms a pipe at depth. The ultrabasic pegmatoid rocks intruded the pyroxenite in three localities. In the central one, phoscorite (a magnetite–olivine bearing rock) and carbonatite form the Loolekop pipe (1.4 by 0.8 km). This pipe has been intruded by a dike-like banded carbonatite. In the late carbonatite at Loolekop repeated fracturing was associated with fluid percolation responsible for the deposition of chalcopyrite and minor cubanite in vertical veins. Sets of parallel veins may occur over a width of 10 m, but individual veinlets are less than 1 cm thick and less than 1 m long. The ore grade is about 1% Cu. In the phoscorite, magnetite with up to 4 wt.% TiO_2 may reach 25–50 vol.%. Apatite reaches economic grade in the phoscorite. Baddeleyite occurs in both the phoscorite and the carbonatite.

Sulfur isotopes and fluid inclusions show that the fluids depositing Cu were derived from carbonatitic magma (Eriksson 1989). The Cu ore body is hosted in a carbonatite pipe with grades highest (1.0% Cu) at the core. Drilling has shown that the ore body extends beyond a depth of 1000 m. Ore reserves are in the order of 300 Mt Cu at 0.69% Cu.

The main U- and Th-bearing mineral is uranothorianite, $(U,Th)O_2$, a quite exceptional mineral in U deposits. Its crystallization necessitates the absence of quartz in the host rock, because the presence of silica leads to the formation of uranothorite. It is recovered as a heavy mineral together with baddeleyite and processed for U production. Thucholite, a variety of Th–U rich pyrobitumen. has been observed in fractures in the center of the transgressive carbonatite. The average U content of the ore body is 25 ppm (Verwoerd 1986).

Palabora Mining Company started U production in 1994 as a by-product of the Palabora Cu mine. The mine yielded a cumulative production of 640 t U and the U treatment circuit was stopped in 2002. Th may become a significant product in the future, with the development of a Th reactor. The uranothorianite contains more than twice the Th compared to U (55.82 wt.% ThO_2, 26.65 wt.% UO_2, 13.40 wt.% PbO, 4.12 wt.% REE_2O_3). With an average grade of 0.01 % Th, the carbonatite should contain about 10,500 t Th for every 100 m of depth (Verwoerd 1986).

Another carbonatite with potential U and Th resources is the Eldor in the Labrador Trough, Québec. Commerce Resources Corp. reported an average U content of 200 ppm on 60 rock samples (85–1400 ppm U). However, the most common U- and Th-bearing phase in this carbonatite is pyrochlore, which cannot be easily leached for production of U.

REFERENCES

ABDEL-MONEN, A.A., HUSSEIN, H. A., EL-TAHER, M.A. & SALEH, E.A. (1994): Radioactivity and origin of U-mineralization at the Kab Amiri area, Central Eastern Desert, Egypt. *Radiation Phys. & Chem.* **44**, 207-214.

ALMEIDA FILHO, R. & PARADELLA, W.R. (1976): Estudo do Maciço Alcalino de Poços de Caldas Através de Imagens Landsat com Ênfase em Mineralizações Radioativas. MSc. Thesis in Remote Sensing, São José dos Campos, INPE Report **1112**-TPT/06, 130 p.

ANDERSEN, S., BAILEY, J.C. & BOHSE, H. (1981): Zr–Y–U stratigraphy of the kakortokite–lujavrite sequence, southern Ilímaussaq intrusion. Report *Grønlands Geologiske Undersøgelse* **103**, 69–76.

ARMOUR-BROWN, A., TUKIAINEN, T. & WALLIN, B. (1982): Pitchblende vein discoveries in the Proterozoic Ketilidian granite of South Greenland. *Internat. J. Earth Sci.* **71**, 73-80.

BAILEY, J.C. (2006): Geochemistry of boron in the Ilímaussaq alkaline complex, South Greenland. *Lithos* **91**, 319-330.

BAILEY, J.C., GWOZDZ, R., ROSE-HANSEN, J. & SØRENSEN, H. (2001): Geochemical overview of the Ilímaussaq alkaline complex, South Greenland. In: Sørensen, H. (ed.): The Ilímaussaq complex, South Greenland: status of mineralogical research with new results. *Geology of Greenland Survey, Bulletin* **190**, 35-53.

BAILEY, J.C., SØRENSEN, H., ANDERSEN, T., KOGARKO, L.N. & ROSE-HANSEN J. (2006): On the origin of microrhythmic layering in arfvedsonite lujavrite from the Ilímaussaq alkaline complex, South Greenland. *Lithos* **91**, 301-318.

BALASHOV, Y. A. (1968): The geochemistry of the Lovozero alkaline massif: Canberra, Australian Natl. Univ. Press, 395 p. (English translation by D.A. Brown).

BOHSE, H., ROSE-HANSEN, J., SØRENSEN, H., STEENFELT, A., LOVBORG, L. & KUNZENDORF, H. (1974): On the behavior of uranium during crystallization of magmas – with special emphasis on alkaline magmas *In* Formation of Uranium Ore Deposits. Vienna, Internat. Atomic Energy Agency, p. 49-60.

BONDAM, J. & SØRENSEN, H. (1959): Uraniferous nepheline syenites and related rocks in the Ilímaussaq area, Julienhab district, South West Greenland. *Proc. 2nd Intern. Conf. U.N. Peace. Atom. Energy* **2**, 555-559.

BOULVAIS, P., RUFFET, G., CORNICHET, J. & MERMET, M. (2007): Cretaceous albitization and dequartzification of Hercynian peraluminous granite in the Salvezines Massif (French Pyrénées). *Lithos* **93**, 89-106.

BOWDEN, P. & TURNER, D.C. (1974): Peralkaline and associated ring-complexes in the Nigeria–Niger Province, West Africa. *In* The Alkaline Rocks, Sørensen J. (*ed.*). John Wiley and Sons, New York, 330-352.

BOWRING, S A, VAN SCHMUS, W.R. & HOFFMAN, P.F. (1984): U-Pb zircon ages from Athapuscow aulacogen, East Arm of Great Slave Lake, N.W-T., Canada. *Can. J. Earth Sci.* **21**, 1315-132.

BRIDGWATER, D. & HARRY, W.T. (1968): Anorthosite xenoliths and plagioclase megacrysts in Precambrian intrusions of South Greenland. *Bulletin Grønlands Geologiske Undersøgelse* **77**, 243 pp.

CATHELINEAU, M. (1987): U-Th-REE mobility during albitization and quartz dissolution in granitoïds: evidence from south-east French Massif Central. *Bull. Minéralogie* **110**, 249-259.

CHURKIN, M. & EBERLEIN, G.D. (1977): Ancient borderland terranes of the North American Cordillera; correlation and microplate tectonics. *Geol. Soc. Am., Bull.* **88**, 769-786.

CINELU, S. & CUNEY M. (2006): Sodic metasomatism and U–Zr mineralization: A model based on the Kurupung batholith (Guyana). Abstract, *Geochim. Cosmochim. Acta* **70**, A103.

CLAUSEN, F.L. (1982): A Geostatistical Study of the Uranium Deposit at Kvanefjeld, the Ilímaussaq Intrusion, South Greenland. Risø National Laboratory, Roskilde, Denmark, Report Risø-R-**468**, 289 p.

COLLOT, B. (1981): Le granite albitique hyperalcalin de Bokan Mountain (SE Alaska) et ses minéralisations U-Th. Sa mise en place dans la cordillière canadienne. Unpubl. PhD Thesis, Montpellier University, 238 p.

COSTI, H.T., DALL'AGNOL, R., BORGES, R.M.K., MINUZZI, O.R.R. & TEIXEIRA, J.T. (2002): Tin-Bearing Sodic Episyenites Associated with the Proterozoic, A-Type Água Boa Granite, Pitinga Mine, Amazonian Craton, Brazil. *Gondwana Res.* **5**, 435-451.

DAVIDSON, A. (1982): Petrochemistry of the Blachford Lake complex near Yellowknife, Northwest Territories. In Y. T. Maurice, Ed , Uranium in Granites, *Geol. Surv. Can. Paper* **8l-23**, 71-80.

DEBON, F. & LEFORT P. (1988): A cationic classification of common plutonic rocks and their magmatic associations: principles, method, applications. *Bull. Minéralogie* **111**, 493-510.

DE SAINT ANDRÉ, B., LANCELOT, J.R. & COLLOT, B. (1983): U–Pb geochronology of the Bokan Mountain peralkaline granite, southeastern Alaska. *Can. J. Earth Sci.* **20**, 236–245.

ERIKSSON, S.C. (1984): Age of the carbonatite and phoscorite magmatism of the Phalaborwa Complex (South Africa). *Isotope Geosci.* **2**, 291-299.

ERIKSSON, S. C. (1989): The Phalaborwa Complex: A Saga of Magmatism, Metasomatism and Miscibility. *In* K. Bell (*ed*), Carbonatites, Allen and Unwin, Toronto, 221-254.

FERGUSON, J. (1964): Geology of the Ilímaussaq alkaline intrusion, South Greenland. *Bull. Grønlands geol. Unders.* **39**.

FERGUSON, J. (1970): The differentiation of agpaitic magmas: The Ilímaussaq intrusion, South Greenland, *Can. Mineral.* **10**, 335-349.

FRAENKEL, M.O., SANTOS, R.C. DOS, LOUREIRO, F.E.V., DE, V.L. & MUNIZ, W.S. (1985): Jazida de urânio no Planalto de Poços de Caldas - Minas Gerais. - Capítulo V . IN: Ministério das Minas e Energia - Recursos Minerais Energéticos – Departamento Nacional da Produção Mineral - Companhia Vale do Rio Doce. Volume I. Principais Depósitos Minerais do Brasil. Brasília, 89-103.

GAMBORG-HANSEN, J.K. (1977): Sulphatising roasting of a Greenlandic uranium ore, reactivity of minerals and recovery. *RISØ Nat. Lab. Rep.* **355**.

GERASIMOVSKY, H.R.I., VOLKOV, V.P., KOGARKO, L.N., POLYAKOV, A. I., SAPRYKINA, T. V., PETERSSONA, J. & ELIASSON, T. (1997): Mineral evolution and element mobility during episyenitization (dequartzification) and albitization in the postkinematic Bohus granite, southwest Sweden. *Lithos* **42**, 123-146.

HANSEN, J. (1968): A study of the radioactive veins containing rare earth minerals in the area surrounding the Ilímaussaq alkaline intrusion in South Greenland. Contrib. to the Mineralogy of Ilimaussaq, **12**. *Greenland Geol. Surv.* 47 p.

JAVOY, M. & WEISS, D. (1987): Oxygen isotopic composition of alkaline anorogenic granites as a clue to their origin: the problem of crustal oxygen. *Earth Planet. Sci. Lett.* **84**, 415-422.

KARUP-MØLLER, S. (1978): The ore minerals of the Ilímaussaq intrusion: their mode of occurrence and their conditions of formation. *Bulletin Grønlands Geologiske Undersøgelse* **127**, 51 pp.

KHOMYAKOV, A.P. (1995): Mineralogy of Hyperagpaitic Alkaline Rocks, 223 pp. Oxford, Clarendon Press.

KHOMYAKOV, A.P. & SØRENSEN, H. (2001): Zoning in steenstrupine-(Ce) from Ilímaussaq alkaline complex, South Greenland: a review and discussion. *Geol. Greenland Surv. Bull.* **190**, 109-118.

KONNERUP-MADSEN, J. & ROSE-HANSEN, J. (1984): Composition and significance of fluid inclusions in the Ilímaussaq peralkaline granite, South Greenland. *Bull. Minéralogie* **107**(2), 317–326.

KONNERUP-MADSEN, J., DUBESSY, J. & ROSE-HANSEN, J. (1985): Combined Raman microprobe spectrometry and microthermometry of fluid inclusions in minerals from igneous rocks of the Gardar province (south Greenland). *Lithos* **18**, 271–280.

KONNERUP-MADSEN, J., KREULEN, R. & ROSE-HANSEN, J. (1988): Stable isotope characteristics of hydrocarbon gases in the alkaline Ilímaussaq complex, South Greenland. *Bull. Minéralogie* **111**, 567–576.

KRUMREI, T.V., VILLA, I.M., MARKS, M.A.W. & MARKL, G. (2006): A 40Ar/ 39Ar and U/Pb isotopic study of the Ilímaussaq complex, South Greenland: Implications for the 40K decay constant and for the duration of magmatic activity in a peralkaline complex. *Chem. Geol.* **227**, 258–273.

LARSEN, L.M. & SØRENSEN, H. (1987): The Ilímaussaq intrusion – progressive crystallization and formation of layering in an agpaitic magma. *In* Fitton, J.G. and Upton, B.G.J. (*eds.*) Alkaline Igneous Rocks. *Geol. Soc. London Special Publ.* **30**, 473–488.

LICHTNER, P.C. & WABER, N. (1992): Redox front geochemistry and weathering: theory with application to the Osamu Utsumi uranium mine, Poços de Caldas, Brazil. *J. Geochem. Explor.* **45**, 521-564.

LUSTRINO, M., DALLAI, L., GIORDANO, R., GOMES, C.B., MELLUSO, L., MORBIDELLI, L., RUBERTI, E. & TASSINARI, C.C.G. (2003): Geochemical and Sr-Nd-O isotopic features of the Poços de Caldas alkaline massif (SP-MG, SE Brazil): relationships with the Serra do Mar analogues. in *IVth South American Symposium on Isotope Geology*, 593-595.

MACKEVETT, E.A. (1963): Geology and ore deposits of the Bokan Mountain uranium-thorium area, southeastern Alaska: *U.S. Geol. Survey Bull.* **1154**, 125 p.

MAKOVICKY, M., MAKOVICKY, E., NIELSEN, B.L., KARUP-MØLLER, S. & SØRENSEN, E. (1980): Mineralogical, radiographic and uranium leaching studies on the uranium ore from Kvanefjeld, Ilímaussaq Complex, South Greenland. Risø R-416, 186 pp. Roskilde, Denmark: Risø National Laboratory.

MARKL, G., MARKS, M., SCHWINN, G. & SOMMER, H. (2001): Phase Equilibrium Constraints on Intensive Crystallization Parameters of the Ilímaussaq Complex, South Greenland. *J. Petrol.* **42**, 2231-2257.

OLIVEIRA A.G. (1974): Mineralizaçao de uranio e molbdenio no Planalto de Poços de Caldas, Minas Gerais. Ann XXVIII Congr. Bras. Geol., Vol. I, 207-221.

ORAJAKA, I. P. (1986): Geochemistry of Kaffo Valley albite-riebeckite-granite, Liruei granite ring-complex northern Nigeria. *Chem. Geol.* **56**, 85-92.

PLIVO, R.G., WILLIAMS-JONES, A.E. (1999): Hydrothermal REE-rich Eudialyte from the Pilanesberg complex, South Africa. *Can. Mineral.* **37**, 653-663.

RECIO, C., FALLICK, A.E., UGIDOS, J.M. & STEPHENS W.E. (1997): Characterization of multiple fluid-granite interaction processes in the episyenites of Avila-Béjar, Central Iberian

Massif, Spain. *Chem. Geol.* **143**, 127-144.

SCHORSCHER H.D. & SHEA M.E. (1992): The regional geology of the Poços de Caldas alkaline complex: mineralogy and geochemistry of selected nepheline syenites and phonolites. *J. Geochem. Explor.* **45**, 25-51.

SEMENOV, E.I. (1997): Minerals and ores of the Khibiny–Lovozero alkaline massif, Kola, 1, 2, 42 pp., 70 pp. Moscow: Russian Academy of Sciences, Fersman Mineralogical Museum.

SHEA, M.E. (1992): Isotopic geochemical characteristics of selected nepheline syenites and phonolites from the Poços de Caldas alkaline complex, Minas Gerais, Brazil. *J. Geochem. Explor.* **54**,173-214.

SØRENSEN, H. (ed.) (2001): The Ilímaussaq complex, South Greenland: status of mineralogical research with new results. *Geol. Greenland Surv. Bull.* **190**, 167 pp.

SØRENSEN, H. & LARSEN, L.M. (2001): The hyper-agpaitic stage in the evolution of the Ilímaussaq alkaline complex, South Greenland. *In* Sørensen, H. (*ed.*): The Ilímaussaq complex, South Greenland: status of mineralogical research with new results. *Geol. Greenland Surv. Bull.* **190**, 83-94.

SØRENSEN, H., BOHSE, H. & BAILEY, J.C. (2006): The origin and mode of emplacement of lujavrites in the Ilímaussaq alkaline complex, South Greenland. *Lithos* **91**, 286-300.

SØRENSEN, H., ROSE-HANSEN, J., NIELSEN, B. L., LØVBORG, L., SØRENSEN, E. & LUNDGAARD, T. (1974): The uranium deposit at Kvanefjeld, the Ilímaussaq intrusion, South Greenland. *Report Grønlands Geologiske Undersøgelse* **60**, 54 pp.

STAATZ, M.H., ARMBRUSTMACHER, T.J., OLSON, J.C., BROWNFIELD, I.K., BROCK, M.R., LEMONS, J.F., COPPA, L.V. & CLINGAN, B.V. (1979): Principal thorium resources in the United States: *U.S. Geol. Surv. Circular* **805**, 42 p.

THOMPSON, T.B. (1988): Geology and uranium-thorium mineral deposits of the Bokan Mountain Granite Complex, southeastern Alaska. *Ore Geol. Rev.* **3**, 193-210.

TOLBERT, J. (1966): The uraniferous zirconium deposits of the Poços de Caldas plateau, Brazil. *U.S. Geol. Surv. Bull.* **1185 C**, 28p.

ULBRICH, H.H.G.J., VLACH, S.R.F., ULBRICH, M.N.C. & KAWASHITA, K. (2002): Penecontemporaneous syenitic-phonolitic and basic-ultrabasic-carbonatitic rocks at the Poços de Caldas alkaline massif, SE Brazil: geological and geochronological evidence. *Revista Brasileira de Geociências* **32**, 15-26.

VERWOERD, W.J. (1986): Mineral deposits associated with carbonatites and alkaline rocks. *In* Anhaeusser, C.R., and Maske S. (*eds*). Mineral Deposits of South Africa, Vol. I and II. Geol. Soc. S. Afr., Johannesburg, 2173-2192.

VLACH, S.R.F., VILALVA, F.C.J., ULBRICH, M.N.C., ULBRICH, H.H.G.J. & VASCONCELOS P.M. (2002): Phlogopite from carbonatitic veins associated with the Poços de Caldas alkaline massif, SE Brazil: mineralogy and $^{40Ar}/^{39}$Ar dating by the laser step heating method. in IVth South American Symposium on Isotope Geology, 702-705.

WABER, N., SCHORSCHER, H.D. & PETERS, T. (1992): Hydrothermal and supergene uranium mineralization at the Osamu Utsumi mine, Poços de Caldas, Minas Gerais, Brazil. *J. Geochem. Explor.* **45**, 53-112.

CHAPTER 5: DEPOSITS RELATED TO PARTIAL MELTING

Michel Cuney
G2R, Nancy-Université, CNRS, CREGU,
B.P. 239,
F-54506 Vandoeuvre lés Nancy, France
michel.cuney@g2r.uhp-nancy.fr

and

Kurt Kyser
Department of Geological Sciences and Geological Engineering,
Queen's University,
Kingston, Ontario, K7L 3N6, Canada
kyser@geol.queensu.ca

INTRODUCTION

The genesis of a uranium deposit is rarely related to a single mechanism, but we will classify deposits by the mechanism that appears to have been responsible for the formation of the major part of the metal stock. For example, partial melting is considered by the authors as the main primary genetic process for the Rössing deposit, although part of the mineralization results from the percolation of late magmatic fluids and another part from supergene enrichment as hexavalent U minerals.

There are four styles of U mineralization related to granite plutons. Three of these correspond to distinct magma chemistry involving peralkaline, metaluminous and peraluminous granite (see chapter 4), with each being characterized by a specific accessory mineral assemblage (Cuney & Friedrich 1987). The fourth style corresponds to granitoid rocks in migmatitic environments, which will be referred to as alaskite. Only this last type of granite and peralkaline granite are associated with U mineralization generated by high temperature magmatic to late-magmatic processes. The geneses of U deposits related to the two other granite types are not directly related to magmatic processes, but to lower temperature hydrothermal processes and therefore will be described in a separate chapter.

Deposits related to partial melting are those corresponding to uraninite enrichment disseminated in pegmatitic dikes and injected into high-grade migmatitic gneiss. They are called "pegmatoid" because the zonation that is commonly observed in pegmatite bodies derived from fractionation of large plutonic bodies is generally absent. The Rössing U deposit in Namibia is the most significant deposit related to partial melting processes (Berning *et al.* 1976, Cuney 1980, 1982). These deposits represent the most extreme temperature and pressure conditions for economic U mineralization, although the Rössing U deposit is one of the lowest grade U deposits ever mined.

THE RÖSSING DEPOSIT, NAMIBIA

General geology

Uranium mineralization associated with leucogranite dikes has been known since 1928. These granite dikes have been termed pegmatite by Smith (1965), potash granite by Nash (1971) and alaskite by the geologists of Rio Tinto Exploration. Rio Tinto began the first serious evaluation of alaskite-related deposits in 1966 and mining at Rössing started in 1976. The open pit presently extends over 3.5 km and down to 350 m. The U resources at a cost of US $80/kg are 142,000 metric tonnes of U at an average grade of about 300 ppm U. Total production by the end of 2007 was slightly over 90,000 tonnes U. In December 2005 the operational life of the mine was extended to 2016, with potential to extend to 2021. The deposit is situated approximately 55 km northeast of Swakopmund (Fig. 5-1), in the Namibian Desert. Several other deposits of the same type have been discovered in a similar geological setting, such as the SH and SK deposits immediately east and west of the Rössing deposit, respectively, and the Goanikontes, Ida, and Valencia deposits some tens of kilometres to the southwest and northeast.

Granitoid dikes hosting the U mineralization at Rössing appear to be derived from the partial melting of U-rich sedimentary rocks. U mineralization is further enriched during

Short course co-sponsored by the the SGA and MAC, Québec City, May 2008, p. 79-95

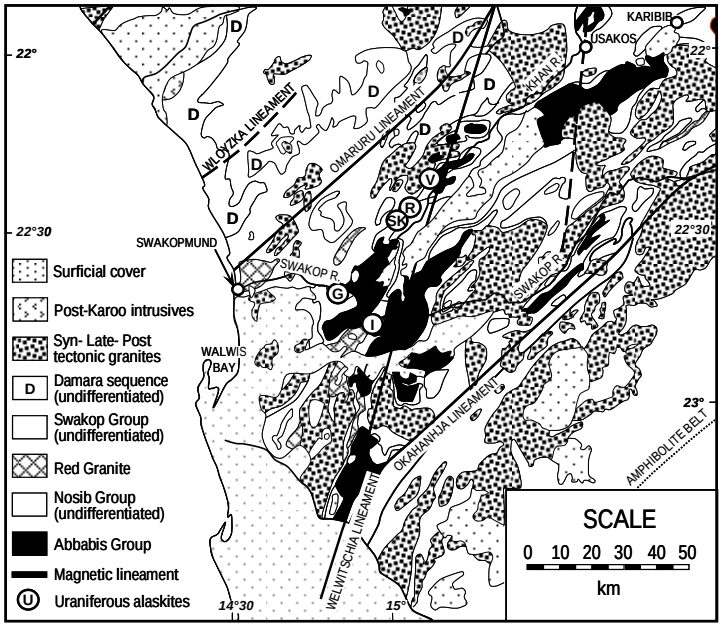

FIG. 5-1. Geological map of the southern part of the Damara Belt with the location of the main alaskitic U deposits: (V) Valencia, (R) Rössing, (SK) SK, (G) Goanikontes, (I) Ida (after Jacob *et al*. 1986).

emplacement of the alaskite by percolation of magmatic fluids through reducing metamorphic host rocks and by recent supergene weathering mainly in the upper part of the deposit.

Uraniferous alaskite bodies are located in strongly metamorphosed and partially migmatized rocks of the central and deeper portion of the Damara Pan-African belt between the Omaruru and Okahandja Lineaments (Fig. 5-1). The Damara Orogen belt belongs to the Neoproterozoic–Cambrian Pan-African mobile belt system composed of two branches, one parallel to the Atlantic coast, the Kaoko belt, separated from the Ribeira belt along the eastern coast of Brazil by the opening of the Atlantic Ocean, and another one transecting the African continent, oriented northeast. The orogen results from a triple continental collision between the Kalahari craton to the south, the Congo craton to the north, and São Francisco craton to the west. The ''Matchless Amphibolite'' to the south (Fig. 5-1) comprises tholeiitic metabasalt with N-MORB to E-MORB compositions (Schmidt & Wedepohl 1983) and represents the sliced upper part of an oceanic crust. This formation therefore corresponds to the suture formed by the northerly dipping subduction of the Damaran Ocean between 750 and 520 Ma ago. Early crustal thinning took place around 700 Ma ago and may have been accompanied by limited seafloor spreading.

The Central Zone of the northeast branch comprises metamorphic polyphase deformed rocks of the Damara sequence, resting uncomfortably on the Mesoproterozoic gneissic and volcano-sedimentary Abbabis Complex, which has a minimum age of 1038 Ma from the Kibaran granitoid rocks that intruded them (Kröner *et al.* 1991). The metamorphic grade increases from east to west reaching high-grade conditions with local partial melting in the coastal area.

The sedimentary package (Table 5-1 and Fig. 5-2) was deposited in an epicontinental platform of a passive margin environment. In the western part of the 400 km wide northeastern branch of the Damara belt, sedimentation began at 900–800 Ma on the Mesoproterozoic Abbabis granite-gneiss, in three independent intracontinental rifts oriented nearly east–west. The 40 km wide grabens are mainly filled with high-energy siliciclastic

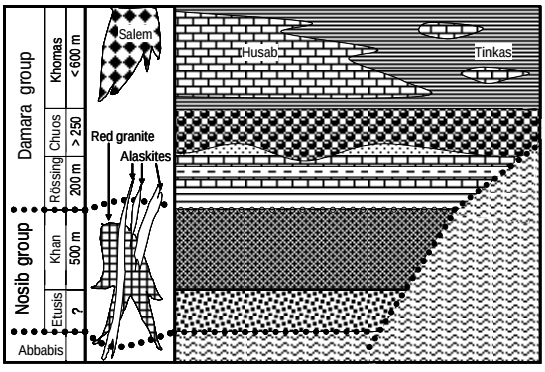

FIG. 5-2. Lithostratigraphic succession of the Damara sedimentary rocks and level of emplacement of the different types of granitoid rocks in the Rössing area.

Table 5-1. LITHOSTRATIGRAPHY OF THE CENTRAL PART OF THE DAMARA BELT

Formation			Lithology	Accessory minerals
Swakop Group	Khomas	Tinkas (Kuiseb)	Pelitic schist (biotite, muscovite, cordierite, sillimanite)	
		Karibib (Husab)	Dolomitic and calcitic marble	
		Chuos < 250 m	Glaciomarine diamictite	
	Rössing 200 m to absent		Metaquartzite, calcsilicate rocks Upper metapelitic gneiss Upper marble Lower metapelitic gneiss Lower marble	graphite, sulfides, zircon
~~ Minor unconformity ~~~~~~				
Nosib Group	Khan (500 m)		Amphibole biotite schist Upper gneiss (hornblende, biotite, quartz, plagioclase ± K-feldspar ± pyroxene ± calcite) Pyroxene – garnet amphibole gneiss Lower gneiss	titanomagnetite, zircon, allanite, titanite, monazite,
	Etusis (up to 6000 m)		Conglomerate, quartzite, migmatized feldspathic gneisses Rhyolitic volcanic rocks (?)	titanomagnetite, anatase, zircon, monazite, apatite, tourmaline
≈≈≈≈≈≈≈≈≈≈≈≈≈≈≈≈≈≈≈≈≈≈≈≈≈≈≈≈≈≈≈≈≈≈ Major unconformity ≈≈≈≈≈≈≈≈≈≈≈≈≈≈≈≈≈≈≈≈≈≈≈≈≈≈≈≈≈≈				
Abbabis			Migmatized granite gneisses/basement	monazite, zircon, apatite

Modified from Nash (1971), Smith (1965), Martin & Porada (1977).

sedimentary rocks corresponding to the Nosib Group. Rhyolitic volcanic rocks have been recognized in the less metamorphosed northern and southern grabens and evaporitic sedimentary rocks occur in the southern one (Porada & Behr 1988). Evidence of former evaporite in the Khan Formation is given by the presence of marialitic scapolite (Cuney 1981) and by the common occurrence of anhydrite, forming up to 20 vol.% of some of the gneiss associated with carbonate rocks (Nash 1972). The degree of metamorphism is too high in the central graben to identify the original lithologies easily. The total thickness of the Nosib Group may locally reach up to 6000 m. Subsequently, low energy epicontinental sedimentation of the Swakop Group extended over the width of the Damara Basin.

In the Rössing area, the Nosib Group includes the Etusis and Khan Formations. From the Etusis Formation to the Khan Formation, there is an increase of Ca content, corresponding to a previous carbonate cement in essentially siliciclastic sedimentary rocks. The Etusis Formation consists mainly of cream colored, pink to reddish feldspathic metaquartzite ringing the dome structure. Biotite may be more abundant in some units and pyroxene and hornblende appear in the uppermost part of the Etusis Formation. In the Etusis Formation quartz-rich units, sedimentary magnetite–monazite–zircon ± tourmaline-rich heavy mineral layers and cross-bedding structures are very well preserved, reflecting continental or near shore deposition. Biotite abundance varies within the Etusis Formation lithologies. Muscovite may occur in small amounts and is always secondary. The initial structure of the feldspar-rich quartzite was affected

by partial melting, in which quartz and feldspar become coarser and tend to form layered to diffuse segregations or pegmatite veins crosscutting the original stratigraphy defined by heavy mineral layers. Frequently, tourmaline is concentrated in recrystallized graphic segregations with quartz, or in the pegmatitic veins. Almost the entire Rössing dome, formerly considered as consisting of Abbabis granite gneiss, corresponds in fact to more or less intensively partially melted Etusis Formation (Nex *et al.* 2001) so that the Etusis Formation is much thicker than the 800 m previously estimated by Berning *et al.* (1976).

The overlying Khan Formation is 100 to 250 m thick and comprises the Lower Banded Gneisses, the Upper Banded Gneisses and the amphibole schist units. These are mainly composed of hornblende ± clinopyroxene, quartz–plagioclase–K-feldspar gneiss enclosing disrupted amphibolite layers. Garnet or calcite may appear in some of these gneiss units. Zircon, monazite, and titanomagnetite are more common than allanite, titanite, and anatase. The foliation is commonly enhanced by coarser grained quartz–plagioclase ± K-feldspar ± biotite ± magnetite segregations. Numerous felsic dikes are generally emplaced parallel to the metamorphic foliation, but discordant dikes also exist. Scapolite with 51% meionite, locally occurs in fractures perpendicular to the foliation.

Subsequently, marine sedimentation progressively invaded the entire Damara Basin. The Damara Group is composed of four formations, the Rössing, Chuos, Karibib (Husab) and Kuiseb (Tinkas). The Rössing Formation comprises six units: a basal, impure forsterite, phlogopite, and graphite marble (Lower Marble) overlain by the lower biotite–cordierite gneiss, a conglomerate, the upper marble, the upper biotite–cordierite gneiss, and a feldspathic quartzite layer. The local occurrence of veinlets of marialite-rich scapolite (up to 49 % marialite) in the upper Khan gneiss and in a quartzite of the Rössing Formation may reflect the former presence of evaporite in the sedimentary succession.

The tillite of the Chuos Formation corresponds to an important glaciation event and is deposited all over the Damara Basin. The tillite has a grey, massive to schistose matrix containing unsorted, elongate, and angular erratic blocks, measuring up to one metre in diameter. The superimposed Karibib Formation comprises a succession of white to bluish grey, well-bedded marble units containing thin layers of calcsilicate rocks. The Kuiseb Formation consists of biotite–cordierite–sillimanite schist intruded by numerous pegmatite dikes.

The collision between the Congo and Kalahari cratons resulted in thrusting and associated folding and foliation development at high structural levels, still preserved in the Usakos–Karibib area to the northeast of the Rössing area. At deeper structural levels in the southernmost metamorphosed Central Zone, regional migmatization is associated with voluminous synkinematic granitoid emplacement. Crustal shortening has produced pure shear-dominated deformation and an orogen-parallel ductile flow of the rocks with constrictional-type strain and a southwest sense of displacement (Kisters *et al.* 2004).

Four structural domains are distinguished in the Damara orogen: a weakly metamorphosed northern platform, a 40 km wide transition zone with metamorphic grade increasing southwards, a 160 km wide highly metamorphosed central zone where the Rössing deposit is located, and a 100 km wide southern zone with a southwards decrease of metamorphic grade. In the central zone, medium-pressure, high-temperature granulite-facies conditions with temperatures of *ca*. 750°C, pressures of 5–6 kbar (Masberg *et al.* 1992, Jung & Mezger 2003) and partial melting. This area is characterized by the development of kilometre-scale, NE-trending elongate domes. According to Poli & Oliver (2001) these domes are overturned and verging to the southwest. Many of them present a core of basement gneiss or Etusis Formation. The overlying Swakop sequence is draped around the domes and folded into tight and geometrically complex synclines striking northeast–southwest. The main structural orientation in this area is northeast and results from an F3 deformation event. The early phases of folding produced the overturned and recumbent structures that were accompanied by intense shearing and limited thrusting. Several less intense phases of folding occurred after F3 and produced NE and NW trending folds.

Several generations of granitoid plutons have been recognized in the Central Zone including the Red and Grey granites, the syn- to post-tectonic Salem granite, post-kinematic Donkerhuk and Bloedkoppie leucogranite and the late-to post-tectonic layered leucogranite, also called the G4 granite or alaskite. The Salem granitoid rocks have batholitic dimensions and are the most abundant. They comprise different generations of granodiorite,

granite, and quartz monzonite, dated at 601±79 Ma.

Deformation and plutonism related to D2 is considered to have occurred before *ca*. 540 Ma, because at that time, D3 produced not only the dome structures, but also the intrusion of voluminous granitic bodies. All monazite fractions from the metasedimentary rocks and migmatite from the Central Damara orogen are nearly concordant and define three different events: (1) at 540 Ma, attributed to the prograde metamorphic event M1 associated with thrusting and D3 dome formation, corresponding to the main collisional phase between the Kalahari and Congo cratons (Kisters *et al.* 2004); (2) at *ca*. 520–510 Ma, related to the peak regional metamorphism M2 during which partial melting of the metasedimentary rocks occurred; and (3) *ca*. 490–470 Ma (Jung & Mezger 2003), corresponding to a late metamorphic event M3, during which voluminous intrusions of post-collisional A-type and S-type granite occurred.

The equigranular homogeneous, fine to medium grained Red or Grey Granites form irregular bodies within the Etusis Formation. They were dated by U–Pb in zircon from the Goanikontes area at 525±5 Ma and were thus formed at the beginning of the M2 phase. The 508 ±2 Ma age obtained on zircon and monazite and the 509 ±1 Ma age obtained on uraninite from an alaskite from Goanikontes (Briqueu *et al.* 1980) confirm emplacement of the alaskite during the final stage of the M2 event associated with partial melting.

All uranium-bearing occurrences related to alaskite discovered in Namibia (Rössing, Goanikontes, Ida, Valencia, *etc*., Fig. 5-1) are situated in the southern Central Zone. The alaskite dikes are widely distributed in all the formations of the Damara metasedimentary package, but are not always uraniferous. They were emplaced post-F3 and are mainly oriented NNE.

The alaskite of the Rössing U deposit occurs in a migmatitic zone to the southwest of a dome structure comprising an intensely migmatitic core (Fig. 5-3). In the open pit, granitic rocks vary widely in texture, color, grain size, thickness, and emplacement habit. They range from centimetre-thick quartzofeldspathic anatectic lenses to several tens of metres-thick dikes, to a few hundreds of metres-thick stocks. Uraniferous alaskite tend to be parallel to the major foliation of the hosting metamorphic rocks, but they can be locally discordant where emplaced along the axial planes of F3 folds, transgressing the concentric envelopes consisting of various lithologies. Their contact with

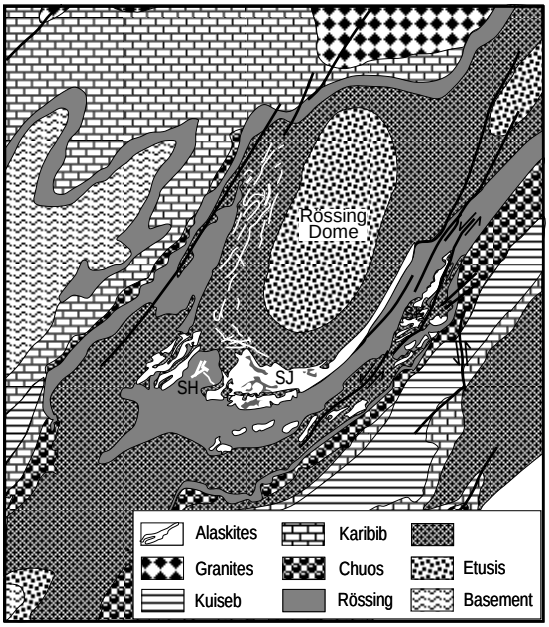

FIG. 5-3. Geological map of the Rössing Dome area with the main U deposits: SJ, SH, and SK (modified after Basson & Greenway 2004).

enclosing rock is commonly sharp as observed in the Rössing open pit, but progressive transitions between quartz-rich meta-arkose and pegmatoid lithologies can be observed where extraction of the melt was limited. In the western part of the open pit, the more massive alaskite bodies contain large host rock xenoliths more than 100 m in size. Their texture and grain size are highly variable: they are commonly pegmatitic, but also granitic, and more rarely aplitic, orbicular and graphic. Such textures may alternate in the same dike and define layering. Biotitic schlieren commonly occur at the margin of the dikes. The rarity of garnet and the absence of cordierite in this granite suggest that the water needed for partial melting has not been provided by biotite incongruent dehydration-melting reactions.

Nex and Kinnaird (1995) have shown that the layered leucogranite of Goanikontes can be divided into six types, which have been also recognized at Rössing by Basson & Greenway (2004). Types A, B, and C are deformed by D3 and D4, and types D, E and F are post-D3. Types A and B granites are pale pink to white, irregular to boudinaged, notably folded by D3, but with a weak S3 foliation. Type C granite is white to pale pink and abundant in relatively undeformed parts of the cover sequence, being occasionally boudinaged and emplaced in F3 'flexures'. Type D granite is white, 0.2–3 m wide, and corresponds to that which can be mineralized in

U. They contain smoky quartz, take irregular to anastomosing forms and are typically confined to high strain zones between the Khan and Rössing Formations. Type E granite dominates in high-strain, post-D3 zones and form 30 m wide massive bodies parallel to the metamorphic foliation, with highly variable grain size and color. Type F granite bodies are distinctively red, post-kinematic, having parallel sides and cross-cutting all pre-existing structures (Nex & Kinnaird 1995, Nex *et al.* 2001, Basson & Greenway 2004).

The alaskite is preferentially emplaced into the pyroxene–hornblende gneiss and biotite–amphibole schist units of the Khan Formation in the northern part of the pit, and into biotite–amphibole schist–lower marble–lower biotite-cordierite gneiss of the Rössing Formation in the central part of the pit. Skarn bodies from a few centimetres to several metres wide are widespread at the contact between the alaskite and the marble of the Rössing Formation. The majority of skarn contacts are composed of green clinopyroxene, brown calcic garnet and varying amounts of scapolite. Pyroxene, garnet, phlogopite and titanite up to several tens of centimetres in size may occur locally.

General characteristics of the U mineralization

Primary U mineralization is observed only in the felsic rocks. Some alaskite bodies can be entirely barren or only slightly mineralized, whereas only a few restricted sections are sufficiently rich to support mining. The mineralized felsic rocks are mainly located in the upper part of the Khan Formation and in the lower part of the Rössing Formation, with U enrichments in the vicinity of the marble of the Rössing Formation and the amphibolite from the Khan Formation. Mineralized alaskite contains smoky quartz, tends to be richer in biotite, is generally pink to reddish, and commonly corresponds to the latest intrusions. Barren alaskite is white to pale pink, although white mineralized alaskite exists. Within mineralized alaskite, the distribution of U can be extremely variable and enrichments are commonly observed at the margin of the dikes and along biotite selvages. Pinkish K-feldspar is generally predominant, but plagioclase-rich occurrences also exist (Fig. 5-4). Biotite generally represents less than a few percent of the volume of the rock, and has high fluorine and chlorine contents up to 1.8% F and 800 ppm Cl (Cuney, unpub. data). Biotite clusters are most common near the contact with the host rocks and muscovite occurs in very limited amounts as alteration of plagioclase and K-feldspar, and associated with chloritized biotite commonly associated with calcite. These rocks have been called "alaskite" at Rössing because of their granitic, predominantly potassic character and their low biotite content in accordance with the original definition of Spurr (1900).

Euhedral Th-bearing uraninite (3.3–8.0 wt.% ThO_2) is commonly the predominant ore mineral. Y and REE contents are elevated (1.6–7.14 wt.% Y_2O_3 and 2.3 wt.% ΣREE) as commonly observed in uraninite formed at high temperature. More surprising is the high and variable Ca contents (0.3–9.5 wt.% CaO) for uraninite formed from a leucocratic granite, which generally has a low Ca content. The high Ca content of some of the Rössing uraninite is interpreted as reflecting the interaction of the alaskite melts with enclosing calcium-rich lithologies of the Khan and Rössing formations as observed in pitchblende from vein-type deposits hosted by calcium-rich lithologies, formed at lower temperature. Uraninite occurs as finely disseminated grains ranging in size from a few micrometres to 0.3 mm, with the majority in the 0.05–0.1 mm fraction. Uraninite grains are included in quartz, feldspar, and biotite, but also appear interstitially to these minerals. Uraninite can be also

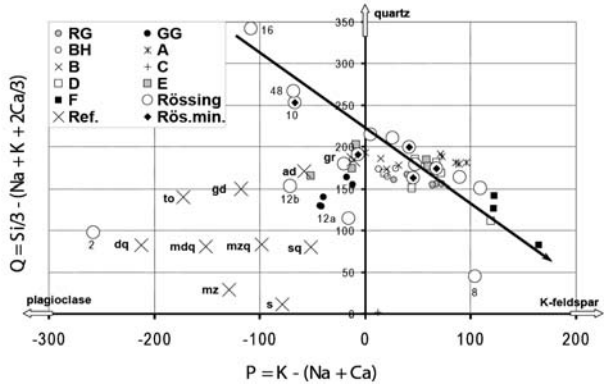

FIG. 5-4. Q–P chemical–mineralogical diagram of Debon & Lefort (1988) representing variations of the proportions of quartz relative to plagioclase and K-feldspar for the granite (RG = Red Granite, GG = Grey Granite) and alaskite (BH = basement hosted alaskite and type A to F) from Goanikontes (data from Nex *et al.* 2001) and alaskite (min. = mineralized alaskite represented with a black diamond) from Rössing (data from Cuney 1981). Only Rössing samples are numbered. Ref. = average composition of the main types of plutonic rocks.

included in zircon and apatite crystals, indicating that its crystallization started very early. Uraninite enrichments are also common in the biotite selvages, in which the uraninite crystals tend to be distributed as trails. This type of uraninite has crystallized from a late magmatic fluid.

Other high- and low-temperature U-bearing minerals can also occur. Nb–Ta–Ti oxides are the most common high-temperature U-bearing minerals, commonly with about 27 wt.% UO_2, occurring as 1–3 mm octahedral to dodecahedral crystals of betafite, isolated or in clusters. Hosting only a few percent of the total U content of the alaskite in the Rössing deposit, betafite becomes the predominant uranium-bearing mineral in the SH mineralization (Fig. 5-2). No specific mineralogical or textural features seem to control the occurrence of betafite in the alaskite.

Monazite is a common mineral in most occurrences at Rössing, but is generally not abundant because of the low solubility of monazite in low temperature peraluminous melts (Montel 1993). However, monazite may be enriched in some alaskitic granite, such as those from southern Finland (Lauri *et al.* 2007). Such monazite accumulations can tentatively be explained as restitic to cumulative enrichments after partial melting of paleoplacers in meta-arkosic conglomerate. Zircon is universally present in the alaskite, but its abundance is generally very low, also because of its low solubility in low temperature peraluminous melts (Watson & Harrison 1983). However, it can also be very abundant in late orogenic alaskitic granite from southern Finland (Lauri *et al.* 2007). As with other U–Th-rich silicate minerals, such zircon is strongly metamict. Allanite and titanite are rare at Rössing and occur in the vicinity of Ca-rich rocks (marble, calcsilicate rocks, amphibolite). Dark purple fluorite is commonly present in the vicinity of chloritized biotite and as coatings of fracture planes at Rössing. Apatite, xenotime, pyrite, chalcopyrite, bornite, molybdenite, arsenopyrite, anatase, magnetite, hematite, and ilmenite are encountered locally.

Hexavalent U minerals are common in the Rössing ore body and contribute to its U enrichment, particularly in the upper part of the deposit. Oxidizing meteoric fluids have dissolved uraninite in the eroded part of the deposit and redeposited U in small fractures, mainly as uranophane, but also as metatorbernite, metahaweeite, and carnotite.

Alaskite geochemistry

Major and trace element compositions of mineralized and barren alaskite from the Rössing area are presented in Table 5-2. Silica and alkali contents range widely and the alaskite can be divided into quartz–plagioclase-rich compositions to quartz-poor–K-feldspar-rich compositions, through granitic compositions with about the same proportion of quartz, K-feldspar, and plagioclase (Fig. 5-4). Mineralized alaskite can belong to any group. Most of these granite bodies have a low peraluminosity (low A parameter in Fig. 5-5 and low normative corundum in Table 5-2) and very low amounts of mafic minerals as shown by the low B parameter in the A *versus* B chemical mineralogical diagram (Fig. 5-5). The low peraluminosity of such granite, despite its derivation from the partial melting of metasedimentary rocks, results from the preferential melting of weakly peraluminous quartzofeldspathic metasedimentary rocks or acidic metavolcanic rocks, materials with nearly eutectic compositions. Another specific characteristic of this type of melt is the highly variable trace and major element composition of the pegmatoid rocks that reflects the diversity of the material being melted and the complex interplay between restite unmixing, mineral–melt fractionation, and fluid–rock equilibration between the injected sheets of granite and the host rocks of highly variable chemistry. Restite unmixing is the most visible mechanism from the common occurrence of biotite-rich schlieren and anorthite-richer plagioclase in the plagioclase-rich pegmatoid rocks.

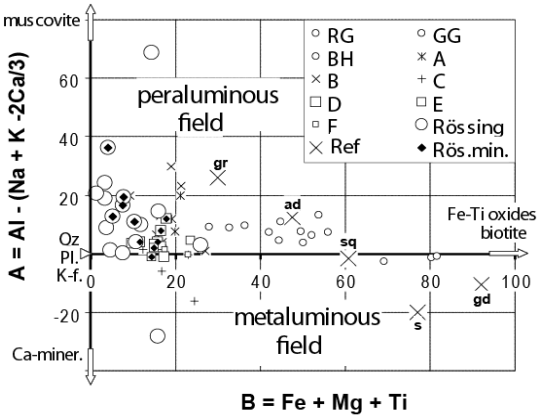

FIG. 5-5. A–B chemical–mineralogical diagram of Debon & Lefort (1988) representing the variations of the peraluminous index (A) *versus* a differentiation index (B) for the granite of the Rössing area. Same legend as Figure 5-4.

TABLE 5-2. SELECTED ANALYSES OF ALASKITE FROM THE RÖSSING OPEN PIT AND DOME GORGE WITH CATANORM CALCULATION (CUNEY, UNPUB. DATA).

	2	**8**	**10**	**14**	**16**	**47a**	**50**	**51a**	**52k**
SiO_2 (wt %)	69.02	65.16	80	77.76	84.61	76.89	74.09	73.35	76.45
Al_2O_3	19.11	16.96	10.96	12.03	8.82	13.13	13.34	13.7	12.32
Fe_2O_3 tot	0.36	0.39	0.34	0.16	0.18	0.13	0.25	0.76	0.28
MnO	nd	nd	0.01	0.01	nd	nd	nd	0.01	0.02
MgO	0.06	0.41	0.11	0.03	0.02	0.12	0.16	0.01	nd
CaO	0.88	1.83	0.3	nd	0.89	0.36	0.21	0.54	nd
Na_2O	8.01	2.46	3.86	3.29	3.25	3.6	2.53	2.84	2.84
K_2O	0.77	10.16	2.97	5.22	0.57	5.45	7.2	6.91	6.27
TiO_2	0.67	0.05	0.04	0.04	0.05	0.04	0.04	0.04	0.04
P_2O_5	0.07	1.1	0.02	nd	0.05	0.07	0.04	0.37	0.01
P.F.	0.24	0.62	0.6	0.64	0.75	0.7	0.76	0.31	0.39
TOTAL	99.14	99.14	99.21	99.18	99.19	100.49	98.62	98.84	98.62
FeO	0.04	0.1	0.09	0.04	0.06	0.09	0.14	0.16	0.22
Fe_2O_3	0.32	0.28	0.24	0.11	0.11	0.03	0.09	0.58	0.04
Fe^{2+}/Fe^{3+}	0.14	0.39	0.41	0.44	0.66	3.48	1.8	0.3	5.67
Fe/Mg	6.3	1.1	3.4	5.6	12.6	1.3	1.7	53.2	
Catanorm									
Q	17.78	10.48	45.46	38.62	61.76	34.33	31.19	30.15	35.78
Or	4.55	60.1	17.57	30.88	3.37	32.24	42.59	40.87	37.09
Ab	67.7	20.79	32.62	27.81	27.47	30.43	21.38	24	24
An	3.91	1.91	1.36	0	4.09	1.33	0.78	0.27	0
Di	0	0	0	0	0	0	0	0	0
Hy	0.15	1.13	0.27	0.07	0.05	0.37	0.52	0.27	0.37
Wo	0	0	0	0	0	0	0	0	0
Ma	0	0	0.21	0.05	0.05	0.04	0.13	0	0
il	0.08	0.09	0.08	0.08	0.09	0.08	0.08	0.08	0.08
He	0.32	0	0.1	0.08	0.08	0	0	0	0
Sp	0	0	0	0	0	0	0	0	0
Ru	0.63	0	0	0	0	0	0	0	0
Cor	3.66	1.19	0.89	0.95	1.35	0.81	1.08	1.43	0.84
Ap	0.15	2.4	0.04	0	0.11	0.15	0.09	0.81	0.02
% An	5.4	8.4	4	0	13	4.2	3.5	1.1	0
U (ppm)	**6.1**	**5.5**	**185**	**61.6**	**39.5**	**423**	**504.5**	**840**	**565**
Th	**68.4**	**10.8**	**39**	**41.1**	**54.5**	**14**	**65**	**95.0**	**35**
Th/U	11.2	20	0.2	0.7	1.4	0.03	0.13	0.11	0.06
Pb	9	24	388	206	16	33	49	60	37
V	27	11	<10	<10	<10	28	16	15	25
Ni	<10	<10	10	<10	22	<10	<10	<10	<10
Cr	17	<10	<10	<10	<10	<10	<10	<10	<10
Cu	<10	<10	<10	<10	<10	<10	<10	<10	<10
S	300	300	200	200	200	200	200	1600	500
Ba	64	314	67	81	72	55	94	205	96
Rb	14	794	200	395	44	319	493	508	439
Sr	34	41	42	30	51	23	20	64	46

nd = not detected.

U and Th contents are not correlated (Fig. 5-6) and do not correlate with any other major or trace elements. The increase of Th content is moderate because the solubility of Th-rich minerals like monazite is limited in low temperature crustal melts.

Parameters controlling the location of the ore bodies at Rössing

At a regional scale, the accumulation of alaskite dikes forming the Rössing deposit is located at the southwestern margin of a dome structure (Fig. 5-2). According to Anderson & Nash (1997) the emplacement of the Rössing alaskite bodies occurs within an ENE jog along a regional NNE sinistral strike-slip structure, the ''Welwitschia Trend'' (Fig. 5-1), which separates two regions of different structural style, and may thus represent a detachment structure. Other alaskite intrusions are related to late sinistral transtensional ladder veins associated with the NNE sinistral strike slip faults (Fig. 5-2). More recently, Basson & Greenway (2004) suggested that the alaskite emplacement is also closely linked to the late kinematic evolution of the Rössing Dome, during a north–south transpressional tectonic episode, causing a rotation of the dome's long axis, with a concomitant southward dome impingement. A wedge-shaped zone was produced, in which the alaskite was emplaced. From the 3D modelling of the U content distribution at Rössing, Basson & Greenway (2004) proposed that the U mineralization is transgressive with respect to the granite types and their host lithologies. Such an interpretation is contradictory with the field observations that show that the mineralization is strictly confined to specific alaskite bodies with no mineralization in the hosting metamorphic rocks. The proposed transgressive distribution of the mineralization results from an interpolation of the U contents measured in the exploration drill cores without taking into account the lithological boundaries. Basson & Greenway (2004) also proposed a control for preferential emplacement of leucogranite in the SJ area by the late-D3 to D4 brittle–ductile deformation that was the site of protracted and elevated fluid flux. However, brittle–ductile fracturing represents a late feature, it cannot occur in a high-grade metamorphic zone with incipient partial melting. The mineralized granitic bodies have the shape of elongate, centimetre to 100 m thick, relatively boudinaged, and sub-parallel sets of pegmatoid dikes, the emplacement of which is controlled mostly by the opening of the foliation of the enclosing metamorphic rocks under highly ductile conditions. The granitic dikes locally merge to form larger granitic bodies a few hundreds of metres thick, as observed in the western part of the Rössing open pit (Figs. 5-7 and 5-8). Such a phenomenon may explain the apparent transgressive character of the largest alaskite accumulations. Economically, they represent the most interesting ore bodies because of

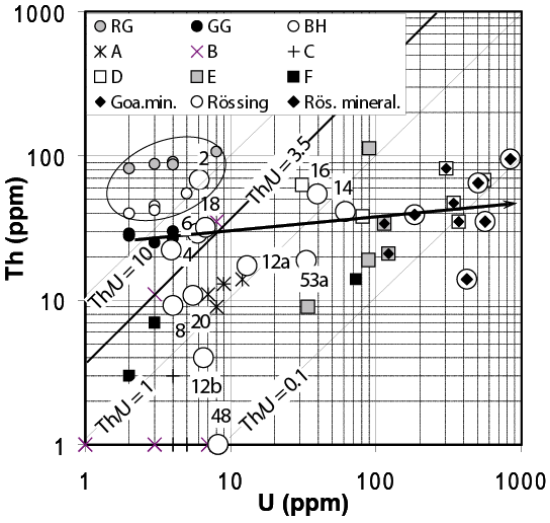

FIG. 5-6. Th–U contents for the granite from the Rössing area. Legend as in Fig. 5-4. Th/U = 3.5 represents the average crustal ratio. The arrow indicates the limited Th enrichment associated with U enrichment. The field defined by the red and grey granite is circled.

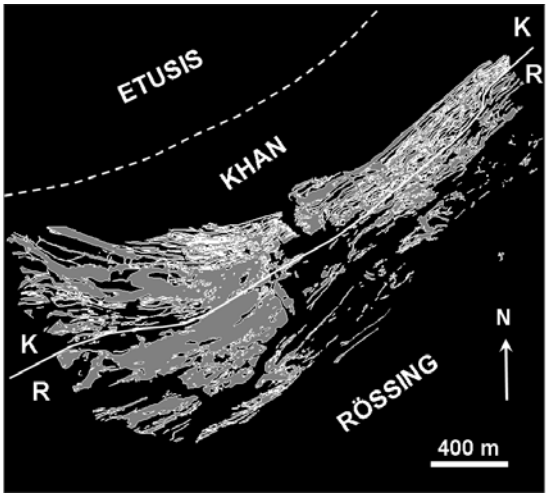

FIG. 5-7. Map of the Rössing deposit emphasizing the location of the alaskite at the interface between the Khan and Rössing formations and their complex ramifications essentially parallel to the schistosity of the enclosing metamorphic rocks (modified from Berning *et al.* 1976).

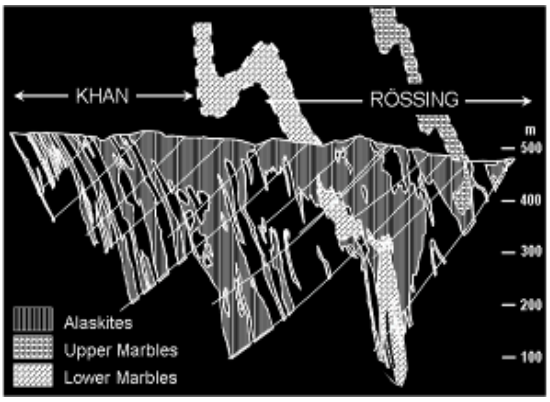

FIG. 5-8. North-south cross section through the Rössing deposit. The two marble levels of the Rössing Formation are emphasized and their presumed extension is extrapolated above the outcrop surface to underline their role as a barrier for the ascension of the granite melts (modified from Berning *et al.* 1976).

the paucity of U-poor host rocks intercalations. Two of the largest granitic bodies are located in the Rössing Formation at the level of the Lower and Upper Marbles as shown in the cross section of the open pit (Fig. 5-8). In marble, being extremely ductile at high temperature, the structures controlling the opening of the metamorphic rocks have been preferentially developed at the rheological transition between the marble and the more competent biotite–cordierite gneiss. The other major granitic body is developed in the only level of pyroxene–garnet gneiss of the Khan Formation between two layers of pyroxene–hornblende gneiss that may also represent a zone of strong rheological contrast. Finally, if a protracted and elevated fluid flux would have existed, as proposed by Basson & Greenway (2004), the U mineralization would not have been restricted to the alaskite bodies, but would have also occurred in the hosting metamorphic rocks.

The carbonate units have also exerted a strong chemical control on the accumulation of alaskite dikes in their vicinity. Many of the large alaskite bodies are located below the marble levels and the Rössing Formation at the Rössing mine, such as the SH anomaly and most of the G.P. Louw Deposits (see below). They also occur below the Husab marble where the Rössing Formation does not exist, as over the Nosib Group at the Ida Dome. Carbonate is also common in the Khan Formation.

The preferential accumulation of alaskite in the vicinity of carbonate-bearing lithologies can be explained as follows. The solidus of a granitic system strongly increases when the molar fraction of CO_2 increases relative to water in the coexisting fluid. The development of skarn at the contact between injected silicate melts and carbonate-bearing lithologies has produced decarbonation reactions such as:

$$CaCO_3 \text{ (calcite)} + SiO_2 = CaSiO_3 \text{ (diopside)} + CO_2$$

The production of CO_2 reduced the water partial pressure in the metamorphic fluid in equilibrium with the silicate melts and thus in the silicate melts themselves. The shift of the solidus of the silicate melts to higher temperature forced them to crystallize preferentially at the level of the Rössing Formation. The marble would thus have acted as a chemical barrier favoring the accumulation of alaskite melts. This interpretation is supported by the decrease of the CH_4/CO_2 ratios in fluid inclusions in the mineralized alaskite of the Rössing open pit compared to the trend of increasing CH_4/CO_2 ratios of the metamorphic fluid extracted from the metamorphic rocks along a profile from the Etusis Formation to the Rössing Formation (Cuney, unpub. data). The CO_2 produced by the skarn reactions has probably migrated along the structural zones controlling the emplacement of the alaskite and thus had an influence on alaskite crystallization over a much larger volume than the skarn formation zones. The preferential accumulation of alaskite bodies in the Rössing deposit is particularly evident in the vicinity of the Upper Marble Unit (Fig. 5-8). The second large accumulation of alaskite bodies occurs between the Khan and Rössing formations below the Lower Marble Unit, which may have extended above, as drawn in the section (Fig. 5-8).

The existence of chemical exchange between the marble units and the alaskite magma is indicated by several features: high Ca contents in the uraninite crystals (up to 9.5 wt.% CaO), local occurrence of allanite, titanite, or amphibole in some of the dikes, and metaluminous chemistry of some of them (Fig. 5-5). In leucocratic granite, the Ca content of uraninite varies between 1 and 3 wt.% CaO and allanite and titanite should not be stable because of the low Ca contents of the silicate melts from which such granite crystallizes (Cuney & Friedrich 1987).

Inasmuch as CO_2-rich fluids have been observed along the entire lithostratigraphic sequence at Rössing and in other mineralized alaskite type occurrences (*e.g.*, Mont Laurier; Cuney 1981, 1982; Bancroft, Baffin Island, Cuney,

unpub. data), X_{CO2} may have been instrumental in the genesis of mineralized alaskite by limiting the rate of melting of metamorphic rocks in the source area. The alaskite consists of quartz and feldspars and few mafic minerals, so the degree of partial melting has been relatively low, which has facilitated high U enrichments in the melts during anatexis.

When a fluid phase exsolves from a silicate melt during progressive crystallization of U-rich granite, part of the U fractionates into the fluid phase and may escape from the system if the fO_2 conditions of the environment are oxidizing. The Rössing mineralization is located just below and within graphite–sulfide bearing schist and marble of the Rössing Formation, the first reducing barrier encountered by the silicate melts during their injection into the lithostratigraphic succession. Sulfide enrichment also occurs in the upper part of the Khan Formation as demonstrated by a Cu exploration shaft close to the Rössing and Ida mines. The increasingly reducing conditions from the base to the upper part of the lithostratigraphic succession are also indicated by the progressive increase of the CH_4/CO_2 ratios of the metamorphic fluid extracted from metamorphic rocks sampled along a section from the Etusis to the Rössing formations (Cuney, unpub. data). The progressive increase of the CH_4/CO_2 ratios along the section shows that the methane-rich fluids don't remain in the immediate vicinity of the reduced formations, but tend to diffuse towards the Khan Formation and probably upwards. Reducing conditions would limit the fractionation of U into the magmatic fluids, forcing uraninite to crystallize as disseminations within alaskite, and induce the precipitation of U from magmatic fluids exsolved from the silicate melts that crystallized in oxidized conditions at lower structural levels. This last type of U precipitation probably corresponds to the uraninite trails observed in the biotitic selvages of alaskite, which has enhanced the grade of the mineralization.

Origin of mineralized alaskite

Two models have been proposed for the origin of the U-mineralized leucocratic granite dikes of the Rössing type. They can result either from (1) extreme fractionation of a larger granitic body located at depth, such as proposed for Rössing (Bowden *et al.* 1995), and mineralized pegmatoid bodies from the Grenville belt in Quebec (Lentz 1996) or from (2) partial melting of U-rich metasedimentary or metavolcanic rocks, such as proposed for Rössing (Cuney 1981, 1982) and for Mont Laurier alaskite and pegmatoid units in Quebec (Cuney 1982). The partial melting model for the origin of the mineralized leucocratic granite dikes of the Rössing type is preferred for the following reasons:

- the larger granitic bodies that exist in the southern central part of the Damara belt are either older or younger than these dikes.
- this type of granitic dike, globally parallel to the regional metamorphic foliation, always occurs in high-grade migmatitic domains where partial melting remains limited. The foliation of the original metamorphic rocks is always well preserved, except where meta-arkoses or meta-acidic volcanic rocks allowed high degrees of melting, as observed in the Etusis Formation of the Rössing area.
- no correlation between U enrichment of the granitic dikes and other major and trace elements is evident, but should be if fractionation were important (Figs. 5-9, 5-10 and 5-11).
- mineralogy and major element contents define three groups of compositions: a plagioclase-rich group generally with a more restite-rich composition, a granitic group with near eutectic composition, and a K-feldspar-rich group generally poorer in quartz and coarse pegmatitic.
- there is evidence for restite material, such as biotite schlieren, but also garnet in some occurrences, such as in the late orogenic granite of southern Finland.
- internal zonation of the pegmatitic granitic dikes is generally absent.
- rather than diverging from a deeper granitic body, the granitic dikes tend to merge to form small (10 to 100 m thick) granitic lenticular bodies.
- the high and variable initial $^{87}Sr/^{86}Sr$ ratios (0.724 to 0.759) obtained from alaskite (only one from Rössing) implies an old crustal source for the magmas (Hawkesworth *et al*. 1981). Their low initial $^{143}Nd/^{144}Nd$ ratios (0.51126 to 0.51117) and high T_{DM} (2.34–2.35 Ga) indicate their derivation from Paleoproterozoic crustal sources. But, as the Etusis sedimentary rocks are derived from the Paleoproterozoic basement, and because of the diversity of the alaskite types, more information is needed on the isotopic signature of alaskite and of the Etusis siliciclastic sedimentary rocks to constrain the source of these magmas better.

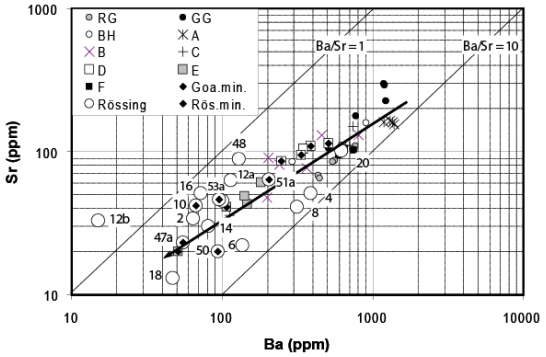

FIG. 5-9. Ba–Sr variations for the Rössing and Goanikontes granite. Same legend as Figure 5-4.

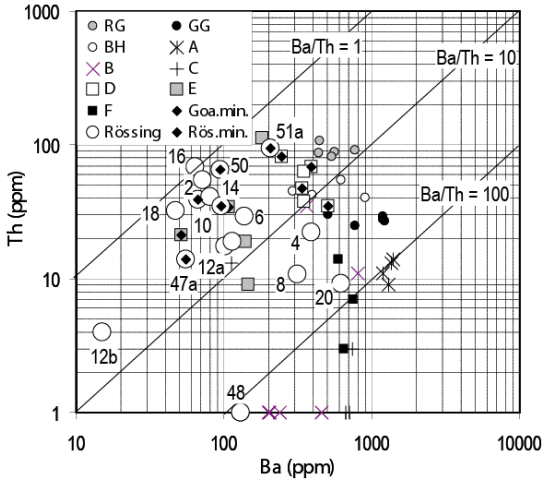

FIG. 5-10: Ba–Th variations for the Rössing and Goanikontes granites. Same legend as Figure 5-4.

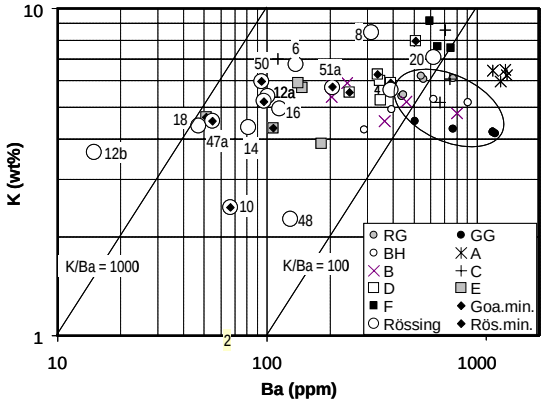

FIG. 5-11: K-Ba variations for the Rössing and Goanikontes granites. Same legend as Figure 5-4.

OTHER WORLD OCCURRENCES OF RÖSSING TYPE MINERALIZATION

Disseminated uraninite mineralization in synmetamorphic pegmatoid rocks are known worldwide and in most of the major orogens. They typically occur in metasedimentary associations initially corresponding to epicontinental successions comprising arkose, quartzite, siltstone, carbonaceous shale, marl, and marble metamorphosed to the upper amphibolite facies with partial melting, and locally up to granulite facies. Occurrences of synsedimentary U enrichment are sometimes still recognizable, mostly in quartz-rich meta-arkose and calcsilicate rocks which have avoided melting because of their refractory compositions.

Archean occurrences

Occurrences in the Litsk area of the northeastern Kola Peninsula, Russia, are probably the only known examples of disseminated U–Th–REE mineralization related to pegmatitic granite with ages of 2.75–2.65 Ga located in a migmatitic domain of Archean age (Savitskii *et al.* 1995). In the literature, they are generally referred to as potassic metasomatite rather than partial melting products. The host rocks are metamorphosed peraluminous sedimentary rocks (biotite, garnet, and two-mica gneiss) and minor amphibolite of the Lower Tundra series. The mineralization is mainly located in the NW-striking Voron'ya–Kolmozersk tectonic zone between the Kola and Murmansk cratons. The Dikoe Lake showing represents one of the most important ones, with mineralized pegmatoid rocks occurring as a series of elongate lenses up to a few tens of metres long and a few metres wide. More than 400 U-bearing bodies have been discovered in two NW-trending bands, 6 km long and 1.5 km wide. Drilling indicates a discontinuous extension of these bodies down to 400 m. Their average U content is in the order of 100 ppm U and up to 0.2 wt.% U, with relatively low Th/U ratios of 0.5 to 0.8. The main ore mineral is uraninite, locally concentrated in biotite selvages. Other U–Th minerals are monazite, uranothorite, and metamict zircon. Other minor minerals present are tourmaline, garnet, pyrite, magnetite and ilmenite. Yttrium and REE concentrations may reach thousands of ppm.

"Hudsonian" *S.L.* occurrences

The Wollaston and Mudjatik domains in Saskatchewan, Canada, have metasedimentary associations corresponding to an epicontinental sequence metamorphosed to amphibolite to granulite facies and with partial melting. Many occurrences of synsedimentary U enrichment occur in meta-arkose at Duddridge Lake and calcsilicate rocks at Burbridge Lake and Cup Lake (Parslow & Thomas 1982, Sibbald *et al.* 1976). Partial melting

has produced pegmatoid and leucocratic granite rich in monazite and uraninite throughout the belt (Annesley & Madore 1999, Madore *et al.* 2000). The most common group are the A pegmatites of Parslow & Thomas (1982), which have low Th/U ratios with the highest and most variable U contents (30 to 4650 ppm). The Charlebois occurrence represents the largest accumulation of pegmatoid dikes in the area, mineralized with disseminated uraninite ± molybdenite ± pyrrhotite ± pyrite ± magnetite (Mawdsley 1957). A thucolite-type occurrence was reported from one sample, underlining the importance of carbon-bearing sedimentary rocks as a redox control for U mineralization in high-grade metamorphic conditions. Some of the mineralized zones may extend continuously over 1 km with a width of 25 to 35 m ("Row" showing) and average 960 ppm U over 21 m. Assay values up to 0.71 wt.% U have been reported. Th/U ratios vary widely, from 0.1 to 4.4, but the average ratio of 0.3, based on 27 samples, is quite low. The mineralized zones are always located between calcic metasedimentary rocks and the greatest uraninite enrichments are generally associated with biotite schlieren. These occurrences share many of the geological characteristics of the Rössing alaskite.

Steward Lake, Quebec, Canada, is located 175 km NE of Schefferville in the Churchill Province. The mineralization is located in coarse-grained pegmatite subcrops and large boulders traced by prospecting over a distance of at least 2.6 kilometres and over a width of up to 700 metres (Freewest Resources Canada Inc).

In northern Quebec, Ungava Bay and Baffin Island, uraniferous pegmatoid bodies have been recognized over an extremely wide area (Maurice 1977) and are being explored by several companies. They occur in the Paleoproterozoic metasedimentary Lake Harbour Group comprising quartzite, graphitic gneiss, calcitic and dolomitic marble, and calcsilicate rock: an association typical of a deposition in an epicontinental environment. Metamorphism during the Torngat orogeny at 1.86–1.74 Ga reached high-grade amphibolite facies with partial melting.

In the Litsk district, Kola Peninsula, Russia, uraniferous pegmatoid bodies, dated between 2.2 and 1.85 Ma, have been reported mainly at Polyarnoe and Litskoe. They are hosted by highly peraluminous sillimanite–biotite migmatitic gneiss. The mineralization is mainly represented by euhedral Th-bearing uraninite. Remobilization of the U is locally observed in veins.

Mineralized pegmatoid bodies in the Wheeler Basin, Colorado (Young & Hauff 1975) are hosted in migmatitic gneiss, and are particularly concentrated in zones injected by the 1.4-Ga-old Silver Plume granite. Uraninite is mostly concentrated in biotitic schlieren. A major difference with the Rössing deposit is the high Th/U ratios of up to 10 (Phair & Gottfried 1964).

The Orrefjell mineralized pegmatite located 70 km north of Narvik, Norway, forms a large (3 x 0.5 km) irregular body alternating with amphibolite and emplaced in mica schist rich in graphite and sulfide minerals, and quartzite (Lindahl *et al.* 1985). The main U mineral is uraninite associated with molybdenite. The best hole gives intersections of 1 m at 3,000 ppm and 2 m at 2,300 ppm.

The late orogenic potassic granite of Southern Finland is strongly enriched in U. The suite was emplaced between 1.85 and 1.79 Ga along a 100–150 km-wide zone of Paleoproterozoic basement, extending for *ca*. 500 km from SW Finland to Russia, and represents one of the most U–Th–K enriched areas in Fennoscandia (Lauri *et al.* 2007). The basement is composed of Paleoproterozoic metavolcanic and metasedimentary rocks belonging to a presumed arc complex formed at *ca*. 1.90–1.87 Ga and accreted to central Finland during the Svecofennian orogeny at *ca*. 1.88 Ga. The mineralized granite is leucocratic, generally pegmatitic, and assumed to be derived from a low degree of partial melting of supracrustal rocks during a low-P, high-T metamorphic event. The granite usually forms relatively thin undulating sheets, dikes, and pods, and commonly exhibits a gradual transition with the migmatized host rocks, rarely forming small granite plutons. The composition of the granite varies from plagioclase-rich to K-feldspar-rich through eutectic granite compositions, as generally observed in migmatitic domains, with minor amounts of biotite (< 5 vol.%) ± muscovite ± cordierite ± garnet. Abundance and paragenetic association of magmatic U-bearing accessory minerals are highly variable from one intrusion to another and include zircon, apatite ± monazite ± uraninite ± uranothorite ± allanite, and rare yttriocolumbo–tantalite. Most granite is slightly

peraluminous (1.04 < A/CNK < 1.10) and a few, with garnet and cordierite schlieren, may reach an A/CNK ratios of 1.55. Its variable U, Th, Zr, Y, and total REE contents reflect the extremely variable abundance of accessory minerals. Most samples have low Th/U ratios (≤ 1) indicating strong U enrichment relative to the average crustal Th/U ratio of 3.5. The late orogenic potassic granite of southern Finland shares many characteristics with Rössing alaskite, but accumulations large enough to form an economic deposit remain to be discovered. The only significant accumulation of potassic pegmatite bodies is represented by the Palmottu deposit, with about 1,000 t U at 0.1 wt.% U (Räisänen 1989).

***At Crocker Well, Olary Province*, South Australia**, U resources are estimated at 7,300 t U at 407 ppm U distributed in six deposits. Mineralization is primarily thorian-brannerite with some davidite, which occurs as disseminations in granite, but also as veins and breccias (Campana & King 1958, Thompson 1965).

At the Six Kangaroos area of Cloncurry–Mt. Isa District, Australia (Brooks 1960; Carter *et al.* 1961).

At Nanambu, Nimbuwah, and Rum Jungle complexes of Katherine–Darwin area, Australia (Dodson *et al.* 1974, Ayers & Eadington 1975).

"**Grenvillian" occurrences**

In the Grenville orogen an extremely large number of U occurrences related to anatectic pegmatoid and pegmatite are known (see Lentz 1996, for a review). One of them, located at Bancroft, Ontario (Satterly 1957, Robinson 1960) was home to four mines, which produced a total of 5,700 t U between 1956 and 1982. The Faraday mine alone has produced 2,544,716 tons of ore averaging 0.1074% U_3O_8 (about 2320 t U). The principal ore minerals were uraninite, with up to 10 wt.% ThO_2, and uranothorite, whereas allanite, fergusonite, and betafite were more sporadic.

Other major occurrences are those of the Mont Laurier area in Quebec, with a decrease of the Th/U ratios of the pegmatoid from south to north that corresponds to a variation of the U–Th mineral paragenesis from uranothorite only, to uranothorite + Th-bearing uraninite, and to Th-bearing uraninite only (Allen 1971, Cuney 1982, Fowler & Doig 1983).

Many other occurrences are situated along the northern shore of the St Lawrence River: Johan Beetz (Rimsaïte 1981), Havre St-Pierre, Sept Îles, Port Cartier with up to 2,920 ppm U and 995 ppm Th in pegmatite, and St-Augustin. Epicontinental platformal sedimentary rocks, as described in the Wollaston belt, typically host most, if not all, of these occurrences. Moreover, there are many indications of the former presence of evaporite, such as highly magnesian gneiss, marialite-bearing gneiss, occurrence of anhydrite in gneiss or in the core of pegmatite, as at Bancroft, and of highly saline brines in the pegmatite (Cuney, unp. data).

"Pan-African" occurrences

In addition to Rössing, all other mineralized alaskite occurrences of the Damara belt are found in Namibia. Some are located in the vicinity of the Rössing mine, including the SH deposit, situated 1.5 km southwest of the Rössing ore body, with a size of 500 x 250 m and a high proportion of betafite, and the G.P. Louw deposits, a series of individual alaskite bodies 2 km east of the Rössing open pit, most of them emplaced in marble of the Rössing or Karibib formations. Others are located in the Central Damara zone along the same NE trend (Fig. 5-1).

The Valencia deposit, located about 35 km to the NE of Rössing, is much smaller with reserves of 12,000 t U at 0.105 % U and probable resources of 12,000 t U at 0.1 % U. These estimates take into account a mining to a depth of –350 m. The alaskite here tends to form a large body of 500 m x 400 m enclosing xenoliths of the host rocks, from tiny fragments to bodies several tens of metres long. Their strikes and dips do not vary significantly compared to those of the country rock. Little tilting and disorientation seems to have taken place during alaskite emplacement.

At Ida, mineralized alaskite occurs along the contact between the Khan Formation and marble of the Husab Formation, the Rössing Formation being absent. Patchy radioactivity has been detected over 9 km along strike and a width of 80 to 90 m. On the eastern side, skarn zones are developed against the marble and can be also mineralized when adjacent to mineralized alaskite. The skarns are generally small, but southeast of the Ida Dome some of them reach several hundred metres in length and more than ten metres in width. Biotite schist schlieren in the mineralized alaskite are enriched in U compared

to alaskite. Schist with K-feldspar porphyroblasts surrounding the alaskite bodies may be more mineralized than the intrusions over 1–2 metres from the contacts.

At Goanikontes, the major mineralized alaskite bodies are restricted to the lower part of the Khan Formation and occur within 400 m of the contact between the Etusis and Khan formations (Valois & Walgenwitz 1979, Mouillac *et al.* 1986). The Rössing Formation is very thin here. Surface exposures show that the alaskite bodies do not seem to merge significantly to produce granitic bodies as large as those in the Rössing, SH, or Valencia deposits. However, recent drilling showed mineralized sections of up to 124 m at 300 ppm U. Uraninite is the most abundant primary U mineral, but betafite is also present. Indicated resources are 4,960 t U at 200 ppm U and 22,800 t U at 170 ppm U.

At Holland's Dome, a weak occurrence, the mineralization has been detected in calcsilicate rocks and skarns with higher grade (1.4% eU) than in adjacent alaskite. The best drilling intersections are 221 m at 430 ppm U and 29 m at 1580 ppm U.

At Currais Novos, Brazil, one occurrence of possible Rössing type mineralization is known (Favali 1973, Ramos & Fraenkel 1974).

REFERENCES

ALLEN, J.N. (1971): The Genesis of Precambrian Uranium Deposits in Eastern Canada, and the Uraniferous Pegmatites of Mont Laurier, Quebec: *Unpub. M.Sc. thesis*, Queen's Univ., Kingston, Ontario.

ANDERSON, H.F. & NASH, C.R. (1997): Integrated lithostructural mapping of the Rössing area, Namibia, using high resolution aeromagnetic, radiometric, Landsat data and aerial photographs. *Explor. Geophys.* **28**, 185-191.

ANNESLEY, I. & MADORE, C. (1999): Leucogranites and pegmatites of the sub Athabasca basement, Saskatchewan: U proto-ore ?, In: C. Stanley (ed.), Mineral Deposits: *Processes to Processing., Balkema, Rotterdam*, 297-300.

AYERS, D. E. & EADINGTON, P. J. (1975): Uranium mineralization in the South Alligator River valley: *Mineral. Deposita* **10**, 27-41.

BASSON, I.J. & GREENWAY, G. (2004): The Rössing Uranium Deposit: a product of late-kinematic localization of uraniferous granites in the Central Zone of the Damara Orogen, Namibia. *J. African Earth Sci.* **38**, 413–435.

BERNING, J., COOKE, R., HIEMSTRA, S.A. & HOFFMAN, U. (1976): The Rössing uranium deposit. South West Africa: *Econ. Geol.* **71**, 351-368.

BOWDEN, P., HERD, D. & KINNAIRD, A. (1995): The significance of uranium and thorium concentrations in pegmatitic leucogranites (alaskites), Rössing mine, Swakopmund, Namibia: *Comm. Geol. Surv. Namibia* **10**, 44-49.

BRIQUEU, L., LANCELOT, J., VALOIS, J.P. & WALGENWITZ, F. (1980): Géochronologie U-Pb et genèse d'un type de minéralisation uranifère : les alaskites de Goanikontes (Namibie) et leur encaissant. *Bull. CREP Elf Aquitaine* **4**, 759-811.

BROOKS, J.M. (1960): The uranium deposits of northwestern Queensland. *Queensland Geol. Survey, Pub*. **297**, 48 p.

CAMPANA, B. & KING, D. (1958): Regional geology and mineral resources of the Olary province: *South Australia Geol. Survey Bull.* **34**, 1-91.

CARTER, E. K., BROOKS, J. H. & WALKER, K. R. (1961): The Precambrian mineral belt of northwestern Queensland: Australian Bur. Mineral Resources, *Geology Geophysics Bull*. **51**, 228-234.

CUNEY, M. (1980): Preliminary results on the petrology and fluid inclusions of the Rössing uraniferous alaskites: *Trans. Geol. Soc. South Africa*, **83**, 39-45.

CUNEY, M. (1981): Comportement de l'uranium et du thorium au cours du métamorphisme. Rôle de l'anatexie dans la genèse des magmas riches en radioéléments. Doctoral thesis, INPL, Nancy, 511 p.

CUNEY, M. (1982): Processus de concentration de l'uranium et du thorium au cours de la fusion partielle et de la cristallisation des magmas granitiques: In "*Les méthodes de prospection de l'uranium*", OCDE (ed), Paris, 277-292.

CUNEY, M. & FRIEDRICH, M. (1987): Physicochemical and crystal-chemical controls on accessory mineral paragenesis in granitoids. Implications on uranium metallogenesis. *Bulletin de Minéralogie* **110**, 235-247.

DEBON, F. & LE FORT, P. (1988): A cationic classification of common plutonic rocks and their magmatic associations; principles, method,

applications. Bulletin de Mineralogie, **111**, 493-510.

DODSON, R. G., NEEDHAM, R. S., WILKES, P. G., PAGE, R. W., SMART, P. G. & WATCHMAN, A. L., (1974): Uranium mineralization in the Rum Jungle-Alligator River province, Northern Territory, Australia. *In* "*Formation of uranium ore deposits: Vienna*", IAEA, Vienna, Austria, 551-567.

FAVALI, J. C. (1973): Mineralizacao uranifera na area do geosyncline do Serido: *Congreso Brasileiro do Geologico* **1**, 48-49.

FOWLER, A. D. & DOIG, R. (1983): The age and origin of Grenville Province uraniferous granites and pegmatites. *Can. J. Earth Sci.* **20**, 92-104.

HAWKESWORTH, C.J., KRAMERS, J.D. & MILLER, R.McG. (1981): Old model Nd Ages in Namibian Pan African rocks. *Nature* **289**, 278-282.

JACOB, R.E., CORNER, B. & BRYNARD, H.J. (1986): The regional geological and structural setting of the uraniferous granitic provinces of Southern Africa. In: Anhaeusser, C.R. and Maske, E. (Eds) Mineral Deposits of Southern Africa, II, *Spec. Pub. Geol. Soc. S. Afr*., 1807-1818.

JUNG, S. & MEZGER, K. (2003): Petrology of basement-dominated terranes: I. Regional metamorphic T-t path and geochronological constraints on Pan-African high-grade metamorphism (central Damara orogen, Namibia). *Chem. Geol.* **198**, 223–247.

KISTERS, A.F.M., JORDAAN, LS. & NEUMAIER, K. (2004): Thrust-related dome structures in the Karibib district and the origin of orthogonal fabric domains in the south Central Zone of the Pan-African Damara belt, Namibia. *Precamb. Res.* **133,** 283–303.

KRÖNER, A., RETIEF, E.A., COMPSTON, W., JACOB, R.E. & BURGER, A.J. (1991): Single-grain and conventional zircon dating of remobilised basement gneisses in the central Damara Belt of Namibia. *South African J. Geol.* **94**, 379–387.

LAURI, L., RAMO, T. & CUNEY, M. (2007): Source characteristics of U-enriched leucogranites of the Svecofennian orogen in southern Finland. *In* "Digging Deeper" C.J. Andrew *et al.* (*eds.*), *Proc. SGA Meeting*, Dublin, Ireland, 1165-1168.

LENTZ, D. (1996): U, Mo, and REE mineralization in late-tectonic granitic pegmatites, southwestern Grenville Province, Canada. *Ore Geol. Rev.* **11**, 197-227.

LINDAHL, I., ANDRESEN, A., RINDSTAD, B.I., & RUNDBERG, Y. (1985): Age and tectonic setting of the uraniferous Precambrian basement rocks at Orrefjell, Salangen, Troms. *Norsk Geologisk Tidsskrift* **65**, 167-178.

MADORE, C., ANNESLEY, I. & WHEATLEY, K. (2000): Petrogenesis, age and uranium fertility of peraluminous leucogranites and pegmatites of the McClean Lake / Sue and Key Lake / P-Patch deposit areas, Saskatchewan, *Geocanada 2000 Program with Abstracts – Geol. Assoc. Can.-Mineral. Assoc. Can.: Joint Annual Meeting,* **25**.

MARTIN, H. & PORADA, H. (1977): The intracratonic branch of the Damaran Orogen in Namibia. I. Discussion of geodynamic models. *Precamb. Res.* **5**, 311–338.

MASBERG, HP, HOFFER, E & HOERNES, S. (1992): Microfabrics indicating granulite-facies metamorphism in the low-pressure central Damara Orogen, Namibia. *Precamb. Res.* **55**, 243–257.

MAURICE, Y.T. (1977): Geochemical methods applied to uranium exploration in Southwest Baffin Island. *CIM Bulletin* **70**, 96-103.

MAWDSLEY, J.B. (1957): The geology of the Charlebois Lake area, Northern Saskatchewan. *Sask. Dept. Mineral. Res.* Rpt 24.

MONTEL, J.-M. (1993): A model for monazite/melt equilibrium and application to the generation of granitic magmas. *Chem. Geol.* **110**, 127-146.

MOUILLAC, J.L., VALOIS, J.P. & WALGENWITZ, F. (1986): The Goanikontes uranium occurrence in South West Africa/Namibia. *In* Anhaeusser C.R. & Maske S. (*Eds*.). *Mineral Deposits of South Africa*, 1834-1843.

NASH, C.R. (1971): Metamorphic petrology of the SJ area, Swakopmund District, Namibia. *Bull. Chamber Min. Precambr. Res. Unit, Univ. Cape Town* **9**, 77 p.

NASH, C.R. (1972): Primary anhydrite in Precambrian gneisses from the Swakopmund district, South West Africa. *Contrib. Mineral. Petrol.* **36**, 27-32.

NEX, P. & KINNAIRD, J.A. (1995): Granites and their mineralisation in the Swakop River area around Goanikontes, Namibia. *Comm. Geol. Surv. Namibia* **10**, 51-56.

NEX, P.A.M., KINNAIRD, J.A. & OLIVER, G.J.H. (2001): Petrology, geochemistry and mineralization of post-collisional magmatism in

the southern Central Zone, Damaran Orogen, Namibia. *J. African Earth Sci.* **33**, 481–502.

PARSLOW, G.R. & THOMAS, D.J. (1982): Uranium occurrences in the Cree Lake Zone, Saskatchewan, Canada. *Mineral. Mag.* **46**, 164-171.

PHAIR, G. & GOTTFRIED, D. (1964): The Colorado Front Range as a uranium and thorium province. *In* Adams, J.A.S. & Lowder, W.E., *eds*., *The natural radiation environment*: Houston, Rice Univ. 7-38.

POLI, L.C. & OLIVER, G.J.H. (2001): Constrictional deformation in the Central Zone of the Damara Orogen, Namibia. *J. African Earth Sci.* **33**, 303–321.

PORADA, H. & BEHR, H.J. (1988): Setting and sedimentary facies of late Proterozoic alkali lake (playa) deposits in the southern Damara belt of Namibia. *Sedimentary Geol.* **58**, 171-194.

RÄISÄNEN, E. (1989): Uraniferous granitic veins in the Svecofennian schist belt in Nummi-Pusula, southern Finland. *In* "Uranium Deposits in Magmatic and Metamorphic Rocks", Proc. IAEA Tech. Comm. Meeting, Salamanca. IAEA Report TC-571.

RAMOS, J.R., DE ANDRADE, A. & FRAENKEL, M. (1974): Uranium occurrences in Brazil. *In* Formation of uranium ore deposits: Vienna, Internat. Atomic Energy Agency, 637-658.

RIMSAÏTE, J., (1981): Petrogeochemical and mineralogical evolution of radioactive rocks in the Baie Johan Beetz area, Québec: a preliminary report. *Curr. Res., Geol. Surv. Can.* **81-1a**, 115-131.

ROBINSON, S.C. (1960): Economic uranium deposits in granitic dykes, Bancroft district, Ontario. *Can. Mineral.* **6**, 514-521.

SATTERLY, J. (1957): Radioactive mineral occurrences in the Bancroft area. *Annual Report of the Ontario Department of Mines* **65**, 179 p.

SAVITSKII, A.V., GROMOV, A.YU., MEL'NIKOV, E.K. & SHARIKOV, P.I. (1995): Uranium ore mineralization of the Litsk District in the Kola Peninsula (Russia). *Geol. Ore Deposits*, **37**, 351-362.

SCHMIDT, A. & WEDEPOHL, K.H. (1983): Chemical composition and genetic relations of the Matchless amphibolite (Damara orogenic belt). *Spec. Publ. Geol. Soc. South Africa* **11**, 139–145.

SIBBALD, T.I.I., MUNDAY, R.J.C. & LEWRY, J.F. (1976): The geological setting of uranium mineralization in northern Saskatchewan. *Sask. Geol. Soc. Spec. Pub.* **3**, 51-98.

SMITH, D.A.M. (1965): The geology of the area around the Khan and Swakop Rivers in Namibia. *Mem. Geological. Surey. Survey Africa (S.W.A. Series)* **3**, 113 p.

SPURR, J.E. (1900): Classification of igneous rocks according to composition. *Amer. Geol.* **25**, 210-234.

THOMPSON, B. P. (1965): Geological mineralogy of South Australia, in McAndrew, J., ed., Geology of Australian ore deposits, 2nd ed., v. 1: *Commonwealth Mining Metallurgy Cong*., 8th, Melbourne, 270-284.

VALOIS, J.P. & WALGENWITZ, F. (1979): Pétrographie des alaskites et de la série métamorphique de Goanikontes, Namibie. *Bull. Cent. Rech. Explor.-Prod. Elf Aquitaine* **3**, 351-367.

WATSON, E.B., & HARRISON, T.M. (1983): Zircon saturation revisited: temperature and composition effects in a variety of crustal magma types. *Earth Planet. Sci. Lett* **64**, 295-304.

YOUNG, E.J. & HAUFF, P.L. (1975): An occurrence of disseminated uraninite in Wheeler Basin, Grand County, Colorado: *U.S. Geol. Survey Jour. Research* **3**, 305-311.

CHAPTER 6: DEPOSITS RELATED TO NA-METASOMATISM AND HIGH-GRADE METAMORPHISM

Michel Cuney
G2R, Nancy-Université, CNRS, CREGU,
B.P. 239,
F-54506 Vandoeuvre lés Nancy, France
michel.cuney@g2r.uhp-nancy.fr

and

Kurt Kyser
Department of Geological Sciences and Geological Engineering,
Queen's University,
Kingston, Ontario, K7L 3N6, Canada
kyser@geol.queensu.ca

Alkali metasomatism is a widespread geological process that occurs in a large variety of geological conditions, some of which are associated with U ore-forming processes. Alkali metasomatism is most commonly associated with albite enrichment and quartz dissolution, although K-feldspathization may occur instead of albite enrichment. Albite enrichment can also be related to purely magmatic processes rather than hydrothermal–metasomatic processes, as in the case of Rare Metal Granites (Linnen & Cuney 2005, Cerný *et al.* 2005). Their albite-rich compositions are due to the high F contents of such extremely fractionated melts which expand the stability field of quartz and shift eutectic melt compositions toward albite in the quartz–K-feldspar–albite system (Manning 1981). Although such granite has been referred to by some as albitite, it is distinct in process from the albitite resulting from fluid–rock interactions.

This chapter is concerned with high temperature hydrothermal processes forming discontinuous occurrences of rock affected by Na-metasomatism over several tens of kilometres. Individual Na metasomatic zones are normally several metres wide and several hundred metres to several thousands of metres long. Granitic rocks are most commonly altered to albitite, but metavolcanic or metasedimentary rocks can be as well. One extreme example is the banded iron formations of the Krivoy-Rog district in Ukraine, which are altered to aegirinite by addition of Na from fluid percolation. Some of these areas may be totally barren, such as the albitized granite of Salvezines from the French Pyrenees (Boulvais *et al.* 2007), whereas others may be mineralized. This type of alteration may form either pre-ore alteration halos around the mineralization, as for the IOCG deposits of the Cloncurry district in Australia (Hitzman 2000), or may be a synmineralization process associated with regional deep structures as in the uranium district of Krivoy-Rog, Ukraine (Belevtsev & Koval 1968). However, even in the U-mineralized districts, only a small proportion of the rocks altered by Na-metasomatism contain U ore.

Uranium mineralization associated with Na-metasomatism occurs mainly during two discrete periods of earth history. The major one corresponds to the 1.9–1.7 Ga highly mineralized Krivoy-Rog district in the Ukraine (Belevtsev & Koval 1968), the Otish Basin in Quebec (Ruhlmann *et al.* 1986), at Mistamisk and other occurrences of the Labrador trough in Quebec (Kish & Cuney 1981), the Kurupung district in Guyana (Cinelu & Cuney 2007), Skuppesavon (Smellie & Laurikko 1984) and Bjorkramyran (Kullman 1989) in northern Sweden, and Liangshanguan in northeastern China (Jiarong & Zhutian 1988, Shen 1990). Another example may be the Lagoa Real district in Brazil, which may be younger (~1.4 Ga, Turpin *et al.* 1988; ~1.5 Ga, Cordani *et al.* 1992), but has been overprinted by the Brazilian event. However, the Valhalla deposit in Queensland (Polito *et al.* 2007) has ages similar to Lagoa Real, suggesting that a Na-metasomatism episode associated with U mineralization may have occurred at 1.4–1.5 Ga. A less widespread Na–U event is associated with the Pan-African–Brazilian (500 ± 50 Ma) deposit of Espinharas, northeastern Brazil (Ballhorn *et al.* 1981, Fuchs *et al.* 1981, Porto de Silveira *et al.* 1991), during the early hydrothermal phase in the granite sheets of the

Short course co-sponsored by the the SGA and MAC, Québec City, May 2008, p. 97-116

Itataia deposit (Netto 1983, Netto *et al.* 1991) and at Kitongo, Cameroon, (Vels & Fritsche 1988).

Na-metasomatism-related deposits of Ukraine

Exploration for U deposits started in Ukraine in 1944, with discovery of the Pervomayskoye deposit in 1945, the Zheltorechenskoye deposit in 1946, and the non-economical Annovskoye and Kremenchugskoye deposits in the Krivoy Rog district. In this district, Na-metasomatism affects metasedimentary rocks. Further exploration in the Kirovograd region led to the discovery in 1964 of the first U deposits considered as economic, the Michurinskoye, Severinskoye and Vatutinskoye deposits, with Na-metasomatism here developed in granite and gneiss of the Ukrainian Shield. The U contents in the ores of these deposits do not exceed 0.2%. Deposits in the area associated with K metasomatism (*i.e.*, Yuzhnoye, Kalinovskoye, Lozovatskoye), in fact correspond to intragranitic disseminated uraninite deposits of the Rössing type.

Regional geology. The Ukrainian U province associated with Na-metasomatism is located within the Sarmatia craton, which is composed of Archean (up to 3.5 Ga) to Proterozoic units exposed in the Ukrainian Shield and in the Voronezh Massif in Russia. The Sarmatia craton with the Fennoscandian and Volgo-Uralian cratons to the north form the East European Craton (Fig. 6-1, Bogdanova *et al.* 2008). Sarmatia first joined with the Volgo–Uralia craton at 2.0 Ga to form the Volgo-Sarmatia craton, during which all rocks within the suture zone underwent metamorphism, migmatization, and S-type granitic magmatism from 2.05 to 2.02 Ga. At *ca*. 1.8–1.7 Ga, Fennoscandia joined with Volgo-Sarmatia. The Fennoscandia–Sarmatia suture represents a major lithospheric boundary marked by the Osnitsa–Mikashevichi Igneous Belt (OMIB) of *ca*. 2.0–1.95 Ga age (Gorbatschev & Bogdanova 1993).

Sarmatia is composed of a series of north-south elongate cratonic blocks separated by major N–S structures. Each of these blocks seems to have a distinct tectono-metamorphic evolution and represents separate Archean microcontinents. They were partly reworked along 2.2–2.1 Ga north–south trending orogenic belts. The collision of the Volgo-Sarmatia craton with Fennoscandia caused extensive reworking of the Archean and Paleoproterozoic upper lithosphere of Sarmatia, with major anorthosite–charnockite–granite magmatism between 1.80 and 1.74 Ga. Finally,

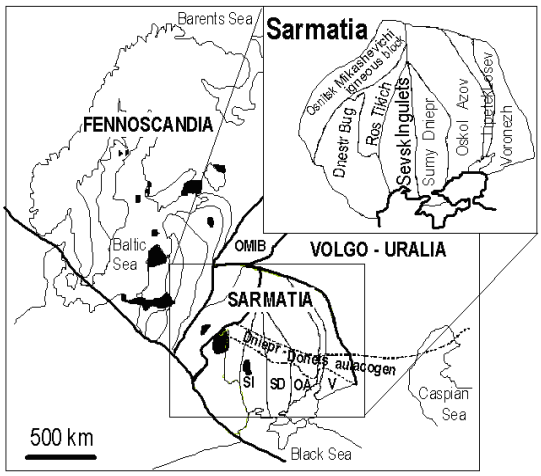

FIG. 6-1. Location of Sarmatia relatively to the Volgo-Uralian and Svecofennian shields. The U deposits associated with Na-metasomatism are located within the Sevsk-Ingulets block within the Samartia megablock (simplified from Bogdanova *et al*., 2008).

from Devonian to Tertiary, a 20-km deep rift filled with sediments and basic volcanism forming the Dniepr-Donetsk Basin.

Uranium mineralization associated with Na-metasomatism in Ukraine is situated along several north-south, deeply rooted continental scale structures occurring between and within the blocks of the central part of Sarmatia (Fig. 6-1). From west to east, these are:

(i) the Krivorozhsk–Kremenchung structure located at the western margin of the Kirovograd-Novoukrainsk (or Sevsk–Ingulets) block, where the city of Krivoy-Rog is located. The Zheltorechenskoye, Pervomaiskoye, Annovskoye, and Kremenchugskoye deposits are located within the Paleoproterozoic metasedimentary formations of the Krivoy-Rog–Zheltorechensk syncline hosting major banded iron formation deposits.

(ii) The Kirovograd structure occurs in the middle of the Kirovograd-Novoukrainsk block, where the Mitchurinskoye, Severinskoye, and Vatutinskoye deposits are located. Underground mining of the Vatutinskoye deposit occurs down to depths of 500 m. The Ingulskoye mine, south of Kirovograd, is operating with three shafts down to a depth of 700 m. The Kirovograd structure hosts high-grade metamorphic formations and granite (Kirovograd or Kirovograd-Zhitomirsky amphibole–biotite and cordierite–biotite granite), dated at *ca*. 2.1–2.2 Ga at the Eastern margin of the Novoukrainsk granite complex.

(iii) The Novokonstantinovka structure has a more limited extension and is hosted by the northern central part of the porphyritic Novoukrainsk granite. The granite underlies an area of *ca*. 3500 km^2. The Novokonstantinovka, Lesnoye, and Dokuchayevskoye deposits are located along this structure. Within the Novokonstantinovka lineament, the density of aplite and pegmatite dikes increases greatly, a feature interpreted as evidence of an early zone of weakness in the granite (Tarasov 2004). The mylonitic zones, associated with the altered and mineralized bodies are clearly intersected by the Korsun-Novomirgorodsk (named Korosternsky in Fig. 6-2) rapakivi granite dated at 1.8 Ga. This indicates that Na-metasomatism and U mineralization are older than 1.8 Ga, at least in the deposit of Novokonstantinovka.

(iv) Other uranium showings of less importance also occur at the eastern margin of the Novoukrainsk granite.

The altered zones and the U mineralization are controlled by ductile tectonic structures that were active at temperatures in excess of 500°C as evidenced by the formation of garnet–aegirine and the occurrence of mylonite in the center of the structure. Deformation continued under brittle conditions with crystallization in fractures of euhedral albite capped by pitchblende. Macroscopically, the altered zones are purple-red and generally maintain the original rock structure except in the most deformed zones. Uranium-ore bodies are typically lenticular, several metres to dozens of metres wide, dozens of metres to several hundred metres long, and hundreds of metres deep. Ore bodies have been drilled to depths greater than 1200 m.

Na-metasomatic alteration in quartz–feldspar-bearing rocks has an external non-mineralized zone in contact with the unaltered host rocks within which K-feldspar is albitized. In the internal zone with variable quartz dissolution, albite crystallization accompanied by hematite hosts the U mineralization. The rocks correspond to nearly pure albitite with minor amount of aegirine and riebeckite. Ca-metasomatism may occur in the internal alteration zone with new formation of pyroxene, garnet, epidote, carbonate minerals or a combination of these. Such a zonation is well illustrated by the detailed maps and cross sections of the Novokonstantinovka deposit (Fig. 6-3). Aegirine may be the sole alteration mineral in the case of banded iron formation in the Krivoy-Rog district.

Uranium is present as uraninite, brannerite, davidite, coffinite, and secondary hexavalent U minerals. Albitite always contains hematite, magnetite, apatite, variably metamict zircon, and rutile. In Ukraine, the U–Ti minerals are generally the most abundant and form aggregates with a range of compositions. They are commonly pseudomorphs of former Ti-minerals such as titanite and ilmenite in the source rock. Brannerite may occur as euhedral columnar crystal but is usually metamict.

The Krivoy-Rog district comprises two north-south striking synclines located along the Krivorozhsk structure (Fig. 6-2). The Saksagansk syncline to the south hosts the largest Fe deposits of the Krivoy-Rog district and the mined-out Sevgok U deposit. The Zheltorechensk syncline to the north (Fig. 6-3), comprises late Archean and Paleoproterozoic metavolcanic and metasedimentary rocks deposited in a passive continental margin environment, and

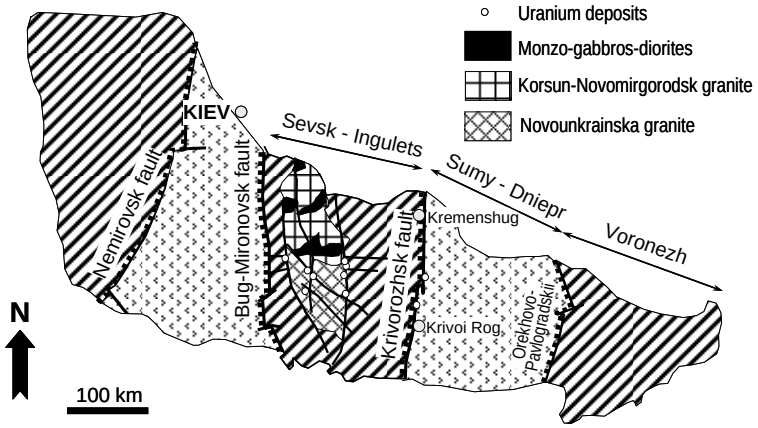

FIG. 6-2. Geologic map of the Ukrainian shield with the location of the main ore deposits and the major lineaments. Modified from Tarasov (2004).

FIG. 6-3. Geologic map of the Zheltorechensk syncline with the location of the U ore bodies and alteration zones (from Shcherbak & Bobrov 2005). 1, Kirovograd Zhitomir granitoid basement; 2, Sur-Tokov tonalite and granite basement; 3, Novokrivoyrog metavolcanic rocks; 4, Skelevatsk conglomerate and schist; 5, Saksagan Suite, including 6, banded iron formations; 7, Gdanzev sandstone, schist and conglomerate; 8, weakly Na-metasomatized zones; 9, strongly Na-metasomatized zones; 10, U ore bodies; 11, mylonites; 12, faults.

hosts the Novaya U mine. These formations are intruded by granitoid rocks of the Dniepr complex. Uranium mineralization is represented by a first generation of small euhedral uraninite crystals, disseminated in albite exhibiting granoblastic polygonal recrystallization. The texture of albite indicates a high temperature mineralization episode. Ti–U oxides, mostly brannerite, are coeval with the uraninite. Albite may also occur along fractures and can be associated with pitchblende deposition, variably altered to coffinite. In all U-minerals, Th is less than 200–300 ppm, but uraninite, brannerite, and pitchblende can contain up to several wt% ZrO_2. The mobility of Zr during Na-metasomatism is also indicated by high Zr contents in the mineralized aegerinite and albitite with 400 and 300 ppm Zr, respectively (Table 6-1).

Selected geochemical data from the Novaya U mine in the Krivoy-Rog district are given in Table 6-1. The protoliths of the quartzite–conglomerate–mica schist association were a mixture of quartz and K-minerals as shown by the mixing line in the mineral–geochemical diagram of Figure 6-4. The orthogneiss and the garnet–biotite gneiss have granitic compositions.

Most of the sedimentary rocks have average U and Th contents and Th/U ratios similar to average crustal values (Fig. 6-5), except for conglomerate and granitic orthogneiss, which have high U and Th and Th/U ratios close to 1. Uranium enrichment of conglomerate is a common feature in this area (Belevtsev *et al.* 1984). The low Th contents of banded iron formation samples indicate an origin essentially by chemical precipitation. No Th enrichment occurred in mineralized samples.

The Michurinskoye deposit occurs along the major brittle–ductile Kirovograd north–south structure (Fig. 6-2). In the northern part of the deposit, the structure is weakly dipping (40°W) compared to its southern part (70°W). The structures controlling the alteration and mineralization diverge from the main structure and tend to form flower structures (Fig. 6-6). The Michurinka mining district comprises three underground mines located within the suburbs of Kirovograd, and one mine extends below Kirovograd city. The alteration envelopes and mineralized zones are distributed along an average N170° direction, parallel to the N–S Kirovograd structure (Fig. 6-1). Variably migmatitic biotite gneiss, fine to medium grained biotite granite, and altered to strongly reddish albitite host the U mineralization. Deformation is very intense and varies from ultramylonite to brecciation.

In the Michurinka deposit, the U mineralization consists mainly of brannerite. Uraninite occurs as very small crystals and in subordinate amounts.

Resources. Uranium mineralization related to Na-metasomatism in Ukraine is usually of low grade, generally 0.01% U, but can reach 0.3% locally. The Reasonably Assured Resources (RAR) and Estimated Additional Resources according to the IAEA classification are 25,500 t U for the Vatutinskoye deposit, 27,000 t U for the Michurinskoye deposit, and 50,000 t U for the Severinskoye deposit. The domains with alkali-metasomatism developed between the Vatutinskoye deposit and the Michurinskoye deposit are the most

TABLE 6-1. CHEMICAL COMPOSITION OF METAMORPHIC ROCKS HOSTING THE KRIVOY-ROG DISTRICT U MINERALIZATION AND ALTERED AND MINERALIZED ROCKS FROM THE NOVAYA MINE.

	1105-6	KR2	KR0	1105-8	KR3	1105-3	1105-1b	1245-R	1245Ae	1245Ab	1245-9	1245Ca1	1245Ca2
SiO_2 (wt%)	95.27	92.61	83.84	76.15	73.70	62.67	52.02	45.58	47.08	47.18	63.48	8.93	0.57
Al_2O_3	2.83	5.55	7.95	13.14	18.50	14.39	0.16	0.10	0.07	6.20	19.24	0.49	0.14
Fe_2O_3	0.14	0.17	2.79	1.29	0.27	16.41	47.41	50.28	40.10	31.55	3.86	1.83	62.77
MnO	0.004	0.003	0.01	0.03	nd	0.03	0.011	0.062	nd	0.023	0.009	0.201	0.077
MgO	0.13	0.06	0.45	0.30	0.07	3.93	0.20	2.57	0.11	0.22	0.88	19.47	6.95
CaO	0.07	0.03	nd	0.96	0.03	0.16	0.11	0.38	0.16	0.89	0.07	27.51	11.09
Na_2O	nd	0.09	nd	3.67	0.42	0.15	0.07	1.74	11.75	9.85	9.96	0.61	0.10
K_2O	0.86	1.55	2.56	4.30	4.98	1.31	nd	nd	nd	nd	0.67	0.08	nd
TiO_2	0.02	0.05	0.25	0.14	0.34	0.37	nd	nd	0.01	0.78	0.34	0.04	0.02
P_2O_5	nd	0.04	0.07	0.07	0.04	0.16	0.12	0.18	0.13	0.48	0.07	1.42	0.13
I.L.	0.47	0.68	2.89	0.76	2.38	0.90	-0.16	-0.61	0.15	0.33	1.83	37.74	16.96
Total	99.78	100.82	100.81	100.82	100.72	100.47	99.94	100.27	99.58	97.51	100.42	98.31	98.81
P	17	30	54	-44	92	20	-4	-63	-382	-334	-308	-509	-201
Q	510	478	411	201	289	313	285	192	-120	-66	16	-299	-132
B	5	4	49	25	9	308	598	693	504	410	75	510	959
A	35	72	102	13	242	244	-3	-68	-383	-228	39	-994	-397
Ba (ppm)	21.64	34.27	151.00	277.40	87.89	451.00	341.90	4.80	90.76	66.45	364.10	4.98	4.65
Cu	10.08	5.62	77.25	10.55	9.95	7.24	11.05	5.35	6.43	15.02	98.14	6.51	6.20
Mo	2.35	2.16	6.15	1.98	2.12	3.16	2.10	0.76	1.33	1.61	1.62	1.66	1.96
Zn	9.20	23.66	41.19	38.61	13.63	72.94	16.21	11.89	26.08	14.54	48.02	72.30	90.87
Ni	19.59	5.40	71.65	17.40	4.98	90.21	14.27	6.77	9.14	33.63	30.35	41.07	20.90
Rb	19.57	37.73	81.57	305.80	110.90	59.34	0.92	nd	nd	0.59	15.55	2.93	0.53
Sr	3.88	4.33	6.64	71.78	12.03	8.75	8.62	6.75	5.25	28.18	105	431	62
Th	1.60	1.82	22.66	25.39	8.80	10.51	0.09	0.15	0.12	25.00	17.72	67.61	1.10
U	0.87	0.88	34.03	13.55	1.91	2.51	2.41	0.40	13.51	238	525	60	520
Pb	5.00	2.44	23.01	39.96	3.50	19.71	2.86	2.02	6.06	93	266	29	181
V	3	5	49	10	29	70	10	20	45	8197	707	260	1490
Sn	< L.D.	0.56	0.66	2.09	1.54	1.62	0.37	< L.D.	0.38	3.65	2.37	0.37	1.18
Nb	0.62	0.63	4.24	14.94	5.80	6.78	0.26	0.19	0.25	23.57	7.07	0.62	2.74
Ta	1.56	1.45	1.94	2.90	1.44	1.81	1.26	0.62	0.45	2.30	1.77	0.26	0.19
Y	1.52	1.48	8.92	8.90	2.86	14.33	30.82	3.32	19.41	24.86	10.52	115	3.65
Zr	38	50	101	97	165	84	2.89	17	4.07	399	303	102	49
Hf	0.17	0.33	2.23	2.72	4.34	1.65	nd	0.11	0.04	8.45	5.42	2.38	0.69
La	3.10	2.36	17.74	24.41	22.03	29.58	3.88	1.00	1.45	47.43	42.33	8.74	0.92
Ce	5.25	3.59	31.81	46.91	41.93	56.18	10.81	1.84	2.52	91.30	77.73	17.44	1.48
Pr	0.53	0.36	3.31	4.73	4.43	6.05	1.98	0.23	0.32	9.87	8.05	2.13	0.18
Nd	1.80	1.15	11.15	15.03	14.28	21.09	10.98	0.90	1.44	36.40	27.28	8.97	0.77
Sm	0.30	0.20	2.15	2.18	1.66	3.63	3.31	0.22	0.49	6.82	4.03	3.40	0.20
Eu	0.09	0.11	0.42	0.31	0.37	0.91	1.34	0.19	0.54	1.36	0.71	1.37	0.11
Tb	0.04	0.04	0.28	0.22	0.10	0.45	0.65	0.04	0.22	0.80	0.36	1.93	0.05
Gd	0.23	0.22	1.80	1.55	0.78	2.95	4.33	0.30	1.13	5.71	2.55	7.45	0.24
Dy	0.27	0.26	1.71	1.29	0.54	2.66	4.10	0.31	1.69	4.40	2.09	15.80	0.37
Ho	0.05	0.05	0.32	0.26	0.11	0.49	0.90	0.08	0.44	0.78	0.40	3.75	0.09
Tm	0.02	0.02	0.13	0.14	0.05	0.21	0.37	0.04	0.19	0.27	0.23	2.01	0.06
Yb	0.18	0.16	0.90	1.04	0.45	1.47	2.49	0.28	1.29	1.61	1.67	14.24	0.44
Er	0.16	0.15	0.88	0.79	0.34	1.49	2.55	0.24	1.33	2.03	1.28	12.09	0.33
Lu	0.03	0.03	0.14	0.18	0.08	0.23	0.39	0.05	0.21	0.23	0.27	2.19	0.07

1105-6 and KR2: quartzite, KR0: conglomerate, 1105-8: migmatite, KR3: phyllite, 1105-3: biotite-garnet schist, 1105-1b: banded iron formation, 1245-R: riebeckitite, 1245Ae: aegirinite, 1245Ab: mineralized albitite, 1245-9: mineralized aegirinite, 1245Ca1: slightly mineralized talc-actinolite metasomatite, 1245Ca2: mineralized iron-carbonate metasomatite. Nd =below detection limit (data from Maruéjol *et al.* 1989 and Cuney, unpub.).

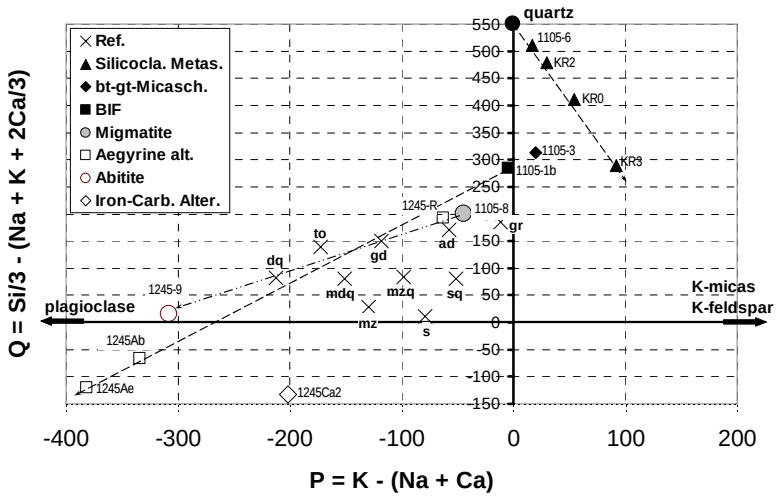

FIG. 6-4. Evolution of quartz (Q parameter) relatively to K-bearing minerals (K-feldspar and micas) and Na–Ca-bearing minerals (P parameter) contents in the Novaya mine metamorphic and metasomatic rocks associated with the U mineralization. The arrows joining the siliciclastic sedimentary rocks indicate mixing between detrital quartz and K minerals. The two other arrows indicate the dissolution of quartz and associated Na-metasomatism corresponding either to albite new formation for quartz-feldspar protoliths or to aegirine ± riebeckite for banded iron formation protoliths. For the most dequartzified samples, the new formation of aegirine ± riebeckite leads to quartz-undersaturated compositions (negative Q values). Chemical-mineralogical diagram in thousands of cations from Debon & Lefort (1988). Average compositions of reference rocks (mz, monzonite; mzdq, Qz-monzodiorite; dq, Qz-diorite; s, syenite; sq, Qz-syenite; to, tonalite; gd, granodiorite; ad, adamellelite (quartz monzonite); g, granite). Data from Table 6-1.

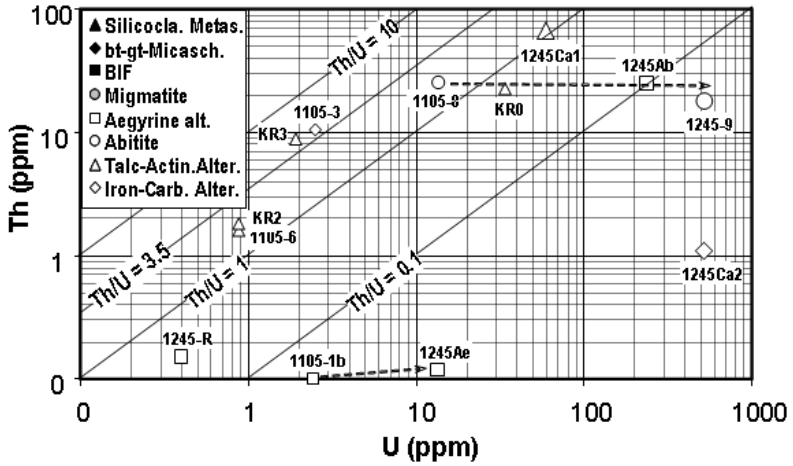

FIG. 6-5. Th–U relations in the Novaya mine metamorphic and metasomatic rocks associated with the uranium mineralization.

promising for the discovery for new Na-metasomatism-related U deposits. It is important to notice that the outcrop conditions in the area are very poor. The deposits have been discovered thanks to systematic drilling.

Genetic model. Na–Ca metasomatism and U mineralization are clearly controlled by tectonic structures at all scales. At a regional scale, the mineralized districts are clearly located along large lineaments, extending over several tens of km (Fig. 6-1). All these lineaments in the central Ukrainian Uranium Province are located within the Krivoy-Rog–Kremenshug structure or are parallel to continental block boundaries. These lineaments were first active at high temperature with formation of mylonite and polygonal granoblastic structures in albite, the orientation of which is parallel to the

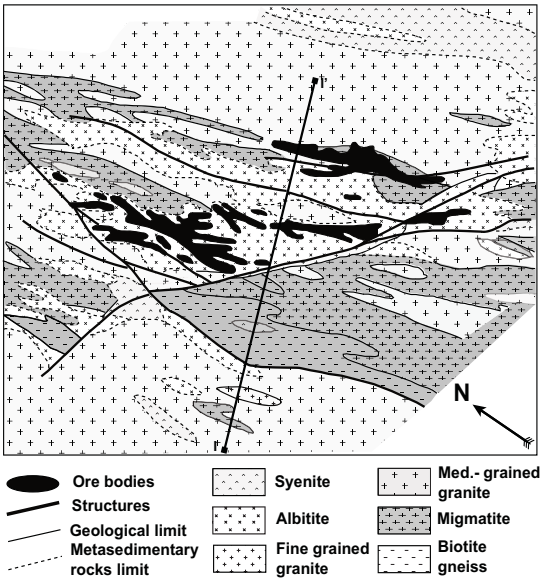

FIG. 6-6: Geological map of the Michurinka deposit. Line I–I' represents the cross section for Figure 6-7 (from Shcherbak & Bobrov 2005).

regional foliation of the metamorphic rocks. The lineaments continued to be active at lower temperatures in the brittle structural regime with the formation of albite, pitchblende, and carbonate in fractures and chlorite–epidote alteration in the host rocks. At the scale of the deposit, the alteration envelopes and the U mineralization are strictly controlled by nearly vertical to moderately dipping structures, which tend to diverge upwards as flower-like structures (Fig. 6-7). Possible U sources in the deposits include protoliths with high initial U, such as orthogneiss for those deposits hosted in granite, or conglomerate which may have been the equivalent of Archean quartz-pebble conglomerate with detrital uraninite. The source of the fluid responsible for the Na metasomatism and quartz dissolution is presumed to be metamorphic, derived from anatectic zones and ascending upward along deep and large fractures (Kushev 1972). However, there is a difference of 200 m.y. between regional metamorphism and the mineralization processes according to Kazansky & Laverov (1978), with Na metasomatism and U mineralization related to a Late Proterozoic tectonic-magmatic activity along long-lived, deep-seated structures, long after peak metamorphism. However, considerable variations in the reported ages for host granite (1800 to 2200 Ma) and mineralization do not allow a reliable genetic model related to them to be validated.

FIG. 6-7. Vertical section of the Michurinka deposit along the I–I' line of Fig. 6-6. Same symbols as in Fig. 6-3 (Shcherbak & Bobrov, 2005).

Lagoa Real (Bahia, Brazil)

Regional geology. The Lagoa Real U district is located in the south-central part of the São Francisco Craton, 500 km west of Salvador (Fig. 6-8). The Lagoa Real granite-gneiss complex is part of the Paleoproterozoic to Archean gneiss of the Paramirim-Gavião blocks (Inda & Barbosa 1996, Fig. 6-9). Lenses of the Lagoa Real complex preserved from deformation are called the San Timoteo granite. The Lagoa Real granitic gneiss has the same major and trace element composition as the San Timoteo granite and both will be refered to as the Lagoa Real granite *s.l.* It extends over an area

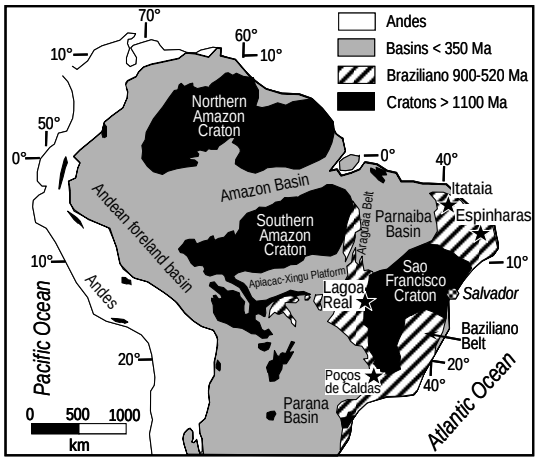

FIG. 6-8. Location of the Lagoa Real and other major U deposits of Brazil (stars) with respect to the different geotectonic units of South America.

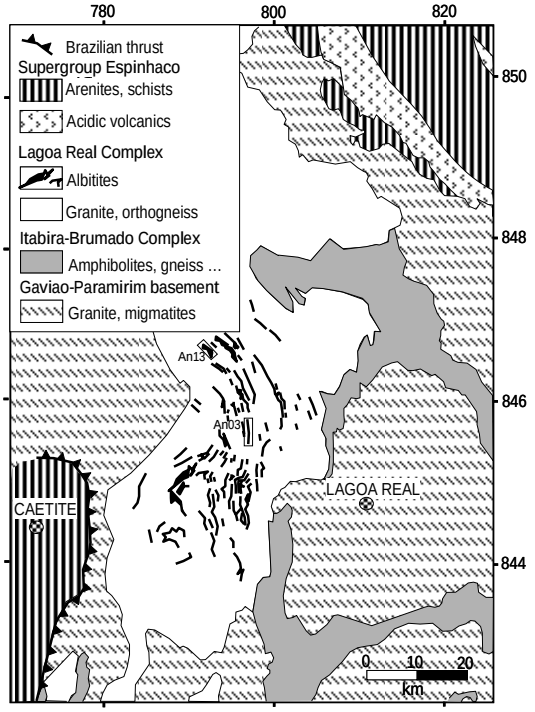

FIG. 6-9: Geologic map of the Lagoa Real district with the location of the main albitized bodies and of anomaly 03 (Fig. 6-10) and 13 (Cachoeira deposit); modified from Pascholati *et al.* (2003).

of about 2,000 km^2 and was thrust to the west over the Mesoproterozoic Espinhaço Supergroup during the Brazilian event at *ca*. 500 Ma. The Espinhaço Supergroup comprises from base to top: acidic volcanic rocks, conglomerate and sandstone with interlayered shale, locally graphitic, and quartzite deposited in a continental platform to marine environment (Jardim de Sa 1978). Below the thrust, the Espinhaço sequence shows inverted metamorphism, with increasing foliation, lineation and metamorphic grade towards the thrust (Caby & Arthaud 1987). Such features are typical of collisional orogens (Lefort 1975).

The Lagoa Real granite. The structure varies from undeformed strongly porphyritic granite, preserved as lenses mostly in the eastern part of the complex, to strongly foliated augen gneiss. The granite is composed of strongly perthitic K-feldspar phenocrysts (40 ± 5vol.%), $An_{5–26}$ plagioclase (25 ±5 vol.%), quartz (30 ±5 vol.%), Al-poor–Fe-rich biotite, ferropargasite to hastingsite, and locally Fe-rich-hedenbergite preserved as relicts in amphibole crystals in the undeformed granite (up to 15 vol.% for all mafic minerals). Accessory minerals are magnetite, ilmenite, titanite, fluorapatite, zircon, allanite, Nb–Ti–REE–U oxide and silicate minerals with up to 5.1 wt.% UO_2, REE-rich titanite, monazite, uranothorite, LREE fluoro-carbonates, and fluorite (Maruéjol *et al.* 1987, Maruéjol 1989). In deformed granite, the structure becomes granoblastic polygonal and a streching lineation is defined by biotite–amphibole aggregates. Perthite is unmixed into microcline and plagioclase, pyroxene is totally altered to amphibole, and amphibole + ilmenite are partly altered to a biotite + titanite + magnetite ± calcite assemblage. The Lagoa Real granite was presumed to be Archean from Rb–Sr dating (Lobato *et al.* 1983a, 1983b), but U–Pb dating of zircon revealed that they were emplaced during late Paleoproterozoic at 1724 ±5 (Turpin *et al.* 1988) to 1750 Ma (Cordani *et al.* 1992).

Na-metasomatism. The south-central part of the Lagoa Real granite contains a very large number of discontinuous lenticular bodies of albitized and dequartzified granite (Fig. 6-9) developed over about 50 km along approximately meridional shear zones (Turpin *et al.* 1988, Lobato & Fyfe 1990, Cordani *et al.* 1992). From south to north the albitized and dequartzified bodies trend from N40E to N30W and dip from 30^o to the west to 70^o to the east, respectively (Costa *et al.* 1985). Each albitite body may be up to 3 km long, up to 30 m wide, and extends down to more than 300 m below the surface, the maximum depth reached by drill cores (Fig. 6-10). The albitite bodies may contain several U-mineralized levels or be barren. The altered zones present zonation from orthogneiss to albitized and dequartzified orthogneiss with albite(1), albite(2), ± pyroxene, ± garnet, uraninite, titanite and magnetite. Because of the extensive recrystallization of the rocks during the deformation event related to the Brazilian orogeny, the typical replacement texture of K-feldspar by albite (chess-board twinning) and the vugs left by quartz dissolution and filled by euhedral albite crystals classically observed in such alteration processes, as in the U–Zr mineralized albitites of Guyana (Cinelu & Cuney 2006), are not observed at Lagoa Real. The metamorphic fabric crosscuts the compositional layering of the altered zones, generally at low angles, and thus clearly post-dates the alteration event (Caby & Arthaud 1987).

Uranium mineralization. Uraninite is the only primary U mineral in the albitite. It occurs as finely disseminated crystals included in all minerals, in

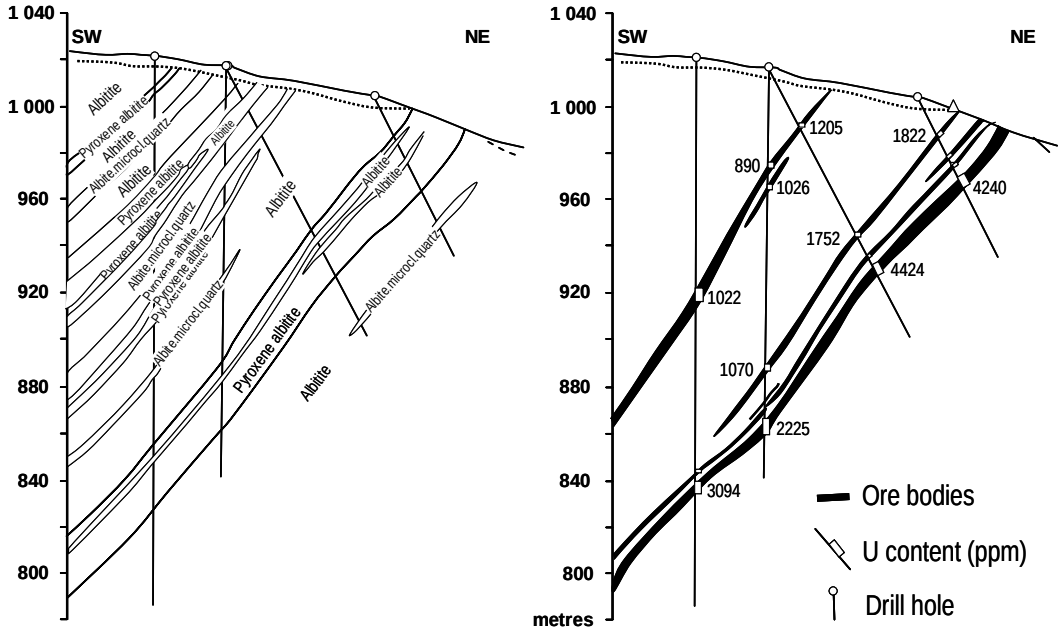

FIG. 6-10. Distribution of metasomatic alteration zones (left) and mineralization (right) in a cross section through Anomaly 03, the location of which is given in Fig. 6-9. Modified from a Nuclebras document (unpublished).

some places regrouped in stringers, in association with titanite and magnetite. Ca and Y contents reach several percent (1.8 to 2.6 wt.% CaO and 1.5 to 2.2 wt.% Y_2O_3). Local weathering has produced small amounts of uranophane. Magnetite is frequently partly martitized, probably also by meteoric fluids. Of the 35 major U anomalies discovered by Nuclebras in the Lagoa Real district, 11 are considered U deposits.

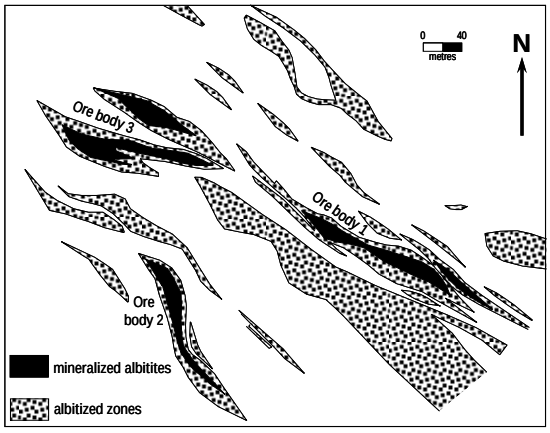

FIG. 6-11. Map of the distribution of the different ore bodies in the Cachoeira deposit (anomaly 13) (modified from a document of Industrias Nucleares Brasileras).

The presently mined Cachoeira deposit, (Fig. 6-11) located 40 km East of Caetité city, has measured geological reserves of 20,460 tons U at 0.35% U, of which 5,500 tons U can be extracted by open pit mining with a cut-off grade of 800 ppm and sulfuric acid consumption of 35 kg/t. The nominal capacity of the ore plant is 400 t/year.

Geochemistry. The Lagoa Real granite and orthogneiss have the same major and trace element composition. They correspond to highly potassic, iron-rich, metaluminous calcalkalic granite (A2 type granite of Eby 1992), strongly enriched in Th, U, Nb, Ba, and Zr (Table 6-2). Two groups can be distinguished, a more fractionated group rich in Th (20–108 ppm), Nb (36–111 ppm), and REE (400–3000 ppm), which is the most leucocratic, less metaluminous (Fig. 6-12), and rich in quartz and K-feldspar (Fig. 6-13), and a less fractionated group poorer in Th (7–27 ppm), Nb (20–63 ppm), and REE (200–400 ppm) and richer in mafic minerals and plagioclase. Granite of the first group has either positive, or slightly negative, Eu anomalies that may correspond to plagioclase accumulation. Th–Nb-rich granite has significant negative Eu anomalies, and some is HREE-enriched. The first group has affinities with peralkaline granite (A1 type granites of Eby 1992) by its very high Th, Nb,

TABLE 6-2. CHEMICAL COMPOSITION OF THE HOST ROCKS AND ALTERED AND MINERALIZED ROCKS OF THE LAGOA REAL DISTRICT.

	1	2	3	4	5	6	7	8	9	10	11	12	13	14	15
SiO_2 wt%	48.24	71.1	72.79	73.12	70.95	67.22	67.5	67.27	69.61	71.16	50.73	56.00	58.96	64.28	62.91
TiO_2	1.82	0.19	0.27	0.14	0.32	0.43	0.31	0.41	0.28	0.29	1.10	0.52	0.72	0.46	0.54
Al_2O_3	14.59	12.85	12.38	12.53	13.2	14.93	14.9	15.52	14.28	13.61	16.25	16.47	15.44	15.46	18.47
Fe_2O_3t	12.17	3.37	3.96	2.17	3.94	4.49	4.66	5.06	4.05	4.23	8.19	6.65	6.83	7.84	5.59
Fe_2O_3	5.00	2.4	2.00	0.57	1.23	1.51	1.26	2.96	1.71	3.19	5.07	3.65	5.74	4.54	5.00
FeO	6.45	0.87	1.76	1.44	2.44	2.68	3.06	1.89	2.11	0.94	2.81	2.70	0.98	2.97	0.53
MnO	0.13	0.03	0.06	nd	0.05	0.06	0.07	0.04	0.08	0.03	0.16	0.15	0.10	0.07	0.03
MgO	7.43	nd	0.10	nd	nd	nd	0.36	nd	1.26	0.46	7.18	1.90	0.52	0.15	0.72
CaO	8.97	1.14	0.86	0.95	1.41	2.11	2.32	1.27	2.39	1.25	7.57	5.48	7.82	1.09	2.86
Na_2O	4.27	3.19	3.17	2.88	3.11	3.66	3.65	5.10	7.10	5.60	4.62	7.90	7.90	8.40	9.20
K_2O	1.43	6.24	5.72	6.13	5.37	5.25	5.34	4	0.51	1.93	2.88	1.03	0.24	0.45	0.46
P_2O_5	0.20	nd	nd	nd	nd	nd	nd	0.05	0.02	nd	0.20	nd	0.02	nd	nd
CO_2	0.10	0.00	0.07	0.00	0.00	0.00	0.00	0.11	0.15	0.00	0.10	3.13	0.00	0.00	0.05
LOI	0.67	0.68	0.41	0.57	0.34	0.49	0.41	0.12	0.21	0.15	1.15	2.77	0.59	0.13	0.21
Total	99.30	98.69	99.59	98.37	98.42	98.34	99.18	98.74	99.71	98.61	99.82	101.7	99.03	98.00	101.0
P	-267	9	4	21	-11	-44	-46	-102	-261	-162	-223	-331	-389	-281	-338
Q	-7	146	170	171	163	118	116	109	118	159	19	31	-26	63	9
B	361	44	55	29	53	61	71	68	86	68	296	137	107	108	95
A	-202	-24	-12	-11	-6	-12	-22	10	-45	1	-161	-15	-236	-16	-46
A/CNK	0.59	0.91	0.95	0.96	0.98	0.96	0.93	1.03	0.86	1.00	0.66	0.68	0.56	0.95	0.89
NK/A	0.59	0.93	0.92	0.91	0.83	0.78	0.79	0.82	0.86	0.83	0.66	0.85	0.86	0.92	0.85
Ba ppm	397	746	413	1300	1067	1632	1434	1661	347	536	466	257	434	409	167
Rb	49	300	277	217	156	154	166	110	13	38	111	60	13	nd	nd
Sr	319	51	52	184	168	343	200	142	101	97	351	292	240	75	156
Nb	12	76	102	55	29	24	41	39	nd	nd	70	101	100	157	42
Y	na	483	262	120	102	41	119	na	61	159	na	na	210	na	64
Zr	136	479	540	651	488	489	596	682	nd	nd	771	862	1406	678	732
U	3	6	12	4	4	2	3	3	5	6	3075	5400	1578	11190	19
Th	1	55	72	20	16	7	20	15	15	36	19	17	19	17	21
Cr	125	nd	nd	18	nd	nd	nd	nd	nd	28	26	20	nd	13	nd
Ni	122	nd	nd	nd	nd	nd	nd	36	nd	21	nd	nd	173	14	66
V	305	10	13	54	nd	58	nd	31	19	nd	440	161	202	193	39
F	1700	4400	3400	1200	870	510	740	360	1600	310	5900	570	nd	290	360
La	na	1260	325	11	123	64	156	na	82	355	na	na	248	na	112
Ce	na	611	624	216	173	113	284	na	146	407	na	na	385	na	222
Nd	na	909	321	122	94	47	130	na	70	302	na	na	201	na	75
Sm	na	164	63	26	19	9	24	na	14	55	na	na	42	na	13
Eu	na	15	5	4	4	3	5	na	5	10	na	na	8	na	4
Gd	na	103	55	22	15	7	20	na	12	37	na	na	34	na	11
Dy	na	77	49	19	13	7	16	na	10	29	na	na	31	na	10
Er	na	33	23	10	7	3	9	na	5	14	na	na	16	na	5
Yb	na	26	21	10	7	3	8	na	6	14	na	na	17	na	6
Lu	na	3	3	1	1	1	1	na	1	2	na	na	2	na	1

1, amphibolite; 2, 3, 4, Th-Nb-rich Lagoa Real granite and orthogneiss; 5, 6, 7, Lagoa Real granite and orthogneiss; 8, 9, 10, albitized Lagoa Real orthogneiss; 11, 12, 13, 14, mineralized dequartzified and albitized Lagoa Real orthogneiss; 15, barren dequartzified and albitized Lagoa Real orthogneiss. nd = not detected (data from Maruéjol, 1989), na = not analyzed.

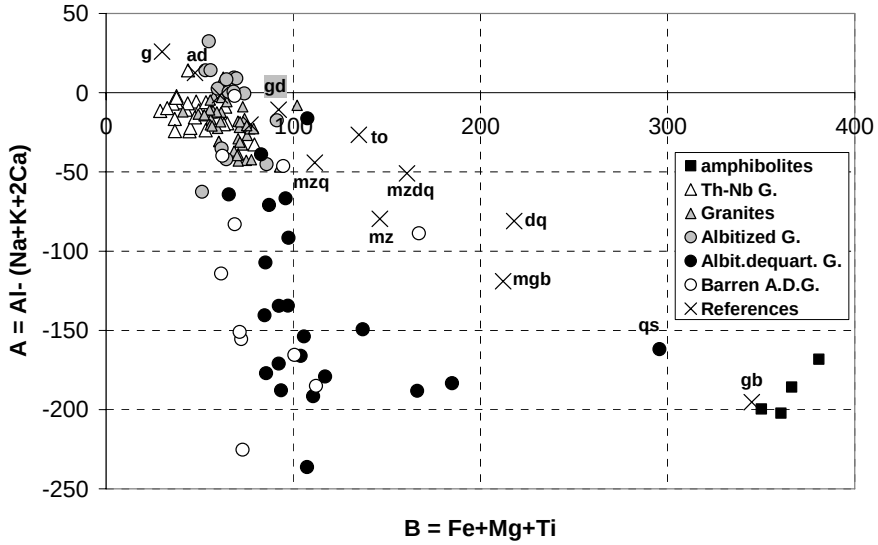

FIG 6-12. Evolution of the peraluminous index (A parameter) with differentiation (B parameter) in the Lagoa Real granite and metasomatized zones associated with U mineralization. The Lagoa granite is metaluminous and the altered samples become increasingly metaluminous with increase Ca addition. Barren and mineralized albitized rocks have the same range of compositions. The average composition of reference rocks are also given: gb, gabbro; mgb, monzogabbro; mz, monzonite; mzdq, quartz monzodiorite; dq, quartz diorite; to, tonalite; gd, granodiorite; ad, adamellelite (quartz monzonite); g, granite. Data from Maruéjol (1989).

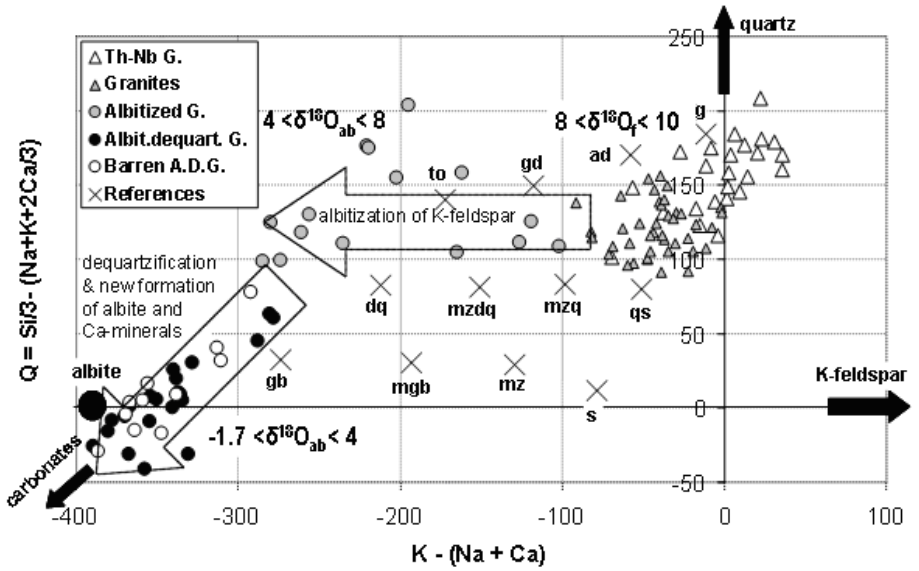

FIG. 6-13. Evolution of the quartz content (Q parameter) relative to K-feldspar and Na-Ca bearing mineral contents (P parameter) in the Lagoa Real granite and altered zones associated with U mineralization. The horizontal arrow indicates the replacement of K-feldspar by albite at constant quartz content. The inclined arrow corresponds to dequartzification and new formation of albite and Ca-minerals. For the most extremely albitized samples, the addition of Ca in the system leads to quartz-undersaturated compositions. Barren and mineralized albitized rocks have the same range of compositions. Diagram is from Debon & Lefort (1988). A.D.G = albitized desilicified granite. The average composition of reference rocks are also given: gb, gabbro; mgb, monzogabbro; mz, monzonite; mzdq, quartz monzodiorite; dq, quartz diorite; s, syenite; sq, quartz syenite; to, tonalite; gd, granodiorite; ad, adamellelite (quartz monzonite); g, granite. Data from Maruéjol (1989).

REE, and Zr contents, but remains always meta-aluminous.

During the alteration process, the same geochemical evolution described for the Bokan Mountain mineralized albitite includes a first stage with only albitization of K-feldspar (albite 1) and a second stage with progressive dissolution of quartz and crystallization of albite (albitite 2) and Ca minerals. Only albitite with quartz dissolution is mineralized with uraninite. Mass balance calculations show that dequartzified gneiss has a volume loss of about 10 to 15% (Lobato *et al.* 1983a, 1983b; Maruéjol 1989), with enrichment in Na as albite, Ca as pyroxene ± garnet ± epidote ± carbonate minerals, Zr as zircon (Fig. 6-14), and U (up to 1 wt.%; Fig. 6-15), Y (up to 570 ppm) and V (up to 500 ppm) related to uraninite deposition. The REE do not appear to have been significantly mobilized during the alteration, except for a slight HREE enrichment in some mineralized albitite, associated with neoformation of garnet.

Oxygen isotope thermometry on the alteration minerals of albitite yields temperatures of 500 to 550°C (Lobato *et al.* 1983a), which are compatible with the alteration assemblage (andradite–hedenbergite). As no hydrous minerals were formed in most samples, there was probably no significant infiltration of fluids. The gradual transition toward lower $\delta^{18}O$ values of feldspars from the granite to the albitized granite and to the desilicified-albitized granite (Fig. 6-13) reflects an increasing water/rock ratio with an ^{18}O-depleted fluid (Lobato *et al.* 1983a, 1983b) producing increasing alteration of the granitic protolith.

Genetic model. Sobrinho (1981) first proposed a late-magmatic origin for the genesis of the Lagoa Real U mineralization. However, the ore deposits are not located preferentially in the most fractionated part of the granite as is usually the case for deposits related to extreme magma fractionation. The enrichment in Ca in a large proportion of albitite and the much lower age of 400 Ma for the U mineralization (Turpin *et al.* 1988), compared to the granite emplacement age of 1724–1750 Ma is also inconsistent with such an origin.

Lobato *et al.* (1983a, 1983b) and Lobato & Fyfe (1990) proposed that the mineralization and the associated Na–Ca metasomatism resulted from the infiltration of pore waters expelled from the Espinhaço metasedimentary formations during their overthrusting by the Lagoa Real Archean gneisses during Brazilian orogenesis at ca. 500–700 Ma. However, this model is not consistent with either the structural observations, showing that the metamorphic foliation in the Lagoa Real granite-gneiss is discordant with the layering of the albitite (Caby & Arthaud 1987) or the older U–Pb ages of

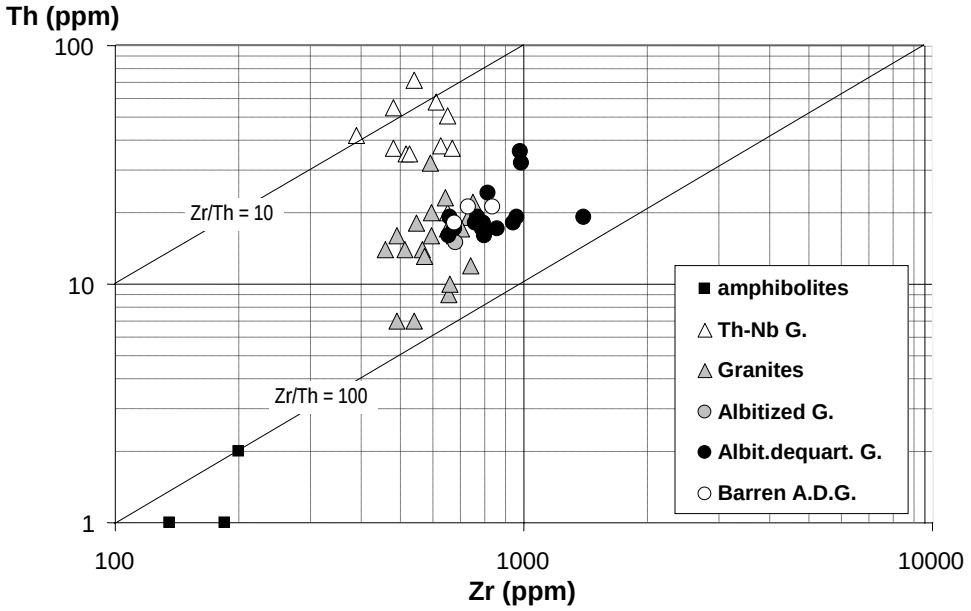

FIG. 6-15. Th-Zr relations in Lagoa Real amphibolite, granite and altered–mineralized zones. The mineralized albitized dequartzified rocks are also enriched in Zr relatively to granite and non-mineralized altered rocks. Data from Maruéjol (1989).

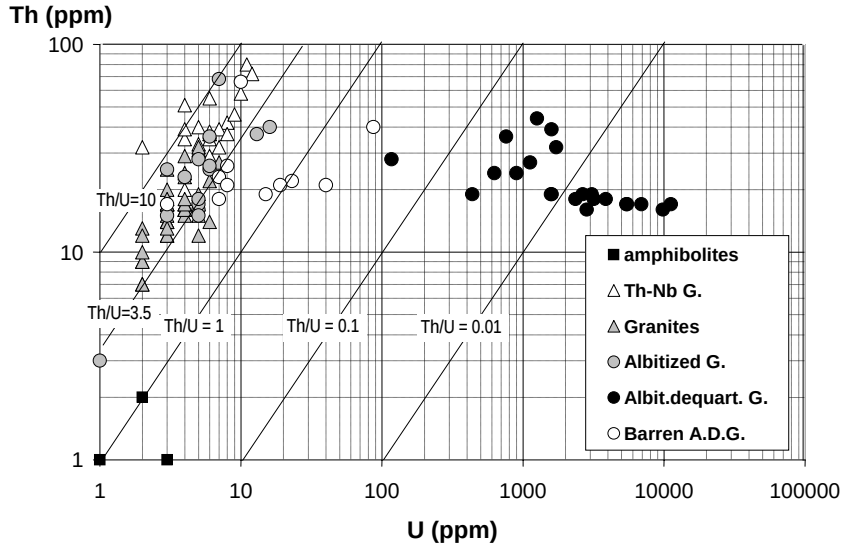

FIG. 6-15. Th-U relations in Lagoa Real amphibolite, granite and altered–mineralized zones. Most Th/U ratios of granite are below 3.5, indicating possible U loss from these rocks. Th-Nb-rich granite is the richest in U. Th content does not increase in U-mineralized samples. Data from Maruéjol (1989).

the uraninite relative to the Brazilian event (Turpin *et al.* 1988). Moreover, the Himalayan-type thrusting observed in the Espinhaço sequence cannot have expelled pore water of the sedimentary rocks without oxygen isotopic signatures of water or marine pore water because the latter were expelled during the low-grade metamorphic stage. Instead, the overthrust metasedimentary rocks must have generated high-temperature metamorphic fluids resulting from dehydration reactions occurring in the upper part of the thrust metasedimentary rocks to produce the garnet, staurolite, and kyanite metamorphic mineral association.

Maruéjol *et al*. (1987), Maruéjol (1989), and Turpin *et al.* (1988) proposed that the Paleoproterozoic Lagoa Real host granite (1725–1750 Ma), which is a highly potassic calcalkalic granite, represents the best source of the U. The granite is enriched in Th (up to 108 ppm) and U (up to 31 ppm) and exhibits higher Th/U ratios than average crust, consistent with U loss (Fig 6-15). However, it is not known whether U has been lost during the mineralization event or the Brazilian metamorphic event. Mineralizing fluids have ages and isotopic compositions consistent with derivation from the Mesoproterozoic Espinhaço sedimentary rocks that should have been lying over the Lagoa Real granite at that time. The basinal fluids led first to albitization of K-feldspar along fracture zones and with further fluid–rock interaction to dequartzification of the granite and simultaneous filling of the created space by albite and Ca-minerals, and deposition of U mineralization. The calculated volume loss of 10 to 15%, obtained for mineralized albitite, indicates that the space resulting from quartz dissolution has not been totally filled by secondary minerals. Therefore, the rock may have been porous at a certain stage during the alteration process as commonly observed in Variscan episyenite (Cathelineau 1986). As in Variscan episyenite, U may have been deposited at a later stage in these vugs. Lobato & Fyfe (1990) proposed that hexavalent U in solution would have been reduced by oxidation of Fe^{2+} to Fe^{3+} from iron minerals of the enclosing granite.

The deposits have been strongly deformed during the Brazilian event at about 500 Ma and the mineral paragenesis has been totally recrystallized with formation of granoblastic polygonal structures for quartz as well as for feldspar, implying a high temperature for the deformation (500–600°C). Such a deformation event has led to the complete disappearance of the initial texture, precluding the reconstitution of a paragenetic succession, and of any fluid inclusion study to characterize the fluids responsible for the alteration and mineralization processes, and preventing the definition of the tectonic conditions prevailing in the area when the mineralization formed.

Other world occurrences of uranium deposits associated with Na-metasomatism

Valhalla (NW Queensland. Australia) The Valhalla U deposit, located 40 km north of Mount Isa, represents another occurrence of U mineralization associated with Na metasomatism. It is one of 107 U occurrences that have been recorded in Paleoproterozoic metasedimentary rocks of the Leichhardt River Fault Trough (McKay & Miezitis 2001) dated from 1800 to *ca*. 1700 Ma (Neumann *et al.* 2006). Host rocks consist of interbedded arkose, fine-grained sandstone, and gritty siltstone bounded by basalt belonging to the Eastern Creek Volcanic Group (1790 Ma) in the Western part of the Mount Isa Basin. The southern Mt. Isa Basin in the vicinity of the Valhalla deposit was metamorphosed to upper greenschist and amphibolite facies (Rubenach 1992) during the 1555 ± 15 Ma to 1532 ± 7 Ma Isan Orogeny (Connors & Page 1995).

The Valhalla U deposit was discovered in 1954 and has since been drilled by government and several private companies. In August 2006, indicated resources were of 14,331 t U at 0.068% U and inferred resources of 7,632 t U at 0.064% U (http://www.wise-uranium.org/). The richest part of the ore body presents 0.6 wt.% U over 10.2 m, with brannerite as the dominant ore mineral. The mineralization is controlled by two vertical structures striking NNW and the ore bodies dip 50° to the south. The larger of the two ore bodies extends for 675 m below the surface, whereas the other one, occurring 1200 m to the south, is much smaller and extends down only for 200 m. According to Polito *et al.* (2007), the rocks hosting the U mineralization were first altered with the development of an albite, F-rich magnesio-riebeckite, calcite, Ti–V-rich magnetite ± brannerite ± uraninite ± dolomite in a strongly foliated rock. Then the rocks were brecciated, further altered and cemented by albite, riebeckite, calcite, apatite, hematite, anatase and the main ore minerals, brannerite, U-rich zircon (up to 1 wt.% Zr in the whole rocks), and uraninite, which represent the main mineralization. Zircon occurs as subhedral to rounded crystals associated with magnesio-riebeckite and albite and sometimes as veins indicating a hydrothermal origin and U contents vary up to 20 wt.%. A late stage of mineralization corresponds to the deposition of dolomite, calcite, chlorite, quartz, hematite, and small amounts of uraninite variably altered to coffinite and Pb–Fe–Cu sulfide minerals in veins. Mass balance calculations show that the mineralization involved the removal of K, Ba, and Si and the addition of Na, Ca, U, V, Zr, P, Sr, F and Y. Grades of about 0.13% V_2O_5 are associated with the U mineralization.

Brannerite U–Pb and Pb–Pb dates are between 1555 and 1510 Ma and overlap the $^{40}Ar/^{39}Ar$ ages of 1533 ±9 Ma and 1551 ±7 Ma obtained from early and main-stage riebeckite (Polito *et al.* 2007). These dates are interpreted as corresponding to the timing of U mineralization and coincide with the age of peak metamorphism in the Mount Isa area during the Isan Orogeny. A Pb loss at *ca*. 1200 Ma is attributed to the assembly of Rodinia.

The hydroxyl site of apatite and riebeckite within the ore zone contains a large proportion of F, suggesting that fluoride-U complexes may have been important for the transport of U. $\delta^{18}O$ values of co-existing calcite and riebeckite give temperatures of 340 and 380°C for the mineralization stage. The $\delta^{18}O_{fluid}$ and δD_{fluid} values, timing of the U mineralization and temperatures are most consistent with fluids derived from regional metamorphism of the proximal metasedimentary rocks, especially given the absence of syn-Isan granite in the western Mt. Isa Basin (Polito *et al.* 2007). Possible sources for a metamorphic fluid containing anomalous U, V, Zr, P, Sr and Y include the proximal fluvial Bottletree Formation and the fluvial Mt. Guide Quartzite that underlie the Eastern Creek Volcanic Group.

Skuppesavon (northern Sweden).

Skuppesavon represents U mineralization within a sequence of mostly rhyolitic to trachytic metavolcanic units. The U mineralization has been deposited in fractures along which fluids have caused albitization of K-feldspar, partial to complete dissolution of quartz and crystallization of new mineral phases in the space left by quartz (Smellie & Laurikko 1984). Uranium occurs as uraninite disseminated in the alteration minerals and only very rarely in fractures. Like at Lagoa Real, uraninite is associated with titanite. The hydrothermal fluids responsible for the alteration and mineralization are assumed to be contemporaneous with Svecofennian metamorphism (Smellie & Laurikko 1984).

Uranium deposits related to very high temperature metasomatism, Tranomaro, Madagascar

Regional geology. Southern Madagascar is composed of Lower Proterozoic metasedimentary and metavolcanic rocks of granulite facies as part of the Mozambique mobile belt that formed during the

Pan-African orogeny and extends into Sri Lanka and southern India (Paquette *et al.* 1994, Nicollet *et al.* 1995). The Tranomaro and the Highland Complex in central Sri Lanka contain comparable metasedimentary lithologies that were metamorphosed to granulite facies during the Pan-African orogeny, before the breakup of Gondwana. The Tranomaro basement is divided into three blocks by north–south, vertical, lithospheric-scale, shear zones (Pili *et al.* 1997). The three blocks experienced granulite-facies metamorphism (750–800°C) with decreasing pressure from 11 kbar in the western block, to 8 kb in the middle one and 4–5 kbar in the eastern one. More specifically, the Tranomaro gneiss indicates low-pressure (4–4.8 kbar) granulitic conditions (750–850°C) from Qtz–Pl–Opx–Grt assemblages, (Rakotondrazafy *et al.* 1996) and high X_{CO2} of 0.82 in the fluid phase from Qtz–Bt–Grt–Sil–Kfs assemblages (Ramambazafy *et al.* 1998).

Th–U mineralization in the Tranomaro area is located in the eastern lowest pressure block (Rakotondratsima 1983, Moine *et al.* 1985). The Tranomaro gneiss comprises metapelite, commonly graphitic, abundant calc-silicate rocks and marble, as well as siliceous feldspathic gneiss; some of which correspond to former acidic volcanic rocks (Fig. 6-16). The depositional environment of the sedimentary protoliths was typically a passive epicontinental margin setting. The marble layers are from a few metres up to a few hundred metres thick, and extend over several kilometres. In the north-western part of the area, the marble layers form closed structures similar to those located more to the west and have been interpreted by Martelat *et al.* (1995) as the result of superimposed deformation events. Because of the high ductility of marble layers, complex folding and boudinage of the more competent calc-silicate layers are common. Calc-silicate rocks are closely associated with marble. Some of them may have formed by metamorphism of impure limestone or marl, interlayered with the marble, producing polymineralic assemblages; others have a metasomatic origin, resulting from the coupled element transfer between marble and granitic rocks or fluid injections, producing mostly monomineralic assemblages. The metasomatic calc-silicate rocks occur either as reaction zones between granite intrusions and host marble or as isolated masses within marble. Granite intrusions are numerous, generally small in size and derived from dehydration melting of biotite-bearing gneiss located at depth, as described in the western deeper level blocks (Nicollet 1985, Kröner *et al.* 1996). Large granitic intrusions occur in the Anosyan Ranges, East of the Tranomaro block.

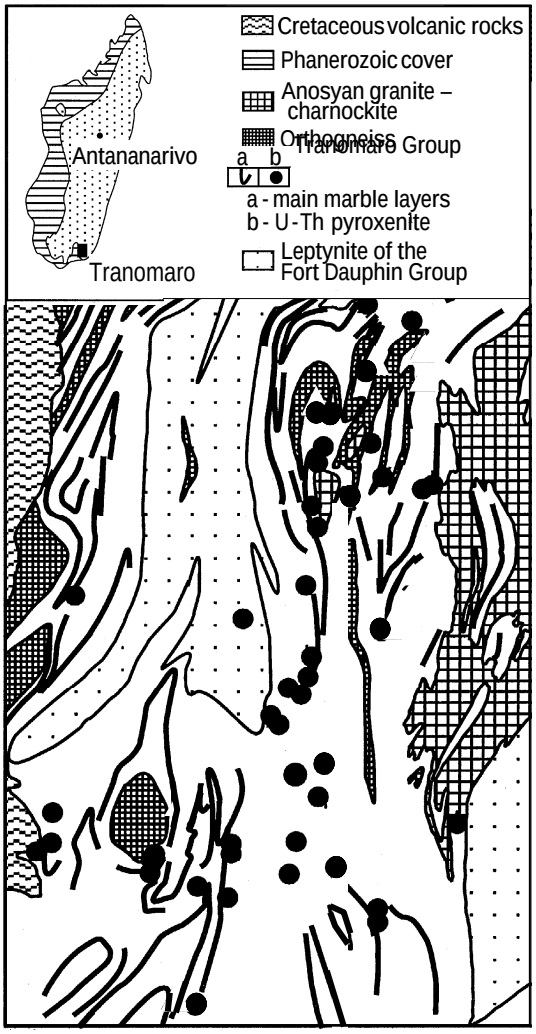

Fig. 6-16. Simplified geological map of the Tranomaro area (modified after Boulvais *et al*., 1998). Only the largest granitic intrusions are represented. A map of Madagascar showing the location of the Tranomaro area is inserted.

Metasomatic skarns are generally well zoned, with the following successions that may extend over several metres to several tens of metres:

- biotite ± hypersthene granite
- diopsidic syenite, the protolith being the granite from which quartz has been dissolved, silica has infiltrated into the enclosing marble, and Ca has migrated toward the granite to form diopside from biotite or hypersthene,

- scapolitite, essentially composed of the meionite end-member, with subordinate diopside, typically corresponding to an endoskarn,
- pyroxenite, essentially composed of pure Ca or Ca–Mg diopside, ± F-rich phlogopite ± scapolite, which corresponds to an exoskarn,
- marble, which can be composed only of carbonates or may have a complex mineralogy with forsterite ± F-rich phlogopite ± diopside ± dark green to light-colored spinel ± F-rich humite ± wollastonite ± pargasite, depending on the amount of detrital Si–Al silicates in the protolith. Minor exsolution of dolomite is locally observed in calcite, K-feldspar is sometimes present as small intergranular lenses and neither garnet nor graphite is present in the marble. Forsterite-bearing marble generally has a MgO content higher than 12 wt.%, whereas most diopside marble has a MgO content lower than 5 wt.%.

Granite is not always observed in the metasomatic zoning. For example the Marosohy occurrence represents a small-scale profile of a metasomatic lens not related to a granitic intrusion. Here, the nearly monomineralic pyroxenite with some spinel and residual calcite is in sharp contact with a calcite–dolomite–forsterite–spinel marble. The amount of dolomite diminishes in the marble towards the pyroxenite with relative increase of calcite and forsterite without appearance of a new mineral phase. Free dolomite disappears inside the marble and is only observed as exsolution in calcite near the contact. At the contact, diopside forms as forsterite disappears. The mineralogical zoning results from two successive reactions induced by the infiltration of a silica-rich fluid and producing carbon dioxide:

(i) disappearance of dolomite:

$$CaMg(CO_3)_2 + SiO_2 \rightarrow CaCO_3 + MgSiO_4 + 2CO_2$$

(ii) new formation of diopside:

$$2CaCO_3 + MgSiO_4 + SiO_2 \rightarrow CaMg(SiO_4)_2 + 2CO_2$$

Under retrograde granulite-facies conditions, F-rich phlogopite, which is mined locally, is associated with calcite, diopside, and occasional anhydrite, and forms veins and lenses crosscutting pyroxenite. Late-stage REE- and zircon-rich calcitic veins crosscut the calcsilicate complex. These may contain up to several centimetres-long euhedral zircon crystals.

Th–U mineralization. Numerous Th–U mineralized showings are known in metasomatic calcsilicate rocks (Moreau 1963, Moine *et al.* 1985). The main ore mineral is uranothorianite occurring as disseminated euhedral crystals, predominantly in diopsidic pyroxenite, which is always the most mineralized layer, but also occasionally in meionitic scapolitite and neighboring marble. The mineralized pyroxenite may also form lenses from a few metres to several tens of metres in length, not closely related to any visible intrusion. For example, in the Marosohy profile, the U–Th mineralization increases rapidly from the barren marble (3.8 ppm Th) towards the contact (up to 2000 ppm Th) and reaches a maximum in the pyroxenite (4000 ppm Th). Several centimetre-scale uranothorianite crystals may also occur in the veins with phlogopite. REE–Th–U-rich hibonite and corundum may crystallize in some extremely Al-rich metasomatic rocks (Rakotondrazafy *et al.* 1996).

Genetic model. Two main stages of metasomatism have been identified in the Tranomaro region (Rakotondrazafy *et al.* 1996). The first stage includes aluminous diopside–scapolite–meionite–titanite–spinel–wollastonite–corundum–uranothorianite that records P–T conditions of 5 kbar and 850°C at 565 Ma (Andriamarofahatra *et al.* 1990) as the main stage of the Th–U mineralization. The second stage comprises F-phlogopite–F-pargasite–uranothorianite–REE-rich hibonite formed at 800°C and 3 kbar at 545 Ma (Paquette *et al.* 1994), but is of minor importance for the mineralization. The similarity of the ages and of the P–T conditions demonstrates the synchronicity between granulite-facies metamorphism and fluid circulation responsible for the first stage metasomatism and U–Th mineralization. Fluid inclusions in minerals from gneiss and skarn are CO_2-rich (Ramambazafy *et al.* 1998). Primary inclusions in growth zones of euhedral corundum crystals have isochores that intersect the P–T field defined by the geothermobarometry on silicate minerals, indicating that they are synchronous with the peak metamorphic conditions (Rakotondrazafy *et al.* 1996, Ramambazafy *et al.* 1998).

Carbon dioxide was not the only fluid involved in the metasomatic reactions. In the Tranomaro metasomatic zones, the hydroxyl sites of phlogopite, pargasite, humite, and apatite are nearly saturated with F, suggesting that fluoride complexes may have transported simultaneously Th, U, REE, and Zr, which all appear to be mobile in the

metasomatic zones, together with Si and Ca (Moine *et al.* 1997). In particular, most of the Th/U ratios of the mineralized rocks are between 2 and 3, close to the average crustal ratio, and thus with no strong difference in mobility between U and Th. Also, unmixed aqueous brines may have coexisted with the carbonic fluids, as shown by Touret (1996) for granulite terrains, but not yet identified in the Tranomaro.

The $\delta^{13}C$ values near 0‰ for the Tranomaro marbles are typical of marine carbonate and thus provide no evidence for massive streaming of mantle-derived fluids during granulite-facies metamorphism. Localized but strong fluid flow occurred in the metasomatic mineralized zones, but also without any contribution of a deep-seated C source as evidenced by the C isotopic compositions of infiltrated marble and pyroxenite. The O isotopic compositions of pyroxenite are consistent with a crustal origin for the metasomatic reactions and U–Th mineralization and rock-buffered fluids for marble. In addition, Nd isotopic compositions of metasomatized marble are similar to those of the metasedimentary rocks and granite intrusions, indicating that the source of the REE is either within the marble or in the host crustal rocks (Boulvais *et al.* 1998).

A possible source for the U–Th is *via* syn-sedimentary pre-concentration of Th, U, Zr, and REE in marl. This is unlikely because these elements in sediments are mainly hosted by detrital monazite (for Th, U, and REE) and zircon (for Zr mainly) that occur in relatively coarse siliciclastic sediments as placers. Marl, even that with a significant detrital component, never has high levels of these elements.

Another possible source, based mainly on the association of U with Th–REE–Zr and the presence of carbonate rocks with pyroxenite, could be a protolith corresponding to metamorphosed carbonatite. For example, the Th–U mineralization in Palabora (South Africa) is associated with carbonatite and pyroxenite, and uranothorianite is the main ore mineral (Eriksson 1989). However, U and Th concentrations in carbonatite are much lower, reaching only 25 ppm U at Palabora, and such an origin will not explain the zoning observed between the different lithologies. Moreover, carbonatite bodies have high Nb contents that are not observed in the Tranomaro pyroxenite and carbonate rocks, and the C isotopic composition of Tranomaro marble is typical of marine carbonate rocks.

Consequently, the geological, geochemical and isotopic data are most consistent with a syn-metamorphic origin for the Th–U–REE–Zr mineralization, although these elements, especially U, are not usually expected to be enriched in granulite-facies rocks (Barbey & Cuney 1982). The classic metasomatic zonation observed between the granite injections and marble, dominantly controlled by the bimetasomatic exchange of Ca and Si between the two lithologies, and the isotopic compositions of the metasomatic rocks imply that the Th–U–REE–Zr mineralization is derived from metasomatic fluids exsolved from granitic magmas injected in the Tranomaro metamorphic series or from fluids derived from devolatization reactions occurring at depth during granulite-facies metamorphism. The simultaneous mobility of U, Th, REE, and Zr is probably due to high fluorine contents of the fluids as a result of dehydration of biotite.

REFERENCES

ANDRIAMAROFAHATRA, J., DE LA BOISSE, H. & NICOLLET, C. (1990): Datation U–Pb sur monazites et zircons du dernier épisode tectono-métamorphique granulitique majeur dans le Sud-Est de Madagascar. *Comptes Rendus à l'Académie des Sciences* **310**, 1643–1648.

BALLHORN, R.K., THAKUR, V.K., DA FONTE, J.E.C. & SUCKAU, V. (1981): Geology of the Uranium Deposit. Brazil. In : Uranium Deposits in Latin America – Geology and Exploration. IAEA Proceedings. Vienna.

BARBEY, P. & CUNEY, M. (1982): K, Rb, Sr, Ba, U and Th geochemistry of the Lapland granulites (Fenno Scandia). Lile fractionation controlling factors. *Contrib. Mineral. Petrol.* **81**, 304-316.

BELEVTSEV, Y.N. & KOVAL V.B. (1968): Genesis of uranium deposits associated with sodium metasomatism in crystalline rocks of shields. *Geologicheskiy Zhurnal* (Kiev.) **28**, 4-17.

BELEVTSEV, Y.N., BATASHOV, B.G. & KOVAL, V.B. (1984): The Zholtyz Vody uranium deposit and the iron ore deposits of Krivoy Rog. Guide Book, XXVIIth IGC, Moscow. 32 p.

BOGDANOVA, S.V., BINGEN, B., GORBATSCHEV, R., KHERASKOVA, T.N., KOZLOV, V.I., PUCHKOV, V.N. & VOLOZH, Y.A. (2008): The East European Craton (Baltica) before and during the assembly of Rodinia. *Precamb. Res.* **160**, 24-45

BOULVAIS, P., FOURCADE, S., GRUAU, G., MOINE, B.

& CUNEY M. (1998): Persistence of pre-metamorphic C and O isotopic signatures in marbles subject to Pan-African granulite-facies metamorphism and U–Th mineralization. Tranomaro. Southeast Madagascar. *Chem. Geol.* **150**, 247–262.

BOULVAIS, P., RUFFET, G., CORNICHET, J. & MERMET, M. (2007): Cretaceous albitization and dequartzification of Hercynian peraluminous granite in the Salvezines Massif (French Pyrénées). *Lithos* **93**, 89-106.

CABY R. & ARTHAUD M. (1987): Petrostructural evolution of the Lagoa Real subalkaline metaplutonic complex (Bahia. Brazil). *Revista Brasilia de Geocienças* **17**, 636.

CATHELINEAU, M. (1986): The hydrothermal alkali metasomatism effects on granitic rocks; quartz dissolution and related subsolidus changes. *J. Petrol.* **27**, 945-965.

CERNÝ, P., BLEVIN, P.L., CUNEY, M. & LONDON, D. (2005): Granite-Related Ore Deposits. *Economic Geology* 100th Anniv. Vol. 1905-2005, 337-370.

CINELU, S. & CUNEY, M. (2006): Sodic metasomatism and U–Zr mineralization: A model based on the Kurupung batholith (Guyana). Abstract, *Geochim. Cosmochim. Acta* **70**, A103.

CONNORS, K.A. & PAGE, R.W. (1995): Relationships between magmatism, metamorphism and deformation in the western Mount Isa inlier, Australia. *Precamb. Res.* **71**, 131–153.

CORDANI, U.G., IYER, S.S., TAYLOR, K., KAWASHITA, K., SATO, K. & MCREATH, I. (1992): Pb-Pb, Rb-Sr, and K-Ar systematics of the Lagoa Real uranium province (south-central Bahia. Brazil) and the Espinhaço Cycle (ca. 1.5-1.0 Ga). *J. S. Amer. Earth Sci.* **5**, 34-46.

COSTA, P.H.O., ANDRADE, A.R.F, LOPES, G.A. & SOUZA S.L. (1985): Projeto Lagoa Real: Mapeamento Geológico, 1:25.000. Salvador: CBPM, v.1.

DEBON, F. & LEFORT P. (1988): A cationic classification of common plutonic rocks and their magmatic associations: principles, method, applications. *Bull. Minéralogie* **111**, 493-510.

EBY, G.N. (1992): Chemical subdivision of the A-type granitoids: petrogenetic and tectonic implications: *Geology* **20**, 641-644.

ERIKSSON, S.C. (1989): Phalaborwa: a saga of magmatism, metsomatism and miscibility. *In* Carbonatites : Genesis and Evolution. Keith Bell (*Ed.*) Ottawa-Carleton Geoscience Center, Carleton University, Ottawa, 221-253.

FUCHS, H.D., DA FONTE, J.E.C., SUCKAU, V. & THAKUR, V.K. (1981): The Espinharas Uranium occurrence. Brazil (IAEA AG. 250/2). In : Uranium Exploration Case Histories. IAEA Proceedings, Vienna.

GORBATSCHEV, R. & BOGDANOVA, S., (1993): Frontiers in the Baltic shield. *Precamb. Res.* **64**, 3–21.

HITZMAN, M.W. (2000): Iron oxide–Cu–Au deposits: what, where, when and why. *In* PORTER. T.M. (*Ed.*). Hydrothermal Iron Oxide Copper–Gold and Related Deposits: A Global Perspective. Australian Minerals Foundation, 9– 26.

INDA, H.V.A. & BARBOSA, J.S.F. (1996): Texto explicativo para o mapa geológico do Estado da Bahia (1:1.000.000). *In* J.S.L. Barbosa & J.M.S. Dominguez. Geologia da Bahia (texto explicativo). Salvador, Secretaria da Industria, Comércio e Mineração, Superintendência de Geologia e Recursos Minerais, 400 p.

JARDIM DE SA, E.F (1978): Geologia da Chapada Diamantina e faixa Santo Onofre, Bahia, e geoquimica do vulcanism acido associado: Unpub. M.Sc. thesis, Salvador, Brazil, Univ. Federal Bahia, 180 p.

JIARONG, Z. & ZHUTIAN, G. (1988): The geological characteristics and metallogenetic control factors of the Lianshanguan uranium deposit. northeast China. *Precamb. Res.* **39**, 51-64

KAZANSKY, V.I. & LAVEROV, N.P. (1978): "Uranium", in Ore Deposits of the USSR, V.I. Smirnov Edt, Nedra, Moscow, 327-333. (in Russian).

KISH, L. & CUNEY, M. (1981): Uraninite - albite veins from the Mistamisk Valley of the Labrador Trough. Québec. *Mineral. Mag.* **44**, 471-483.

KRÖNER, A., BRAUN, I. & JAECKEL, P. (1996): Zircon geochronology of anatectic melts and residues from a high-grade pelitic assemblage at Ihosy, southern Madagascar: evidence for Pan-African granulite metamorphism. *Geol. Mag.* **133**, 311–323.

KULLMAN, F. (1989): A uranium-zirconium mineralization in Revsund Granite at Bjorkramyran northern Sweden. *In* Uranium deposits in magmatic and metamorphic rocks. International Atomic Energy Agency. Vienna, Austria, 45-56.

KUSHEV, V.G. (1972): Alkaline Metasomatites of the Precambrian (Nedra, Leningrad). 191 p. (in Russian).

LEFORT, P. (1975): Himalaya: the collided range. Present knowledge of the continental arc. *Am. J. Sci.* **275-A**, 1-44.

LINNEN, R.L. & CUNEY, M. (2005): Granite-related rare-element deposits and experimental constraints on Ta-Nb-W-Sn-Zr-Hf mineralization. *In* LINNEN. R.L. AND SAMSON. I.M.. *eds.* Rare-Element Geochemistry and Mineral Deposits: Geological Association of Canada. *Geol. Assoc. Can. Short Course Notes* **17**, 45-67.

LOBATO, L.M. & FYFE, W. (1990): Metamorphism. metasomatism and mineralization at Lagoa Real. Bahia. Brazil. *Econ. Geol.* **85**, 968-989.

LOBATO, L.M., FORMAN, J.M.A., FUZIKAWA, K., FYFE, W.S. & KERRICH, R. (1983a): Uranium in overthrust Archaean basement. Bahia. Brazil. *Can. Mineral.* **21**, 647-654.

LOBATO, L.M., FORMAN, J.M.A., FYFE, W., KERRICH, R. & BARNETT, R.L (1983b): Uranium enrichment in Archaean crustal basement associated with overthrusting. *Nature* **303**, 235-237.

MANNING, D.A.C. (1981): The effect of fluorine on liquidus phase relationships in the system Qz-Ab-Or with excess water at 1 kb: *Contrib. Mineral. Petrol.* **76**, 206-215.

MARTELAT, J-E., VIDAL, G., LARDEAUX, J.-M., NICOLLET, C. & RAKOTONDRAZAFY, M. (1995): Images spatiales et tectoniques profondes des continents: l'exemple du Sud-Ouest de Madagascar. *Comptes Rendus à l'Académie des Sciences*, Paris **321**, 325–332.

MARUÉJOL, P. (1989): Métasomatose alcaline et minéralisations uranifères: les albitites du gisement de Lagoa Real (Bahia. Brésil) et exemples complémentaires de Xihuashan (SE Chine). Zheltorechensk (Ukraine) et Chhuling Khola (Népal central). Thèse Doctorat. – Mémoire 18 Centre de Recherches sur la Géologie de l'Uranium, Nancy, France.

MARUÉJOL, P., CUNEY, M. & FUZIKAWA K. (1989): U versus Th; concentration processes associated to Na-metasomatism in granites, the Lagoa Real District, S. Bahia, Brazil. *In* XIIIth International Geochemical Exploration Symposium abstracts). *Anais do Congresso Brasileiro de Geoquimica* **2**, 103

MARUÉJOL, P., CUNEY, M., FUZIKAWA, K., NETTO, A.M. & POTY, B. (1987): The Lagoa Real subalkaline granitic complex (South Bahia. Brazil): a source for uranium mineralizations associated with Na-Ca metasomatism. *Revista Brasileira de Geociências* **17**, 578-594.

MCKAY, A.D. & MIEZITIS, Y. (2001): Australia's uranium resources, geology and development of deposits. Australian Geological Survey Organisation, Geoscience Australia, Canberra, *Mineral Resource Report* **1**, 171 p.

MOINE, B., RAKOTONDRATSIMA, C. & CUNEY, M., (1985): Les pyroxénites à uranothorianite du Sud-Est de Madagascar: conditions physico-chimiques de la métasomatose. *Bull. Mineralogie* **108**, 325–340.

MOINE, B., RAKOTONDRAZAFY, M., RAMAMBAZAFY, A., RAKOTONDRATSIMA, C., CUNEY, M. (1997): Controls on the urano-thorianite deposits in S-E Madagascar. *In* Cox. R., Ashwal. L.D., *eds*. Proc. Int. Symp. Field Workshop on Proterozoic Geology of Madagascar, *Gondwana Research Group Miscellaneous Publication* **5**, Antananarivo, 55–56.

MOREAU, M. (1963): Le gisement des minéralisations de thorianite à Madagascar. *Annnales Géologiques de Madagascar* **33**, 175–178.

NETTO, A.M. (1983): Le gisement d'uranium d'Itataïa (Ceara. Brésil). PhD Thesis, Université de Clermont Ferrand.

NETTO, A.M., MEYER, A., CUNEY, M. & POUPEAU, G. (1991): A thermo-geochronological study of the Itataia phospho-uraniferous deposit (Ceará, Brazil) by apatite fission track analysis: genetic implications. *In.* Proc. 25 years SGA meeting: Source, Transport and deposition of metals. M. PAGEL AND J. LEROY. Edit., A.A. Balkema Publ., Rotterdam, 409-412.

NEUMANN, N., SOUTHGATE, P.N., MCINTYRE, A. & GIBSON, G. (2006): New SHRIMP geochronology for the Western Fold Belt of the Mount Isa Inlier: Developing a 1800-1650 Ma Event Framework. *Aust. J. Earth Sci.***53**, 1023-1039.

NICOLLET, C. (1985): The banded cordierite and garnet-bearing gneisses from Ihosy; a thermobaric tracer in southern Madagascar. *Precamb. Res.* **28**, 175-185.

NICOLLET, C., MONTEL, J.-M., FORET, S., MARTELAT, J.E. & LARDEAUX, J.-M. (1995): E-probe monazite dating of the uplift of the

Precambrian in the south of Madagascar. EUG 8 Strasbourg, *Terra Abstract* **7**, 124.

PAQUETTE, J-L., NÉDÉLEC, A., MOINE, B. & RAKOTONDRAZAFY, M. (1994): U–Pb. single zircon Pb-evaporation, and Sm–Nd isotopic study of a granulite domain in SE Madagascar. *J. Geol.* **102**, 523–538.

PASCHOLATI, M.E., LIMA, DA SILVA C., DOS SANTOS, COSTA S., SAYURI OSAKO, L., AMARAL, G. & PADILLA RODRIGUEZ, I. (2003): Novas ocorrências de urânio na região de Lagoa Real, a partir da superposição de dados geofísicos, geológicos e de sensoriamento remoto. *Revista Brasileira de Geociências* **33**, 91-98.

PILI, E., RICARD, Y., LARDEAUX, J.-M. & SHEPPARD, S.M.F. (1997): Lithospheric shear zones and mantle–crust connections. *Tectonophysics* **280**, 15–29.

POLITO, P.A., KYSER, K.T. & STANLEY, C. (2007): The Proterozoic, albitite-hosted, Valhalla uranium deposit, Queensland, Australia, a description of the alteration assemblage associated with uranium mineralisation in diamond drill hole. *Mineralium Dep.* **39**, in press.

PORTO DE SILVEIRA, C.L., SHORSCHER, H.D. & MIEKELEY, N. (1991): The geochemistry of albitization and related uranium mineralization, Espinharas, Paraiba, Brazil. *J. Geochem. Expl.* **40**, 329-347.

RAKOTONDRATSIMA, C. (1983): Les pyroxénites à urano-thorianite du Sud-Est de Madagascar. Etude pétrographique. minéralogique et géochimique. Conséquences métallogéniques. Unpub. PhD thesis. Université Claude Bernard Lyon I, 226 p.

RAKOTONDRAZAFY, M.A.F., MOINE B. & CUNEY M. (1996): Mode of formation of hibonite ($CaAl_{12}O_{19}$) within the U–Th skarns from the granulites of S-E Madagascar. *Contrib. Mineral. Petrol.* **123**, 190–201.

RAMAMBAZAFY, A., MOINE, B., RAKOTONDRAZAFY, M. & CUNEY M. (1998): Signification des fluides carboniques dans les granulites et les skarns du Sud-Est de Madagascar. *C. R. Acad. Sci. Paris* **327**, 743–748.

RUBENACH, M.J. (1992): Proterozoic low-pressure/high-temperature metamorphism and an anticlockwise P-T-t path for the Hazeldene area, Mount Isa inlier, Queensland, Australia. *J. Metamorphic Geol.* **10**, 333–346

RUHLMANN, F., RAYNAL, M. & LAVOIE S. (1986): Un exemple de metasomatisme alcalin albite-uranium dans le bassin des Monts Otish. Québec. *Can. J. Earth Sci.* **23**, 1742-1752

SHCHERBAK, M.P., & BOBROV, O.B. (2005): Mineral deposits of Ukraine. Vol. I. Metalliferous mineral deposits, 783 p.

SHEN J.S. (1990): The relationship between soda metasomatism and uranium mineralization in No. 375 and No. 326 ore deposits. *Mineral Deposits Kuangchuang Dizhi* **9**, 64-69

SMELLIE, J.A.T. & LAURIKKO, J. (1984): Skuppesavon, northern Sweden: a uranium mineralisation associated with alkali metasomatism. *Mineral. Dep.* **19**,184-192

SOBRINHO, E.G. (1981): Apresentação de uma hipótese genética para o Distrito Uranífero de Lagoa Real. Nota Técnica EBHO.PM 3, Nuclebrás, 35p.

TARASOV, N.N. (2004): Geotectonic position and structure of the Novoukrainsk uranium ore field (Ukrainian Shield). *Geology of Ore Deposits* **46**, 237-251.

TOURET, J.R.L. (1996): LILE-depletion in granulites: myth or reality? In: Demaiffe, D. Ed.., Petrology and Geochemistry of Magmatic Suites of Rocks in the Continental and Oceanic Crusts, a volume dedicated to Pr. J. Michot., Université libre de Bruxelles, Royal Museum for Central Africa, Tervuren, 53–72.

TURPIN, L., MARUÉJOL, P. & CUNEY, M. (1988): U-Pb-Rb-Sr and Sm-Nd chronology of granitic basement, hydrothermal albitites and uranium mineralization (Lagoa Real, South-Bahia. Brazil). *Contrib. Mineral. Petrol.* **98**, 139-147.

VELS, B. & FRITSCHE, R. (1988): Sodium metasomatism in the Kitongo uranium occurrence near Poli, Cameroon. *Uranium* **4**, 365-383.

CHAPTER 7: HYDROTHERMAL URANIUM DEPOSITS RELATED TO IGNEOUS ROCKS

Michel Cuney
G2R, Nancy-Université, CNRS, CREGU,
B.P. 239,
F-54506 Vandoeuvre lés Nancy, France
michel.cuney@g2r.uhp-nancy.fr

and

Kurt Kyser
Department of Geological Sciences and Geological Engineering,
Queen's University,
Kingston, Ontario, K7L 3N6, Canada
kyser@geol.queensu.ca

Hydrothermal uranium deposits represent an extremely diverse category of deposits generally exhibiting vein-type morphology; however, they may also occur as disseminated ore in episyenite bodies. They may be hosted by granite, as in the Saint Sylvestre district (Massif Central, France), within volcanic rocks (Streltsovskoye Caldera, Transbaikalia, Russia), in the immediate vicinity of granite, as in the Erzgebirge district (south-east Germany and Czech Republic), or without any direct relation with granite (Schwartzwalder, USA). In the present chapter, after an introduction about the different types of granite and volcanic rocks which may represent favorable sources for the generation of U deposits, we will present typical examples of intragranitic U deposits from the Limousin U district, and an example of a caldera-related deposit from the largest U district related to volcanic rocks, the Streltsovskoye U district in Russia.

IGNEOUS ROCK TYPES AND URANIUM METALLOGENESIS

Felsic igneous rocks, plutonic or volcanic, represent the most common U source for most deposits. However, to represent an efficient U source, an igneous rock has to be sufficiently enriched in U and U should be hosted by minerals from which the metal can be leached by common hydrothermal fluids. Three types of igneous rocks, distinguished according to their chemistry, can be enriched in U. These are the peralkaline, metaluminous, and peraluminous felsic igneous rocks. Each of the plutonic varieties of these rock types is characterized by a specific magmatic fractionation of Th and U and a specific accessory mineral paragenesis (Cuney & Friedrich 1987). The distribution of U between different accessory minerals is of critical importance for the genesis of U mineralization associated with these rocks. A fourth type of igneous rock, generally referred to as alaskite, corresponds to disseminated U mineralization hosted by granitoid rocks in migmatitic domains as discussed in Chapter 5.

Peraluminous leucogranite and volcanic rocks

Peraluminous leucogranite and volcanic rocks are classically referred as S-type granite, according to the classification by White & Chappell (1977), to indicate their derivation from the partial melting of sedimentary rocks and their peraluminous character. Specific parameters have been devised using the variation of the peraluminosity in granite relative to a magmatic fractionation parameter (Debon & Lefort 1988, Stussi & Cuney 1993) to characterize peraluminous granite associated with U mineralization (Fig. 7-1).

The peraluminosity is calculated as the difference between the total amount of Al present in the rock and the amount of Al bound to the feldspars: $A = Al–(Na+K+2Ca)$, instead of the ratio (A/CNK) used more commonly in the literature. This index indicates the excess or the deficiency of Al with respect to the quantity needed to make the feldspars. Values higher than zero (or $A/CNK > 1$) indicate peraluminous compositions, corresponding mineralogically in granite to the presence of one or several of the following minerals: Al-biotite, muscovite, garnet, cordierite, topaz, Al-silicate minerals (Fig. 7-1). Values lower than zero (or $A/CNK < 1$) indicate metaluminous or peralkaline compositions, characterized mineralogically by the

Short course co-sponsored by the the SGA and MAC, Québec City, May 2008, p. 117-160

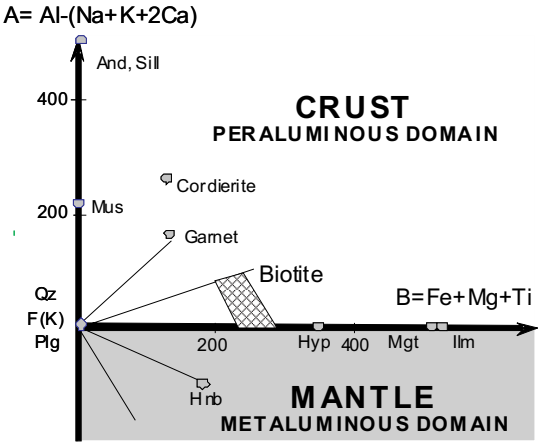

Fig. 7-1. Peraluminous index (A = Al–(Na+K+2Ca) *versus* differentiation index (B = Fe+Mg+Ti) diagram of Debon & Lefort (1988) used to decipher various magmatic fractionation trends among peraluminous and metaluminous granite bodies. Main rock-forming minerals are also plotted: And = andalusite, Sill = sillimanite, Mus = muscovite, Qz = quartz, F(K) = K-feldspar, Plg = plagioclase, Hyp = hypersthene, Mgt = magnetite, Ilm = ilmenite, Hnb = Hornblende.

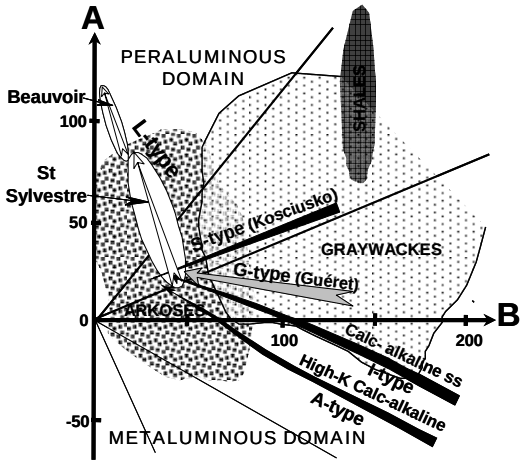

Fig. 7-2. Peraluminous index *versus* differentiation index diagram of Debon & Lefort (1988), showing trends defined by the various types of peraluminous and metaluminous granite. Compositions of major types of sedimentary rocks are also plotted. Graywacke and arkose may be metaluminous if they have carbonate cement.

presence of Al-poor biotite ± amphibole ± pyroxene ± titanite (Fig. 7-1). Quartz and feldspars are located at the origin in this diagram, and represent the eutectic composition of the granite system. The differentiation parameter is the sum of Fe + Mg + Ti, which also represents a coloration index of the rock and is thus easy to evaluate in the field. The more fractionated rocks have the lowest B-values.

Plotting the compositions of the major types of granite (Fig. 7-2) reveals several trends (Debon & Lefort 1988, Stussi & Cuney 1993). Each trend corresponds to a different granite type, resulting from different genesis processes and reflecting the possibility of granite being associated with hydrothermal vein-type U deposits as described below.

Highly fractionated calc-alkaline granite may become peraluminous as a result of (i) extreme magmatic fractionation of metaluminous minerals like amphibole or pyroxene; (ii) assimilation of peraluminous material during ascent of the magma through the continental crust; (iii) late magmatic to hydrothermal alteration leading to the fractionation of Na, K, or Ca into Cl-bearing late magmatic to hydrothermal fluids; or (iv) a combination of any of these processes. This may lead to the crystallization of muscovite in the miarolitic cavities of some granite when fluid oversaturation of the magma occurs at shallow levels, or to the sericitization of the feldspars during post-magmatic hydrothermal circulation. Generally, this type of peraluminous granite represents a small volume of the whole calc-alkaline plutonic complex and its peraluminosity remains limited, except for the most fractionated examples of this type (Linnen & Cuney 2005, Černý *et al*. 2005). Such peraluminous granite bodies derived from extreme fractionation of high-K calc-alkaline magmas is characterized by moderate enrichment in Th, REE, and Zr. Uranium, mainly as uraninite, requires extreme differentiation, forming too small a stock to represent sizable ore deposits.

S-type granite bodies, as exemplified by the biotite-cordierite-bearing Kosciusko batholith (south-eastern Australia), and as described first by White & Chappell (1977), have compositions that define a trend in which the less fractionated compositions (the most mafic) are in the center of the greywacke field and have the highest peraluminous index (Fig. 7-2). Such compositions result from a high degree of partial melting (> 50 %) of metagreywacke or metapelite at temperatures above 800°C and up to 1000°C, and dry conditions (Burkhard 1991, Vielzeuf & Holloway 1988). During this process, there is no selective partial melting of the protolith, hence the U concentrations of the various lithological layers are averaged by the large degree of melting and U is not selectively fractionated into

the melt. During subsequent fractionation, the granite compositions become less peraluminous and evolve towards eutectic compositions (the origin of the A–B diagram), defining a positive correlation between the A and B parameters (Fig. 7-2). This model is in complete agreement with the restite unmixing model of Chappell & White (1974), wherein the Fe–Mg–Ti-enriched and highly peraluminous restitic material (mostly garnet and/or cordierite) is progressively unmixed during the extraction of the magmas from their source. This process should lead to a slight enrichment in U in the residual melts, but never to a level sufficient to obtain crystallization of a large proportion of U as uraninite. This type of granite is not known to be associated with U deposits.

The Guéret-type biotite-cordierite granite (G-type), from the French Massif Central, has the same mineral content as the S-type Kosciusko Batholith, but the correlation between the A and B parameters is negative, and thus corresponds to different processes. The less fractionated granite bodies, the richest in mafic minerals (mainly biotite), are less peraluminous and the more leucocratic bodies are more peraluminous, with increasing cordierite content. Rb–Sr and Sm–Nd isotopic studies (Turpin *et al.* 1990a) have shown that this type of geochemical trend can be explained by the mixing of a peraluminous leucocratic granitic melt derived from a limited amount of partial melting of crustal material with a metaluminous melt derived from the partial melting of metaluminous rocks at the base of the continental crust or from the partial melting of the mantle. Consequently, even if the crustal protolith undergoing partial melting was enriched in U, leading to U enrichment of the corresponding silicate melt, the U content of this melt will decrease because of mixing with a metaluminous melt poor in U. Such granite is not known to be associated with U deposits.

The two-mica leucogranite (L-type), as exemplified by the peraluminous leucogranite complexes from Limousin (French Massif Central), is characterized by the presence of biotite and muscovite. It also defines a negative fractionation trend, but much steeper than the G-type. It has a very limited range of composition (Fig. 7-2). The mafic mineral content of such granite, mainly biotite, is always very low, generally below 10%, corresponding to a B parameter value of about 50 regardless of the extent of fractionation. This type forms from low degrees of partial melting (less than about 30%) of essentially quartz-feldspar-rich protoliths such as meta-arkose, felsic metavolcanic rocks, or metagranite. Such source rocks are the most favorable for syngenetic U enrichment. When the protoliths are enriched in U, a low degree of partial melting will lead to further U enrichment in the resulting silicate melt. Subsequent melt extraction from the source and crystal fractionation will produce peraluminous U-rich granite.

If the granite sources have high HFSE contents, U will be predominantly hosted in the lattice of accessory minerals such as monazite, zircon, and apatite (Friedrich *et al.* 1987) and will not enter the silicate melt because these accessory minerals are only sparingly soluble (Watson & Harrison 1983, Montel 1993). These accessory minerals will be enriched in the restite material together with U, as shown by Friedrich *et al*. (1987) from the St Malo migmatites in Brittany, France.

In U-enriched peraluminous granite, U is dominantly hosted by Th-poor uraninite, which represents an easily leachable source of metal (Cuney & Friedrich 1987). The preferential crystallization of U as uraninite results from the low solubility of monazite and zircon in peraluminous low temperature melts. Saturation of the melts with respect to these accessory minerals leads to their early fractionation, first in the restite during partial melting at the level of the source, and then during progressive fractional crystallization. As a result, Zr, Th, and REE are strongly depleted in strongly acidic peraluminous magmas and a limited amount of U enters the structure of the accessory minerals. As a consequence, the U remaining in the melt, not retained in the structure of the accessory minerals, continues to be enriched during fractionation until the silicate melt reaches uraninite saturation and Th-poor uraninite will crystallize (Cuney & Friedrich 1987). Uranium contents of only a few tens of ppm are sufficient to reach uraninite saturation in peraluminous low temperature melts (Peiffert *et al*. 1994, 1996).

Two-mica peraluminous leucogranite is by far most commonly associated with vein-type or episyenite-type U deposits. The largest province of this type is the mid-European Variscan Belt with Carboniferous granite plutons, followed by the Jurassic granite plutons of the Indosinian-Yanshanian belt of southeast China and the Argentinian Achala Batholith of Devonian age. The most fractionated members of this type of

peraluminous granite are represented by rare metal, high-P highly peraluminous granite or pegmatite (LCT-type), extremely depleted in Th (down to less 1 ppm), Zr (~20 ppm), and REE (close to or below chondritic abundances) (Linnen & Cuney 2005, Černý *et al.* 2005). In a Th (Zr, REE) *versus* U diagram, these elements are inversely correlated (Fig. 7-3). Hence, the Th/U ratio of such granite decreases during fractionation.

Strongly acidic, highly peraluminous volcanic rocks equivalent to two-mica peraluminous leucogranite are quite rare. Peraluminous melts are generally generated at relatively low temperature and are rich in water, two parameters favoring the intersection of the granitic solidus by these magmas during their rise before they reach the surface. The only well known occurrence associated with U mineralization is the Macusani volcanic suite in Peru, which forms thick and extensive sheets of ignimbritic tuffs (Pichavant *et al.* 1988a). Such rhyolite has the same composition as peraluminous leucogranite with about the same levels of U enrichment (up to about 20 ppm), and is also depleted in Th, Zr, and REE. It represents a potential source of U via devitrification of the glass by oxidizing fluids.

Peralkaline granite, syenite and volcanic rocks

Peralkaline granite and syenite equivalent to A1-type granite of Eby (1992) is always enriched in U together with Th and other large highly charged elements, such as Zr and REE, as a result of the large solubility of these elements in highly depolymerized melts (Peiffert *et al.* 1994, 1996, and Chapter 3). In contrast to peraluminous melts, Th, Zr, and REE are continuously enriched with U in peralkaline melts during fractionation. Extreme fractional crystallization of peralkaline melts leads to the formation of the peralkaline rare metal granite (Linnen & Cuney 2005). Th, Zr, and REE concentrations may reach several thousands of ppm and in some cases up to several weight percent. During crystallization of highly fractionated peralkaline melts, large amounts of complex Zr, REE, Th, Nb, and Ta minerals form, with U as a minor element substituted in the structure of all these minerals. Individual crystals of uraninite will generally not be able to crystallize. As a consequence, even though the U contents of deposits related to peralkaline melts may be high, they have generally not been mined until now because of the cost of extraction of U from such highly refractory minerals. However, highly fractionated peralkaline rocks become significant U sources when U and Th are hosted by silicate minerals and when they become metamict after a period of at least 100 million years. In a Th (Zr, REE) *versus* U diagram, peralkaline complexes define a positive correlation (Fig. 7-3) and their Th/U ratio remains close to the average crustal ratio, or slightly lower during magmatic fractionation.

The Kvanefjeld deposit in the Ilímaussaq peralkaline complex (Sorensen *et al.* 1974), presented in Chapter 4, is one of the best examples of a U deposit associated with the most highly fractionated syenite of a peralkaline complex. The resources of the deposit are over 20,000 tU and U is mainly hosted by steenstrupine. In the Bokan Mountain Granite of Alaska, the Ross Adams deposit represents another example of U associated with highly fractionated peralkaline magmas, but in this case saturated in silica, corresponding to aegirine–arfvedsonite granite.

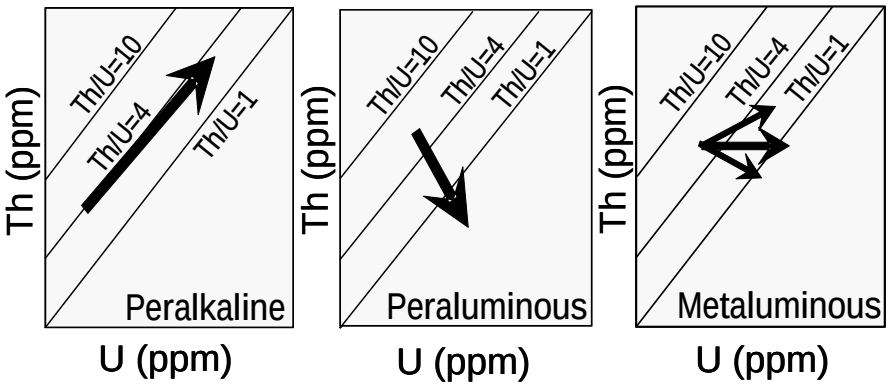

Fig. 7-3. General evolution of Th and U contents and Th/U ratios during magmatic fractionation in peralkaline, peraluminous and metaluminous U-rich magmas. In metaluminous granite Th and U may behave differently depending on the degree of peraluminosity of the most fractionated magmas and their temperature.

Peralkaline felsic volcanic rocks, generally called liparite, are quite common relative to peraluminous felsic volcanic rocks. They represent an excellent U source, because most of the U is in the glassy matrix. When the glass becomes devitrified during alteration, U can be easily mobilized. These units form extended and thick layers of pyroclastic tuff (ignimbrite) in and outside calderas. The Latium Province in Italy represents a very recent example of such a pyroclastic tuff sheet enriched in U, and extending over more than 2000 km^2 (Villemant & Palacin 1987). A large part of the Stretsovkoye Caldera in Transbaikalia, Russia, hosting the largest U district related to volcanic rocks is partly filled with peralkaline liparitic tuff (Chabiron *et al.* 2001). Liparitic tuff can also be a significant component in siliciclastic sedimentary rocks associated with U deposits, as in the arkosic sandstone hosting the U deposits of the Akouta area in Niger (Forbes *et al.* 1984).

High K calc-alkaline granite

Some members of the metaluminous calc-alkaline granite family (I-type granite) are enriched in K, which generally correlates with enrichments in Th, U, and other incompatible elements (Fig. 7-4). Such granite is called high-K calc-alkaline granite (A2-type granite of Eby 1992) or even shoshonitic granite when K enrichment reaches very high levels. The intermediate to high temperature of these melts and their metaluminous composition lead to an intermediate behavior of Th, Zr, and the REE (Fig. 7-3). With magmatic fractionation and increasing U concentrations, these elements may increase slightly in the melt, remain constant, or decrease slightly, depending on the melt temperature and composition. These magmas are also characterized by higher Ca contents than peraluminous and peralkaline granite. When the CaO content of high-K calc-alkaline silicate melts exceeds about 1 wt.%, crystallization of Ca-rich minerals such as amphibole, titanite and allanite can occur, which incorporate REEs and minor Th and U. If the Th/REE ratio of the melt is sufficiently high, Th and U will crystallize together as thorite (Th-silicate), which may incorporate up to 30 wt.% UO_2 in its structure. This mineral is a very refractory U source for hydrothermal fluids circulating relatively early after the granite emplacement (Cuney & Friedrich 1987). Thorite and other Th- and U-rich silicate phases may become U sources during later fluid events when they become metamict as a result of alpha-recoil from U decay. When such granite is rich in Nb, complex Nb and Nb–Ti oxides rich in U may crystallize. When the Th/U ratio of the melt

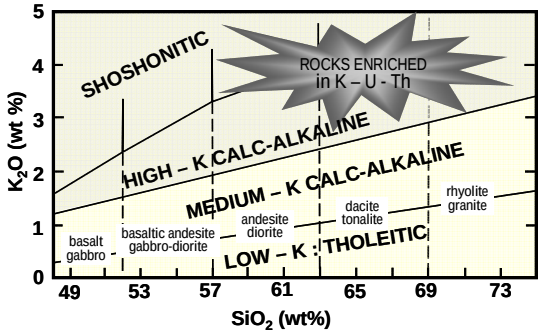

Fig. 7-4. Classification of calc-alkaline metaluminous igneous and volcanic rocks based on their SiO_2 and K_2O contents (modified from Ewart, 1982). The K_2O enrichment generally parallels Th and U enrichment.

decreases sufficiently during magmatic fractionation, small amounts of uraninite may crystallize in highly fractionated high-K calc-alkaline granite. However, such granite generally represents a minor amount of high-K calc-alkaline complexes so that the proportion of U occurring as uraninite is quite small. When uraninite does form in high-K calc-alkaline granite in equilibrium with Th-rich minerals (uranothorite), it is characterized by high Th contents (8 to 15 wt.% ThO_2).

Therefore, U-rich high-K calc-alkaline granite bodies may become a significant U source and may be associated with U deposits, but only when their accessory minerals have become metamict and if they contain some uraninite. However, high uraninite contents in such granite are exceptional relative to peraluminous leucogranite, and the deposits have more limited resources.

INTRA- AND PERI-GRANITIC URANIUM DEPOSITS

The mid-European Variscan U province, which extends over more than 2000 km from Spain to the Erzgebirge through Cornwall, Brittany, Vendée, the Massif Central, the Vosges, and the Black Forest, represents a major U, Sn, W, and Au province, in which the mineralization is related to Late Carboniferous peraluminous two-mica leucogranite emplaced between 335 and 310 Ma (Fig. 7-5). The granite is derived entirely from the partial melting of the continental crust (Bernard-Griffiths *et al.* 1985) during the collision between the Eurasian and African continental plates at about 400 Ma. The deposits are located either in the granite, such as in the French Massif Central and Brittany, or in their enclosing metamorphic rocks, such as in the Erzgebirge district, and are predominantly of Permian age.

France has approximately 140,000 MtU resources representing most of the U resources of

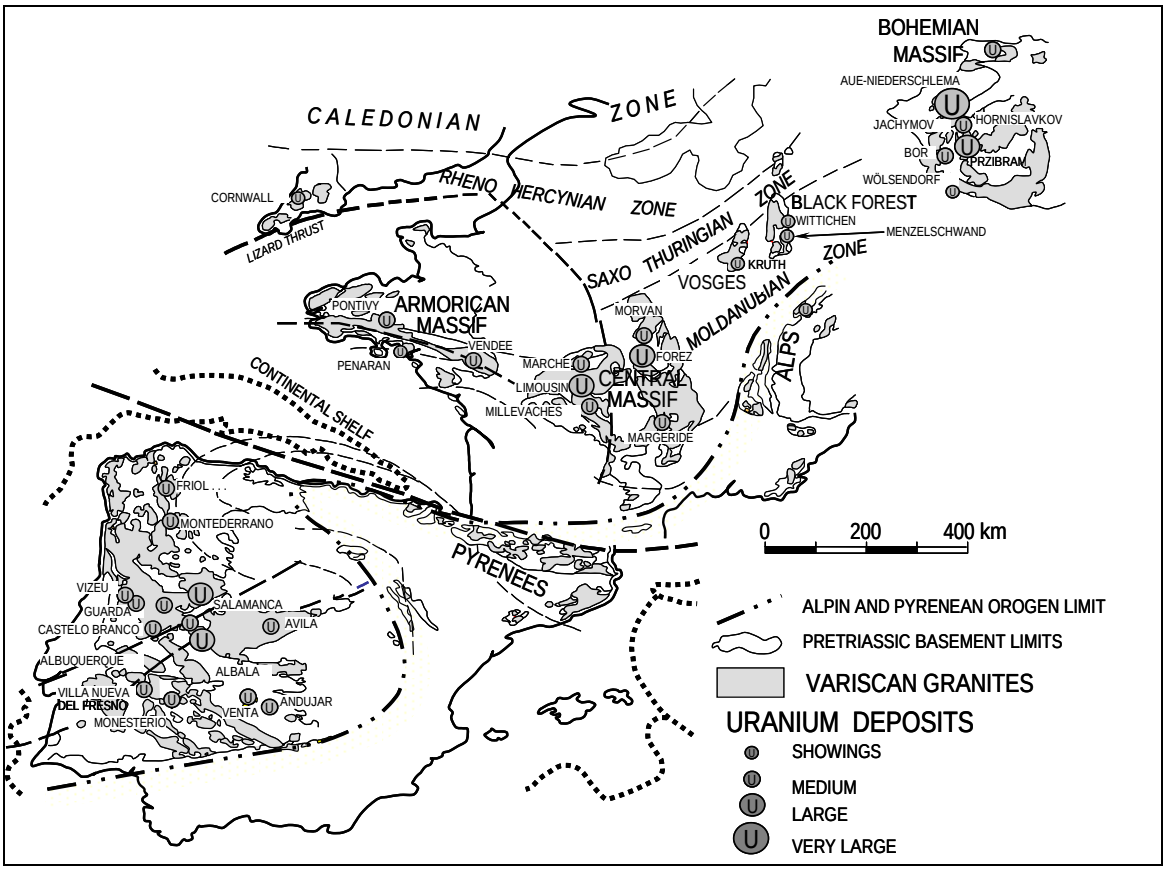

Fig. 7-5. Distribution of the Variscan granite bodies and U deposits related to granite in the mid-European Variscan belt before the opening of the Gulf of Biscay (from Cuney, 1978, modified)

Western Europe. Vein-type U deposits represent the main part of these resources and occur mainly in the Massif Central within the Saint Sylvestre, Marche, Millevaches, Forez, Morvan, and Margeride districts and the Armorican Massif in the Mortagne, Guérande, and Pontivy districts. In addition, numerous minor occurrences have been discovered in other parts of the Massif Central and Armorican Massif, as well as in the Vosges, Esterel, Corsica, and the Western Alps.

The occurrence of numerous ore deposits of the same metal or metal association of different ages is generally attributed to elevated concentrations of these metals in the crustal segment compared to average crustal abundances (Routhier 1980, Plimer 1980, Strong 1985). This is the origin of the metallogenic province concept. For other authors, metal enrichment results either from the extreme fractionation of magma with average metal contents, as proposed by Lehman (1982) for Sn, or from the efficiency of hydrothermal fluids to dissolve, transport, and precipitate the metal from granitic or metamorphic protoliths having average metal concentrations. For the western part of the mid-European Variscan belt, we will show that the U deposits hosted in peraluminous leucogranite are derived primarily from a U-rich crustal segment.

Relations between Variscan granite types and U mineralization

During the Variscan orogeny, large amounts of granitic magma were generated from either melting of recycled pre-Variscan crust to produce peraluminous leucogranite, or from mixing of pre-Variscan material with a mantle contribution. Many types of granite were produced in the French part of the Variscan orogen from 360 to 290 Ma including low- to medium-K calc-alkaline, high-K calc-alkaline, and various types of peraluminous granite (Stussi 1989).

There is no distinct temporal or spatial distribution of different types of granite throughout the Variscan orogen. However, the earliest granitoid magmatism is related to the "tonalitic line" extending NW–SE for 350 km along the eastern margin of the French Massif Central and Vendée (Fig. 7-6). It consists of low to medium-K calc-alkaline granitoid bodies emplaced with high-K calc-alkaline granitoid bodies between 350 and 300 Ma (Cuney *et al.* 2001, Bertrand *et al.* 2001). Low

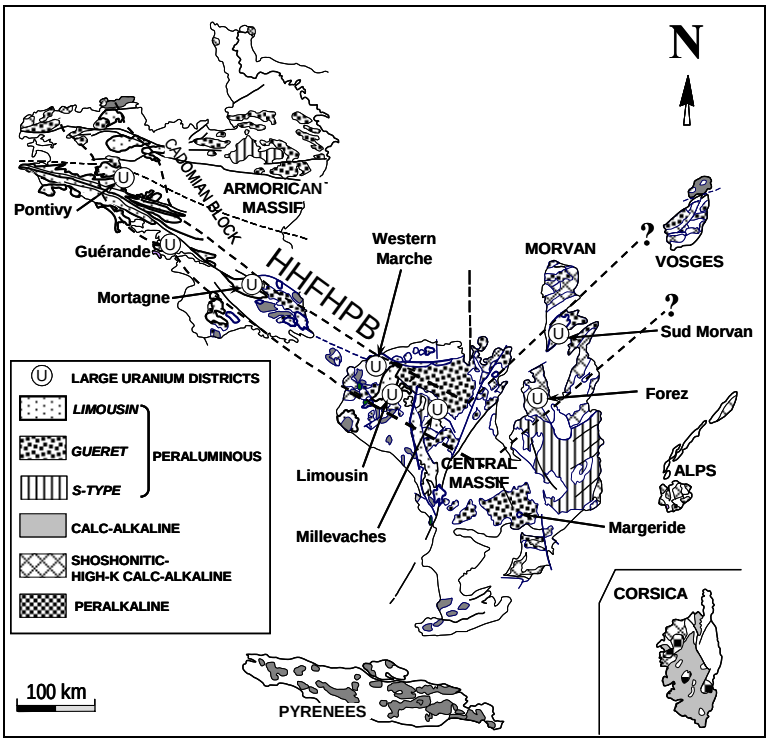

Fig. 7-6. Distribution of different granite types and main U districts in the French part of the Variscan orogen. Some preserved Cadomian granite bodies in northern Brittany and Normandy are also indicated. Modified from Stussi (1989).

to medium-K calc-alkaline granitoid bodies are predominantly located in the Pyrenees whereas high-K calc-alkaline granitoid rocks occur to the east of the Massif Central in the Vosges and the Alps, and were emplaced between 340 and 330 Ma (Pin & Duthou 1990). Guéret-type peraluminous granite was emplaced from 355 to 320 Ma throughout the French Massif Central. Variscan S-type granite, compositionally similar to that of the Kosciusko batholiths, is rare and occurs mainly in the southeastern part of the Massif Central and in the northern Millevaches area. Peraluminous two-mica leucogranite (L-type) was mainly emplaced between 335 and 310 Ma, along a belt extending from western Brittany to the core of the French Massif Central, and coincident with the High Heat Flow High Pressure belt (HHFHP). Alkaline granite occurs only in Corsica.

Low to medium-K calc-alkaline granite is never associated with U mineralization, because most of the U is hosted by refractory accessory minerals. Similarly, high-K calc-alkaline granite, which has high U (12–20 ppm) and Th (30–60 ppm) contents, is not directly associated with U deposits in the Variscan belt (Pagel 1982) because the U is mainly hosted in uranothorite ($(U,Th)SiO_4$). Uranothorite is very resistant to leaching when hydrothermal circulation occurred some tens of millions of years after granite emplacement (Pagel 1982, Cuney & Friedrich 1987).

Most Variscan U deposits formed during hydrothermal circulation that occurred some tens of millions of years after the emplacement of the calc-alkaline granite. The deposits are related to Late Carboniferous peraluminous two-mica leucogranite, variably enriched in incompatible elements (F, Li, Rb, Sn, U, W). Their Rb–Sr, Sm–Nd, and $\delta^{18}O$ signatures and their high peraluminous index indicate derivation from partial melting of the continental crust (Pin & Duthou 1990, Turpin *et al.* 1990a, b). All two-mica leucogranite plutons have similar major element compositions and, thus, were likely derived from similar degrees of partial melting of crustal material and magmatic fractionation. Concentrations of incompatible elements should reflect the abundance of these elements in the crust that melted. The St Sylvestre two-mica leucogranite complex shows enrichment in F during fractionation, whereas the Western Marche two-mica leucogranite complex does not, although both bodies have similar major element composition, are enriched in U, and are associated with U deposits.

To understand the successive U fractionation steps that led to formation of economic metal concentrations within two-mica leucogranitic complexes, we will examine the Saint Sylvestre complex. This granite has been one of the most thoroughly studied and has the largest U total resource among hydrothermal U deposits hosted in granite, with over 40,000 metric tons of metal at 0.2%.

Radioelement distribution in the Variscan crust

Correlations between heat production and heat flow data can be used to estimate the global radioelement distribution in the lithosphere, particularly the upper crust, which concentrates a large portion of radioelements over a relatively limited thickness. For example, in the French Massif Central, the measured surface heat flow is 90 to 120 $\mu W/m^2$, which is 2–3 times higher than the average continental heat flow of 40 $\mu W/m^2$. The crustal-integrated heat production contributes 50 to 60% of the total heat flow (Lucazeau & Vasseur 1981), whereas globally it is only 40% of the total heat flow (Chapman *et al.* 1979). The high radioelement content of the crust in the French Massif Central as suggested from the high crustal-integrated heat production is complicated because recent mantle uplift and active volcanism disturbs the heat flow in many parts of this region. However, the basement block in Limousin, which continues beneath the sedimentary cover into Brittany, and which has been stable basement since the Variscan Orogeny at about 300 Ma, has high heat flow that correlates with high heat production of 2.0 to 8.2 $\mu W/m^2$. This belt has been referred to as the High Heat Flow and Heat Production (HHFHP) belt (Vigneresse *et al.* 1987, 1988) at the southern margin of a Cambrian Cadomian block (Fig. 7-6). The thermal depth of 15.6 ± 0.6 km, estimated from the correlation between heat production and heat flow, is much larger than the average thickness of 2 to 7 km for granitic plutons deduced from gravimetric modelling (Vigneresse 1983). Thus, a 15 km-thick layer of Pre-Variscan formations is enriched in radioelements by more than two times that of the average crust. The HHFHP belt rims the Precambrian Cadomian block, but crosscuts the Central Armorican, South Armorican, and the West Vendean Variscan structural domains (Fig.7-6), suggesting that the distribution of the HHFHP belt should correspond to a Pre-Variscan feature.

All two-mica leucogranite bodies enriched in U and having U deposits are located within this high heat flow-production belt. Since such granite is derived from partial melting of crustal material based on its peraluminous character and Sr–Nd isotopic composition (Bernard-Griffiths *et al.* 1985, Vidal *et al.* 1984), it should be derived from partial melting of U-enriched metamorphic protoliths. Leucogranite located outside of the HHFHP belt has lower U content and is not associated with U deposits.

Characterization of the protoliths of U-enriched peraluminous leucogranite

Shale represents the most commonly proposed source for peraluminous leucogranite. Among Pre-Variscan sedimentary rocks, Early Paleozoic black shale should theoretically represent the best protolith for the Variscan U-rich, ilmenite-bearing peraluminous leucogranite, because it is strongly peraluminous, generally rich in U, and reduced as a result of its organic matter. However, the isotopic composition of most Variscan leucogranite is not compatible with its derivation from lithologies similar to outcropping Early Paleozoic formations (Vidal *at al.* 1984, Duthou *et al.* 1984, Bernard-Griffiths *et al.* 1985, Peucat *et al.* 1988). In particular, the $^{87}Sr/^{86}Sr$ initial ratios of this granite are lower than those of the metasedimentary rocks occurring in the area. To explain the so called "Sr paradox", Bickle *et al.* (1988) proposed that the $^{87}Sr/^{86}Sr$ ratios of the sediments may have been lowered by their interaction with aqueous fluids during diagenetic or prograde metamorphic episodes before anatexis. Downes & Duthou (1987) have shown that metasedimentary granulite of the lower crust sampled by Tertiary volcanoes has Sr and Nd isotopic compositions compatible with that of the peraluminous leucogranite, and thus may represent the source of the leucogranite. However, as granulite is typically depleted in U, such rocks cannot represent the source of the U-rich peraluminous leucogranite.

Turpin *et al.* (1990b) analyzed the Sr and Nd isotopic compositions of felsic metamorphic rocks outcropping in Limousin and concluded that Late Precambrian to Early Paleozoic felsic orthogneiss represents a possible source lithology for peraluminous leucogranite. In particular, the Saint Sylvestre granite, highly mineralized in U, may be derived from the partial melting of such rocks. Partial melting modelling of felsic orthogneiss (Bourguignon 1988) also supports this hypothesis and many examples of this orthogneiss, such as the Dronne potassic calc-alkaline orthogneiss from central Limousin, are rich in U, averaging 6.9 ppm U (Table 7-1). The Limousin basement is composed of a series of lithotectonic units overthrust during the early stages of the Variscan orogeny (Floc'h *et al.* 1983), so that outcropping lithotectonic units may represent exhumed slices equivalent to the more deeply buried lithologic units, which could have been melted to generate the peraluminous leucogranite.

High-K calc-alkaline granite, such as the Dronne orthogneiss, is typically derived from the fractionation of melt generated during subduction from a lithospheric mantle enriched in incompatible elements by the dehydration or melting of subducted sediments (McKenzie 1989). Thus, the ultimate origin of the U-enrichment of the Late Proterozoic to Early Paleozoic highly potassic calc-alkaline

orthogneiss is by metasomatism of the Late Proterozoic to Early Paleozoic lithospheric mantle.

The existence of the pre-Variscan vein-type U deposit at Le Retail in southern Brittany, dated at 425 Ma (Holliger & Cathelineau 1986), represents additional evidence for U-rich source rocks favorable for the formation of U mineralization already in the Pre-Variscan basement before the genesis of the Carboniferous two mica leucogranite.

Successive fractionation in the Saint Sylvestre granite complex

The Saint Sylvestre leucogranitic complex (Fig. 7-7) was emplaced during the Late Carboniferous. Different types of ore deposits associated with this granite show a remarkable regional zonation. U deposits are located in the central part of the leucogranitic complex, whereas minor Sn or W mineralization occurs near the granite–metamorphic rocks contact, and gold mineralization is hosted by the enclosing metamorphic rocks a few kilometres from the granite contact.

The Saint Sylvestre complex results from the accretion of successive batches of magma, all corresponding to more or less leucocratic peraluminous granite. The main part of the complex corresponds to coarse-grained porphyritic leucogranite (γ1) dated at 324 ±4 Ma from zircon and monazite (Holliger *et al.* 1986). The emplacement of γ1 leucogranite was nearly synchronous with γ2 fine-grained leucogranite. Emplacement of the γ3 fine-grained small granitic stocks at 308 Ma marks the end of granite magmatism in the complex. Three magmatic metal fractionation stages correspond to the three successive magma injections (from γ1 to γ3). Emplacement of the magmas was controlled by the regional tectonics.

The γ1 granites have a laccolith shape as deduced from the 3D inversion of gravimetric and seismic data (Audrain *et al.* 1989) and from the horizontal to gently dipping magmatic foliation and lineation (Fig. 7-7), defined by the orientation of K-feldspar megacrysts and biotite laths (Mollier 1984). The main magmatic lineation in the granite is oriented N110°E, parallel to that of enclosing gneiss and migmatite, and reflects the synkinematic emplacement of γ1 granite in the flat-lying thrusted metamorphic pile (Mollier & Bouchez 1982). The granite is presently about 2 km thick on average and extends over 50 km. Numerous root zones, some down to 6 km, generally correspond to fine grained granite intrusions (Fig. 7-7). The magmatic foliation of γ1 granite becomes locally vertical within north–south striking corridors mainly between the three main structural blocks constituting the Saint Sylvestre granite complex, which are, from west to east, the Brame, St Sylvestre and Saint Goussaud blocks. The largest corridor with vertical structures is located between the Brame and Saint Sylvestre blocks.

The γ1 granite slab is composed of a succession of magmatic injections, which have been mapped in more detail in the central–southern part of the granitic complex (Fig. 7-7). For example, along 3 km of the cross-section from Pény to Margnac (Fig. 7-7) are three coarse-grained sub-units, identified by their structural, major and trace element signatures (Cuney *et al.* 1984). The contacts between each of these sub-units are magmatic and commonly marked by fine-grained granite or pegmatite. In the central-southern zone of the complex, two major leucogranite sub-units can be distinguished (Fig. 7-7), the first corresponding to coarse-grained porphyritic leucogranite forming lenses several kilometres long, which are enveloped by the second unit of slightly porphyritic medium- to coarse-grained granite. The two units have the same magmatic structure and contacts between the two units are purely magmatic and tend to strike north-south on average.

Despite this local scale complexity, the γ1 granite slab is zoned from east to west, with the

TABLE 7-1. AVERAGE URANIUM CONTENTS OF THE PRE-VARISCAN METAMORPHIC FORMATIONS OF LIMOUSIN.

Formation	I	II	III	IV	V	VI	VII	VIII	Total
N	79	71	77	97	70	69	51	46	560
M (ppm)	3.3	3.2	4.4	3.7	6.9	4.1	4.2	6.8	4.4
min-max	0-11.8	0.2-9.9	1.3-9.4	0-13.3	1.1-19.6	0-17.7	0-17.1	1-27.5	0-27.5
s.d.	1.6	1.6	1.7	2.0	3.9	2.7	3.6	5.7	3.1

I = Mica schist Unit; II = metagreywacke of the Upper Gneiss Unit; III = metagreywacke and mica schist of the Lower Gneiss Unit; IV = anatexite of the Lower Gneiss Unit; V = Dronne felsic orthogneiss of the Lower Gneiss Unit; VI = Meuzac felsic orthogneiss of the Lower Gneiss Unit; VII = felsic metavolcanic rocks of the Lower Gneiss Unit; VIII = Thaurion felsic orthogneiss of the Lower Gneiss Unit (Cuney *et al.* 1990).

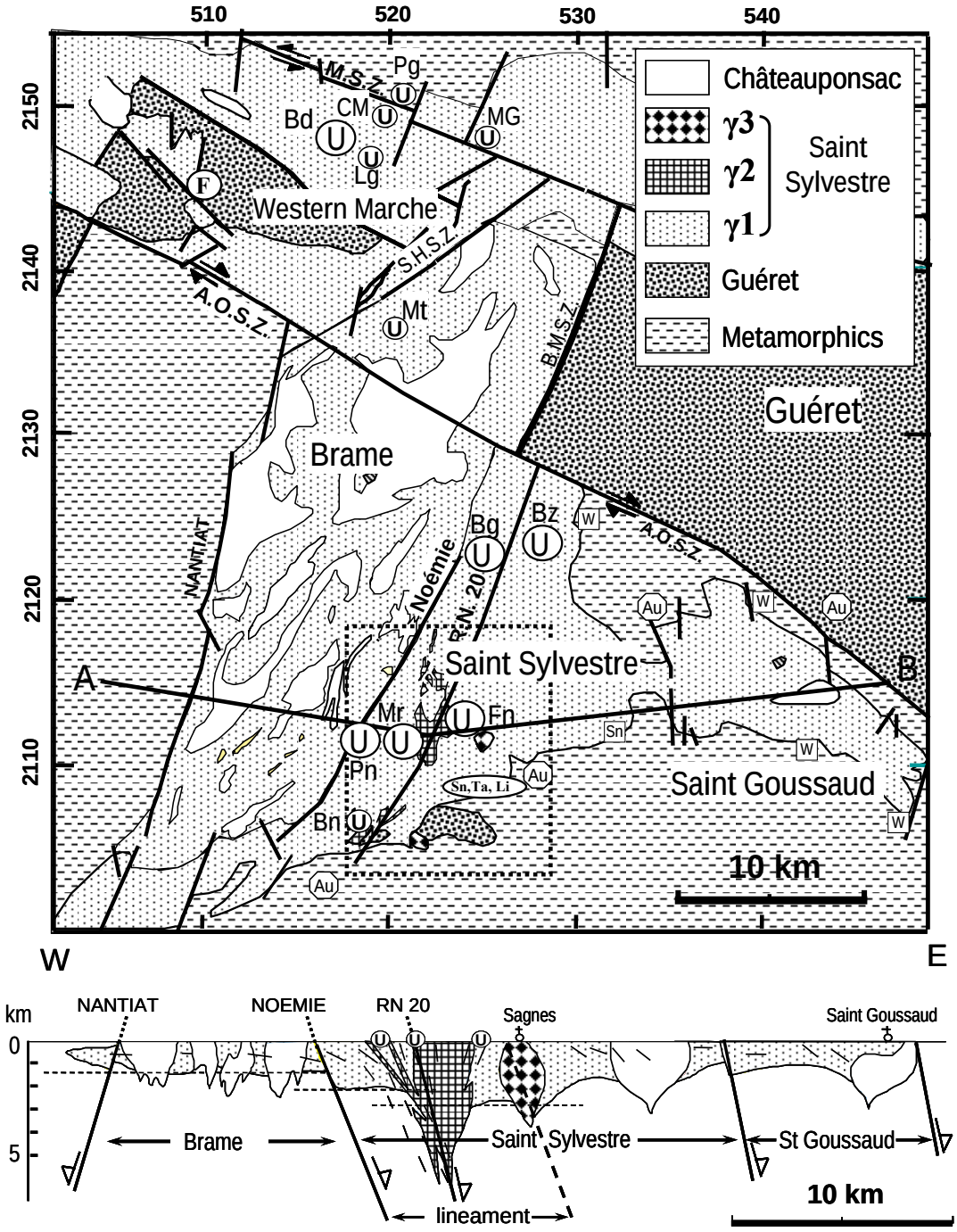

Fig. 7-7. Simplified geologic map and west to east cross-section of the Saint Sylvestre and Western Marche peraluminous complexes. The main uranium deposits and other metallic ore deposits (Au) and showings (F, Sn, W, Ta, Li) are indicated. Abbreviations of major shear zones (SZ) are: AOSZ = Arrènes–Ouzilly, CMSZ = Bussières–Madeleine, SHSZ = Saint Hilaire, MSZ = Marche. Abbreviations of the uranium deposits: Bd = Bernardan, Bg = Brugeauds, Bn = Bonnac, Bz = Bellezane, CM = Cote Moreau, Fn = Fanay, Lg = Loges, Mg = Mas Grimaud, Mr = Margnac, Mt = Montulat, Pg = Piégut (the only metamorphic deposit), Pn = Pény. The location of the cross section A-B, and the location of the map in Fig. 7-8 are also given.

west portion having a very penetrative horizontal magmatic foliation, and horizontal restitic biotitic schlieren rich in Th because of clusters of monazite crystals. The main rock-forming minerals, in decreasing order of abundance, are euhedral and elongated K-feldspar megacrysts, oligoclase, quartz, 5–8 vol.% Mg-rich F-poor biotite, sillimanite and muscovite and abundant accessory minerals of U-poor monazite and zircon generally occurring as clusters, apatite, anatase, ilmenite, ± pyrite, ± uraninite. Relatively high concentrations of elements compatible in peraluminous melts include 30 to 50 ppm Th, several hundred ppm Zr, several hundred ppm REE, as well as Ba, Sr, and transition elements (Table 7-2), and low contents of Rb, Li, Sn, F, and Be and moderate U contents (8–12 ppm U). Whole rock Th/U ratios are generally higher than 4 and are close to the average Th/U ratios of monazite (5 to 4), indicating that Th and U are almost entirely hosted by monazite.

Eastwards the magmatic foliation becomes increasingly less penetrative, the granite becomes nearly isotropic, the biotitic schlieren disappear and the contact with enclosing metamorphic rocks becomes relatively steep (45–50°). Quartz, albite, and muscovite (2 to 10 vol. %) increase in abundance, K-feldspar decreases in abundance and tends to become more isometric and biotite becomes more Fe–F–Li-rich. Accessory mineral contents decrease, as do concentrations of incompatible elements. Whole rock Th/U ratios decrease down to 0.4, and monazite hosts less and less of the whole-rock U. The fraction of U in the rocks hosted by uraninite increases steadily eastwards, from nearly zero to more than 80%.

As uraninite represents the most easily leachable U source by hydrothermal solutions, the eastern part of the γ1 granite should represent the most favorable area for U deposits. In fact, even though most of the Sn and W mineralization is located in the eastern, most fractionated part of the granitic complex, the main U-mineralization is

TABLE 7-2. REPRESENTATIVE CHEMICAL COMPOSITIONS OF THE MAIN PLUTONIC UNITS OF THE SAINT SYLVESTRE PERALUMINOUS LEUCOGRANITE COMPLEX.

N°	C2	C24	C36	4164	4135	89.1	89.38	89.36	C47	89.57	89.49	87.96	7128
Unit	1	1	1	1	1	1	1	1	1	2	2	3	3
SiO_2	70.87	71.99	72.58	72.14	73.59	71.77	73.18	73.65	72.16	68.29	71.50	73.47	73.96
Al_2O_3	14.95	14.76	15.26	14.71	14.07	14.50	14.38	13.71	15.59	15.19	14.61	14.54	14.38
Fe_2O_{3t}	1.99	1.74	1.39	1.86	1.52	1.63	1.38	1.06	1.63	2.87	1.72	0.92	1.03
MnO	0.02	0.02	0.03	0.03	0.04	0.00	0.02	0.02	0.04	0.02	0.01	0.06	0.02
MgO	0.52	0.38	0.34	0.34	0.42	0.41	0.25	0.17	0.41	0.76	0.38	0.05	0.28
CaO	0.69	0.00	0.31	0.16	0.52	0.96	0.48	0.58	0.70	1.29	0.81	0.32	0.54
Na_2O	3.02	3.06	3.23	3.39	3.39	2.99	3.45	3.50	3.48	2.67	3.22	3.83	3.19
K_2O	5.68	5.80	5.32	4.89	5.08	5.98	5.70	5.10	4.84	6.16	5.73	4.47	4.92
TiO_2	0.37	0.29	0.32	0.21	0.23	0.26	0.15	0.14	0.21	0.63	0.32	0.03	0.17
P_2O_5	0.31	0.32	0.26	0.24	0.17	0.41	0.36	0.41	0.29	0.46	0.41	0.43	0.33
LOI	1.15	0.84	0.95	0.89	0.74	1.04	0.93	1.00	1.14	1.24	1.05	0.97	1.19
Total	99.57	99.20	99.99	98.86	99.77	99.95	100.28	99.34	100.49	99.58	99.76	99.09	100.01
B	42	35	30	34	32	34	25	19	33	63	35	13	22
A	51	68	71	70	40	27	33	27	66	35	32	55	55
Ba	359	324	376	202	178	378	182	151	173	744	286	77	145
Rb	376	406	562	406	398	299	454	472	407	386	503	595	505
Sr	70	87	163	58	65	111	50	42	63	166	63	26	47
Th	51.0	35.0	23.0	21.3	23.0	19.0	14.4	14.1	11.3	94.5	52.5	10.9	20.2
U	13.8	16.0	16.0	22.1	20.9	14.5	18.6	23.2	21.0	13.9	17.1	10.4	19.9
Li	88	140	110	134	180	66	200	262	171	123	329	390	255
Sn	10	10	16			5.5	19	30	17.5	6.5	34	69	47
F				1400	1600	1100	1500	2300		4800	4000	4050	4200

Unit 1, 2 and 3 correspond respectively to γ1, γ2 and γ3 leucogranites (see text). The analyses of γ1 leucogranites are ordered from left to right according to increasing magmatic fractionation which occurs from West to East in the leucogranitic complex. Oxides are given in percent. The color index (B = Fe+Mg+Ti) and aluminous index (A = Al-(K+Na+2Ca)) are given in thousands of cations. Trace elements are given in ppm.

located in the central part, "anomalous" with respect to the general geochemical fractionation trend of the granite.

The γ2 granitic suite (Fanay type) forms a series of fine- to medium-grained small intrusions mainly elongate in the N–S direction that were injected into the central part of the γ1 main granitic body (Fig. 7-8) before its complete crystallization. In this area, magmatic foliation of the γ1 granite is nearly vertical and strikes N to N20°E, and becomes N60°E to the south in the Bonnac area (Fig. 7-9). The magmatic lineation is vertical. The contact between the γ1 and γ2 granite units is magmatic and their respective magmatic structures are concordant. Gravimetric modelling shows that the γ2 granite bodies are deeply rooted, down to 6–8 km, corresponding to a 5 km-size structure between the Noémie and RN20 normal fault (Fig. 7-9). This structure was active only during emplacement of the γ1 and γ2 granite bodies. No significant ductile structure is known in the area. The γ2 granite bodies crosscut the entire granitic slab and are rooted in the basement (Mollier 1984). This structure has been interpreted to correspond to a major crustal-scale lineament that controlled successive U concentration steps leading to the formation of economic U deposits in the Saint Sylvestre granite (Cuney *et al.* 1990). Thick, layered aplito-pegmatitic complexes with biotite-rich selvages are commonly present at the contact within the enclosing granite and at a few hundred metres from the contacts. Widespread beryl-bearing potassic

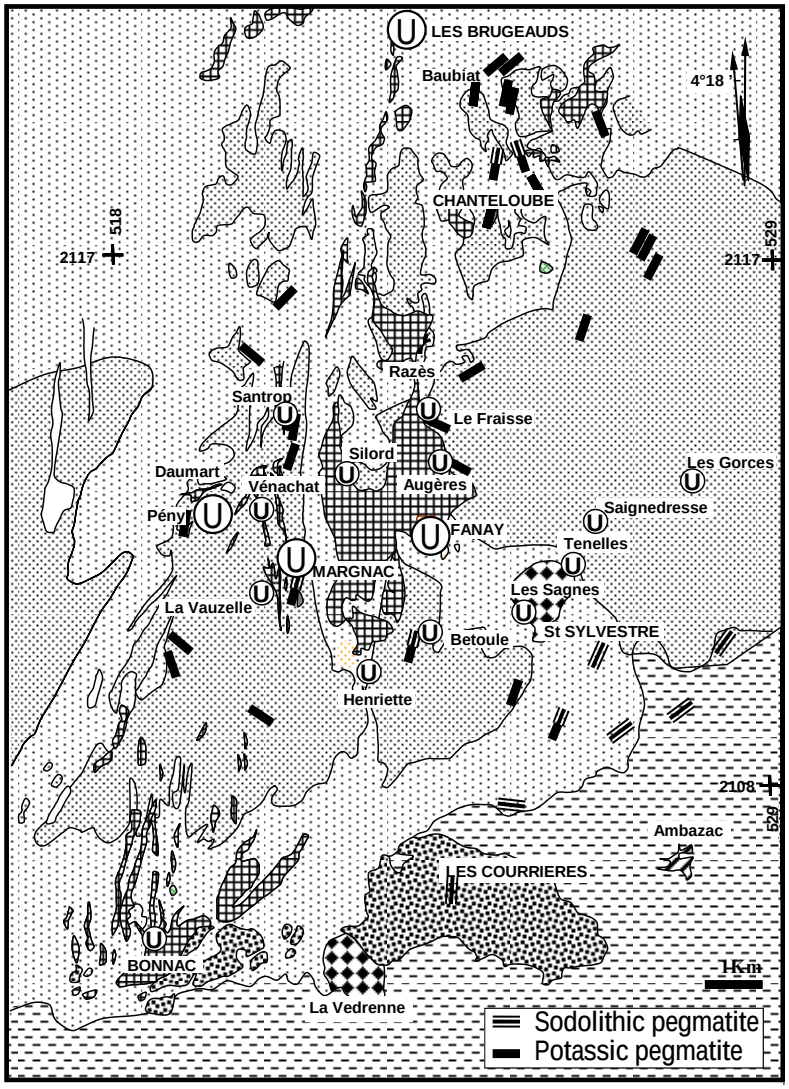

Fig.7-8. Detailed geologic map of the central-southern part of the Saint Sylvestre peraluminous leucogranite complex showing the relations between the major granitic units, the pegmatites and the major U deposits. The legend of the granitic units is the same as for Fig. 7-7, except that γ1 granites have been subdivided in two facies: γ1a (fine dots) and γ1b (larger dots) sub-units (see text for explanation).

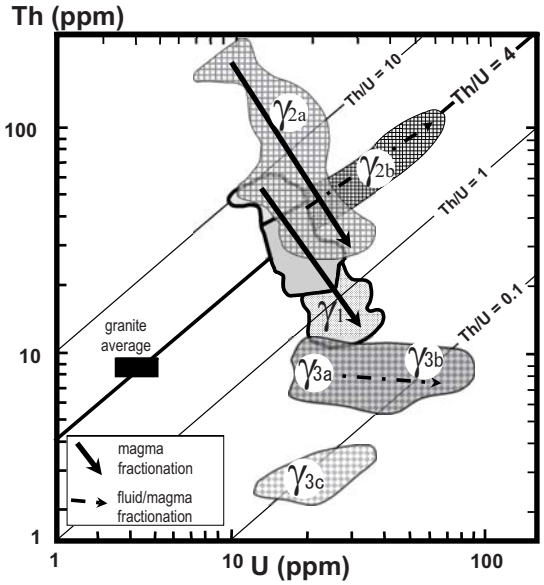

Fig. 7-9. Fractionation of U relative to Th in the main granitic units of the Saint Sylvestre leucogranitic complex (Friedrich *et al.* 1987). The symbols are the same as in Fig. 7-7 and 7-8. Only data for unaltered samples from drill cores and mining galleries have been used. The grey area in the γ1 granite field contains Th and U values of this granite hosting later fine grained γ2 leucogranitic intrusions.

pegmatite is spatially and genetically associated with this granite (Fig. 7-8).

The emplacement dynamics of the γ2 granite bodies have been reconstructed in the Margnac underground mine. Two facies have been distinguished. Fine-grained granite (γ2a) was emplaced as N–S to N165E vertical sheets, a few tens of metres to one kilometre thick with layering parallel to the magmatic foliation of enclosing γ1 granite. The layered zones result from discontinuous magmatic injections. The shortening direction during the syntectonic emplacement of γ2a is N50E–40 SW. Above the apex of some γ2a granite bodies, NNE-striking shear zones dipping 10 to 40°E or W, some centimetres to tens of metres thick, control the syntectonic emplacement of γ2b layered granite. The main stress direction became E–W and horizontal through a clockwise rotation during the intrusion of the γ2b layered zones. At that stage, crystallization of γ1 was complete and the deformation regime evolved from a viscous to a plastic state.

The γ2b layers have the same whole rock geochemical characteristics and the same biotite compositions as γ2a granite, but they are richer in U (up to 50 ppm) and their Th/U ratios tend to decrease. Uraninite therefore represents the most important U-bearing mineral in γ2b leucogranite. Uraninite in γ2 granite is in equilibrium with monazite crystals that have up to 7 wt.% UO_2 in their external growth zones.

Biotite in γ2 leucogranite are slightly more abundant (6 to 10 vol. %) and higher in Ti and incompatible elements (Th and Zr, Table 7-2) than in γ1 bodies, implying a higher temperature of formation for the γ2 biotite. It is also rich in U, with an inverse correlation between U and Th, and its Th/U ratios vary from 15 to 1 (Fig. 7-9, Table 7-2).

Intrusions of γ2b leucogranite occur as small cupolas or dikes throughout the south-central part of the Saint Sylvestre peraluminous complex (Fig. 7-8). They are less abundant northward where they form thinner dikes and disappear north of Les Brugeauds (Fig. 7-9).

Injections of γ2 granite into γ1 granite resulted in numerous magmatic shear zones, several metres thick, and considerably enriched in uraninite crystals (Friedrich *et al.* 1987). For example, along the Compreignac drill hole, U contents increase from 8 ppm in the undeformed granite up to 35 ppm in the shear zones (Fig. 7-9). This type of uraninite distribution is attributed to saturation of uraninite in magmatic fluids derived from γ2 granitic magma, which percolated into the shear zones that developed during emplacement of the γ2 granitic magma into the enclosing γ1 leucogranite. The trace element patterns of these shear zones are identical to those of the γ2 granite (Friedrich *et al.* 1987). Fractionation of U into the fluid phase expelled from this peraluminous leucogranite is in accordance with the experimental data presented in Chapter 2 that show the fluid/melt partition coefficients of U are the highest for peraluminous melts equilibrated with acidic chlorine-rich fluids (Peiffert *et al.* 1996). Hence, the present U content of this granite is significantly lower than the initial U content of the magma.

The γ3 granite (Sagnes type) was emplaced after crystallization of γ1 granite. It always presents sharp and discordant contacts with enclosing granite. It forms three small circular intrusive bodies, 100 m to 1 km in diameter, located at the eastern margin of the lineament in the central part of the Saint Sylvestre complex (Fig. 7-8). They are medium-grained and represent the most peraluminous plutonic units of the Saint Sylvestre complex with up to 10 vol.% trilithionite and F–Li-rich muscovite, scarce biotite, albite contents in excess of K-feldspar, and amblygonite, topaz,

cassiterite, Nb–Ta oxides and beryl as the main accessory minerals. The Sagnes granite is highly fractionated and probably related to rare metal pegmatite, the so-called "sodolithic pegmatites", located in the southern part of the Saint Sylvestre leucogranite. In the La Betoulle underground mine, the early and main intrusions of γ3a form several metre-thick, nearly vertical, E–W trending (N80°E to 110°E) dikes. The γ3b leucogranite corresponds to strongly layered units developed at the margins of γ3a dikes. The layering consists of a succession of 10 cm thick, strongly micaceous, granitic layers alternating with leucogranitic muscovite-poor layers. The γ3c intrusions form E–W, vertical, fine-grained, leucocratic dikes associated with pegmatite.

Pegmatites having the same mineralogical geochemical composition as the γ3 granite have the lowest compatible element content compared to γ1 and γ2 and the highest enrichment in U, Sn, Li, and Rb (Table 7-2). Concentrations in compatible elements decrease from γ3a to γ3b. The fractionation of Th-rich monazite and U-enrichment of the residual melts have led to a decrease of the Th/U ratios from 2 to 0.1 from γ3a to γ3c (Fig. 7-9). The average U content of γ3a granite is 24 ppm and the Th/U ratio is 1.8. Layers of γ3c have the highest U contents (50–60 ppm) and the lowest Th/U ratios (down to 0.1). Thus, in γ3 granite, U is almost entirely located in uraninite. The same type of uraninite-enriched shear zone that characterizes the γ1 and γ2 granite bodies is also observed in the vicinity of the γ3 granite bodies, with a geochemical signature specific to the γ3 granite (Friedrich *et al.* 1987).

Numerous other granitic intrusions of fine- to medium-grained biotite–muscovite granite occur in the Saint Sylvestre peraluminous complex, but will not be presented here, as they are not related to the U mineralization. For example, the Brame tectonic block is injected by numerous N–S elongate bodies of fine-grained biotite–muscovite granite named the Chateauponsac granite (Fig. 7-8), but these are devoid of U mineralization.

Lamprophyre and microgranite dikes striking NNE–SSW represent the latest intrusions in the area, emplaced in the central part of the Saint Sylvestre complex at 285–295 Ma (Leroy & Sonet 1976). The age of these dikes is between the time of formation of the episyenite pipes and overlaps with the U mineralization.

Relations between magmatic U enrichment and hydrothermal deposits

The first stage of hydrothermal U deposition in veins largely postdates the magmatic processes by 30 to 40 m.y. (Leroy & Holliger 1984). Despite this large gap, the mechanical aspects controlling the emplacement of γ2 and γ3 intrusions also controlled the emplacement of the brittle structures channelling the hydrothermal fluids. For example, the structures hosting the hydrothermal U mineralization at La Betoulle spatially overlap the early magmatic U enrichment that occurred at a late magmatic stage (Fig. 7-10). The BTL2 U vein is entirely located within or at the margin of several thick EW γ3a, γ3b, and γ3c dikes within γ2a leucogranite bodies (Fig. 7-8).

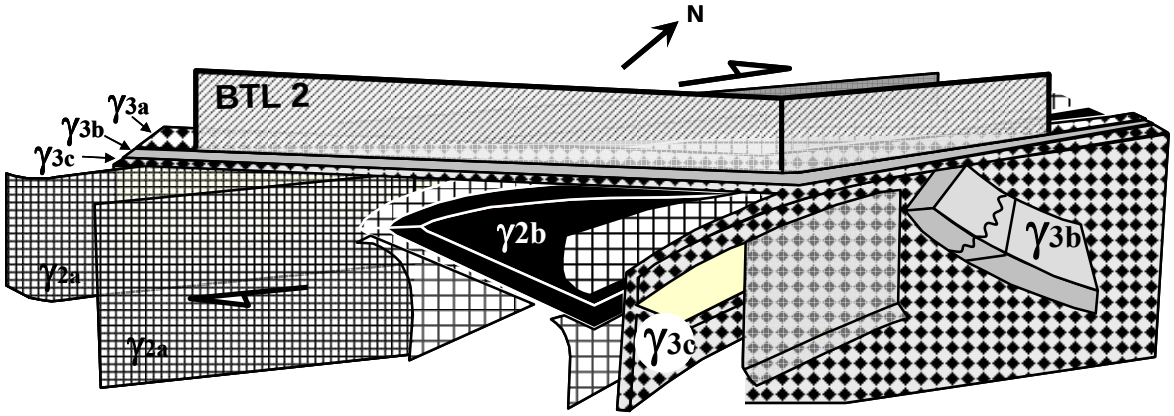

Fig. 7-10. Three dimensional representation of the relation between the magmatic structures defined by the striking of the injections of γ2 and γ3 leucogranitic injections and the brittle structure controlling the deposition of the hydrothermal uranium mineralization along the structure of La Betoule in the Saint Sylvestre peraluminous leucogranitic complex (modified from Cuney *et al.* 1990). The symbols for granite types are the same as in Figs. 7-7 and 7-8.

The most favorable U sources are located in the vicinity of the late stage endogranitic intrusions, the emplacement of which was structurally controlled in the 5 km long lineament located the central part of the Saint Sylvestre peraluminous complex. These intrusions strongly enhance the U enrichment of the surrounding γ1 leucogranite. Moreover, this U enrichment essentially corresponds to the crystallization of uraninite with small shear zones, which represents a U source easily leachable by oxidizing hydrothermal fluids. The degree of overlap between magmatic structures enriched in uraninite and brittle structures channelling hydrothermal fluids several tens of millions of years later is one of the main parameters controlling the efficiency of U concentration that formed these vein-type deposits. The U mineralization associated with peraluminous leucogranite in the Variscan orogen resulted from multistage processes, beginning with Late Proterozoic to Early Paleozoic partial melting of a metasomatized mantle, followed by several stages of partial melting of metal-rich portions of the continental crust and finally by hydrothermal circulation which was controlled by long-lived structures deeply rooted in the continental crust.

Alteration and uranium mobility

Various authors have proposed several types of alteration that may have influenced U distribution within granite bodies and increased their capacity to form U deposits. For example, albitization is a common feature in many peraluminous leucogranite bodies. However, albite enrichment in this type of granite appears to be a late magmatic process related to the high F and Li contents of the most fractionated melts. Increasing F and Li contents in the melts enlarge the stability field of quartz and shift their eutectic composition towards albite (Manning 1981). Because of the incompatible behavior of U until uraninite saturation is reached at tens of ppm in peraluminous melts (see Chapter 2), U tends to increase with increasing albite content, as observed in the eastern part of the Saint Sylvestre leucogranitic complex. Hydrothermal albitization may occur in some episyenite bodies, but they are never mineralized in the Saint Sylvestre leucogranite complex.

The occurrence of muscovite in peraluminous leucogranite has frequently been attributed to post-magmatic alteration of the feldspars. Ranchin (1971) suggested that uraninite crystallization occurred during a subsolidus event related to muscovitization. Detailed work by Monier & Robert (1986a, b) on muscovite stability, and by Friedrich *et al.* (1987) on uraninite distribution, have shown that both minerals result from crystallization at the magmatic stage. Very limited amounts of muscovite with phengitic compositions result from hydrothermal alteration.

During typical greisenization of peraluminous leucogranite from Brittany (France), and Cornwall (England), Pagel (1981) showed that U concentrations have remained constant. This is in agreement with the reducing nature of fluids involved in the formation of Sn–W mineralized greisen (Dubessy *et al.* 1987).

Chloritization of biotite is a common alteration in peraluminous leucogranite. Studies of Variscan leucogranite plutons have shown that there is no direct relation between the intensity of chloritization of the leucogranite and their U contents. In some leucogranite plutons with relatively limited U resources, such as Guérande in Brittany (Ouddou 1984) and Grandrieu in Margeride (Peyrou 1981), biotite is nearly totally chloritized, whereas in the central part of the St. Sylvestre peraluminous leucogranite complex, which hosts large U resources, chloritic alteration is limited. Chloritization may lead to *in situ* redistribution of U (Le 1975, Renard 1974) because chlorite generally contains more U than unaltered biotite. In zones of chlorite alteration, U is located in microfractures, along grain boundaries, and adsorbed on Fe- and Ti-oxides associated with the chloritization.

One pre-ore alteration feature controlling the location of the U ore bodies are “episyenite” pipes (Leroy 1978a, b, Cathelineau 1986). These pipes may extend over more than 800 m vertically as in the Bernardan deposit (Western Marche granite bodies), with diameters of a few tens of centimetres to a few tens of metres. These rocks are characterized by complete quartz leaching. The cavities left by quartz may remain open with no further mineral deposition, although the high porosity created in these rocks by quartz dissolution from circulating hydrothermal fluids, may lead to the deposition of a great variety of minerals (Cathelineau 1986). Some of these pipes were initially mineralized with uraninite and pyrite, with limited illitic alteration.

$^{40}Ar/^{39}Ar$ dates for muscovite from barren episyenite are *ca*. 305 Ma by Scaillet *et al.* (1996a, b), which corresponds to a late orogenic event and uplift of the Limousin domain (Cuney *et al.* 2002)

and the beginning of post-collisional extension in the western part of the Variscan belt (Bouchot *et al.* 2005). Exhumation and extension favored the infiltration of meteoric fluids (Turpin *et al.* 1990b), which were heated to at least 400°C, rose rapidly, boiled and subsequently condensed in the alteration zones (El Jarray *et al.* 1994). The solubility of silica is lower in water vapor than in the equivalent mass of liquid water, so that condensation of the vapor formed from the boiling of the meteoric fluids led to the dissolution of quartz in the granite and creation of the episyenite. Episyenitization developed preferentially at the intersection of fracture systems (Pécher *at al.* 1985). In the Saint Sylvestre granite these occur mainly at the intersection between the E–W and N to NNE structures.

Kaolinitization is the latest alteration event that affected the peraluminous granite. The most intensely altered zones occur within the most evolved parts of the granitic massifs. Compared to fresh granite, kaolinitized granite always has very low U contents (Allman-Ward 1985, Simpson *et al.* 1979). Kaolinitization may have been initiated at the hydrothermal stage (Charoy 1981), but a large part is from supergene meteoric alteration. Meteoric oxygenated fluids are very effective in dissolving uraninite, with U loss reaching 30 to 50% in uraninite-rich peraluminous leucogranite (Barbier 1967). In kaolinitized granite, the remaining U is hosted mainly in monazite, zircon, and apatite, adsorbed on Ti–Fe oxy-hydroxides, and redistributed along microfractures and grain boundaries.

Peraluminous leucogranitic complexes, which have been subjected to recent uplift, will still contain uraninite grains in surface-near sections. For example, the Monts d'Ambazac area in the Saint Sylvestre leucogranitic complex, which exhibits rugged topography, contains uraninite preserved in many outcrops. In contrast, meteoric fluids dissolved uraninite at depths exceeding 100 m and precipitated autunite in microfractures in peraluminous granite in the much less rugged Western Marche (NW Massif Central), Grandrieu (Margeride, south Massif Central), and Guérande (Armorican Massif). Autunite in weathered granites generally indicates uraninite at depth below the weathering zones.

Characteristics of vein uranium deposits

Primary U deposition at the scale of the Variscan belt occurred at 270–280 Ma during the Stephanian to Permian transition (Leroy & Holliger 1984, Holliger & Cathelineau 1986, Cathelineau *et al.* 1989, Golubev *et al.* 2000). This period corresponds to a major extensional event with deposition of siliciclastic sediments in small intracontinental basins. Some of these basins also host stratabound U deposits (Landais 1996).

Most of the vein type U deposits from the French part of the Variscan orogeny are monometallic. Uraninite, with minor coffinite and hexavalent U minerals, are the principal U minerals. Associated minerals include pyrite, marcasite, quartz, fluorite, calcite, and barite. Occasionally, chalcopyrite, galena, bismuth, and bismuthinite may occur in telescoping veins deposited later in the same structures as the U veins, as observed in the Bois Noirs Limouzat deposit (Cuney 1978). After fracturing or brecciation of the host rock, the following mineral succession is commonly observed (Geffroy 1971, Leroy 1978a, Cuney 1978, Poty *et al.* 1986):

(1) Millimetre- to centimetre-thick comb quartz is first deposited on the vein walls or the breccia fragments. Hematite may occur in the finely crystallized base of the quartz comb, but when the quartz crystals become euhedral, uraninite half spherulites are deposited on the growth zones of quartz, sometimes together with pyrite. This comb quartz may be absent and direct deposition of uraninite may occur on the wall rocks. Alteration of the wall rocks is generally limited to an illitization and hematization of the feldspars.

(2) Spherulitic uraninite is deposited together with iron disulfide. Simultaneous growth of uraninite and sulfide has been observed in some deposits (Leroy 1978b), but generally where uraninite deposition is massive the iron disulfides are less abundant. Uraninite within granites contains several percent CaO, with the highest contents (up to 8–9 wt.% CaO) in deposits hosted by metamorphic rocks that are generally richer in Ca than the peraluminous leucogranite (Cathelineau *et al. 19*82). Thorium contents in uraninite are generally below 400 ppm, the detection limit of the electron microprobe. Alteration results in increase of the silica content of the uraninite, whereas Pb contents decrease. In the northeastern part of the Massif Central (Morvan), fluorite may be synchronous with pitchblende deposition.

(3) After another brecciation episode, microcrystalline hematitic silica (red jasper), evolving progressively to euhedral quartz crystals, may be deposited. Iron is oxidized to hematite, but

sometimes löllingite from the As contained in the initial pyrite crystals may be observed. During this episode, uraninite can be partly altered to coffinite.
(4) In the Bois Noirs deposit, this episode was followed by deposition of banded quartz veins, with alternating smoky, white, amethyst, and hyaline bands associated with chalcopyrite. Occasionally, concretionary coffinite can be deposited in fractures at this stage.
(5) After another fracturing or brecciation episode, minor quantities of carbonate (calcite, dolomite, or ankerite), fluorite or barite may be deposited.
(6) The last event that occurred in the veins corresponds to oxidation of primary U minerals and formation of roll-front type structures in the episyenite and development of clay alteration (mainly montmorillonite), fluorite, and secondary uraninite (Cathelineau 1982). Uranium was redeposited in variable amounts by infiltration of meteoric fluids. Sooty pitchblende occurs in the reduced zones and hexavalent U minerals, mainly uranophane, autunite, and chalcolite, in the oxidized zones. This remobilization can be an important source of U. For example, in the Bois Noirs Limouzat deposit it has been estimated that more than the half of the mined mineralization corresponds to remobilized ore (Cuney 1978).

Ore bodies occur as veins or stockwork in granite or the enclosing rocks, or disseminated in the episyenite. Episyenitic alteration is generally developed at the expense of the host granite but also occasionally at the expense of enclosing gneiss. The mineralized veins extend over a length of a few metres to several hundreds of metres. The thickness of the ore bodies is commonly 1 to 2 m but ranges from a few centimetres up to 15 m and their vertical extent varies between 10 m and hundreds of metres. The grade averages 0.1–0.3% U, but is highly variable ranging from a few hundred ppm to several % U. Uranium enrichment also occurs at the intersection with lamprophyric dikes.

Mineralized episyenite bodies have vertical extensions typically from ten to a few hundreds of metres. The largest episyenite system from the Bernardan deposit (Western Marche), consisting of complex continuous episyenite columns, extends from the surface down to 800 m. However, the total vertical extent of the system was certainly over one kilometre if the eroded part of the granite is taken into account. The diameter of the columns is variable, from a few centimetres up to several tens of metres.

Several hundreds of U occurrences have been discovered in the Limousin area since the beginning of exploration in the late 1940s, and more than fifty deposits have been mined by underground and open pit methods. Resources of individual ore bodies of both vein and episyenite type range from a few tonnes up to 7,000 tonnes. The average grade of the episyenite-hosted ore bodies tends to be higher than the vein-type mineralization. For example, the Bernardan episyenitic type deposit in Western Marche has produced 7000 tonnes U at an average grade of 0.55 %, whereas the Bois Noirs vein type deposit at Forez has produced 5,400 tonnes U at an average grade of 0.26 %. The district has been the most important U district in France with cumulative original resources of over 40,000 MtU, from which about 25,000 MtU have been mined from 1949 to 1995, at an average mining grade close to 0.2% U and a cutoff of 0.07% U.

OTHER VEIN-TYPE URANIUM DEPOSITS

Hercynian granite bodies similar to the Saint Sylvestre peraluminous leucogranite occur in other parts of the Massif Central (Western Marche, Millevaches, Margeride) and in the Armorican Massif (Mortagne, Guérande, Pontivy) in France, and the mid-European Variscan belt in Portugal and Spain, Cornwall, Erzgebirge in Germany and the Czech Republic, and its extension in North America with the South Mountain Batholith (Nova Scotia, Canada). Elsewhere in the world, other districts with vein type U mineralization related to peraluminous leucogranite occur mainly in South America within the Hercynian Achala Batholith, Argentina (Cuney *et al.* 1989), and in Asia in the Indosinian and Yanshanian granite intrusions of southeastern China (Min *et al.* 1999).

METALLOGENETIC MODELS FOR THE VARISCAN GRANITE-RELATED URANIUM DEPOSITS

A number of metallogenetic models have been proposed for the formation of Hercynian uraninite veins within peraluminous leucogranite. Geffroy & Sarcia (1958) and Geffroy (1971) proposed an epithermal origin for the genesis of these deposits. Roubault & Coppens (1955, 1958) first suggested a lateral secretion process, but without specifying the nature of fluids involved in the process. A series of authors (Moreau *et al.* 1966, Barbier 1974, Langford 1974, 1977, 1978, and Knipping 1974) favored a supergene origin (the "*per descensum*"

theory) for many U deposit types, wherein leaching of U was favored by the development of tropical climatic conditions at the time of the formation of the deposits. More recently, Leroy & Poty (1969), Leroy (1978a), Cuney (1978), Poty *et al.* (1986) and others have shown from fluid inclusion studies that the fluids involved in the genesis of the Variscan vein-type U deposits are of hydrothermal origin. These fluids are relatively low salinity fluids with temperatures from 100–120°C for the Bois Noirs deposit (Cuney 1978) up to 200°C in Limousin (Dubessy *et al.* 1987). The CO_2-rich fluids initially attributed to uraninite deposition at Margnac in Limousin (Leroy 1978a) are related to earlier fluids associated with arsenopyrite deposition (André *et al.* 1999). Stable isotope studies by Turpin *et al.* (1990b) have shown that U deposition results from the mixing of two types of fluids, an oxidizing meteoric water able to leach uraninite from the enclosing granite and a connate fluid with high $\delta^{18}O$ = +8 to +15‰ and δD = –45 to –30‰. These latter fluids infiltrated from overlying Permian formations and provided hydrocarbons or H_2S to reduce the U, also resulting in low $\delta^{13}C$ values of the syngenetic carbonates of –17.6‰. Later deposited fluorite, barite and calcite are associated with more saline fluids at temperatures of 100–150°C.

VOLCANIC-RELATED URANIUM DEPOSITS

Mid-oceanic ridge basalts (MORB) are by far the most abundant volcanic rocks on the Earth's surface, with very limited U-enrichment (70–100 ppb U in average MORB glasses; White 1993). However, they represent the first major U fractionation process in the geological cycle. Uranium enrichment results mainly from the preferential fractionation of the incompatible elements in basaltic melts during partial melting of the mantle initially containing about 18 ppb U (abundance for the Bulk Silicate Earth estimated from chondrites), which represents an upper limit for U content in the depleted mantle source for the MORBs. Subsequently, the thermal anomaly created by the extrusion of MORBs induces convective hydrothermal circulations along the ridge, which leads to a further U enrichment of the upper part of the basaltic crust. The 3.22 ppb U from seawater is essentially trapped by reduction processes within the sea floor basalt. The reduced hydrothermal fluids escaping from the mid-oceanic ridge contain two orders of magnitude less U (0.06 to 0.18 ppb U) than the seawater (Chen *et al.* 1986), but the levels of U enrichment in the basalt remain at the ppm level. The global amount of U trapped by the hydrothermal circulation is estimated at 1.5 to 4 x 10^3 tU/year (Elliott *et al.* 1999). Chen *et al.* (1986) estimated that about 98% of the U from seawater has been trapped in the oceanic crust. Although these two successive processes are largely insufficient to approach economic grade concentrations, they are of major interest for the generation of enriched mantle wedges during the subduction process. As a volume of oceanic crust equivalent to 10% of the entire mantle has been recycled throughout Earth's history, using present subduction rates, this process has significantly changed mantle composition through time, especially for U. The U-enriched oceanic lithosphere produced at mid-ocean ridges is then re-injected into the mantle at

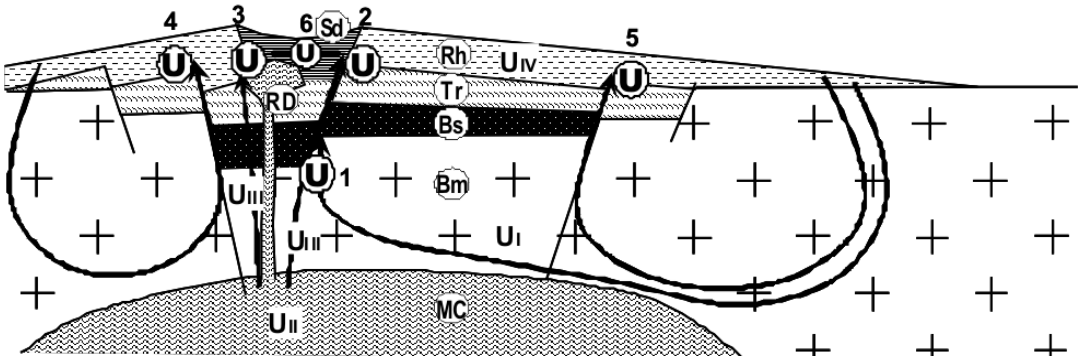

Fig. 7-11. Conceptual model for volcanic-related U deposits. MC = magmatic chamber, Bm = basement, Bs = basalt, Tr = trachyte, Ry = rhyolite, RD = resurgent dome, Sd = sediments. Uranium sources: U_I = basement, U_{II} = magmatic chamber, U_{III} = magmatic fluids, U_{IV} = rhyolite. Type of uranium deposits: 1 = basement-unconformity-hosted low-medium temperature vein-type deposit, 2 = high temperature vein-type deposit related to magmatic fluids, 3 = low-medium temperature vein-type deposit associated with resurgent domes, 4, 5: low-medium temperature vein-type deposit associated with intracaldera or ring faults, 6: stratabound deposit in interlayered sedimentary rocks.

convergent plate boundaries. During subduction, with increasing temperature, a progressive dehydration of the oceanic crust occurs with a loss of incompatible elements. At still higher temperatures, partial melting of the oceanic crust produces melts enriched in incompatible elements (except Nb, Ta, and Ti), which will fertilize the overlying mantle wedge and produce the enriched mantle sources of arc basalt and related felsic rocks generated by magmatic fractionation. Depending on the degree of enrichment in incompatible elements of the mantle source and the rate of partial melting, these elements, especially K, Th, and U, will be variably enriched in the resulting magmas. The formation of peralkaline melts necessitates a very low degree of partial melting. Alkali basalt with up to 1–2 ppm U contents (Jannot *et al.* 2005) can be produced in the most favorable conditions. The fractionation of these magmas may ultimately lead to the formation of rhyolite with up to 20 ppm U as in the Streltsovskoye Caldera, Transbaikalia, Russia (Chabiron *et al.* 2001).

Volcanic rocks mainly occur in four types of geotectonic environment: (i) mid-ocean rift where two oceanic plates are spreading apart, (ii) subduction zone at the boundaries of two plates either in an oceanic arc or continental arc setting, (iii) hot spots which usually occur under the oceanic crust, but can also be located under the continental crust, (iv) intracontinental setting associated with rifting. The relative role of subduction, hot spots and rifting is frequently debated for the origin of the intracontinental volcanism.

Besides mid-oceanic ridge volcanic activity, volcanic eruptions may generate more or less complex edifices, in a variety of geotectonic setting, comprising highly variable quantities of volcanic material, deriving from different type of sources, variably enriched in U, more or less fractionated and with variable degrees of crystallization when they cool down. Each of these parameters has an importance for the genesis of highly fractionated volcanic rocks strongly enriched in U, which may ultimately represent an efficient source for the formation of U deposits.

Shield volcanoes are almost exclusively composed of basalt, the Hawaiian volcanoes being one of the best examples. They are commonly considered as the product of hotspot volcanism but they can also be found along subduction-related volcanic arcs. The high magma supply rates typical of these volcanoes do not allow significant fractionation of the lavas, and thus prevent the formation of significant amounts of highly fractionated, U enriched melts.

Flood basalt, such as the Columbia River Basalt province (SE Washington State, USA) or the Deccan Traps (western India) extend over thousands of square kilometres in intracontinental settings. Individual flows may be more than 50 m thick, and extend for hundreds of kilometres. But, despite the large size of these volcanic systems, they also do not produce highly fractionated, U enriched melts.

Monogenetic volcanic fields consist of a collection of hundreds to thousands of separate vents and flows spread out both temporally and spatially. No preferred conduit structure ever gets established. Even if some highly fractionated magmas can be produced locally, the amount of U-enriched magma is too small to represent a significant U source, and the duration of the magmatic activity is too short to promote important convective hydrothermal circulation to remobilize U. However, local U showings may be formed.

Strato-volcanoes, as illustrated by Mt. St. Helens, Pinatubo and Fuji volcanoes, are characterized by eruptions of andesitic to dacitic lava formed at lower temperature. Thus, they are more viscous than basalt, and often suffer explosive eruptions leading to the formation of large amounts of pyroclastic material in association with lavas. Strato-volcanoes are commonly found along subduction-related volcanic arcs, and the magma supply rates to strato-volcanoes are lower, allowing the formation of more differentiated magma compositions. However, the amount of highly fractionated melts of rhyolitic composition that can be enriched in U remains limited. Hence their ability to represent significant U sources for the genesis of U deposits remains also limited.

Caldera complexes are at the origin of the most explosive of Earth's volcanic eruptions and often do not look like volcanoes. They are usually associated with magmatic chamber collapse, forming large depressions, called calderas, rather than building a volcanic cone. The collapsed depressions indicate that the magma chambers associated with the eruptions are situated at a relatively shallow level in the crust. Their origin is either attributed to an intracontinental hotspot, such as at McDermitt or Yellowstone, or to subduction-related arc settings. Caldera complexes comprise a large range of magma composition from basalt to highly fractionated rhyolite. Rhyolite generally represents the largest proportion of the extruded

magmas mostly occurring as layers of ash fall or flows (ignimbrite) often extending over thousands of square kilometres in all directions from these calderas. When such rhyolite is strongly enriched in U it represents a very important U source for hydrothermal U deposits associated with the caldera system or for sandstone-hosted deposits from intracontinental basins. As the pyroclastic material can be transported in the atmosphere over several tens to hundreds of kilometres, this type a volcanism may represent an essential component for an additional U source in sedimentary basins located far away from these volcanoes. Hence, caldera complexes, comprising large amounts of highly fractionated pyroclastic rhyolitic material, represent the best setting for the genesis of U deposits related to volcanic rocks. Another, highly favorable character of this type of volcanic environment is the existence of a relatively shallow magmatic chamber inducing convective hydrothermal fluid circulations lasting over a long period of time allowing an important alteration of the rocks and thus an important remobilization of the U from the volcanic rocks.

Streltsovskoye caldera (Transbaikalia, Russia)

Geological setting: the Streltsovskoye caldera is located in the general vicinity of the eastern Russian–Chinese–Mongolian border. The caldera is part of a Late Jurassic–Cretaceous volcanic belt, which extends from Siberia to Kazakhstan, through Mongolia. More locally, Streltsovskoye represents one of the volcanic centers spread along the Tulukaevskii volcanotectonic structure (TVTS) within the Argun River region–Mongolian volcanic belt (Ishukova 1989; Fig. 7-12). Similar U mineralization settings include Dornot in Mongolia (Mironov *et al.* 1993), Maureen and Ben Lomond in Australia (O'Rourke 1975), Marysvale and Thomas Range in the United States (Cunningham *et al.* 1982 1998), Sierra Pena Blanca in Mexico (George-Aniel 1988, George-Aniel *et al.* 1991) and the Xiangshan volcanic complex in China (Yaohui Jiang *et al.* 2005a, b).

The Streltsovskoye caldera represents the largest U ore field associated with volcanism in the world. The ore resource estimates grading above 0.2% U reach more than 232,000 tU in the cost category lower than 80 USD/kg (Laverov *et al.* 1992), and are distributed in 18 deposits. About 25,000 tU of additional and possible reserves are included in the IAEA cost category 80–130 USD/kg. Since 1968, about 115,000 tU have been produced by the Krasnokamensk Kombinat from open pit and underground operations.

The caldera has a diameter of about 20 km (180 km^2) and was filled with a pile of volcanic rocks (basalt, andesite, trachydacite, rhyolite) and interlayered sedimentary horizons (Fig. 7-13). The present thickness of the pile locally reaches more than 1 km. The caldera filling occurred during the Late Jurassic. Liparitic tuff corresponding to the last erupted volcanic rocks was dated at 142 ±7 Ma by K–Ar (Chernyshev & Golubev 1996). It may have

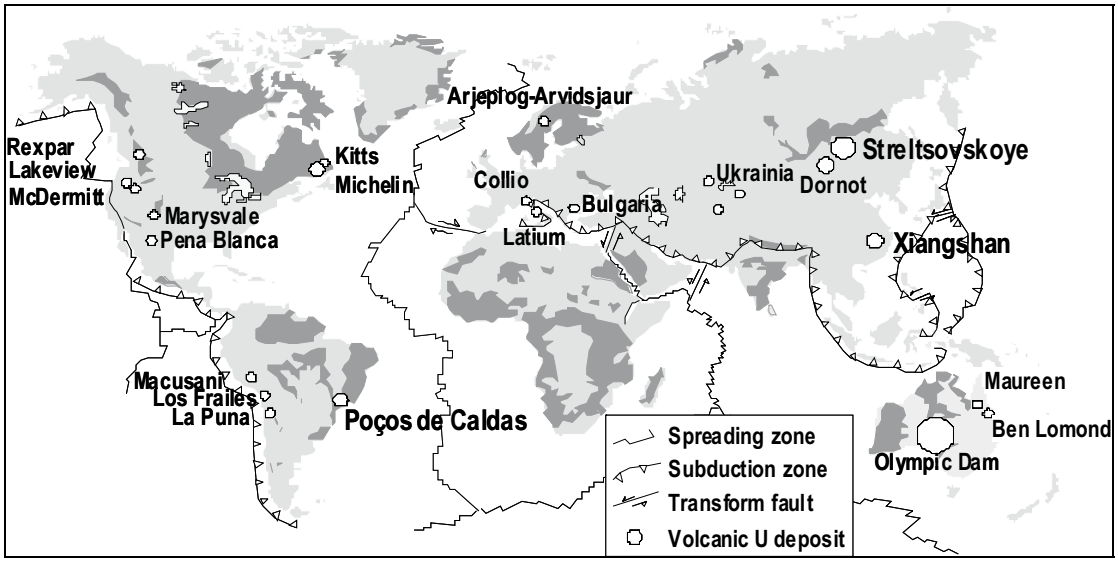

Fig. 7-12: World distribution of the major uranium deposits related to volcanism. The darker gray fields correspond to Archean and Proterozoic basement.

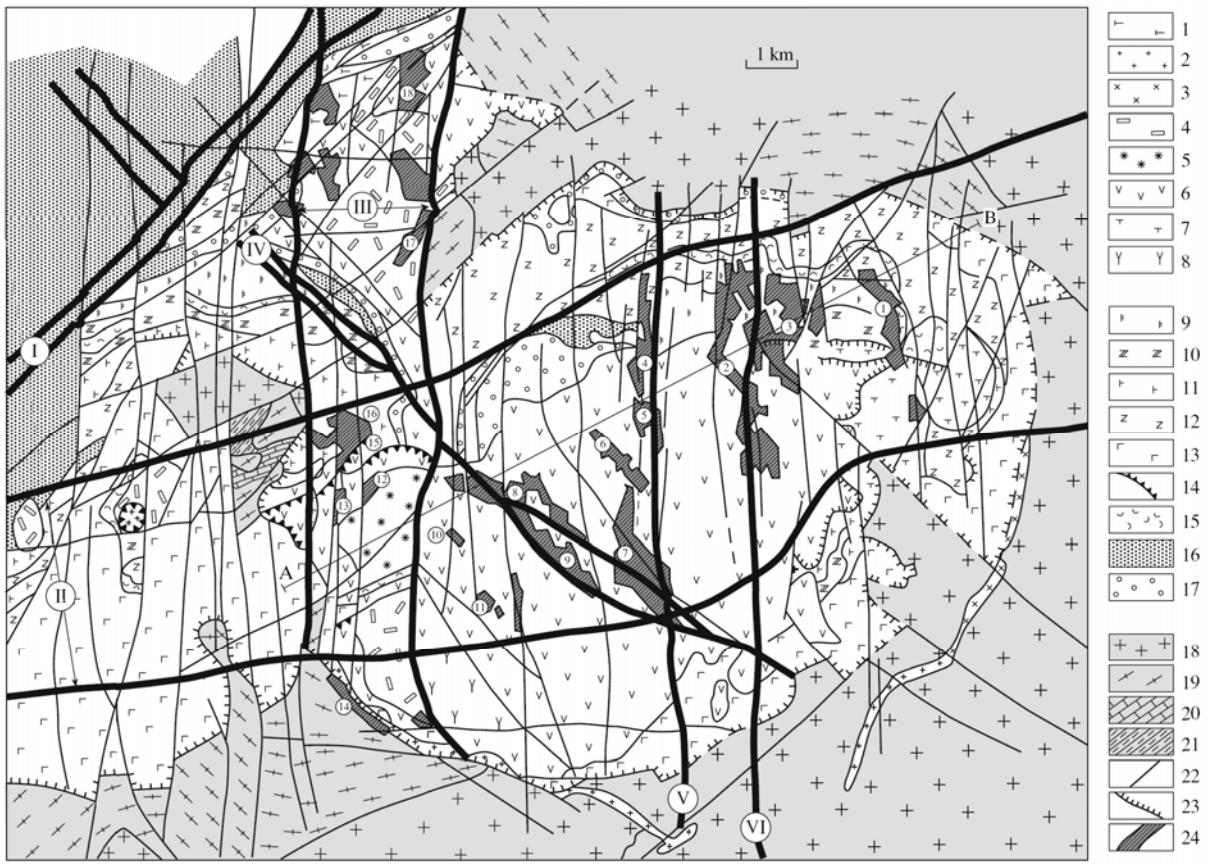

Fig. 7.13. Geologic map of the Streltsovskoye caldera with the location of the U ore deposits. A SW–NE cross section is given below. Major tectonic structures: I = Urulunghuyevskaya shear zone, II, = Argunskaya shear zone, III = Meridional fault zone, IV = Malo-Tulukuyevskaya fault, V = central fault, VI = Streltsovskoye fault. Uranium ore deposits: 1: Shironoskoye, 2: Streltsovskoye, 3: Antei, 4: Oktabraskoye, 5: Luchistokoye, 6: Martoskoye, 7: Malo-Tulukuyevskoye, 8: Tulukuyevskoye, 9: Yubilenoye, 10: Vesenneye, 11: Novogodneye, 12: Pyatletneye, 13: KranyKamen, 14: Yugo-Zapadnoye, 15: Zherlovoye, 16: Argunskoye, 17: Berzrechnoye, 18: Dal'nee. Legend of the figure: Turginskaya Suite (Cretaceous): 1: basalt, 2: dikes and subvolcanic bodies of finely porphyritic latite, 3: syenite, syenite-porphyry, granosyenite-porphyry, 4: upper sheet of liparite, 5: spherulitic liparite, 6: massive and fluidal rhyolite and tuff, 7: andesite, 8:lower sheet of fine-fluidal spherulitic and glassy liparite, Priargunskaya Suite (Jurassic): 9: upper sheet of basalt and andesitic basalt, 10: upper trachyte sheet, 11: medium sheet of basalt, 12: lower sheet of trachydacite, 13: lower sheet of andesitic basalt, 14: volcanic centers, 15: tuff, 16: sandstone, 17: conglomerate, basement: 18: Variscan granite, 19: Caledonian orthogneiss, 20: marble, 21: metasedimentary gneiss, 22: steeply dipping faults, 23: caldera ring structure, 24: U ore deposits projected to the surface.

represented between 30 and 35% of the volume of the volcanic pile, but at the present time, liparite is mainly preserved in the center of the caldera. The thickness of the sedimentary layers varies from some metres to 100 metres. From bottom to top the lithologic succession is the following:

- a basal conglomerate, filling the depressions of the basement;
- the Priargunski Formation, which marks the beginning of the formation of the caldera, during Mid to Late Jurassic with an alternation of sedimentary and various types of volcanic rocks;
- the Turginski Formation, of Late Jurassic age (155–135 Ma), which corresponds to the paroxysm of the volcanic activity in the caldera with powerful emissions of rhyolite and ignimbrite, with a few basaltic horizons;
- the Kutinsky Formation, of Early Cretaceous age (135 Ma), which is composed of conglomerate, sandstone with coal intercalations and thin layers of basalt and andesite. The main volcanic centers are located at the intersection between NE or N-S extensional faults and NW faults.

The basement is mainly composed of Paleozoic granitoid rocks and Precambrian metamorphic formations (biotite gneiss, amphibole gneiss, and dolomitic marble). The age of the granite ranges from Early Paleozoic (510 Ma), Caledonian, and Hercynian to 121 Ma. No regolith alteration has been observed below the basal conglomerate at the unconformity. Drilling down to depths of 2,700 m through the Streltsovskoye

caldera and basement has provided a unique opportunity to evaluate the role of the different source rocks that may be involved in the genesis of the deposits. The granite of the basement from the Streltsovskoye caldera is mainly biotite granite (Andreeva *et al.* 1996). A biotite leucogranite was recognized in drill core below 2,644 m (Chabiron *et al*. 2003). The granite bodies are equigranular to porphyritic and characterized by the accessory mineral paragenesis of magnetite, titanite, apatite, zircon, thorite, and allanite, typical of subalkaline granite (Cuney & Friedrich 1987). Leucogranite is characterized by an accessory mineral paragenesis of magnetite, apatite, zircon, xenotime, monazite, thorite, and pyrochlore. The granite and leucogranite are variably altered with sericitization, chloritization, and carbonatization (Andreeva *et al.* 1990, 1996). Despite the numerous drill cores studied in thin section and the fact that some of them reached a depth of 2,700 m, fresh plutonic rocks with non-chloritized biotite and non-altered allanite are unusual. A detailed geochemical study was performed on the freshest samples of the 7c drill hole (Chabiron *et al*. 2003), which crosscuts the basement from 891 to 2,670 m and intersects the most common basement lithologies and some of the major structures of the area. The selected samples in Table 7-3 record moderate alteration, as indicated by their low A/CNK index, close to one.

Uranium distribution in the granite. In highly potassic calc-alkaline meta-aluminous granite rich in Ca, Th, and U, the U is located mainly in uranothorite and allanite (Cuney & Friedrich 1987). Uraninite is sometimes present. In the Streltsovskoye granite, allanite and uranothorite have been observed. Uraninite may have been present but was leached during hydrothermal alteration of the granite, because of its high solubility in oxidizing fluids. Fission track distribution shows that U is mainly located in allanite, monazite, zircon, and uranothorite. However, U is not easily leached by common hydrothermal solutions from such accessory minerals. Metamictization or specific hydrothermal alteration may alter their structure, and allow the leaching of U. Metamictization affects more efficiently U and Th-rich silicates such as zircon, allanite, and uranothorite (Ewing *et al.* 1988). At Streltsovskoye, hydrothermal alteration occurred during the Early Cretaceous (Chernyshev & Golubev 1996), *ca*. 150–200 m.y. after crystallization of the Hercynian granite plutons. Therefore, after such a time span, zircon, thorite, and allanite had already undergone a significant degree of metamictization, which enabled the leaching of U from their structures.

Allanite presents a specific alteration style in Streltsovskoye granite (Chabiron & Cuney 2001). Euhedral, fresh allanite crystals have only been identified in a few samples. Altered allanite consists of an Fe-oxide skeleton, which mimics the typical zonation of allanite crystals, filled with newly formed monazite and REE carbonates. Rare earth elements, Th and part of U from allanite are trapped in these newly formed minerals. Monazite has a highly variable Th content (from 0 to 12 wt.% ThO_2) and a low U content (from 0.1 to 0.2 wt.% UO_2). REE carbonates were only detected by SEM because of their small size. They mainly contain LREEs with some Y.

Uranium deposits. The area is marked by an important radioactive anomaly, mostly due to the high Th background of liparite. In Transbaikalia, exploration was first directed to find U mineralization related to granite. More than 3,000 U showings have been identified in the area. The first U deposit was discovered in the Streltsovskoye caldera in 1963, more than 10 years after the start of the exploration in this region. Structural guides were used because all the deposits are blind and are not related to surface radioactive anomalies. The only anomalies occur at the periphery of the caldera and are only slightly above the local radioactive background and not related to any deposit. Most of the deposits start at about 200 m below the surface and the largest ones are located at depths from 400 to 900 m. Just a few small deposits occur in the upper 100 m.

Uranium mineralization is located in any of the different volcano-sedimentary horizons and was also recognized by drilling down to 2,400 m into the granitic basement. Each deposit exhibits specific characteristics. The two most important, Argunskoye and Antei, are located in the basement, thirteen are located in the volcanic-sedimentary formations, and four in volcanic necks. The main control of ore deposition is structural; the chemistry of the host rocks does not seem to have a significant control. Nearly all types of rocks in the caldera (basalt, trachyte, rhyolite, and sedimentary layers) or the basement (granite and dolomitic marble) can be mineralized. Mineralization generally occurs as sub-vertical veins or stockwork in the caldera fill and in the basement, and in some places expands along stratigraphic levels in sandstone, conglomerate and tuff of the caldera. All enclosing rocks are deeply altered. Uranium contents generally amount to about 0.15 wt.%, up to 0.6 wt.% in large stockwork, and up to 1.0 wt.% in veins. Small deposits were also discovered in the

TABLE 7-3. CHEMICAL COMPOSITION OF GRANODIORITE, GRANITE AND LEUCOGRANITE (WITH DEPTH IN THE 7C DRILL HOLE INDICATED) FROM THE BASEMENT OF THE STRELTSOVSKOYE CALDERA, AND OF THE RHYOLITES (WR = WHOLE ROCK) AND ASSOCIATED MELT INCLUSIONS (MI) HOSTED BY QUARTZ PHENOCRYSTS (FROM CHABIRON *et al.*, 2001; 2003)**.

	Granodiorite		Granite		Leucogranite		Tulukuevskoye		Krasny Kamen		Streltsovskoye	
	2360	2398	1231	2630	2658	2665	WR	M.I.	WR	M.I.	WR	M.I.
SiO_2	69.26	68.66	70.91	73.85	76.12	76.38	77.77	71.54	73.18	74.68	78.03	71.78
TiO_2	0.30	0.40	0.28	0.17	0.04	0.05	0.12	0.15	0.12	0.09	0.11	0.17
Al_2O_3	14.90	14.86	14.48	13.28	12.60	12.41	12.54	12.90	11.85	12.43	12.13	13.49
FeO	2.69	3.24	2.18	1.86	1.22	1.16	1.08	1.09	2.69	0.73	1.18	1.19
MnO	0.08	0.09	0.06	0.08	0.04	0.03	–	0.13	0.04	–	0.04	0.04
MgO	0.65	0.91	0.48	0.29	–	0.02	0.05	–	0.15	–	0.16	–
CaO	2.11	2.44	1.82	1.03	0.28	0.39	–	0.19	0.04	0.20	0.41	–
Na_2O	4.74	4.55	3.85	4.33	4.52	4.44	3.90	4.70	1.67	5.17	0.95	4.90
K_2O	3.34	3.13	4.49	3.97	4.30	4.21	2.96	4.85	5.47	4.81	4.38	5.76
F	n.d.	n.d.	n.d.	n.d.	n.d.	n.d.	0.21	1.83	0.22	1.39	nd	1.77
P_2O_5	0.11	0.13	0.03	0.03	–	–	–	–	0.07	–	–	nd
L.O.I.	0.42	0.88	1.19	0.91	0.72	0.77	1.36	nd	3.25	nd	2.31	nd
Total	98.59	99.29	99.77	99.80	99.85	99.86	98.42	97.59	95.50	99.70	97.39	99.10
A/CNK	0.98	0.97	1.00	1.00	1.00	0.99	1.30	0.97	1.35	0.88	1.72	0.94
La	35.2	64.4	38.5	36.7	16.1	15.6	53.6	67.3	54.6	53.8	51.3	72.5
Ce	71.7	120.3	81.4	78.8	49.9	45.6	99.2	154.0	74.0	109.7	95.8	138.6
Pr	7.0	11.2	8.7	9.5	7.5	6.9	8.7	11.8	8.7	9.7	9.4	11.9
Nd	23.4	37.5	30.1	33.7	33.0	29.3	23.5	32.1	24.0	28.5	24.7	40.9
Sm	4.0	6.4	5.5	7.7	10.9	9.1	4.2	6.4	4.2	6.9	4.4	10.6
Eu	0.8	1.0	0.9	0.4	0.0	0.0	0.1	0.12	0.08	0.16	0.1	0.20
Gd	3.9	4.6	4.4	7.0	11.7	9.5	3.7	5.8	3.7	5.5	3.9	10.0
Tb	0.6	0.7	0.7	1.2	2.1	1.9	0.7	n.d.	0.7	n.d.	0.7	n.d.
Dy	3.6	3.8	4.5	8.4	13.6	12.1	4.9	8.2	4.8	8.1	5.2	13.5
Ho	0.7	0.7	0.9	1.9	3.1	2.7	1.1	n.d.	1.1	n.d.	1.3	n.d.
Er	2.1	2.0	2.5	4.8	7.9	7.1	3.7	6.0	3.4	6.5	3.6	11.7
Tm	0.3	0.3	0.4	0.8	1.3	1.2	n.d.	n.d.	n.d.	n.d.	n.d.	n.d.
Yb	2.3	2.2	2.7	5.8	8.2	7.3	4.7	6.5	4.5	11.9	4.8	14.9
Lu	0.4	0.3	0.5	0.8	1.2	1.2	0.7	1.0	0.7	1.7	0.8	2.4
Ba	801	913	796	258	13	20	n.d.	2.2	50.3	1.9	n.d.	2.0
Nb	13.0	10.6	14.9	20.8	28.4	16.2	58.3	202.7	61.7	121.2	59.4	138.8
Rb	144	125	190	208	227	200	289	n.d.	475	n.d.	338	n.d.
Sr	215	275	205	70	7	15	n.d.	1.1	1.6	24.7	n.d.	n.d.
Ta	1.2	0.6	1.5	2.7	1.2	1.1	5.6	n.d.	5.3	n.d.	5.8	n.d.
Th	18.3	14.6	22.4	29.5	53.4	38.9	66.7	[46]	61.9	[49]	68.4	n.d.
U	6.3	3.4	5.7	9.5	14.1	11.8	7.4	[15]	28.1	[14]	21.5	n.d.
Y	24.5	24.7	26.3	52.7	83.3	70.3	38.4	34.5	39.8	30.8	39.4	61.5
Zr	225	263	165	173	161	174	245	n.d.	259	n.d.	250	n.d.

**The two rhyolite samples from Streltsovskoye and Krasny Kamen are slightly mineralized. U and Th contents of melt inclusions are bracketed because they have not been determined exactly on the same magmatic inclusion as the rest of the analyses. n.d. = not determined. Whole rocks have been analyzed by ICP-AES and –MS, whereas melt inclusion have been anayzed *in situ* by ion microprobe after rehomogenization.

surroundings of the caldera. They correspond to remobilization in younger sediment rocks. The major deposits inside the Streltsovskoye caldera are the mined-out Tulukuevskoye open pit, and the presently operating Streltsovskoye and Antei underground mines.

The Tulukuevskoye deposit is located in the center of the caldera and represents the most complete volcano-sedimentary sequence (rhyolite, trachy-dacite, dacite, andesite, basalt, and conglomerate, about 800 m thick; Fig. 7-14). It was exploited until 1996 by open pit mining down to a depth of –300 metres and subsequently by underground mining down to –700 metres. The pitchblende–molybdenite mineralization occurred as a stockwork and lenses of complex morphologies and was restricted to the volcano-sedimentary pile. The U resources were of 37,000 tU (Laverov *et al.* 1992).

The Argunskoye deposit is entirely located in basement composed of biotite–amphibole gneiss, schist, marble, and amphibolite and Early Paleozoic granitoid rocks. The mineralization is overlain by a basalt layer and starts 140 m below the surface. It is located in a thick lenticular breccia body (50–100 m) developed in carbonate rocks below a contact with granite, dipping steeply to the NE down to more than 1,000 m. Its lateral extension is 500 m and its maximum thickness is 70 m. The grades are highly variable: 0.1–3.5 % U, 0.15–0.26 % Mo. The resources are estimated to 39,000 tU and the deposit is not mined. The ore minerals are pitchblende, coffinite–pitchblende associated with small amounts of brannerite, pitchblende–coffinite–molybdenite and fluorite–molybdenite. Pyrite, marcasite, galena, sphalerite, chalcopyrite, freibergite, native Cu boulangerite, and arsenopyrite occur in small amounts. Enclosing granite and volcanic rocks are highly altered with clay minerals, quartz, kaolinite, and siderite. Marble is silicified and fluoritized.

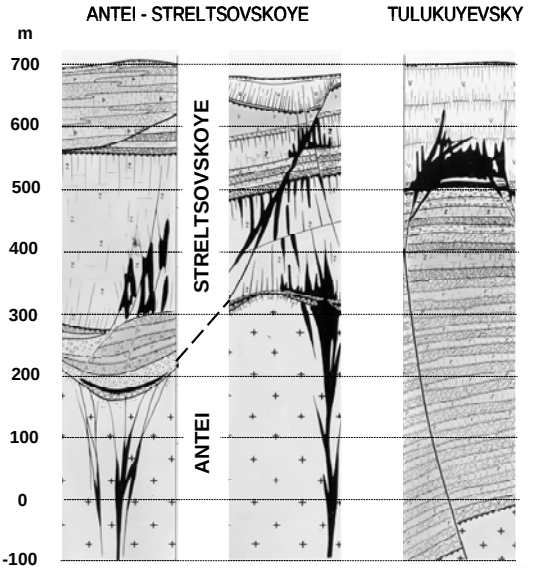

Fig. 7-14. Cross sections of Antei, Streltsovskoye and Tulukuevsky U deposits from the Streltsovskoye caldera. Same symbols as Fig. 7-13. Note that the ore bodies never reach the surface and they may extend deep into the basement.

The Streltsovskoye-Antei deposit has vein-type mineralization hosted in volcanic rocks and the basement (Fig. 7-14). It is the most important one with resource estimates greater than 60,000 tU. Uranium contents vary from 0.1 to 50 wt.%. Vein thickness varies from a few metres up to 60 m. The Streltsovky vein was 750 m long with an average thickness of 6 m, and an average grade of 0.33% U and 0.2–0.4% Mo. Fluorite veins are also abundant in the caldera and were discovered first. The Streltsovskoye deposit is composed of six interconnected mineralized bodies, localized along N–S and NE structures, mainly hosted by trachy-andesitic tuff, whereas the Antei deposit is entirely located in the granitic basement along vertical N–S structures at depths from 350 to 1400 m. The upper part of the Streltsovskoye deposit has been mined by an open pit down to –220 m.

The paragenesis of the U mineralization is mainly based on mineralogical studies of the Streltsovskoye deposit (Melnikov *et al*. 1980; Fig. 7-15; recently revised by Krylova *et al*. 2006). The first stage corresponds mainly to local albitization in the deep part of the deposit and intense illite–phengite alteration ("hydromicas" of the Russian authors; Andreeva *et al*. 1996). In the 2,700 m deep drill hole from the Streltsovskoye-Antei deposit, illite–phengite, or chloritization, or both, occur along nearly the entire length of the drill core. The phengite–illite stage was dated at 139–130 Ma by Andreeva *et al.* (1996), and at 133 ±5 Ma by Chernyshev & Golubev (1996) by K–Ar geochronology. Quartz veins with variable quantities of carbonate, pyrite, and jordisite also occur (Ishukova *et al*. 1991). In the Antei deposit, breccia with cryptocrystalline quartz cement and stockwork of thin cryptocrystalline quartz veinlets with finely dispersed pyrite, jordisite, and low Fe sphalerite were deposited. High U contents were locally observed with pre-ore stage paragenesis, but

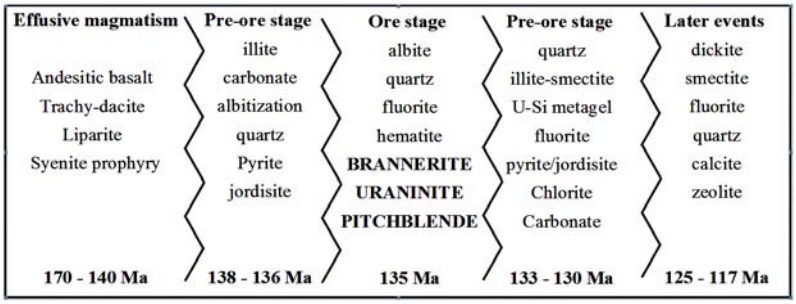

Fig. 7-15. Simplified paragenetic succession of the Streltsovskoye-Antei deposit (from Melnikov *et al.* 1980; Krylova *et al.* 2006)

without any visible U minerals, particularly at the periphery of the caldera (Ishukova *et al*. 1991). The pre-ore stage was developed at temperatures of 280 to 300°C

The main U deposition occurred during the quartz–pitchblende ore stage, followed by purple and black fluorite. In fact, several quartz generations were formed during this stage. The early quartz generation is weakly developed, fine-grained, impregnated by iron oxide–hydroxide minerals and cements host rock fragments. The later generation of quartz is widely developed, especially in the Antei deposit, forms short-prismatic bi-pyramidal crystals from some tenths to several millimetres, and is devoid of solid inclusions. The bulk of the quartz was formed before pitchblende, but the latest growth zones were formed with the first nucleation of fine spherulitic pitchblende. Pitchblende also occurs as spherulites capping idiomorphic minerals, as isolated spherulites, or as disseminated grains in the cement of breccia. Typically, for U deposits related to volcanic rocks, the pitchblende contains up to 1.5 wt.% ZrO_2. The syn-ore stage developed at temperatures of 180–220°C. However, new fluid inclusion data on syn-ore quartz indicate that the formation conditions of the primary pitchblende–brannerite ores took place at temperatures up to 350–460°C from Na–Cl–(HCO_3) fluids (Krylova *et al.* 2006). Uranium transport may have occurred as chloride or fluoride complexes of U^{6+} and the decrease of the fluid temperature was the main cause of the ore deposition. Xenomorphic coffinite was developed later at the margin of pitchblende spherulites, and is associated with pitchblende in the breccia cement, and with pyrite. Fibrous coffinite crystals are locally present at the contact with pitchblende. Brannerite occurred as small idiomorphic, rectangular elongated crystals deposited earlier than coffinite or pitchblende. Pyrite, galena, and molybdenite may be associated with the U minerals. Brannerite ores occur at depths of more than 1,300 m in the basement, mixed pitchblende–coffinite–brannerite ores between 800 and 1,300 m, and molybdenite–pitchblende ores occur at higher levels (Ishukova *et al.* 1991). A first generation of fluorite was deposited during the syn-mineralization stage, and a second generation of fluorite (yellow to colorless) was deposited with calcite, comb quartz (up to 1 cm crystals), and zeolites during the post-ore stage. Temperatures of the post-ore stage were between 160–210°C.

Massive pitchblende has given $^{206}Pb/^{238}U$ and $^{207}Pb/^{235}U$ concordant ages between 134 and 136 Ma, and finely disseminated pitchblende and pitchblende with galena and Fe-molybdenite inclusions give discordant ages at 133 ±4 Ma (Chernyshev & Golubev 1996). The age of the radiogenic Pb from a pitchblende–molybdenite aggregate, calculated using a two-stage model, is 250 to 260 Ma, which is older than the pitchblende deposition age and has been interpreted as the age of the possible source of U for the Streltsovskoye deposit. This age is concordant with K–Ar ages of some of the granites from the basement of the Tulukuevsky volcano-tectonic structure. The isotopic composition of Pb from galena from the Streltsovskoye ore deposit corresponds to a two-component mixture between a Pb with a model age of 460 Ma, an age obtained for dispersed U mineralization in Precambrian rocks of the Tulukuevsky VTS basement (457–459 Ma), and a Pb with the same composition as the radiogenic Pb of the Streltsovskoye U ores. From the K–Ar ages of the mica alteration and the U–Pb ages of pitchblende, the total time span of the hydrothermal process responsible for the formation of the Streltsovskoye deposit cannot exceed 3 m.y. The isotopic data from the Streltsovskoye U mineralization in the basement and in the caldera indicate that U concentration processes had already operated in the basement from Ordovician until Jurassic times for the formation of this giant ore district.

Uranium sources Four main types of sources may have contributed to the formation of the U deposits from the Streltsovskoye caldera:

1. peralkaline rhyolite filling the caldera, particularly the trachyte;
2. fluids expelled from volcanic melts or from the underlying magma chamber;
3. subalkaline granitoid rocks of the basement;
4. Ordovician mineralization.

Rhyolitic tuff, which represents 30–35 vol.% of the volcanic pile, seems the most important potential U source. As it is aphyric, nearly all the U is hosted by the volcanic glass, which has been strongly devitrified by hydrothermal alteration. Devitrification facilitates liberation of U and Zr from the rhyolite. Mass balance calculations based on the initial U contents of silicate melt inclusions trapped in quartz phenocrysts of the rhyolite (15–23 ppm, 17 ppm on average), measured *in situ* by SIMS, and average present-day U content of the rhyolite (7 ppm U), (Table 7-3) show that the hydrothermal alteration of 1 km^3 of rhyolitic rocks liberated 18,000 to 21,000 tU. Thus, the leaching of 14–15 km^3 rhyolite is sufficient to explain the total U resources of all the deposits of the Streltsovskoye caldera, if total efficiency of U deposition from the hydrothermal fluids is postulated (Chabiron *et al.* 2003). Such a rhyolite volume would represent a thickness of 40 to 45 m over the entire caldera surface. This is less than the presently preserved thickness of the rhyolite of up to 100 m and much less than the presumed initial total thickness of the rhyolitic eruptive rocks. Also, comparison of the Th/U of the melt inclusions (Th/U = 2 to 3) with those of the altered non-mineralized rhyolite (Th/U = 9 to 10), indicates that 70–80% of the initial U from the rhyolite has been lost during the hydrothermal alteration process. A further argument for rhyolite being one of the major U sources is the presence of high Zr contents in the U oxides. This is systematically observed in U deposits related to acidic volcanic rocks. For example, at the Moonlight mine (McDermitt Caldera, Nevada), the Zr content of the ore is higher than its U content because of deposition of hydrothermal zircon (Castor & Henry 2000). Similarly, where volcanic rocks are present in the sedimentary sequence, such as the Akouta deposit in Niger (Forbes 1989) and the Müllenbach deposit in Germany (Pironon 1986), U mineralization also occurs. The high Zr content of those U minerals result from the fact that Zr localized in volcanic glass after devitrification is much more soluble than Zr located in the zircon structure. Besides U, the rhyolite also represents a huge source for fluorine.

Magmatic fluids have been expelled from extruded rhyolite and from the melts that have crystallized in the underlying magmatic chamber. The experimental data of Peiffert *et al.* (1996), in the haplogranite–$UO_{2.x}$–H_2O–NaF system for such peralkaline ($1.04 < Na+K/Al < 1.10$) and F-rich (1.4 to 2.7 wt.%) compositions, indicate that:

1. the Streltsovskoye rhyolitic melts were strongly undersaturated in U: up to 1.1 wt.% U can be dissolved for such melt compositions at 800°C and 2 kbar, and even more at the temperature possibly reached by the Streltsovskoye rhyolitic magma (1,014±30 °C; Chabiron *et al.* 2001)
2. the U fluid–melt partition coefficient is strongly in favor of the melt (K_{DU}fluid/melt = 3×10^{-2} to 4×10^{-2}; Peiffert *et al*. 1996).

Based on these K_{DU} values, the U content of the aqueous fluids expelled from the Streltsovskoye rhyolitic melts was 0.6 to 0.8 ppm. The average amount of water in the melt inclusions was estimated at 2 wt.% from ion microprobe measurements on homogenized inclusions (Chabiron *et al.* 2003). This water content is a minimum estimate because water may have been lost at several stages during melt ascent. Therefore, the minimum mass of fluid released by the rhyolite magma corresponds to 31.4 km^3 x 0.02 x 2.6 (average rhyolite density) = 1.63 Gt, taking into account the already eroded part of the volcanic pile. Then, the resulting mass of U released is less than 1,630 t. This amount of U may be increased if we take into account the fluids expelled from the large underlying magma chamber. Caldera-related magma chambers usually have a volume in the 100–1,000 km^3 range. Thus, taking the same fluid content as in the rhyolite, the volume of fluid released from the whole magma chamber would be 5.2 to 52 Gt. The resulting mass of U released by the magmatic fluids, also considering the same U content in the fluid (<1 ppm), will be in the order of 5,200 to 52,000 tU. These results probably represent an overestimation, because mafic and intermediate magmas from the chamber are likely to have lower water and U contents. The quantities of U that may have been released by magmatic fluids remain well below the amounts necessary to explain the estimated resources of the Streltsovskoye caldera. The fluids released from the underlying magmatic chamber may have served to enrich slightly the granite of the basement along

fractures and may be responsible for the high-temperature brannerite mineralization found in the deepest part of the ore system.

The main source of U in the basement is represented by high-K calc-alkaline granite (Table 7-3). Uranium is difficult to mobilize from accessory minerals such as silicates (zircon, thorite, and allanite), a typical assemblage in high-K calc-alkaline granite. However, the hydrothermal system associated with the formation of the U deposits operated 150 to 200 m.y. after the emplacement of the granite, a duration sufficient for metamictization of the structure of the richest of the U–Th minerals to facilitate the liberation of U from their structure. Although it was not possible to determine the initial U content of the granite magma from melt-inclusion studies, such granite is known for high U content. Taking into account only the alteration of allanite, 1,638 t U/km^3 may have liberated. Assuming a minimum 1.8 km thick layer of granite below the caldera (crosscut by the deepest drill holes) and allanite alteration in 80% of the granite, the granite may have liberated 750,000 tU. Metamict thorite and uraninite would represent still larger U sources, but their contribution cannot be accurately estimated. Uranium liberated from the accessory mineral structures and other labile U sources was mobilized by oxidized meteoric fluids that infiltrated the granitic basement during the development of convection cells above the caldera magma chamber.

Therefore, the juxtaposition of two major U sources, U-rich peralkaline rhyolite and 150 to 200 m.y. older, U-rich subalkaline granite, is one of the key parameters contributing to the large size of the U resources in the Streltsovskoye caldera. The total amount of U that may have been liberated from these sources represents several times the total U resources estimated for the caldera. An additional U source is represented by the Ordovician U mineralization already occurring in the basement. The acidic hydrothermal solutions, probably partly of magmatic origin, responsible for the pervasive alteration of accessory minerals in the caldera basement, also were essential.

Other volcanic-related uranium districts of Asia

Numerous other similar volcanic districts associated with U mineralization exist in eastern and central Asia. They all occur in caldera-like structures filled by alternating andesitic–basaltic to rhyolitic lava layers, with clastic and pyroclastic intercalations. Extrusive bodies may intersect these layers. The volcanic structures are developed within cratonic areas, frequently of granitic nature. The mineralization is controlled by deep structures and characterized by a U–Mo–F association. Some of the districts are:

- Chatkalo-Kumarinski district, Karamazar region, Uzbekistan, south of Tashkent, with the Taboshar, Adrasman, Chouli, and Kattasay–Alatanga deposits (12–13,000 tU), hosted by Permian–Jurassic volcanic rocks
- Betpakdalinskii district, Balkhash Lake area, Kazakhstan, with the deposits of Botta-Burum, Kysylsay, Dzhideli, and Kostobe, (15–16,000 tU), hosted by Silurian-Devonian volcanic rocks
- SW of the Kokchetov region, in Kazakhstan with the Vostoh-Ishymsky and Balkashinsky deposits, also hosted by Silurian-Devonian volcanic rocks
- Chukotka region close to the Bering Strait, hosted by Cretaceous volcanic rocks
- northeastern Mongolia in the Dornot caldera
- southeastern China in the Xiangshan caldera.

Dornot (northeastern Mongolia): The Dornot volcano-tectonic structure (DVTS) is one of several volcanic mineralized structures located in northeastern Mongolia (Mironov *et al.* 1993). The basement of the DVTS consists of Late Proterozoic–Early Paleozoic deformed granodiorite and quartz diorite, plagiogranite, and granite. Carboniferous plutonic rocks and Permian volcanic rocks and granite are less developed than in Streltsovskoye. The alkaline to peralkaline volcanic rocks that fill the caldera comprise the following successive associations: basalt–trachy-andesite–rhyolite, rhyolite–trachy-rhyolite, and trachy-andesite. The caldera hosts U, Au, Pb–Zn, fluorite, and Mo hydrothermal deposits. The U deposits are located at the northern margin of the DVTS and occur as veins and stockwork in all sedimentary–volcanogenic series, but rarely in the basement. Pitchblende U–Pb ages between 138 and 135 Ma are similar to those of the Streltsovskoye mineralization. Coffinite and U-titanate minerals are the main U-bearing minerals; pitchblende is less common.

Volcanic-related U deposits, also associated with Mesozoic volcanic units, occur in Eastern China and Southern China (Jiang *et al.* 2005a, 2005b). The main one is the Xiangshan district, Jiangxi province. The caldera extends for about 300 km^2. Two cycles of volcanic activity occurred from Middle Jurassic to Early Cretaceous (114–163 Ma).

The first cycle corresponds to air-fall and ash-flow deposits interbedded within rhyolitic crystal tuff, rhyolitic vitric crystal tuff, rhyolitic welded tuff and clastic sedimentary rocks followed by the emplacement of a rhyodacite dome. Then a caldera formed. The second cycle was dominated by rhyolitic slightly welded tuff of ash-flow facies accompanied by rhyolitic crystal tuff followed by intrusions of biotite monzonitic granite porphyry and biotite quartz monzonite porphyry.

One of the most typical deposits, Zoujiashan, is located in rhyolitic porphyroclastic lava and rhyodacite, in the western part of the Xiangshan caldera. Pitchblende, Th-bearing pitchblende, and uranothorite are associated with molybdenite, pyrite, and galena. The mineralization was dated at 100 Ma. Small ore bodies are tens of metres to about 100 m long and 1–3 m thick. Large ones are 100–300 m long and 5–8 m thick. Ore grade is 0.1–0.3% U and estimated U resources are estimated at about 20,000 tU. The occurrence of Th in the U mineralization suggests high temperature processes, possibly in relation with magmatic fluids exsolved from the melts.

Other volcanic-related uranium districts of the world

In other parts of the world, U mineralization associated with volcanism represents much smaller occurrences. This situation may result from insufficient exploration of this type of model during the 1970s and 1980s by western companies. The main occurrences are described below.

The U–Mo Kitts-Michelin deposit in Labrador, Canada (Gandhi 1978), hosted by Paleoproterozoic felsic volcanic rocks of the Aillik Group (1.9–1.7 Ga) with measured resources of 5,000 tU at 0.1–0.07% U (respective grades for underground and open pit mining), but with 21,000 tU indicated at 0.11–0.05% U and 13,600 tU inferred at 0.1–0.04% U (http://www.aurora-energy.ca/). The Kitts-Michelin deposit and a number of other radioactive occurrences are located in bimodal volcanic sequences comprising metabasalt and metarhyolite with interbedded clastic sedimentary rocks belonging to the Paleoproterozoic Aillik Group, along the central Labrador coast. The Aillik Group was affected by the Hudsonian orogeny and was intruded by numerous Hudsonian intrusions. From the base to top, the Aillik Group consists of:

- paragneiss and schist (1,000 m), lying on the Hopedale basement gneiss
- tholeiitic mafic lava and tuff (up to 200 m)
- coarse clastic metasedimentary rocks (500 m)
- metarhyolite flows, fragmental and felsic tuffs (up to 700 m)
- metamorphosed quartz-feldspar porphyry, concordant to subconcordant (1500 m thick).

Metamorphism of the Aillik Group ranged from upper greenschist to amphibolite facies. The regional structure corresponds to that of an arcuate fold belt. Deposition of the Aillik Group seems to have occurred in an intracratonic basin controlled by faults, which may have corresponded to a rift type structure. Greenschist–amphibolite facies metamorphism is overprinted by contact metamorphism by a gabbro pluton.

In the Michelin deposit, mineralization is localized in rhyolite, which have been albitized and locally dequartzified (episyenite-type alteration). Hence, the original typology of the rhyolite magma is difficult to determine. Rb–Sr age determinations on the rhyolite are between 1659 and 1676 Ma, but these ages have been reset by metamorphism and do not correspond to the emplacement age of the rocks.

Uranium mineralization has yielded discordant ages of 1730 to 1745 Ma, but these ages correspond to resetting during Hudsonian metamorphism. Ages at 1364, 1244, and 934 Ma represent rejuvenation ages related to later intrusive and metamorphic events.

The cumulate resource estimates of the Michelin and Jacques Lake deposits are 5,645 t U at 0.08% (measured) and 24,300 tU at 0.08% (indicated; http://wise-uranium.org).

The U occurrences are distributed along four fold belts:

1. Kitts-Post Hill: the mineralization is located in andalusite-garnet schist with an albite, amphibole, and biotite matrix overlying basaltic pillow lava and chert and overlain by basaltic flows. Graphite (1–2.5%) and pyrrhotite-bearing beds (less than 10 m thick and elongated over 10–300 m) are the major hosts for the mineralization.
2. White Bear Mountain-Walker Lake: most of the occurrences are located in coarse feldspar porphyritic rhyolite alternating with subporphyritic members and minor tuff layers. The larger ones, including the Michelin deposit, are located in an area of 1 by 15 km parallel to the ENE trend of the belt. The mineralization also occurs along stratigraphic horizons about 40 m thick over 1 km enriched in Na (7–12%

Na_2O). Uranium minerals are finely disseminated in the rocks.

3. Cape Makkovik-Monkey Hill: the U mineralization is confined to 2 m thick zones parallel to the foliation of albitized granoblastic rhyolite.
4. Falls Lake-Shoal Lake-Bernard Lake: the mineralized lenses are generally less than 1 m thick and located in mafic and felsic lavas flows and tuff.

All the mineralized occurrences appear as lenticular or tabular bodies with disseminated mineralization parallel to the foliation of the rocks. The U mineral is pitchblende with very low Th contents. Calcite, hematite, pyrite, titanite and fluorite are associated minerals.

The relative influence of volcanic-related hydrothermal activity, Na-metasomatism and metamorphism in the genesis of the U mineralization in the Kitts-Michelin deposit remains to be assessed. Na-metasomatism associated with felsic volcanism also occurs in the Valhalla district, Australia, described in Chapter 6, which has been attributed to basinal brines released during metamorphism (Polito *et al*. 2007).

Th–U–REE Rexpar deposits**,** British Columbia, Canada are hosted by metamorphosed trachytic flows and hypabyssal intrusive rocks, tuff and pyritic schist of rhyolitic composition belonging to the Mid Paleozoic to Permian Eagle Bay Formation (Morton *et al*. 1978). Combined reserves of only 1,300 tons of ore at 0.066% U have been estimated. The simultaneous enrichment of Th and REE together with U suggests high temperature processes with involvement of magmatic fluid and a peralkaline chemistry of the magma. A similar element association is found in some of the mineralization from the Xiangshan U district in China.

U–Zr–F Moonlight and U–Hg Aurora deposits in Nevada (Roper & Wallace 1981, Wallace & Roper 1981, Rytuba & Conrad 1981, Rytuba & McKee 1984: Dayvault *et al.* 1985, Noble *et al.* 1988, Castor & Henry 2000) are hosted by peralkaline rhyolitic tuff of the Tertiary McDermitt volcanic caldera, dated at 17 Ma. At the Moonlight mine the U mineralization is associated with abundant hydrothermal zircon. The global U resources of the caldera are estimated at 8,000 t U.

U–Mo–F Marysvale deposit**,** located between the Colorado plateau and the Basin and Range Provinces, is hosted by a bimodal sequence of mildly peralkaline rhyolite occurring as domes, lava flows, and ash-flow tuff and basaltic lava flows. It was emplaced from 22 to 14 Ma (Cunningham *et al.* 1982, 1998, Budding *et al.* 1987). A tonnage of about 600 tU has been mined.

The Lakeview district U mineralization, in south-central Oregon, hosted by intrusive metaluminous to weakly peraluminous rhyolite domes dated at 7.0 ± 0.4 to 7.90 ± 0.09 Ma has produced nearly 170 tons of U (Castor & Berry 1981).

U–Be–Li–F Spor Mountain mineralization, west-central Utah, is hosted in slightly peraluminous topaz-bearing rhyolitic lavas within the Beryllium Tuff unit erupted at least from 12 separate vents at 21 Ma. The Beryllium Tuff unit is underlain and bordered by pyroclastic rocks of minor importance (Burt *et al.* 1982). The eruptions were related to faults associated with the collapse of an earlier unrelated caldera (Lindsey 1981). Hydrothermal U concentrations rarely exceed 100 to 300 ppm except very locally at the Yellow Chief U mine, which gave small bodies of weeksite and beta-uranophane.

U–Mo mineralization of the Sierra Peña Blanca, located to the east of the Sierra Madre Occidental, is hosted by rhyolitic ash-flow sheets belonging to the upper volcanic sequences of a Tertiary rhyolitic pile (53.8–37.3 Ma) extending over 125,000 km^2 and related to the emplacement of 200 to 400 calderas (Alba & Chavez 1974, Magonthier 1984). In the Sierra Peña Blanca area, the volcanic rocks are more likely related to large fissure eruptions through a Cretaceous calcareous basement. The youngest member of the sequence corresponds to the thick peralkaline Mesa pyroclastic formation (Leroy *et al.* 1987), but the lower members are slightly peraluminous. Mineralization occurs in three small deposits: Nopal I (280 tU at 0.26% U), Las Margaritas (300 tU_3O_8 at about 0.085% U) and Puerto III (423 tU), and total U resources are in the order of 2,400 tU, from which only 49 tons of U have been extracted.

U–Mo Ben Lomond deposit, Queensland, Australia is hosted by Carboniferous ignimbrite (O'Rourke 1975, Bain 1977), with estimated resources of 6800 tU at 0.23 % U.

U–Mo–Sn–F Maureen uranium deposit, Queensland, Australia, is hosted by Permo-Carboniferous Galloway rhyolitic ignimbrite and

volcaniclastic sedimentary rocks. In the basement of the Maureen U deposit, felsic leucocratic granite enriched in Li, Be, Rb, F, Th, and U are particularly abundant. In 1978, resources of 2500 tU with a grade of 0.105% U_3O_8 were estimated.

The Arjeplog-Arvidsjaur U province, northern Sweden (Adamek & Wilson 1979), is located in a volcanosedimentary belt. The most important mineralization is epigenetic and formed during peak metamorphism associated with the Svecofennian orogeny at about 1750 Ma. The Pleutajokk U deposit is hosted by metamorphosed metaluminous rhyolitic tuff composed of quartz, albite, oligoclase, K-feldspar, and aggregates of magnetite, biotite, hornblende, titanite, zircon, apatite, allanite ± fluorite. Na-metasomatism with biotite + hematite + riebeckite + epidote occurs prior to the mineralization. The U mineralization is uraninite ± brannerite that occurs as veins and lenses in association with chlorite, titanite, hematite ± fluorite ± calcite. The mineralization location is controlled by rock lithology and tectonic structure. The resources have been estimated about 10,000 tU.

***The Duobblon deposit*,** northern Sweden, which is hosted by Paleoproterozoic ignimbrite, occurs as stratabound tabular bodies with estimated resources over 4000 tons U at 200–300 ppm U (Lindroos 1980, Lindroos & Smellie 1979, Smellie 1982). A basal breccia lying unconformably on the deeply weathered Revesund Granite (1750 Ma) was followed by rhyolitic ignimbrite, overlain by thick fluvial red bed-type conglomerate and sandstone, in turn capped by felsic to intermediate volcanic rocks. The Sorsele Granite (1590 Ma) to the north is intrusive into this series. The ignimbrite layers are metaluminous, highly potassic (up to 7.9 wt.% K_2O) calc-alkaline, highly siliceous (up to 77.6 wt.% SiO_2), rich in Th (up to 41 ppm), Zr (up to 540 ppm), Mo (Up to 2,000 ppm) and U (highly variable), strongly devitrified and welded to various extents. The rocks are composed of about 80% matrix and the phenocrysts are 2–6% quartz, 6–9% albite (possibly replacing primary K-feldspar), 3.6–4.8% Fe–Ti–Mn oxides, and 0.5–9% fragments. Accessory minerals are: titanomagnetite, ilmenite, magnetite, zircon, apatite, titanite, epidote, calcite, and pyrite. The mineralization is believed to be syngenetic and related to the devitrification of the tuff (Lindroos & Smellie 1979). The main ore mineral is uraninite associated with pyrite, sphalerite, galena, arsenopyrite, chalcopyrite, pyrrhotite, and molybdenite. Alteration phases are: calcite, quartz, muscovite, epidote, chlorite, and fluorite. The reserves were estimated at 4,000 tU at 0.03%.

The Skuppesavon uranium district is hosted in metavolcanic rocks, and rhyolitic to trachytic tuff, with 2–3 m interlayered amphibolite sills (up to 50 m), located about 30 km SW of the Pleutajokk deposit. The metavolcanic rocks were intruded by the Hällnäs granite, which is older than 1700 Ma. Unaltered rhyolite is composed of quartz, plagioclase, K-feldspar, and mafic aggregates of biotite and magnetite with subordinate apatite, titanite, and zircon. It is moderately siliceous (63–68 wt.% SiO_2), potassic when not albitized, and have moderate Th contents (15–28 ppm). The alteration associated with the mineralization is rather typical of ore deposits associated with Na-metasomatism, with albitization and dequartzification, andradite and hedenbergite rather than of that associated with volcanism. Low Th (up to 0.9 wt.%) uraninite occurs as finely disseminated crystals, rarely in fractures, and commonly associated with titanite. Complex uranotitanate minerals occur in minor amounts. The Skuppesavon mineralized zone is tabular, 400 m long, 150 m wide and up to 20 m thick. Reserves were estimated at 700 tU at 700 ppm. The proposed genetic model involves hydrothermal mineralization during peak metamorphism of the Svecofennian orogeny.

Macusani mineralization of the Carabaya province (SE Peru) occurs in the upper part of a 1,400 m thick pile of strongly peraluminous ignimbritic ash-flow tuff (17–4 Ma) emplaced synchronously with small Tertiary peraluminous granite stocks (27–8 Ma), (Valencia-Herrera *et al.* 1984, George-Aniel 1988, Pichavant *et al.* 1988a, 1988b, Cheilletz *et al.* 1992). Pitchblende–pyrite–chalcopyrite mineralization occurs in fractures (Aniel & Leroy 1985), but autunite disseminated in vitroclastic tuffs with 200–300 ppm average U content is the most common (Arribas & Figueroa 1985). Reserves are estimated at 8,500 tU.

The Los Frailes U occurrences (Sevaruyo district, central Bolivia) are hosted in a 500 m thick pile of tuff, ignimbrite and lavas emplaced between 16 and 3.6 Ma and occasionally in associated sedimentary rocks (Jimenez 1985) overlying a Silurian metasedimentray basement and Permo-Triassic, Cretaceous to Tertiary coarse detrital sediments.

According to Leroy *et al.* (1987), the potential of this district is small because the tuffs are moderately fractionated to weakly peraluminous, a large part of the U is in refractory accessory minerals and hydrothermal alteration was limited (Leroy & George-Aniel 1992).

La Puna uranium mineralization, located at the southern end of the Bolivian Altiplano, is hosted by rhyodacitic ignimbrite belonging to Tertiary (19.7–3.6 Ma) volcanic-sedimentary sequences on highly folded and metamorphosed Ordovician marine sedimentary basement rocks intruded by intermediate magmatic rocks. (Salfity *et al.* 1984, Seggiaro & Aniel 1987). Most of the ignimbrite is well crystallized (50–60 vol.%) and moderately fractionated.

Novazza (U–Mo–Zn) and Val Vedello (U, Cu, Pb, Zn, Sb, As, and Hg) deposits, Northern Italy, are hosted by the Late Carboniferous–Early Permian Collio Formation, composed mainly of rhyolitic welded tuff units occurring within a caldera and overlying a thick basement composed of polycyclic Early Paleozoic greenschist to amphibolite facies metasedimentary rocks and orthogneiss (Cadel 1986, Cadel *et al*. 1987, Fuchs 1989). The reserves of the Val Vedello deposit were estimated at 4,250 tU at 0.085% U, and those of the Novazza deposit are of 1,530 tU at 0.07% U. Dravite occurs a few kilometres around the Novazza mine mostly in the lower rhyolite, with up to 0.5 % B.

The very recent (0.4 and 0.06 Ma) Vulsini fissures and calderas and the ***Vico caldera*** (Italy) have mineralization associated with ignimbrite. Volcanoes from the Latium province are composed of potassic peralkaline undersaturated magmas in the Roman province and of oversaturated shoshonitic basalt and basaltic andesite and high-K trachyte in the Tuscan province (Holm *et al.* 1982, Rogers *et al.* 1985, Palacin 1985, Villemant & Palacin 1987). All the lavas are interpreted as mantle-derived magmas, highly fractionated by crystal fractionation (up to 250 ppm Th and 60 ppm U) of primitive melts previously contaminated by fluids derived from a subducted oceanic plate and associated sediments. The Vico volcanism is more evolved than is Vulsini and thus richer in U. U–Fe–S concentrations containing up to 500 ppm U occur on the flanks of the Vulsini. The mineralized zones with average grades of 300 to 500 ppm (locally up to 0.2–0.3% U) correspond to fault-controlled altered volcaniclastic and vitric volcanic rocks.

Uranium deposits related to volcanic units in Bulgaria are located in the East Rhodope massif (Simov & Bojkov 1992) and hosted in Miocene (Smolian, Platinetz, and Sarnitza deposits) and Cretaceous (Sliven and Rosen deposits) tectonized rhyolite and tuffaceous sedimentary rocks. The sizes of the ore bodies vary from 500 to 5000 tU with average grades varying from 0.1 to 1% U, and 0.03 to 0.1% U.

MODEL FOR URANIUM DEPOSITS ASSOCIATED WITH VOLCANISM

Nature of the magmatism

Peralkaline extrusive magmatism, generally silica-oversaturated, presents the most interesting U source because of the high U solubility in such magmas. The accessory mineral phases that may trap part of the U in their lattice during fractional crystallization do not crystallize because of their high solubility in highly depolymerized peralkaline melt (see Chapter 2). Consequently, U is continuously enriched during fractional crystallization of peralkaline magmas, and can be easily leached during hydrothermal alteration by devitrification of the glass. Peralkaline rhyolite is quite common and occurs in anorogenic settings. Peralkaline felsic pyroclastic eruptive rocks may also significantly contribute to the U fertility of siliciclastic sedimentary basins as exemplified by the Tim Mersoï basin in Niger, which hosts the Arlit and Akouta tectono-lithologic U deposits (Forbes 1989).

Peraluminous eruptive rocks may also represent a favorable U source because of the early fractionation of Th-, REE-, and Zr-rich accessory minerals, allowing enrichment of U in the residual silicate melts, but only in the case of U-rich systems (see Chapter 2). However, this type of magmatism is scarce because peraluminous magmas are generally water-rich and thus tend to crystallize at depth in the form of peraluminous leucogranite. The Macusani strongly peraluminous ignimbrite of Peru represents an exception. One has to be careful with aluminous indexes calculated from the analysis of more or less altered whole rock samples, which give peraluminous values because of the leaching of the alkalis and Ca during alteration. The most reliable way to obtain the aluminous index of volcanic rocks is the analysis of magmatic inclusions trapped in quartz phenocrysts, which preserve the pristine composition of the melts and their initial U content.

High-K calc-alkaline metaluminous volcanic rocks generally represent less favorable U sources

for U deposits because a large part of the U can be trapped in accessory minerals (Leroy & George-Aniel 1992). The most favorable melts are the Fe-rich highly fractionated highly potassic magmas, such as the most fractionated Gawler Range volcanic units associated with the Olympic Dam deposit, which tend to be transitional with the peralkaline magmatism.

Melt chemistry recorded by magmatic inclusions

Figure 7-16 synthesizes the chemistry of the magmatic inclusions after homogenization from different types of volcanic sequences associated with U deposits (Chemillac 2004). The inclusions have been analyzed by electron microprobe. The diagram involves two peraluminous indexes: the classical A/CNK (Al/(Na+K+2Ca)) parameter separating peraluminous melts from metaluminous and peralkaline melts and the Al/(Na+K) parameter allowing discrimination between metaluminous and peralkaline melts. In this diagram, Macusani glass is clearly the most peraluminous. Magmatic inclusions from the Xiangshan volcanic sequence in China have the most variable compositions of peralkaline lavas, but the initial magma was probably mildly peralkaline as indicated by the composition of the best-preserved inclusions. The composition of the Peña Blanca magmatic inclusions is also somewhat peralkaline and inclusions from the Ben Lomond rhyolite are homogeneous and slightly peraluminous. Those from McDermitt are variable and peralkaline whereas those from Streltsovskoye, which host the largest U district associated with volcanic rocks, are very homogeneous and entirely peralkaline.

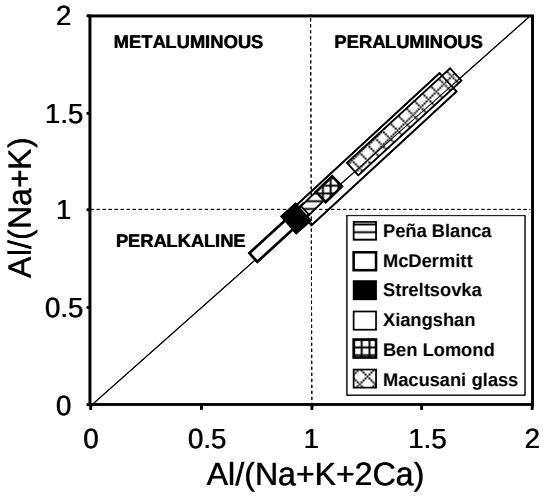

Fig. 7-16. Composition of the melt inclusions trapped in quartz phenocrysts from rhyolitic lavas from different U districts in the world in the Al/(Na+K+2Ca) *versus* Al/(Na+K) diagram (Chabiron *et al.* 2003, Chemillac 2004).

The U and Th contents of the same magmatic inclusions presented in Figure 7-17 have been analyzed *in situ* by SIMS (Chabiron *et al.* 2003, Chemillac 2004). Magmatic inclusions with the highest U contents up to more than 20 ppm are from the Streltsovskoye and Dornot calderas, the two largest volcanic-hosted U districts in the world. Inclusions from the McDermitt caldera are distinctly lower in U content and those from Ben Lomond are only moderately enriched in U, averaging 7 ppm. The few data available on magmatic inclusions from the Xiangshan district are not rich in U, with a maximum value of about 5 ppm. This may be due in part to the relatively poor preservation of the magmatic inclusions, as also indicated by their anomalously high Th/U rations between 4 and 10. Macusani glasses is enriched in U, with up to 20 ppm, but has low Th contents, typical of highly fractionated peraluminous melts. All other melts, except those from Xiangshan, have low Th/U ratios of about 2.

Nature of the volcanic system

The most favorable types of volcanic eruptive are weakly porphyritic ignimbritic tuffs, in which U is hosted in the glass and accessible to hydrothermal fluids. Also, ignimbritic tuffs accumulate as thick layers, over wide areas and thus constitute significant U sources.

The best volcanic structures are wide calderas (1 to 20 km across), mostly filled with pyroclastic

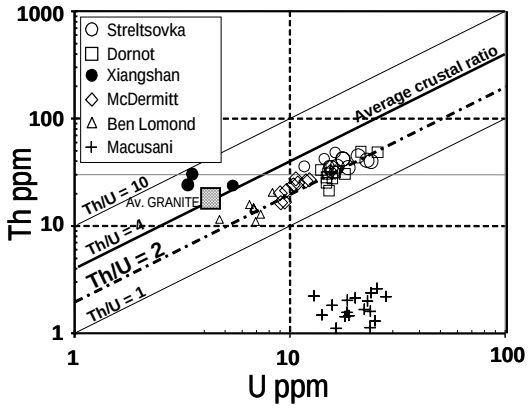

Fig. 7-17. Th *versus* U contents in magmatic inclusions in quartz phenocrysts from rhyolitic lavas from different U districts in the world (Chabiron *et al.* 2003, Chemillac 2004).

tuff of mafic and felsic volcanic rocks and sediments. The presence of rheological and compositional contrasts is favorable for the formation of traps for U deposition. The collapse of the caldera provides extensive fracturing of the rocks promoting fluid circulation. The formation of such structures indicates eruption of a large volume of lavas, and therefore a large potential source of U. A magmatic system should be active over several millions of years to provide the necessary heat flux to promote focused and long-lasting convective fluid circulation.

The development of such volcanic systems within "fertile" basement already enriched in U in the form of U-rich granitoid rocks, or older U mineralization in the basement of the Streltsovskoye caldera in Russia, represents an additional favorable criterion for the genesis of important U districts.

Olympic Dam

The Olympic Dam Iron Oxide Cu–Au (U–Ag–REE) deposit (IOCG deposit) is located on the Gawler Craton, South Australia. This deposit was discovered in 1975 and represents about 30 million tons of Cu, 1,907,000 tU at 0.025% (in 2007), 1,200 tons of Au and 6,700 tons of Ag (Reynolds 2000). Mineralization occurs in a zoned hematite breccia complex hosted by the Roxby Downs Granite (Roberts & Hudson 1983, Creaser 1996). The Olympic Dam deposit is described in this chapter because the breccia hosting the mineralization is attributed to a huge volcanic explosion in a diatreme within the Roxby Downs granite. Unlike previous examples discussed, there is no evidence for a caldera (Drummond *et al*. 2006).

Geological setting The Olympic Dam breccia complex is covered by a thick Mesoproterozoic to Cambrian sedimentary sequence of the Stuart Shelf. The breccia complex is hosted in the Roxby Downs granite of the Hiltaba Granite Suite, dated at 1588 ±4 Ma (Creaser 1996). The breccia complex extends approximately over 5 to 7 km along a NW–SE trend. It is zoned and presents a central barren quartz–hematite breccia associated with volcaniclastic rocks which are relict from an eroded volcanic suite equivalent to the Gawler Range Volcanics (GRV) rimmed by a variably mineralized hematite–granite breccia (Kamenetsky *et al.* 2000, Morrow & McPhie 2000). Several types of breccia have been documented and result from many processes including hydraulic fracturation, tectonic faulting, chemical corrosion, phreatomagmatism, and gravity collapse (Reeve *et al.* 1990, Reynolds 2000). Clasts of surficial sedimentary and volcaniclastic rocks are found within heterolithic breccia. Volcanic rocks range from lapilli tuffs to felsic porphyritic lavas but all show systematic hematite alteration. Mafic to felsic dikes intruded the breccia complex and mark the final steps of magmatic activity associated with hydrothermal circulations.

The Roxby Downs Granite represents the most fractionated member of the large Mesoproterozoic Burgoyne Batholith. This batholith belongs to the Hiltaba Suite, a voluminous unit across the Gawler Craton. The suite ranges from quartz-monzonite to granite. These rocks are enriched in K_2O, Rb, Ba, Th, U, REE, Nb, Y, and Zr, typical of A-type high-K calc-alkaline granite. The Roxby Downs granite is comagmatic with the Gawler Range Volcanic Complex (Giles 1988, Garner & McPhie 1999, Morrow & McPhie 2000).

The Gawler Range Volcanic Complex underlies an area of 25,000 km^2 in the Gawler Craton and consists mainly of felsic lava with lesser amounts of mafic to intermediate lava. Three rhyolitic facies are distinguished: plagioclase rhyolite, vesicular rhyolite, and quartz rhyolite (Morrow & McPhie 2000). They have been dated at 1592 Ma (Fanning *et al.* 1988, Morrow & McPhie 2000) and are coeval and cogenetic with the Hiltaba Granite Supersuite (Fanning *et al.* 1988, Johnson & Cross 1995). Together these magmatic units represent a huge episode of intracontinental anorogenic magmatism of the same geochemistry as the rapakivi granite plutons of western Europe.

The IOCG mineralization Hydrothermal activity is presumed to be related to the magmatic episode related to the emplacement of the Roxby Downs Granite and the extrusion of the Gawler Range Volcanic Complex (Roberts & Hudson 1983, Reeve *et al.* 1990, Reynolds 2000). Dating of the breccia complex rocks indicates the contemporaneity among magma emplacement, brecciation, and mineralization (Johnson & Cross 1995). The typical alteration mineralogy is sericite-hematite, minor chlorite, quartz, carbonate, and magnetite and the intensity of alteration is generally linked to the extent of brecciation (Roberts & Hudson 1983, Hitzman *et al.* 1992, Reynolds 2000). The main Cu-bearing phases are chalcopyrite, bornite, and chalcocite; the U-bearing phases are uraninite,

coffinite, and brannerite. REE are mainly found in bastnaesite, florencite, monazite, and xenotime (Roberts & Hudson 1983, Oreskes & Einaudi 1992). The Olympic Dam ore genesis is related to the unmixing of a hot, high salinity fluid from a granitic magma, which subsequently mixed with an oxidizing meteoric fluid (Hitzman *et al.* 1992, Oreskes & Einaudi 1992, Haynes *et al.* 1995, Pollard 2000). Oxygen and H isotope studies are consistent with a magmatic source for the fluids (Oreskes & Einaudi 1992). Most Fe–Cu–Au deposits represent shear zone controlled, distal magmatic-hydrothermal mineralization with variable amounts of non-magmatic fluids, and high Cl/S ratios compared to most other hydrothermal systems, leading to very low enrichments in Pb and Zn, which have low solubilities in S-poor fluids. If magmas effectively play a major role, the tectonic settings, and geochemical processes leading to the generation of Fe–Cu rich fluids remains poorly understood. Intrusive rocks linked to the Fe-oxide Cu–Au deposit are commonly accepted as the sources for metal. However, Johnson & McCulloch (1995) inferred a mafic origin for Cu and REE at Olympic Dam on the basis of Sm–Nd data.

Compared to the other deposits, Olympic Dam has unique characteristics that include:

- it is the most enriched in U
- it is entirely hosted within a highly potassic Fe-rich calc-alkaline granite, and associated with felsic volcanic rocks of the same nature
- it was formed at shallow depths
- the influence of meteoric fluids in its genesis was very important and thus the main Fe-oxide is hematite instead of magnetite.

Uranium mineralization Uranium is mainly present as fine crystals of uraninite dispersed within the mineralized breccia as well as pitchblende, coffinite, and U–Ti oxides (brannerite and davidite). Uraninite is disseminated within hematite-rich breccia and is commonly intergrown with sulfide minerals and hematite. Its distribution and abundance are correlated with copper sulfide minerals and locally enriched in discontinuous zones (10–20 m) within the bornite–chalcocite ore. Gangue minerals are hematite, barite, fluorite, quartz and magnetite. Grades of U greater than 0.17% U are known to occur in the deposit. Since 1988, about 40,000 tU have been already produced.

Pitchblende and coffinite seem to be the major U ore minerals deposited in veins in close association with Fe and Cu sulfide minerals. An age of 1400 Ma on a U oxide from an unpublished report by Trueman *et al.* (1988) would indicate that U deposition is 190 Ma younger than the age of the magmatism. Therefore, new and precise age determinations of the different types of U minerals are crucially needed for a better understanding of the genesis of the U mineralization at Olympic Dam.

Other IOCG prospects include:

- in Australia: Manxman with U contents up to 1200 ppm and Prominent Hill, located 60 km NW of the Olympic Dam deposit, have mineral parageneses similar to Olympic Dam (uraninite, pitchblende and coffinite). Oak Dam East, located in the northeastern Gawler Craton, contains uraninite. Cu–Au–U-bearing, massive Fe-oxide mineralization occurs in the northeastern Gawler Craton beneath more than 500 m of younger cover (Davidson *et al.* 2007). Monakoff, in the Cloncurry District, has minor uraninite.
- in Brazil: Archean IOCG deposits of Igarapé–Bahia (up to 160 ppm U), Salobo (30–60 ppm U), and Alemao all contain uraninite. In the Palaborwa Cu deposit hosted in a carbonatite, which has been classified as an IOCG deposit by some authors, 90 tU/year have been mined until 2002, the U-bearing mineral being uranothorianite.

In the Oak Dam East Cu–Au–U-bearing, massive Fe oxide deposit (~560 Mt of 41–56 wt.% Fe) which lies beneath more than 500 m of younger cover rocks, U mineralization has been studied in more detail (Davidson *et al.* 2007). Uraninite is the main U mineral and has been deposited with chalcopyrite, illite, hydromuscovite, florencite and carrolite, the Cu–U–(Au) mineralization stage. The Cu–U mineralized zones resemble Olympic Dam ore in terms of geometry, being nearly horizontal, 10–70 m thick, and crosscutting the host breccia. A brine system analogous to the Salton Sea geothermal system is proposed for the genesis of the mineralization. Cu, Fe, and S were transported by a deep brine reservoir and chalcopyrite–uraninite veins formed as a result of mixing with steam-heated, U-rich, oxidized saline ground water. High grade ore occurs centrally within the chalcopyrite zone (*e.g.*, 10 m of 0.46.% Cu and 0.32.% U), straddling a boundary between K mica + illite alteration and underlying Fe–Mg chlorite alteration and was formed when the deep brine upflow decreased.

REFERENCES

ADAMEK, P.M. & WILSON, M.R. (1979): The evolution of a uranium province in northern Sweden. Phil. *Trans. R. Soc. Lond.* **291**, 355-368.

ALBA, L.A. & CHAVEZ, R. (1974): K-Ar ages from volcanic rocks from the Central Pena Blanca, Chihuahua, Mexico. *Isochron West* **10**, 21-23.

ALLMAN-WARD, P. (1985): Distribution of uranium and thorium in the Western Lobe of the St. Austell granite and the effects of alteration processes. In: High Heat Production (HHP) Granites, hydrothermal circulation and ore genesis; papers presented at an international conference, St. Austell, September 1985. London: *Inst. Mining & Metallurgy*, **437**.

ANDRE, A.S., LESPINASSE, M., CATHELINEAU, M., BOIRON, M.C., CUNEY, M. & LEROY, J.M. (1999): Percolation de fluides tardi-hercyniens dans le granite de Saint Sylvestre (NW Massif Central français): données des inclusions fluides sur un profil Razès-Saint Pardoux. *C. R. Acad. Sci.* **329**, 23-30.

ANDREEVA O.V., WOLFSON F.I., GOLOVIN V.A. & ROSSMAN G.I. (1990): The behavior of uranium during low- temperature alteration of host rocks in uranium deposits. *Geokhimiya* **28**, 206–215.

ANDREEVA, O.V., ALYESHIN, A.P. & GOLOVIN & V.A. (1996): Vertical zonality of ore formations in uranium deposits of Antei-Streltsovskoye (Transbaikalia, Russia). *Geol. Rudn. Mestorozhdeny* **38**, 396-411 (in Russian).

ANIEL, B. & LEROY, J. (1985). The reduced uraniferous mineralisations associated with the volcanic rocks of the Sierra Pena Blanca (Chihuahua, Mexico). *Am. Mineral.* **70**, 1290-1297.

ARRIBAS, A. & FIGUEROA, E. (1985): Geologia y metalogenia de las mineralizaciones uraniferas de Macusani, Puno (Peru). Proc. IAEA Vienna, Symp. *Uranium deposits in volcanic rocks*, El Paso, TX 1984, 237-254.

AUDRAIN, J., VIGNERESSE, J.L., CUNEY M. & FRIEDRICH, M. (1989): Modèle gravimétrique et mise en place du complexe granitique hyperalumineux de Saint-Sylvestre (Massif Central français). *C.R. Acad. Sci.*, Paris **309** 1907-1914.

BAIN, J.H.C. (1977): Uranium mineralisation associated with late Palaeozoic acid magmatism in northeast Queensland. *J. Austr. Geol. Geoph.* **2**, 137-147.

BARBIER, J. (1967): Etude pétrographique et géochimique du granite à deux micas des Monts de Blond (Limousin - France). *Sc. de la Terre, Nancy* **VII**, 183–206.

BARBIER, J. (1974): Continental weathering as a possible origin of vein-type uranium deposits: *Mineral. Dep.* **9**, 271-288.

BERNARD-GRIFFITHS, J., PEUCAT, J.J., SHEPPARD, S. & VIDAL, P. (1985): Petrogenesis of Hercynian leucogranites from the southern Armorican Massif: contribution of REE and isotopic (Sr, Nd, Pb and O) geochemical data to the study of source rock characteristics and ages. *Earth Planet. Sci. Lett.* **74**, 235-250.

BERTRAND, J.M., LETERRIER, J., CUNEY, M., BROUAND, M., STUSSI, J.M., DELAPIERRE, E. & VIRLOGEUX, D. (2001): Géochronologie U-Pb sur zircons de granitoïdes du Confolentais, du massif de Charoux-Civray (seuil de Poitou) et de Vendée. *Géologie de la France* **1-2**, 167-181.

BICKLE, M.J., WICKAM, S.M., CHAPMAN, H.J. & TAYLOR, JR. (1988): A strontium, neodymium and oxygen isotope study of hydrothermal metamorphism and crustal anatexis in the Trois Seigneurs Massif, Pyrénées, France. *Contrib. Mineral. Petrol.* **100**, 399-417.

BOUCHOT, V., LEDRU, P., LEROUGE, C., LESCUYER, J.L. & MILESI, J.P. (2005): Late Variscan mineralizing systems related to orogenic processes: The French Massif Central. *Ore Geology Reviews* **27**, 169-197.

BOURGUIGNON, A. (1988): *Origine des formations paradérivées et orthodérivées acides du Limousin central. Une source possible pour les leucogranites uranifères*. Unpub. Thesis, Lyon Univ. 208 p.

BUDDING, K.E., CUNNINGHAM, C.G., ZIELINSKI, R.A., STEVEN, T.A. & STERN, C.R. (1987): Petrology and chemistry of the Joe Lott Tuff member of the Mount Belknap Volcanics, Marysvale volcanic field, west-central Utah. *US Geol. Surv. Prof. Pap.* **1354**, 47p.

BURKHARD, D.J.M. (1991): Temperature and redox path of biotite-bearing intrusives: A method of estimation applied to S- and I-type granites from Australia. *Earth Planet. Sci. Let.* **104**, 89-98.

BURT, D.M., SHERIDAN, M.F., BIKUN, J.V.& CHRISTIANSEN E.H. (1982): Topaz rhyolites-Distribution, origin, and significance for exploration. *Econ. Geol.* **77**, 1818-1836

CADEL, G. (1986): Geology and uranium mineralisation of the Collio Basin (Central Southern Alps, Italy). *Uranium* **2**, 215-240.

CADEL, G., FUCHS, Y. & MENEGHEL, L. (1987): Uranium mineralisation associated with the evolution of a Permo-Carboniferous volcanic field - Examples from Novazza and Val Vedello (northern Italy). *Uranium* **3**, 404-421.

CASTOR, S.B. & BERRY, M.R. (1981): Geology of the Lakeview uranium district, Oregon. *In* P.C. Goodell, A.C. Waters (*Eds.*), Uranium in Volcanic and Volcanoclastic Rocks, **13**, *AAPG Stud. Geol.* 55-62.

CASTOR, S.B. & HENRY, C.D. (2000): Geology, geochemistry, and origin of volcanic rock-hosted uranium deposits in north-western Nevada and south-eastern Oregon, USA. *Ore Geology Reviews* **16**, 1-2, 1-40.

CATHELINEAU, M. (1982): Les mécanismes de type «roll-front» dans les granites: un modèle de remobilisation dans les gisements hydrothermaux d'uranium. *C.R. Acad. Sci.* Paris **294**, 865-868.

CATHELINEAU, M. (1986): The hydrothermal alkali metasomatism effects on granitic rocks: quartz dissolution and related subsolidus changes. *J. Petrol.* **27**, 945-965.

CATHELINEAU, M., CUNEY, M., LEROY, J., LHOTE, F., NGUYEN, C.T., PAGEL, M. & POTY B. (1982): Caractères minéralogiques des pechblendes de la province hercynienne d'Europe. Comparaison avec les oxydes d'uranium du protérozoïque de différents gisements d'Amérique du Nord, d'Afrique et d'Australie. In *Vein type and similar uranium deposits in rocks younger than Proterozoic* Proc. Symp. Lisbon 1979, IAEA, 159-177.

CATHELINEAU, M., BOIRON, M.C., HOLLIGER, P. & POTY, B. (1989): Metallogenesis of the French part of the Variscan orogen. Part II: time-space relationships between U, Au, Sn-W ore deposition and geodynamic events: mineralogical and U-Pb data. *Tectonophysics* **177**, 59-79.

ČERNÝ, P., BLEVIN, P.L., CUNEY, M. & LONDON, D. (2005): Granite-Related Ore Deposits. *Econ. Geol.* 100th Anniv Vol. 1905-2005, 337-370.

CHABIRON, A., ALYOSHIN, A., CUNEY, M., GOLUBEV, V., VELITCHKIN, V., DELOULE, E. & POTY, B. (2001): Geochemistry of the rhyolitic magmas associated with the Streltsovskoye uranium deposits (Tranbaikalia): a magmatic inclusion study. *Chem. Geol.* **175**, 273-290.

CHABIRON, A. & CUNEY, M. (2001): Allanite alteration in the Streltsovskoye granites: A source of uranium. *C. R. Acad.Sci.* **332**, 99-105.

CHABIRON, A., CUNEY, M. & POTY B. (2003): Possible uranium sources for the largest uranium district associated with volcanism: the Steltsovka caldera (Transbaïkalie, Russia). *Mineral. Dep.* **38**, 127-140.

CHAPMAN, D.S., POLLACK, H.N. & CERMAK, V. (1979): Global heat flow with special reference to the region of Europe. In: *Terrestrial heat flow in Europe*, V. Cermak & L. Rybach, Springer Verlag, Berlin, 41-48.

CHAPPELL, B.W. & WHITE, A.J.R. (1974): Two contrasting granite types. *Pacific Geol.* **8**, 173-174.

CHAROY, B. (1981): Post-magmatic processes in south-west England and Brittany. *Proc. Ussher Soc.*, **5**, 101-115.

CHEILLETZ, A., CLARK, A.H., FARRAR, E., ARROYO PAUCA, G., PICHAVANT, M., & SANDEMAN, H.A. (1992): Volcano-stratigraphy and 40Ar/39Ar geochronology of the Macusani ignimbrite field: monitor of the Miocene geodynamic evolution of the Andes of southeast Peru. *Tectonophysics* **205**, 307-327

CHEMILLAC, R. (2004): *Géochimie des magmas associés aux gisements d'uranium intravolcaniques.* Unpub. PhD thesis, Nancy University.

CHEN, G.J., WASSERBURG, K.L. & VON DAMM EDMOND, J.M. (1986): The U-Th-Pb systematic in hot springs of the East Pacific Rise at 21°N and Guaymas Basin. *Geochim. Cosmochim. Acta* **50**, 2467-2479

CHERNYSHEV, I.V. & GOLUBEV, V.N. (1996): The Strel'tsovskoe deposit, Eastern Transbaikalia: isotope dating of mineralisation in Russia's largest uranium deposit. *Geokhim.* **10**, 924-937 (in Russian).

CREASER, R.A. (1996): Petrogenesis of a Mesoproterozoic quartz latite-granitoid suite from the Roxby Downs area, South Australia. *Precamb. Res.* **79**, 371-394

CUNEY, M. (1978): Geologic environment, mineralogy, and fluid inclusions of the Bois Noirs-Limouzat uranium vein, Forez, France: *Econ. Geol.* **73**, 1567-1610.

CUNEY M. & FRIEDRICH M. (1987): Physico-chemical and crystal chemical controls on accessory mineral paragenesis in granitoids. Implications on uranium metallogenesis. *Bull. Minéral.* **110**, 235-247.

CUNEY, M., ALEXANDROV, P., LE CARLIER, C., CHEILLETZ, A., RAIMBAULT, L. & RUFFET, G. (2002): The Sn-W-Rare Metals mineral deposits of the Western Variscan chain in their orogenic setting: the case of the Limousin area (French Massif Central). In: BLUNDELL, D., NEUBAUER, F. & VON QUADT, A. (eds), The timing and location of major ore deposits in an evolving orogen: *Geol. Soc. London, Special Publ.* **206**, 213-228.

CUNEY, M., FRIEDRICH, M., BLUMENFELD, P., BOURGUIGNON, A., BOIRON, M.-C., VIGNERESSE, J.-L. & POTY, B. (1990): Metallogenesis in the French part of the Variscan orogen. Part I: Preconcentration in Pre-Variscan and Variscan formations-a comparison with Sn, W and Au: *Tectonophysics* **177**, 39-57.

CUNEY, M., BROUAND, M., STUSSI, J.M. & VIRLOJEUX, D. (2001): Le complexe plutonique de Charroux-Civray (Vienne): témoin du magmatisme infra-carbonifère dans le segment occidental de la chaîne varisque européenne. *Géologie de la France* **1-2**, 143-166

CUNEY, M., FRIEDRICH, M. & POTY, B. (1984): Pétrologie et géochimie des radioéléments dans les granites et dans les leucogranitiques en particulier. Conséquences génétiques et applications à la prospection. *Documents du BRGM* **79**, 91-125.

CUNEY, M., LEROY, J., VALDIVIEZO, P.A., DAZIANO, C., GAMBA, M., ZARCO, A.J., MORELLO, O., NINCI, C., MOLINA P. (1989): Geochemistry of the uranium mineralized Achala granitic complex, Argentina: comparison with Hercynian peraluminous leucogranites of Western Europe. IAEA-TC-542/16, 211-232.

CUNNINGHAM, C.G., LUDWIG, K.R., NAESER, C.W., WEILAND, E.K., MEHNERT, H.H., STEVEN, T.A. & RASMUSSEN, J.D. (1982): Geochronology of hydrothermal uranium deposits and associated igneous rocks in the eastern source area of the Mount Belknap volcanics, Marysvale, Utah. *Econ. Geol.* **77**, 453-463.

CUNNINGHAM, C.G., RASMUSSEN, J.D., STEVEN, T.A., RYE, R.O., ROWLEY, P.D., ROMBERGER, S.B. & SELVERSTONE, J. (1998): Hydrothermal uranium deposits containing molybdenum and fluorite in the Marysvale volcanic field, west-central Utah. *Mineral. Dep.* **33**, 477-494.

DAVIDSON, G.J., PATERSON, H., MEFFRE, S. & BERRY R.F. (2007): Characteristics and Origin of the Oak Dam East Breccia-Hosted, Iron Oxide Cu-U-(Au) Deposit: Olympic Dam Region, Gawler Craton, South Australia. *Econ. Geol*. **102**, 1471 - 1498

DAYVAULT, R.D. CASTOR, S.B. & BERRY, M.R. (1985): Uranium associated with volcanic rocks of the McDermitt caldera, Nevada and Oregon. In: Uranium deposits in volcanic rocks; Proc. Tech. Com. Meet., Panel Proc. Ser. *IAEA STI/PUB/690*, 379-409.

DEBON, F. & LEFORT, P. (1988): A cationic classification of common plutonic rocks and their magmatic associations: principles, method, applications: *Bull. Minéral.* **111**, 493-510.

DOWNES H. & DUTHOU J.L. (1987): Isotopic trace element arguments for the lower crustal origin of Hercynian granitoids and pre-Hercynian orthogneisses (Massif Central, France). *Chem. Geol.* **68**, 291-308.

DRUMMOND, LYONS, B.P., GOLEBY, B. & JONES L. (2006): Constraining models of the tectonic setting of the giant Olympic Dam iron oxide–copper–gold deposit, South Australia, using deep seismic reflection data. *Tectonophysics* **420**, 91-103

DUBESSY J., RAMBOZ C., NGUYEN TRUNG C., CATHELINEAU M., CHAROY B., CUNEY M., LEROY J., POTY, B. & WEISBROD, A. (1987): Physical and chemical control (fO_2, T, pH) of the opposite behaviour of U and Sn-W as examplified by hydrothermal deposits in France and Great Britain, and solubility data. *Bull. Minéral.* **110**, 262-281.

DUTHOU, J.L., CANTAGREL, J.M., DIDIER, J. & VIALETTE, Y. (1984): Paleozoic granitoids from the French Massif Central: age and origin studied by 87Rb-87Sr system. *Phys. Earth Planet. Int.* **35**, 131-144.

EBY, G.N. (1992): Chemical subdivision of the A-type granitoids: Petrogenetic and tectonic implications: *Geology* **20**, 641-644.

EL JARRAY, A., BOIRON, M.-C. & CATHELINEAU, M. (1994): Percolation microfissurale des vapeurs aqueuses dans le granite de Pény (Massif de Saint Sylvestre, Massif Central): relations avec la dissolution du quartz: *C. R. Acad. Sciences, Paris* **318**, 1095-1102.

ELLIOTT, T., ZINDLER, A. & BOURDON, B. (1999): Exploring the kappa conundrum; the role of recycling in the lead isotope evolution of the mantle. *Earth Planet. Sci. Lett.* **169**, 139-145.

EWART, A. (1982): The mineralogy and petrology of Tertiary-Recent orogenic volcanic rocks, with special reference to the andesitic- basaltic compositional range. *In* R.S. Thorpe, *Ed*. Andesites: Orogenic andesites and related rocks, p. 25-95. Wiley, New York.

EWING, R.C., CHAKOUMAKOS, B.C., LUMPKIN, G.R., MURAKAMI, T., GREEGOR R.B. & LYTLE, F.W. (1988): Metamict minerals: natural analogues for radiation damage effects in ceramic nuclear waste forms. *Nuclear Instruments Methods Phys Res*. **B32**, 487–497

FANNING, C.M., FLINT, R.B., PARKER, A.J., LUDWIG, K.R. & BLISSETT, A.H. (1988): Refined Proterozoic evolution of the Gawler Craton, South Australia, through U-Pb zircon geochronology. *Precamb. Res.* **40-41**, 363-386

FLOC'H, J.P., GUILLOT, P.L., SANTALLIER, D. & AUTRAN, A. (1983): Le Limousin: un empilement de grandes unités lithotectoniques d'âges précambrien et paléozoïque? Coll final ATP géodynamique, Sophia Antipolis, III: 7.

FORBES, P. (1989): Rôles des structures sédimentaires et tectoniques, du volcanisme alcalin régional et des fluides diagénétiques hydrothermaux pour la formation des minéralisations à U-Zr-Zn-V-Mo d'Akouta (Niger). *Géol. Géochim. Uranium Mém.* Nancy **17**: 376 p

FORBES, P., PACQUET, A., CHANTRET, F., OUMAROU, J. & PAGEL M. (1984): Marqueurs du volcanisme dans le gisement d'uranium d'Akouta (République du Niger). *C. R. Acad. Sci.*, Paris, 298.

FRIEDRICH, M., CUNEY, M. & POTY B. (1987): Uranium geochemistry in peraluminous leucogranites. *Uranium* **3**, 353-385.

FUCHS Y.A. (1989): Hydrothermal alteration at the Novazza volcanic field and its relation to the U, Mo, Zn Novazza deposit, Northern Italy. *In* Metallogenesis of uranium deposits, IAEA, Vienna, 137-151.

GHANDI, S.S. (1978): Geological setting and genetic aspects of uranium occurrences in the Kaipokok Bay-Big river area, Labrador. *Econ. Geol.* **73**, 1492-1522.

GARNER, A. & MCPHIE, J. (1999): Partially melted lithic megablocks in the Yardea Dacite, Gawler Range Volcanics, Australia: implications for eruption and emplacement mechanisms: *Bull. Volcan.* **61**, 396-410.

GEFFROY, J. (1971): Les gites uranifères dans le Massif Central, in Symposium Jung: Géologie, Géomorphologie et structure profonde du Massif Central Français: Clermont, Plein Air Service Ed., 541-579.

GEFFROY, J. & SARCIA, J. (1958): La notion de "gite épithermal uranifère" et les problèmes qu'elle pose: *Soc. Géol. France Bull*. **6**, 173 - 190.

GEORGE-ANIEL, B. (1988): Comportement naturel de l'uranium en milieu volcanique et approche expérimentale. *Géol. Géochim. Uranium, Mém.* Nancy **16**, 311 p.

GEORGE-ANIEL, B., LEROY, J., & POTY, B. (1991): Volcanogenic Uranium mineralisations in the Sierra Pena Blanca district, Chihuahua, Mexico: three genetic models. *Economic Geology* **86**, 233-286.

GILES, C.W. (1988): Petrogenesis of the Proterozoic Gawler Range Volcanics, South Australia. *Precamb. Res.* **40-41**, 407-427

GOLUBEV, V.N., CUNEY, M. & POTY, B. (2000): Phase composition and U-Pb isotopic systems of pitchblende of quartz-calcite-pitchblende veins at the Schlema-Alberoda deposit (Erzgebirge). *Geol. Ore Dep.* **42**, 761-773.

HAYNES, D.W., CROSS, K.C., BILLS, R.T. & REED, M.H. (1995): Olympic Dam Ore genesis: A fluid-mixing model. *Econ Geol.* **90**, 281-307

HITZMAN, M.W., ORESKES, N. & EINAUDI, M.T. (1992): Geological characteristics and tectonic setting of Proterozoic iron oxide (Cu-U-Au-REE) deposits. *Precamb. Res.* **58**, 241-287

HOLLIGER P. & CATHELINEAU, M. (1986): Le chronomètre U-Pb en milieu uranifère: application aux gisements hydrothermaux d'U associés spatialement au batholite de Mortagne (Vendée, France). *Chron. Rech. Min.* **485**, 33-43.

HOLLIGER P., CUNEY M., FRIEDRICH M. & TURPIN L. (1986): Age Carbonifère de l'unité de Brame du complexe granitique peralumineux de Saint Sylvestre (NO Massif Central) défini par les données isotopiques sur zircon et monazite. *C. R. Acad. Sci*. 1309-1314.

HOLM, P.M., LOU, S. & NIELSEN, A. (1982): The Geochemistry and Petrogenesis of the Lavas of the Vulsinian District, Roman Province, Central Italy. *Contrib. Mineral. Petrol*. **80**, 367-378.

ISHUKOVA, L.P. (1989): Geological structure of south-Priargun in Transbaikalia. *Izv An SSSR, Geol*, **8**, 102-118 (in Russian).

ISHUKOVA, L.P., MODNIKOV, I.S. & CITCHEV, I.V. (1991): Uranium ore-forming systems of continental volcanism regions. *Geol. Rudn. Mestorozhd*. **3**, 16-25 (in Russian).

JIANG, Y.H. LING, H.F., JIANG, S.Y., FAN, H.H., SHEN, W.Z. & NI, P. (2005a): Petrogenesis of a Late Jurassic Peraluminous volcanic Complex and its High-Mg, Potassic, Quenched Enclaves at Xiangshan, Southeast China. *J. Petrol.* **46**, 1-34.

JIANG, Y.H. LING, H.F. & JIANG, S.Y. (2005b): Mantle derived fluid and uranium mineralization: Evidence from the world-class Xiangshan uranium deposit, SE China. Mineral Deposit Research, *Proceedings of the Eighth Biennial SGA Meeting*, Jingwen Mao, Bierlein F.P. (Ed.), 269-27.

JIMENEZ, N. (1985): *Evolucion del vulcanismo terciario en la meseta Los Frailes suroccidental (sector Cotaje-Tihua Alti).* Unpub. Thesis UMSA, La Paz.

JOHNSON, J.P. & CROSS, K.C. (1995): U-Pb geochronological constraints on genesis of the Olympic Dam Cu-U-Au-Ag deposit, South Australia. *Econ. Geol.* **90**, 1046-1063

JOHNSON, J.P., & MCCULLOCH, M.T. (1995): Sources of mineralizing fluids for the Olympic Dam Deposit (South Australia); Sm-Nd isotopic constraints. *Chem. Geol.* **121**, 177-199

KAMENETSKY, V.S., MORROW, N. & MCPHIE, J. (2000): Origin of high-Si dacite from rhyolitic melt: evidence from melt inclusions in mingled lavas of the 1.6 Ga Gawler Range Volcanics, South Australia. *Mineral.& Petrol.* **69**, 183-185

KNIPPING, H.D. (1974): The concepts of supergene versus hypogene emplacement of uranium at Rabbit Lake, Saskatchewan, Canada. *In* Formation of Uranium Deposits, International Atomic Energy Agency, Vienna, 531-548

KRYLOVA, T.L., ALESHIN, A.P., LHOMME, T., VELICHKIN V.I. & CUNEY M. (2006): New data on the formation conditions of the uranium ores at the Streltsovskoye and Antei deposits (Eastern Transbaikalia, Russia). *Proceedings of the 12th IAGOD meeting*, 21-24 Août 2006, Moscow.

LANDAIS, P. (1996): Organic geochemistry of sedimentary uranium ore deposits. *Ore Geol. Rev.* **11**, 33-51.

LANGFORD, F.F. (1974): A supergene origin for vein-type uranium ores in the light of the western Australian calcrete-deposit. *Econ. Geol.* **69**, 516–526.

LANGFORD, F.F. (1977): Surficial origin of North American pitchblende and related uranium deposits. *AAPG Bulletin* **61**, 28-42.

LANGFORD, F.F. (1978): Origin of unconformity-type pitchblende deposits in the Athabasca Basin of Saskatchewan. *In* Kimberly, M.M., *ed*., Uranium Deposits: their Mineralogy and Origin, Short Course: Mineralogical Association of Canada, University of Toronto, 485-499.

LAVEROV, N.P., VELITCHKIN, V.I. & SHUMILIN, M.V. (1992): Uranium deposits of the CIS: the main economic genetic types and their distribution. *Geol. Rudn. Mestorozhd.* **2**, 3-18 (in Russian).

LE, V.T. (1975): Géochimie de l'uranium et du thorium dans les granitoides et formations associées de la Montague Bourbonnaise (Massif Central Francais). Liaisons possibles avec les minéralisations uranifères des Bois-Noirs: Unpub. *Doctoral thesis, Univ. Nancy* I, 372 p.

LEHMAN, B. (1982): Metallogeny of tin/ magmatic differentiation versus geochemical heritage. *Econ. Geol.* **77**, 50-59.

LEROY, J. (1978a): The Margnac and Fanay uranium deposits of the La Crouzille district (Western Massif Central, France), geologic and fluid inclusion studies. *Econ. Geol.* **73**, 1611-1634.

LEROY, J. (1978b): Métallogénèse des gisements d'uranium de la division minière de la Crouzille (COGEMA, Nord Limousin France), *Mem. Sci.Terre. Nancy*, 36, 278p.

LEROY, J. & GEORGE-ANIEL, B. (1992): Volcanism and uranium mineralisations: the concept of source rock and concentration mechanism. *J. Volcan. & Geotherm. Res.* **50**, 247-272.

LEROY, J. & HOLLIGER, P. (1984): Mineralogical, chemical and isotopic (U/Pb method) studies of Hercynian uraniferous mineralizations (Fanay and Margnac mines, Limousin, France). *Chem. Geol.,* 45, 121-134.

LEROY, J. & POTY, B. (1969). Recherches préliminaires sur les fluides associés et la genèse des minéralisations en uranium du Limousin (France): *Mineral. Deposit.* **4**, 395-400.

LEROY, J. & SONET, J. (1976): Contribution à l'étude géochronologique des filons de lamprophyres recoupant le granite à deux micas de St Sylvestre (Limousin, Massif Central français). *C.R. Acad. Sci. Paris* **283**, 1477-1480.

LEROY, J., GEORGES-ANIEL, B. & POTY, B. (1987): The Sierra Peña Blanca (Mexico) and the Meseta Los Frailes (Bolivia): the uranium concentration mechanisms in volcanic environment during hydrothermal processes. *Uranium* **3**, 211-234.

LINDROOS, H. (1980): Internal Report SGU, in Smellie J. 1982.

LINDROOS, H. & SMELLIE, J. (1979): A stratabound Uranium Occurrence within Middle Precambrian Ignimbrites at Duobblon, Northern Sweden. *Econ. Geol.* **74**, 1118-1130.

LINDSEY D.A. (1981): Volcanism and uranium mineralization at Spor Mountain, Utah. In: Goodell, P.C. and Waters A.C. eds., Uranium in Volcanic and Volcaniclastic Rocks, *AAPG Stud. Geol.*, **13**, 89-98.

LINNEN, R.L. & CUNEY, M. (2005): Granite-related rare-element deposits and experimental constraints on Ta-Nb-W-Sn-Zr-Hf mineralization. *In* Rare-Element Geochemistry and Mineral Deposits, Linnen, R.L. & Samson, I.M., *eds.*, *Geol. Assoc. Can, Short Course Notes* **17**, 45-67.

LUCAZEAU, F. & VASSEUR, G. (1981): Production de chaleur et régime thermique de la croûte du Massif Central, *Ann. Géophys.* **37**, 493-513.

MAGONTHIER, M.C. (1984): Les ignimbrites de la Sierra Madre Occidental et de la province uranifère de la Sierra Pena Blanca, Mexique. *Mém. Sci. Terre, Univ. P. et M. Curie*, Paris, **84-17**, 351 p.

MANNING, D.A.C. (1981): The effect of fluorine on liquidus phase relationships in the system Qz-Ab-Or with excess water at 1 kb. *Contrib. Mineral. Petrol.* **76** 206-215.

MCKENZIE, D.P. (1989): Some remarks on the movement of small melt fractions in the mantle. *Earth Planet. Sci. Lett.* **95**, 53–72.

MELNIKOV, I.V., TIMOFEEV, A.V, KOTOV, I.I., CHTEINCHNEIDER, T.L. & GORBOUNOV. V.I. (1980): Thermobarogeochemical particularities of hydrothermal uranium deposits in Phanerozoic folded areas. *Termobarogeokhim Rudogenez*, 210-217 (in Russian)

MIN, M.-Z. LUO, X.-Z., DU, G.-S., HE, B.-A. & CAMPBELL, A.R. (1999): Mineralogical and geochemical constraints on the genesis of the granite-hosted Huangao uranium deposit, SE China. *Ore Geol. Rev.* **14**, 105–127

MIRONOV, Y.B., FILONENKO, Y.D., SOLOV'EV, N.S., PETROV, V.A., GOLOVIN, V.A. & STREL'TSOV, V.A. (1993): Lead-zinc, uranium, and fluorite deposits in the Dornot volcano-tectonic structure (East Mongolia). *Geol. Ore Dep.* **35**, 26-37.

MOLLIER, B. (1984): Le granite de Brame - St Sylvestre - St Goussaud: ses structures magmatiques, une étude de la distribution de l'uranium ˆ l'échelle du grain. *Géol. Géochim. Uranium, Mém. Nancy* **7**, 145 p.

MOLLIER B. & BOUCHEZ J.L. (1982): Structuration magmatique du complexe granitique de Brâme-St-Sylvestre-St-Goussaud (Limousin, Massif central français). *C. R. Acad. Sc. Paris* **294**, 1329-1334.

MONIER G. & ROBERT, J.L. (1986a): Muscovite solid solutions in the system K_2O-MgO-FeO-Al_2O_3-SiO_2-H_2O: an experimental study at 2 kbar P_{H2O} and comparison with natural Li-free white micas. *Mineral. Mag.* **50**, 257-266.

MONIER G. & ROBERT, J.-L. (1986b): Evolution of the miscibility gap between muscovite and biotite solid solutions with increasing lithium content: an experimental study in the system K_2O−Li_2O−MgO−FeO−Al_2O3−SiO_2−H_2O−HF. *Mineral. Mag.* **50**, 641-651

MONTEL, J.M. (1993): A model for monazite/melt equilibrium and application to the generation of granitic magmas. *Chem. Geol.* **110**, 127-146.

MOREAU, M., POUGHON, A., PUYBARAUD, Y. & SANSEHNE, H. (1966): L'uranium et les granites: *Chronique des Mines et de la Recherche Minière* **350**, 47-50.

MORROW, N. & MCPHIE, J. (2000): Mingled silicic lavas in the Mesoproterozoic Gawler Range Volcanics, South Australia. *J. Volcan. Geotherm. Res.* **96**, 1-13

MORTON, R.D., ABUT, A. & GANDHI, S.S. (1978): Fluid inclusion studies of the Rexpar uranium fluorite deposit, Birch Island, British Columbia. In Current Research, B, *Geol. Surv. Canada paper* **78-1B**, 137-140.

NOBLE, D.C., MCCORMACK, J.K., MCKEE, E.H., SILBERMAN, E.H. & WALLACE, A.B. (1988): Time of mineralisation in the evolution of the McDermitt caldera complex, Nevada-Oregon, and the relation of middle Miocene mineralisation in the northern Great Basin to coeval regional basaltic magmatic activity. *Econ. Geol.* **83**, 859-863.

ORESKES, N. & EINAUDI, M.T. (1992): Origin of hydrothermal fluids at Olympic Dam: Preliminary results from fluid inclusions and stable isotopes. *Econ. Geol.* **87**, 64-90

O'ROURKE, P.J. (1975): Maureen Uranium Fluorine Molybdenum Prospect, Georgetown in Knight C.L. (Ed.) Economic Geology of Australia and Papua New Guinea. *The AusIMM, Monograph Series* **5**, 764-769.

OUDDOU, D. (1984): *Le massif de Guérande – Le Croisic (Loire Atlantique). Caractérisation géochimique et minéralogique de l'évolution magmatique. Comportement de l'uranium et du thorium*. Unpb. Thesis, INPL, Nancy, 220 p.

PAGEL, M. (1981): *Les facteurs de concentration de l'uranium et du thorium dans quelques granites de la chaîne hercynienne d'Europe.* Unpb. Doctoral thesis, INPL, Nancy, 520 p.

PAGEL, M. (1982): The mineralogy and geochemistry of uranium, thorium, and rare-earth elements in two radioactive granites of the Vosges, France. *Mineral. Mag.* **46**, 152-163.

PALACIN, P. (1985): *Etude géologique et géochimique du volcanisme du Latium (Italie): exemples du Vico et du Vulsini*. Unpub. thesis, Paris VI University, 254 p.

PÉCHER, A., LESPINASSE M. & LEROY J. (1985): Relations between fluid inclusion trails and regional stress field: a tool for fluid chronology - An example of an intragranitic uranium ore deposit (northwest Massif Central, France). *Lithos* **18**, 229-237.

PEIFFERT, CH., CUNEY, M. & NGUYEN TRUNG, CH. (1994): Uranium in granitic magmas. Part I: Experimental determination of uranium solubility and fluid-melt partition coefficients in the UO_2-haplogranite-H_2O-Na_2CO_3 system at 720-770°C 200 MPa. *Geochim. Cosmochim. Acta* **58**, 2495-2507.

PEIFFERT, CH., NGUYEN TRUNG, CH. & CUNEY, M. (1996): Uranium in granitic magmas. Part II: Experimental determination of uranium solubility and fluid-melt partition coefficients in the UO_2 - haplogranite - H_2O-halides system at 720-770°C 200 MPa. *Geochim. Cosmochim. Acta* **60**, 1515-1529.

PEUCAT, J.J., JEGOUZO P., VIDAL, P. & BERNARD GRIFFITHS, J. (1988): Continental crust formation seen through the Sr and Nd isotope systematics of

S-type granites in the Hercynian belt of France. *Earth Planet. Sci. Lett*. **88**, 60-68.

PEYROU, E. (1981): *Pétrographie et géochimie du granite de Grandrieu (Margeride, Massif Central).* CREGU, Vandoeuvre les Nancy, Report 81-3.

PICHAVANT, M., KONTAK, D.J., BRIQUEU, L., VALENCIA-HERRERA, J. & CLARK A.H. (1988a): The Iocene-Pliocene Macusani volcanics, SE Peru. II - Geochemistry and origin of a felsic peraluminous magma. *Contrib. Mineral. Petrol.* **100**, 325-338.

PICHAVANT, M., KONTAK, D.J., VALENCIA-HERRERA, J., CLARK, A.H. (1988b): The Miocene-Pliocene Macusani volcanics, SE Peru. I. Mineralogy and magmatic evolution of a two-mica aluminosilicate-bearing ignimbrite suite. *Contrib. Mineral. Petrol.* **100**, 300-324.

PIN, C. & DUTHOU, J.L. (1990): Sources of Hercynian granitoids from the French Massif Central: Inferences from Nd isotopes and consequences for crustal evolution. *Chem. Geol.* **83**, 281-296.

PIRONON, J. (1986): Zonalités géochimiques et minéralogiques dans les bassins continentaux uranifères. Exemples de St. Hippolyte (Massif Vosgien), Müllenbach (Forêt Noire, R. F. A.), Salmanière (Massif Central français). *Géol. Géochim. Uranium Mém.* Nancy **13**: 296 p

PLIMER, I.R., (1980): Exhalative Sn and W deposits with mafic volcanism as precursors to Sn and W deposits associated with granites. *Mineral. Dep.* **22**, 282-291.

POLITO, P.A., KYSER, K.T. & STANLEY, C. (2007): The Proterozoic, albitite-hosted, Valhalla uranium deposit, Queensland, Australia, a description of the alteration assemblage associated with uranium mineralisation in diamond drill hole. *Mineral. Dep.* **39**, in press.

POLLARD, P.J. (2000): Evidence of a magmatic fluid and metal source for Fe-Oxide Cu-Au mineralization. *In* Porter, T.M., *ed*., Hydrothermal iron oxide copper-gold & related deposits, 1: Linden Park, Porter Geoconsultancy Pty Ltd, 27-41

POTY, B., LEROY, J., CATHELINEAU, M., CUNEY, M., FRIEDRICH, M., LESPINASSE, M. & TURPIN L. (1986): Uranium deposits spatially related to granites in the french part of the Hercynian orogen. *In*: Vein-type U deposits, *IAEA-TECDOC-361*, 215-246

RANCHIN, G. (1971): La géochimie de l'uranium et la différenciation granitique dans la province uranifère du Nord Limousin. *Rapport CEA R.4034*, 467 p.

REEVE, J.S., CROSS, K.C., SMITH, R.N. & ORESKES, N. (1990): Olympic Dam Copper -uranium - gold - silver deposit. *In* Geology of the Mineral Deposits of Australia and Papua New Guinea, F.E. Hughes, *ed.*, Melbourne. Australasian Inst. Mining & Metallurgy, 1009-1035

RENARD, J.P. (1974): Etude pétrographique et géochimique des granites du district uranifère de Vendée. Liaisons entre l'évolution minéralogique et le comportement de l'uranium. Conséquences pour la prospection: *Comm. Energie Atomique, Rap.* R-4407, 216 p.

REYNOLDS, L.J. (2000): Geology of the Olympic Dam Cu-U-Au-Ag deposit. *In* Hydrothermal iron oxide copper-gold & related deposits, 1: Linden Park, Porter, T.M., *ed*. Porter Geoconsultancy Pty Ltd, 93-104.

ROBERTS, D.E. & HUDSON, G.R.T. (1983): The Olympic Dam Copper-Uranium - Gold deposit, Roxby Downs, South Australia: *Econ. Geol.* **78**, 799-822

ROGERS, N.W., HAWKESWORTH, C.J., PARKER, R.J. & MARSH, J.S. (1985): The geochemistry of potassic lava Pichavant s from Vulsini, central Italy and implications for mantle enrichment processes beneath the Roman region. *Contrib. Mineral. Petrol.* **90**, 244-257.

ROPER, M.W. & WALLACE, A.B. (1981): Geology of the Aurora uranium prospect, Malheur County, Oregon. In: P.C. Goodell, A.C. Waters (Eds.), Uranium in Volcanic and Volcaniclastic Rocks, *AAPG Stud. Geol.* **13**, 81-88.

ROUBAULT, M. & COPPENS, R. (1955): Sur les relations entre certains gites filoniens d'uranium et la présence d'inclusions radioactives dans les roches encaissantes. *C.R. Acad. Sci. Fr.* **240**, 214-216.

ROUBAULT, M. & COPPENS, R. (1958): Migration of uranium in crystalline rocks and the possible

relation of this phenomenont the genesis of certain deposits. *Proc. Int. Conf. Peaceful Uses Atomic Energ.,* Geneva, 335-337

ROUTHIER, P. (1980): Où sont les métaux pour l'avenir? Les provinces métalliques. Essai de métallogénie globale. *Mémoire BRGM* **105**, 410p.

RYTUBA J.J. & CONRAD, W.K. (1981): Petrochemical characteristics of volcanic rocks associated with uranium deposits in the McDermitt caldera complex. *In*: P.C. Goodell, A.C. Waters (*Eds*.), Uranium in Volcanic and Volcaniclastic Rocks, *AAPG Stud. Geol.* **13**, 63-72.

RYTUBA, J.J. & MCKEE, E.H. (1984): Peralkaline ash flow tuffs and calderas of the McDermitt volcanic field, Southeast Oregon and north central Nevada. *J. Geophys. Res.* **89**, 8616-8628.

SALFITY, J., GORUSTOVICH, S., MOYA, M. & AMENGAL, R. (1984): Marco tectonico de la sedimentacion y efusidad cenozoicas en la Puna de Argentina. *Abst. Proc. 9th Argentinian Geological Congress*, Bariloche **1**, 539-554.

SCAILLET, S, CHEILLETZ, A., CUNEY, M., FARRAR, E. & ARCHIBALD, D. (1996a): Cooling patterns and mineralization history of the Saint Sylvestre and Western Marche leucogranite plutons, French Massif Central. I - 40Ar/39Ar isotopic constraints. *Geochim. Cosmochim. Acta* **60**, 4653-4671.

SCAILLET, S, CUNEY M., LE CARLIER DE VESLUD, CH., CHEILLETZ A. & ROYER J.J. (1996b): Cooling patterns and mineralization history of the Saint Sylvestre and Western Marche leucogranite plutons, French Massif Central. II - Thermal modelling and implications for the mechanisms of U-mineralization. *Geochim. Cosmochim. Acta* **60**, 4673-4688.

SEGGIARO, R.E. & ANIEL, B. (1987): Los ciclos piroclasticos del area Tiomayo-Coranzuli, Provincia de JuJuy, Argentina. Abst. Int. Symp. Andean Volcanism, *10th Argentinian Geological Congress*, Tucuman, 358-360.

SIMOV, S.D. & BOJKOV, I.B. (1992): Case histories and new areas for uranium exploration in Bulgaria. *IAEA-TECDOC-650*, Vienne, Autriche, 81-88.

SIMPSON, P.R., BROWN, G.C., PLANT, J. & OSTLE, D. (1979): Uranium mineralisation and granite magmatism in the British Isles. *Phil. Trans. R. Soc. Lond*. **A291**, 385-412.

SMELLIE, J. (1982): The mineralogy and genesis of uranium in rhyolitic ignimbrites of Precambrian age from Duobblon, Sweden. In "Uranium 81", Simpson (Ed.) Mineral. Soc., Londres.

SØRENSEN, H., ROSE-HANSEN, J., NIELSEN, B. L., LØVBORG, L., SØRENSEN, E. & LUNDGAARD, T. (1974): The uranium deposit at Kvanefjeld, the Ilímaussaq intrusion, South Greenland. *Grønlands Geologiske Undersøgelse report* **60**, 54 pp.

STRONG, D.F. (1985): Mineral deposits associated with granitoid rocks of Eastern Canada and Western Europe: a review of their characteristics and their depositional controls by source-rock compositions and late-stage magmatic processes. *In*: R.P. Taylor & D.F. Strong *eds.*, "Granite-related Mineral Deposits". Extended abstracts, *Canadian Inst. Mining & Metallurgy, Spec. Publ. Conference*, 248-257.

STUSSI, J.M. (1989): Granitoid chemistry and associated mineralization in the French Variscan. *Econ. Geol.* **84**, 1363-1381.

STUSSI, J.-M. & CUNEY, M. (1993): Modèles d'évolution géochimique de granitoïdes peralumineux. L'exemple du complexe plutonique varisque du Millevaches (Massif central français): *Bull. Soc. Géol. France* **164**, 585-596.

TRUEMAN, N.A., LONG, J.V.P., REED, S.J.B. & CHINNET, G.A. (1988): The lead-uranium systematics, and rare earth element distributions of some Olympic Dam and Stuart shelf mineralisation: Adelaide, Australia, Western Mining Corporation, unpub. report K/3143, 46 p.

TURPIN, L., CUNEY, M., FRIEDRICH, M., BOUCHEZ, J.-L. & AUBERTIN, M. (1990a): Meta-igneous origin of peraluminous granites in NW French Massif Central: implications for crustal history reconstructions: *Contrib. Mineral. Petrol.* **104**, 163-172.

TURPIN, L., LEROY, J. & SHEPPARD, S.M.F. (1990b): Isotopic systematics (O, H, C, Sr, Nd) of surimposed barren and U-bearing hydrothermal systems in a Hercynian granite, Massif Central, France. *Chem. Geol.* **88**, 85-96.

VALENCIA-HERRERA, J. & ARROYO PAUCA, G. (1985): Consideraciones geoquimicas de los indicios uraniferos de Macusani, Puno (Peru). *Proc. IAEA Vienna, Symp. Uranium Deposits in Volcanic Rocks*, El Paso, TX 1984, 275-288.

VIDAL, P., BERNARD-GRIFFITHS, J., COCHERIE, A., LE FORT, P., PEUCAT, J.J. & SHEPPARD, S.M.F. (1984): Geochemical comparison between Himalayan and Hercynian leucogranites. *Phys. Earth Planet. Inter.* **35**, 179-190.

VIELZEUF, D. & HOLLOWAY, J.R. (1988): Experimental determination of the fluid-absent melting relations in the pelitic system. *Contrib. Mineral. Petrol.* **98**, 257-276.

VIGNERESSE, J.L. (1983): Enracinement des granites armoricains estimé d'après la gravimétrie. *Bull. Soc. Min. Bretagne* **15C**, 1-15.

VIGNERESSE, J.L., JOLIVET, J., CUNEY, M. & BIENFAIT, G. (1987): Heat flow, heat production and granites depth in western France. *Geophy. Res. Letters* **14**, 275-278.

VIGNERESSE, J.L., CUNEY, M., JOLIVET, J. & BIENFAIT, G. (1988): Selective heat producing elements enrichment in a crustal segment of Brittany (France). *Tectonophysics* **159**, 61-72.

VILLEMANT, B. & PALACIN, P. (1987): Différenciation magmatique et mécanismes de concentration de l'uranium: exemple du volcanisme du Latium (Italie centrale). *Bull. Minéral.* **110**, 319-333.

WALLACE, A.B. & ROPER, M.W. (1981): Geology and ore deposits along the north-eastern margin, McDermitt caldera complex, Oregon. In: P.C. Goodell, A.C. Waters (Eds.), Uranium in Volcanic and Volcaniclastic Rocks, *AAPG Stud. Geol.* **13**, 73-80.

WATSON, E.B. & HARRISON, T.M. (1983): Zircon saturation revisited: temperature and composition effects in a variety of crustal magma types. *Earth Planet. Sci. Lett.* **64**, 295–304.

WHITE, W.M. (1993): $^{238}U/^{204}Pb$ in MORB and open system evolution of the depleted mantle. *Earth Planet. Sci. Lett.* **115**, 211-226

WHITE, A.J.R. & CHAPPELL, B.W., (1977): Ultrametamorphism and granite genesis: *Tectonophysics* **43**, 7-22.

CHAPTER 8: UNCONFORMITY-RELATED URANIUM DEPOSITS

Kurt Kyser
Department of Geological Sciences and Geological Engineering,
Queen's University,
Kingston, Ontario, K7L 3N6, Canada
kyser@geol.queensu.ca

and

Michel Cuney
G2R, Nancy-Université, CNRS, CREGU,
B.P. 239,
F-54506 Vandoeuvre lés Nancy, France
michel.cuney@g2r.uhp-nancy.fr

UNCONFORMITY-RELATED DEPOSITS

Paleoproterozoic basins in Canada and Australia host world-class unconformity-related U deposits that currently supply 33% of the global U market (Sibbald & Quirt 1987, Thomas *et al.* 2000). The formation of these deposits is related to a reduction front near the unconformity between Paleoproterozoic sandstone and underlying metamorphosed basement lithologies. The deposits are structurally-hosted either in the basement or in overlying sandstone (Fig. 8-1). Current models for the formation of the deposits can be divided into two general end members. One involves the basement as the source of the U and the basins as the source of the fluids (Cuney *et al.* 2003), and the other involves the overlying basin as a source for both the U and fluid (Kyser *et al.* 2000). The former model sources U from the breakdown of monazite along fault zones as basinal brines interact with the basement. In the basin model, U is precipitated when the oxidized basinal brine carrying U interacts with a reduced basement lithology (basement-hosted deposits; Hoeve & Sibbald 1978), encounters reductants in the basin such as volcanic units (Holk *et al.* 2003), or mixes with basement-derived, reduced fluids (Fayek & Kyser 1997). The source of the U in the basin model is from the breakdown of U-bearing detrital phases, such as

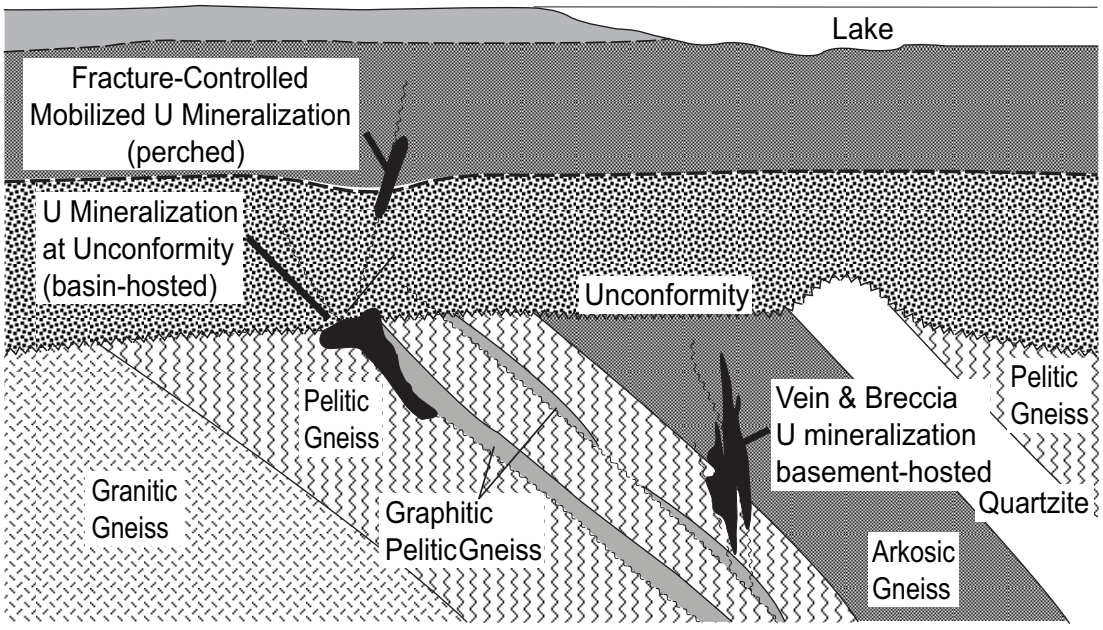

Fig. 8-1. General components and geology of Proterozoic unconformity-related uranium deposits.

Short course co-sponsored by the the SGA and MAC, Québec City, May 2008, p. 161-219

phosphates, tourmaline, monazite, zircon and uraninite, by basinal fluids in deep basin paleoaquifers. In either model, the composition of the basin fill influences the prospectivity of a basin because both use basinal brines to form the deposit.

Fluids associated with these deposits can produce significant alteration zones in the overlying sandstone or in the basement rocks around the U mineralization (Hoeve & Quirt 1984). This alteration tends to be different in both character and extent in basin-hosted and basement-hosted deposits. In the former, illite or kaolin alteration, both distal and proximal, is predominant over chlorite. In contrast, basement-hosted deposits have illite predominant in the distal alteration zone up to about 100 m from the U mineralization, and chlorite is normally the major alteration mineral in the proximal (within 10 m) alteration zone. The presence of a reductant, such as graphite, and of alteration zones are among the major indicators of U enrichment (Fig. 8-1). Exploration techniques that exploit these features include airborne and ground geophysics, surface geochemistry and clay typology (Sibbald & Quirt 1987). These methods help define favorable target zones, which normally are subject to further investigation via drilling (Thomas *et al.* 2000).

Sedimentary basins are segments of the Earth's crust that have been down-warped and filled with sediment during intermittent relative uplift and subsidence. They are the largest structures on the surface of our planet, host to all of the oceans, and comprise a significant proportion of the continents. Their sedimentary fill is an unrivalled record of Earth history, including the evolution of the biosphere, the geosphere, and how they relate to each other. Sedimentary basins are also the most significant sources of the energy-related commodities petroleum, gas, coal, and uranium. As with petroleum deposits, both syn-depositional and post-depositional processes are important in the formation of U deposits. Consequently, understanding critical processes involving fluid flow in basins is paramount for formulating genetic models and exploration strategies for U deposits.

Clastic sedimentary rocks, especially shale, sandstone and conglomerate, normally act as principal aquifers or aquitards for early fluids in basins, and control later basin-wide fluid events because of their variable permeability (Nesbitt 1990, Bjørlykke 1994, Kyser 2007). Moreover, the chemical and mineralogical heterogeneity of clastic rocks makes them highly sensitive indicators of fluid events, including those that form U deposits. Associated with the generation of aquifers and aquitards is a transfer of the inherently unstable original mineralogy in basin sediments to a more stable assemblage during burial diagenesis, with the release and removal of various components by the fluid. The typical change in the mineralogy of pelitic sediments is from quartz, montmorillonitic clays, plagioclase and zeolites to a mixture of quartz, feldspar, chlorite and muscovite (*e.g.*, Harrison & Tempel 1993, Hutcheon 2000). Quartz in these rocks is normally stable, but may be mobilized during pressure solution or as the temperature increases during burial. Sedimentary carbonates in these systems are inherently unstable at the outset, but most diagenetic fluids become saturated or nearly saturated with Ca–Mg–Fe carbonate during diagenesis.

Basin analysis has been used extensively by academic investigators to decipher Earth history, and by industry in the search for petroleum and gas products, but less so by those exploring for U. Most Earth scientists broadly define basin analysis as reconstructing the history of a sedimentary basin to understand the processes and mechanisms by which a basin formed (*e.g.*, Allen & Allen 1990, Miall 2000, Einsele 2006). Most basin analysis studies are done by those who work on Phanerozoic basins hunting for petroleum and who use fossils to indicate time. A critical question in analyzing basins for their metal potential is whether all basins were created equal throughout Earth history and why only a few have U deposits. The basic tenets of basin analysis for evaluating the potential of a basin to host mineral deposits have been discussed by Kyser (2007), particularly for Proterozoic basins in northern Australia that host world-class Zn–Pb–Ag, Cu, and U deposits.

Proterozoic Basins—why so much uranium?

Proterozoic basins, which host all known unconformity-related U deposits, are numerous, are extensive and are spatially related to Proterozoic orogens that helped create and fill them (Fig. 8-2). Preservation of so many Proterozoic basins poses a myriad of basic questions for those exploring for U including what processes formed them, what was the character of their basin fill, what was the nature of the fluid events that produced such vast concentrations of U and how do we use this information to find U deposits? The answers to these questions require an analysis of how the basins, and the fluids therein, originated and

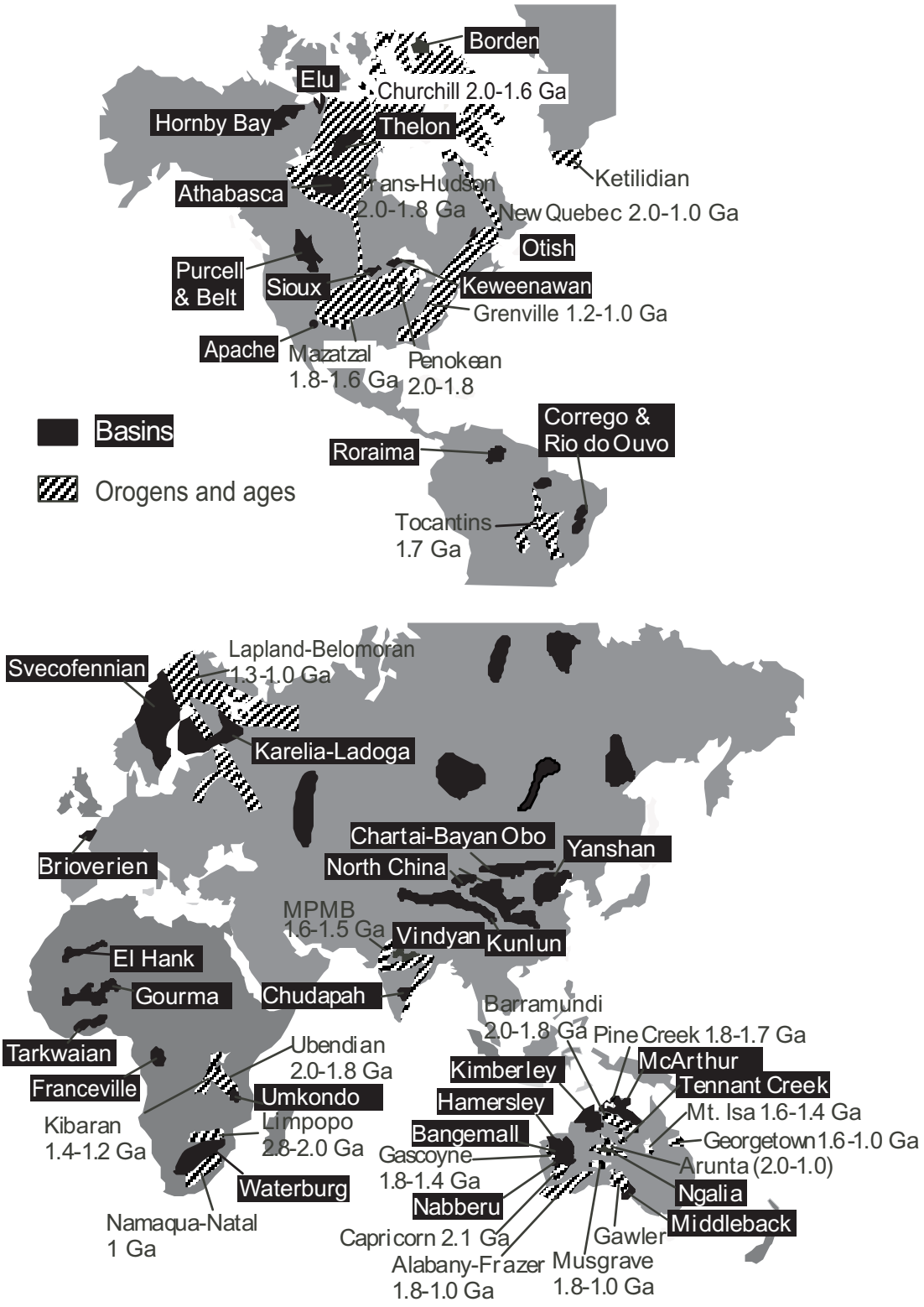

Fig. 8-2. Present global distribution of major Proterozoic basins and orogens. Modified from Kyser *et al.* (2000) and references therein.

changed with time and which factors are critical for the formation of unconformity-related U deposits.

All unconformity-related deposits currently being exploited occur in the Athabasca Basin in Canada or the Kombolgie Basin, a sub-basin of the McArthur Basin in northern Australia (Fig. 8-2). As a consequence, these two basins have been the focus of efforts to understand how the deposits form, with many studies focused on the deposits themselves, and a few on a more holistic view of the hydrothermal systems involved. Indeed, these two basins, which have several similarities, also have some marked differences in their evolution, fluid histories and styles of U mineralization (Kyser *et al.* 2000). Although deposit models are guiding much of the current exploration effort for unconformity-related deposits, they lack predictability given the low success rate of finding new deposits, and so must be refined to expose the critical elements needed to form the deposits.

Other Proterozoic unconformity-related deposits not yet exploited but under study include the Kiggavik trend deposits proximal to the Thelon Basin in Canada, the Karku deposit in the Pasha-Ladoga Basin in northwestern Russia and the Kintyre deposit associated with the Gascoyne orogeny in the Yeneena Basin of Western Australia (Fig. 8-2). Uranium showings associated with other Proterozoic basins include the Otish Basin in Quebec, and these bear resemblance to unconformity-related U deposits (Fig. 8-2). Some of the deposits that were exploited in the Beaverlodge area of Canada and the Rum Jungle area of the Alligator River Uranium Field (ARUF) in Australia also have affinities to unconformities, but these deposits are older than the U-rich Athabasca and Kombolgie basins. Although all of these deposits and showings share some of the same attributes as unconformity-related deposits in the Athabasca Basin, there are some important differences, and both reveal the key processes involved to refine deposit models for exploration. For any model to be effective in exploration, it must have the predictive capacity for locating favorable areas for deposits as well as for indicating why seemingly favorable areas lack any significant mineralization.

The Paleoproterozoic era (2500–1600 Ma) was a period of Earth history characterized by substantial orogens associated with the assemblage of the megacontinents (Fig. 8-3) of Arctica

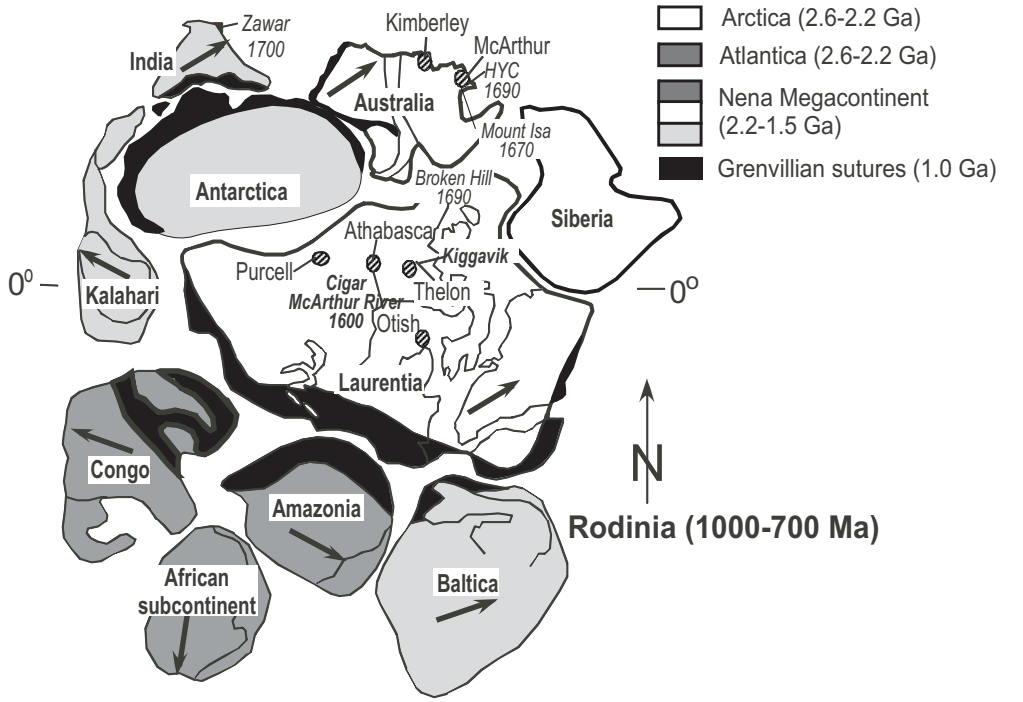

Fig. 8-3. One possible scenario for the assemblage of continents at 1000-700 Ma. Also shown are the continents of Arctica, Atlantica, the Nena megacontinent, and Grenvillian sutures. The arrows indicate direction of drift with the breakup of Rodinia and also shown are the locations of major Proterozoic basins and ore deposits on Laurentia and Australia. After Kyser *et al.* (2000).

(Canada, Siberia and parts of Greenland) and Atlantica (Africa and South America). Growth of Arctica occurred during the Paleoproterozoic through the beginning of the Mesoproterozoic with the accretion of Baltica, North America and East Antarctica into the larger continent of Nena (Rogers 1996, Zhao *et al.* 2002, Cawood *et al.* 2007). Among these orogens, the coeval Barramundi orogen in Australia and Trans-Hudson Orogen in Canada (2.0–1.8 Ga) are particularly significant for the formation of basins that host unconformity-related U deposits (Fig. 8-2).

The end of the Paleoproterozoic and beginning of the Mesoproterozoic was marked by the general termination of orogens, and a period of continental readjustment and relative tectonic quiet for about 500 m.y., during which several large intracratonic basins formed and evolved. During this period, the basins and the fluids they contained would have been affected by far-field tectonic events associated with the readjustment, which resulted in changing the hydraulic gradients within the basins. Atlantica and other continental blocks would have been accreted to Nena during the Grenville event at *ca*. 1.0 Ga to form the supercontinent Rodinia (Fig. 8-3). Near the termination of the Proterozoic, the Earth became agitated once again as the megacontinent Rodinia was tectonically dissected into several fragments, mainly along suture zones formed previously (Rogers & Santosh 2003). As a consequence, many of these basins remained intact, and would remain so unless affected by later tectonic events.

During the Paleoproterozoic, blue-green algae, simple bacteria, and simple eukaryotic green algae in the oceans produced organic matter that occasionally resulted in accumulations of microbial matter (Knoll *et al.* 2006). For unconformity-related deposits, some of these accumulations were deformed and metamorphosed into graphite in the steeply dipping Paleoproterozoic metasedimentary rocks that would comprise favorable basement rocks that floored the basins. More importantly, the absence of land plants and the resulting lack of stable soils would have rendered the alluvial plain environment without cohesive riverbanks, preventing streams from developing meandering systems and producing instead braided streams that dominated the terrestrial landscape, forming extensive sand and gravel-covered braid plains (Miall 2000). As a result, very little mud is found in Proterozoic sedimentary successions deposited in fluvial environments, and these serve as the aquifers for later fluid events related to the deposits (Hiatt 2000).

Minerals that can be used to infer paleoenvironmental conditions during the Paleo-proterozoic to Mesoproterozoic, such as pyrite produced by bacterially mediated sulfate reduction, are preserved in sedimentary rocks, as are "evaporites" in the form of bedded sulfate phases and casts of halite crystals. Substantial deposits of Mn occur and enormous deposits of banded iron gave way to abundant red-bed Cu deposits. During the Archean and early Paleoproterozoic, U was deposited in placer deposits as quartz-pebble conglomerate, but these become rare after the Paleoproterozoic, perhaps related to changes in oxygen levels in the atmosphere. In the Late Paleoproterozoic to Mesoproterozoic, formation of economic U deposits shifted to the subsurface of intracratonic basins as oxidized ground waters and basinal brines mobilized and transported U^{6+} that could be concentrated by effective reductants.

Reconstruction of the continents during the Neoproterozoic indicates that many of the large intracratonic basins that host unconformity-related U deposits were spatially associated with orogens initiated during the Paleoproterozoic (Fig. 8-2) and subsequently reactivated (Tack *et al.* 2001). Much of the reactivation occurred near the end of the Mesoproterozoic and beginning of the Neoproterozoic during the Grenville event and the subsequent initial break-up of the megacontinent (Fig. 8-3). Break-up finally was achieved at *ca*. 900–700 Ma, although paleomagnetic data suggest it was a drawn-out and complex process (Li *et al.* 2004, Zhao *et al.* 2006).

Unconformity-related deposits are composed of veins, pods and massive accumulations of uraninite that were deposited close to basal unconformities between Proterozoic red-bed sedimentary rocks and underlying metamorphosed Archean and Paleoproterozoic basement rocks, particularly metasedimentary rocks. Most of the basins that still exist are at most 1–3 km thick and most are flat-lying, unmetamorphosed and pervasively altered. When preserved, the sedimentary units of these basins are mainly fluvial sandstone sequences derived from U-rich source areas and overlying basement rocks that have been paleoweathered, with variable preservation of a clay-altered hematitic regolith grading down through a chloritic zone into fresh rocks. However, the basin fill can be absent, having been removed by erosion, exposing basement rocks at the surface that

were originally just below the unconformity, such as around the Roraima Basin in Guyana and the Proterozoic basement rocks in much of Scandinavia.

THE ATHABASCA BASIN

The Athabasca Basin (Fig 8-4) has been the subject of several studies because of the world-class, unconformity-type U deposits it hosts, and serves as the "standard" to which other basins are compared for their U potential. It is possible that the Athabasca is a unique basin for the breadth, size and grades of unconformity-related U deposits it hosts, and that all basins hosting such deposits have some of the same properties as well, but were different in their evolution. Most studies have focused on the U deposits themselves or on the sedimentology of the basin, which are somewhat myopic approaches to take if the goal is to understand why mineralization occurs where it does. The results from these studies have been aptly summarized by a consortium of industry and government geologists associated with EXTECH IV (Jefferson & Delaney 2007), an effort to understand the Athabasca Basin and the deposits therein.

The Athabasca Basin hosts the largest and highest grade U deposits globally, which are currently the sole sources of U from Canada. The average grade for all mined unconformity deposits in the Athabasca Basin is 2% U (Gandhi 2007), five times the average grade of 0.4% for the Australian unconformity-related deposits. The major deposits include Key Lake, Cluff Lake and Rabbit Lake, which have been mined out, and McClean Lake and McArthur River deposits (Fig. 8-5). Other large, exceptionally high grade unconformity-related deposits currently being developed include Cigar Lake, which averages almost 20% U, only slightly less than McArthur River.

General geology

The Athabasca and Thelon Basins are located in the western Churchill province between the eroded remnants of two major orogenic belts, the 1.8 Ga Trans-Hudson orogen to the southeast and

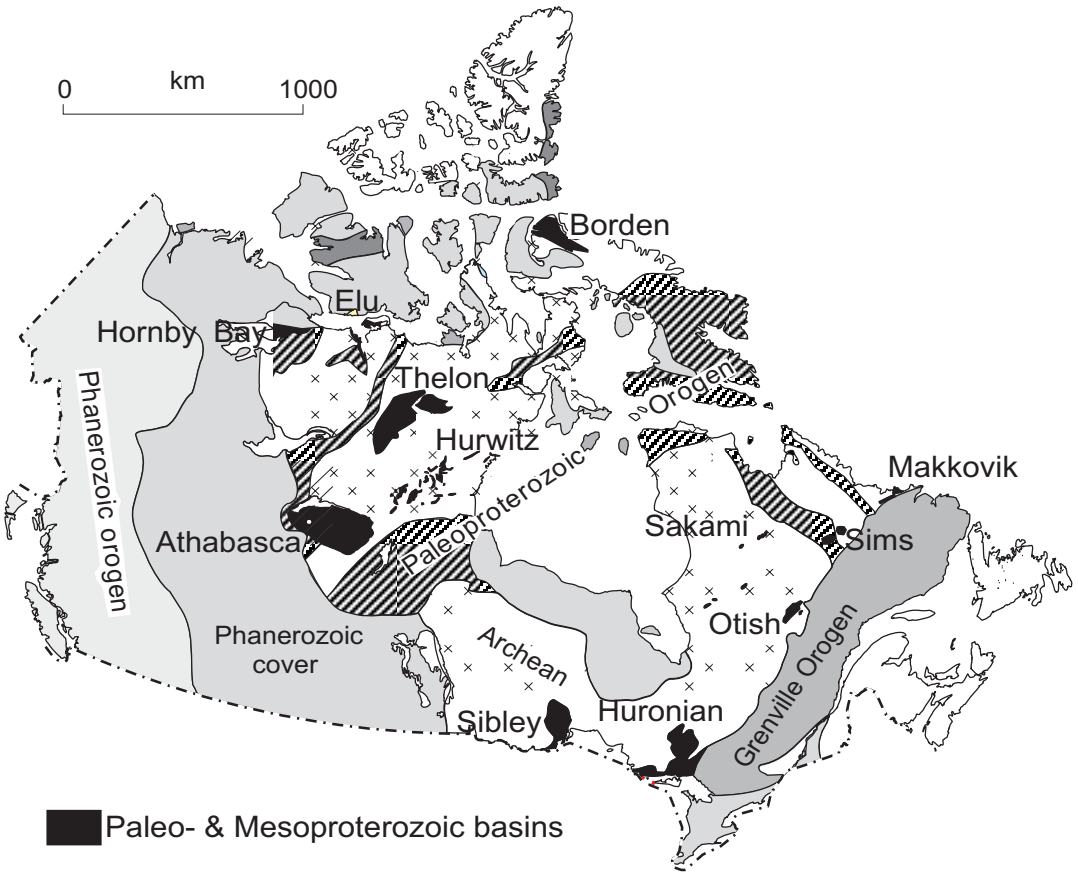

Fig. 8-4. General geology and locations of major Paleoproterozoic and Mesoproterozoic basins and major orogens in Canada. Modified from Jefferson *et al.* (2007).

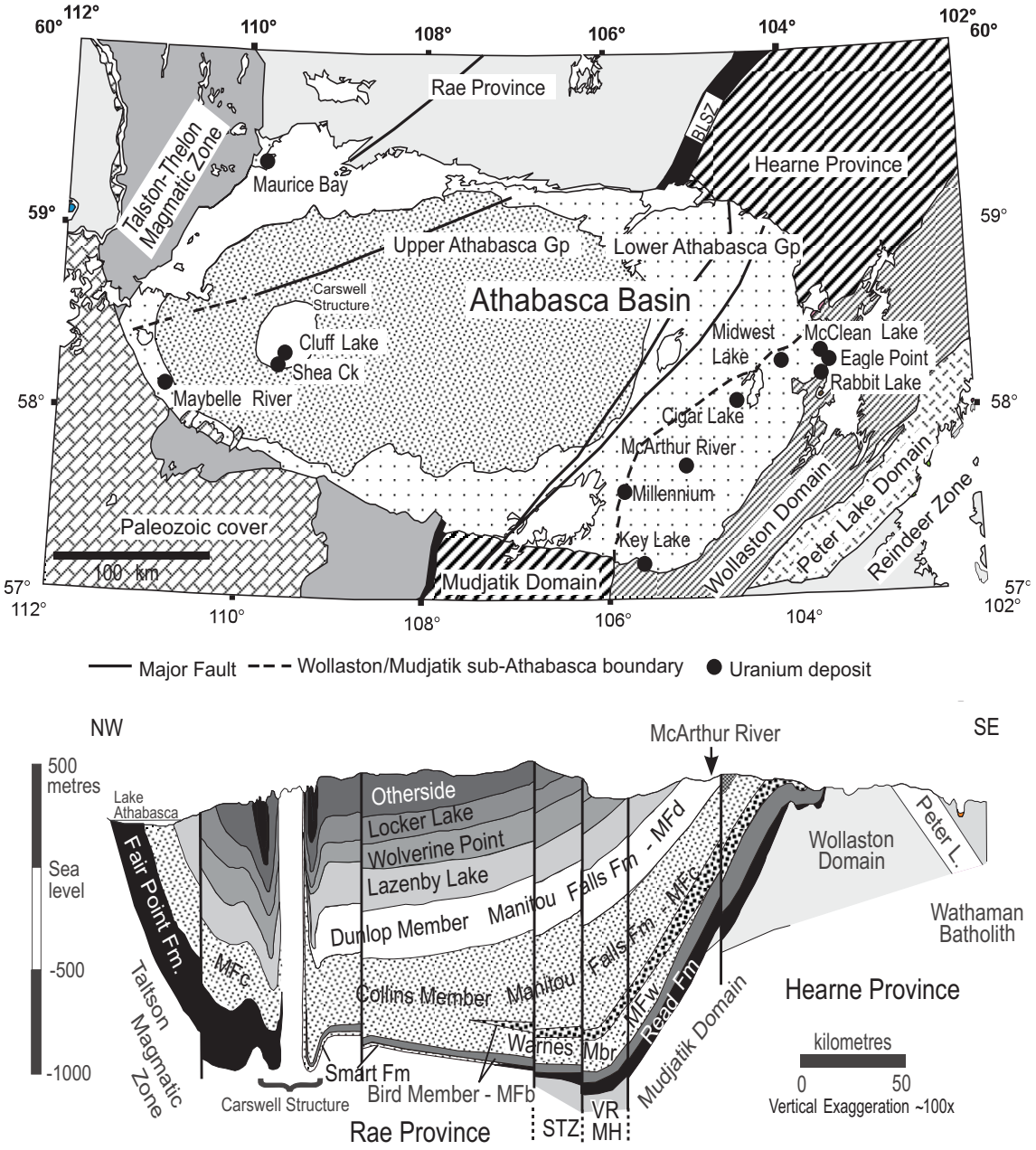

Fig. 8-5. **(a)** General geology of the Athabasca Basin showing various domains that make up the basement units and location of various unconformity-related deposits. **(b)** Generalized cross section from NW to SE of the Athabasca Basin showing the stratigraphic units and their distribution. Formation and member names from Jefferson *et al.* (2007).

the 1.9 Ga Talston magmatic zone to the northwest (Fig. 8-5). These orogenic belts accommodated the convergence of the Slave and Superior provinces (*e.g.*, Hoffman 1988) and formed the Rae and Hearne provinces. Voluminous granitoid intrusive rocks within these orogens were probably the major source of the U in the deposits.

In the eastern part of the Athabasca Basin, the great majority of mines and prospects are located where the Athabasca Group unconformably overlies the transition between the western Wollaston and eastern Mudjatik basement domains (Fig. 8-5). The basal Wollaston domain includes graphitic units, with many deposits located at the metamorphosed contact between Archean granitoid gneisses and these graphitic metapelite units (Fig. 8-5).

Deposits and prospects in the basement complex of the Cluff Lake area are also associated with graphitic units close to the overturned basal unconformity of the Athabasca Group (Laine *et al.* 1985). High grade U intersections have also been reported from Maybelle River and Shea Creek in the western Athabasca Basin (Fig. 8-5). These intersections are also associated with graphitic shear zones in the underlying basement in the Taltson Magmatic Zone that can be traced as EM conductors under the Athabasca Basin toward the Virgin River shear zone (Wheatley & Cutts 2006, Pană *et al.* 2007, Card *et al.* 2007).

The Athabasca Basin (Fig. 8-6) formed as a series of NE–SW-oriented sub-basins (Armstrong & Ramaekers 1985). The maximum age of the Athabasca Basin is constrained by the timing of rapid exhumation of the Trans-Hudson orogenic belts to the east of the basin at 1750 Ma (Kyser *et al.* 2000, Alexandre *et al.* 2007) whereas the minimum age comes from dates of 1640–1620 Ma for early diagenetic fluorapatite (Rainbird *et al.* 2003a) and constraints on deposition of the Wolverine Point Formation at 1644 ±13 Ma (Rainbird *et al.* 2007). Carbonaceous marine shale of the Douglas Formation (Fig. 8-6) was deposited later at 1541 ±13 Ma (Creaser & Stasiuk 2007). Sub-basin formation was controlled by major NE–SW Hudsonian-age faults rooted in underlying Paleoproterozoic metasedimentary rocks and Archean gneiss.

The Athabasca Group makes up the sedimentary basin fill, and consists of flat-lying, quartz-rich sandstone and conglomerate that is interpreted to have been deposited in major river systems and near-shore to shallow shelf environments (Ramaekers 1990, Ramaekers *et al.* 2007).

Fill in the Athabasca Basin is fluvial deposits of gravel and sand, with four major depositional sequences separated by basin-wide unconformities that record deposition and erosion during 200 m.y. (Jefferson *et al.* 2007). The Athabasca Basin has been interpreted as an intracontinental basin, although the basin is capped by marine sandstone and carbonate units. There is no evidence that the Athabasca Basin region was associated with mafic magmatism (Buchan & Ernst 2004).

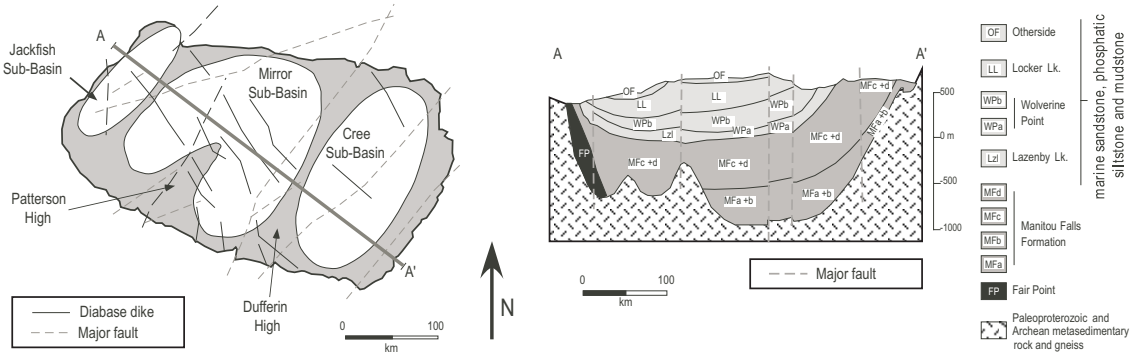

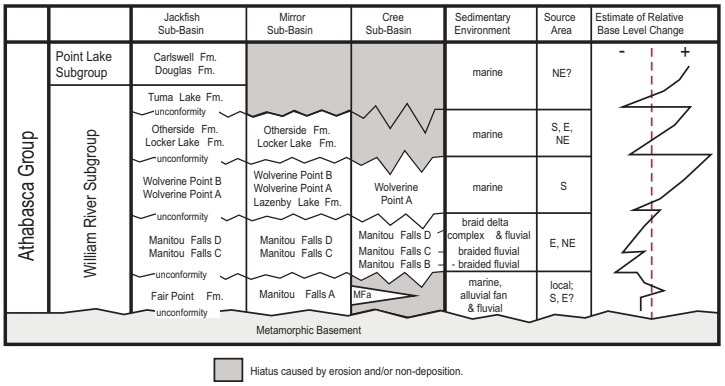

Fig. 8-6. General stratigraphy of the Athabasca Group in various sub-basins of the Athabasca Basin along with sedimentary environment and source based on paleocurrents. Modified from Hiatt & Kyser (2007).

The basal sequence of the Athabasca Group (Manitou Falls and Fair Point formations) consists of permeable coarse- to medium-grained, hematite-rich conglomerate and sandstone (Fig. 8-6) with paleocurrent directions predominantly from the east (Ramaekers *et al.* 2007). In the Manitou Falls Formation (or Read Formation and Warnes, Collins and Dunlop Members shown in Fig. 8-5), hematite and brookite are disseminated along thin stratigraphic horizons, indicating local oxidation of heavy mineral suites and removal of soluble components (Jefferson *et al.* 2007). The basal portion of the Manitou Falls Formation, primarily Manitou Falls A and B and most associated with the deposits (Fig. 8-6), is composed of coarse-grained conglomerate beds with attributes that reflect deposition in high energy braided streams, or alluvial fan settings. This lower coarse-grained interval is overlain by finer grained sandstone with minor conglomerate that is marked by abundant trough cross bedding and relatively rare siltstone layers that average three to five centimetres thick. This middle interval represents deposition in more distal braided stream environments, and due to the much better sorting, has coarse-grained textures, more extensive quartz cement, and lower hydraulic conductivity.

The sandstone layers that make up the upper third to half of the Manitou Falls Formation, primarily Manitou Falls B, C and D (Fig. 8-6), consist of medium-grained sandstone with abundant ripple marks, rare thin mudstone layers that average one to three centimetres thick, and mud rip-up clasts. This sandstone is consistent with deposition in lower energy distal braided stream systems to possibly braid deltas. The detrital material that makes up the Manitou Falls sandstone units is composed of 95–100% well rounded quartz with minor muscovite and rare heavy minerals, such as zircon and apatite. The absence of feldspar and rarity of any other minerals further suggests relatively long distance transport and intense weathering in the source area.

Tracking stratigraphic units in drill core reveals that there are two unconformity-bounded stratigraphic sequences in the deposit-rich eastern portion of the Athabasca Basin (Hiatt & Kyser 2007). These are marked first by coarse-grained units that appear in association with topography on the basal unconformity. As suggested by Ramaekers (1990), the Athabasca Basin can be divided into sub-basins (Fig. 8-6). These early coarse-grained basal units probably mark the time when subdivision of the overall Athabasca was at its greatest with alluvial fans forming adjacent to paleo-highs, and high energy braided streams flowing in the deeper parts of the sub-basins. After this initial stage of basin formation, the source area shifted further to the east and the braided streams flowing into the Athabasca sub-basins began filling them with sediment. Sedimentation and basin subsidence continued, resulting in a rise in base level, so that by the time the uppermost portion of the Manitou Falls Formation was deposited, the braided stream systems had become low energy and distal. This relationship is reflected in stratigraphic cross sections that indicate that the upper portion of the Manitou Falls on-laps onto the basal unconformity in the easternmost parts of the basin (Hiatt & Kyser 2007). One consequence of this basin evolution is that the basin fill was composed in large part of weathered equivalents of the basement rocks that floored the basin and the terranes to the east of the basin.

The sandstone units of the Manitou Falls Formation are unconformably overlain (Figs. 8-5 and 8-6) by a succession of less permeable marine sandstone, phosphatic siltstone, and phosphatic mudstone layers, the Lazenby Lake Formation, Wolverine Point Formation, respectively, which are in turn overlain first by sandstone (Locker Lake, Otherside and Tuma Lake Formations, and the William River Subgroup), then by shale (Douglas Formation), and finally by stromatolitic dolomite (Carswell Formation). These marine units in conjunction with the unconformities would be ideal environments in which evaporated seawater could permeate into the lower units.

There is a well developed paleo-regolith on the crystalline basement rocks underlying the Athabasca Group that extends to a depth of several metres. The paleo-regolith has an upper portion of strong red hematitic alteration that grades downward through greenish chloritic alteration into fresh basement rock (Fraser *et al.* 1970, MacDonald 1985, Ramaekers 1990). A downward progression from kaolinite to illite and chlorite is common through the regolith profile and a bleached zone overprints the top of the red zone of the paleo-weathered basement and basal units of the Athabasca Group, particularly proximal to mineralization.

Graphitic units, which are stratigraphically low in the metasedimentary sequences of the western Wollaston and eastern Mudjatik basement domains, unconformably overlie older granitoid

gneiss and form the basal interface with the overlying Wollaston Supergroup. Many significant deposits are located at the metamorphosed contact between Archean granitoid gneiss and graphitic metapelite in the late Paleoproterozoic basal Wollaston Supergroup (Yeo & Delaney 2007). These graphitic units are less competent than proximal quartz-rich lithologies and so were more affected by regional deformation. Quartzite ridges, which are compressional pop-up structures bounded by outward-divergent faults often associated with graphitic units (Earle & Sopuck 1989), splay out into kink folds and bedding-parallel shears in the Manitou Falls Formation.

The Athabasca Group sedimentary rocks and the basement complex are cut by a series of northwest-trending mafic dikes, which were emplaced along reactivated fractures during post-Athabasca tectonic activity at 1270 Ma (LeCheminant & Heaman 1989). The dikes are believed to be related to the Mackenzie dike swarm, and represent the only igneous activity throughout the evolution of the basin. The sedimentary fill in the Athabasca Basin is presently 1 to 2 km thick (Fig. 8-6). Temperature estimates derived from fluid inclusions, however, indicate that the sedimentary sequence may have reached a thickness of *ca.* 5 km during peak diagenesis (Pagel *et al.* 1980).

Alteration

A detailed paragenesis of alteration minerals in the Athabasca Group and basement rocks was developed by Kotzer & Kyser (1995), and refined by Fayek & Kyser (1997) and Alexandre *et al.* (2007). These paragenetic relationships are based on petrography, isotopic compositions, geochronology and analyses of fluid inclusions in altered sandstone and metasedimentary rocks proximal to, and distal from, the U deposits. A revised paragenesis based mainly on these studies is shown in Figure 8-7. This paragenesis is generally applicable throughout the basin.

The basin-filling sandstones presently consist of *ca*. 95–100% detrital quartz (+ minor heavy minerals) and 0–5% secondary minerals by volume (Fig. 8-7). Fluid inclusions in the detrital quartz are aqueous or CO_2+H_2O and most have high homogenization temperatures (*ca*. 400°C), consistent with derivation from relatively high-grade metamorphic rocks not unlike those of the basement and adjacent terranes in the Trans-Hudson Orogen. Detrital fluorapatite, monazite and zircon occur within the detrital quartz grains, but rarely as detrital interstitial minerals, indicating that these heavy minerals may have been removed by fluids flowing through the sandstone. Zircon is variably preserved in some fine-grained units, but is absent

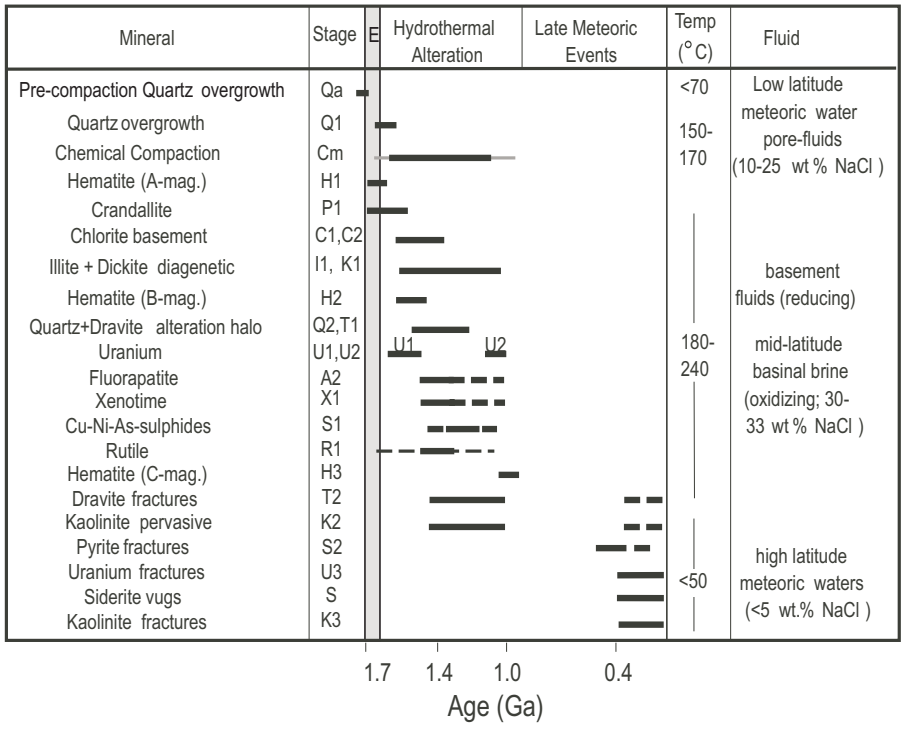

Fig. 8-7. Generalized mineral paragenesis of alteration in the Athabasca Group sandstone and underlying basement rocks. Also indicated are the types of alteration, their temperatures and the origin of the fluids. E means Early diagenesis. Modified from Kotzer & Kyser (1995) and Hiatt *et al.* (2007).

or altered elsewhere despite its common occurrence as inclusions in detrital quartz grains (Fayek & Kyser 1997). Detrital zircon studies in the Athabasca Basin (Rainbird *et al.* 2007) tend to be focused in well cemented or fine-grained units where zircon is preserved and many of the zircon grains analyzed are probably from within detrital quartz grains.

As with most basins, the first major diagenetic events recorded in the clastic sedimentary rocks of the Athabasca Basin are early hematite and quartz overgrowths. However, the apparent character of the basin fill is different than most modern basins where detrital smectite and plagioclase generally result in authigenic illite, feldspar and carbonate as the main diagenetic phases rather than the kaolinite–illite assemblage without carbonate that characterizes the Athabasca Basin. In addition to quartz and heavy minerals, kaolinite and muscovite with minor amounts of montmorillonite and chlorite were detrital components in the basin (Hoeve & Quirt 1984, Kotzer & Kyser 1995, Hiatt & Kyser 2007). Regional diagenesis converted this to a mixture dominated by dickite, with lesser amounts of illite and chlorite (Quirt & Wasyliuk 1997, Earle *et al.* 1999, Quirt 2003, Wasyliuk 2002). Illite crystallinity indicates that burial diagenetic temperatures were near 200°C (Hoeve & Quirt 1984, Alexandre *et al.* 2007), similar to temperatures from fluid inclusions in quartz (Pagel *et al.* 1980). Altered mafic heavy mineral laminae consist of zircon and quartz framework grains surrounded by a matrix of secondary hematite, clay minerals, and Th-rich Al phosphate ± sulfate (APS) minerals (Percival 1993, Mwenifumbo & Bernius 2007). Thorium anomalies in coarse-grained beds correlate with APS minerals and are interpreted as alteration products of monazite that would have released U (Jefferson *et al.* 2007, Mwenifumbo *et al.* 2007).

Early diagenesis of the Athabasca Basin (Fig. 8-7) produced quartz overgrowths (Q1), a crandallite-group phosphate mineral (P1) and hematite (H1) on detrital quartz in the Manitou Falls Formation (Kotzer & Kyser 1993, 1995, Derome *et al.* 2005). Kotzer *et al.* (1992) suggested that the early hematite (H1) throughout the Athabasca corresponds to a paleomagnetic direction (A-type) with an age of 1600–1750 Ma. The quartz overgrowths have fluid inclusions with homogenization temperatures of 150–170°C, between 10 and 25 wt.% NaCl and isotopic compositions are characteristic of low latitude, near coastal meteoric waters (Kotzer & Kyser 1995, Hiatt *et al.* 2007). The high salinity values suggest that these waters interacted with evaporites and minerals in the basin and the high temperatures indicate burial depths of 3–4 km or a steeper than average geothermal gradient. The crandallite-group diagenetic mineral present (APS) has a composition consistent with solid solution between goyasite and crandallite and is F-poor (Fayek & Kyser 1997). An abundance of the crandallite-group mineral and authigenic xenotime overgrowths on altered detrital zircon is associated with the hydrothermal clay and silicate minerals that comprise the alteration halo around U deposits in the basin.

A basin-wide mineral assemblage consisting of variable proportions of *cv*-1M illite (I1) and dickite (K1) was produced by the alteration of detrital silicates during peak diagenesis of the Athabasca Group sedimentary rocks (Percival 1993, Kotzer & Kyser 1995, Laverret *et al.* 2006). Thus, in the Athabasca Basin, the predominant diagenetic clay assemblage is kaolin ± illite. Areas proximal to faults, fractures and the ore deposits in sandstone are hydrothermally altered to illite (I1) and kaolinite (K2) intergrown with euhedral quartz (Q2) and dravite (T1), Al–Mg chlorite (C2) and hematite (H2), with varying amounts of uraninite (U1) (Fig. 8-7) This hydrothermal alteration is largely contemporaneous with the later stages of basin-wide, peak diagenetic clay mineral assemblage of illite and postdates the early overgrowths of quartz (Q1).

In metasedimentary basement rocks and in sandstone proximal to the unconformity throughout the basin, rosettes of trioctahedral chlorite (clinochlore, C1) infill pore spaces. However, varying amounts of dioctahedral chlorite (sudoite, C2) occur in hydrothermally altered sandstone and metasedimentary rocks of the basement near unconformity-related U deposits and fault zones that intersect the unconformity (Hoeve & Quirt 1984, Wilson & Kyser 1987, Kotzer & Kyser 1995). Sudoite also occurs in fault zones up to 300 m above the basal unconformity, suggesting that these faults allowed fluid from the basement access to much higher stratigraphic levels (Kotzer & Kyser 1995). Up to five types of chlorite have been documented in the basement (Quirt & Wasyliuk 1997), with Fe-rich chlorite normally associated with the mineralizing event (Alexandre *et al.* 2005).

Illite from the Shea Creek deposit in the Athabasca Basin occurs in two populations, a tv-1M

polytype that occurs in altered sandstone near the unconformity or along faults and a cv-1M poly-type that is bigger, lath-shaped and is dominant in barren regional sandstone (Laverret *et al.* 2006). Differences between these two polytypes are interpreted to reflect kinetics or a change in flow of the fluids wherein the tv-1M illite is favored in environments with high fluid–rock ratios and supersaturation of the fluids proximal to mineralization. However, comparison with other areas where alteration occurs but there is no U mineralization (*i.e.*, barren areas) such as the Spring Point area, eastern Athabasca (Alexandre *et al.* 2008) and the Wheeler River area in the west, suggests that the distribution of these two polytypes is not related to the presence or lack of U mineralization.

A regional anomaly in illite, chlorite and dravite relative to dickite occurs in a corridor 10 to 20 km wide that extends 100 km northeast from Key Lake to Cigar Lake (Earle *et al.* 1999) over an aeromagnetic low (Fig. 8-8). The dravite is concentrated along fractures and disseminated in altered zones, overprinting illite, chlorite, and kaolinite. The illite anomaly encompasses all known U deposits and prospects in the southeastern part of the basin, including Key Lake, McArthur River, and the Millennium prospect, and is discontinuous around the Cigar Lake mine and the Dawn Lake–Rabbit Lake areas. Regional illite + kaolinite assemblages represent terrestrial strata (most of the Athabasca Group) whereas illite + chlorite (sudoite) assemblages represent marine strata (Wolverine Point and Douglas formations) (Hoeve & Quirt 1984). Separate linear tourmaline and chlorite alteration zones (Fig. 8-8) suggest discrete basement sources for B and Mg+Fe (Jefferson *et al.* 2007). Despite the favorable alteration and basement rock lithologies throughout the entire area, deposits are very localized.

Uranium deposits

Unconformity-related U deposits can be classified on the basis of associated metals as (1) simple, being primarily U and having a simple mineralogy of uraninite, or (2) complex, being polymetallic and having a diversity of sulfides and arsenides along with the uraninite (Everhart & Wright 1953, Beck 1969, Ruzicka 1989, 1996, Fayek & Kyser 1997, Thomas *et al.* 2000). Simple deposits (Fig. 8-9) are hosted in fractures and faults in the basement more than 50 m below the

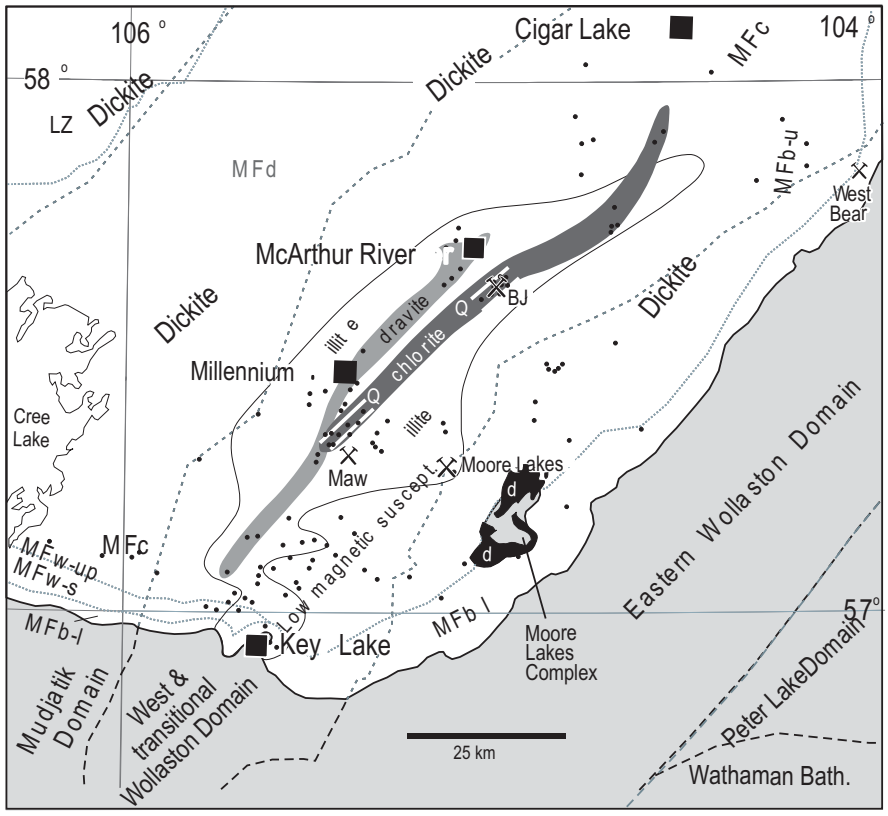

Fig. 8-8. General geology and alteration of the Athabasca Group along the corridor from the Key Lake to Cigar Lake deposits showing the areas of illite, dravite and chlorite relative to the background alteration of dickite. Squares represent deposits, dots are drill holes and white area is the extent of the basin, with subunits indicated. Q=quartz, d=dravite. Modified from Earle *et al.* (1999).

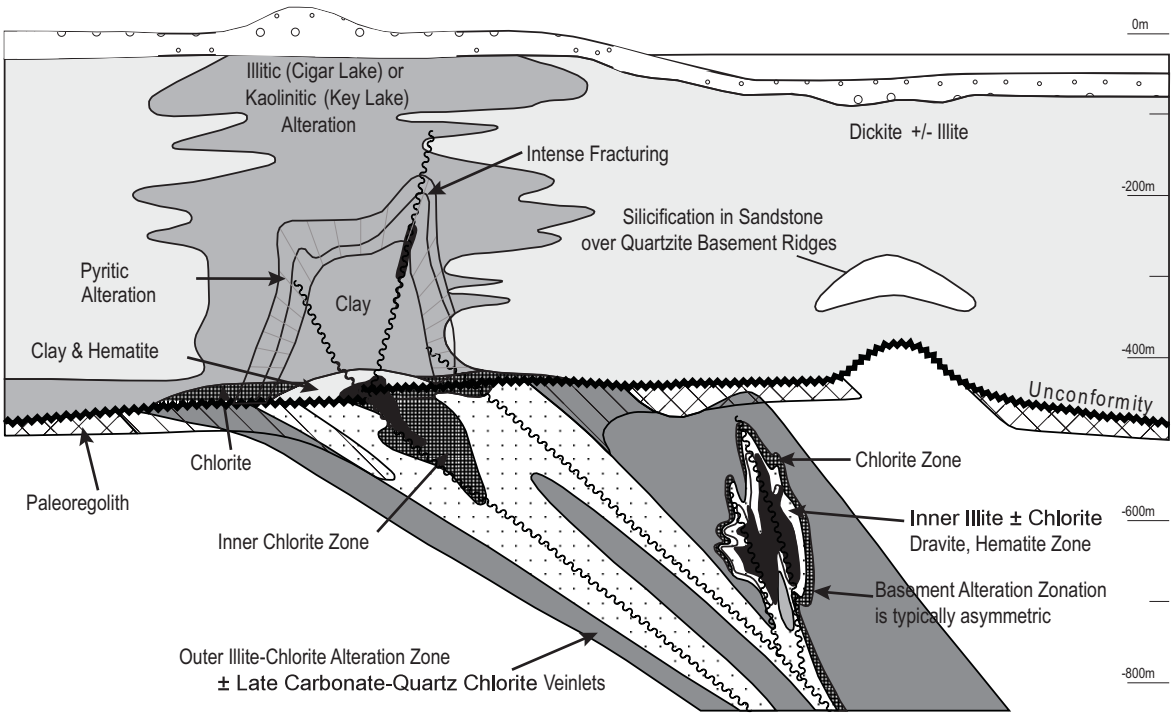

Fig. 8-9. General geological features of unconformity-related ore deposits in the Athabasca Basin. Basement-hosted, simple type deposit and basin-hosted, complex-type deposit and their associated alteration are shown.

unconformity and are composed primarily of uraninite (*e.g.*, McArthur River, Rabbit Lake, Eagle Point, McClean–Sue C deposits). In contrast, complex deposits (Fig. 8-9) are typically hosted by clay-altered Athabasca Group sandstone and conglomerate within 50 m of the unconformity and are characterized by Ni, Co, Cu, Pb, Zn, and Mo sulfide and arsenide minerals in addition to uraninite. Clay-bounded, massive ore occurs as elongate pods and linear ore bodies of a high grade core and lower grade halo along the unconformity and just above it in the overlying Athabasca Group (*e.g.*, Cigar Lake, Key Lake, Collins Bay and Midwest). At Cigar Lake, one pod is 1.9 km long, 50 to 100 m wide and 20 m thick (Andrade 2002). Many deposits have both these end-members.

The McArthur River deposit is hybrid, comprising one basement-hosted and three basin-hosted ore bodies, with the basement-hosted P2 ore body containing about half of the U in the total deposit (McGill *et al.* 1993). The sub-Athabasca basement host rocks at McArthur River consist of two distinct metasedimentary sequences, a hanging-wall pelitic sequence of cordierite- and graphite-bearing pelitic and pelitic gneiss, and a footwall sequence consisting of metaquartzite and silicified meta-arkose (McGill *et al.* 1993). This is characterized by an abrupt transition from nearly unaltered basement host rock into intense chloritic alteration and then into monomineralic high grade U mineralization (Fig. 8-9).

The Dawn Lake deposit consists of four zones, each having three or four separate NE–SW elongated, cigar-shaped ore bodies between 100 and 190 m long and 20 to 45 m wide. The Dawn Lake deposit is hosted by metapelite, calc-silicate rocks, biotite gneiss and pegmatite of the Wollaston Group (Chan *et al.* 2000). Alteration of the basement rocks around the deposit consists mainly of chlorite and illite (Quirt 1997). The orientation of the main controlling structure is a steeply west-dipping strike-slip fault system with predominantly horizontal displacement (Chan *et al.* 2000), which is atypical of basement-hosted unconformity type deposits in the eastern Athabasca Basin that are controlled by major NE/SE oriented reverse fault systems.

The Rabbit Lake deposit is hosted by Paleoproterozoic Wollaston Group supracrustal rocks, comprising interlayered meta-arkose and calc-silicate rocks in the hanging wall (upper gneisses), massive meta-arkose in the core of the ore zone, and partly graphitic calc-silicate rocks and dolomitic marble in the footwall (Wallis 1971,

Knipping 1974, Chandler 1978). Evidence of faulting is widespread and two major structures are recognized. The younger Rabbit Lake thrust fault, underlies the deposit, dips 30°SSE, and downthrows the Athabasca Group sedimentary rocks to the northeast at least 75 m against the crystalline basement. An older northeasterly trending and steeply dipping fault bounds the ore zone to the southeast (Sibbald 1978). Mineralization comprises several different generations of uraninite and coffinite, accompanied by several other minerals including euhedral quartz, dolomite, calcite, hematite, chlorite, and sulfide phases. A high-grade mineralized core is surrounded by a lower grade envelope of mineralization (Hoeve & Sibbald 1978).

Despite some differences, alteration assemblages of basement-hosted deposits are generally the same (Fig. 8-10). The earliest alteration phase involves intense illitization of feldspar, biotite and amphibole followed by alteration of biotite and illite

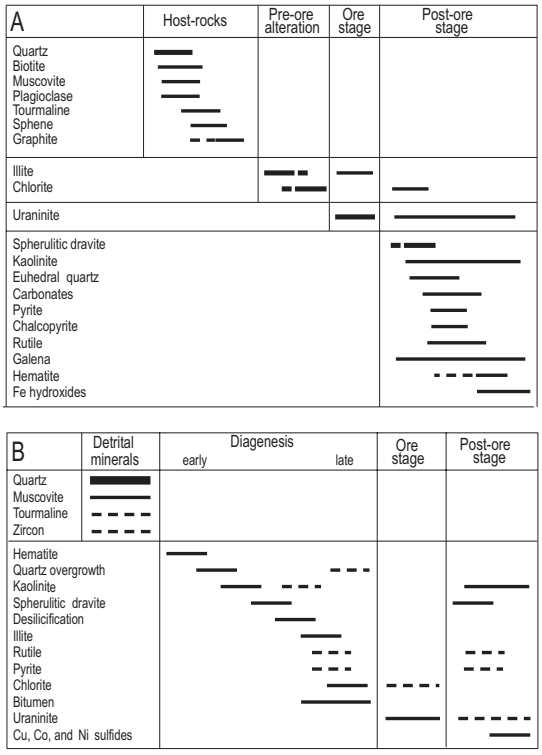

Fig. 8-10. Detailed mineral paragenesis of basement-hosted, simple-type deposits **(A)** and basin-hosted, complex-type **(B)** unconformity-related U deposits in the Athabasca Basin. The thickness of the lines indicates the relative abundance, while dashed lines indicate uncertain position in the paragenesis. From Alexandre *et al.* (2007).

to chlorite. The illitization process results in creation of voids, whereas chloritization is void-filling and can result in alteration without U mineralization if the voids are filled with chlorite (Alexandre *et al.* 2005). Illite is dominant distal to the ore zone, whereas chlorite is dominant proximal to the ore body. Initial U mineralization is manifest as uraninite (U1), which is massive at the McArthur River deposit, and precipitates in voids and open fractures created by pre-ore alteration at the Dawn Lake and the Rabbit Lake deposits. Uraninite crystals are commonly euhedral to subhedral or colloform, particularly at the McArthur River deposit, or have irregular shape as at the Dawn Lake and the Rabbit Lake deposits. Coarse-grained, 30 to 50 μm, euhedral illite (I2) is the only phase that accompanies uraninite precipitation (Fig. 8-10). Post-ore alteration is manifest as vein chlorite, euhedral quartz, spherulitic dravite, dolomite, and rare kaolinite. Uraninite has variably recrystallized to coffinite with release of radiogenic Pb, some of which precipitates as microscopic grains of galena in the uraninite. Pyrite, rutile, and rare chalcopyrite, bornite, pentlandite, cobaltite, and magnetite precipitated late as disseminated euhedral to subhedral grains.

The general paragenesis in the basin-hosted prospects is dominated by diagenetic and hydrothermal alteration. Early diagenesis during initial burial was characterized by hematite staining that indicates oxidizing fluids preceded quartz overgrowths and the precipitation of fine-grained kaolin and minor spherulitic dravite (Fig. 8-10). Desilicification is manifest as quartz dissolution accompanied by minor coarse-grained kaolinite and illite during peak diagenesis. Near the U mineralization, pre-ore alteration is manifest as illite preceding minor pyrite and rutile, indicating reducing conditions, followed by chlorite and minor euhedral quartz formed in open fractures. The ore stage is characterized by disseminated uraninite grains with chlorite rims or with no other minerals. The post-ore stage is characterized by kaolinite and some spherulitic dravite, pyrite and rutile, and occasionally abundant copper, nickel, and cobalt sulfide phases (Fig. 8-10). Uraninite alteration and recrystallization also occurred at this stage. Non-mineralized areas are characterized by the absence of pyrite, much lower amounts of clay alteration in general and chlorite in particular, and the absence of coarse-grained kaolinite.

Faults were important for focusing mineralizing fluids in these deposits (*e.g.*, Hoeve &

Sibbald 1978). Reactivated faults rooted in the basement and initially associated with the Trans-Hudson Orogen offset the unconformity by hundreds of metres, and some are associated with mineralization (Baudemont & Paquet 1996). In the McArthur River area, ore pods are localized where cross-faults intersect the P2 fault (Györfi *et al.* 2007) with mineralization mainly in reverse faults along graphitic units and in quartzite. Faults that were active during sedimentation appear to have been reactivated after lithification, and were conduits for hydrothermal fluid flow in the vicinity of ore deposits (*e.g.*, Hoeve & Quirt 1984). However, structure is not a definitive indicator of mineralization, except perhaps within the deposit itself to find additional ore (LeMaitre 2005). This is because there are identical structural environments to those that host the deposits, but contain no U. As with graphitic units in the basement or illite–chlorite alteration, a favorable structural environment is necessary for the deposit, but such an environment rarely hosts mineralization.

Anomalously high proportions of illite are observed in the 1 to 5% clay matrix of the Athabasca Group strata and in altered basement rock in the vicinity of the U deposits. This results in anomalous K_2O/Al_2O_3 ratios in the sandstone (Earle & Sopuck 1989), evident from spectral K–Th–U gamma ray and till geochemical data (Shives *et al.* 2000, Campbell *et al.* 2007). Illite–kaolinite–chlorite alteration halos are up to 400 m wide at the base of the Athabasca Group, thousands of metres in strike length, and extend several hundred metres above Cigar Lake (Bruneton 1993), McArthur River (Thomas *et al.* 2000) and Shea Creek (Kister *et al.* 2006). This alteration typically envelops the main ore-controlling structures. Pre-ore alteration minerals developed in the basement at 1670 to 1620 Ma and formation of the U deposits occurred at 1600 Ma (Alexandre *et al.* 2007), beneath at least 1500 m of strata, after early diagenesis and during peak, high temperature diagenesis.

Constraints on ore genesis

The isotopic compositions, phase relations and fluid inclusion characteristics indicate that the basinal fluid throughout the basin underwent salinity, temperature and ^{18}O increases relative to the fluid present when the quartz overgrowths formed from 15–30 wt.% NaCl, from 120–250°C and became more ^{18}O-rich (Kyser *et al.* 2000, Hiatt *et al.* 2007, Alexandre *et al.* 2007). These changes resulted from increasing burial depth and sustained water–rock interactions with the basinal sedimentary rocks over substantial time periods. Lack of any appreciable change in the δD values of the basinal fluid, except that associated with preferential hydrogen isotope exchange of alteration minerals near fractures with recent fluids having very low δD values (Wilson *et al.* 1987, Kyser *et al.* 2000), indicates that the basin-wide fluid in the basal units was not diluted with, or replaced by, other fluids (Fig. 8-11). Fluid compositions and pH were buffered in the basin by kaolin–illite at 200°C and by chlorite–illite in the basement, which fixed the pH to 5 (Kotzer & Kyser 1995, Kyser *et al.* 2000, Cuney *et al.* 2003, Kister *et al.* 2005). These fluids were oxidized, saline basinal brines capable

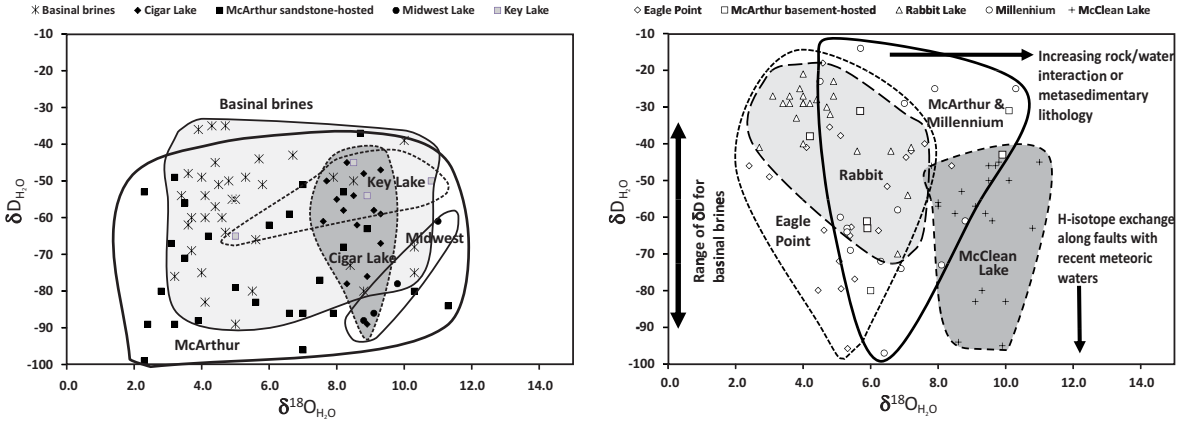

Figure 8-11. Left diagram shows the relationship between H and O isotopic compositions of fluids associated with diagenetic minerals that record basinal brines and fluids related to unconformity- or basin-hosted deposits in the Athabasca Basin. Right diagram shows same relationship for basement-hosted deposits, along with the effect of increasing interaction between fluids and metasedimentary lithologies having high $\delta^{18}O$ vales as well as the effect of preferential exchange of H isotopes on minerals near fractures that interact with modern meteoric fluids. Data from sources described in text.

of transporting U (Kotzer & Kyser 1995, Ruzicka 1996, Cuney *et al.* 2003).

The isotopic compositions of sudoite and clinochlore in the alteration haloes in metasedimentary basement rocks (Fig. 8-9) within the alteration haloes reflect a basement-derived fluid with a similar temperature, but different isotopic compositions relative to the basinal fluid (Fig. 8-11).

Calculated isotopic compositions of H and O for fluids associated with pre- and syn-ore alteration minerals in the basin-hosted deposits indicate that the isotopic compositions of the fluids that formed them are almost identical to those measured in peak diagenetic minerals (Fig. 8-11). Moreover, each deposit has quite a range of both H and O isotopic compositions. The range in O isotopic compositions reflects interactions of the fluid with distinct lithologies in the basement. The H isotopic compositions in all deposits in the Athabasca Basin are complicated by preferential exchange of H isotopes between alteration minerals near fractures and recent meteoric waters, resulting in δD values as low as –160‰ (Kotzer & Kyser 1995). This exchange has affected the δD value of the alteration minerals used to reflect the H isotopic composition of the mineralizing fluid, but also diagenetic minerals in fracture systems throughout the basin (Wasyliuk 2002).

In basement-hosted deposits, the ore fluid is also isotopically similar to the basinal fluid, indicating that the dominant fluid in the basement-hosted deposits is also from incursion of the basin fluid into the basement. However, there is also a fluid with a higher δD value recorded in some basement deposits that reflects a distinct origin in the basement (Wilson & Kyser 1987). Differences between the $\delta^{18}O$ values in fluids that formed basement-hosted deposits result from interaction of basinal fluids with various lithologies, some of which are ^{18}O-rich and thus change the O isotopic composition of the fluid. For example, the $\delta^{18}O$ values of fluids associated with the basement-hosted McClean Lake deposit are generally higher than those for the proximal Rabbit Lake. Given that H isotopic compositions of fluids are unlikely to be changed during rock/fluid interaction because rocks have very little H in them whereas the fluids do, the H isotopic compositions of the fluids reflect the origin of the fluid whereas the O isotopic compositions reflect the lithologies and conditions during rock/fluid interactions. The similarity in H and O isotopic compositions of both basin- and basement-hosted deposits with the basinal brines is consistent with this fluid being dominant in formation of the deposits. However, a basement-derived fluid is also involved, particularly evident from the compositions of fluids in basement-hosted deposits.

Initial Sr isotopic compositions of fluids in the basin and basement rocks, reflected by the $^{87}Sr/^{86}Sr$ ratios of chlorite, illite and dravite (Fig. 8-12), are also consistent with mixing of two isotopically and chemically distinct fluids in the vicinity of faults as the process by which U was precipitated, similar to that suggested by isotopic systematics in the clays and silicate minerals (Kotzer & Kyser 1995) and chemical compositions of fluid inclusions in quartz (Derome *et al.* 2005, Richard *et al.* 2008). The $^{87}Sr/^{86}Sr$ ratio in typical basement rocks and basin rocks in the Athabasca Basin as a function of time indicate that basin-hosted (complex-type) U mineralization has Sr isotopic compositions in its uraninite that have a significant input of basement Sr, whereas basement-hosted uraninite (simple type) is more consistent with the ratios expected from basinal fluids (Kotzer & Kyser 1995). The low $\delta^{18}O$ values of the uraninite indicate it has exchanged oxygen isotopes with relatively recent meteoric waters.

Rb–Sr and Ar–Ar isotope systems in illite from the Manitou Falls Formation record oldest ages of 1500 Ma (Bray *et al.* 1988, Wilson *et al.* 1987, Kotzer & Kyser 1995), which is coincident with the paleomagnetic age of 1450–1600 for peak diagenetic hematite (Kotzer *et al.* 1992), but younger than the ages of 1600 Ma for the primary uraninite in the deposits (*e.g.*, Fayek & Kyser 1997, Alexandre *et al.* 2007). This would indicate that fluids were resident in much of the Manitou Falls Formation during and after the initial U mineralizing event at 1600 Ma. Ages for some illite associated with later kaolinite and dravite (K2, T2) are 900–1000 Ma, which are coincident with another distinct paleomagnetic age for later hematite (H3) and recrystallization ages of uraninite (U2). This age is found in the U–Pb system in uraninite as either a lower intercept or as younger concordant uraninite (*e.g.*, Kotzer & Kyser 1993, Alexandre *et al.* 2007) and marks the end of the Grenville Orogeny and the beginning of the demise of Rodinia. Only minerals near structures, such as the uraninite ores, or along lithostratigraphic boundaries were affected by these later events.

Late kaolinite (K3) in reactivated fault zones has isotopic compositions indicative of low

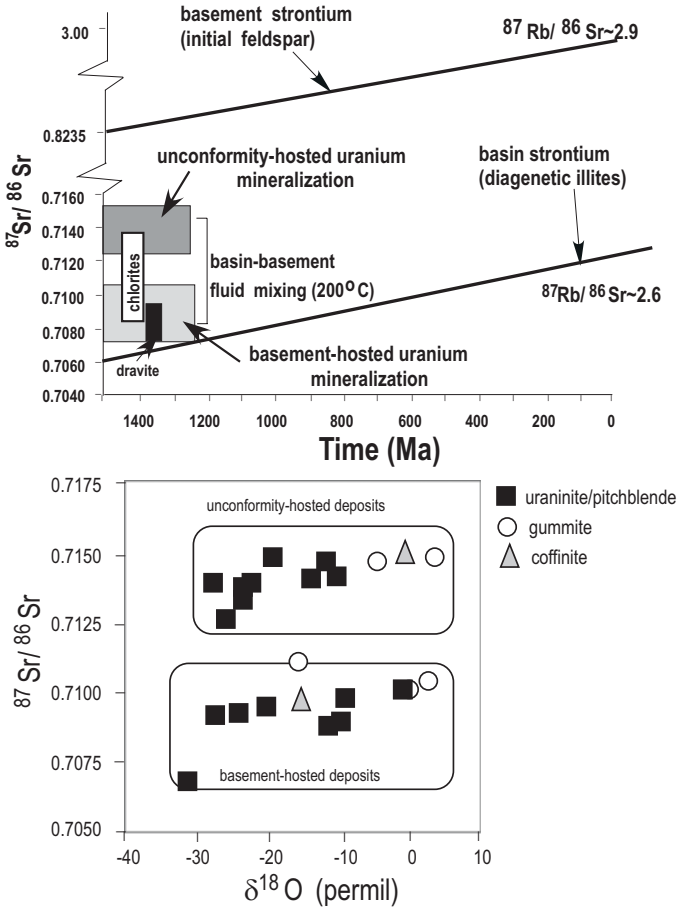

Fig. 8-12. **(A)** Evolution of the $^{87}Sr/^{86}Sr$ ratio in typical basement rocks and basin rocks in the Athabasca Basin as a function of time. Also shown are the ratios of uraninite from unconformity-hosted (basin-hosted, complex-type) uranium mineralization , basement-hosted mineralization (simple-type) and the ratios in dravite and late chlorite. Modified from Kotzer & Kyser (1995). **(B)** Relationship between $^{87}Sr/^{86}Sr$ ratios and $\delta^{18}O$ values of uraninite from unconformity-hosted (basin-hosted) and basement-hosted deposits, showing that the latter have a more significant contribution from basinal fluid Sr. The low $\delta^{18}O$ values of the uraninite indicate they have exchanged oxygen isotopes with relatively recent meteoric waters.

temperature (25–50°C) fluids having isotopic compositions similar to recent meteoric waters in the area. Indeed, many uraninite analyses are highly discordant, have lower intercept U–Pb ages of less than 300 Ma (*e.g.*, Kotzer & Kyser 1993), have low and variable $\delta^{18}O$ values (Fig. 8-11), all consistent with re-equilibration with Tertiary or Quaternary meteoric waters (Kotzer & Kyser 1993, Fayek & Kyser 2000). Illite, dravite and kaolin minerals associated with the uraninite and in fracture zones without mineralization can have low δD values (*i.e.*, less than –100 ‰), and also young K–Ar ages of *ca*. 300 Ma, further attesting to the influx and partial retrograde reaction between minerals in the basin and recent meteoric waters (Wilson *et al.* 1987, Kotzer & Kyser 1995, Kyser *et al.* 2000). Late siderite (S) precipitated in vugs typically has fluid inclusions with homogenization temperatures < 50°C and low salinity fluids, also forming from meteoric waters. The significance of late kaolinite (K3) and minerals that have undergone preferential hydrogen isotope exchange with relatively modern waters is that late influx of meteoric waters occurred, but primarily along faults where permeabilities are enhanced. From an exploration point of view, these results coupled with the extreme loss of radiogenic Pb from the deposits (Holk *et al.* 2003, Kister *et al.* 2004) indicate that components from the deposits have been mobilized into the basin along high permeability structures such as unconformities, fractures and lithostratigraphic boundaries.

Aluminum phosphate sulfate minerals (APS) are widespread in the Athabasca Basin as well as the Kombolgie Basin in Australia (Gaboreau *et al.* 2005, 2007). These APS minerals are divided into three associations, one hosted in the sandstone several metres above the unconformity, another associated with chlorite and illite close to regional faults, and one APS mineral associated with trioctahedral chlorite proximal to U deposits. Variations in the Sr, S and LREE contents of these APS minerals show that those closest to the mineralization are LREE-rich whereas those far from mineralization are Sr- and S-rich. As such the types of APS mineral were suggested to be

controlled by the same factors that control deposition of U, namely Eh, pH and fluid composition and could reflect proximity to the mineralizing process.

Primary detrital heavy minerals in the Athabasca Group are essentially absent except for rare zircon and tourmaline, but fluorapatite and zircon are relatively abundant as inclusions in detrital quartz. Possible original detrital carriers of U include rock fragments and heavy minerals such as zircon, apatite, monazite and uraninite that should have been eroded from source terranes but are now absent in the matrix, except for zircon. Zircon in the matrix is commonly corroded and shows evidence of U increases relative to Zr (Cuney *et al.* 2003). Zircon grains in the matrix can be unaltered, particularly in better sorted fine-grained facies or where cementation is more extensive. *In situ* alteration of monazite results in formation of U-poor APS minerals (Cuney & Mathieu 2001), as has been suggested for the lower Manitou Falls Formation of the Athabasca Basin (Mwenifumbo *et al.* 2007). The former presence of detrital monazite is also suggested by high Th contents of 18 ppm in the lower Manitou Falls Formation of the eastern Athabasca Basin (Quirt 1985).

In addition to U sourced by basinal brines interacting with detrital minerals in the basins, alteration of basement rocks is another possible source (Hecht & Cuney 2000) because U contents in the basement are an order of magnitude higher than the overlying Athabasca Group, which are generally < 1 ppm. Altered areas of zircon grains are depleted in Zr and Si and enriched in P, Y, Fe, Ca and U as well as OH, so that they may not be a good source for U unless they are completely altered (Hecht & Cuney 2000). Monazite is the dominant U-bearing phase in much of the basement and near the deposits has been altered. Calculations suggest that 75% of its U was leached, and this is evident to a depth of 200 m below the unconformity. Leaching of U during monazite alteration was suggested to be from oxidizing fluids originating in the overlying Athabasca Group. However, the basement rocks altered along faults would have to be aberrantly enriched in monazite to produce enough U for a deposit because transitions to unaltered basement rocks are sharp outside of shear zones and permeability in unfractured basement rocks is low. Nevertheless, fluid inclusions observations indicate that basinal brines reacted with basement rocks both pre- and post-ore and in so doing, may have resulted in monazite releasing U into the fluids.

Pagel *et al.* (1980), Kyser *et al.* (2000) and Cuney *et al.* (2003) proposed that ore was deposited during peak diagenesis at 180 to 250°C, suggesting a geothermal gradient in the order of 35°C/km at depths of about 5 km. Ramaekers & Catuneanu (2004) suggested that either the geothermal gradient beneath the Athabasca Basin was 40–50°C/km for a 5 km thick basin fill or that the basin fill was much thicker before erosion. Fluid inclusions in quartz in sandstone and pre- and post-ore quartz cement in breccia at McArthur River record possible mixing between an NaCl-rich brine and a $CaMgCl_2$-rich brine. The latter brine formed during alteration of the Ca-rich basement rocks by the NaCl brine, and mixed with the NaCl-rich brine during U mineralization (Derome *et al.* 2005). Pressure–temperature conditions during ore formation are purported to be 0.5–0.9 kbar, reflecting a pressure decrease from lithostatic to hydrostatic conditions during brecciation and possibly lower temperatures of only 140°C (Derome *et al.* 2005). U concentrations in the $CaCl_2$-rich inclusions are higher than those in the NaCl brines, suggesting that the basement may be an important source for U in the McArthur River deposit (Richard *et al.* 2008).

Fayek & Kyser (1997) suggested that much of the fluid involved in basement-hosted deposits had not interacted significantly with basement rocks whereas basin-hosted deposits indicate a significant input of Sr from the basement rocks (Fig. 8-12). High concentrations of phosphate minerals occur with the U mineralization and the uraninite has high REE contents and is HREE-enriched (Fayek & Kyser 1997). They suggest that there was extensive REE mobility during diagenesis of the Athabasca Group and that REE and U were most likely derived from detrital diagenetic clay minerals, fluorapatite and zircon in the sandstone and garnet and zircon in the basement. Monazite certainly played a role as a source for REEs, Sr and U, whether from the basin fill, basement rocks or both.

Timing of fluid events and their relationship to mineralization

Fayek *et al.* (2000) reported a discordia age near 1500 Ma for the Cigar Lake deposit using SIMS. However, the degree of discordia was significant so the age is not very precise. Similarly, Fayek *et al.* (2002) suggested an initial age of mineralization near 1500 Ma for the McArthur River and Sue Zone U deposits using SIMS with significant overprinting by later fluid events. Again,

the degree of discordia was significant so that the upper intercepts were not very precise.

Post-peak metamorphic cooling during the Trans-Hudson Orogen is indicated by dates of 1750 Ma from mica in the basement rocks underlying the Athabasca Basin and throughout the domains to the east of the Athabasca Basin (Kyser *et al.* 2000, Alexandre *et al.* 2007). This gives a maximum age of formation of the basin of 1750 Ma (Fig. 8-13). Pre-ore alteration occurred simultaneously near basement- and basin-hosted deposits beginning at 1670 Ma, based on the $^{40}Ar/^{39}Ar$ dates from pre-ore illite and chlorite proximal to the deposits. The major U mineralization event occurred at 1600 Ma based on U/Pb dates of uraninite and Ar/Ar dates of syn-ore illite, and is constant throughout the basin in both basement- and basin-hosted deposits (Alexandre *et al.* 2007). Several subsequent fluid events affected all the minerals in the structurally hosted deposits, and the ages of these events correspond to far field, continent-wide tectonic and metamorphic events such as the Mazatzal Orogeny at 1600 Ma, the Berthound Orogeny at *ca*. 1400 Ma, the Mackenzie dike swarm at 1270 Ma, the Grenville Orogeny at 1100 Ma and the assemblage and break-up of Rodinia, up to 850 Ma. Given that the major U mineralization event occurred 150 million years after the basin began to form, the basin architecture and hydrogeology at that time is critical to understand what factors controlled formation of the deposits.

Multiple fluid events, involving isotopically and chemically distinct fluids that migrated laterally for considerable distances and along fault zones, produced a paragenetically identifiable assemblage of clay, silicate and oxide minerals in the basin and basement rocks. Isotopic, chemical, microthermometric and petrologic data indicate that the major sandstone aquifers in the Athabasca Basin, which were most pronounced in the poorly sorted basal

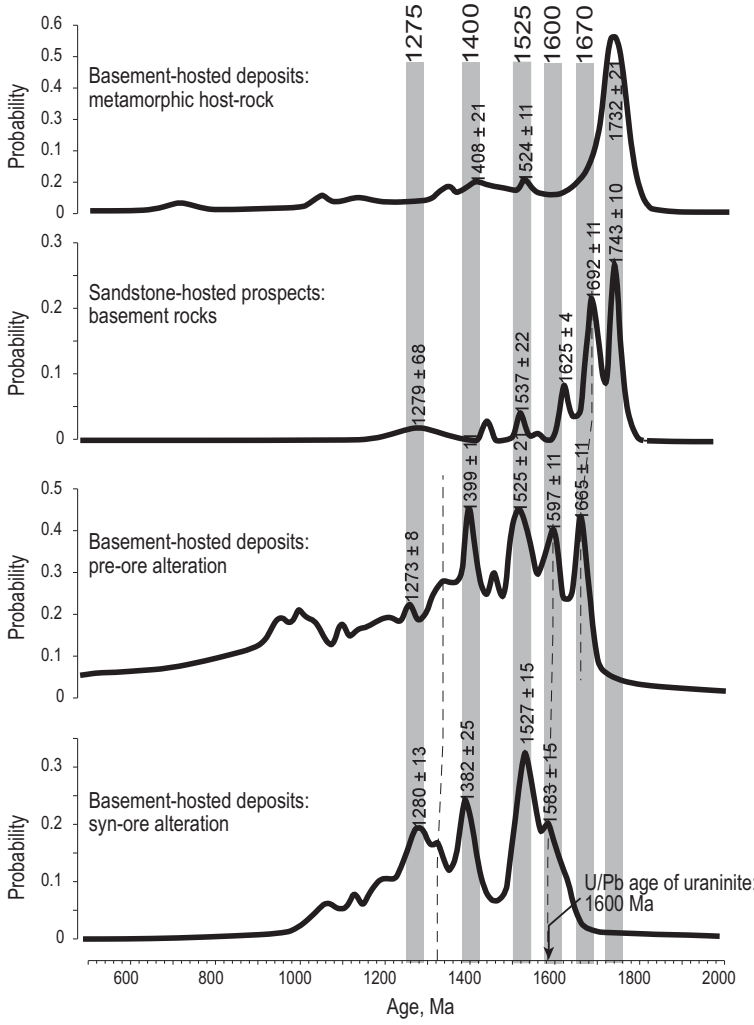

Figure 8-13. U/Pb ages of uraninite and $^{40}Ar/^{39}Ar$ ages of mica from the basement rocks, pre-ore alteration phases and ores from various basement-hosted and sandstone-hosted (basin-hosted) U deposits in the Athabasca Basin, indicating ore formation throughout the entire basin at 1600 Ma and perturbations coincident with major tectonic events in North America. 1750 Ma corresponds to rapid uplift of Trans-Hudson units to the east and beginning of basin formation, 1670 Ma is pre-ore alteration event, 1525 Ma corresponds to the Mazatzal Orogeny, 1400 Ma to the Berthoud Orogeny, 1275 Ma to emplacement of the McKenzie mafic dike swarm, with younger dates related to the Grenville Orogeny (1.1 Ga) and the assemblage and break-up of Rodinia (0.85 Ga). Modified from Alexandre *et al.* (2007).

units, have been affected by widespread lateral flow of diagenetic fluids over distances of hundreds of kilometres (Fig. 8-14). These fluids appear to have been resident in basinal units at temperatures in excess of 200°C for at least 300 m.y., but reacted with minerals in the basin during flow in response to orogenic events during evolution from massive paleoaquifers to fracture-controlled flow. These fluid migration paths followed stratigraphic units and flowed up dip from the basin center. The stratigraphic pathways, however, were modified by cross-formational fluid flow near active fault zones until fault zones became the exclusive pathways.

The first refereed publication of a geological model for a new class of U deposit called 'unconformity type' was by Hoeve & Sibbald (1978). This and subsequent models suggest that oxidizing, U-bearing, basin fluids heated by the geothermal gradient eventually attained 200°C (burial depths of ~5–6 km) at the unconformity and reacted with reducing fluids coming out of reactivated basement shear zones to produce complex deposits, or directly with the basement rocks to produce the simple type deposits (Fig 8-9). Other models involve leaching of U from basement rocks as they reacted with basinal brines (Derome *et al.* 2005). Uranium precipitated as uraninite in fault zones where reduced and oxidized fluids were mixed. Uraninite precipitated during active faulting was repeatedly brecciated during precipitation of newly formed uraninite. Ore deposits accumulated where these conditions were focused for very long periods of time (Hoeve & Quirt 1987), perhaps hundreds of millions of years (Kyser *et al.* 2000). Zones of inferred fluid mixing are characterized by alteration halos that contain illite, kaolinite, dravite, chlorite, euhedral quartz, and locally, Ni–Co–As–Cu sulfide minerals (Hoeve & Quirt 1984, Kotzer & Kyser 1995, Kister *et al.* 2006). Pre-ore to post-ore alteration halos dominated by chlorite (Alexandre *et al.* 2005) developed around sites of ore deposition where reduced basement fluids circulated upward into the overlying oxidized basin-fluid environment (Fayek & Kyser 1997). Flow of basinal fluids downward into the basement developed inverted and condensed alteration zones, mainly in host basement rocks, with a more subtle and complex expression in overlying conglomeratic sandstone (Fayek & Kyser 1997). Although there are many variations on the unconformity-associated U deposit model (*e.g.*, Quirt 2003, Alexandre *et al.* 2005), most are mere refinements of the original model presented by Hoeve & Sibbald (1978). Critical elements are still missing, however, as the models can identify favorable areas and are intellectually pleasing, but they are not yet predictive.

THELON BASIN, CANADA

The Paleoproterozoic Thelon Basin straddles the border between Nunavut and the Northwest Territories of Canada (Fig. 8-4). It is a potential analog of the Athabasca Basin in terms of its sedimentological history and potential metallogeny. Also, the Thelon Basin is host to two areas of U mineralization, one in the eastern portion of the basin at Kiggavik–Andrews Lake, and the other in the western portion at Boomerang.

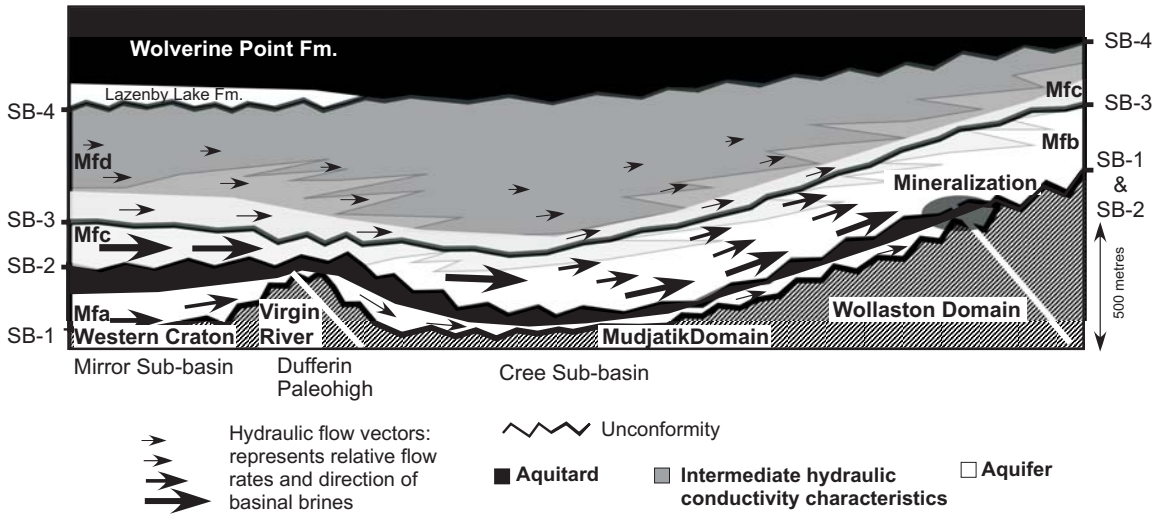

Fig. 8-14. Schematic illustration of the possible hydraulic flow vectors in the eastern Athabasca Basin at 1600 Ma, the time at which unconformity-related U deposits formed throughout the Athabasca Basin. Modified from Hiatt & Kyser (2007).

Geologic setting

The Paleoproterozoic Thelon Basin occupies an intracratonic setting within the Archean Churchill Province in Nunavut, approximately 200 km west of the Inuit hamlet of Baker Lake (Fig. 8-15). Sedimentary fill lies unconformably on Archean granitic and metasedimentary rocks, and Paleoproterozoic volcanic and metasedimentary rocks (Hiatt *et al.* 2003, Rainbird *et al.* 2003b). Graphitic units underlying the western Thelon Basin are identified as part of the Paleoproterozoic Amer Group (Miller & LeCheminant 1985), but graphitic metapelite is absent beneath the eastern part of the Thelon Basin along the Kiggavik trend (Fuchs & Hilger 1989).

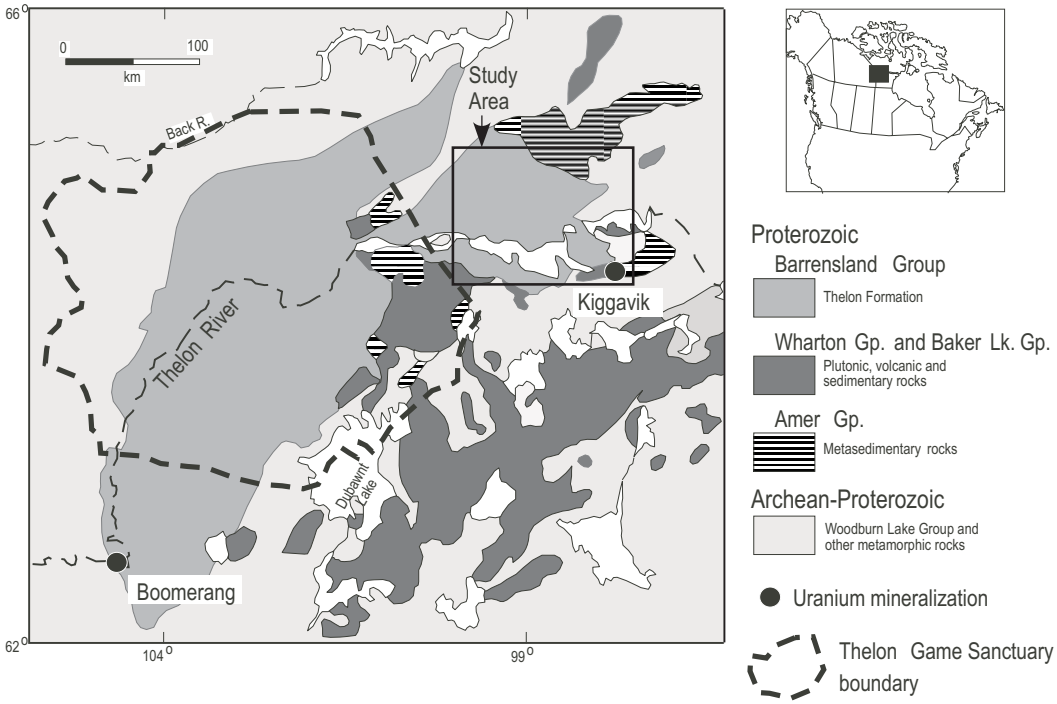

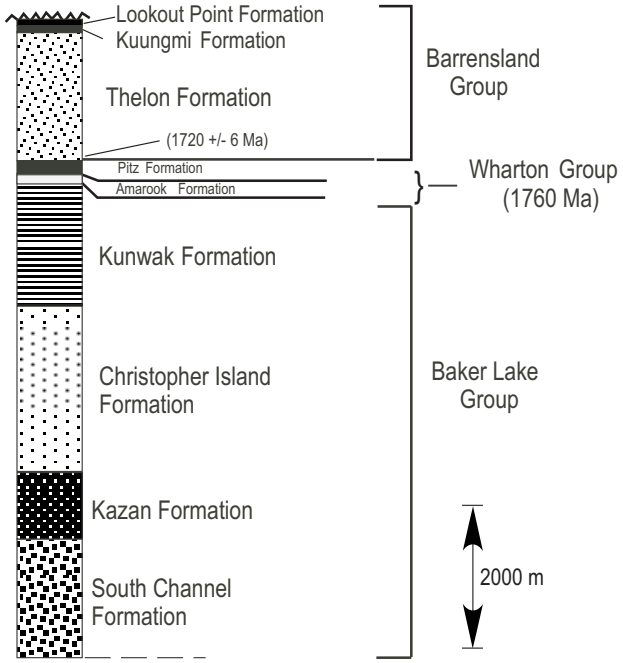

Fig. 8-15. Regional map showing the location and general stratigraphy of the Thelon Basin, including areas of known U mineralization and area in the eastern basin that has been well studied. Based on Gall *et al*. (1992), Rainbird & Hadlari (2000), Renac *et al*. (2003) and Hiatt *et al*. (2003). Modified from Gandhi (1989).

A maximum age for the basal Thelon Basin is provided by a 1753 Ma fluorite-bearing granite that intruded basement lithologies (Miller 1995). A minimum age for the Thelon Basin is inferred from authigenic fluorapatite within basal units of the basin that has U–Pb dates ranging from 1720–1760 Ma (Miller *et al.* 1989), indicating an age near that of the Athabasca Basin. The basin was intruded by 1270 Ma Mackenzie diabase dikes.

Sedimentary rocks of the Thelon Basin belong to the Dubawnt Supergroup (Gall *et al.* 1992). The Dubawnt Supergroup consists of three sedimentary sequences (Fig. 8-15), in stratigraphic order, the Baker Lake Group, the Wharton Group, and the Barrensland Group (Rainbird *et al.* 2003b). The latter includes the Thelon Formation conglomerate and coarse-grained sandstone. The Thelon Formation is up to 1800 m thick (Overton 1977) and overlies a well developed paleo-regolith (Gall 1994, Gall *et al.* 1992). Sedimentary facies of the Thelon Formation generally fine upward and consist of sublithic to subarkosic conglomerate and coarse-grained sandstone, and thinly bedded to cross-bedded quartz arenite (Hiatt *et al.* 2003). The Thelon Formation in the western Thelon Basin is overlain by isolated exposures of the basaltic Kuungmi Formation and the Lookout Point Formation consisting of stromatolite-bearing dolomite and evaporites (Gall *et al.* 1992). The overall fining-upward of facies and the presence of overlying carbonate lithologies are interpreted to represent transgression and increasing marine influence in the Thelon Basin during the Barrensland sequence (Hiatt *et al.* 2003, Rainbird *et al.* 2003b).

Sedimentology and stratigraphy

The unmetamorphosed and flat-lying Thelon Formation reaches a thickness of 1 km in the eastern sub-basin, and is composed of thick (metres to tens of metres), poorly sorted, trough cross-bedded conglomerate and coarse-grained sandstone units, and to a lesser extent, well sorted, medium to coarse-grained sandstone units (Hiatt *et al.* 2007). Thin, clay-rich, fine-grained sandstone and siltstone punctuate the coarser grained lithofacies. The basal conglomerate layers contain abundant clasts of the underlying Pitz Formation volcanic rocks and clasts of the older Pitz and Amarook Formation sandstone (Rainbird & Hadlari 2000).

Hiatt *et al.* (2007, 2008) have divided the Thelon Formation into four broad lithofacies types (Fig. 8-16). The first is a coarse-grained trough-cross bedded, sublithic arenite and conglomerate lithofacies. This is composed of pebbly and cobbly coarse-grained sandstone and conglomerate that is very poorly sorted, and contains abundant well rounded quartzite pebbles and cobbles that sometimes make up >50% of the rock. The gravel fraction of this lithofacies contains minor volcanic rocks from the underlying Pitz Formation,

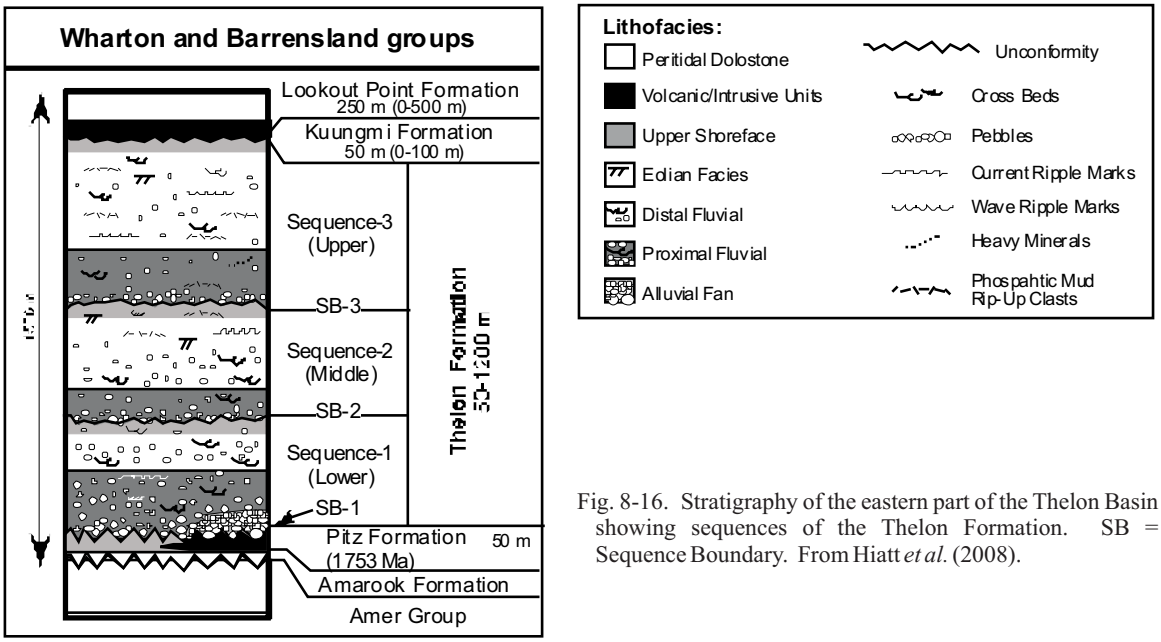

Fig. 8-16. Stratigraphy of the eastern part of the Thelon Basin showing sequences of the Thelon Formation. SB = Sequence Boundary. From Hiatt *et al.* (2008).

sandstone from the Pitz and Amarook formations, and metapelite clasts from the underlying Amer Group. The coarse-grained units are marked by abundant trough cross-bedding, scour surfaces, and asymmetrical ripple marks. This coarse-grained lithofacies suggests deposition in high energy braided fluvial systems, and is located both at the base of the basal unit and at the basal sequences within the Thelon Formation over intra-formational unconformities. Fluvial paleocurrent directions are predominantly west to northwest-directed. Locally, this lithofacies contains lithic pebble-cobble conglomerate with angular clasts of metapelite and a muddy to sandy matrix suggestive of alluvial fan deposition.

The second lithofacies is composed of poorly sorted subarkosic arenite that is coarse to fine-grained, contains 6–10% white clay grains that are assumed to represent replacement of original feldspar grains, and minor lithic fragments (primarily volcanic and quartzite). This lithofacies is composed of beds that are generally massive and thickly bedded. Beds fine upward stratigraphically and are pebbly at their base but grade into fine-grained sand near top; these units are commonly capped by clay-rich, red Fe-stained fine-grained sandstone to siltstone horizons. This lithofacies is interpreted to represent low-energy braided stream bar to sheet channel and braid plain deposition.

The third lithofacies is composed of thinly bedded, medium to coarse-grained, well sorted quartz arenite with large-scale, low-angle cross bedding and abundant wave and current ripple marks. This lithofacies is most common in the western and northern parts of the sub-basin and is interpreted to represent deposition in upper shore-face settings.

The fourth, and most distinctive lithofacies in the Thelon Formation is made up of thinly bedded, medium-grained, well sorted quartz arenite with large-scale, high angle wedge cross bedding with foresets 2 to 3 m long, dipping 20–25°. This lithofacies is spatially limited and interpreted to represent eolian deposition (Hiatt *et al.* 2008).

Three third order sequences are identified in the Thelon Formation (Fig. 8-15). Systems tracts can be defined using lithofacies analysis and distinct breaks in fining upward cycle thickness (Hiatt *et al.* 2003). The thicknesses of fining upward cycles in the Thelon Formation varies in a systematic way that reflects changes in accommodation space through time. Intervals that record minimums in accommodation space are composed of conglomerate and coarse-grained lithic arenite with abundant large scale trough cross-bedding and relatively thin fining upward cycles. These intervals mark periods in which most sand is transported into the basin center and are interpreted as low-stand system tracts. Transgressive surfaces are defined by abrupt increases in the thicknesses of fining upward cycles. Above these surfaces, rapid creation of accommodation space produces cycles that average 9 m thick, are laterally continuous and punctuated by weakly developed paleosol horizons. These are interpreted as transgressive system tract deposits. Intervals with fining upward cycles of intermediate thickness and laterally continuous beds of sandstone marked by sedimentary structures and fabrics characteristic of upper shore-face and eolian deposition are interpreted to represent high-stand system tracts. Recognition of accommodation space relationships and multiple intervals of braided fluvial, shore-face, and eolian sedimentation reveal a complex depositional history for the Thelon Basin that is much more dynamic than that of the Athabasca Basin (Hiatt *et al.* 2003).

The Thelon Formation in the western portion of the basin is capped by thin basaltic flows of the Kuungmi (or Sanctuary) Formation. Dolomite of the Mesoproterozoic Lookout Point Formation stratigraphically overlie these volcanic rocks and contain evidence of marginal marine and evaporative conditions (Gall *et al.* 1992). The Kuungmi Formation flows attest to late igneous activity, albeit limited, during basin evolution, and the Lookout Point Formation to evaporitic brines that may have charged the early Thelon aquifers, and later circulated and diagenetically altered the rocks of the Thelon Formation, at least in the western portion of the basin.

Uranium deposits

The Kiggavik-Sissons deposits consist of 3 separate basement-hosted unconformity U deposits containing approximately 123 million pounds U (56 million kg U) and a grade of 0.27% U (AREVA Annual Report 2005). The deposits lie ~2–4 km south of the present day eastern extent of the Thelon Basin (Fig. 8-15) and presumably were once unconformably overlain by the Thelon Formation. Kiggavik is hosted in flat-lying quartzite of the Ketyet River Group near a *ca*. 1.7 Ga Hudsonian granite pluton and are cross-cut by late 1.27 Ga, diabase intrusions that post-date mineralization (Fuchs *et al.* 1986). The U mineralization occurs as

plunging, elongate pods located at the intersection of two major deposit-scale faults/shear zones, one trending ENE and dipping SSE intersecting an east–west trending fault dipping northward (Fuchs & Hilger 1989). Mineralization in the form of coffinite occurs as colloform aggregates close to fractures and finely disseminated granules near altered pyrite grains (Fuchs & Hilger 1989). Mineralization is associated with pyrite altered to hematite and illite formed by hydrothermal processes (Fuchs *et al.* 1986). Although there are no direct absolute dates for the U minerals, associated illite dated using whole rock K–Ar gives 1648 and 1563 Ma, and 1358 and 1073 Ma from quartzite bearing mineralization (Fuchs *et al.* 1986). The ore and alteration mineralogy of the Kiggavik deposit is similar to simple type U deposits of the Athabasca Basin. Renac *et al.* (2002) detailed the paragenesis of the eastern Thelon Basin proximal to the Kiggavik deposit and concluded that mineralizing fluids responsible for ore deposition in the Athabasca and Thelon Basins were chemically distinct. Although similar in size, age and geology to the Athabasca Basin, so far the U resources of the Thelon Basin are only 10% of those of the Athabasca Basin.

The Boomerang Lake prospect is located in the western Thelon Basin (Fig. 8-15), but has not been studied. Uranium and Au mineralization is hosted by Thelon Formation sandstone at the unconformity overlying a graphitic and garnetiferous metapelite unit (Gandhi 1989). Davidson & Gandhi (1989) summarized results of exploration by Urangesellschaft Canada, Ltd., at Boomerang Lake. Three of 36 drill holes intersected significant concentrations of U and Au. The best intersection assayed 0.42% U and 25 ppm Au over 0.5 m. Two uraninite samples give a U–Pb date of 1300 Ma, but this is probably reset and unlikely to be the primary age of the U mineralization. Uranium is correlated with Cu, As, Ni, Co, Cr, V, Au, Pb, and Zn associated with sulfides, arsenides, and Ni–Co–Cd selenides. Additionally, selenides minerals from one sample contained 82 ppb Pt and 160 ppb Pd. This complex metal inventory is similar to complex-type U deposits in the Athabasca Basin.

Paragenesis and fluid evolution in the Thelon Basin

Petrographic examination reveals a complex history of post-sedimentation events recorded in the Thelon Formation of the eastern sub-basin (Fig. 8-17). Detrital phases preserved include rare clasts of metamorphic rocks, occasional zircon and muscovite grains, and fluorapatite clasts (P0). The detrital quartz, which normally comprises >95% of the Thelon Formation, occasionally contains inclusions of apatite, rutile, and zircon. In the southern portion of the sub-basin, the most basal unit contains detrital microcline (F0) that is still preserved as a result of early extensive quartz cementation. The paleoregolith still preserves kaolinite (K) and hematite (H1) from the original weathering.

In units that had very high initial hydraulic conductivities, such as eolian sand, the earliest diagenesis is expressed by a phase of quartz cement that forms isopachous rims of fine crystals (IQC). Cements of this morphology are characteristic of phreatic zone diagenetic environments, and their high $\delta^{18}O$ values and low temperatures of formation of <50°C (Fig. 8-17) support such an interpretation (Hiatt *et al.* 2007). Although not widespread, this cement suggests that porosity and permeability networks in some units were being modified soon after deposition (Hiatt *et al.* 2007). In most lithologies, however, early diagenesis is commonly manifested by fine veneers of reddish-brown or black iron oxides (H2) and syntaxial, syn- and post-compaction quartz overgrowths (Q1) on detrital quartz grains. UV optical microscopy reveals the presence of detrital feldspar ghosts in the present pore space in sandstone, although these spaces are now filled with quartz cement and illite (Renac *et al.* 2002). Local variations include areas that lack quartz overgrowths but display specular hematite (100 μm diameter, H2) and associated neoformed hydroxyphosphate cement of *ca*. 50 μm diameter (P1). In the Thelon, Hornby Bay, and Elu basins, Al phosphate sulfate (APS) minerals occur at the base and in the paleoregolith (Gall & Donaldson 2006). These APS are pseudocubic and appear to postdate uraniferous fluorapatite. Small, millimetre-wide quartz veins containing euhedral quartz (Q2) along the margins and later minerals in the center occur locally in the basal Thelon Formation. Early diagenesis resulted in syntaxial quartz (Q1) on detrital quartz (Q0) and detrital feldspar, and later quartz veining (Q2), at 100–160°C from NaCl brines having *ca*. 17 wt.% NaCl (Hiatt *et al.* 2008). The $\delta^{18}O$ value of this brine was *ca.* 0‰, identical to seawater, and it was distributed throughout the Thelon sub-basin.

A period of silica dissolution occurred prior to precipitation of illite (I1 and I2) in pore spaces during peak diagenesis (Fig. 8-17). Dissolution

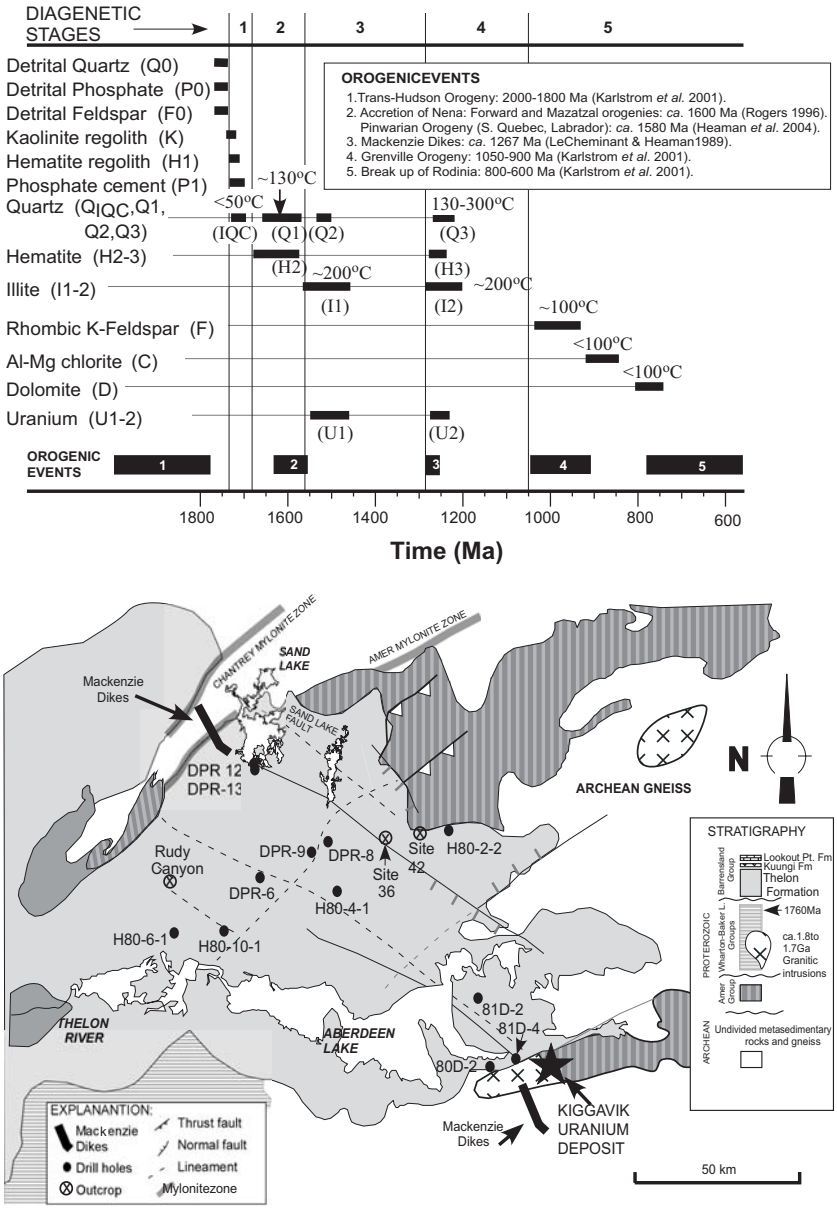

Fig. 8-17. Paragenetic relationships for the Thelon Basin showing five phases of diagenesis based on Renac *et al.* (2002) and Hiatt *et al.* (2007). Major tectonic events are shown in numbered black boxes and described in the inset. Bottom figure shows the locations of drill core and outcrop on which the stratigraphy and paragenesis is based.

most likely occurred in response to an increase in temperature of the pore fluids as burial proceeded. Although dissolution of overgrowths is present in other Proterozoic basins, it is more widespread and substantial in the Thelon Basin (Hiatt *et al.* 2007). Peak diagenesis is manifest as illite crystals (I1 and I2) distributed radially around quartz grains or remnant quartz overgrowths. Throughout the Thelon Formation, the basal units have only *cv*-1M illite (I1), consistent with fluid temperatures near 200°C, whereas some of the stratigraphically higher units of the Thelon Formation have mixtures of *cv*-1M and *tv*-1M polytypes of illite. Ar–Ar total fusion ages of illite produced during peak diagenesis from the basal units (I1) range from 1516 to 1690 Ma (Fig. 8-18). In contrast, those from stratigraphically higher areas from the central portion (I2) have younger ages of *ca.* 1300 Ma. The separation in Ar–Ar ages and relative stratigraphic position of this illite indicates the illite formed at different times. In addition, there was either an evolution in the $\delta^{18}O$ values of these fluids from *ca.* 9‰ for illite (I1) in the basal Thelon Formation to *ca.* 3.9‰ for illite (I2) in the more permeable upper stratigraphic units, or a decrease in temperature of 50°C (Fig. 8-17). However, δD values of the fluids were

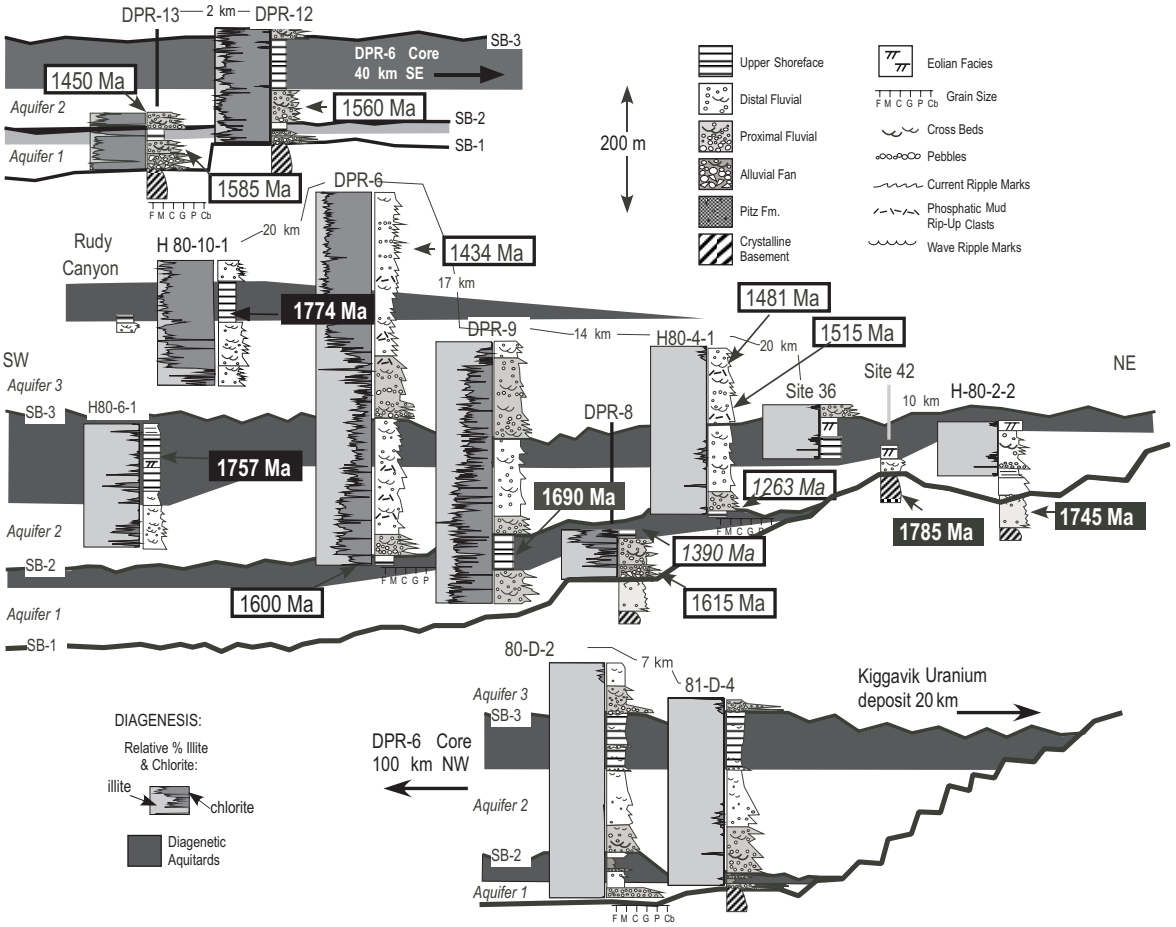

Fig. 8-18. Lithology, sequence boundaries (SB), location of diagenetic aquitards and aquifers in the Thelon Formation and Ar–Ar ages of I1 illite and I2 illite (italics) for the eastern Thelon Basin. Locations of drill cores are shown in Fig. 8-17. Ar–Ar dates in black boxes are from basement lithologies or upper shore-face units, the latter cemented early in basin evolution forming extensive diagenetic aquitards. Those dates in italics are from I2 illite, which is normally found along lithostratigraphic boundaries where late fluids could flow. Modified from Hiatt *et al.* (2008).

relatively constant and like those of the low latitude meteoric–marine waters that affected the Athabasca Basin. The substantially higher $\delta^{18}O$ values of the peak diagenetic fluids relative to those for the quartz overgrowths imply that the peak diagenetic fluids represent ^{18}O-enrichment as a result of more extensive evaporation or water–rock interaction, the latter during evolution of the basin.

Also associated with late illite (I2), which maybe a degradation product of earlier formed illite (I1), is quartz veining (Q3) having a wide range of fluid inclusion homogenization temperatures from 130 to 300°C and variable but low salinity. Veins of hematite (H3) also appear to be nearly contemporaneous with the Q3 veins. The variable temperatures, low salinities and fracture control of these fluids are consistent with heating of small amounts of fluids in fractures during emplacement of the Mackenzie dike swarm. Similar effects are recorded in late quartz veins in U deposits in the Kombolgie Basin in Australia.

Late diagenetic features are characterized by widespread rhombic K-feldspar cement (adularia) (F) and paragenetically later Al–Mg chlorite (C) in the uppermost sandstone of the central Thelon subbasin (Fig. 8-17). The K-feldspar is poorly ordered, consistent with temperatures of precipitation of <150°C (Kastner & Siever 1979). The K-feldspars have total fusion Ar–Ar ages of *ca*. 1000 Ma (Figs. 8-17), substantially younger than the illite. Fluids related to the K-feldspar had high salinity of 21 wt.% NaCl and $\delta^{18}O$ values of –3 to 1‰, whereas those for the chlorite had much higher $\delta^{18}O$ values near 5‰ and δD values of –30‰. The paragenesis,

mineralogy, high salinity and heavy isotopic compositions of these authigenic minerals are consistent with an evaporitic source for the fluids well after the sediments in the basin had lithified.

The youngest fluid event preserved in the Thelon Basin is that associated with the precipitation of minor dolomite cement (D) in fractures of reactivated quartz veins (Q3) in the basal units. Although the exact age is uncertain, the fluid was *ca*. 100°C, with low salinity between 1 and 5 wt.% NaCl equiv., and low $\delta^{18}O$ values of –8 to –5–5‰. The distinct occurrence, salinity, and composition of this fluid imply that enough time had passed to expel totally the brines that had formed the chlorite, even along fractures. The dolomite represents the last of seven distinct fluid events preserved in the authigenic minerals of the Thelon Basin.

The fluids in the eastern Thelon Basin during peak diagenesis are similar to those of the Athabasca Basin in terms of their origin, evolution and temperature, but they were buffered by illite–quartz rather than quartz–kaolin–illite. The major difference between the basins, however, is a more pronounced compartmentalized diagenetic aquifer system that developed in the Thelon Basin as a result of early quartz cementation in well sorted lithologies. This is reflected in the older Ar–Ar ages of illite in the well sorted facies relative to diagenetic illite in the more poorly sorted facies (Fig. 8-18). Because Ar–Ar ages represent the time at which cessation of fluid–mineral interactions occurred, the older ages as well as early, low temperature and extensive quartz cementation of well sorted lithologies based on their high $\delta^{18}O$ values indicate they had little fluid shortly after the basin began to form (Hiatt *et al.* 2007). Confined diagenetic aquifers in the Thelon Basin differ from the extensive and permeable Manitou Falls Formation that comprise the basal units in the Athabasca Basin, where dates of diagenetic illite are almost uniformly much younger than the age of the U deposits and quartz cement formed from high temperature diagenetic fluids (Hiatt *et al.* 2007). This would suggest that favorable horizons are where the paleoaquifers and reducing lithologies in the basement intersect, which would be more limited and total fluid reservoirs less substantial for the eastern Thelon Basin, but the locations of possible deposits are easier to predict.

In contrast, the western Thelon Basin has less developed confined diagenetic aquifers, but a major diagenetic aquifer in the lower half of the stratigraphy. It also has a peak diagenetic assemblage of dickite and illite, similar to the Athabasca Basin.

THE KOMBOLGIE BASIN, AUSTRALIA

The Kombolgie Basin is located on the Arnhem Land Plateau area and is the northern part of the larger McArthur Basin in the Northern Territory of Australia (Fig. 8-19). Like the Athabasca Basin in Canada, the Kombolgie Basin is also host to large world class U deposits and evolved from a thick (1–2 km) sequence of flat-lying clastic basin-filling sediments that were deposited in fluvial, eolian, and marine paleo-environments. In contrast to the Athabasca Basin, all the deposits in the Kombolgie Basin are basement-hosted, although in the McArthur Basin, deposits such as the Westmoreland (Polito *et al.* 2005a), are associated with intrusive units in the basin.

Unconformity-related deposits constitute a major proportion (20%) of Australia's total U resources, and much of Australia's total production since 1980 has been mined from two of these deposits – Nabarlek (now mined out) and Ranger 1 & 3. Other major deposits in the Alligator Rivers region are Jabiluka, Koongarra and Ranger 68. Uranium exploration in the Alligator Rivers region and Arnhem Land has been restricted since the late 1970s because of political factors. Much of the Alligator Rivers region and Arnhem Land have only been subjected to first pass exploration designed to detect outcropping deposits and extensions of known deposits, *e.g.*, Jabiluka 2 was found by drilling along strike from Jabiluka 1. Until recently, there has been limited exploration to locate deeply concealed basin-hosted deposits lying above the unconformity similar to those in Canada. The Australian deposits are of lower grade than the Athabasca Basin deposits and are confined to the Alligator River Uranium Field (ARUF), a relatively small area in the Northern Territory which includes the eastern Pine Creek Inlier and the western Kombolgie Basin. The other probable unconformity-related deposit in Australia is the Kintyre deposit in Western Australia, which is a large tonnage and low grade deposit similar to those in the ARUF.

The Paleoproterozoic to Mesoproterozoic McArthur Basin (Fig. 8-19) is filled with a thick (5–15 km) sequence of nearly flat-lying sedimentary rocks interpreted to have formed in terrestrial and marine environments. Volcanic rocks deposited

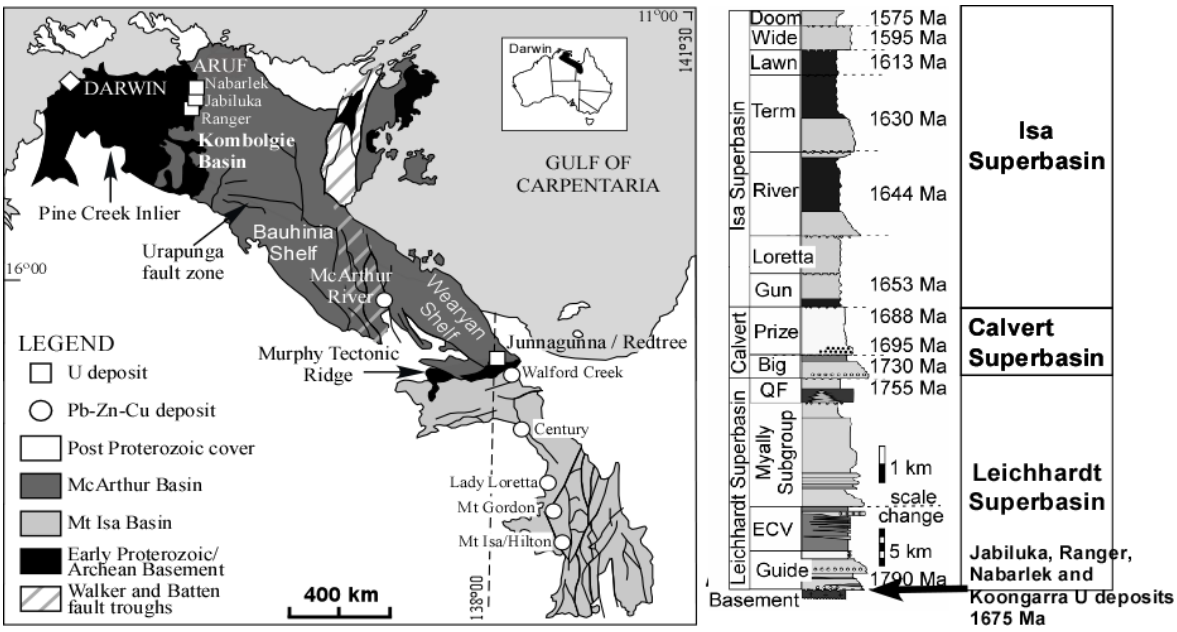

Fig. 8-19. Left: generalized geological map of the Mt. Isa and McArthur Basins showing locations of Zn-Pb-Ag, Cu and unconformity-related U deposits. The Kombolgie Basin is the northwestern part of the McArthur Basin. Right: generalized stratigraphic sequence of the Mt. Isa and McArthur River basins showing the stratigraphy of the three superbasins, ages of the units determined from U-Pb dates of felsic volcanic rocks or detrital zircon and stratigraphic positions of unconformity-related U deposits and their ages (modified from Polito *et al.* 2006a).

on the North Australian craton (Fig. 8-19) periodically punctuate these sedimentary successions, and are indicative of rifting periods. Deposition of the mixed siliciclastic–carbonate successions and minor volcanic units occurred in a variety of intracratonic settings so that the McArthur Basin actually consists of several adjoining sub-basins (*e.g.*, Rawlings 1999, Rawlings & Page 1999). The McArthur Basin is host to Precambrian petroleum deposits, the largest Pb–Zn–Ag district in the world, and its northernmost sub-basin contains world-class unconformity-type U deposits. The basin is bounded by Paleoproterozoic crystalline basement rocks of the Pine Creek Inlier to the northwest and by other inliers to the southeast and north.

The Northern McArthur Basin begins east of the Pine Creek Inlier and is represented by the Kombolgie sub-basin, here after referred to as the Kombolgie Basin (Fig. 8-19). Units in the Kombolgie Basin are equivalent to the basal units of the Leichhardt Superbasin in the McArthur and Mt. Isa basins (Figure 8-19) and have a similar mineral paragenesis. A detailed chronostratigraphic framework for the McArthur Basin has been elegantly elucidated by integrating sequence stratigraphy (Southgate *et al.* 2006), U–Pb geochronology on the volcanic rocks (Page *et al.* 2000), paleomagnetic directions in the sedimentary units (Idnurm & Giddings 1995, Idnurm *et al.* 1995, Idnurm 2000) and diagenesis (Polito *et al.* 2006a, 2006b). Correlations between the Kombolgie and McArthur–Mt. Isa basins suggest that the Kombolgie Basin began to form at about 1793 Ma (Fig. 8-18).

The Kombolgie Basin is floored by the equivalent rocks that comprise the Alligator River Uranium Field (ARUF) of the Pine Creek Inlier exposed to the west, and is equivalent to the basal units of the McArthur Basin to the southeast (Fig. 8-19). The dominant tectonic extensional and compressional structures and the main metamorphic event within the Pine Creek Inlier were due to the Barramundi Orogeny, which occurred between 1890 and 1870 Ma (Riley *et al.* 1988, Page & Williams 1988) and continued with the Nimbuwah Event of the Top End Orogeny from 1863–1847 Ma (Needham *et al.* 1980). During the Barramundi Orogen metamorphic event, Paleoproterozoic sedimentary, volcanic and plutonic rocks were metamorphosed in the western portion of the ARUF to amphibolite facies (Snelling 1990) and to granulite facies in the eastern portion (Ferguson 1980). The Nimbuwah Event was followed by post-peak regional retrogression that ended prior to *ca*.

1820 Ma based on U/Pb ages of 1829 ±5 Ma and 1825 ±5 Ma from the Pul Pul Rhyolite and the Plum Tree Creek Volcanic rocks that were deposited on the basement rocks in the South Alligator Rivers Uranium Field and the Alligator Rivers Uranium Field, respectively (Jagodzinski 1998, Page unpub.).

The metasedimentary basement is domed by Archean to Paleoproterozoic pre-orogenic granitic intrusions (Dodson *et al.* 1974) and the Zamu Dolerite, which was emplaced at 1884 Ma. The late Paleoproterozoic is characterized by post-orogenic intrusions, such as the Jimbu microgranite, which is restricted to the southeast portion of the basin (Rawlings & Page 1999), and the Oenpelli Dolerite, which occurs throughout the Kombolgie Basin (*e.g.*, Kyser *et al.* 2000). Both of these intruded the Kombolgie Subgroup and have ages of 1720 Ma. Subsequent magmatic episodes are characterized by minor intrusions of phonolitic and doleritic dikes that occurred between 1370 and 1200 Ma (Page 1988).

Sedimentology and stratigraphy

Overlying the steeply dipping Paleoproterozoic basement metasedimentary rocks (Fig. 8-20) is the relatively undeformed and flat-lying Kombolgie Subgroup, formerly the Kombolgie Formation, and part of the Katherine River Group. The Kombolgie Subgroup consists of sandstone and conglomerate, and interlayered volcanic units of the Nungbalgarri Formation and Gilruth Member (Page & Williams 1988). Economic deposits of U have primary mineralization ages of 1650–1675 Ma (Maas 1989, Polito *et al.* 2004, 2005a, 2005b) and are hosted in the Paleoproterozoic basement rocks, but near the unconformity between the basement and overlying Kombolgie Subgroup. The Kombolgie Subgroup consists predominantly of sandstone and arkose that were deposited in fluvial and eolian environments with occasional marine incursions that deposited marine sandstone and evaporite. Marine conditions dominated in the McKay Formation, as suggested by the presence of glauconite, halite crystal casts, and wave ripple marks in sandstone (Fig. 8-21). Sandstone of the McKay Formation shows minimal diagenesis relative to the rest of the units in the Subgroup.

The Kombolgie Subgroup is composed of at least three stratigraphic sequences (Hiatt *et al.* 2007). The lowermost, like that of the Thelon and Athabasca basins, is coarse-grained and represents the early stages of basin formation. This lower sequence is composed of coarse-grained sandstone and conglomerate with abundant trough cross-bedding. These lower stratigraphic units are interpreted to primarily represent deposition in high energy braided river systems that transported sediment to the south and east from a proximal source region. After this initial stage of basin evolution, coarse to medium-grained quartz arenite was deposited and represents deposition in much lower energy, more distal braided streams. These

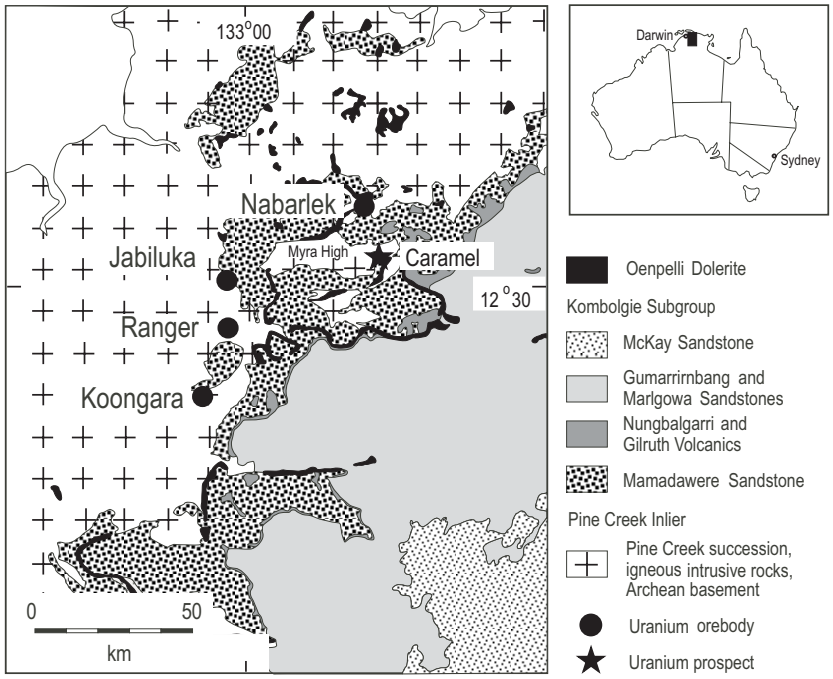

Fig. 8-20. General geology and locations of unconformity-related U deposits and prospects in the Kombolgie Basin. Modified from Holk *et al.* (2003) and Polito *et al.* (2005b).

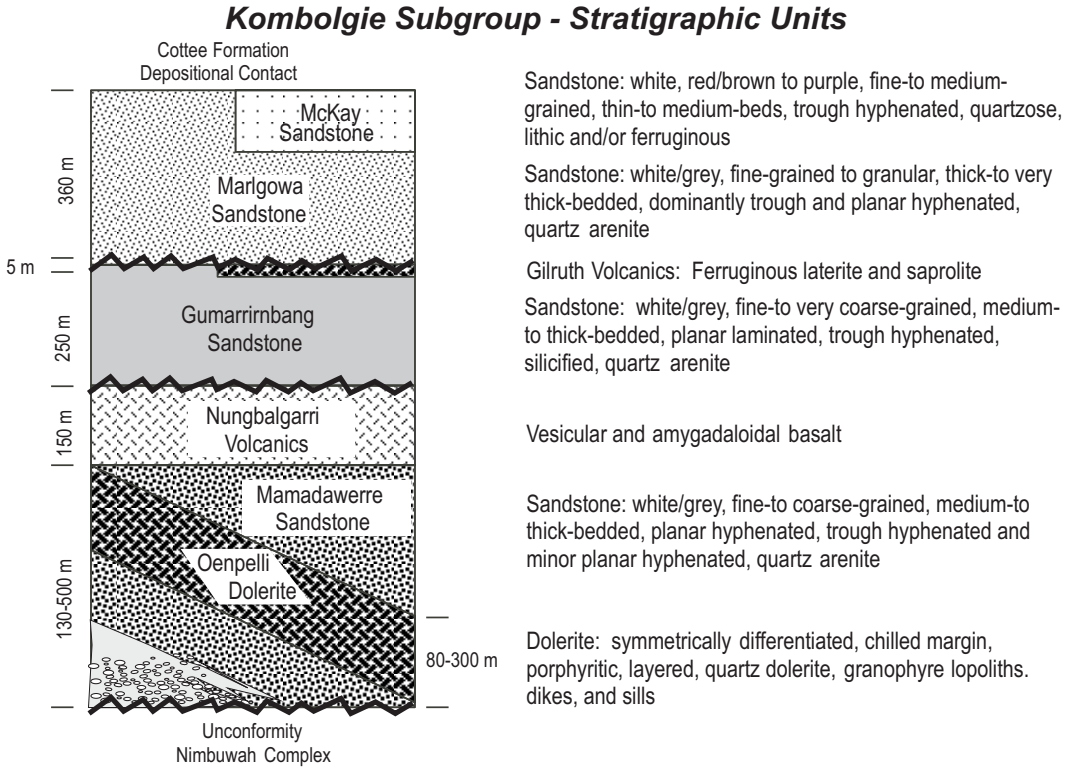

Fig. 8-21. Stratigraphic units of the Kombolgie Subgroup. After Kyser *et al.* (2000) and Hiatt *et al.* (2007).

sandstone layers were deposited by sand bar migration and sheet flow across braid plains and exhibit much better sorting than sediments laid down by the higher energy streams that preceded this interval. This evolution from proximal to more distal fluvial environments occurs in the sandstone units of the Gumarrirnbang Formation (Fig. 8-21). This facies of fluvial deposition is overlain by very well sorted, medium-grained quartz arenite that exhibits large-scale wedge to trough cross bedding. Foresets are up to 3 m in length, dip 18–20° and exhibit reverse grading. The unit is interpreted as representing eolian dune deposition. Overlying the dune field is an interval marked by mud-rich, fine-grained sandstone and mud-cracked siltstone with wave ripple marks and minor flaser bedding, which are interpreted to represent tidal flat deposition. The overlying Marlgowa Formation marks a return to distal fluvial deposition. Basin subsidence or sea level rise late in the depositional history of the Kombolgie Subgroup resulted in marine conditions returning to the basin in the McKay Formation (Fig. 8-21). Evaporite deposits and evaporated seawater associated with the marine stages are likely sources of brines that eventually evolved into mineralizing fluids.

Paragenesis and fluid evolution in the Kombolgie Basin

Sandstone in the Kombolgie Basin is typically mature quartz arenite with detrital phases consisting of quartz (90–100%), lithic fragments (0–10%), and trace hematite, zircon, and apatite. Moderate to well sorted detrital quartz sand grains range from 0.1–2.5 mm in diameter and well rounded lithic fragments are generally 0.2–1.0 mm in diameter. Detrital quartz separated from sandstone of the Gumarrirnbang and Mamadawerre formations have $\delta^{18}O$ values consistent with a provenance similar in isotopic composition to the basement rocks.

The generalized paragenetic sequence recorded in the lower Kombolgie Subgroup sandstone layers (Fig. 8-22) is characterized by formation of early stage quartz overgrowths (Q1) that formed at 80–130°C from low salinity NaCl fluids with <10 wt.% NaCl having δD values typical of evaporated seawater (Kyser *et al.* 2000, Polito *et al.* 2006b, Derome *et al.* 2003, 2007). The first stage of hematite (H1) occurs along the interface between the detrital and overgrowth quartz. Initial alteration of lithic fragments and detrital feldspar to clay (probably smectite, precursor to illite) + quartz + hematite also occurred

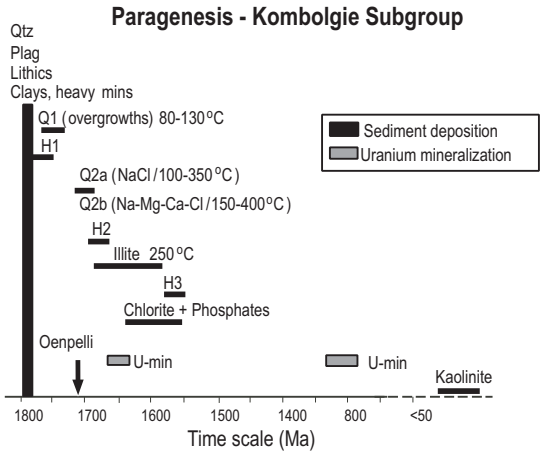

Fig. 8-22. Paragenesis of minerals in the Kombolgie Subgroup as a function of age. Modified from Kyser *et al.* (2000).

during this stage of diagenesis, and served as the most dominant source of silica (Q1) in the Kombolgie Subgroup. This early quartz cement event resulted in the most pronounced porosity reduction, particularly in the well sorted lithologies (Hiatt *et al.* 2007). The common presence of unaltered detrital zircon and apatite in quartz overgrowth-rich rocks suggests that early fluids related to Q1 cementation did not significantly mobilize components hosted in detrital zircon and apatite in these units. The principal impact of these silicified zones on basin hydrology is in the creation of basin-wide impermeable zones of diagenetic aquitards, capable of focusing later fluid flow within and toward zones of higher permeability, such as fault zones and zones without quartz cements.

The next paragenetic stage recorded in the fluid evolution in sandstone of the Kombolgie Subgroup is associated with filling of remaining pore space with diagenetic illite or less commonly, chlorite, coincident with peak diagenesis (Fig. 8-22). Hematite and rare occurrences of phosphates are also formed at this stage. The illite has a *vt*-1M crystal structure (Beaufort *et al.* 2005), thereby requiring temperatures of formation greater than 200°C. The Ar–Ar ages of the illite are 1650 ± 80 Ma and fluids in equilibrium with peak diagenetic illite were basinal brines with $\delta^{18}O$ = +6‰ and δD = –30‰, consistent with derivation from evaporated seawater and meteoric waters from low latitudes.

Chlorite follows and is coeval with illite in the lowermost parts of the Kombolgie Subgroup (Fig. 8-22), indicating a change of fluid properties in some parts of the basin to one that contained Mg. Euhedral quartz (Q2a & Q2b) that postdates the quartz overgrowths occurs with, and after, illite as massive veins, breccia pipes and cement in some sandstone from around the Myra High (Fig. 8-20), but always proximal to the Oenpelli Dolerite, which intruded throughout the basin at 1720 Ma (Kyser *et al.* 2000). This quartz has fluid inclusions with distinct characteristics that depend on their location relative to the Oenpelli Dolerite. Those farthest (up to several tens of metres) from the dolerite (Q2a; Fig. 8-22) have fluids with 20 wt.% NaCl, isotopic compositions identical to those recorded by peak diagenetic illite and homogenization temperatures from 100 to 350°C. In contrast, those proximal to the Oenpelli (Q2b) formed from fluids with the same isotopic compositions, but they are saline (20–30%) Na–Mg–Ca–Cl brines having temperatures from 150 to 400°C (Fig. 8-22). In rare instances, euhedral quartz can contain zones of primary Na-rich inclusions with earlier, or later, zones of Na–Mg–Ca–Cl inclusions and substantial variations in homogenization temperatures between the zones. In detail, silicified zones (200–250°C) occur proximal to the dolerite just beyond an inner zone of desilicification (250–400°C). This association formed in response to changes in SiO_2 solubility as convective circulation of basinal brines occurred during crystallization and cooling of sills. The fluid properties are consistent with shallow convective circulation of evolved formation fluids during the emplacement of the mafic intrusive rocks, but only in the basin near the Myra High. In the King River sub-basin located north of the Myra High (Fig. 8-20), intrusion of the hot dolerite resulted primarily in limited contact metamorphism of the sandstone because of the lack of basinal brines in the area. Intrusion of the Oenpelli Dolerite was early peak diagenesis as indicated by the age of the intrusion, older Ar–Ar ages of illite adjacent to the Oenpelli, and spilitization of the Oenpelli. Thus, after 1720 Ma, there were both NaCl and Na–Ca–Mg–Cl brines in the basin near the Myra High but not in the King River sub-basin.

The third stage in the fluid evolution of the Kombolgie Subgroup is related to fracturing, faulting, and quartz vein formation. Veins filling heavily fractured and slightly desilicified sandstone have primary aqueous fluid inclusions with δD values near –30‰, homogenization temperatures of *ca*. 200–400°C and salinities of 22 wt.% Na–Mg–Ca–Cl brines. Fluids in isotopic equilibrium with this vein quartz have isotopic compositions similar to those of peak diagenetic fluids. These relatively

^{18}O- and D-rich fluids are similar to those related to the hydraulic breccias (Q2) in the basin and likely reflect overpressured fluids that formed from the same extensive fluid–rock interaction with volcanic rocks and sedimentary rocks in the basin during emplacement of the Oenpelli and with basement rocks during the mineralizing process (Kyser *et al.* 2000, Derome *et al.* 2003, 2005) or thereafter (Polito *et al.* 2006b).

The McKay Formation (Fig. 8-21) is predominantly composed of submature to mature quartz arenite, but feldspathic arenite is common. Like the underlying sandstone of the rest of the Kombolgie Subgroup, quartz is the primary detrital phase (70–100%), but feldspar (0–30%), albeit altered, is much more common. Other detrital phases include lithic fragments (up to 10%), hematite, zircon, and apatite. Early stage authigenic quartz overgrowths are not as pronounced as in the underlying Kombolgie units. Stable isotope data for the quartz overgrowths and peak diagenetic illite from the McKay Formation are similar to those for the underlying formations described above, indicating a common fluid between the Kombolgie and McKay at early and peak diagenesis. The difference is that the McKay Formation was much less permeable and saw much lower fluid/rock ratios than the lower Kombolgie Formation.

The final stage of alteration of the Kombolgie Subgroup is pervasive kaolinite that permeates the Kombolgie Subgroup at the surface, and down to several hundreds of metres depth. This kaolinite is pervasive along fractures and in the center of pores where it replaces illite (I1). This late stage kaolinite has isotopic compositions typical of those expected from modern weathering (last 50 m.y.) associated with the development of the vast Australian regolith (Fig. 8-22).

Uranium Deposits

Jabiluka

The Jabiluka unconformity-related U deposit is located in the Alligator Rivers Uranium Field within the Pine Creek Inlier, approximately 225 km east of Darwin and 20 km north of the township of Jabiru in the Northern Territory (Figs. 8-19, 8-20). It comprises two areas of mineralization, Jabiluka I and Jabiluka II (Fig. 8-23). Jabiluka I has a resource of 1.3 Mt of ore grading 0.20% U, whereas Jabiluka II is a world class mineral resource of 31.1 Mt grading 0.45% U for 138,550 tonnes of contained U. Jabiluka II also contains a significant Au resource that is estimated to be 5–6 Mt at a grade of 3.07 g/t Au. The deposit was discovered in 1971, but has never been mined.

Mineralisation is hosted by shallow to steeply dipping Paleoproterozoic basement rocks comprising graphitic units of chlorite–biotite–muscovite schist belonging to the Cahill Formation (Fig. 8-23). These rocks are overlain by flat-lying coarse-grained sandstone of the Kombolgie Subgroup. The south-facing basement–sandstone contact with up to 300 m of displacement is a normal unconformity contact that may have been offset by minor faulting (Gustafson & Curtis 1983, Polito *et al.* 2006b). Jabiluka sits on the south-western margin of the Myra High, which probably had a paleotopographic shoulder in the vicinity of the Jabiluka deposit. The U mineralization is structurally controlled within brittle shears that are subconformable to the basement stratigraphy, and breccia that is developed within the hinge zone of fault-related folds adjacent to the shears (Polito *et al.* 2006b).

Jabiluka has an alteration halo in the basement rocks that extends at least 200 m beyond known U ore (Binns *et al.* 1980a, 1980b). Alteration associated with U mineralization can be loosely divided into an outer and inner halo, with the principal difference being an increase in fine-grained chlorite and sericite associated with brecciation in the inner halo. This alteration contrasts with the Nabarlek U deposit where the inner and outer alteration halos in the basement rocks are mineralogically distinct from one another (Wilde & Wall 1987, Polito *et al.* 2004). Alteration in the outer halo at Jabiluka is represented by chlorite that pseudomorphs metamorphic biotite, garnet, amphibole, feldspar and sillimanite, void and matrix-filling chlorite adjacent, fine-grained sericite that replaces metamorphic biotite, muscovite, amphibole and feldspar and traces of fine-grained red translucent hematite. Metamorphic zircon, muscovite, quartz and carbonaceous graphitic material are not visually altered in this area despite the alteration of adjacent phases (Binns *et al.* 1980a).

Uraninite is the dominant U mineral at Jabiluka and is intimately associated with chlorite, sericite and hematite (Fig. 8-24). Cross-cutting relationships show that multiple generations of uraninite cut chlorite and *vice versa*. Uraninite also occurs with sericite and euhedral quartz in high angle cross-cutting veins. Graphite is obliterated in strongly bleached zones adjacent to massive uraninite veins, but is generally preserved where

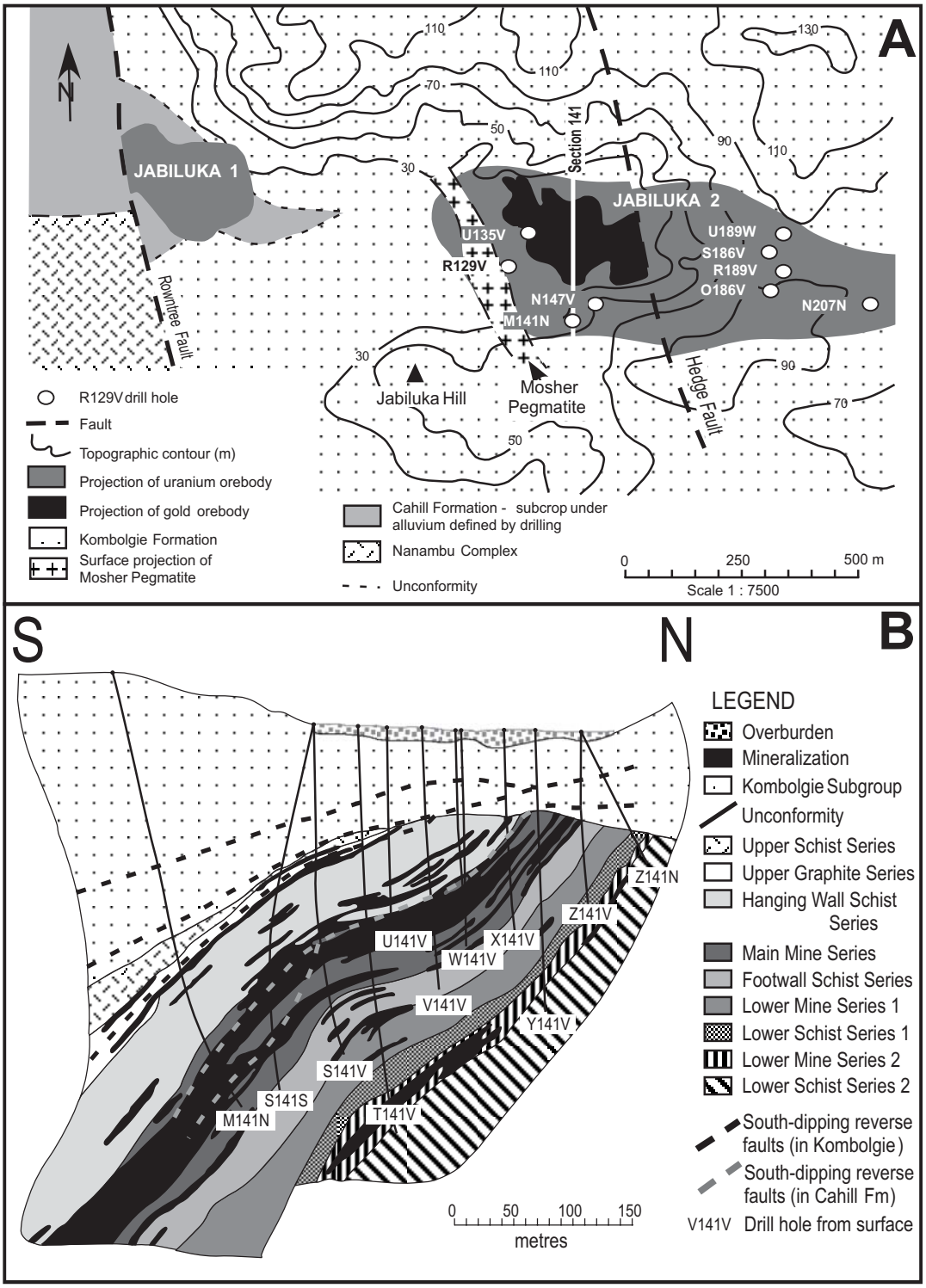

Fig. 8-23. **(A)** Plan map of geology and surface topography of the Jabiluka U deposit, with Jabiluka I and II and the Mosher pegmatite projected through the cover of the Kombolgie Subgroup (Ewers *et al.* 1984) and location of drill holes. **(B)** Interpreted cross section through section 141 of the Jabiluka deposit showing nature of the unconformity over the northern part of the deposit and the steeply south-dipping contact over the southern part of the deposit. The reverse fault structures indicated along the unconformity are from Johnston (1984). Figure modified from Polito *et al.* (2006b).

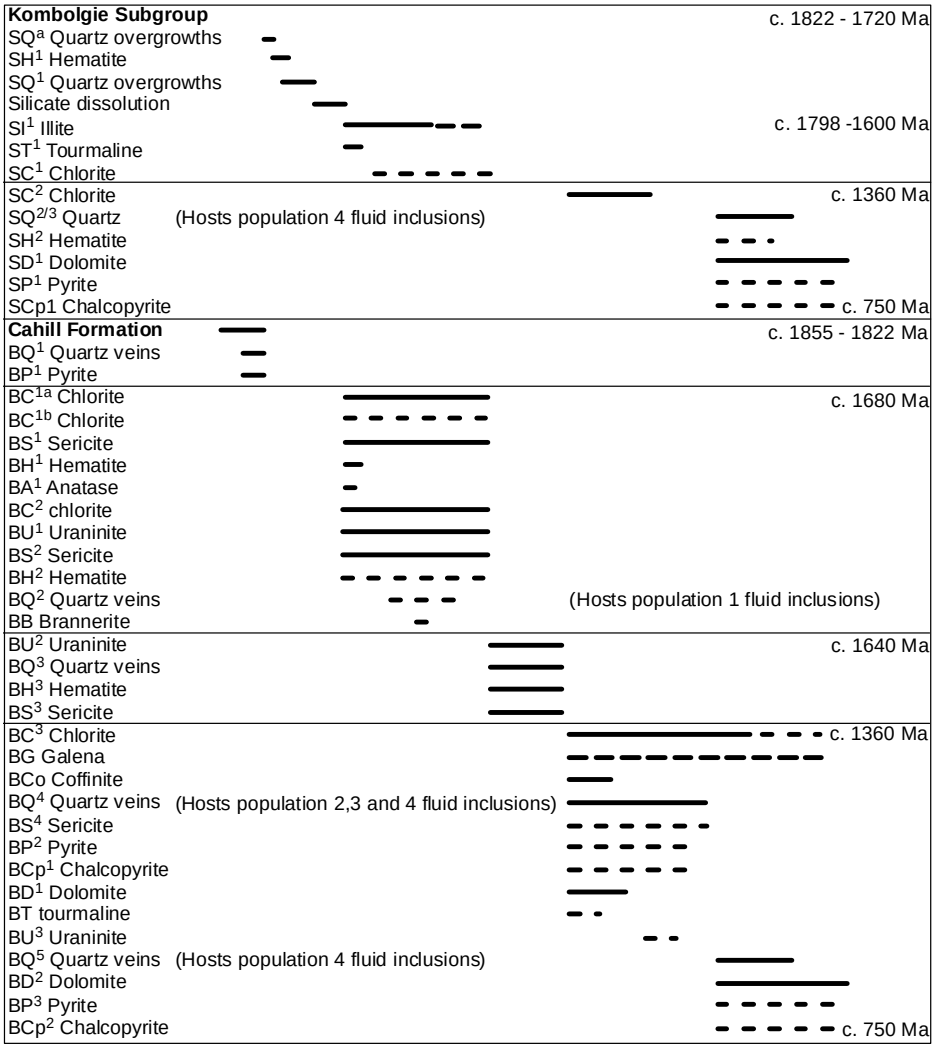

Fig. 8-24. Paragenesis of minerals in the sandstone and basement lithologies around the Jabiluka deposit. The S and B before each phase denotes sandstone diagenesis/alteration and basement alteration, respectively. The ages presented for each event are based on cross-cutting relationships that have been constrained by K-Ar ages (Page *et al.* 1980) and $^{40}Ar/^{39}Ar$ and $^{207}Pb/^{206}Pb$ ages (Polito *et al.* 2006b).

chlorite, sericite and disseminated uraninite comprise the mineralization. A later generation of monomineralic uraninite veins and uraninite–quartz veins form an interconnected stockwork. These veins occur with hematite and sericite that cross-cut and obliterate all earlier structures, metamorphic textures and minerals. The style and timing of this alteration is similar, but at a much smaller scale to that observed at Nabarlek where phengitic illite, hematite and uraninite obliterate all pre-ore textures and minerals, including quartz, in the mineralized zone (Polito *et al.* 2004).

Brannerite forms <5% of the ore and is likely coeval with uraninite, but coffinite cross-cuts and replaces uraninite, indicating its later formation (Fig. 8-24). Syn-ore illite and chlorite record mineralization temperatures of 200 ± 20°C. Pre- and syn-ore minerals from the Kombolgie Subgroup overlying the deposit and syn-ore alteration minerals in the Cahill Formation have $\delta^{18}O_{fluid}$ and δD_{fluid} values that are indistinguishable from illite from diagenetic aquifers that occur in the Kombolgie Subgroup up to 70 km south and east of the deposit and are the likely source of the mineralizing fluid.

U–Pb and $^{207}Pb/^{206}Pb$ ratios of uraninite suggest that massive uraninite first precipitated at 1680 Ma, after the cessation of brine migration out

from the Kombolgie Subgroup where illite has $^{40}Ar/^{39}Ar$ ages equal to or younger than the initial mineralization ages. Distinct $^{207}Pb/^{206}Pb$ age populations in the uraninite occur at 1300, 1190 and 800 Ma, which correlate with the intrusion of the Maningkorrirr/Mudginberri phonolitic dikes and the Derim Derim Dolerite between 1370 and 1316 Ma, the amalgamation of Australia and Laurentia during the Grenville Orogen at *ca*. 1140 Ma, and the break-up of Rodinia between 1000 Ma and 750 Ma.

Unmineralized breccia cemented by chlorite, quartz and sericite cross-cut mineralized breccia and is in turn cut by straight-sided, high-angle veins of drusy quartz, sulfide and dolomite. Drusy quartz ± dolomite ± pyrite ± chalcopyrite veins up to 10 cm wide occur in the basement units and the overlying sandstone. A cross-cutting relationship with unmineralized breccia excludes these veins from being related to the quartz in the breccias. These post-ore minerals formed when mixing between two fluids occurred sometime between *ca*. 1450 and 550 Ma.

Fluid inclusion data from a syn-ore quartz–uraninite vein indicates that the mineralizing brine was saline, but neither saturated, nor Ca-dominated (Polito *et al.* 2006b). This brine could have originated from marine fluids, in contrast to the post-ore brines, which are Ca-dominated with Na/Ca ratios as low as 0.07 (Wilde *et al.* 1989, Derome *et al.* 2003). A marine origin for the mineralizing fluid is consistent with the stable isotope values from pre- and syn-ore phyllosilicates. The $\delta^{18}O_{fluid}$ values from the pre- and syn-ore phyllosilicates in the sandstone and basement rocks are too low to be derived from a metamorphic fluid, whereas the high δD_{fluid} values rule out normal magmatic and pure meteoric sources (Taylor 1997), thus ruling out basement-derived fluids for the origin of the U.

A scenario proposed by Polito *et al.* (2006b) that adequately explains the paragenesis of minerals in the deposit involves basinal fluids in diagenetic aquifers being drawn into the basement after faulting and brecciation, thus precipitating uraninite and other alteration minerals. The basinal fluids equilibrate with the basement and those that did not hydrate the basement assemblage are driven into the sandstone during compression related to increased stress post-failure. These Mg-rich fluids precipitate chlorite until the next rupturing event occurs and fluids are again drawn into the basement. Sibson (1984) noted that dilational fault jogs such as those described for Jabiluka are often "characterised by multiple re-cemented wall-rock breccias resulting from repeated hydraulic implosion", exactly as observed at Jabiluka.

Nabarlek

The Nabarlek unconformity-related U deposit in the Alligator Rivers Uranium Field (Fig. 8-20) is hosted by Paleoproterozoic amphibolite-facies metamorphosed semipelitic sedimentary rocks and amphibolite schist on the north side of the Myra High. High grade ore is confined to the Nabarlek fault, a reverse fault/shear zone that crosscuts a series of interbedded muscovite–quartz–biotite schist and amphibolite. No graphite was present in the host lithologies, suggesting that Fe was the reductant. Eight significant fluid events were identified by Polito *et al.* (2004), beginning with the precipitation of early quartz veins during uplift of the Myra Falls Metamorphics at 1830 Ma and ending with limited uraninite recrystallization during reactivation of the Nabarlek Fault between 1380 and 750 Ma.

Quartz veins that likely formed toward the end of the Top End Orogeny represent the earliest recorded fluid event (Fig. 8-25). Fluid inclusion data and $\delta^{18}O$ and δD values indicate that these veins formed from basement-derived fluids associated with intrusion of the Nabarlek Granite during circulation through reverse fault or shear zones. The next fluid event, represented by fine-grained sericite and chlorite occurred when fluids passed into these faults and altered the metamorphic minerals following the exhumation of the basement and deposition of the Kombolgie Subgroup at about 1760 Ma. The intrusion of the Oenpelli Dolerite at 1720 Ma resulted in local mobilization of silica and precipitation of quartz associated with minor pyrite and dolomite around the reverse faults.

Uranium mineralization is associated with an inner and outer alteration halo that extends as far as 1 km from the Nabarlek fault. Alteration in the outer halo began as early as 1700 Ma and is dominated by chlorite and sericite, which formed when a 200ºC fluid flowed into the Nabarlek fault from the overlying Kombolgie Subgroup (Polito *et al.* 2004). U–Pb and $^{207}Pb/^{206}Pb$ dating reveals that massive uraninite precipitated at *ca*. 1640 Ma and formed together with illite and hematite at *ca*. 200ºC. Chlorite was not coeval with uraninite (Fig. 8-25). Stable isotopic compositions indicate that the pre-ore and syn-ore alteration assemblage formed from basinal brines derived from marine sources.

Reactivation of the Nabarlek fault at *ca*. 1360, 1100 and 900 Ma is indicated by U–Pb and

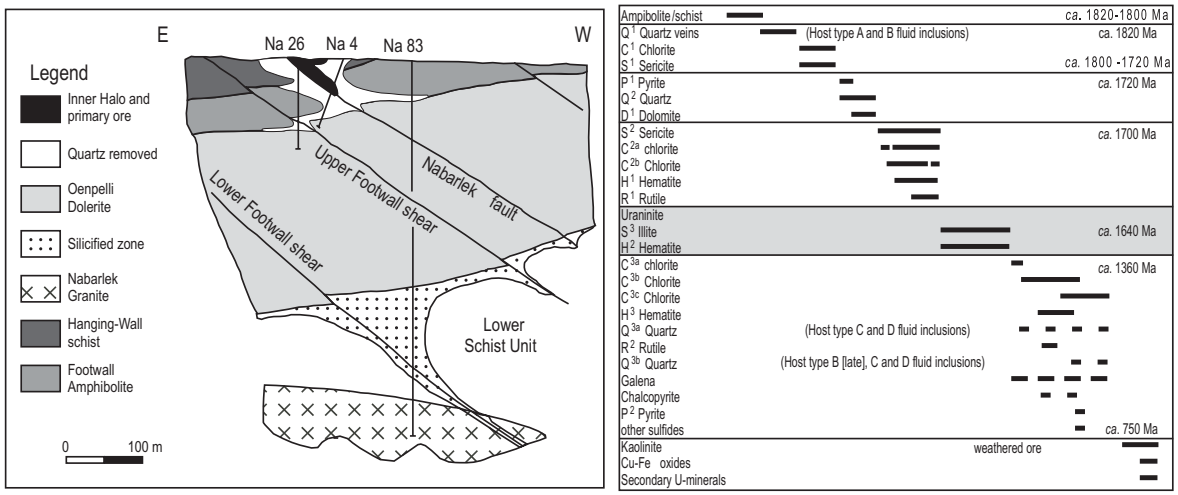

Fig. 8-25. Left: cross section through the Nabarlek orebody showing the inner alteration halo and the area identified to be devoid of quartz in relation to the Nabarlek fault. Modified after Wilde & Wall (1987) and Wilde & Noakes (1990). Right: paragenesis of alteration assemblages around the Nabarlek deposit. From Polito *et al.* (2004).

$^{207}Pb/^{206}Pb$ dates for uraninite. These ages correlate with the intrusion of the Maningkorrirr phonolitic dikes and the Derim Derim Dolerite at *ca*. 1316 and 1324 Ma, respectively, the amalgamation of Australia and Laurentia during the Grenville Orogen at *ca*. 1140 Ma, and the break-up of Rodinia between 1000 Ma and 750 Ma. Fluid incursions associated with these events precipitated much of the chlorite that has previously been related to uraninite precipitation. Drusy quartz veins that host high salinity fluid inclusions and sulfides, particularly galena, also formed after the initial uraninite-forming event.

Erosion of the Kombolgie Subgroup and subsequent weathering of the deposit resulted in kaolinite and numerous secondary U minerals. These data constrain individual events more precisely than previous studies and thus advance the current genetic model to a level that takes into account the multiple stages of fluid overprinting that occurred over a period of at least 800 million years.

Westmoreland

The northern and southern ends of the McArthur Basin share numerous geological attributes including correlative stratigraphic lithology and metal inventories (Rawlings 1999). However, whereas all of the known U deposits in the Alligator Rivers Uranium Field are hosted by amphibolite- and granulite-facies basement meta-sedimentary schist (Ewers & Ferguson 1980, Snelling 1990, Wilde & Wall 1987, Polito *et al.* 2004), the majority of the deposits in the Westmoreland U field are hosted by undeformed sandstone (Ahmad & Wygralak 1989). The Westmoreland U field comprises at least 50 U prospects of various size and grade (Ahmad & Wygralak 1989). Polito *et al.* (2005a) compared results from the two largest known deposits in the Westmoreland area, the Redtree and Junnagunna deposits (Fig. 8-26), with those in the Alligator Rivers Uranium Field. Collectively, these deposits have an average grade of 1% U and a contained resource of 15,215 tU (Rheinberger *et al.* 1998).

The Westmoreland Conglomerate, which is coeval with the basal Kombolgie Subgroup, is up to 1800 m thick and is divided into five fining upward units termed Ptw_1, Ptw_{2a}, Ptw_{2b}, Ptw_3 and Ptw_4 (Ahmad & Wygralak 1989). Each unit comprises proximal fluvial deposits typical of debris flows, alluvial fans and braided river systems that are overlain by medium- to coarse-grained, well sorted sandstone (Wygralak *et al.* 1988, Ahmad & Wygralak 1989). Cobbles and coarse sand grains within the basal conglomerate are dominated by reworked quartz veins, chert and clasts of felsic to mafic volcanic rocks that were likely derived from the Murphy Tectonic Ridge or similar basement rocks that once existed to the north (Wygralak *et al.* 1988, Ahmad & Wygralak 1989, Croaker 1996).

The Seigal Volcanics conformably overlie the Westmoreland Conglomerate. The unit is generally less than 20 m thick in the Westmoreland area occurring predominantly as basaltic lava flows, but is known to be as much as 1600 m thick in the

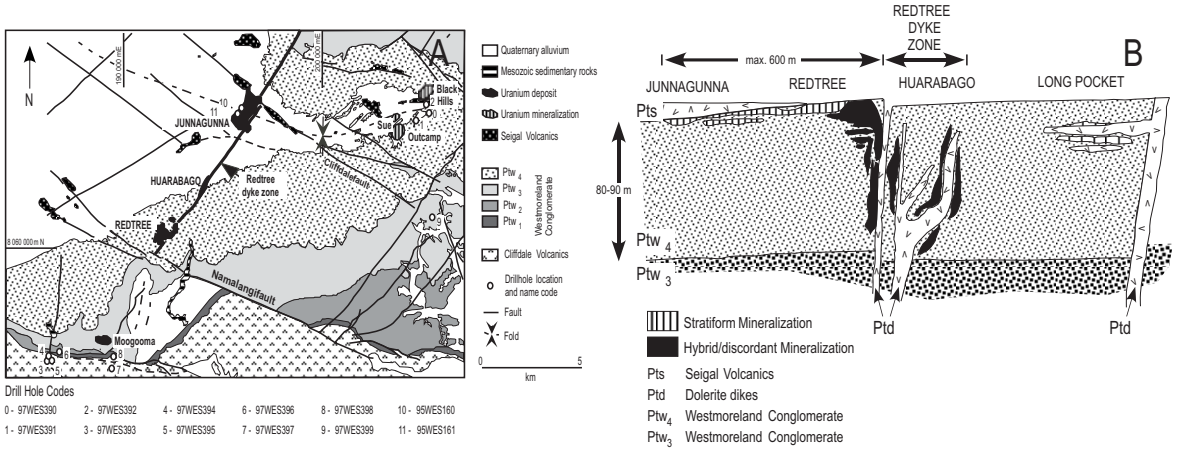

Fig. 8-26. **(A)** Location of the Redtree, Junnagunna and Huarabagoo deposits and the general geology of Westmoreland region (after Rheinberger *et al.* 1998). **(B)** Schematic cross section looking NE through the Redtree and Junnagunna uranium-deposits (after Schindlmayer & Beerbaum, 1984). The deposits comprise horizontal mineralization up to 15 m thick and vertical mineralization up to 30 m thick. From Polito *et al.* (2005a).

north-central part of the McArthur Basin (Ahmad & Wygralak 1989). The volcanic rocks are strongly altered to chlorite, illite, Fe-oxides and rare quartz and plagioclase (Ahmad & Wygralak 1989).

A number of aphyric, medium-grained dolerite dikes cut the Westmoreland Conglomerate and basement units belonging to the Murphy Inlier (Rawlings & Page 1999). These dikes commonly occur in NE-trending structures that likely reflect zones of weakness in the underlying basement. The Redtree Dike (Fig. 8-26) is one such dolerite dike. The geochemistry of the Redtree Dike is consistent with that of the Seigal Volcanics, suggesting that the dikes may have been feeders for these lava flows. The Redtree U deposit flanks the Redtree dike zone immediately north of the NW-trending Namalangi fault (Fig. 8-26). It comprises stratiform and discordant U mineralization with grades ranging from 0.15 % to > 2% U in four lenses (Rheinberger *et al.* 1998). Stratiform mineralization up to 15 m thick is hosted entirely within Ptw_4 of the Westmoreland Conglomerate below the Seigal Volcanics (Rheinberger *et al.* 1998). Vertically discordant mineralization occurs in the Westmoreland Conglomerate and dolerite of the Redtree dike zone and can be up to 30 m in thickness.

The Junnagunna U deposit occurs at a fault intersection west of the Redtree dike zone and south of the NW-trending Cliffdale Fault (Fig. 8-26). Uranium mineralization in the Junnagunna deposit is predominantly flat-lying (Fig. 8-26) and concentrated within unit Ptw_4 of the Westmoreland Conglomerate, immediately below the Seigal Volcanics (Fig. 8-26). Minor discordant mineralization occurs within the Westmoreland Conglomerate adjacent to the Redtree dike. The stratiform mineralization is 0.5 to 10 m thick, and grades from 0.3 to 1 per cent U (Rheinberger *et al.* 1998). Limited mineralization occurs on the northern side of the Cliffdale Fault and the eastern side of the Redtree dolerite dike zone.

Uranium mineralization in these deposits consists of uraninite with hematite and illite and occurs within a zone of chlorite alteration that formed prior to the uraninite. Oxygen and hydrogen isotopic compositions of syn-mineralization illite show that U was transported to the site of deposition by a basinal brine evolved from evaporated seawater, but not with hot, oxidized fluids derived from underlying uraniferous granite or volcanic rocks as previously suggested (Schindlmayer & Beerbaum 1984). Illite crystallinity indicates that the uraninite–illite–hematite assemblage formed at 200 ±50ºC and $^{40}Ar/^{39}Ar$ ages of illite and $^{207}Pb/^{206}Pb$ ages of uraninite indicate that mineralization occurred at 1655 ±83 Ma, coincident with major tectonic events in northern Australia, and was later remobilized at 1150 and 850 Ma. Fe^{2+} in the Fe-rich chlorite adjacent to the Seigal Volcanics may have provided the chemical trap that reduced the U^{6+} to precipitate uraninite. A similar precipitation mechanism occurred at the Nabarlek U deposit, where graphite is rare or absent and Fe-rich chlorite was the primary reductant (Polito *et al.* 2004). At the same time, the relatively impermeable Redtree Dike coupled with higher fluid flow created by fault

ramps that offset the Redtree Dike by up to 30 m (Croaker 1996, Rheinberger *et al.* 1998) provided the structural trap that focussed the U-bearing brine. The mineralogy, paragenesis and geochemistry of the Redtree and Junnagunna U deposits are largely indistinguishable from the basement-hosted Nabarlek U deposit in the northern McArthur Basin, suggesting that the Westmoreland U field might also be prospective for basement-hosted U deposits where suitable structural and chemical traps can be found.

Timing and spatial extent of the mineralizing fluids

Recent Rb/Sr, Sm/Nd and U/Pb isotope data on the U deposits in the ARUF indicate that primary U mineralization at Koongarra, Jabiluka and Nabarlek took place at 1640–1680 Ma (Ludwig *et al.* 1987, Maas 1989, Polito *et al.* 2004, 2005a, 2005b, 2006b). Paleotemperatures for U mineralization indicate a formation temperature near 200°C (Gustafson & Curtis 1983, Wilde 1988, Wilde *et al.* 1989, Polito *et al.* 2006a, b), although some studies have suggested lower temperatures (Beaufort *et al.* 2005). Paleomagmatic studies in the adjacent McArthur Basin show a significant change in the apparent polar wander path (APWP) at 1640–1680 Ma (Idnurm & Giddings 1995) which is related to major tectonic events in the overall McArthur Basin region (Fig. 8-27). These tectonic events match the mineralizing ages and later events, indicating that these events may have stimulated fluid flow possibly related to primary U-mineralization in the Kombolgie.

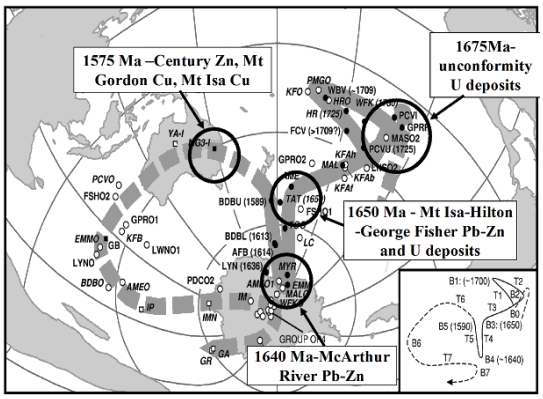

Fig. 8-27. Relationship between the apparent polar wander path for northern Australia and dates of unconformity-related U deposits, several Zn-Pb deposits and the Mt. Isa Cu deposits. APWP is from Idnurm (2000) and figure from Kyser (2007).

Recent results from the Paleoproterozoic Mt. Isa and McArthur basins in northern Australia serve as a template for exploring for mineral deposits in basins. Basinal fluids were saline, 200–300ºC and evolved primarily from meteoric water in the Mt Isa Basin and from seawater in the McArthur Basin during burial to depths of 4 to 12 km. The δD_{fluid} and $\delta^{18}O_{fluid}$ values in these brines were isotopically identical to those in the Zn–Pb, Cu and U deposits. Geochemical changes of various lithologies during alteration support either detrital minerals as the major source of the U or from monazite in the basement that reacted with the basinal brines. Ages of diagenetic phases extracted from aquifer lithologies reveal that fluid migration from the diagenetic aquifers effectively covers the period of formation for U mineralization and that the deposits formed in response to tectonic events reflected in the apparent polar wandering path for the area. Sequence stratigraphic analysis and models of fluid flow also indicate that basinal reservoirs were likely sources for the mineralizing fluids (Fig. 8-28). Thus, diagenetic aquifer lithologies were being drained of fluids at the same time as the deposits were forming from fluids that were chemically and isotopically similar, linking diagenesis and fluid events within the basin to the formation of the deposits.

OTHER BASINS HOSTING UNCONFORMITY-RELATED URANIUM MINERALIZATION

Kintyre

The Kintyre project is located on the edge of the Great Sandy Desert in the eastern Pilbara craton, about 1200 km north-northeast of Perth. CRA Exploration Pty discovered the deposits in 1985, and by 1988, they had delineated reserves totaling 30,600 tU at a grade of 0.20% U in five ore bodies (Jackson & Andrew 1990, Hickman & Clarke 1994). It is currently owned by Cameco Corp.

The Kintyre U deposit is spatially associated with the unconformity between the Rudall Metamorphic Complex and the overlying Coolbro Sandstone, which sit within the Neoproterozoic Yeneena Basin, (Fig. 8-29). The U deposits in the Rudall River area are reportedly similar to the deposits in the Alligator Rivers region and may be unconformity-related, but not much has been published about the deposit.

The ore zone at Kintyre consists of uraninite veins and lenses within chlorite–quartz schist, chlorite–carbonate schist and chloritic and

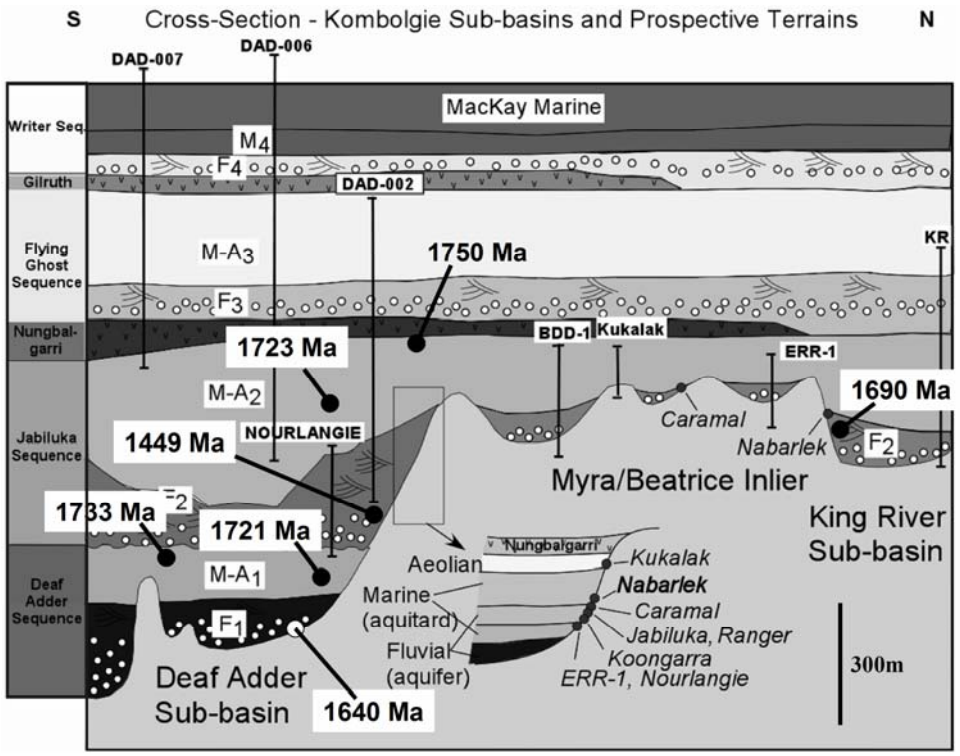

Fig. 8-28. Cross section through the Kombolgie Basin showing sequences and drill-cores used in conjunction with outcrop observations to construct this cross section. The inset shows the stratigraphic location of various U deposits, which lie near the boundary between major paleoaquifers and aquitards. Units labeled as F are fluvial facies (diagenetic aquifers) whereas those labeled M and A are marine and eolian facies (diagenetic aquitards). Also shown are the $^{40}Ar/^{39}Ar$ dates of illite from this area, which record the time that fluid was no longer interacting with the illite. From Kyser (2007) and Hiatt (pers. comm.).

garnetiferous quartzite of the Rudall Metamorphic Complex (Jackson & Andrew 1990). The age of the mineralization is uncertain, however, the veins occur in a major northwest-trending shear zone that has faulted the Coolbro Formation sandstone and therefore the mineralization is younger than 1070 Ma, the maximum age of the Yeneena Basin, and older than the Miles Orogeny that affected the deposit at about 700 Ma (Durocher *et al.* 2003). Other basement-hosted U showings in the region include the Tracy and Lead Hills prospects (Hickman & Clarke 1994) and the Mount Cotton prospect where U mineralization occurs in veins within graphite–garnet–chlorite schist in the Connaughton Terrane of the Rudall Complex (Bagas *et al.* 2000). To the east of Kintyre, within the Coolbro Formation, U–Cu prospects have been identified at Sunday Creek within the sandstone (Swingler 1981) and at Mt. Sears, where mineralization occurs within a shear zone at the top of the Coolbro Formation near its contact with the Broadhurst Formation (Schwabe 1981).

The Yeneena Basin has similar lithological characteristics to the Paleoproterozoic Athabasca Basin, Canada, and Kombolgie Basin, Australia. In comparison to the Athabasca Basin and Kombolgie Basin, the Yeneena Basin is younger (Neo-proterozoic) and has been subjected to regional deformation and greenschist-facies metamorphism, thereby complicating both the evaluation of its U potential and exploration for mineralization (Hanly 2005). The mineral paragenesis of the Coolbro Formation is similar to that of the U-rich Kombolgie Basin, with early quartz overgrowths, peak diagenetic tourmaline, muscovite, and chlorite and quartz veining that occurred during the latest stages of diagenesis (Hanly 2005). Some of the primary fluid inclusions in these quartz veins have not reequilibrated during regional metamorphism and record homogenization temperatures of 225˚C and salinity values that range from 3 to 23 wt.% eq. NaCl. The isotopic compositions of fluids that formed peak diagenetic muscovite at *ca*. 225˚C in the Coolbro Formation sandstones are consistent

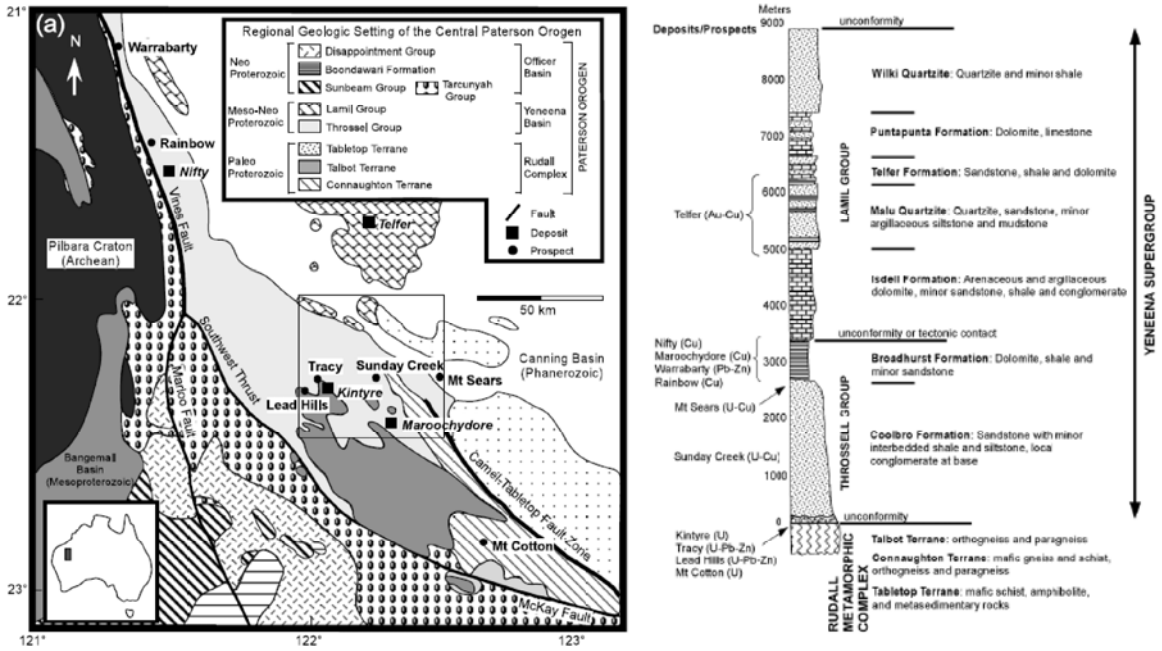

Fig. 8-29. Left: regional geologic map of the Paterson Orogen indicating major stratigraphic subdivisions and the deposits and prospects associated with the Yeneena Supergroup and Rudall Metamorphic Complex. The box corresponds to the Broadhurst 1:100 000 map sheet. Right: general stratigraphy of the Yeneena Basin and the stratigraphic location of mineral deposits and prospects. Figures from Hanly (2005).

with evolved meteoric water and seawater present during peak diagenesis, similar to the fluids associated with alteration and unconformity-type U mineralization in the U-rich Athabasca Basin and Kombolgie Basin. In contrast, secondary fluid inclusions in the quartz veins that formed later during regional metamorphism have much lower salinity of 0–8 wt.% eq. NaCl and higher homogenization temperatures of 250 to 378˚C. The isotopic compositions of diagenetic minerals and fluid inclusions were preserved because regional metamorphism was rock-dominated resulting in "dry" metamorphism. As such, regional metamorphism can have minimal effect on the mobilization of U from pre-existing deposits.

Hornby Bay

The Hornby Bay and Elu basins of northwestern Canada (Fig. 8-4) began forming at about the same time as the Thelon and Athabasca basins, also culminating in volcanism at about 1670 Ma (Bowring & Ross 1985). The Hornby Bay Basin (Fig. 8-30) is viewed as correlative with the Athabasca and Thelon Basins (Rainbird *et al.* 1994) as is the Elu Basin which extends from Bathurst Inlet north to Hadley Bay on Victoria Island (Campbell 1979). The Hornby Bay Basin is associated with the Port Radium deposit, which produced 5,800 tU at 0.6%, and also hosts the Mountain Lake showing (Bell 1996, Trueman 2005).

The Hornby Bay Basin is composed of Paleo- and Mesoproterozoic clastic–carbonate sedimentary rocks of the Hornby Bay Group and the overlying Dismal Lakes Group, which unconformably overlie Paleoproterozoic granitic and metasedimentary rocks of the Great Bear Magmatic Zone (Fig. 8-30). Present stratigraphic thickness of the Hornby Bay Group is 1500 m, with the Dismal Lakes Group being about 1100 m thick. The Hornby Bay Group is dominated by shallow marine and fluviatile clastic sedimentary rocks with minor oolitic dolomite and shale. The lower part of Dismal Lakes Group is mainly shallow marine and fluviatile siliciclastic rocks that grade upwards into stromatolitic dolomites. Both groups have basal conglomerate units (Fig. 8-30).

The Mountain Lake showing is tabular, stratabound and hosted within silicified sandstone and conglomerate of the Dismal Lakes Group, near the upper contact with the overlying laminated black shale (Armitage 2007). The showing occurs in a northeast-trending graben bounded by the steeply dipping Aquitaine and Imperial faults. Disseminated

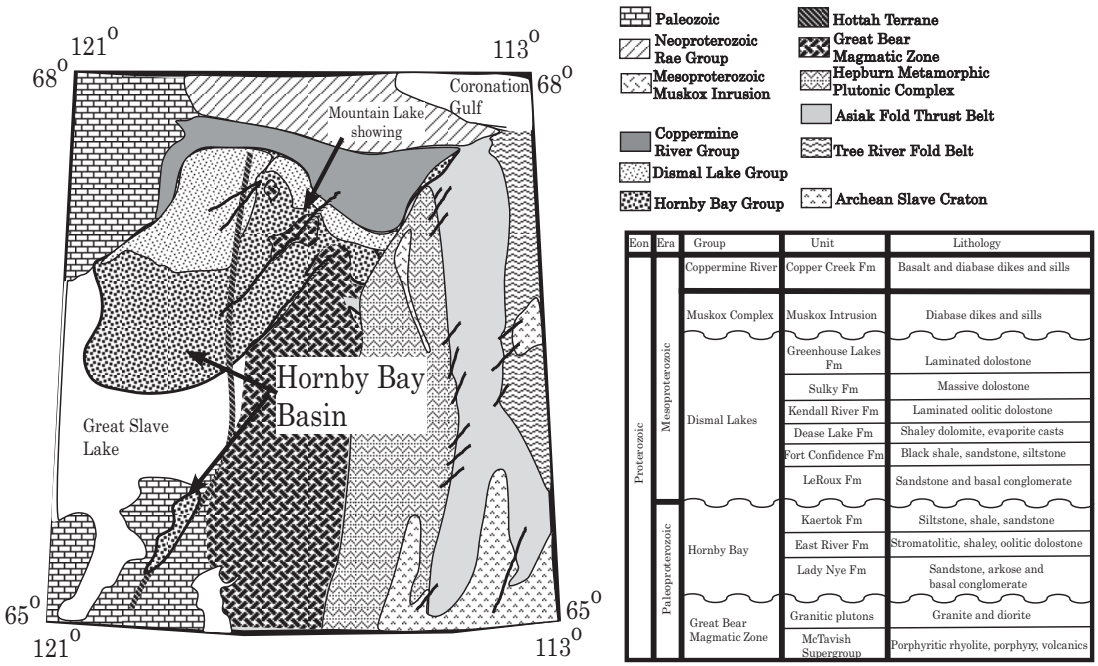

Eon	Era	Group	Unit	Lithology
Proterozoic	Mesoproterozoic	Coppermine River	Copper Creek Fm	Basalt and diabase dikes and sills
		Muskox Complex	Muskox Intrusion	Diabase dikes and sills
		Dismal Lakes	Greenhouse Lakes Fm	Laminated dolostone
			Sulky Fm	Massive dolostone
			Kendall River Fm	Laminated oolitic dolostone
			Dease Lake Fm	Shaley dolomite, evaporite casts
			Fort Confidence Fm	Black shale, sandstone, siltstone
			LeRoux Fm	Sandstone and basal conglomerate
	Paleoproterozoic	Hornby Bay	Kaertok Fm	Siltstone, shale, sandstone
			East River Fm	Stromatolitic, shaley, oolitic dolostone
			Lady Nye Fm	Sandstone, arkose and basal conglomerate
		Great Bear Magmatic Zone	Granitic plutons	Granite and diorite
			McTavish Supergroup	Porphyritic rhyolite, porphyry, volcanics

Fig. 8-30. General geology and stratigraphy of the Hornby Bay Basin, showing location of the basin and the Mountain Lake U showing. Modified from Kerans *et al*. (1981) and Ross (1983).

U oxides grading up to 0.35% U occur in several horizons and fracture-controlled mineralization grades up to 5% U across 0.3 m (Armitage 2007). The Mountain Lake showing is estimated to contain an Inferred Resource of 3,500 tU at an average grade of 0.2% U.

The Mountain Lake showing is classified as sandstone type and is akin to some of the deposits in the Paleoproterozoic Franceville Basin of Gabon (Trueman 2005), which is described in the next chapter on basin-hosted deposits. Paleocurrents in the Hornby Bay Basin were from the west for basal units (Kerans *et al.* 1981), with units of variable thicknesses (Fig. 8-30) as a result of syn-depositional compression (MacLean & Cook 2004). Much of the Hornby Bay Group is feldspathic (Kerans *et al.* 1981), although the basal sedimentary rocks that comprise the lower part of the stratigraphy have characteristics that are conducive to formation of diagenetic aquifers.

Disseminated uraninite in sandstone from a dug trench at the surface in the Mountain Lake showing (Aquitaine discovery showing) has a U–Pb date of 1221 ±83 Ma using laser–ablation high resolution–multicollector ICP–MS. Highly altered feldspars and micas surround the uraninite grains in the sample from the Mountain Lake showing. This assemblage is crosscut by a chlorite vein (1 cm width) partially altered to biotite. Quartz grains from the original sandstone are preserved principally in areas with little or no disseminated uraninite. An additional mineralized sandstone section from the Mountain Lake deposit area included barite, chalcopyrite, pyrite, trogerite/metazeunerite (U–As minerals), uraninite, gersdorfite (Ni–As) and a Cu–As–S–U mineral. They replace the chlorite–clay matrix between quartz grains. The uraninite age obtained is similar to the age of 1160 ±83 Ma reported by Davis *et al.* (2008) for early fluoroapatite cements, and both are consistent with the Mackenzie magmatic event in the area that affected both the Athabasca and Thelon basins (Kotzer & Kyser 1995, Renac *et al.* 2002). This age is significantly younger than that of the basin or basement and reflects Pb loss and resetting of the U–Pb ages coincident with the Mackenzie dikes. Thus, the age of original mineralization has yet to be revealed and the date obtained indicates that the deposits have interacted significantly with fluids along structures that were reactivated during later tectonic events.

Otish Basin

The Paleoproterozoic Otish Basin and the related Mistassini Basin are located at the margin of the Archean Superior Province adjacent to the Grenville Front (Fig. 8-31) in central Quebec, approximately 500 km north of Quebec City (Fig. 8-

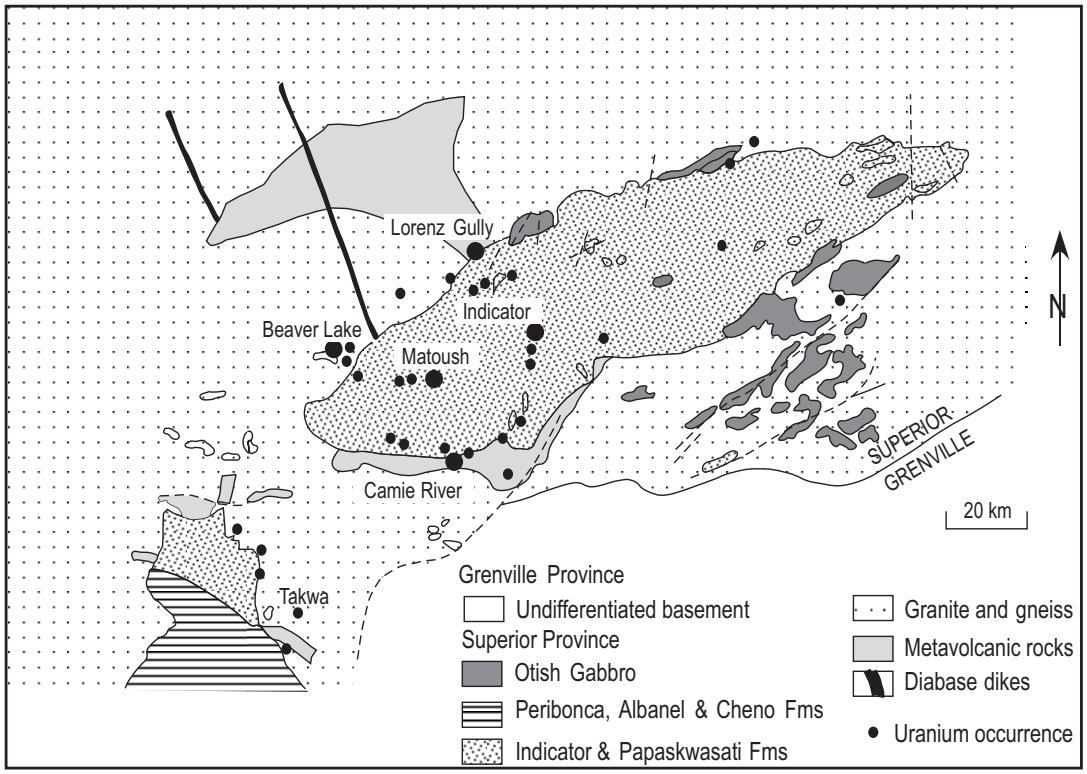

Fig. 8-31. Geology of the Otish Mountains area and location of the uranium occurrences (after Gatzweiler, 1987).

4). Sedimentary fill lies unconformably on quartz–biotite–feldspar gneiss and migmatite, metavolcanic and metasedimentary belts ("greenstone belts"), felsic intrusive complexes, and minor garnet cordierite gneiss and graphite schist of the Superior Province (Gatzweiler 1987). These basement lithologies are intruded by NNW-trending diabase dikes that date between 1926 and 2150 Ma (Heaman, pers. comm.), and do not penetrate basin fill, thus providing a maximum age of deposition of 1926 Ma. Sedimentary fill in the basin is intruded by sills and dikes of the Otish Gabbro with a presumed age of 1750 Ma (Chown & Archambault 1973), a minimum age of deposition for basin fill.

Sedimentary rocks of the Otish and Mistassini Basins overlie a well developed paleosol that extends several metres into basement lithologies at all locations where the unconformity has been observed (Chown & Caty 1983). Strata are horizontal to shallow dipping and of greenschist to sub-greenschist metamorphic facies in the northwest and central portions of the area. Strata closest to the Grenville Front to the southeast are faulted and folded, steeply dipping and have locally reached amphibolite-facies metamorphism.

Units of the Otish Basin include the basal Indicator Formation and the overlying Peribonca Formation (Fig. 8-31). Rocks of the Mistassini Basin are the clastic-dominated Papaskwasati and Cheno Formations, present to the east, and the overlying carbonate-dominated Lower Albanel, Upper Albanel, and Temiscamie Formations, present in the western part of the basin (Fig. 8-31). Chown & Caty (1973) proposed a correlation between the basins and envisioned a terrestrial-dominated Otish Basin that laterally transitioned to a marine-dominated Mistassini Basin, with increasing marine influence in the Otish Basin throughout time. Gatzweiler (1987) suggested a transition from a reducing environment during deposition of the Indicator Formation to an oxidizing environment during deposition of the Peribonca Formation.

Exploration in the western Otish Basin from 1974 to 1984 resulted in the discovery of approximately 30 U showings (Gatzweiler 1987). Information regarding the majority of these discoveries and others in the eastern Otish area is limited. Gatzweiler (1987) described five ore-grade U showings (Fig. 8-31) at Beaver Lake and Lorenz Gully (basement-hosted veins and breccia), Camie River (unconformity-related), and Matoush and

Indicator Lake (basin-hosted; proximal to diabase intrusions). Typical ore minerals include uraninite, ±uranophane, ±brannerite, ±coffinite. Typical alteration minerals include illite, chlorite, hematite, tourmaline, and quartz. Geochemical associations with Cu, As, Ni, Co, Cr, and V are observed with U mineralization at Camie River, Matoush, and Indicator. Additionally, the Camie River and Matoush showings contain late Cu–Ni–Fe–Pb sulfides, arsenides, and selenides similar to complex-type unconformity-related U deposits in the Athabasca Basin.

Hoehndorf *et al.* (1989) examined the U–Pb isotope systematics of the five U showings in the Otish Basin along with stratiform showings in basement schist at the Takwa River occurrence, where a date of 1882 Ma is interpreted as the oldest preserved mineralization in the Otish system. Deposition of the Otish Group sedimentary rocks is constrained by the age of the Otish Gabbro and dikes at 1730 Ma which intruded the sedimentary rocks and the Mistassini dikes that cut only the basement at 2140 Ma. Uranium mineralization is nearly contemporaneous with intrusion of the Otish Gabbro and dikes, with ages of 1710–1725 Ma for mineralization as veins and breccia in the basement at Beaver Lake and Lorenz Gully, at the unconformity at Camie River and in the Otish Group sedimentary rocks at Matoush and Indicator Lake. The latter two deposits also record later U mobilization at 1359 Ma, 1070 Ma and 622 Ma (Hoehndorf *et al.* 1989).

More recent studies on the Beaver Lake, Camie River, and Matoush showings (Polito & Kyser, unpub.) indicate they have paragenetic relationships that reflect three major events recorded by sedimentary and volcanic rocks around the deposits. These events correspond to early diagenesis, late diagenesis and U mineralization, and the Grenville Orogeny. Isotopic compositions of O and H in late-diagenetic illite and chlorite are consistent with formation from basinal brines that evolved from a marine-dominated fluid. Two groupings of Pb–Pb ages on uraninite indicate a likely mineralization age of 1734 Ma and a remobilization age of 1050 Ma, the former near the age of the Otish Gabbro and the latter coincident with the Grenville Orogeny. Radiogenic Pb leached from the sedimentary rocks from the Indicator Formation has a Pb–Pb model age near 1287 Ma, consistent with mobilization of radiogenic Pb from a U deposit during post-depositional events.

Karku, Russia

Discovered in 1989, the Karku unconformity-related deposit is associated with the small Pasha-Ladoga Basin in northeastern Russia (Fig. 8-32). This deposit, located just north of St. Petersburg on

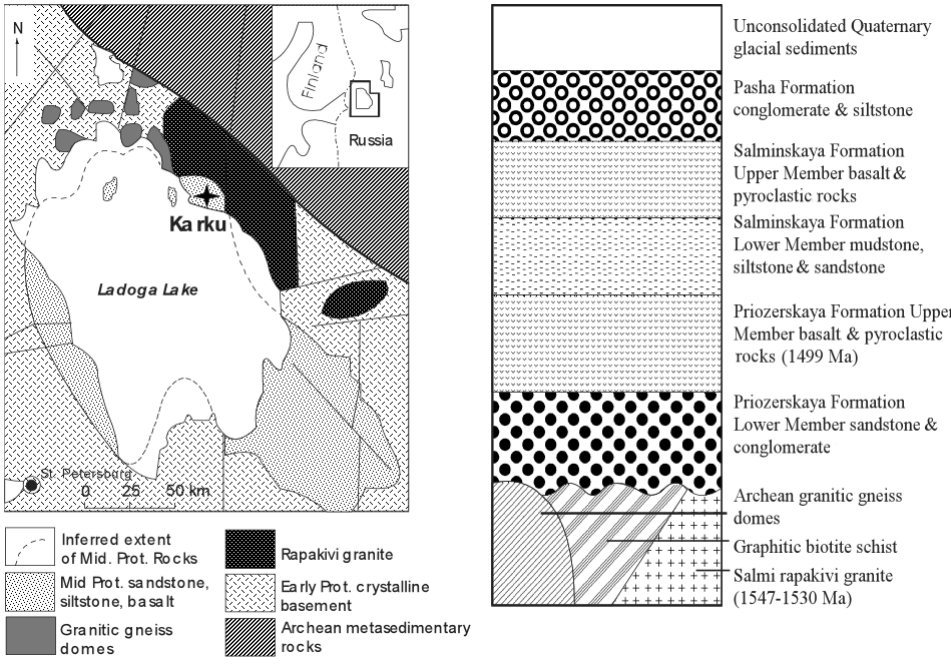

Fig. 8-32. Plan map of the Pasha-Ladoga Basin and surroundings (after Andreeva & Golovin, 2005) and stratigraphic section of the Pasha-Ladoga Group and basement rocks (after Lobaev *et al.* 2003).

the northeastern shore of Lake Ladoga, appears to be unconformity-related, but is different from the Athabasca and Kombolgie basins in several key aspects. The age of the basin itself is younger, having formed during the Mesoproterozoic after emplacement of rapakivi granite at 1530 Ma that make up the basement rocks to the east of the deposit (Andreeva & Golovin 2005, Amelin *et al.* 1997). The sedimentary rocks in the area of Karku are immature, feldspathic, clay and lithic-rich sandstone and conglomerate with significant amounts of calcite cement, distinct from the clean arenite of the Athabasca, Kombolgie and Thelon basins.

The Pasha-Ladoga Basin is located on the southeast margin of the Baltic Shield over the Ladoga geological block (Fig. 8-32). The basin is in a depression created by the intersection of two major fault zones, the Ladoga-Barents belt striking northwest and the Ladoga-Barents tectonic zone striking north–south. Tectonic movements have created horst and graben structures in the area, with the Karku deposit located over a block in the Pasha-Ladoga Basin called the Central Horst, uplifted by 200–300 m from surrounding basement rocks. (Velichkin *et al.* 2005). The basement rocks belong to the Ladoga Supergroup, with biotite–amphibole schist, graphitic biotite schist, amphibolite and granite gneiss dated at 2100–1800 Ma (Lobaev *et al.* 2003) and deformed and folded during the Svecofennian Orogeny from 1900–1800 Ma (Velichkin *et al.* 2005). The large Salmi rapakivi granite pluton intruded into the basement rocks at 1530–1547 Ma (Amelin *et al.* 1997) at the northeastern edge of the basin. A sharp angular unconformity, dipping gently southwest and marked by a regolith from a few centimetres to 30 m thick, overlies both the metamorphic and rapakivi granite basement rocks (Velichkin *et al.* 2005).

The Riphean Pasha-Ladoga Group basin rocks (Fig. 8-32) consist of several volcano-sedimentary packages up to 2.6 km thick and comprise the basal Priozerskaya Formation with lower sandstone and upper flood basalt members dated at 1499 ±68 Ma (Andreeva & Golovin 2005). The Priozerskaya Formation is only preserved over the Central Horst, indicating significant erosion (Velichkin *et al.* 2005). Overlying this is the Salminskaya Formation with lower sandstone and upper flood basalt members, and conglomerate and siltstone of the Pasha Formation (Lobaev *et al.* 2003). The lower units are complicated by multiple faults and fractures, mostly likely formed due to subsidence and post-depositional tectonic movement (Velichkin *et al.* 2005). The area is covered by unconsolidated Quaternary glacial moraine sediments, ranging from 24 to 85 m thick.

Original clasts include quartz (10–35%), potassium feldspar as microcline with characteristic tartan twinning and as orthoclase (20–50%), detrital zircon and muscovite, and corroded lithic fragments including plagioclase and pyroxene. Hematite occurs both as distinct grains and as staining throughout the sandstone. Detrital quartz shows hematite rim staining and syntaxial quartz cements on original grain boundaries, with corrosion of the euhedral cements by matrix clays postdating quartz cement. There is 0–15% green chlorite in the matrix, but in unmineralized samples at the unconformity in the ore zone, there is 20–30% bright green chlorite in the matrix. Large orthoclase clasts show cracking and alteration inside the grains as well as on the edges, and plagioclase and pyroxene clasts have been almost completely replaced by matrix clay minerals including chlorite. Small microcline grains appear to be unaltered, with only slightly corroded grain edges.

High grade ore zones ranging from 0.3% up to 19% U occur within the sandstone at the unconformity, with some mineralization up to 20 m above and 10 m below the unconformity along faults (Fig. 8-33). Mineralization is associated with intense fracturing, more than what is normally present along the unconformity (Velichkin *et al.* 2005). Matrix clays have been identified as illite–kaolinite–smectite (Lobaev *et al.* 2003) and illite–smectite mixed-layer minerals (Velichkin *et al.* 2005). Widespread Fe-rich chloritization along the unconformity contact (Lobaev *et al.* 2003, Velichkin *et al.* 2005, Andreeva & Golovin 2005) is accompanied by carbonates, pyrite, and fluorite (Shurilov *et al.* 2003, Velichkin *et al.* 2005). Uraninite occurs as complete replacement of the matrix minerals and intrudes the chlorite crusts, indicating that chlorite formed prior to the uraninite (Fig. 8-33). Reflected light microscopy reveals considerable inhomogeneity within the uraninite, including many small euhedral cubes of galena scattered throughout representing post-ore alteration that added sulfur to the system, also responsible for the pyrite grains in the chlorite. Post-ore calcite veinlets cut the clasts, chlorite and uraninite.

Uraninite has been dated by U–Pb SIMS at 1405 ± 76 Ma and a lower intercept of 412 ± 11 Ma (Shurilov *et al.* 2006), whereas LA–ICP–MS gives ages of 1467 ± 39 Ma. There is a purported second

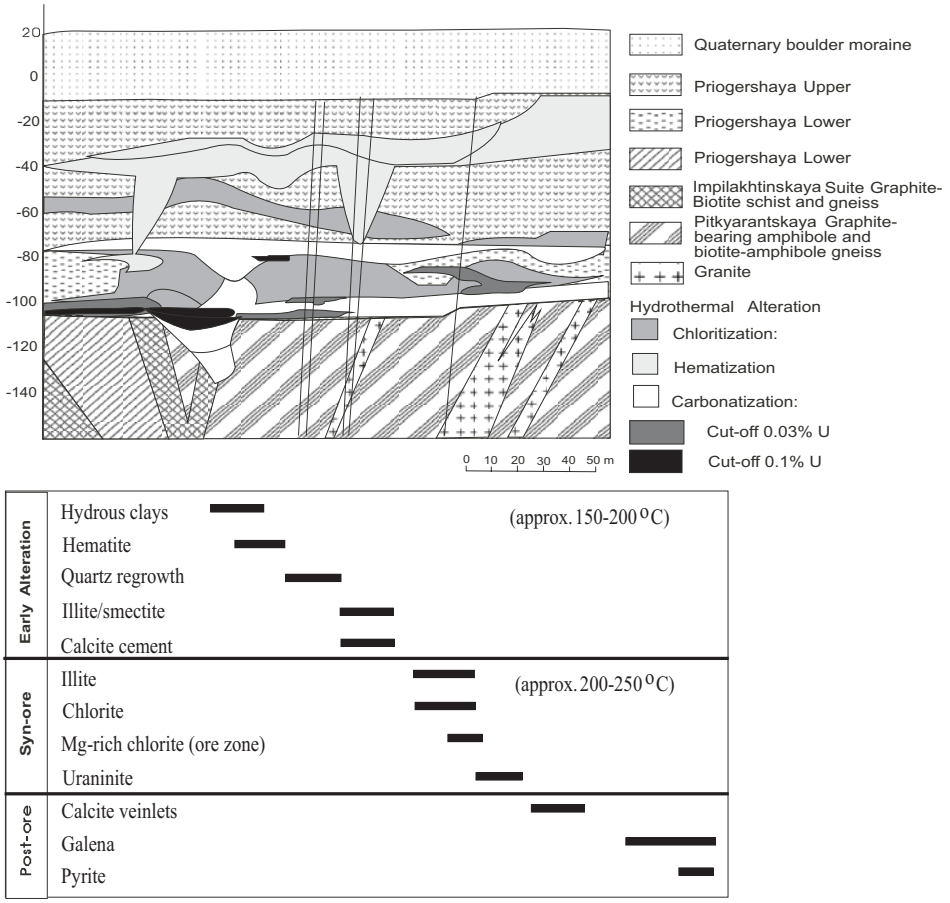

Figure 8-33. Geologic and alteration cross section of the Karku deposit and simplified mineral paragenesis around the deposit, including approximate temperatures. Interstitial swelling clays and hematite staining formed early in the diagenetic history of the basin and with increased burial, swelling clays and mud recrystallized into mixed-layer illite-smectite and quartz cements. Calcite in the matrix is coeval with mixed-layer clays in the matrix. First-generation chlorite is a pervasive alteration product in all lithologies, particularly in areas near the deposit, but before deposition of uraninite. A second generation of Mg-rich chloritization occurring as crusts around quartz and feldspar clasts is particularly prevalent in the ore-bearing zones. Uraninite replaces all matrix minerals, and is later cut by calcite veinlets. Sulfur is added to the system through post-ore fluid movement forming microscopic pyrite grains occurring in 2nd-generation chlorite.

generation dated at 1131 ± 31 Ma (Shurilov *et al.* 2006), although this is likely a reset associated with assembly of Rodinia. Areas within the uraninite that give discordant ages reflect reset uraninite, dominantly at 1100 Ma, where Pb has left the uraninite structure and Si, Fe, Ca and Mg have entered. Alteration varies considerably over micrometre scales as shown by the mottled appearance of the uraninite in back-scattered electron images. A complex fluid history with multiple resetting events is recorded in the $^{206}Pb/^{207}Pb$ dates from the uraninite, with ages at 1300 Ma coinciding with the start of the Grenville orogeny, and at 1100 Ma resulting from the initial breakup of Rodinia and at 300 Ma representing reactivation of old fault structures caused by far-field effects of the Caledonian Orogeny (Shurilov *et al.* 2006).

Samples of the basal Priozerskaya Formation away from the ore zone consist of a matrix of 10–85% smectite and illite with occasional dickite (10–55%) whereas samples near the unconformity in the ore zone consist of 40–100% chlorite and 10–65% muscovite (Fig. 8-33). Early calcite cements have homogenization temperatures of 130–190ºC (Velichkin *et al.* 2005), consistent with relatively low temperature diagenesis occurring early, while calcite syngenetic with uraninite has fluid inclusions with higher homogenization temperatures of 170–240ºC (Fig. 8-33). Illite crystallinity and chlorite compositions indicate temperatures of 190–300ºC, a level of heating at which smectite layers in the

interstratified clays should have been destroyed (Freed & Peacor 1989). The Fe-rich chlorite in unmineralized samples record temperatures near 200ºC, similar to fluid inclusion temperatures from the syn-ore calcite, confirming that Fe-rich chlorite is the result of hotter fluids flowing along the unconformity prior to mineralization. The isotopic compositions of the pre-ore fluids indicate formation from dominantly meteoric waters at low latitudes, whereas the syn-ore brines have isotopic compositions consistent with a marine source.

Karku exhibits many similarities to other unconformity U deposits in Canada and Australia. Stable isotopes indicate that mineralization reflects mixing of basinal brines and basement fluids and precipitation of high-grade U ore minerals near the unconformity. Temperatures in the ore zone recorded by clay minerals and fluid inclusions are 200°C, similar to those of the Athabasca and Kombolgie basins. The major difference is the lack of wide-scale circulation of mineralizing fluids in the deposit area itself and the silicified, immature, clayey nature of the Priozerskaya Formation rocks, which would have acted as an effective paleo-aquitard (Fig. 8-33), isolating it from fluid movement during early diagenesis. Radiogenic Pb is not very mobile outside of the deposit itself, instead remaining in the ore as galena, so that a halo of radiogenic Pb is not dispersed around the deposit as it is in the Athabasca and Kombolgie basins (Holk *et al.* 2003). Chlorite chemistry varies widely over a small distance and the clay assemblage in Karku is very different from that in the Athabasca Basin, owing to the nature of the host rocks. The basal sandstone unit of the Priozerskaya Formation represents distal, basin edge mud-rich sediment that developed early swelling clays during low temperature diagenesis, forming a diagenetic paleo-aquitard. Perhaps fluids circulated through the deeper, basal paleoaquifers at depth, leached U into solution, flowed along the unconformity in response to the far-field tectonic event that caused extensive rifting and grabens in the area and were focused into structures near the unconformity below the paleoaquitard unit. The structure was developed as a result of less competent graphite-rich units on the margin of a granitic gneiss dome. Interaction of the U-bearing fluids with the graphitic schist reductant caused precipitation of U ore.

SUCCESSOR BASINS

A different, and older, style of basement-hosted U mineralization occurs in the Beaverlodge area, Saskatchewan, Canada, and in the South Alligator River Uranium Field, Northern Territory, Australia. Uranium mineralization occurs in basement rocks beneath, and within, Paleoproterozoic basins that are stratigraphically older than, but are spatially related to, the younger U-rich Athabasca and Kombolgie basins. Igneous rocks and clastic sedimentary rocks belonging to the Martin Lake Basin in the Beaverlodge area of Canada and the El Sherana Group in the South Alligator River Uranium Field of Australia are hosts to, or overlie basement host rocks for U mineralization, but whether the deposits are unconformity-related similar to the younger Athabasca and Kombolgie basins is inconclusive. The Martin Lake Basin and the El Sherana Group represent successor basins and are distinguished from the Athabasca and Kombolgie basins by an unconformity, their smaller size and temporal relationship to older Paleo-proterozoic orogens, hence making them successor basins to an orogen and potentially sources of older U mineralization.

Exploited during 1940–60 before a decline in the price of U led to their closure, research on the genesis of deposits in the older (1720 Ma) Beaverlodge area or the South Alligator River Uranium Field (Sassano *et al.* 1972, Needham & Stuart-Smith 1987, Mernagh *et al.* 1994) has been limited. This is primarily due to the consensus that the older areas are traditionally associated with small, uneconomic deposits or are genetically related to the younger deposits despite the lack of a clear understanding of when the deposits first formed, what fluids formed them and why the deposits in these basins can be enriched in other metals. Given that about 25000 tU was mined from the Beaverlodge district (Sibbald & Quirt 1987) and 875 tU and 370,000 g of Au were recovered from deposits linked with the El Sherana Group (Mernagh *et al.* 1994), these basins have been overlooked in terms of both modern research and exploration potential.

The Martin Basin sits within basement rocks north of Lake Athabasca, from an area referred to as the Beaver Lodge district, a major producer of U from 1950–1980. The deposits in the Beaver Lodge area are spatially associated with the unconformity beneath the Martin Group, a volcaniclastic-filled successor basin (Tremblay 1972). Mafic flows in the upper Martin Group (Gillies Channel Formation) are interpreted to be *ca*. 1820 Ma based on the age of a diabase dike with similar geochemistry (Ashton *et al.* 2004). Uranium occurs

in veins in the basement near the basal unconformity, but these veins are absent where the Martin Group was not present, despite favorable basement lithologies and structures. The Martin Basin, and the prospective Baker Lake Basin east of Thelon Basin (Miller 1980), are formed in pull-apart structures filled by relatively thick but laterally restricted sequences and host low grade, unconformity-related deposits and occurrences.

The El Sherana Group in Australia was deposited at 1830 Ma (Friedmann & Gotzinger 1994) whereas the Kombolgie Group was deposited later at *ca*. 1800 Ma (Kyser *et al.* 2000). Published ages for the Martin Group are between 1630 and 1700 Ma (Tremblay 1972) but must be incorrect because the basin is overlain by the Athabasca Basin, which was likely deposited about 1750 Ma (Kyser *et al.* 2000). Both the basins that host the El Sherana Group and the Martin Lake have basement-hosted, vein-type U deposits composed primarily of U minerals that most likely formed near 1720 Ma (Kotzer & Kyser 1993, Mernagh *et al.* 1994) or older. At present, there is no consensus regarding the origin of the fluids that carried the U, the age of the deposits or their relationship with the younger sediments of the Athabasca and Kombolgie basins, primarily because they are wholly understudied. In addition, there are also complex-type deposits that contain an aberrant abundance of metals as well as U. The Coronation Hill complex-type U–Au + Pt + Pd ± Ni ± Cu ± As deposit is hosted by the El Sherana Group or equivalent in South Alligator Uranium Field (*e.g.*, Mernagh *et al.* 1994), and the Nicholson Bay U–PGE ± Ni deposit occurs in basement rocks in the Beaverlodge area 8 km away from the nearest Martin Lake Basin outcrop (Sibbald & Quirt 1987). These deposits raise additional questions regarding the origin of the precious and base metal inventory as well U.

Diagenetic processes and fluid evolution in the Martin Group and El Sherana Group have never been studied so models regarding basin *versus* basement sources for the U and other metals in the deposits have yet to be addressed. In regard to fluid timing and character, even the most recent studies cover only aspects of a few deposits and older studies dating back to the 1950s often lack the necessary details needed to construct meaningful modern exploration models (*e.g.*, Condon & Walpole 1955, Tremblay 1972, Crick *et al.* 1980). Indeed, there is a lack of basic knowledge on whether the successor basins could form or host an exploitable deposit and what their significance is (if any) to the overlying U-rich Athabasca and Kombolgie basins.

Other successor type basins may include the Baker Lake Group (1833–1785 Ma, Rainbird *et al.* 2003b), which is correlative with the Martin Group (Fraser *et al.* 1970, Rainbird *et al.* 2003b, Ashton *et al.* 2004), but it differs in having significant intercalated ultrapotassic volcanic rocks (Peterson *et al.* 2002). These alkaline units are potential sources of U for basinal fluids. Uranium prospects in the Baker Lake Basin appear to be spatially associated with the basal unconformity (Miller 1980), although only a few attributes support the unconformity model (Gandhi 2007). Supracrustal units in the Central Mineral Belt of Labrador may include red-bed lithologies and unconformities, however in this region the U deposits with reasonably assured resources, such as Michelin, have been classified as volcanic-related (Gandhi 1996).

CONCLUSIONS

The underlying initial difference in the paleohydrologic and diagenetic evolution pathways of basins that host U deposits is in the composition and distribution of the basin-filling sedimentary rocks. In the eastern Thelon and Kombolgie basins there is abundant evidence that detrital feldspar was present in the sediments as they moved into the burial setting. In stratigraphic units that had extremely high hydraulic conductivities initially, early and pervasive quartz cementation sometimes resulted in excellent preservation of this detrital feldspar. This is not the case for the sediments of the Athabasca Basin. Furthermore, the presence of multiple unconformity-bound stratigraphic sequences within the eastern Thelon Formation and the Kombolgie Subgroup indicate a much more dynamic and proximal source region for these basins. In fact, there are clasts of volcanic rock and older sandstone not only near the base, but also near the top of the Thelon Formation indicating that these basement lithologies were exposed to erosion, weathering, and reworking multiple times through the evolution of the basin. In the Athabasca Basin, on the other hand, the Manitou Falls Formation exhibits a much simpler sedimentologic evolution. After initial basin formation, stratigraphic units in the upper half of the formation accumulated as the basin underwent simple subsidence, filling the basin. There is little evidence of feldspar surviving into the deep burial setting in the Athabasca Basin. There is, however, abundant evidence suggesting

that kaolin minerals were present as detrital clay matrix. This suggests that weathering may have been much more intense in the Athabasca source region. This difference in basin-fill composition sets the stage for marked differences in the later diagenetic evolution of these basins that were necessary to form basinal brines that would be instrumental in formation of unconformity-related deposits.

Virtually all models for formation of unconformity-related U deposits invoke a reduction front near the unconformity between Proterozoic sandstone layers and underlying metamorphosed basement lithologies. The deposits are structurally hosted in either the basement, such as the Kiggavik deposit in the eastern Thelon Basin, or in overlying sandstone, such as the Boomerang Lake showing in the western Thelon Basin. The major issue in these models is whether the U is derived from the breakdown of U-bearing detrital phases, so that the source of the basin fill influences the prospectivity of a basin, or from the breakdown of monazite in the basement, so that the basement lithologies and their structural evolution influence prospectivity. Although the source of U is critical for understanding how the deposits formed and the fluids involved, it is their timing, and the critical physical and chemical environments that are probably more important in formulating exploration strategies.

REFERENCES

AHMAD, M. & WYGRALAK, A.S. (1989): Calvert Hills, Northern Territory; 1:250 000 Metallogenic Map Series, sheet SE53-8. *Northern Territory Geol. Surv., Map & Explanatory Notes*: Government Printer of the Northern Territory, 55 p.

ALEXANDRE, P., KYSER, K., POLITO, P. & THOMAS, D. (2005): Alteration mineralogy and stable isotope geochemistry of Paleoproterozoic basement-hosted unconformity-type uranium deposits in the Athabasca Basin, Canada. *Econ. Geol.* **100,** 1547-1563.

ALEXANDRE, P., KYSER, K., THOMAS, D., POLITO, P. & MARLATT, J. (2007): Geochronology of unconformity-related uranium deposits in the Athabasca Basin, Saskatchewan, Canada and their integration in the evolution of the basin. *Mineral. Dep.*, in press.

ALEXANDRE, P., KYSER. K. & JURIKA, D. (2008): Critical geochemical and mineralogical factors for the formation of unconformity-related uranium deposits in the Athabasca Basin, Canada. *Mineral. Dep.* (in review).

ALLEN, P.A. & ALLEN, J.R. (1990): *Basin Analysis: Principles and Applications*, Blackwell Science, Boston, 451p.

AMELIN, Y.V., LARIN, A.M. & TUCKER, R.D. (1997): Chronology of multiphase emplacement of the Salmi rapakivi granite-anorthosite complex, Baltic Shield: implications for magmatic evolution. *Contrib. Mineral. Petrol.* **127**, 353-368.

ANDRADE, N. (2002): Geology of the Cigar Lake uranium deposit. *In*: The Eastern Athabasca Basin and Its Uranium Deposits. Andrade, N., Breton, G., Jefferson, C.W., Thomas, D.J., Tourigny, G., Wilson, W., and Yeo, G.M., *eds*. Geol. Assoc. Can. and Mineral. Assoc. Can. **Field Trip A-1 Guidebook**, 53-72.

ANDREEVA, O.V. & GOLOVIN, V.A. (2005): Altered wall rocks in the Karku unconformity type uranium deposit and their genesis (Northern Ladoga region, Russia). *Geol. Ore Deps.* **47**, 410-428.

AREVA Annual Report, 2005. Table 8-4, page 70.

ARMITAGE, A.E. (2007): Technical Report on the Mountain Lake Property, Nunavut, Canada (NTS 86N/7). Triex Minerals Corp, **43-101**, 46 p.

ARMSTRONG, R.L. & RAMAEKERS, P. (1985): Sr isotopic study of Helikian sediment and diabase dikes in the Athabasca Basin, northern Saskatchewan. *Can. J. Earth Sci.* **22**, 399-407.

ASHTON, K.E., HARTLAUB, R.P., HEAMAN, L.M., MORELLI, R., BETHUNE, K.M., & HUNTER, R.C. (2004): Paleoproterozoic sedimentary successions of the southern Rae Province: Ages, origins, and correlations. Geol. Assoc. Can. and Mineral. Assoc. Can., Proceedings of the Joint Annual Meeting, St. Catharines, 435.

BAGAS, L., WILLIAMS, I.R. & HICKMAN, A.H. (2000): Rudall, Western Australia, second edition: Western Australia Geological Survey, 1:250 000 Geological Series Explanatory Notes, 50 p.

BAUDEMONT, D. & PACQUET, A. (1996): The Sue D and E uranium deposits, northern Saskatchewan: Evidence for structurally controlled fluid circulation in the Athabasca Basin. *In:* MinExpo'96 Symposium-Advances in Saskatchewan Geology and Mineral Exploration. Ashton, K.E. & Harper, C.T., *eds*. Sask. Geol.

Soc. Special Publ. **14**, p. 85-95.

BEAUFORT D., PATRIER P., LAVERRET E., BRUNETON P. & MONDY J. (2005): Clay alteration associated with Proterozoic unconformity-type uranium deposits in the East Alligator Rivers uranium field, Northern Territory, Australia. *Econ. Geol.* **100,** 515-536.

BECK, L.S. (1969): Uranium Deposits of the Athabasca Region, Saskatchewan. Department of Mineral Resources, Geological Science Branch, Precambrian Geology Division, Province of Saskatchewan, Report No. **126**, 140 p.

BELL, R.T. (1996): Sandstone uranium. *In*: Geology of Canadian Mineral Deposit Types, Eckstrand, O.R., Sinclair, W.D., and Thorpe, R.I., *eds.*, **8**: *Geol. Surv. Can.*, Geology of Canada, 212-219.

BINNS, R.A., AYRES, D.E., WILMSHURST, J.R. & RAMSDEN, A.R. (1980a): Petrology and geochemistry of alteration associated with uranium mineralization at Jabiluka, Northern Territory, Australia. In: Ferguson J, Goleby AB (eds) *Uranium in the Pine Creek Geosyncline*. Vienna, International Atomic Energy Agency, 417-438.

BINNS, R.A., MCANDREW ,J. & SUN S-S (1980b): Origin of Uranium at Jabiluka. In: Ferguson J, Goleby AB (eds) *Uranium in the Pine Creek Geosyncline*. Vienna, International Atomic Energy Agency, 543-562.

BJØRLYKKE, K. (1994): Fluid-flow processes and diagenesis in sedimentary basins. *In:* Geofluids. Origin, Migration and Evolution of Fluids in Sedimentary Basins (*ed*. J. Parnell) Geol. Soc. Special Publ. **78**, 127-140.

BOWRING, S.A. & ROSS, M.G. (1985): Geochronology of the Narakay volcanic complex: implications for the age of the Coppermine Homocline and Mackenzie igneous events. *Can. J. Earth Sci.* **22**, 774-781.

BRAY C. J., SPOONER E. T. C. AND LONGSTAFFE F. J. (1988): Unconformity-related uranium mineralization, McClean deposits, north Saskatchewan, Canada; hydrogen and oxygen isotope geochemistry. *Can. Mineral.***26,** 249-268.

BRUNETON, P. (1993): Geological environment of the Cigar Lake uranium deposit. *Can. J. Earth Sci.* **30**, 653-673.

BUCHAN, K.L. & ERNST, R. E. (2004): Diabase dyke swarms and relate units in Canada and adjacent regions: *Geol. Surv. Can., Map* **2022A**, scale: 1:5,000,000.

CAMPBELL, F.H.A. (1979): Stratigraphy and sedimentation in the Helikian El Basin and Hiukitak Platform, Bathurst Inlet-Melville Sound, N.W.T. *Geol. Surv. Can.* **Paper 79-8**, 18.

CAMPBELL, J.E., KLASSEN, R.A. & SHIVES, R.B.K. (2007): Integrated field investigations of airborne radiometric data and drift composition, Nuclear Energy Agency-International Atomic Energy Agency Athabasca Test Area, Saskatchewan. In: Jefferson, C.W., and Delaney, G., eds., *EXTECH IV: Geology and Uranium EXploration TECHnology of the Proterozoic Athabasca Basin, Saskatchewan and Alberta*. *Geol. Surv. Can.*, Bulletin **588**, 533-555-

CARD, C., PORTELLA, P., ANNESLEY, I. & PANĂ, D. (2007): Basement rocks of the Athabasca Basin, Saskatchewan and Alberta. I*n* Jefferson, C.W., and Delaney, G., eds., *EXTECH IV: Geology and Uranium EXploration TECHnology of the Proterozoic Athabasca Basin, Saskatchewan and Alberta. Geol. Surv. Can.*, Bulletin **588**, 69-88.

CAWOOD, P. A., NEMCHIN, A. A., STRACHAN, R., PRAVE, T. & KRABBENDAM, M. (2007): Sedimentary basin and detrital zircon record along East Laurentia and Baltica during assembly and breakup of Rodinia. *J. Geol. Soc. London* **164,** 257-275.

CHAN, D., JIRICKA, D. & MAINVILLE, A. (2000): Geology and uranium resources of the Dawn Lake deposit. Cameco Corp., 2000 assessment report.

CHANDLER F.W. (1978): Geology of part of the Wollaston Lake fold belt, northern Wollaston Lake, Saskatchewan. *Canada Geological Survey Bulletin* **277**, 57 p.

CHOWN, E.H. & ARCHAMBAULT, G. (1987): The transition from dyke to sill in the Otish Mountains, Quebec; relations to host-rock characteristics. *Can. J. Earth Sci.* **24**, 110-116.

CHOWN, E.H. & CATY, J.L. (1973): Stratigraphy, petrography and paleocurrent analysis of the Aphebian clastic formations of the Mistassini-Otish Basin. *Geol. Assoc. Can.* **Special Paper 12**, 49-71.

CONDON M.A. & WALPOLE B.P. (1955): Sedimentary environment as a control of uranium mineralization in the Katherine-Darwin region, Northern Territory. *Bureau of Mineral Resources Geology and Geophysics Australia* **24**, 17p.

CREASER, R.A. & STASIUK, L.D. (2007): Depositional age of the Douglas Formation, northern Saskatchewan, determined by Re-Os geochronology. I*n* Jefferson, C.W., and Delaney, G., eds., *EXTECH IV: Geology and Uranium EXploration TECHnology of the Proterozoic Athabasca Basin, Saskatchewan and Alberta. Geol. Surv. Can.*, Bulletin **588**, 341-346.

CRICK I.H., MUIR M.D., NEEDHAM R.S. & ROARTY M.J. (1980): The Geology and mineralization of the South Alligator Valley Uranium Field. In: J. Ferguson & A. Goleby (eds.), *Uranium in the Pine Creek Geosyncline*. Proceedings of the International Atomic Energy Agency, Vienna. 273-285.

CROAKER, M.R.D. (1996): *The sedimentology of the middle Proterozoic Westmoreland Conglomerate Formation and the relationship to uranium mineralization within Unit 4 at the Redtree uranium prospect.* Unpublished B.Sc. honours thesis, Queensland University of Technology, Queensland. 91p.

CUNEY, M. & MATHIEU, R. (2001): Extreme light rare earth element mobilization by diagenetic fluids in the geological environment of the Oklo natural reactor zones, Franceville Basin, Gabon. *Geology* **28**, 743-746.

CUNEY, M., BROUAND, M., CATHELINEAU, M., DEROME, D., FREIBERGER, R., HECHT, L., KISTER, P., LOBAEV, V., LORILLEUX, G., PEIFFERT, C. & BASTOUL, A.M. (2003): What parameters control the high grade - large tonnage of the Proterozoic unconformity related uranium deposits? *Uranium Geochemistry 2003*, International Conference, Nancy, France, April 2003, Proceedings, 123-126.

DAVIDSON G. I. & GANDHI, S. S. (1989): Unconformity-related U-Au mineralization in the middle Proterozoic Thelon Sandstone, Boomerang Lake Prospect, Northwest Territories, Canada. *Econ. Geol.* **84**, 143-157.

DAVIS, W.J., RAINBIRD, R.H., GALL, Q. & JEFFERSON, C.J. (2008): *In situ* U-Pb dating of diagenetic apatite and xenotime: Paleofluid flow history within the Thelon, Athabasca and Hornby Bay basins. *Geochim. Cosmochim. Acta* **72**, A203.

DEROME, D., CUNEY M., CATHELINEAU, M., DUBESSY, J. & BRUNETON, P. (2003), A detailed fluid inclusion study in silicified breccias from the Kombolgie sandstones (Northern Territory, Australia): Application t the genesis of Middle-Proterozoic unconformity-type uranium deposits. *J. Geochem. Explor.* **80**, 259-275.

DEROME, D., CATHELINEAU, M., CUNEY, M., FABRE, C., LHOMME, T. & BANKS, D.A. (2005): Mixing of Sodic and Calcic Brines and Uranium Deposition at McArthur River, Saskatchewan, Canada: A Raman and Laser-Induced Breakdown Spectroscopic Study of Fluid Inclusion. *Econ. Geol.* **100**, 1529–1545.

DEROME, D., CATHELINEAU, M., FABRE, C., BOIRON, M., BANKS, D. A., LHOMME, T. & CUNEY, M. (2007): Paleo-fluid composition determined from individual fluid inclusions by Raman and LIBS; application to mid-Proterozoic evaporitic Na-Ca brines (Alligator Rivers uranium field, Northern Territories, Australia); New results in fluid and melt inclusion research. *Chem. Geol.* **237,** 240-255-

DODSON, R.G., NEEDHAM, R.S., WILKES, P.G., PAGE, R.W., SMART, P.G. & WATCHMAN, A.L. (1974): Uranium mineralization in the Rum Jungle-Alligator Rivers Province, Northern Territory, Australia. In: International Atomic Energy Agency (ed.), *Formation of Uranium Ore Deposits.* Proceedings of a Symposium, Athens, 551-568.

DUROCHER, K.D., KYSER, T.K., MARLATT J. & HANLY, A. (2003): New $^{40}Ar/^{39}Ar$ ages from the central Paterson Orogen, Western Australia. *Aust. J. Earth Sci.* **50**, 601- 610.

EARLE, S. & SOPUCK, V. (1989): Regional lithogeochemistry of the eastern part of the Athabasca Basin uranium province, Saskatchewan. *In*: Muller-Kahle, E., ed., Uranium Resources and Geology of North America. *International Atomic Energy Agency, Technical Document* **TECDOC-500**, 263-269.

EARLE, S., WHEATLEY, K. & WASYLIUK, K. (1999): Application of reflectance spectroscopy to assessment of alteration mineralogy in the Key Lake area. *MinExpo '96 Symposium - Advances in Saskatchewan geology and mineral exploration*, Saskatoon, November 21, 22, 1996, Proceedings, 109-123.

EINSELE, G. (2006): *Sedimentary Basins: Evolution, Facies and Sediment Budget*. Springer-Verlag, Berlin.

EVERHART, D.L. & WRIGHT, R. (1953): The geologic character of pitchblende veins. *Econ. Geol.* **48**, 77-96.

EWERS, G.R. & FERGUSON, J. (1980): Mineralogy of the Jabiluka, Ranger, Koongarra and Nabarlek uranium deposits. In: Ferguson, J. and Goleby, A.B., eds., *Uranium in the Pine Creek Geosyncline*, Vienna, International Atomic Energy Agency 363 - 375-

EWERS, G.R., FERGUSON, J., NEEDHAM, R.S. & DONNELY, T.H. (1984): Pine Creek Geosyncline NT. *Proterozoic unconformity and stratabound uranium deposits* **TECDOC-315**, Vienna, International Atomic Energy Agency, 135-206.

FAYEK, M. & KYSER, K (1997): Characterization of multiple fluid-flow events and rare-earth elements mobility associated with formation of unconformity uranium deposits in the Athabasca Basin, Saskatchewan. *Can Mineral* **35,** 627-658.

FAYEK M. & KYSER T. K. (2000): Low temperature oxygen isotopic fractionation in the uraninite-UO (sub 3) -CO (sub 2) -H (sub 2) O system. *Geochim. Cosmochim. Acta* 64, 2185-2197.

FAYEK, M., HARRISON, T. M., GROVE, M. & COATH, C.D. (2000): A rapid *in situ* method for determining the ages of uranium oxide minerals: Evolution of the Cigar Lake Deposit, Athabasca Basin. *Internat. Geol. Rev.* **42**, 163-171.

FAYEK, M., KYSER, T.K. & RICIPUTI, L.R. (2002): U and Pb isotope analysis of uranium minerals by ion microprobe and the geochronology of the McArthur River and Sue Zone uranium deposits, Saskatchewan, Canada. *Can. Mineral.* **40**, 1553-1569.

FERGUSON, J. (1980): Metamorphism in the Pine Creek Geosyncline and its bearing on stratigraphic correlation. In: Ferguson, J. and Goleby, A. (eds.), *Uranium in the Pine Creek Geosyncline*, I.A.E.A., Vienna, 91-100.

FRASER, J.A., DONALDSON, J.A., FAHRIG, W.F. & TREMBLAY, L.P. (1970): Helikian basins and geosynclines of the northwestern Canadian Shield, *in* Baer, A.J., ed., Basins and Geosynclines of the Canadian Shield. *Geol. Surv. Canada Paper* **70-40**, 213-238.

FREED, R.L. & PEACOR, D.R. (1989): Variability in temperature of the smectite/illite reaction in Gulf Coast sediments. *Clay Minerals* **24**, 171-180.

FRIEDMANN, S.J. & GROTZINGER, J.P. (1994): Sedimentology, stratigraphy, and tectonic implications of a paleo-Proterozoic continental extensional basin: the El Sherana-Edith River groups, Northern Territory, Australia. *Can. J. Earth Sci.* **31**, 748-765-

FUCHS, H. & HILGER, W. (1989): Kiggavik (Lone Gull): an unconformity related uranium deposit in the Thelon Basin, Northwest Territories, Canada. *Uranium Resources and Geology of North America, Proceedings of a Technical Committee Meeting, Saskatoon, Saskatchewan, International Atomic energy Agency, Vienna* **IAEA-TECDOC-500**.

FUCHS, H., HILGER, W. & PROSSER, E. (1986): Geology and exploration history of the Lone Gull property. In: Uranium Deposits of Canada. E. L. Evans, *Can. Inst. Mining Metal.. Special Volume* **33**, 286-292.

GABOREAU, S., BEAUFORT, D., VIEILLARD, P. & PATRIER, P. (2005): Aluminum phosphate-sulfate minerals associated with Proterozoic unconformity-type uranium deposits in the East Alligator River uranium field, Northern Territories, Australia. *Can. Mineral.* **43**, 813-827.

GABOREAU, S., CUNEY, M., QUIRT, D., BEAUFORT, D., PATRIER, P., MATHIEU, R., COULSON, I. M., EDWARDS, P. R., & LEE, M. R. (2007): Significance of aluminum phosphate-sulfate minerals associated with U unconformity-type deposits; the Athabasca Basin, Canada; Microbeam cathodoluminescence. *Am. Mineral.***92,** 267-280.

GALL, Q. (1994): The Proterozoic Thelon paleosol, Northwest Territories, Canada. *Precamb. Res.* **68**, 115-137.

GALL, Q. & DONALDSON, J.A. (2006): Diagenetic fluorapatite and aluminum phosphate--sulphate in the Paleoproterozoic Thelon Formation and Hornby Bay Group, northwestern Canadian Shield. *Can. J. Earth Sci.* **43**, 617–629.

GALL, Q., PETERSON, T.D. & DONALDSON, J.A. (1992): A proposed revision of Early Proterozoic stratigraphy of the Thelon and Baker Lake basins, Northwest Territories. *Current Research, Part C, Geol. Surv. Can.* **Paper 92-1 C**, 129-137.

GANDHI, S.S. (1989): Geology and uranium potential of the Thelon and adjacent basement in comparison to the Athabasca Basin region. In: Muller-Kahle, E., (ed.), *Uranium resources and geology of North America. International Atomic Energy Agency*, **IAEA-TECDOC-500**, Vienna, 411-428.

GANDHI, S.S. (1996): Volcanic-associated uranium, Chapter 12. *In*: Geology of Canadian Mineral

Deposit Types. Eckstrand, O.R., Sinclair, W.D., and Thorpe, R.I., *eds*, *Geol. Surv. Can., Geology of Canada* **8**, 269-276.

GANDHI, S.S. (2007): Significant Unconformity Associated Uranium Deposits o the Athabasca Basin, Saskatchewan and Alberta, and Selected Relate Deposits of Canada and the World: *Geol. Surv. Can., Open File* **5005**, *Sask. Industry and Resources, Open File* 2007- 11, CD-ROM.

GATZWEILER, R. (1987): Uranium mineralization in the Proterozoic Otish Basin, Central Quebec, Canada. *Monograph Series on Mineral Deposits* **27**, 27-48. Gebruder Borntraeger, Berlin-Stuttgart.

GUSTAFSON. L,B, & CURTIS. L,W, (1983): Post-Kombolgie metasomatism at Jabiluka, Northern Territory, Australia, and it significance in the formation of high-grade uranium mineralization in Lower Proterozoic rocks. *Econ. Geol.* **78**, 26 – 56.

GYÖRFI, I., HAJNAL, Z., WHITE, D.J., TAKÁCS, E., REILKOFF, B., ANNESLEY, I.R., POWELL, B. & KOCH, R. (2007): High-resolution seismic survey from the McArthur River region: contributions to mapping the complex P2 uranium ore zone, Athabasca Basin, Saskatchewan. In: Jefferson, C.W., and Delaney, G., eds., *EXTECH IV: Geology and Uranium EXploration TECHnology of the Proterozoic Athabasca Basin, Saskatchewan an Alberta*. *Geol. Surv. Can.* Bulletin **588**, 397-412.

HANLY, A. (2005) *Evolution of Mesoproterozoic basins and their economic potential*. Ph.D. thesis, Queen's University, 276 p.

HARRISON, W.J & TEMPEL, R.N. (1993): Diagenetic pathways in sedimentary basins. In: *Diagenesis and Basin Development* (eds. A.D. Horbury, A.G. Robinson). *AAPG Studies in Geology* **36**, 69-86.

HEAMAN, L.M., GOWER, C.F. & PERREAULT, S. (2004): The timing of Proterozoic magmatism in the Pinware terrane of southeast Labrador, easternmost Quebec and northwest Newfoundland. *Can. J. Earth Sci.* **41**, 127-150.

HECHT L. & CUNEY M. (2000) Hydrothermal alteration of monazite in the Precambrian crystalline basement of the Athabasca Basin (Saskatchewan, Canada); implications for the formation of unconformity-related uranium deposits. *Mineral. Dep.* **35,** 791-795.

HIATT, E. (2000): Sedimentology and sequence stratigraphy in basin analysis and paleohyrologic studies. In: *Fluid and Basin Evolution* (ed. T.K. Kyser), *Mineral. Assoc. Can. Short Course* **28**, 19-38.

HIATT, E. & KYSER, K. (2007): Sequence stratigraphy, hydrostratigraphy, and mineralizing fluid flow in the Proterozoic Manitou Falls Formation, eastern Athabasca Basin, Saskatchewan. In: Jefferson, C.W., and Delaney, G., eds., *EXTECH IV: Geology and Uranium EXploration TECHnology o the Proterozoic Athabasca Basin, Saskatchewan and Alberta: Geol. Surv. Can., Bulletin* **588**, 489-506.

HIATT, E.E., KYSER, T.K. & DALRYMPLE, R.W. (2003): Relationships among sedimentology, stratigraphy and diagenesis in the Proterozoic Thelon Basin, Nunavut, Canada: implications for paleo-aquifers and sedimentary-hosted mineral deposits. *J. Geochem. Explor.* **80**, 221-240.

HIATT, E.E., KYSER, T.K., FAYEK, M., POLITO, P., HOLK, G.J. & RICIPUTI, L.R. (2007): Early quartz cements and evolution of paleohydraulic properties of basal sandstones in three Paleoproterozoic continental basins: Evidence from in situ $\delta^{18}O$ analysis of quartz cements. *Chem. Geol.* **238**, 19-37.

HIATT, E.E., PALMER, S.E., KYSER, T.K. & O'CONNOR, T.K. (2008): Regional tectonic effects on the diagenesis and uranium mineralization of the Paleoproterozoic Thelon Basin, Nunavut, Canada. Submitted to *Basin Research*.

HICKMAN, A.H. & CLARKE, G.L. (1994): Geology of the Broadhurst 1:1 000 000 Sheet. *Geological Survey of Western Australia*, 40 p.

HOEHNDORF A., BIANCONI F., VON PECHMANN E. & DARDEL J. (1989): Geochronology and metallogeny of vein type uranium occurrence in the Otish Basin area, Quebec, Canada; Metallogenesis of uranium deposits; proceedings of a Technical Committee Meeting. *Panel Proceedings Series - International Atomic Energy Agency* **1989,** 233-260.

HOEVE, J. & QUIRT, D.H. (1987): A stationary redox front as a critical factor in the formation of high-grade, unconformity-type uranium ores in the Athabasca Basin, Saskatchewan, Canada. *Bull. Mineral.***110**, 157-171.

HOEVE, J. & QUIRT, D.H. (1984): Mineralization and Host Rock Alteration in Relation to Clay Mineral Diagenesis and Evolution of the Middle-

Proterozoic, Athabasca Basin, northern Saskatchewan, Canada. *Saskatchewan Research Council, SRC Technical Report* **187**, 187 p.

HOEVE, J. & SIBBALD, T. (1978): On the genesis of Rabbit Lake and other unconformity-type uranium deposits in northern Saskatchewan, Canada. *Econ. Geol.* **73**, 1450-1473.

HOFFMAN, P. (1988): United plates of America, the birth of a craton: Earl Proterozoic assembly and growth of Laurentia. *Ann. Rev. Earth Planet. Sci.* **16**, 543-603.

HOLK, G.J., KYSER, T.K., CHIPLEY, D., HIATT, E.E. & MARLATT, J. (2003): Mobile Pb-isotopes in Proterozoic sedimentary basins as guides for exploration of uranium deposits, *J. Geochem. Explor.* **80**, 297–320.

HUTCHEON, I. (2000): Principles of diagenesis and what drives mineral change *In*: Fluid and Basin Evolution (*ed.* T.K. Kyser), *Mineral. Assoc. Can.* Short Course **28**, 93-115-

IDNURM, M. (2000): Towards a high resolution Late Paleoproterozoic-earliest Mesoproterozoic apparent polar wander path for northern Australia. *Aust. J. Earth Sci.* **47**, 405 – 429.

IDNURM, M. & GIDDINGS, J.W. (1995): Paleoproterozoic-Neoproterozoic North America-Australia link: New evidence from paleomagnetism *Geology* **23**, 149-152.

IDNURM, M., GIDDINGS, J.W. & PLUMB, K.A. (1995): Apparent polar wander and reversal stratigraphy of the Paleo-Mesoproterozoic southeastern McArthur Basin, Australia. *Precamb. Res.* **71**, 1-41.

JACKSON, D.G. & ANDREW, R.L. (1990): Kintyre uranium deposit, in Hughes, F.E. (ed.): Geology of the Mineral Deposits of Australia and Papua New Guinea. *Australasian Inst. Mining Metal.* **Monograph 14**, 653-658.

JAGODZINSKI E.A. (1998): SHRIMP U-Pb dating of ignimbrites in the Pul Pul Rhyolite, Northern Territory; a cautionary tale. *AGSO Research Newsletter* **28,** 23-25.

JEFFERSON, C.W. & DELANEY, G. (2007): *EXTECH IV: Geology and Uranium EXploration TECHnology of the Proterozoic Athabasca Basin, Saskatchewan and Alberta*. *Geol. Surv. Can.*, Bulletin **588**, 644 p.

JEFFERSON, C. W., THOMAS, D. J., GANDHI, S. S., RAMAEKERS, P., DELANEY, G., BRISBIN, D., CUTTS, C., PORTELLA, P. & OLSON, R. A. (2007): Unconformity-associated uranium deposits of the Athabasca Basin, Saskatchewan and Alberta. *EXTECH IV: Geology and Uranium EXploration TECHnology of the Proterozoic Athabasca Basin, Saskatchewan and Alberta* **588,** 23-68.

JOHNSTON, D.J. (1984): *Structural evolution of the Pine Creek inlier and mineralization therein, Northern Territory, Australia.* Unpublished PhD thesis, Monash University, Victoria, 335p.

KARLSTROM, K.E., ÅHÄLL, K-I., HARLAN, S.S., WILLIAMS, M.L., MCLELLAND & GEISSMAN, J.W. (2001): Long-lived (1.8-1.0 Ga) convergent orogen in southern Laurentia, its extensions to Australia and Baltica, and implications for refining Rodinia. *Precamb. Res.* **111**, 5-30.

KASTNER, M. & SIEVER, R. (1979): Low temperature feldspars in sedimentary rocks. *Amer. J. Sci.* **279**, 435-479.

KERANS, C., ROSS, G.M., DONALDSON, J.A. & GELDSETZER, H.J. (1981): Tectonism and depositional history of the Helikian Hornby Bay an Dismal Lakes Groups, District of Mackenzie. In: Campbell, F.H.A., ed., *Proterozoic Basins of Canada: Geol. Surv. Can.* **Paper 81- 10**, 157-182.

KISTER P., CUNEY M., GOLUBEV V. N., ROYER J., LE CARLIER DE VESLUD, CHRISTIAN & RIPPERT J. (2004): Radiogenic lead mobility in the Shea Creek unconformity-related uranium deposit (Saskatchewan, Canada); migration pathways and Pb loss quantification. *C. R. – Acad. Sci. Geoscience* **336,** 205-215.

KISTER, P., VIEILLARD, P., CUNEY, M., QUIRT, D. & LAVERRET, E. (2005): Thermodynamic constraints on the mineralogical and fluid composition evolution in a clastic sedimentary basin: the Athabasca Basin (Saskatchewan, Canada). *Eur. J. Mineral.* **17**, 325-342.

KISTER, P., LAVERRET, E., QUIRT, D., CUNEY, M., MAS, P.P., BEAUFORT, D. & BRUNETON, P. (2006): Mineralogy and geochemistry of the host-rock alterations associated with the Shea Creek unconformity-type uranium deposits (Athabasca Basin, Saskatchewan, Canada). Part 2. Regional-scale spatial distribution of the Athabasca Group sandstone matrix minerals. *Clays & Clay Minerals* **54**, 295-313.

KNIPPING, H.D. (1974): The concepts of a supergene versus hypogene emplacement of uranium at Rabbit Lake, Saskatchewan, Canada. In: *Formation of uranium ore deposits*. Vienna,

International Atomic Energy Agency, 531-548.

KNOLL, A.J., JAVAUX, E.J., HEWITT, D. & COHEN, P. (2006): Eukaryotic organisms in Proterozoic oceans; Major steps in cell evolution; palaeontological, molecular and cellular evidence of their timing and global effects. *Phil. Trans. Royal Soc. London. Biol. Sci.* **361**, 1023-1038.

KOTZER, T.G. & KYSER, T.K. (1993): O, U, and Pb isotopic and chemical variations in uraninite: Implications for determining the temporal and fluid history of ancient terrains. *Amer. Mineral.* **78**, 1262-1275-

KOTZER, T.G. & KYSER, T.K. (1995): Petrogenesis of the Proterozoic Athabasca Basin, northern Saskatchewan, Canada, and its relation to diagenesis, hydrothermal uranium mineralization and paleohydrogeology. *Chem. Geol.* **120**, 45-89.

KOTZER T.G., KYSER T.K. & IRVING E. (1992): Paleomagnetism and evolution of fluids in the Proterozoic Athabasca Basin, northern Saskatchewan, Canada. *Can. J. Earth Sci.* **29**, 1474-1491.

KYSER, T.K. (2007): Fluids, basin analysis and mineral deposits. *Geofluids* **7**, 238-257.

KYSER ,T.K., HIATT, E., RENAC, C., DUROCHER, K., HOLK, G. & DECKART, K. (2000): Diagenetic fluids in Paleo-and Meso-Proterozoic sedimentary basins and their implications for long protracted fluid histories. In: *Fluid and Basin Evolution* (ed. T.K. Kyser), *Mineral. Assoc. Can.* Short Course **28**, 225-262.

LAVERRET, E., MAS, P.P., BEAUFORT, D., KISTER, P., QUIRT, D., BRUNETON, P. & CLAUER, N. (2006): Mineralogy and geochemistry of the host-rock alterations associated with the Shea Creek unconformity-type uranium deposits (Athabasca Basin, Saskatchewan, Canada). Part 1. Spatial variation of illite properties. *Clays & Clay Minerals* **54**, 275-295-

LAINÉ, R., ALONSO, D. & SVAB, M. (1985): The Carswell Structure Uranium Deposits, Saskatchewan. *Geol. Assoc. Can. Special Paper* **29**, 230 p.

LECHEMINANT, A.N. & HEAMAN, L.M. (1989): Mackenzie igneous events, Canada: middle Proterozoic hotspot magmatism associated with ocean opening. *Earth Planet. Sci. Lett.* **96**, 38–48.

LE MAITRE, R. (2005): The Eagle Point mine-structural interpretation and geology are the keys to exploration success in basement rocks. Uranium*: Origin and Exploration Techniques*, Mineral Exploration Roundup, Vancouver B.C.

LI, Z. X., EVANS, D. A. D. & ZHANG, S. (2004): A 90 degrees spin on Rodinia; possible causal links between the Neoproterozoic supercontinent, superplume, true polar wander and low-latitude glaciation. *Earth Planet. Sci. Lett.* **220,** 409-421.

LOBAEV, V., CUNEY, M & TERENTYEV, V. (2003): The Karku uranium deposit (Ladoga District): mineralogical and geochemical characteristics of the sandstone. *In*: Proceedings of the International Conference on Uranium Geochemistry (Nancy, France, 2003), 223-226.

LUDWIG, K.R., GRAUCH, R.I., NUTT, C.J., NASH, J.T., FRISHMAN, D. AND SIMMONS, K.R. (1987): Age of uranium mineralization at the Jabiluka and Ranger Deposits, Northern Territory, Australia: New U-Pb isotope evidence. *Econ. Geol.* **82,** 857-875-

MAAS, R. (1989): Nd-Sr Isotope Constraints on the Age and Origin of Unconformity-type Uranium Deposits in the Alligator Rivers Uranium Field, Northern Territory, Australia. *Econ. Geol.* **84**, 64-90.

MACDONALD, C. (1985): Mineralogy and geochemistry of the sub-Athabasca regolith near Wollaston Lake: Geology of Uranium Deposits. *Can. Inst. Mining-Soc. Econ. Geol., Uranium Symposium, Proceedings*, 155-158.

MACLEAN, B.C. & COOK, D.G. (2004): Revisions to the Paleoproterozoic Sequence A, based on reflection seismic data across the western plain of the Northwest Territories, Canada. *Precamb. Res.* **129**, 271-289.

MCGILL, B.D., MARLATT, J.L., MATTHEWS, R.B., SOPUCK, V.J., HOMENIUK, L.A. & HUBREGTSE, J.J. (1993): The P2 North uranium deposit, Saskatchewan, Canada. *Explor. Mining Geol.* **2**, 321-331.

MERNAGH T.P., HEINRICH C.A., LECKIE J.F., CARVILLE D.P., GILBERT D.J., VALENTA R.K. & WYBORN L.A.I. (1994): Chemistry of low temperature hydrothermal gold, platinum and palladium (± uranium) mineralization at Coronation Hill, Northern Territory, Australia. *Econ. Geol.* **89**, 1053–1073.

MIALL, A.D. (2000): *Principles of Sedimentary Basin Analysis*. Springer-Verlag, Berlin, 616p.

MILLER, A.R. (1980): Uranium Geology of the eastern Baker Lake Basin, District of Keewatin,

Northwest Territories. *Geol. Surv. Can.* **Bull. 330**, 63 p.

MILLER, A.R. (1995): Polymetallic unconformity-related uranium veins in lower Proterozoic Amer Group, Pelly Lake map area, northern Thelon Basin, Churchill Province, Northwest Territories. *Geol. Surv. Can., Current Research* **1995-C**, 151-161.

MILLER, A.R. & LE CHEMINANT, A.N. (1985): Geology and uranium metallogeny of Proterozoic supracrustal successions, central district of Keewatin, N.W.T. with comparisons to northern Saskatchewan. Geology of Uranium Deposits. In: Sibbald, T. I. I., and Petruk, W., eds., *Can. Inst. Mining Metal. Special Volume* **32**, 167-185.

MILLER, A.R., CUMMING, G.L. & KRSTIC, D. (1989): U-Pb, Pb-Pb, and K-Ar isotopic study and petrography of uraniferous phosphate-bearing rocks in the Thelon Formation, Dubawnt Group, Northwest Territories, Canada. *Can. J. Earth Sci.* **26**, 867-880.

MWENIFUMBO C.J. & BERNIUS G.R. (2007): Crandallite-group minerals: host of thorium enrichment in the eastern Athabasca Basin, Saskatchewan; EXTECH IV: Geology and Uranium EXploration TECHnology of the Proterozoic Athabasca Basin, Saskatchewan and Alberta. *Bulletin - Geol. Surv. Can.* **588,** 521-532.

MWENIFUMBO, C.J., PERCIVAL, J.B., BERNIUS, G., ELLIOTT, B., JEFFERSON, C.W., WASYLIUK, K. & DREVER, G. (2007): Comparison of geophysical, mineralogical and stratigraphic attributes in drill holes MAC 218 and R 88, McArthur River uranium camp, Athabasca Basin, Saskatchewan. In: Jefferson, C.W., and Delaney, G., eds., *EXTECH IV: Geology an Uranium EXploration TECHnology of the Proterozoic Athabasca Basin, Saskatchewan and Alberta: Geol. Surv. Can., Bulletin* **588**, 507-520.

NEEDHAM R.S. & STUART-SMITH P.G. (1987): Coronation Hill U-Au mine, South Alligator Valley, Northern Territory: an epigenetic sandstone-type deposit hosted by debris flow conglomerate. *BMR Journal of Australian Geology and Geophysics* **10**, 12 –131.

NEEDHAM, R.S., CRICK, I.H. & STUART-SMITH, P.G. (1980): Regional geology of the Pine Creek Geosyncline: *Proceedings of International Uranium Symposium on the Pine Creek Geosyncline*, 1-22.

NESBITT, B.E. (1990): Fluid flow and chemical evolution in the genesis of hydrothermal ore deposits. In: *Short Course in Fluids in Tectonically Active Regimes of the Continental Crust* (ed. B.E. Nesbitt) *Mineral. Assoc. Can.* **18**, 261-298.

OVERTON, A. (1979): Seismic reconnaissance survey of the Dubawnt Group, districts of Keewatin and Mackenzie. *Current Research, Part B. Geol. Surv. Can.* 397-400.

PAGE, R.W. (1988): Geochronology of early to middle Proterozoic fold belts in northern Australia: a review. *Precamb. Res.* **40/41**, 1-19.

PAGE, R.W. & WILLIAMS, I.S. (1988): Age of the Barramundi Orogeny in northern Australia by means of ion microprobe and conventional U-Pb zircon studies. *Precamb. Res.* **40/41**, 21-36.

PAGE, R.W., COMPSTON, W. & NEEDHAM, R.S. (1980): Geochronology and evolution of the late Archean basement and Proterozoic rocks in the Alligator Rivers uranium fields, Northern Territory, Australia. In: Ferguson J, Goleby AB (eds) *Uranium in the Pine Creek Geosyncline*. Vienna, International Atomic Energy Agency, 36-68.

PAGE, R.W., JACKSON, M.J., KRASSAY, A.A. & SOUTHGATE, P.N. (2000): Constraining sequence stratigraphy in North Australian basins; SHRIMP U-Pb zircon geochronology between Mt Isa and McArthur River; Carpentaria-Mt. Isa Belt; basement framework, chronostratigraphy and geodynamic evolution of Proterozoic successions., *Aust. J. Earth Sci.* **47**, 431-459.

PAGEL, M., POTY, B. & SHEPPARD, S.M.F. (1980): Contributions to some Saskatchewan uranium deposits mainly from fluid inclusion and isotopic data In: Ferguson, S., and Goleby, A., eds., *Uranium in the Pin Creek Geosyncline*. International Atomic Energy Agency (IAEA), 639-655.

PANĂ, D., CREASER, R.A., MUEHLENBACHS, K. & WHEATLEY, K. (2007): Basement geology in the Alberta portion of the Athabasca Basin: context for the Maybelle River area. *In* Jefferson, C.W., and Delaney, G., eds., *EXTECH IV: Geology and Uranium EXploration TECHnology o the Proterozoic Athabasca Basin, Saskatchewan and Alberta*. *Geol. Surv. Can.*, Bulletin **588**, 135-155-

PERCIVAL, J. B. (1993): Clay mineralogy and isotope geochemistry of the alteration halo at the Cigar Lake uranium deposit. *Can. J. Earth Sci.* **30**, 689-705-

PETERSON T. D., VAN BREEMEN O., SANDEMAN H. & COUSENS B. (2002): Proterozoic (1.85-1.75 Ga) igneous suites of the western Churchill Province; granitoid and ultrapotassic magmatism in a reworked Archean hinterland; Granite systems and Proterozoic lithospheric processes. *Precambrian Res.* **119,** 73-100.

POLITO, P.A., KYSER, T.K., MARLATT, J., ALEXANDRE, P., BAJWAH, Z. & DREVER, G. (2004): Significance of alteration assemblages for the origin and evolution of the Proterozoic Nabarlek unconformity-related uranium deposit, Northern Territory, Australia. *Econ. Geol.* **99**, 111–139.

POLITO P. A., KYSER T. K., RHEINBERGER G. & SOUTHGATE P. N. (2005a): A paragenetic and isotopic study of the Proterozoic Westmoreland uranium deposits, southern McArthur Basin, Northern Territory, Australia. *Econ. Geol.* **100,** 1243-1260.

POLITO, P., KYSER, T.K., THOMAS, D., MARLATT, J. & DREVER, G. (2005b): Re-evaluation of the petrogenesis of the Proterozoic Jabiluka unconformity-related uranium deposit, Northern Territory, Australia. *Mineral. Dep.* **40**, 257-288.

POLITO, P.A., KYSER, T.K., SOUTHGATE, P.N. & JACKSON, M.J. (2006a): Sandstone diagenesis and aquifer evolution in the Mt Isa Basin: the isotopic and fluid inclusion history of fluid flow in the Mt Isa Basin. *Econ. Geol.* **101**, 1159-1188.

POLITO, P.A., KYSER, T.K. & JACKSON, M.J. (2006b): The role of sandstone diagenesis and aquifer evolution in the formation of uranium and zinc-lead deposits, southern McArthur Basin, Northern Territory, Australia. *Econ. Geol.* **101**, 1189-1209.

QUIRT, D.H. (1985): Lithogeochemistry of the Athabasca Group: Summary o sandstone data. In: *Summary of Investigations 1985: Saskatchewan Geological Survey, Saskatchewan Energy and Mines*, **Miscellaneous Report 85-4**, 128-132.

QUIRT. D. (1997): Chloritization below the Dawn Lake uranium deposit (11A zone), northern Saskatchewan. *Geol. Assoc. Can. - Mineral. Assoc. Can. Conference Abstracts* **22**, A-122.

QUIRT, D.H. (2003): Athabasca unconformity-type uranium deposits: one deposit type with many variations. *Uranium Geochemistry 2003*, International Conference, Nancy, France, April 13-16 2003, Proceedings, 309-312.

QUIRT, D.H. & WASYLIUK, K. (1997): Kaolinite, dickite, and other clay mineral in the Athabasca Group, Canada, and the Kombolgie Formation, Australia. *11th International Clay Conference*, Ottawa, Ontario, Jun 1997, Proceedings, A61.

RAINBIRD, R.H. & HADLARI, T. (2000): Revised stratigraphy and sedimentology of the Paleoproterozoic Dubawnt Supergroup at the northern margin of Baker Lake Basin, Nunavut. *Geol. Surv. Can. Current Research* **Paper 2000-C8**, 9.

RAINBIRD, R.H., JEFFERSON, C.W., HILDEBRAND, R.S. & WORTH, J.K. (1994): The Shaler Supergroup and revision of Neoproterozoic stratigraphy in the Amundsen Basin, Northwest Territories. In*: Current Research, Part A: Geol. Surv. Can.*, **Paper 94-1A**, 61-70.

RAINBIRD, R.H., RAYNER, N. & STERN, R.A. (2003a): SHRIMP U-P geochronology of apatite cements and zircon bearing tuff clasts in sandstone from the Athabasca Group, Athabasca Basin, northern Saskatchewan and Alberta. *Saskatchewan Industry Resources, Open House Proceedings*, 6.

RAINBIRD, R.H., HADLARI, T., ASPLER, L.B., DONALDSON, J.A., LECHEMINANT, A.N. & PETERSON, T.D. (2003b): Sequence stratigraphy and evolution of the Paleoproterozoic intracontinental Baker Lake and Thelon basins, western Churchill Province, Nunavut, Canada. *Precamb. Res.* **125**, 21–53.

RAINBIRD, R.H., STERN, R.A., RAYNER, N. & JEFFERSON, C.W. (2007): Age, provenance, and regional correlation of the Athabasca Group, Saskatchewan and Alberta, constrained by igneous and detrital zircon geochronology, *in* Jefferson, C.W., and Delaney, G., eds., *EXTECH IV: Geology and Uranium EXploration TECHnology of the Proterozoic Athabasca Basin, Saskatchewan and Alberta*. *Geol. Surv. Can.* Bulletin **588**, 193-210.

RAMAEKERS, P. (1990): Geology of the Athabasca Group (Helikian) in northern Saskatchewan: *Sask. Geol. Surv. Report **195***, 49 p.

RAMAEKERS P. & CATUNEANU O. (2004): Development and sequences of the Athabasca Basin, Early Proterozoic, Saskatchewan and Alberta, Canada; The Precambrian Earth; tempos and events. *Developments in Precambrian Geology* **12,** 705-723.

RAMAEKERS, P., JEFFERSON, C.W., YEO, G.M., COLLIER, B., LONG, D.G.F., CATUNEANU, O., BERNIER, S., KUPSCH, B., POST, R., DREVER, G., MCHARDY, S., JIRICKA, D., CUTTS, C. & WHEATLEY, K. (2007): Revised geological map and stratigraphy of the Athabasca Group, Saskatchewan an Alberta. I*n* Jefferson, C.W., and Delaney, G., eds., *EXTECH IV: Geology and Uranium EXploration TECHnology of the Proterozoic Athabasca Basin, Saskatchewan and Alberta*. *Geol. Surv. Can.* Bulletin **588**, 155-192.

RAWLINGS, D.J. (1999): Stratigraphic resolution of a multiphase intracratonic basin system: the McArthur Basin, northern Australia. *Aust. J. Earth Sci.* **46**, 703-723.

RAWLINGS, D.J. & PAGE, R.W. (1999): Geology, geochronology and emplacement structures associated with the Jimbu Microgranite, McArthur Basin, Northern Territory. *Precamb. Res.* **94**, 225-250.

RENAC, C., KYSER, T.K., DUROCHER, K., DREAVER, G. & O'CONNOR, T. (2002): Comparison of diagenetic fluids in the Proterozoic Thelon and Athabasca basins, Canada: implications for long protracted fluid histories in stable intracratonic basins. *Can. J. Earth Sci.* **39**, 113-132.

RHEINBERGER, G.M., HALLENSTEIN, C. & STEGMAN, C.L. (1998): Westmoreland Uranium deposits. *In*: *Geology of Australian and Papua New Guinean Mineral Deposits*, Berkman, D.A. and Mackenzie, D.H. *eds*., Australasian Inst. Mining and Metallurgy, Melbourne, 807 – 815.

RICHARD, A., BOIRON, M-C., CATHELINEAU, M., DEROME, D., PETTKE, T., BANKS, D., MERCADIER, J. & CUNEY, M. (2008): U concentrations in ore fluids: A LA-ICP-MS investigation of fluids associated with unconformity-related uranium deposits. *Geol. Assoc. Can.*, *Mineral. Assoc. Can.* Program with Abstracts, 158.

RILEY, G.H., BINNS, R.A. & CRAVEN, S.J. (1988), Rb-Sr chronology of micas at Jabiluka. In: *Uranium in the Pine Creek Geosyncline* (eds. J. Ferguson J, AB Goleby) International Atomic Energy Agency, Vienna, 457-468.

ROGERS, J.W. (1996): A history of continents in the past three billion years. *J. Geol.* **104**, 91-107.

ROGERS, J.W. & SANTOSH, M. (2003): Supercontinents in Earth history; Special issue in honour of Prof. John J. W. Rogers on supercontinents and crustal evolution. *Gondwana Research* **6**, 357-368.

ROSS, G.M. (1983): *Geology and depositional history of the Hornby Bay Group, Proterozoic, Northwest Territories, Canada.* Ph.D. Thesis. Carleton University: Ottawa, Canada.

RUZICKA, V.R. (1989): Monometallic and polymetallic deposits associate with the sub-Athabasca unconformity in Saskatchewan. In: *Current Research, Geol. Surv. Can.*, **89-1C**, 67-79.

RUZICKA, V.R. (1996): Unconformity-associated uranium, Chapter 7. In: Eckstrand, O.R., Sinclair, W.D., and Thorpe, R.I., eds., Geology of Canadian Mineral Deposit Types. *Geol. Surv. Can., Geology of Canada*, **8**, 197-210.

SASSANO G.P., FRITZ P. & MORTON R.D. (1972): Paragenesis and isotopic composition of some gangue minerals from the uranium deposits of Eldorado, Saskatchewan. *Can. J. Earth Sci.* **9**, 141–157.

SCHINDLMAYER, W.E. & BEERBAUM, B. (1984): Structure related uranium mineralization in the Westmoreland District, Northern Australia [abs]. Proceedings 27th International Geological Congress, Moscow IX, 95.

SCHWABE, M.R. (1981): Mt Sears Range project, Rudall River Region, Western Australia. Annual Report 1979-80, Temporary reserve 6883H. Occidental Minerals Corporation of Australia. *Western Australia Geological Survey WAMEX Open File Series*, **Item 1695-**

SHIVES, R.B.K., WASYLIUK, K. & ZALUSKI, G. (2000): Detection of K-enrichment, illite chimneys using ground gamma ray spectrometry, McArthur River area, northern Saskatchewan. In: *Summary of Investigation 2000, Volume 2*. Saskatchewan Geological Survey, Saskatchewan Energy and Mines, Miscellaneous **Report 2000-5-2**, 160-169.

SHURILOV, A.N., POLEKHOVSKIY, YU.S., TARASOVA, I.P. & PETROV, YU.V. (2003): Geology and ore paragenesis of the Karku uranium deposit (Northeastern Ladoga region). *In:* Proceedings of the International Conference on Uranium Geochemistry (Nancy, France, 2003), 347-350.

SHURILOV, A.V., POLEKHOVSKIY, YU.S., CUNEY, M. & KISTER, P. (2006): Age determinations of uranium mineralization of Ladoga area. Poster presented at IGOD Conference 2006, Russia.

SIBBALD T.I.I. (1978): Uranium metallogenic studies; Rabbit Lake, geology; Summary of

investigations, 1978, Saskatchewan Geological Survey. *Summary of Investigations by the Saskatchewan Geological Survey* **1978,** 56-60.

SIBBALD T.I.I & QUIRT D. (1987): Uranium deposits of the Athabasca Basin. *Geol. Assoc. Can., Annual Meeting, Saskatoon, 1987. Field trip guidebook. Trip 9: Saskatchewan Research Council Publication* **R-855-1-G-87**.

SIBSON R. H. (1984): Roughness at the base of the seismogenic zone; contributing factors; Special section; Fault behavior and the earthquake generation process. *J. Geophys. Res.* **89,** 5791-5799.

SNELLING, A.A. (1990): Koongarra Uranium Deposits. *In:* The geology of the mineral deposits of Australia and Papua New Guinea. Hughes, F.E. (*ed*.) Australasian Institute of Mining and Metallurgy, Melbourne, 807-812.

SOUTHGATE, P.N., KYSER, T.K., SCOTT, D.L., LARGE, R.R., GOLDING, S.D. & POLITO, P. (2006): A basin system and fluid flow analysis of the Zn-Pb-Ag Mt Isa Type deposits of northern Australia: Identifying metal source, basinal brine reservoirs, times of fluid expulsion and organic matter reactions. *Econ. Geol.* **101**, 1100-1117.

SWINGLER, N. (1981): Sunday Creek Project, Rudall River Region; WA-Final report for TR 7071H. Occidental Minerals Corporation of Australia. *Western Australia Geological Survey WAMEX Open File Series*, **Item 1695-**

TACK, L., WINGATE, M.T.D., LIEGEOIS, J.P., FERNANDEZ-ALONSO, M. & DEBLOND, A. (2001): Early Neoproterozoic magmatism (1000-910 Ma) of the Zadinian and Mayumbian groups (Bas-Congo); onset of Rodinia rifting at the western edge of the Congo Craton: Assembly and breakup of Rodinia. *Precamb. Res.* **110**, 277-306.

TAYLOR, H.P. JR. (1997): Oxygen and hydrogen isotope relationships in hydrothermal mineral deposits. *In:* Geochemistry of hydrothermal ore deposits. Barnes H.L. (*ed.*) John Wiley and Sons, New York, 229–302.

THOMAS, D.J., MATTHEWS, R.B. & SOPUCK, V. (2000): Athabasca Basin (Canada) unconformity - type uranium deposits: Exploration model, current mine developments and exploration directions. In: Geology and Ore Deposits 2000: The Great Basin and Beyond. *Geological Society of Nevada Symposium*, Reno, Nevada, May 15-18, 2000, *Proceedings,* **1**, 103-126.

TREMBLAY L.P. (1972): Geology of the Beaverlodge mining area, Saskatchewan (revised). *Can. Geol. Surv. Memoirs* **367**, 265pp.

TRUEMAN, T. (2005): Geology, classification and global distribution of uranium deposits. *Uranium: Origin and Exploration Techniques*, Mineral Exploration Roundup, Vancouver B.C.

VELICHKIN, V.I., KUSHNERENKO, V.K., TARASOV, N.N., ANDREEVA, O.V., KISELEVA, G.D., KRYLOVA, T.L., DONIKOVA, O.A., GOLUBEV, V.N. & GOLOVIN, V.A. (2005): Geology and formation conditions of the Karku unconformity-type deposit in the Northern Ladoga region (Russia). *Geol. Ore Dep.* **47**, 87-112.

WALLIS, R.H. (1971): The geology of the Hidden Bay area, Saskatchewan. *Sask. Geol. Surv. Report* **137**, 75p.

WASYLIUK, K. (2002): *Petrogenesis of the Kaolinite-Group Minerals in the eastern Athabasca Basin of northern Saskatchewan: Applications to Uranium Mineralization. M.Sc. thesis*, University of Saskatchewan, Saskatoon, Saskatchewan, 140 p.

WHEATLEY, K. & CUTTS, C. (2006): Overview of the Maybelle River uranium mineralization, Alberta, Canada. In: *Uranium production and raw material for the Nuclear Fuel Cycle - supply and demand, economics, the environment and energy security.* International Atomic Energy Agency, Symposium Proceedings, Vienna, 12 p.

WILDE A. R. (1988): *On the origin of unconformity-related uranium deposits.* Ph.D. thesis, Monash University, Clayton, Victoria, Australia (AUS).

WILDE, A.R. & NOAKES, J.S. (1990): Nabarlek uranium deposit. In: Hughes, F. E. ed., *Geology of the mineral deposits of Australia and Papua New Guinea*. Australasian Institute of Mining and Metallurgy, Melbourne, 779-783.

WILDE, A.R. & WALL, V.J. (1987): Geology of the Nabarlek Uranium Deposit, Northern Territory, Australia. *Econ. Geol.* **82**, 1152 – 1168.

WILDE A. R., MERNAGH T. P., BLOOM M. S. AND HOFFMANN C. F. (1989): Fluid inclusion evidence on the origin of some Australian unconformity-related uranium deposits. *Econ. Geol. Bull. Soc. Econ. Geol.* **84,** 1627-1642.

WILSON, M.R. & KYSER, T.K. (1987): The stable isotope geochemistry of alteration associated with the Key Lake uranium deposit, Canada. *Econ. Geol.* **82**, 1540-1557.

WILSON, M.R., KYSER, T.K., MEHNERT, H.H. & HOEVE, J. (1987): Changes in the H-O-Ar isotope composition of clays during retrograde alteration. *Geochim. Cosmochim. Acta* **51**, 869-878.

WYGRALAK, A.S., AHMAD, M. & HALLENSTEIN, C.P. (1988): Sedimentology of the Westmoreland Conglomerate, southern McArthur Basin, Northern Territory, Australia. *Aust. J. Earth Sci.* **35**, 195 – 207.

YEO, G.M. & DELANEY, G. (2007): The Wollaston Supergroup, stratigraphy and metallogeny of a Paleoproterozoic Wilson cycle in the Trans-Hudson Orogen, Saskatchewan, *in* Jefferson, C.W., and Delaney, G., eds., *EXTECH IV: Geology and Uranium EXploration TECHnology of the Proterozoic Athabasca Basin, Saskatchewan and Alberta: Geol. Surv. Can., Bulletin* **588**, 89-118.

ZHAO, G., CAWOOD, P.A., WILDE, S.A. & SUN, M. (2002): Review of global 2.1-1.8 Ga orogens; implications for a pre-Rodinia supercontinent. *Earth Sci. Rev.* **59**, 125-162.

ZHAO, G., SUN, M., WILDE, S. A., LI, S. & ZHANG, J. (2006): Some key issues in reconstructions of Proterozoic supercontinents; The Role of Sri Lanka and Associated Continental Blocks in the Assembly and Break-up of Rodinia and Gondwana. *J. Asian Earth Sci* **28,** 3-19.

CHAPTER 9: SANDSTONE-HOSTED URANIUM DEPOSITS

Kurt Kyser
Department of Geological Sciences and Geological Engineering,
Queen's University,
Kingston, Ontario, K7L 3N6, Canada
kyser@geol.queensu.ca

and

Michel Cuney
G2R, Nancy-Université, CNRS, CREGU,
B.P. 239,
F-54506 Vandoeuvre lés Nancy, France
michel.cuney@g2r.uhp-nancy.fr

Sandstone-hosted uranium deposits are defined as epigenetic concentrations of U minerals occurring as impregnations and replacements primarily in fluvial, lacustrine, and deltaic sandstone formations (Finch & Davis 1985). The deposits occur in medium to coarse-grained sandstone deposited in a continental fluvial or marginal marine sedimentary environment. Impermeable shale/mudstone units are interbedded in the sedimentary sequence and often occur immediately above and below the mineralized sandstone. Uranium precipitated under reducing conditions caused by a variety of reducing agents within the sandstone including carbonaceous material (detrital plant debris, amorphous humate, marine algae), sulfides (pyrite, H_2S), hydrocarbons (petroleum, humate), and interbedded basic volcanic rocks with abundant ferromagnesian minerals (*e.g.*, chlorite). The deposits span a broad range in age from the Paleozoic to the Tertiary and less commonly in the Proterozoic. Typical sedimentary environments conducive to their formation include molasse-like sequences in fluvial-lacustrine systems on wide forelands between a subduction zone and an intracratonic sea, intermontane basins in foreland regions, and fluvial-shoreline systems of marginal marine plains (Everhart 1985).

Sandstone deposits constitute about 30% of world U resources. Ore bodies of this type are commonly low to medium grade (0.05–0.4% U) and individual ore bodies are small to medium in size, ranging up to a maximum of 50,000 tU (OECD 2008). The main primary U minerals are uraninite and coffinite. Conventional mining/milling operations of these deposits have been progressively undercut by cheaper *in situ* leach (ISL) mining methods.

There are four main types of sandstone deposits (Fig. 9-1):

- basal-type deposits, which occur in poorly consolidated and sorted sediments deposited in paleovalleys incised in basement rocks and capped by plateau basalts or sediments;
- tabular deposits, which are irregular, elongate lenticular bodies parallel to the depositional trend, commonly occurring in paleochannels incised into underlying sedimentary units;
- roll-front deposits, which are arcuate bodies of mineralization that crosscut sandstone bedding;
- tectonolithologic deposits, which occur as sandstone adjacent to a permeable fault zone, but are also controlled by paleochannels and roll fronts.

The two main U deposit forms are tabular and roll front.

The United States has large resources of U in sandstone deposits in the Western Cordillera region, and most of its U production has been from these deposits, recently by *in situ* leach (ISL) mining (Fig. 9-2). The Powder River Basin in Wyoming, the Colorado Plateau and the Gulf Coast Plain in south Texas are major sandstone U provinces. Other large sandstone deposits occur in Kazakhstan, Niger, Uzbekistan, Gabon, and South Africa (Karoo Basin). Kazakhstan has substantial reserves in sandstone deposits (615,000 tU) with average grades ranging from 0.02 to 0.07% U (OECD 2008).

Most sandstone-hosted U deposits are strikingly similar, despite occurring in host rocks ranging from Carboniferous to Tertiary and on almost every continent (Finch 1985). Deposits in

Short course co-sponsored by the the SGA and MAC, Québec City, May 2008, p. 221-240

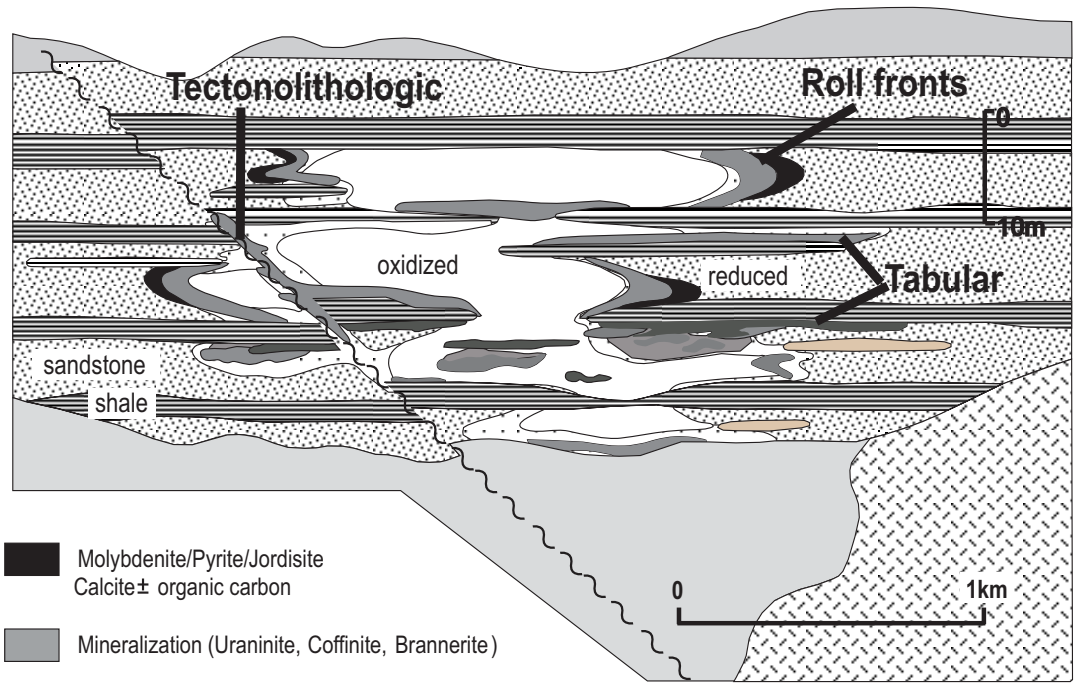

Fig. 9-1. Idealized section showing the distribution and occurrence of three of the major types of sandstone U deposits and the distribution of oxidized and reduced sandstone units.

Ordovician and Devonian host rocks are syngenetic and related to carbonaceous black shale, but the dominant occurrences in Silurian and younger host rocks reflect development of vascular land plants, the primary source of the reductant for fixing U from groundwaters. In most well-studied districts, the timing of the mineralizing process is closely related to the diagenesis of the host rock, which in turn is related to the tectonic evolution of the area. In continental platform and intracratonic basins, Carboniferous, Permian, Jurassic and Cretaceous tabular deposits are found in Argentina, Brazil, Niger, South Africa and USA. Intermontane basins in Australia and USA host Tertiary roll-front deposits whereas graben and regional extensional basins in India, Japan and USA host Permian, Triassic and Tertiary tabular and basal-type deposits. Volcanogenic basins host relatively young Tertiary and Quaternary tabular deposits in Italy and Mexico, and continental margin basins in Brazil, France, India and USA contain roll-front, tabular and tectonolithologic deposits hosted in Devonian, Permian, Cretaceous and Tertiary sandstone units.

Most of the basins that host these deposits were essentially on stable cratons or their margins and closed to the sea, which prevented wholesale oxidation and promoted reducing conditions during and after sedimentation that was essential for U deposition. Adjacent elevated provenance terranes resulted mostly in high energy fluvial systems of variably permeable sedimentary rocks that restricted groundwater flow and concentrated the U. Primary ores were precipitated in host rocks near their initial dips, and in younger host rocks, the primary ores have not been modified. In pre-Tertiary host rocks in some regions, such as the San Juan Basin, USA (Crawley *et al*. 1985), tectonic uplift and exposure of margins of basins allowed introduction of oxidizing ground water to redistribute tabular ores as U minerals in roll fronts and in faults. In other areas, such as the San Rafael District in Argentina (Belluco *et al*. 1985), folding and faulting of the original host rock beds into steeply dipping beds did not redistribute the ore minerals, whereas in others, such as Lodève in France (Comte *et al*. 1985), primary ores were redistributed into fractures and breccia zones.

Wholly marine environments do not host typical epigenetic sandstone-type U deposits, but rather they host syngenetic U deposits in black shale, and thus are not sandstone-hosted. Even in terrestrial environments where lacustrine conditions locally prevail, the deposits are in part syngenetic.

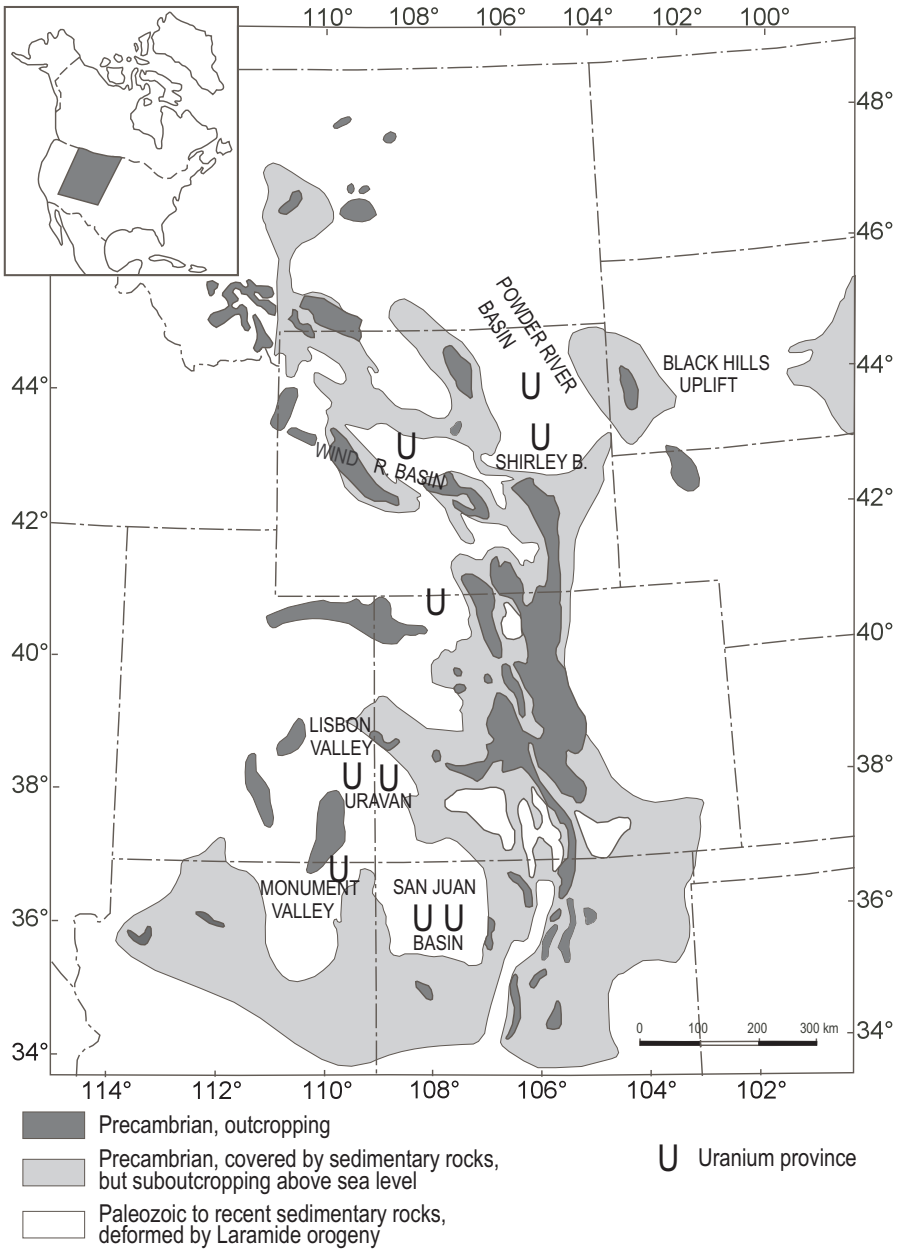

Fig. 9-2. Uranium provinces in the USA (after Finch 1996).

Basal type

These are transitional between surficial and sandstone type U deposits. They occur in poorly consolidated, highly permeable, fluvial to lacustrine carbonaceous gravels and sands deposited in paleovalleys directly incised in basement rocks, generally granitic, and capped by plateau basalts or sediments. Uranium is leached from the granitic basement and precipitates by reaction with the organic matter during groundwater percolation in permeable sediments, between low permeable basement and basalts. The Blizzard deposit in Canada is a typical example of this type (Boyle 1982). The basal type is similar to the "paleovalleys or infiltration type" U deposits in Russia.

Tabular type

The Grants Uranium Region of the San Juan Basin includes five major U districts distributed over an area of 150 km by 30 km on the south-eastern Colorado Plateau in northwestern New Mexico (Fig. 9-3). Within the Region is the

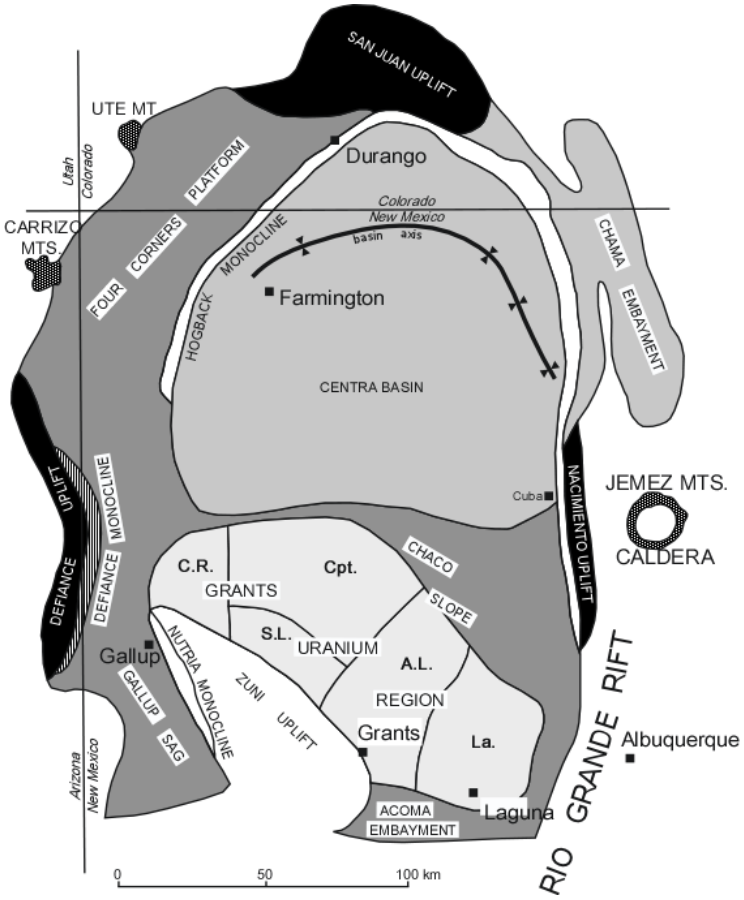

Fig. 9-3. Location of Grants Uranium Region in the San Juan Basin (Fig. 9-2) and other geomorphic features in the Four Corners area of USA. The five major districts include the Church Rock (C.R.), Crownpoint (Cpt.), Smith Lake (S.L), Ambrosia Lake (A.L.) and Laguna (La.).

Ambrosia Lake district, the largest U-producing area in USA, with 238,000 Mt U estimated total resources (Finch 1996). The deposits are tabular sandstone-type in which the U is associated with redistributed carbonaceous material such as humate.

The region extends along the southern border of the San Juan Basin, north of the Zuni Uplift (Fig. 9-3). During late Jurassic time, three broad alluvial fans were deposited in the basin upon Middle Jurassic sedimentary rocks. The fans constitute the Morrison Formation and Salt Wash Member in the north, the Recapture, and the Westwater Canyon–Brushy Basin members in the south (Fig. 9-4). The Morrison Formation was partly eroded in the south during the Late Cretaceous before being unconformably transgressed by the Dakota Sandstone and Mancos Shale.

The Laramide Orogeny (Cretaceous/Tertiary) resulted in the Zuni Mountains in the south, northward tilt of the Morrison Formation, and Tertiary volcanic rocks of Mt. Taylor that cover the Mesozoic sedimentary rocks between Laguna and Ambrosia Lake.

Extensive units of grayish green, montmorillonitic claystone and mudstone beds adjacent to the sandstone units of the upper Morrison Formation (Fig. 9-4) are favorable for uraniferous humate deposits in the Grants U region. Similar beds occur in the Morrison Formation elsewhere in the Colorado Plateau, but they are much more widespread in the southern San Juan Basin. Uranium discoveries were first from random drilling at ever increasing depths, but the geologic trend of the deposits became an exploration strategy in the Grants U region. In addition, important sandstone U deposits in USA were in stream-deposited sediments with ratios of sandstone to mudstone near 2:1. Major ore bodies are restricted

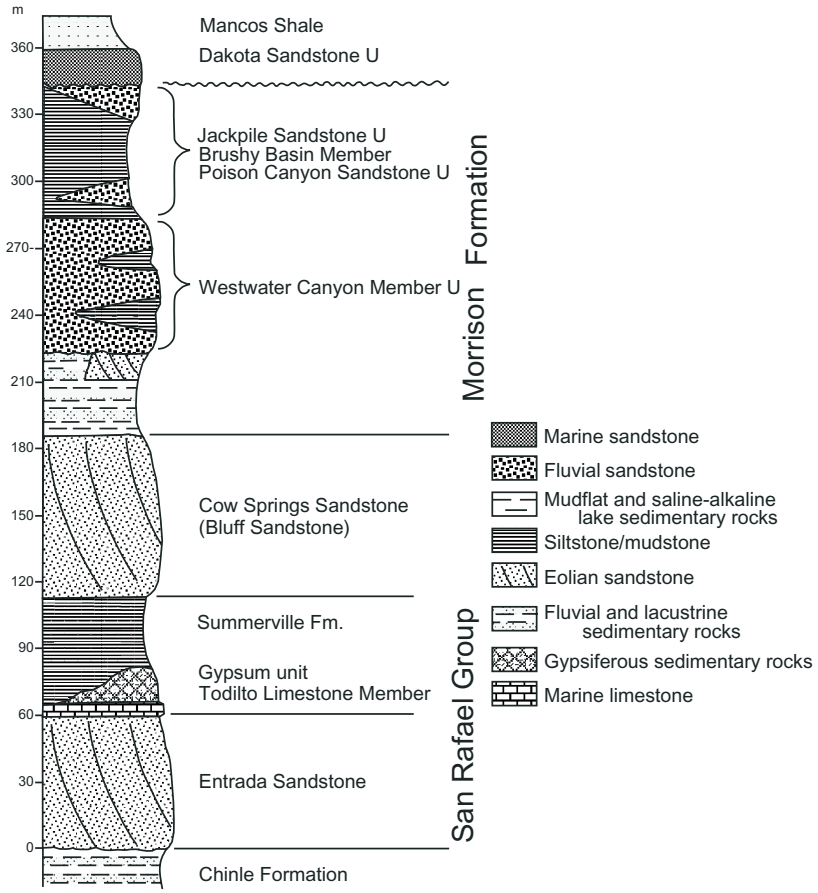

Fig. 9-4. Stratigraphy of sedimentary rocks in the Grants District showing location of Westwater Canyon and Brushy Basin members, sandstone units that host U deposits.

to sand bodies deposited in braided, straight, and sinuous channel environments, which can be imaged using geophysics, and are found near the boundary between oxidized hematitic and limonitic sandstone up-dip, and gray, pyritic sandstone down-dip. Primary ore is at or near the oxidation front because organic carbon and other minerals fix the oxidation front as it progresses down-dip and the ore minerals and humate reduce the permeability of the sandstone. Sandstone bodies that are strongly oxidized are poor targets because pre-existing ore bodies would have been destroyed. Continuous Westwater Canyon sandstone beds may be oxidized many kilometres from the outcrop, so that large deposits occur down-dip in unoxidized Westwater Canyon sandstone, or as islands of unoxidized sandstone up-dip from the regional oxidation front.

Tabular U deposits are primarily hosted in sandstone of the Westwater Canyon and overlying Brushy Basin members of the Morrison Formation (Fig. 9-4). These generally dip <5° to the north and total up to 180 m thick. The Brushy Basin Member consists of a lacustrine greenish gray mudstone and intercalated feldspathic sandstone with mont-morillonite from devitrification of volcanic ash. Uranium is hosted in the Jackpile sandstone, which is up to 75 m thick, in the Laguna district and the Poison Canyon sandstone, up to 25 m thick, in the Mt. Taylor district.

The Westwater Canyon Member is a host for ore bodies in the Ambrosia Lake area, where it is 15–80 m thick. It is composed of poorly sorted, fine- to coarse-grained arkosic sandstone with local intercalations of gray montmorillonitic mudstone and contains variable amounts of humate and organic plant material. The Westwater Canyon member sandstone contains 5 to 15 ppm U and pyrite where reduced, 1 to 2 ppm U and hematite where oxidized (Brookins 1979), and up to 0.5% heavy minerals. Irregularly distributed plant remains and humate serve as a reductant for U. The Recapture Member, which is 10 to 60 m thick,

consists of alternating beds of gray sandstone and gray to maroon mudstones that interfinger with the Westwater Canyon sandstones.

Galloway (1980) suggested that the Westwater Canyon Member was deposited in an alluvial fan derived by rivers flowing from a source to the southwest, probably the ancient Zuni or Mogollon highlands, which provided the igneous and metamorphic detritus complemented by widespread volcanic ash-fall material. Proximal to mid-sections of the fan are braided channel facies which grade down-fan into straight, sinuous, and finally distributary channel facies at the distal front system. All major U deposits occur in the mid-fan facies (Dahlkamp 1993).

Most of the Westwater Canyon and Brushy Basin sandstone lenses are reduced. The reduction, or re-reduction, presumably occurred with humate formation from soluble organic substances during diagenesis. Early alteration of volcaniclastic material resulted in montmorillonite, smectite, illite and mixed layer clays that preceded and partly overlapped the reduction process in the ore hosts. Reduction destroyed detrital magnetite and ilmenite and precipitated pyrite. The humic material subsequently precipitated with the U. Subsequent to the formation of the primary ore lenses, barite and calcite precipitated and kaolinite crystallized in pores within the sands.

The largest ore bodies occur in reduced, pyrite-, vegetation- and humate-bearing continental fluvial sandstone of bedload facies deposited in straight to sinuous streams (Galloway 1980). High sandstone to mudstone ratios, volcaniclastic material in mudstone, good continuity of the sandstone beds with thicknesses of 70–100 m and poorly sorted sandstone are favorable hosts (Fig. 9-5). Mineralized trends have been strongly altered, with corroded quartz, altered plagioclase, albite and K-feldspar cements and mixed layer illite–smectite or chlorite (Fig. 9-6). Chlorite is enriched in the ore zone, and kaolinite and altered montmorillonite are enriched up-dip from the ore. Reduction is indicated by destruction of detrital magnetite and ilmenite, and local formation of authigenic pyrite.

The humate likely originates from plant debris in Brushy Basin Member pelite or an external source from surface vegetation or swamps (Granger *et al.* 1961, Turner-Peterson & Fishman 1986). Subtle structural influences controlled the accumulation of unusually large quantities of uraniferous humate. Humate precipitated as tabular bodies along a shallow, horizontal chemical interface at an oxidation–reduction front separating surface-derived oxidizing waters from deeper perhaps H_2S-rich, reducing groundwaters (Saucier 1980) or from reducing fluids expelled from the Brushy Basin Member.

A later post-Laramide alteration stage produced a regional oxidation front that advanced from the southern outcrop zone of the Morrison Formation north into the San Juan Basin (Fig. 9-3), leaving unoxidized islands behind. Most of the primary U ore is from unoxidized deposits, with

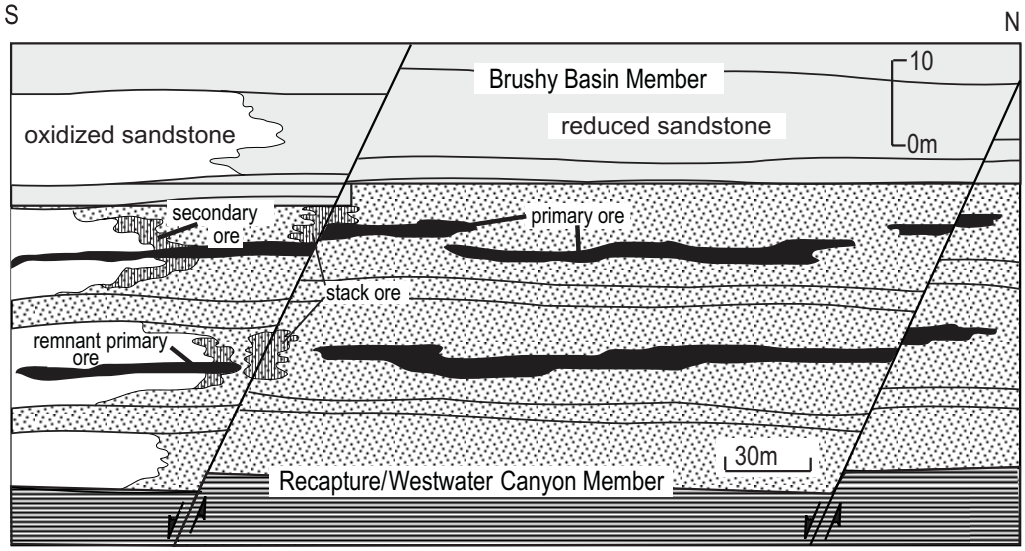

Fig. 9-5. Section from S to N showing the positions of primary ores as tabular lens within reduced sandstone and secondary ore in faults and at boundaries between reduced and oxidized sandstone of the Morrison Formation. After Turner-Peterson & Fishman (1986).

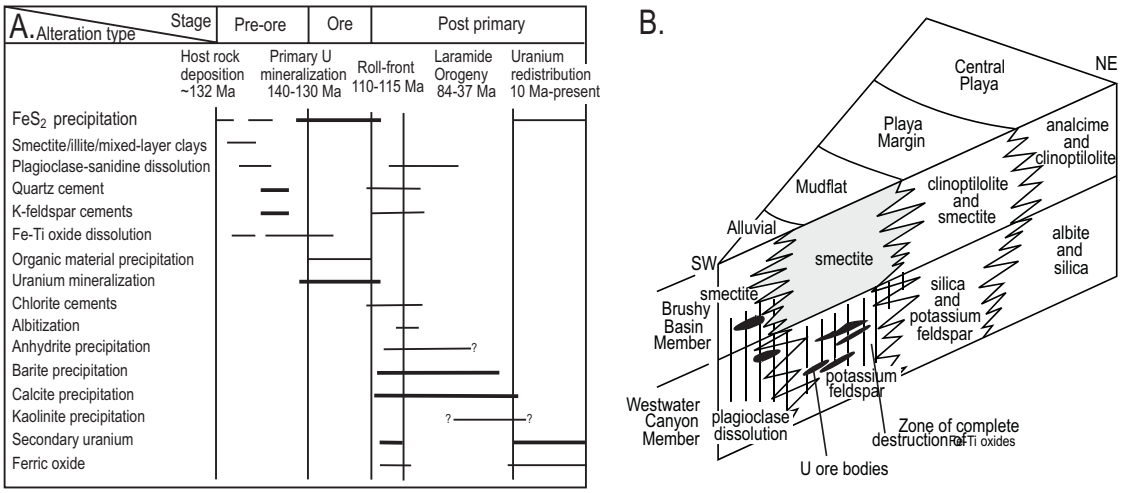

Fig. 9-6. **A**: simplified paragenesis of alteration minerals in the Westwater Canyon Member and Brushy Basin Member sandstones. Also shown are the ages of various events that have affected the units hosting tabular U deposits. **B**: Distribution of alteration minerals in the Westwater Canyon Member and Bushy Basin Member sandstone units. Modified from Turner-Peterson & Fishman (1986).

minor occurrences of secondary oxidized ore (Fig. 9-5). All ore of post-Laramide age, which is only randomly associated with humate, is secondary mineralization with grades of < 0.17% U and coffinite as the major ore mineral. Primary ore consists of coffinite and black amorphous urano-organic complexes interstitial to the sand grains, along with pyrite, marcasite and jordisite (Adams & Saucier 1981, Crawley *et al.* 1985, Granger & Santos 1986). Uranium is associated with enrichments of Cu, Fe, Mn, Mo, Se, V, Y, As, S and organic C, with an average U/humate ratio near 1 (Dahlkamp 1993).

Primary ore is classified as blanket, channel and roll-type ore bodies (Fig. 9-5). Channel ore is facies-controlled, following channels for as much as 2000 m and is associated with silicified vegetation and some humate. Blanket ore displays a more undulating sheet-like shape, with ESE trending "roll"-like thickenings, and is associated with humate. Mineralized blankets can cut across sandstone bedding to a different elevation. Roll-type ore bodies exhibit C-shapes in cross-section similar to the Wyoming roll-front deposits. Tabular and roll-type mineralization is ESE-trending, more or less parallel to the orientation of the sedimentary transport direction. Ore lenses range in length from several tens of metres up to about 2000 m, and in width from several metres up to some hundreds of metres. Their thickness is usually less than 2.5 m.

Primary mineralization has U/Pb dates of 140 to 130 Ma (Brookins 1980, Rosenberg & Hooper 1982). Mobilization occurred at 115 to 110 Ma, perhaps associated with a first roll-type ore formation (Fig. 9-6). Secondary ore associated with hematitic and limonitic alteration zones have U/Pb ages of 13 to 10 Ma and 4 to 3 Ma, respectively (Ludwig *et al.* 1984). Relatively young U/Pb ages of < 1 Ma have been measured for some roll-front ore in the Church Rock district (Ludwig *et al.* 1982).

One possible source of the U is intraformational altered igneous material within sandstone itself or at some distance up the hydrologic gradient from where the deposits are presently located. This is supported by the frequent association of U deposits with tuffaceous sedimentary sequences. However, the Brushy Basin Member has a Th/U ratio of 1.5, suggesting that U has not been mobilized (Brookins 1979), whereas the Th/U ratios are higher in the Westwater Canyon Member and likely provided the U for the ore. Furthermore, the reduced state of the Brushy Basin Member sedimentary rocks implies low U solubility, whereas pervasive mild oxidation prevailed in the lower Westwater Canyon Member sandstone.

The sediment pile provided a particular chemical environment due to the juxtaposition of two inherently unstable components, organic material in the form of plant debris and volcanic glass within the tuffaceous intercalations. The Westwater Canyon Member sandstone is locally oxidized and reduced, depending upon the distribution of organic debris. Groundwaters within

the Westwater Canyon Member were relatively oxidized compared to the organic-rich alkaline and reducing waters of the Brushy Basin Member. Along this interface, the primary U-humate mineralization of the Grants Uranium Region probably precipitated (*e.g.*, Adams & Saucier 1981). Bacteriogenic H_2S and CO_2 from fermentation of the vegetation would cause a drop in pH, altering the silicates and precipitating pyrite and U, the latter from uranyl carbonate and uranyl humate complexes. The favorable site for this process is the mudflat facies of the Brushy Basin Member (Turner-Peterson & Fishman 1986).

Remobilization destroyed part of the deposits and resulted in the formation of the younger types of U deposits during the late Jurassic to late Cretaceous, prior to deposition of the Dakota Sandstone, and during the Miocene to Recent erosional period (Fig. 9-6). Early mobilization of primary ore during late Jurassic to mid Cretaceous time is also considered for some of the breccia pipe ore.

Uravan Mineral Belt & Colorado Plateau

The oldest U mining district in the USA is the Uravan Mineral Belt (Fig. 9-2), where U and V extracted from the Salt Wash Member of the Jurassic Morrison Formation amounted to 48,000 mt U grading 0.17% U and about five times as much vanadium averaging a grade of 1.1% V (Finch 1996). The Salt Wash Member, equivalent to the upper Westwater Canyon Member, is overlain by the Brushy Basin Member and underlain by the Tidwell Member of the Upper and Lower Morrison Formation, respectively. Salt Wash Member sandstone is orthoquartzite to feldspathic orthoquartizite deposited as braided and meandering streams. Clay lenses rich in volcanic debris were deposited locally as basal mud.

Oxidation and reduction are the most prominent alteration features observed in the ore-hosting Salt Wash Member sedimentary rocks (Fig. 9-7). Mineralization occurs in tabular forms and as rolls or C-shaped configurations. Unoxidized primary mineralization, which constitutes the majority of the ore, is uraninite and coffinite commonly associated with carbonaceous debris, sometimes replacing plant material (Thamm *et al.* 1981). Vanadium of low-valence state occurs as oxide minerals. Calcite, dolomite, and barite are present within and close to mineralization as cement in the sandstone. Partially oxidized blue–black ore contains the uranyl vanadate rauvite. Completely

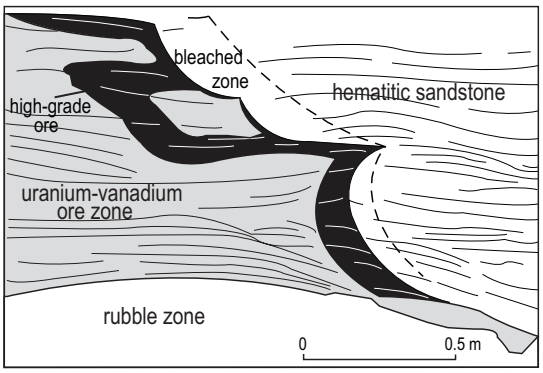

Fig. 9-7. Distribution of redox boundaries and mineralization in the Salt Wash Member as rolls or C-shaped configurations at the Deremo mine, Uravan Mineral Belt. Unoxidized mineralization is commonly associated with carbonaceous debris (after Thamm *et al.* 1981).

oxidized yellow ore contains tyuyamunite and carnotite. There is no loss of U or change in the U/V ratios of the ore during the oxidation processes (Thamm *et al.* 1981).

Zoning of elements is similar to that of the Wyoming roll fronts, particularly for Se, V, U, and Mo across roll and tabular deposits of the Salt Wash Member. Tabular ore bodies, which are controlled by the distribution of plant material, are concordant to the bedding and elongate parallel to the sedimentary trends whereas roll-shaped ore bodies transect the bedding. The ore averages about 1 to 1.5 m thick, but can approach 10 m. The roll-shaped ore bodies are narrow, sinuous and elongate parallel to local sedimentological features, major channels, or axes of good permeability. Distribution of V–U mineralization is rather erratic and unpredictable as compared with other types of sandstone U deposits. Individual ore bodies range in size from less than 1 Mt to more than 1000 Mt U.

The source of the U is the relatively U-rich Precambrian basement rocks or younger uraniferous igneous or volcanic rocks, particularly as tuffaceous material in the Salt Wash Member host sandstone and overlying Brushy Basin Member pelite. Vanadium is derived from either decomposition of detrital magnetite and ilmenite within the host sedimentary rocks, introduced from the overlying Cretaceous sedimentary rocks or from leaching and erosion of Paleozoic sedimentary rocks located to the west of the Colorado Plateau.

Ore bodies occur in reduced channel sand bodies adjacent to oxidized overbank deposits, generally entirely within reduced sandstone, like that of the deposits of the Grants Uranium Region.

The gray Salt Wash Member sandstone and mudstone that fills channels was deposited under reducing environments, as reflected by the presence of pyrite and carbonaceous material, although spotty. Pore water in the sand bodies would have been reducing because of the decay of buried vegetal material, with larger channels with abundant carbonaceous debris being more intensely reduced, leading to the destruction of magnetite and ilmenite. More intensely reduced portions of the channel sand bodies tend to occur near the base of thicker sandstone units along one margin of a major channel system.

The Salt Wash Member was covered by the predominantly oxidized, tuff-interbedded pelite of the Brushy Basin Member. Expulsion of oxidizing pore waters from the Brushy Basin sedimentary rocks into the Salt Wash channel sandstone aquifers produced an element zoning that proceeds from Se and V at the top, through U to Mo at the bottom of the mineralized section (Fig. 9-8). Northrop (1982) added stable isotope data to devise a model wherein U precipitation in the Henry Mountains district of Utah occurred at an interface between brine and meteoric waters (Fig. 9-8). He suggested that mineralization is restricted to intrabasinal synclines where the brine–meteoric water interface intersects sandstone horizons containing concentrations of organic matter, so that more favorable environments were predicted that could aid in exploration.

Monument Valley-White Canyon Districts

The Monument Valley–White Canyon Districts of the Colorado Plateau (Fig. 9-2) have produced 48,000 mt U from the Triassic Chinle Formation. These deposits occur as lenticular ore pods located within the lower part of distinct Triassic sandstone channels. Like the deposits from the Uravan Mineral Belt, the ore host comprises fluvial sedimentary rocks with abundant volcanic material and carbonaceous debris, but in the 50 to 600 m thick Triassic Chinle Formation rather than Jurassic rocks. The Shinarump Member, which hosts most of the deposits, rests unconformably on the Middle Triassic Moenkopi Formation and is composed of feldspathic sandstone and conglomerate with rare mudstone.

Ore minerals in the reduced zone include uraninite, coffinite and montroseite ($(V^{3+},Fe^{3+})O(OH)$). The oxidized zone contains hexavalent U minerals and uranyl vanadates. Ore minerals impregnate sandstone voids, replace quartz grains, clay particles, and abundant fossil plant debris, and fill vertical fractures which extend beneath the scour base. Potential sources of the U are uraniferous volcanic ash preserved in the form of bentonitic clays in the lower Chinle sedimentary rocks or U-enriched granite which supplied the arkosic sands. Host rocks of the ore are reduced and tuffaceous material is incorporated in the sedimentary rocks. Significant alteration is related to redox processes reflected by bleaching around U mineralization and calcite and silica cements in the host rocks.

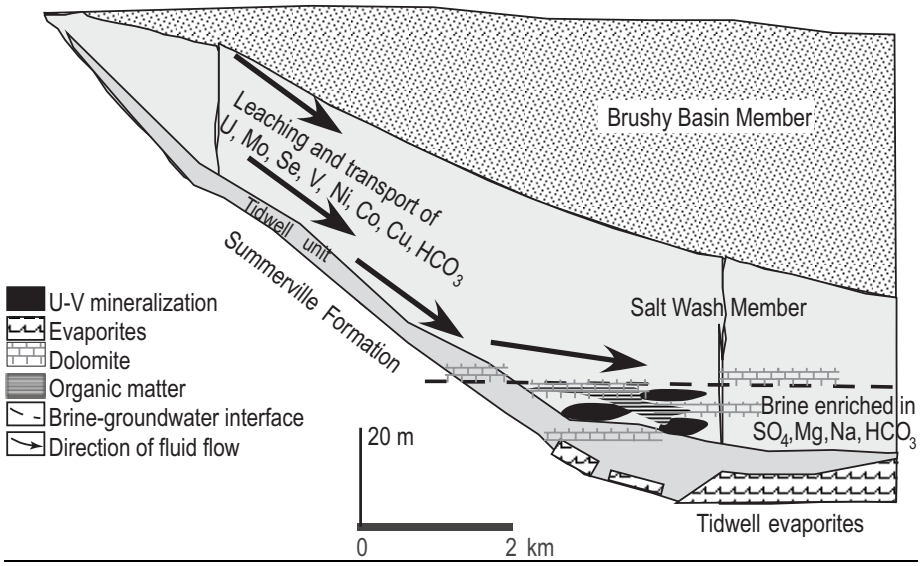

Fig. 9-8. Model for the formation of V–U mineralization at the interface between groundwaters and brines in the Henry Mountains district of Utah (after Northrup 1982).

Powder River Basin, Wyoming

The fluvial architecture and paleohydrology of the Fort Union Formation near the Hyland U mine in the Powder River Basin of Wyoming (Fig. 9-2) has been reviewed by Hunter (1995). Infiltration of paleochannel aquifers by meteoric water occurred after uplift of the basin margins to the south and southwest. The progress of this uplift is reflected in the distribution of hematitic alteration, preserved in the sandy phases. This alteration demonstrates that infiltrating fluids migrated in a northeasterly direction, perpendicular to multiple stacked fluvial channels that were fed by a single regional sand horizon. Sandstone-hosted U deposits in the Shirley Basin in Wyoming have U/Pb ages that indicate significant post-formational interaction with fluids, resulting in data that are difficult to interpret. However, the best age for formation of these deposits is 24 Ma for the youngest ore and >35 Ma for the oldest ore (Ludwig 1979).

Asia

Sandstone-type U deposits occur throughout northwest China in Mesozoic to Cenozoic basins that are part of the network of basins that stretch from China into Kazakhstan, Mongolia and Siberia (Zhou *et al.* 2000). Unlike sandstone-hosted deposits in other areas of the world, these deposits have been studied recently because of the need by China for U. The Sanerlin U deposit in southern China is Early Tertiary in age and located near the margin of the Shaling-Yong Xing Basin (Li *et al.* 2002), a pull-apart basin. The ores occur as breccia and veins mixed with silicified shale and sandstone. Uraninite is the main U mineral and occurs as disseminated grains within quartz veins or coatings on fragments. Fluid inclusions in the quartz veins have homogenization temperatures of 150–280°C and variable salinities of 5.6–13.4 wt.% NaCl. The isotopic compositions of the mineralizing fluids indicate that they were basinal brines from the Shaling-Yong Xing Basin. Precipitation of uraninite is proposed to have occurred when carbonaceous gases were released from the ore fluids due to hydraulic fracturing.

The Olov and Ima U deposits in the Transbaikal region of Russia occur along the flanks of Jurassic depressions between granite gneiss domes and at the intersections of major lineaments. The deposits are stratiform and controlled by low dipping faults developed near the contact between the Jurassic volcanogenic and sedimentary rocks with the underlying granitoid plutons (Kislyakov & Sumilin 1996). The paleovalleys that host the bodies are of variable age and are altered by pre-ore clay minerals and syn-ore biotite. Hematization is widespread, resulting from the mixing of ascending hydrothermal fluids with near surface oxidized water.

Roll-front type

Major roll-front U districts in Wyoming include the Wind River, Shirley, Powder River, and Great Divide basins (Fig. 9-2). The Wyoming basins are the second major U producers in the USA after the Colorado Plateau, with total reserves of 250,000 Mt U at 0.05 to 0.25% U. Significant roll-front U deposits are hosted in the early Eocene Wasatch, Wind River, and Battle Spring formations, and to a lesser extent in the Paleocene Fort Union Formation. The most favorable host rock is friable fine to coarse-grained or pebbly, arkosic sandstone containing considerable pyrite and carbonaceous material. The host sandstone is generally light gray or greenish gray where not altered and occurs preferentially in the central part of the fluvial system in the basins, in large fans that range in length from a few km in the Wind River and Shirley Basins to 100 km in the Powder River Basin (Fig. 9-2).

Oxidation processes associated with the ore-forming process include bleaching of the normal gray sandstone, elevated Se contents, higher $CaCO_3$, organic C, and sulfate contents and destruction of heavy minerals, particularly pyrite and magnetite. Ore minerals are uraninite and coffinite that occur as coatings on sand grains, void fillings in sandstone and replacements of organic matter (Fig. 9-9). Disseminated uraninite ore is found in water-saturated, unconsolidated, immature, coarse-grained arkose. Massive uraninite, pyrite–marcasite, and rare barite are the only non-detrital minerals in the ores. Calcite-cemented ore has the highest grades of up to 12% U.

The distribution of the ore and associated elements in roll-front deposits is strikingly similar (Harshman 1974). The redox interface for U coincides with that for Fe in some of the deposits, whereas in others the U interface is separated from the iron interface by as much as 5 m of pyrite-bearing reduced sandstone. Pyrite has been added to reduced sandstone at the edges of the altered sandstone tongues and decreases away from the edges toward unaltered sandstone. Selenium has been deposited in narrow zones at the edges of the

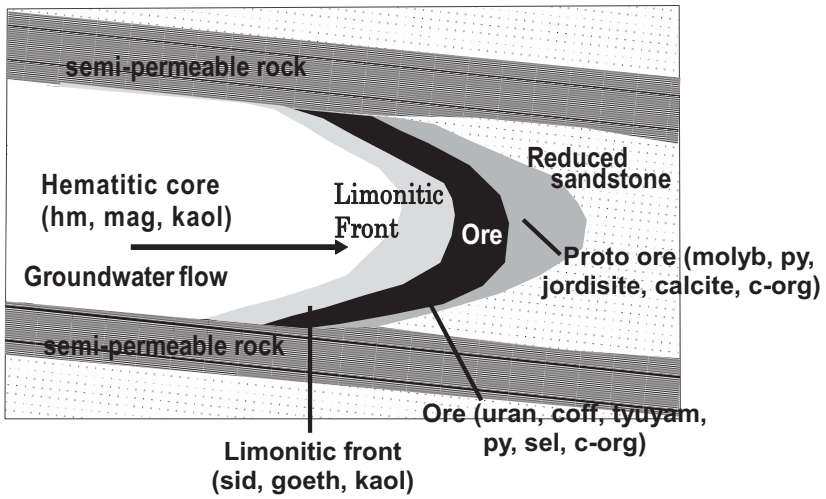

Fig. 9-9. Idealized distribution of alteration zones and minerals in roll-front deposit. After Harshman (1972) and DeVoto (1978). Abbreviations: hm, hematite; mag, magnetite; kaol, kaolinite; sid, siderite; goeth, goethite; uran, uraninite; coff, coffinite; tyuyam ,tyuyamite; py, pyrite; sel, selenite; c-org, organic carbon; molyb, molybdenite.

altered tongues, Mo is concentrated at the distal, down-dip edge of the mineralized zone, and V has been deposited on the convex side of the roll front. Organic C has an erratic distribution, sulfate is high in mineralized sandstone and phosphate is related to high U contents. U/Pb isotope systematics indicate significant migration from the ore of ^{234}U within the last 100,000 years, and dates that vary from 22 to 35 Ma (Dooley *et al.* 1974, Ludwig 1978, 1979) could reflect apparent mineralization times.

The two most probable sources for the U are uraniferous granitic rocks of Lower Proterozoic to Archean age exposed in the ranges that surround the U-bearing basins in Wyoming, and uraniferous tuff and bentonitic volcaniclastic sedimentary rocks of Eocene and younger age that overlie or once overlaid the basins. Granite of the Sweetwater Uplift contains up to 30 ppm U and tuffaceous sedimentary rocks have 250 ppm U in chalcedony. Spring waters in both granitic and sedimentary terrains contain anomalous U contents of up to 8 and 52 ppb, respectively (Harshman 1972), supporting any hypothesis deriving the U for ore formation from either one of these sources.

Harshman & Adams (1981) have comprehensively analyzed all information on the formation of this type of U deposit in Wyoming and elsewhere (Fig. 9-9). They concluded that a roll front is a dynamic feature migrating down a hydrologic gradient, generally basinward, by oxidation and solution on its up-dip side and reduction and deposition on its down-dip side. Uranium ore formation began in Wyoming during the Oligocene when oxygenated groundwater started to enter the exposed or truncated edges of the early Eocene sedimentary rocks in the Wyoming Basins. Correlation between U and organic carbon within the roll-type system is not consistent, so that precipitation of U by organic material must not be the only mechanism.

Microbes functioning in two very restricted environments of different eH and pH zones, sharply separated from one another by the redox front have been proposed as a mechanism for ore deposition (Rackley 1972). The biogenic system is self-perpetuating and needs only oxygen, pyrite, CO_2, and organic matter to complete the oxidation, migration, and reduction cycle required by a dynamic system. Such a process is supported by the wide range in $\delta^{34}S$ values (Jensen 1963, Reynolds & Goldhaber 1983) that suggest oxidation of pyrite at the roll front is accomplished by the ore-bearing solution, but the amount of oxygen in that solution is limited. Pyrite-bearing sandstone is completely capable of establishing and maintaining a roll front, once oxygenated waters are introduced. Two other reductants that have been proposed because of their spatial relation to the deposits are vegetal material, H_2S and hydrocarbons from deeper reservoirs.

The role of microbes as a critical element in roll-front U deposits is exemplified by results from sandstone-hosted deposits in northwestern China (Min *et al.* 2005). In the Xinjiang region in northwestern China, several sandstone-hosted deposits consisting of uraninite and coffinite have structures that indicate that they were biogenically precipitated

and pseudomorphically replaced fungi and bacteria. Uranium was reduced enzymatically by these microrganisms.

A similar model was presented by Arthur *et al.* (2006) for the Tono U deposit in Japan. They suggested that U was leached from the upper weathered zone of the Tokai granite and then reduced by mudstone and sandstone in the overlying Tokai Formation. The U minerals consist of uraninite, coffinite and metastable amorphous U oxide. The deposit has continually evolved since it began to form at 15 Ma, when seawater was flushed out of the sedimentary cover by meteoric waters. The redox environment in which the U was precipitated is suggested to be controlled by microbially mediated sulfate reduction, oxidation of organic matter and precipitation of sulfide minerals.

Roll-type sulfide-uranium deposits occur in Phanerozoic coastal plain sandstones in the south Texas coastal plain, along a 20 to 45 km wide curvilinear belt which approximately parallels the coast of the Gulf of Mexico about 130 km inland. Total reserves in the south Texas region are 72,000 Mt U, although most deposits are low grade (0.1% U) and small (<5000 Mt U).

The Texas coastal plain is underlain by more than 15 km of flat-lying interbedded marine and nonmarine sedimentary rocks of Tertiary age deposited in coastal plains by major river systems on Jurassic and Cretaceous sedimentary rocks. Host rocks of known U occurrences are sandstone deposited between middle Eocene and early Pliocene. Host lithologies include beach sandstone, margins of major fluvial channel systems, sandstone close to faults along which hydrogen sulfide could be introduced into the aquifer and sandstone above salt domes. Abundant pyrite within the host sands of these deposits reflects the introduction of H_2S up along faults from various hydrocarbon reservoirs within the Mesozoic–Tertiary sediment pile.

The mineralization does not occur at the margin of altered sandstone tongues but rather occurs entirely within reduced, pyrite-bearing reduced sandstone, but the host sands contain essentially no carbonaceous plant material, only disseminated pyrite. Reductants for the U include hydrocarbons–H_2S infiltrated from deep seated oil reservoirs in the pyritic fluvial sands and vegetal organic matter in the littoral sands. Uraniferous volcaniclastics are the most favored source of U.

Many roll-type U deposits occur in the Texas U district, hosted by the Miocene Oakville sandstone. The deposits are aligned parallel to or intersect the Oakville fault, which indicates they are structurally controlled (Goldhaber *et al.* 1983). Distribution of U, Mo and Se are typical of roll-type deposits that reflect invasion of reduced host rocks by oxygenated U-bearing fluids. The sulfur content of these deposits is high but organic matter is virtually absent. The altered tongue of these deposits is anomalous in that it contains Fe sulfide rather than Fe oxide phases that typify other Texas and Wyoming roll-type deposits. Goldhaber *et al.*, (1983) suggested that the fault is a site of mixing between saline reducing brines migrating up the fault and oxidized meteoric water near the surface. The saline brines carry organic acids and methane, which provided a favorable environment for sulfate-reducing bacteria, as indicated by the variations in S isotopic compositions of these sulfides. Thus, this U district formed and was preserved because of its proximity to a zone of mixing between connate brines from depth with shallow meteoric waters.

Franceville Basin, Gabon

The Paleoproterozoic Franceville Basin is located about 500 km SE of Libreville, Gabon (Fig. 9-10). All deposits found to date cluster in two groups, 30 km apart, along the southwestern edge of the basin adjacent to the Massif du Chaillu. Total reserves are 42,700 Mt U at an average grade of 0.3% U (OECD 2008). They occur in arenite (FA Formation) below black shale (FB Formation) so that the organic material is from marine origin (*e.g.*, algae) and not, as in the Phanerozoic deposits, of plant origin.

The geology of the Franceville Basin and associated U deposits is described by Gauthier-Lafaye & Weber (1989). The Franceville Basin was formed as an intracratonic structural depression during the Paleoproterozoic. The basement is Archean granite and gneiss, which were dated about 2600 Ma in the Massif du Chaillu. The intracratonic Francevillian sedimentary series is divided into five formations, FA to FE, and is 1,000 to 4,000 m thick. The lowermost formation, FA, is 100 to 1,000 m thick and rests unconformably on the Archean basement. The FA formation, which hosts all of the U deposits in the basin, consists of basal quartz pebble conglomerate and coarse-grained arkosic sandstone, which grade progressively upward into medium- to coarse-grained sandstone a with dolomitic matrix. These are succeeded by alternating fine-, medium-, and coarse-grained sandstone, with occasional intercalations of conglomeratic lenses. The matrix of this younger,

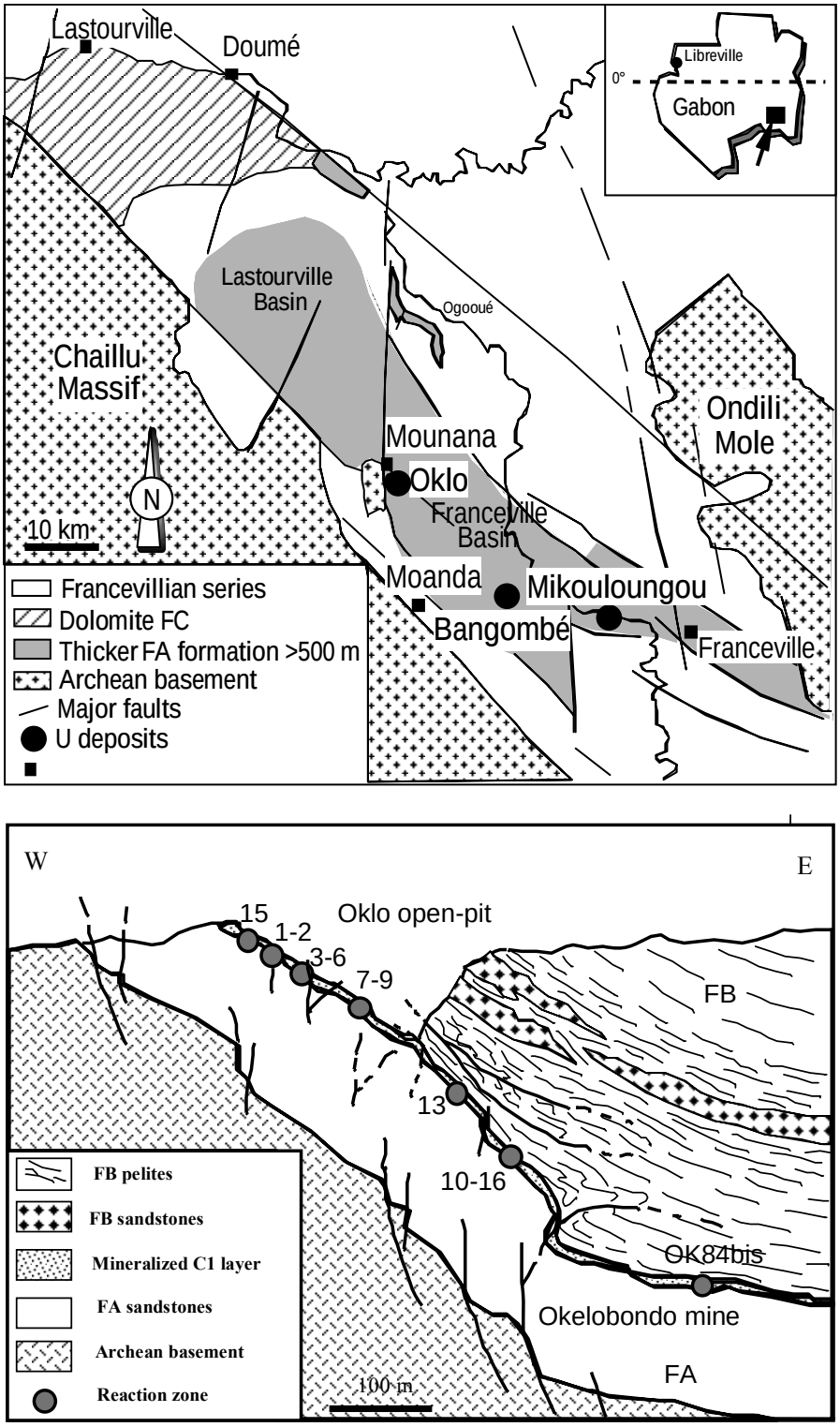

Fig. 9-10. Top: Franceville Basin showing simplified geology and location of selected deposits tabular type at Oko, and Bottom: cross-section showing location of Oklo deposits and Okelobonde mine (after Guathier-Lafaye & Weber 1989).

feldspar-poor sandstone consists of silica or organic material. The individual sandstone layers exhibit cross-bedding and rapid lateral facies change.

The FA Formation is transgressed by the FB Formation which consists of up to 1000 m thick black carbonaceous marine shale carrying kerogen and asphalt/bitumen. The FC to FE formations are composed of shale, chert, dolomite and volcanic rocks. The series is overlain by Mesozoic continental sedimentary rocks of the Congolian basin.

Deformation resulted in slight folding along NW–SE axes, and fault systems trending N–S and NW–SE resulted in displacements of up to several hundred metres. The northwestern group of deposits, which contains all the major ore bodies, is immediately adjacent to the granite–gneiss horst of Mounana, a tectonic outlier of the Chaillu Massif. Pfiffelmann (1975) proposed stratiform (*e.g.*, Oklo), veinlike (*e.g.*, Mounana, Boyindzi), and mixed stratiform-tectonic (*e.g.*, Mikouloungou) as the types of deposits in the area.

Mineralization grades from 0.1 to 1% U, with higher grades up to 10% U in lenses 20 m long, 10 m wide and 2 m. thick. Very high grade mineralization occurs at Oklo, as lensoid bodies, of up to 80% uraninite in a clay gangue, approximately 10 m. long (Gauthier-Lafaye *et al*. 1989).

The U deposits were formed by multistage events around 2050 Ma, about the same time as early diagenesis of the Francevillian sedimentary series (Mathieu *et al.* 2001). During maximum burial, reducing fluids, in the form of oil, migrated from black shale into the upper part of the FA sandstone. At the same time, oxidized fluids in permeable FA sandstone reacted with detrital phases (Cuney & Mathieu 2000), dissolving U and other metals and introducing hematite into the conglomerate and lower sandstone layers during maximum burial. A tectonic event uplifted the basin, hydrofracturing the sandstone to produce secondary porosity and permeability. Uranium was deposited by mixing of oxidized basinal brines, having the same composition and temperatures as the brines of the Athabasca or Kombolgie basins and carrying U, with reduced fluids derived from the maturation of the organic matter of the overlying FB Formation (Mathieu *et al*. 2000). The lower FA sandstone and conglomerate layers are red, and within the upper part of the FA sandstone, there is a green zone whose boundary transgresses stratigraphy. This green zone is capped by a black hydrocarbon-rich zone which hosts the ore within sandstone and immediately below the black shale layer. All of the U deposits of the basin appear to be located in fracture zones and tectonic structures. The U is always accompanied by kerogen or bitumen and pyrite and galena, with minor marcasite and chalcopyrite, digenite, and covellite. Some deposits contain significant vanadium.

Reduced ores are uraninite and coffinite whereas later oxidized ores are francevillite, vanuralite, uranocircite, autunite, torbernite and renardite. The natural reactors of the Oklo area (Boyer *et al.* 1975) are a unique phenomenon among U deposits of the world. They are characterized by a depletion of ^{235}U from 0.72% to between 0.62% and 0.296% and trace fission products.

The Oklo mineralization shows a strong lithologic control, with U concentrated on the flanks or rims of paleo-channels or where intermediate thicknesses of sandstone are combined with high concentrations of organic matter and faulting. The best ore occurs in rocks dipping about 30° and associated with illite and chlorite alteration. A regional ore control may be related to the western bounding fault of the Franceville Basin and the crystalline Massif du Chaillu less than 1000 m to the west of the deposit. Ore controls are structural and lithologic.

Tectonic/lithologic type

Solution collapse breccia-type deposits, Arizona, USA

Thousands of solution-collapse breccia pipes occur in the Grand Canyon region of Arizona because of the widespread Paleozoic carbonate and gypsum-rich rocks that are amenable to formation of karst structures. Breccia pipes hosting Mississippian to Lower Triassic stratigraphic units consist of almost horizontally bedded marine to marginal continental limestone, mudstone, and sandy to silty sedimentary rocks (Wenrich *et al.* 1995). Roof collapse of caverns (paleokarst) in the carbonate strata of the Mississippian Red Wall Limestone initiated the formation of a pipe (Fig. 9-11). The generally circular collapse transgressed chimney-like upwards into the overlying, essentially flat-bedded strata, from the Red Wall Limestone as much as about 1200 m up into the Permian Kaibab Limestone, and locally into the overlying Lower Triassic Moenkopi Formation or Upper Triassic Chinle Formation (Fig. 9-11).

There is no temporal or spatial relationship between the structures and volcanic rocks and most formed as collapse features into solution caverns in

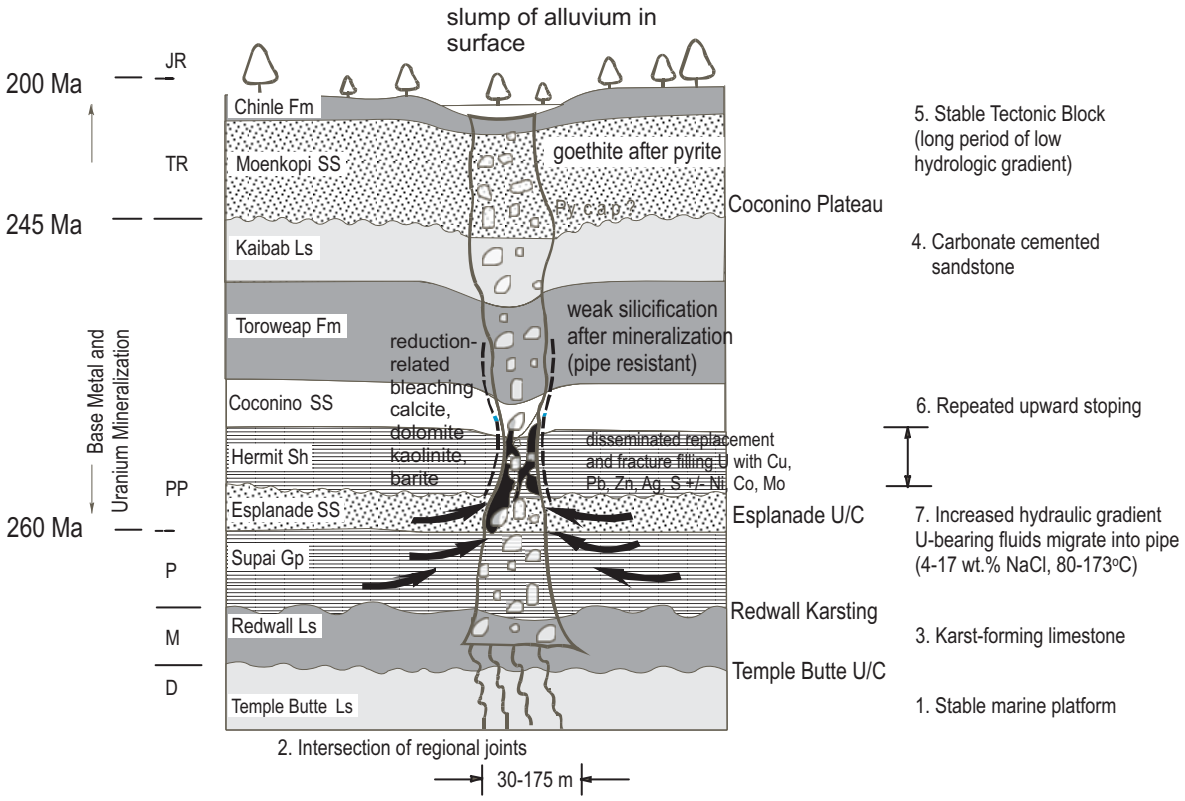

Fig. 9-11. General geology and features of breccia pipes from the Grand Canyon region of Arizona. After Weinrich (2000).

the underlying Mississippian Red Wall Limestone. Most pipes are about 100 m in diameter and of variable extent up to 1000 m in depth. In addition to grades of 0.4–1% U, most pipes have variable concentrations of Ag, Co, Cu, Mo, Ni, Pb, V and Zn. Uranium was not discovered in the pipes until 1951 and during the 1970s to 1990s, the average grade of ore produced was about 1% U (Wenrich 2000).

The main U-mineralizing event occurred after deposition of the Triassic Chinle Formation. Principal alteration in the ore zones includes pyritization, dolomitization, calcitization, silicification, desilicification, Mg-depletion (dedolomitization), gypsum/anhydrite formation, and bleaching. The most common U mineral is uraninite, locally coffinite. Uranium forms irregular ore shoots distributed intermittently over a vertical pipe interval of as much as 200 m from the Coconino stratigraphic level downward. The main event occurred at 200 Ma and a minor event occurred prior to deposition of the Chinle Formation at 160 Ma (Ludwig & Simmons 1992).

The ore bodies can be divided into five stages, beginning with carbonate and sulfate minerals, followed by metallic sulfides in stages two and three and then U in stage four. The U precipitated as uraninite along with coarsely crystalline calcite and minor copper sulfides. Supergene alteration represents the last depositional stage (Wenrich 2000). Most models invoke reduced brines within the limestone layers, which contained base metals, mixed with oxidized U and Cu-bearing groundwaters that were circulating in the sandstone (Wenrich 2000).

Mineralization started during late Mississippian (Billingsley *et al.* 1986) and continued intermittently into the late Triassic. However, all the U–Pb isotopic ages are younger than Mississippian, ranging from 260 and 254 Ma for the Canyon & Pine Nut pipes, to 220–180 Ma for the Kanab North, Hack 1,2,3 and EZ 1,2 pipes, 220 Ma for the Pigeon mineralization, 186 Ma at Orphan, 169 Ma at Arizona-1 and 138 Ma at Hermit (Ludwig & Simmons 1992). There is no evidence for major U introduction with Laramide tectonism, mid Tertiary volcanism, or late Tertiary uplift. Instead, the ages are similar to the timing of deposition of the lower part of the Chinle Formation (Late Triassic), consistent with U being derived by leaching from

volcanic ash in the Chinle and mobilized by groundwater movement during regional uplift in the southwest. Furthermore, the isotopic composition of Pb in galena in mineralized pipes indicates that the fluids had interacted with Proterozoic basement, possibly through vertical fractures rooted in the basement which influenced the location of the pipes.

The presence of calcite suggests that U was probably transported as a uranyl carbonate complex, and effervescence of CO_2 with associated pressure release helped to break up uranyl compounds. Invading hydrocarbons and H_2S derived from sedimentary rocks surrounding the pipe may have been the agent for the required reduction of the U^{6+} ions, but coeval oxidation of some pyrite to hematite associated with the uraninite may be evidence of reduction by Fe^{2+}. Fluid inclusion studies suggest that the ore-forming solutions that deposited the sphalerite, calcite and dolomite had minimum temperatures in the range of 80°C to 173°C, with salinities consistently >9 wt.% NaCl eq. and most commonly >18 wt.% NaCl eq. (Wenrich & Sutphin 1989). Conduits for the U mineralizing fluids are sandy horizons or structures.

The Orphan Mine is a breccia-type deposit that occurs on the Kaibab Plateau near the Colorado River. The ore body is a nearly circular vertical pipe structure from 50–150 m in diameter extending downward from the Permian Coconino sandstone into the Supai Formation. The pipe is filled with displaced Coconino sandstone and fragments from the Supai and Hermit Formations. Gornitz & Kerr (1970) suggested that the pipe probably formed by solution collapse beginning in the underlying Mississippian Red Wall limestone. Uranium ore is concentrated along the border of the pipe and as irregular masses within the pipe. Uraninite and pyrite at the center of the pipe grade into Cu–Ag–Pb sulfides in uraninite at the margins. Bleaching of the red Supai sandstone is evident near the contact with the pipe. The temperature of ore deposition is estimated to be 60–110°C, greater than the burial temperature of the sediments at the time when the deposit formed. A date from U/Pb data indicates a minimum age of 140 Ma (Ludwig & Simmons 1982). Gornitz & Kerr (1970) presented a strong case that the system is of hydrothermal origin that mixed with groundwater along fractures to precipitate the ore.

Breccia bodies in some cases are cut by cave passages, such as at Corkscrew Cave, Arizona, where such structures are exposed along the walls and on the cave ceilings (Onac *et al.* 2007). The abundance of gypsum and barite throughout the cave and their low $\delta^{34}S$ values (–11 to –7) suggest deposition from warm sulfidic solutions that were also responsible, at least in part, for development of the recent cave passages that dissect older paleokarst breccia bodies. The presence of calcite with low $\delta^{18}O$ values (–16.9 to –11.3‰) is considered indicative of a low-temperature hydrothermal episode in the deposition history of cave minerals. Groundwater percolating through the breccia-pipe bodies mobilized and transported ore-related ions into the cave, where they formed a unique assemblage of minerals including carnotite and tyuyamunite that mirror breccia-pipe mineralization.

Shinkolobwe, Dem. Rep. Congo

The Shinkolobwe deposit in the Democratic Republic of the Congo is part of the Katanga Copper Belt. It was discovered in 1915 and mined for radium (Derriks & Vaes 1956), but has achieved recent fame as an environmental, political and social nightmare because of uncontrolled mining of the old workings for U. The deposits graded several percent U, producing cumulatively 25,600 Mt U (OECD 1998), grading about 1% U_3O_8. The mineralization occurs as vein stockwork in sedimentary rocks distant from any known granite.

The Katanga Copper Belt is part of the Katanga Synclinorium, an arcuate fold belt extending about 300 km from Zambia into the Democratic Republic of the Congo. Precambrian basement is overlain by the Neoproterozoic Katanga Group, largely marine sedimentary rocks deposited in a large, but restricted, intracratonic basin at 883 to 620 Ma. Deposition started after 883 ±10 Ma, constrained by the age of the Nchanga Granite (Armstrong *et al.* 2005), and folding and faulting occurred during three phases of deformation of the Lufilian Orogeny at 840 to 710 Ma, 670 Ma and 670 to 620 Ma. The dominant structure that affects the area, the Shinkolobwe Fault Zone, trends E and NE, dipping 60°S.

The ores are hosted in cataclastic zones (breccia zones) in siliceous dolomite and carbonaceous shale of the Mines Series, which is folded into NE–SW-oriented fold and fault wedges, 150–250 m wide and several kilometres long. Longitudinal faults trending NE–SW and NW–SE and NNE–SSW cross faults dissect the Mines Series wedge into four displaced blocks. The breccias have blocks of the units that comprise the Mine Series in

a matrix of dolomitic marl with a variable component of silt, quartz, and Mg-chlorite.

Host rocks were altered by Mg-metasomatism to siliceous dolomite and magnesite replacing dolomite and forming veins, and to chlorite if silt was present, prior to U mineralization (Derriks & Vaes 1956). The principal ore mineral is uraninite in cubes up to 4 cm, which formed with pyrite in open structures. Associated minerals that formed after the uraninite include molybdenite, monazite, and chlorite, which were followed by precipitation of quartz and Co–Ni-sulfides and selenides. Brecciation and dolomitization then occurred, followed by formation of chalcopyrite. The ore and associated minerals occur as discontinuous veins and stringers from a few centimetres to a metre thick along bedding planes and minor faults. In oxidized sections, a large variety of hexavalent U minerals are found. There is a regional zoning in the metallogeny (Ngongo-Kashisha 1975), with U, Cu, Ni, Co, Mo associated with magnesite and monazite prevalent in the southern segment of the arc and Co and Co dominant further to the north.

Meneghel (1979) suggested an origin of the U and associated metals from synsedimentary or syndiagenetic protore in the Mines Series, which were redistributed into favorable structures by convective circulation of basinal brines. A likely source of U and other metals appears to be the Cu-rich horizon of the lower Mines Series (Dahlkamp 1993). U–Pb ages of uraninite are 706 to 620 Ma (Cahen *et al.* 1971), which correlate with the tectonic phases of the Lufilian Orogeny (Cahen 1970), supporting remobilization associated with tectonic processes, but could also reflect resetting.

In the Zambian Copper belt area, U mineralization is found the basal part of the Katanga system at Nkana, Mushoshi, Luanshya and Chibuluma. Mineralization is clearly epigenetic as disseminations or fracture fillings stratigraphically below the Cu ores. Uranium mineralization contrasts with Cu mineralization, for which a synsedimentary origin is commonly proposed (Meneghel 1981).

During the metamorphism of epicontinental platform sedimentary rocks, oxidized brines expelled from evaporitic layers are extremely efficient for transporting U, whereas hydrocarbons produced by black shale, are efficient for the precipitation of U. Hence, the mixing of these two fluids may lead to the formation of U deposits. Typical examples are the Mistamisk U veins from Labrador, Canada (Kish & Cuney 1981), the U deposits of the Copper Belt as exemplified by the Shinkolobwe deposit in the Democratic Republic of the Congo (Ngongo-Kashisha 1975, Audeoud 1982), and deposits from Zambia, such as Kansanshi (Kríbek *et al.* 2005), all of which formed at 350 ±50°C. In fact these deposits are generated by very low grade metamorphism and are distinct from purely sandstone-hosted deposits.

REFERNCES

ADAMS, S.S. & SAUCIER, A.E. (1981): Geology and recognition criteria for uraniferous humate deposits, Grants mineral region, New Mexico. US-DOE, GJBX-2, **81,** 225 pp.

ARMSTRONG, R.A., MASTER, S. & ROBB, S.L. (2005): Geochronology of the Nchanga Granite, and constraints on the maximum age of the Katanga Supergroup, Zambian Copperbelt. *J. Afr. Earth Sci.* **42,** 32–40.

ARTHUR R. C., IWATSUKI T., SASAO E., METCALFE R., AMANO K. & OTA, K. (2006): Geochemical constraints on the origin and stability of the Tono uranium deposit, Japan. *Geochem. - Exploration, Environment, Analysis* **6,** 33-48.

AUDEOUD, D. (1982): *Les minéralisations uranifères et leur environnement à Kamoto, Kambove et Shinkolobwe (Shaba, Zaïre). Pétrographie, géochimie et inclusions fluides.* PhD Thesis, Lyon (France).

BELLUCO, A., RODRIGUEZ, E., GORUSTOVICH, S., OLSEN, H. & VALDIVIEZO, A. (1985): The sedimentary controlled uranium deposits in Argentina and their relation to the geostructural development. *In: Geological environments of sandstone-type uranium deposits,* **TECDOC-328**, IAEA, Vienna, 159-172.

BILLINGSLEY G.H., WENRICH, K.J. & HUNTOON, P.W. (1986): Breccia pipe and geologic map of the southeastern Hualapai Indian Reservation and vicinity, Arizona. *U.S. Geol. Surv. Report,* **86-458B**, 26 pp.

BOYER, R.L. NAUDET, R. & PFIFFELMANN, J.-P. (1975): *Exploration des foyers de réaction, In: The Oklo Phenonmenon,* IAEA, Vienna, 67-81.

BOYLE, D.R. (1982): The formation of basal-type uranium deposits in South Central British Columbia. *Econ. Geol.* **77**, 1176-1209.

BROOKINS, D.G. (1979): *Uranium deposits of the Grants, New Mexico mineral belt (II),* US-DOE

GJBX-141, **79**, 411 pp.

BROOKINS, D.G. (1980): Geochronologic studies in the Grants Mineral Belt. *In:* Rautman C.A., Ed., Geology and mineral technology of the Grants Uranium Region 1979, *New Mex. Bur. Mines Mineral Res. Mem,* **38**, 52-58.

CAHEN, L. (1970): Etat actuel de la géochronologie du Katangien, Mus Royal Afrique Centre, Annales, Ser in 80, *Sci. Geol,* **65**, 7-14.

CAHEN, L., FRANCOIS, A. & LEDENT, D. (1971): Sur l'âge des uraninites de Kambove ouest et de Kamoto principal et révision des connaissances relatives aux minéralisations uranifères du Katanga et du Copperbelt de Zambia*, Soc. Géol Belgique Annales,* **94**, 185-198.

COMTE, D., BLACHÈRE, H. & VARLET, M. (1985): Geological environment of the uranium deposits in the Permian of Lodève Basin, France. *In: Geological environments of sandstone-type uranium deposits,* **TECDOC-328**, IAEA, Vienna, 69-82.

CRAWLEY, R.A., HOLEN, H.K. & CHENOWETH, W.L. (1985): Geology and application of geologic concepts, Morrison Formation, Grants Uranium Region, New Mexico, *USA, In: Geological environments of sandstone-type uranium deposits,* **TECDOC-328**, IAEA, Vienna, 199-214.

CUNEY, M. & MATHIEU, R. (2000): Extreme Light Rare Earth Element mobilization by diagenetic fluids in the geological environment of the Oklo natural reactor zones, Franceville basin, Gabon. *Geology* **28**, 743-746

DAHLKAMP F.J. (1993): *Uranium ore deposits.* Springer-Verlag, Berlin, 460p.

DERRIKS, J.J. & VAES, J.F. (1956): The Shinkolobwe uranium deposit. Current status of our geologic and metallogenic knowledge*, In:* U.N., Intern Conf Peaceful uses of Atomic Energy, 1st, Geneva, Proc, **6**, *Geology of uranium and thorium,* 94-128.

DEVOTO, R.H. (1978): Uranium in Phanerozoic sandstone and volcanic rocks. Short course in uranium deposits; their mineralogy and origin. *Mineral. Assoc. Can. Short Course Handbook* **3,** 293-305.

DOOLEY, J.R., HARSHMAN, E.N. & ROSHOLT, J.N. (1974): Uranium-lead ages of the uranium deposits of the Gas Hills and Shirley Basin, Wyoming, *Econ. Geol.* **69**, 527-531.

EVERHART, D.L. (1985): Tectonic settings of the world's sandstone-type uranium deposits. *In: Geological environments of sandstone-type uranium deposits,* **TECDOC-328**, IAEA, Vienna, 21-46.

FINCH, W.I. (1985)*:* Sandstone-type uranium deposits — Summary and conclusions. *In: Geological environments of sandstone-type uranium deposits,* **TECDOC-328**, IAEA, Vienna, 401-408.

FINCH, W.I. (1996): Uranium provinces of North America – Their definition, distribution, and models. *U.S. Geol. Surv. Bull.* **2141**, 1-18.

FINCH, W.I. & DAVIS, J.F. (1985)*:* Sandstone-type uranium deposits—An introduction. *In: Geological environments of sandstone-type uranium deposits,* **TECDOC-328**, IAEA, Vienna, 11-20.

GALLOWAY, W.E. (1980): Deposition and early hydrologic evolution of the Westwater Canyon wet alluvial fan system, *In:* Rautman, C.A., ed., Geology and mineral technology of the Grants Uranium Region 1979, *New Mex Bur Mines Mineral Res Mem,* **38**, 59-69.

GAUTHIER-LAFAYE F. & WEBER F. (1989): The Francevillian (Lower Proterozoic) uranium ore deposits of Gabon. *Econ. Geol.* **84,** 2267-2285.

GAUTHIER-LAFAYE F., WEBER F. & OHMOTO H. (1989) Natural fission reactors of Oklo. *Econ. Geol. Bull. Soc. Econ. Geol.* **84,** 2286-2295.

GOLDHABER, M.B., REYNOLDS, R.L. & RYE, R.O. (1983): Role of fluid mixing and fault-related sulfide in the origin of the Ray Point Uranium District, South Texas. *Econ. Geol.* **78**, 1043-1062.

GORNITZ, V.M. & KERR, P.F. (1970): *Uranium mineralization and alteration, Orphan mine,* Grand Canyon, Arizona, *Econ. Geol.* **65**, 751-768.

GRANGER, H.C. & SANTOS, E.S. (1986): Geology and ore deposits of the Section 23 mine, Ambrosia Lake district, New Mexico, *In:* Turner-Peterson C.E., Santos, E.S., Fishman, N.S., eds., A basin analysis case study – the Morrison Formation, Grants Uranium Region, New Mexico, *AAPG Studies in Geology* **22**, 185-210.

GRANGER, H.C., SANTOS, E.S., DEAN, B.G. & MOORE, F.B. (1961): Sandstone-type uranium deposits at Ambrosia Lake, New Mexico – an interim report, *Econ. Geol.* **56**, 1179-1210.

HARSHMAN, E.N. (1972): *Geology and uranium deposits, Shirley Basin area, Wyoming, U.S. Geological Survey Prof Paper* **745**, 82 pp.

HARSHMAN, E.N. (1974): *Distribution of elements in some roll-type uranium deposits, In: Formation of uranium ore deposits,* IAEA, Vienna, 169-183.

HARSHMAN, E.N. & ADAMS, S.S. (1981): *Geology and recognition criteria for roll-type uranium deposits in continental sandstones,* US-DOE, GJBX-1, **81**, 185 pp.

HUNTER, J. (1995): Fluvial architecture and paleo-ground water infiltration of the Fort Union Formation near the Highland Uranium Mine, Southern Powder River Basin, Wyoming. *Wyoming Geol. Assoc. Guidebook, Fiftieth Field Conference,* 119-137.

JENSEN, M.L. (1963): Sulfur isotopes and biogenic origin of uraniferous deposits of the Grants and Laguna districts. In*:* Kelley, V.C., ed., Geology and technology of the Grants Uranium Region, *New Mex Bur Mines, Mineral Res Mem,* **15,** 182-190.

KISH, L. & CUNEY, M. (1981): Uraninite - albite veins from the Mistamisk Valley of the Labrador Trough, Québec. *Min. Mag* **44**, 471-483.

KISLYAKOV, Y.M. & SHUMILIN, M.V. (1996): Olovskoye i Imskoye uranovyye mestorozhdeniya v mezozoyskikh vpadinakh Zabaykal'ya (Rossiya). Olov and Ima uranium deposits in Mesozoic depressions of Transbaikalia, Russia Federation. *Geologiya Rudnykh Mestorozhdeniy* **38,** 540-557.

KRÍBEK, B., KNÉSL, I. & PASAVA J (2005): Hydrothermal alteration of the graphitized organic matter at the Kansanshi Cu (Au-, U-) deposit, Zambia. In: Proc 8th SGA Meeting Beijing, China, Mao J, Bierlein FP (eds) *Mineral Deposit Research: Meeting the Global Challenge*, 277-280.

LI, J.-W., ZHOU, M.-F., LI, X.-F., LI, Z.-J. & FU, Z.-R. (2002): Origin of a large breccia-vein system in the Sanerlin uranium deposit, southern China: a reinterpretation. *Mineral. Deposita,* **37**, 213-225.

LUDWIG, K.R. (1978): Uranium-daughter migration and U-Pb isotope apparent ages of uranium ores, Shirley Basin, Wyoming, *Econ. Geol.* **73**, 29-49.

LUDWIG, K.R. (1979): Age of uranium mineralization in the Gas Hills and Crooks Gap districts, Wyoming, as indicated by U-Pb isotope apparent ages, *Econ. Geol.* **74**, 1654-1668.

LUDWIG, K.R. & SIMMONS, K.R. (1992): U-Pb dating of uranium deposits in collapse breccia pipes of the Grand Canyon region. *Econ. Geol.* **87,** 1747-1765.

LUDWIG, K.R., RUBIN, B., FISHMAN, N.S. & REYNOLDS, R.L. (1982): U-Pb ages of uranium ores in the Church Rock uranium district, New Mexico, *Econ. Geol.* **77**, 1942-1945.

LUDWIG, K.R., SIMMONS, K.R. & WEBSTER,J.D. (1984): *U-Pb isotope systematics and apparent ages of uranium ores, Ambrosia Lake, and Smith Lake districts,* Grants Mineral Belt, New Mexico, *Econ. Geol.* **79**, 322-337.

MATHIEU, R., CUNEY M. & CATHELINEAU M. (2000): Geochemistry of palaeofluids circulation in the Franceville basin and around Oklo natural nuclear reaction zones (Gabon); Proceedings of Geofluids III; third international conference on Fluid evolution, migration and interaction in sedimentary basins and orogenic belts. *J. Geochem. Explor.* **69-70,** 245-249.

MATHIEU R., ZETTERSTROM L., CUNEY M., GAUTHIER-LAFAYE F. & HIDAKA H. (2001): Alteration of monazite and zircon and lead migration as geochemical tracers of fluid paleocirculations around the Oklo-Okelobondo and Bangombe natural nuclear reaction zones (Franceville Basin, Gabon). *Chem. Geol.* **171,** 147-171.

MENEGHEL, L. (1979): *Uranium occurrence in the Katanga System of north-western Zambia, In: Uranium deposits in Africa, Geology and exploration,* IAEA, Vienna, 97-122.

MENEGHEL L. (1981): The Occurrence of Uranium in the Katanga System of Northwestern Zambia. *Econ. Geol.* **76**, 56-68

MIN, M., XU, H., CHEN, J. & FAYEK, M. (2005): Evidence of uranium biomineralization in sandstone-hosted roll-front uranium deposits, northwestern China. *Elsevier, Ore Geol. Rev.* **26,** 198-206.

NGONGO-KASHISHA (1975): Sur la similitude entre les gisements uranifères (type Shinkolobwe) et les gisements cuprifères (type Kamoto) au Shaba, Zaïre, *Ann Soc Gèol Belg*, **98**, 449-462.

NORTHRUP, H.R. (1982): *Origin of the tabular-type vanadium-uranium deposits in the Henry structural basin, Utah,* Ph.D. Thesis, Colorado

School of Mines, Golden, 194 pp.

OECD/NEA-IAEA (1998): *Uranium 1997: Resources, Production and Demand, 1997 Red Book*. **OECD/IAEA-TECDOC-650**, Paris, France.

OECD/NEA-IAEA (2008): *Uranium 2007: Resources, Production and Demand, 2007 Red Book*. OECD, Paris, France.

ONAC, B.P., HESS, J.W. & WHITE, W.B. (2007): The relationship between the mineral composition of speleothems and mineralization of breccia pipes; evidence from Corkscrew Cave, Arizona, USA. *Can. Mineral.* **45**, 1177-1188.

PFIFFELMANN, J.-P. (1975): L'uranium dans le bassin de Franceville, *In: The Oklo phenomenon*, IAEA, Vienna, 37-51.

RACKLEY, R.I. (1972): Environment of Wyoming Tertiary uranium deposits, *AAPG Bull,* **56**, 755-774.

REYNOLDS, R.L & GOLDHABER, M.B. (1983): Iron disulfide minerals and the genesis of roll-type uranium deposits, *Econ. Geol.* **78**, 105-120.

ROSENBERG, P.E. & HOOPER, R.L. (1982): Fission-track dating of sandstone-type uranium deposits, *Geology,* **10**, 481-485.

SAUCIER, A.E. (1980): Tertiary oxidation in the Westwater Canyon Member of the Morrison Formation, *In:* Rautman, C.A., ed., Geology and mineral technology of the Grants Uranium Region 1979, *New Mexico Bureau Mines Mineral Res. Mem.* **38**, 151-157.

THAMM, J.K., KOVSCHAK, A.A. & ADAMS, S.S. (1981): *Geology and recognition criteria for sandstone uranium deposits of the Salt Wash type*, Colorado Plateau province, **US-DOE, GJBX-6**, **81**, 136 pp.

TURNER-PETERSON, C.E. & FISHMAN, N.S. (1986): Geologic synthesis and genetic models for uranium mineralization in the Morrison Formation, Grants Uranium Region, New Mexico, *In:* Turner-Peterson, C.E., Santos, E.S., Fishman, N.S., eds., A basin analysis case study: the Morrison Formation, Grants Uranium Region, New Mexico, AAPG *Studies in Geology* **22**, 357-388.

WENRICH, K.J. (2000): Breccia pipe uranium deposits – A provocative insight into global uranium ore genesis and exploration. *Internat. Atomic Energy Agency, Vienna,* 1-5.

WENRICH, K.J. & SUTPHIN, H.B. (1989): Lithotectonic setting necessary for formation of a uranium-rich, solution-collapse breccia-pipe province, Grand Canyon region, Arizona. *Open-File Report - U.S.Geol. Surv.* **89-0173,** 33p.

WENRICH K. J., VAN GOSEN B. S. & FINCH W. I. (1995): Solution-collapse breccia pipe U deposits; Preliminary compilation of descriptive geoenvironmental mineral deposit models. *Open-File Report - U.S.Geol. Surv.* **OF 95-0831,** 244-251.

ZHOU, W., LIU, S., WU, J. & WANG, Z. (2000): Sandstone type uranium deposits in NW China. *East China Inst. Tech. (ECIT)*, IAEA-CN-128/27.

CHAPTER 10: OTHER TYPES OF URANIUM DEPOSITS

Kurt Kyser
Department of Geological Sciences and Geological Engineering,
Queen's University,
Kingston, Ontario, K7L 3N6, Canada
kyser@geol.queensu.ca

and

Michel Cuney
G2R, Nancy-Université, CNRS, CREGU,
B.P. 239,
F-54506 Vandoeuvre lés Nancy, France
michel.cuney@g2r.uhp-nancy.fr

QUARTZ-PEBBLE CONGLOMERATE URANIUM DEPOSITS

Quartz-pebble conglomerate-type U deposits are defined as stratiform and stratabound deposits of uraninite and brannerite hosted in pyrite-rich quartz-pebble conglomerate. Pyrite is the main detrital and authigenic heavy mineral, with pyrite contents generally between 3 and 15%. These deposits are hosted by the basal sequences of Archean and Paleoproterozoic basins and can be of detrital or hydrothermal origin. They make up approximately 2% of the world's U resources. Where U is recovered as a by-product of Au mining, such as the Witwatersrand Basin, the grade may be as low as 0.01% U whereas in deposits mined exclusively for U, average grades range as high as 0.15% U. Individual deposits range in size from 5,000 to 160,000 tonnes contained U.

The major examples of quartz-pebble conglomerate deposits are the Elliot Lake deposits in Canada and the Witwatersrand Au-U deposits in South Africa (Fig 10-1). The mining operations in the Elliot Lake area closed in the early nineties because these deposits were uneconomic in the U market. Other areas that have been examined or mined for their quartz-pebble conglomerate U-type mineralization include the Southern Lake Superior Region, Proterozoic conglomerate of the Black Hills and southeastern Wyoming in USA, and Paleoproterozoic conglomerate of the Koli Area in Eastern Finland (Fig. 10-1), Moeda and Jacobina formations in Brazil (Fig. 10-1), Ghana and Western Australia (IAEA, 1987).

Most economically significant uraniferous conglomerate formed through mechanical or later hydrothermal concentration of U in basins between

Fig. 10-1. Locations of most significant quartz-pebble conglomerate deposits.

Short course co-sponsored by the the SGA and MAC, Québec City, May 2008, p. 241-252

2.2 and 3.1 Ga on an Archean craton. This time-space criterion is essential, as is the presence of oligomictic, fluvial conglomerate that indicate reworking of the sediments, particularly any detrital uraninite essential for placer U concentrations (Anderson *et al*., 1987). Radioactive pyritiferous conglomerate with metamorphic grades lower than amphibolite facies and minimal regional deformation are also features of known economic deposits.

There are two main types of quartz-pebble conglomerate U deposits. Elliot Lake-type deposits (Fig. 10-2) have mineralization affected mainly by sedimentological controls. The ores grade from U through Th to Ti-rich with decreasing pebble size and increasing distance from their source (Fig. 10-2). Although brannerite is an alteration mineral, post-diagenetic remobilization is minimal and subordinate to sedimentological controls.

In contrast, Witwatersrand-type deposits have ores along unconformities, shale and siltstone beds and carbonaceous seams (Fig. 10-2). Regional structures include normal faults while, on the deposit scale, controls are bedding-parallel shears and thrusts, although the main control is still sedimentological. Textural evidence indicates that part of the U and Au have been remobilized to their current sites, however, whether the original deposition was detrital or entirely hydrothermal remains contentious.

In both types of deposit, the host rocks are typically submature to mature, polymictic conglomerate and sandstone deposited in alluvial fan and braided stream environments. The host conglomerate is at the base of the sequence in the Elliot Lake district, whereas the mineralized horizons in the Witwatersrand are mainly along intraformational unconformities.

Blind River-Elliot Lake district

The Blind River-Elliot Lake district is located in southern Ontario at the southern margin of the Canadian Shield to the north of Lake Huron. The major ore trends include the Quirke trend in the Quirke Lake area, the Nordic trend in the Elliot Lake area and the Pronto trend in the Blind River area. Reserves are about 450,000 tonnes U.

The geology comprises Archean basement, Paleoproterozoic Huronian Supergroup and post-Huronian intrusive rocks, Paleozoic sedimentary

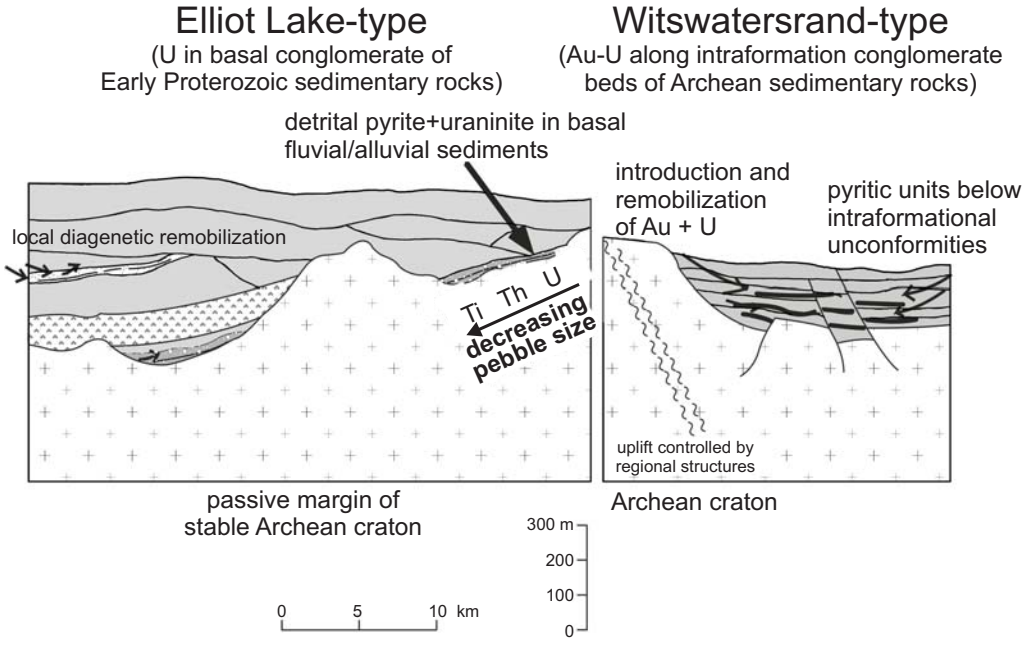

Fig. 10-2. General features of quartz-pebble conglomerate deposits in the Elliot Lake area of Canada (Elliot Lake- type) and the Witwatersrand-type from South Africa. In both cases, there is evidence for detrital uraninite, particularly in the Elliot Lake-type where zoning in detrital components is prevalent and much of the U occurs in basal channel facies. Both types also record diagenetic remobilization of U, although in the case of the Witwatersrand, more U is associated with secondary hydrothermal processes. From Roscoe & Minter (1993) and Dahlkamp (1993).

rocks and Pleistocene to Recent glacial deposits (Fig. 10-3). The Archean includes metavolcanic rocks, metasedimentary rocks, granitic and gabbroic intrusions and the late Archean quartz-monzonitic Algoman Granite. Similar basement rocks north and northwest of Elliot Lake contain anomalous U contents (Richardson *et al.,* 1975). The Huronian Supergroup is a thick clastic sequence with minor tholeiitic basalt. At its base, the Elliot Lake Group consists of psammite and volcanic rocks and includes uraniferous quartz-pebble conglomerate of the Matinenda Formation. Uraniferous conglomerate present in the Elliot Lake mining area is contained within the middle and lower portions of the Matinenda Formation (Robertson 1989). The Supergroup forms a southward thickening wedge composed of three sedimentary megacycles. Each cycle consists of a basal fluvial unit overlain by glacial-marine/lacustrine strata and capped by a turbiditic to lenticular bedded assemblage. The Matinenda Formation represents the basal braided fluvial unit of the lowermost glacial megacycle (Fig. 10-3). Glacial units of the Ramsay Lake Formation and marine/lacustrine strata of the McKim and Pecors Formations complete the assemblage. This is overlain by the Hough Lake and Quirke Lake groups, with a sedimentary cycle starting with polymictic paraconglomerate interpreted as tillite and followed by clastic rocks coarsening upward. Overlying this is the Cobalt Group, which consists of three glacial to fluvial cycles ending with an upper coastal beach facies (Richardson *et al.,* 1975).

The Lower Huronian section contains sulfides, dominantly pyrite, associated with U in near-shore clastic units (Fig. 10-3). The Upper Huronian contains Th and abundant hematite that has been cited as evidence for an increase in the level of atmospheric oxygen. The Matinenda Formation was deposited in regressive cycles, resulting in several quartz-pebble conglomerate horizons interbedded with arkose and sandstone deposited within depressions of the Archean basement from high energy, braided fluvial systems with a S to SE-direction. During the Blezardian (2100 Ma) and Penokean (1900-1750 Ma) orogenies (Fig. 10-3), the rocks were weakly metamorphosed and gently folded, with main fold axes trending roughly E-W. A regional structure in the U region is the Murray Fault, a high-angle reverse fault, north of which all economic deposits are located. In the Blind River-Elliot Lake district, the Huronian strata are folded into a WNW-ESE-oriented syncline, the Quirke Syncline. The area was intruded by the Nipissing Diabase at 2.21 Ga.

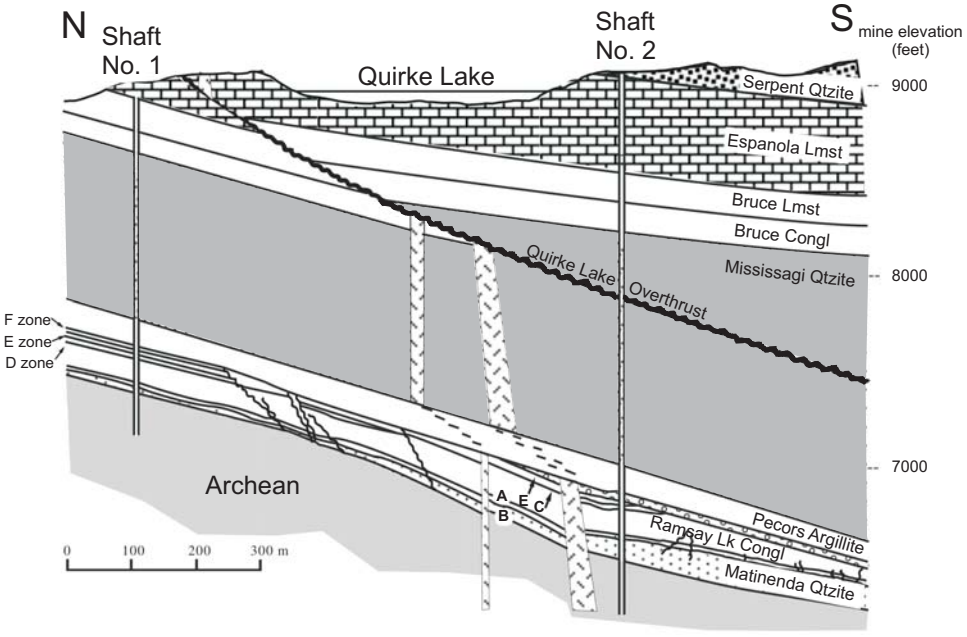

Fig. 10-3. Blind River-Elliot Lake, Denison mine, geological N-S section showing position and attitude of the uraniferous conglomerate horizons (A to F zones). The stratigraphy is from the Lower Huronian Supergroup. The intrusive units are primarily the 2.21 Ga Nipissing Diabase. Modified from Dalhkamp (1993).

Paleoweathering of the Archean basement is best preserved on granitic rocks. The chemical character of the paleosol suggests the weathering processes operated under reducing conditions (Kimberley *et al.* 1984). Post depositional modifications of the Matinenda Formation include pressure solution of quartz, quartz cementation, sericitization of K-feldspars and pyritization, with more than about 90% of the pyrite present being of post-depositional origin (Robinson & Spooner, 1984). Intrusion of Nipissing Diabase dikes and sills caused local albitization, chloritization, and carbonatization of the wall rocks. No major alteration related to the initial U emplacement has affected the host rocks.

Principal ore minerals are uraninite, brannerite and monazite, with minor coffinite, uraniferous kerogen, uranothorite, xenotime, and gummite (*e.g.*, Mossman 1999). The U/Th ratios range within various ore bodies from 5 to 0.3 and in ore milled from 2 to 3. Uraninite grains are up to 0.2 mm in diameter and average 65% UO_2, 6.5% ThO_2, 2.5% Y_2O_3, 0.9% Ce_2O_3 and 18% PbO. Uraninite occurs primarily as small clusters of grains between pebbles and in monomineralic subparallel bands of well-sorted angular grains concentrated proximal to the base of small-scale depositional units within conglomerate (Fig. 10-3). Although rare, uraninite fragments can be cemented by filamentous hydrocarbons (Ruzicka & Steacy 1976, Mossman *et al.* 1993). Uranium content correlates with maximum apparent quartz-pebble diameter (Theis 1979, Roscoe 1969) and is associated with pyrite. Brannerite, which is mainly amorphous U–Ti-oxide mixtures, is the reaction product of U with Ti oxides within conglomerate after its deposition.

Heavy minerals in Matinenda Formation conglomerate give U/Pb dates of 2550 ± 50 Ma for uraninite (Meddaugh & Holland, 1981), 2500 Ma for monazite and 2450 Ma for zircon (Mair *et al.* 1960), all indicative of an Archean source. The uraninite contains up to 9% ThO_2 and 8% REEs, which are typical for uraninite from granite and pegmatite.

Economic U mineralization has been found in three ore trends corresponding to three NW–SE-oriented fluvial systems of the Matinenda Formation (Fig. 10-3). The major ore bodies occur in the Quirke Syncline and are up to 15 km wide, more than 50 km long and slightly more than 1000 m thick. Uranium mineralization is confined to several horizons of quartz-pebble conglomerate, consisting of well-rounded and well-sorted quartz (> 95% of the pebble fraction) and chert pebbles in a matrix of quartz, feldspar, sericite and pyrite (Fig. 10-3). There is a paucity of clay and silt-size particles.

A syn-sedimentary placer deposit modified by post-depositional processes generated by diagenesis or mild metamorphism is the most cited model for these deposits (Robertson 1989). Uraninite grains are rounded in a way that is best explained by fluvial transport and abrasion. The age and character of most of the uraninite are consistent with derivation from uraniferous Archean granite and pegmatite. Lack of magnetite, hematite and ilmenite resulted from conversion to pyrite by sulfurization (Ferris & Ruud 1971). In support of this, pyrite from the 2.45 Ga pyritic uraniferous quartz-pebble conglomerate of the Matinenda Formation has $\delta^{34}S$ values that vary from –9.0 to +5.5‰ (Yamaguchi & Ohmoto 2006). The widest range of approximately 15‰ is in euhedral pyrite grains whereas a much smaller range typifies anhedral, subhedral, and rounded grains of pyrite. Variable concentrations of Co (to 4700 ppm), Ni (to 1900 ppm), and As (to 3400 ppm) among individual pyrite crystals and within single grains with overgrowth textures are markedly different between core and overgrowth parts of pyrite because the pyrites have been isotopically, chemically, and morphologically modified by post-depositional processes and not solely by a detrital process. Therefore, the morphology and chemistry of pyrite (and possibly uraninite) may not always represent the original features at the time of deposition.

The Witwatersrand Basin

The Witwatersrand Basin is located along the border between the Free State and Gauteng, South Africa (Fig. 10-1). Ore horizons are exposed along a 450 km long section on the western and northern sides of the Witwatersrand Basin, the largest Au-U province in the world. Uranium grade of *in situ* ore is generally very low, ranging from 0.013% to 0.06% U (Brynard & Andreoli 1988).

The Witwatersrand Basin covers an area of almost 50,000 km^2 underlain by more than 8000 m of slightly metamorphosed strata of the Dominion Group and Witwatersrand Supergroup, which host ore-bearing, quartz-pebble conglomerate, and the Ventersdorp Supergroup, which is slightly mineralized (Fig. 10-4). The strata rest unconformably upon granitic gneiss, and ultramafic and metasedimentary rocks of the Swaziland Supergroup of the Archean Kaapvaal Craton, with a

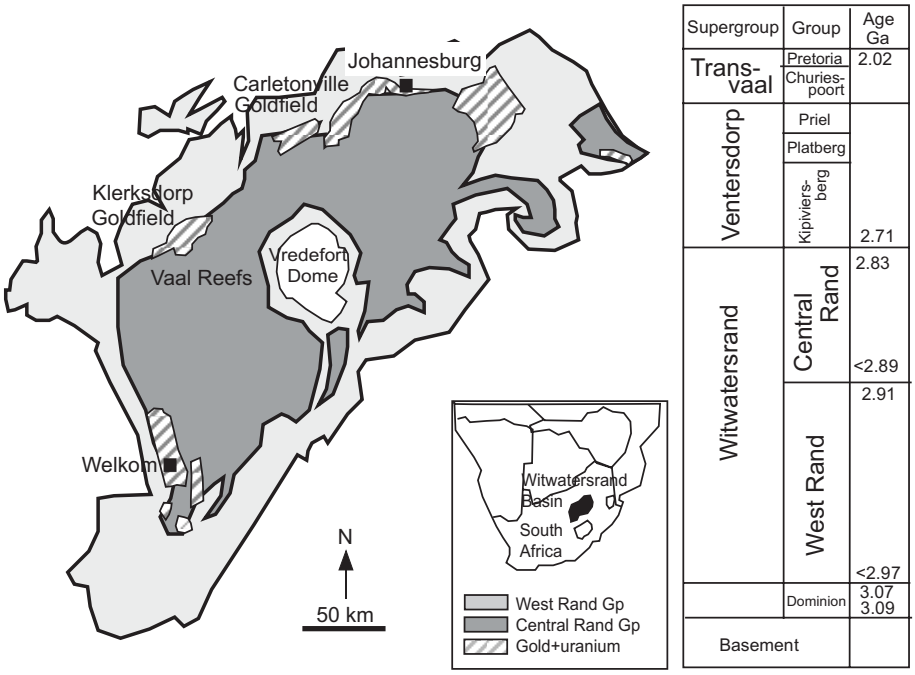

Fig. 10-4. Simplified geologic map of the Witwatersrand Basin showing areas of Au + U mineralization and generalized stratigraphic column showing ages. Modified from Kirk *et al.* (2001).

paleosol just below the unconformity. The lowermost sedimentary unit is the 3074–3086 Ga Dominion Group (Frimmel & Minter 2002), a 40–100 m thick package of conglomerate, arkose, and quartzite capped by lava, tuff and shale with a composite thickness of almost 2700 m. Uranium occurs within the basal section in two oligomictic quartz-pebble conglomerate layers, the Lower Reef and the Upper Reef. The Lower Reef forms narrow lenses within paleo-valleys incised into the Archean basement and the Upper Reef, in contrast, is laterally more continuous.

The overlying 2.970 to 2.837 Ga Witwatersrand Supergroup (Fig. 10-4) is divided into a lower West Rand Group, about 4500 m thick, and an upper Central Rand Group, about 2500 m thick. The West Rand Group includes shale, quartzite, scarce conglomerate, and andesitic lava, but U occurs in only one zone of conglomerate. The Central Rand Group contains predominantly medium to coarse-grained quartzite and conglomerate with minor amounts of interbedded slate and andesitic lava. The amount of conglomerate in the Witwatersrand Supergroup is only 8%, but the Central Rand Group hosts the most important uraniferous reefs, with more than 80% of the total U.

The Vaal Reef (Fig. 10-4) is considered to be the product of a meandering stream system on a broad flood plain with the direction of transport to the southeast. It dips to the southeast from 12 to 60°, has a maximum thickness of 100 cm and overlies a carbonaceous, thucholite-bearing horizon. The Ventersdorp Supergroup unconformably overlies the Witwatersrand sedimentary rocks and contains primarily lava. The Transvaal Sequence sits unconformably on the Ventersdorp Sequence and contains slate, quartzite, conglomerate, dolomitic limestone, and diabase sills.

Principal ore minerals are uraninite and native Au and lesser uranothorite, brannerite, thucholite, coffinite, and hexavalent U minerals. Remobilization by erosional redistribution (Minter 1981) and diagenetic processes (Thiel *et al.* 1979) resulted in modification leading to formation of brannerite and other U–Ti-phases. U mineralization is manifest as detrital grains, with a degree of roundness similar to detrital monazite, uraniferous phyllosilicates in concretionary pyrite nodules, authigenic minerals of U–Ti-phases and uraniferous carbonaceous matter. U accumulated as a matrix constituent in conglomerate, in pyritic sand, in quartzite along unconformity surfaces and in carbonaceous bands on, or adjacent to, unconformity surfaces (Mossman *et al.* 1993).

Uraninite grains from Witwatersrand ores have apparent U/Pb dates of 3065 ± 100 Ma, similar to the age of granite surrounding the Witwatersrand

Basin, and a secondary age of 2040 Ma that is coeval with the emplacement of the Bushveld Complex (Allsopp & Welke 1986) and the large Vredefort impact structure. The uraninite grains have up to 10% ThO_2, which is typical for uraninite from granite and pegmatite. Liberation of detrital minerals by predominantly physical weathering is reflected by the paleosol topping the crystalline basement (Grandstaff *et al.* 1986). However, Law & Phillips (2006) challenged the placer model for the genesis of the Witwatersrand deposits by suggesting that post-burial fluids during diagenesis, deformation and metamorphism were responsible for remobilization of the Au and the U (Fig. 10-2). As is true of most things in complex natural systems, the truth is most likely a combination of the extremes.

Koli

Jatulian meta-arenite forms an extensive part of the Karelian Supergroup in the Baltic Shield, including the Koli region (Fig. 10-1). In eastern Finland, Karelian supracrustal rocks (Jatulian and Sariolian; 2,000–2,500 Ma) trend northwesterly for 150 km along the margin of the Archean basement in the east (Äikäs & Sarikkola 1987). The thickness of this sequence varies from less than 500 m to 2000 m.

Uranium and Th occur in the lower Jatulian Quartzite Member as lenses and at the contacts of Jatulian diabase intrusions where they cut across the uraniferous horizon. Small U bodies also lie in the middle Jatulian Arkosite Member such as at Ipatti, a well-exposed occurrence of U at Koli (Fig. 10-1), where 71,000 tons of mineralized quartz pebble conglomerate and sandstone averaging 0.083% U are situated in the Arkosite. Ipatti arenite is predominantly a pebbly and clayey subarkose indicating poor sorting and, hence, rapid burial in a fluvial-dominated deltaic environment. Mineralization is in the form of cement restricted to beds of sandstone and small-pebbled conglomerate on top of a 5–20 m thick unit of sericite quartzite.

The U mineralization at Ipatti is suggested to have originated from pore fluids in at least three stages of epigenetic precipitation (Äikäs & Sarikkola 1987). Sedimentary control for the migration of the mineralizing fluids is displayed by the host unit that is interpreted as a channel-fill structure with relatively better permeability because it is more pebbly than the wall rocks. Magnetite in the host acted as reductant and Archean granitoid rocks are considered to be the most probable sources of U. Sedimentological, mineralogical, and geochemical evidence for mineralization of U in the Koli area indicate more than one superimposed stage of epigenetic mineralization, and hence not of detrital origin (Äikäs & Sarikkola 1987). However, there are also high Th contents in these conglomerate layers which favor a detrital origin for part of the radioactive material.

SURFICIAL URANIUM DEPOSITS

Surficial U deposits are broadly defined as young (Tertiary to Recent) near-surface U concentrations in sediments or soils. Surficial U deposits form in four major environments (Otto 1984): (1) hot and dry (desert), (2) hot and wet (tropical), (3) temperate and cool (wetlands), and (4) hot climates transitional between wet and dry. Some of the environments where surficial deposits form include non-pedogenic in valley-fill and playas, pedogenic environments, ephemeral evaporative, karst caves, wetland valley-fill and lacustrine deposits, tropical deposits developed in lateritic weathering profiles over U-rich source rocks, supergene enrichment of primary U ore bodies, epigenetic U entrapped in redox fronts above sulfide ore bodies and in alkaline lakes.

Calcrete-hosted uranium deposits

Uranium deposits in calcrete are the most significant of the surficial deposits, wherein U mineralization is in surficial sand and clay, cemented by Ca and Mg carbonates, although gypcrete and silcrete may also be associated. Host sediments are of Tertiary to Quaternary age but U mineralization is usually young, commonly less than 2.0 Ma. Calcrete-hosted U deposits have relatively large tonnages but very low grades, with the average deposit size being 3000 tU at less than 0.05% U, although two deposits are much larger. Calcrete deposits have only recently begun to be exploited, with extraction started at the Langer Heinrich deposit in Namibia and soon to start at the Yeelirrie deposit in Western Australia (Fig. 10-5).

Surficial deposits comprise about <1% of world U resources. They generally form where U-rich granite or felsic volcanic rocks were deeply weathered in a semi-arid to arid climate. Major U deposits in Western Australia (Lambert *et al.* 1996) include the Yeelirrie, Lake Way, Centipede, Thatcher Soak, and Lake Maitland deposits (Fig. 10-5), where calcrete U deposits occur in valley-fill sediments along Tertiary drainage channels, and in playa lake sediments (Fig. 10-6). These deposits

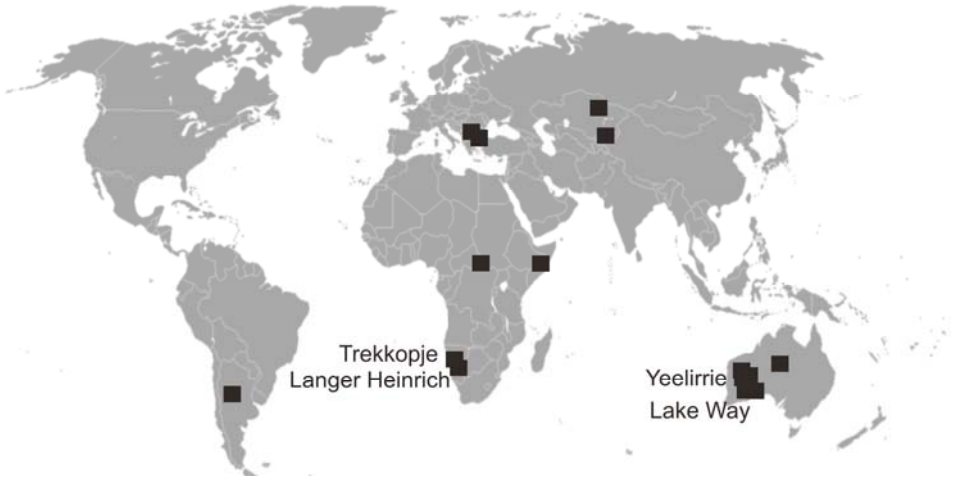

Fig. 10-5. Location of major surficial calcrete-hosted uranium deposits.

overlie Archean granite and greenstone basement of the northern portion of the Yilgarn Craton. The U mineralization is carnotite (hydrated K–U vanadate). In addition to Australia, uraniferous valley-fill deposits also occur in Namibia, South Africa, Mauritania, Somalia, Argentina, and China (Fig. 10-5). The most noteworthy occurrences are the Langer Heinrich, Trekkopje, Tubas, and Aussinanis in Namibia, and Kamasoas and Henkries in the northwestern Cape of South Africa (Fig. 10-5).

The general model for the formation of surficial calcrete-hosted U deposits (Fig. 10-6) involves liberation of U from source rocks by leaching and transport by oxidizing surface waters or shallow groundwaters. In arid lands, U is generally leached from source rocks by slightly alkaline, oxidizing waters and carried as uranyl carbonate or bicarbonate complexes. Oxidizing conditions persist and the alkalinity and salinity of the waters tend to increase down-flow, keeping the uranyl ions in solution until fixation mechanisms intervene.

In tropical environments, the near-surface soil horizons are typically acid and U is probably complexed by sulfate or phosphate ions. In wetlands, the waters are usually acid or close to neutral and are relatively fresh but still carry inorganic or organic complexing agents well in excess of any contained U. In tropical and wetland environments, transport distances are generally short (a metre to a few kilometres), whereas in arid lands, transport distances may be long (several tens of kilometres). During transport from source to eventual host, U may be concentrated first in a protore, such as an older weathering horizon which

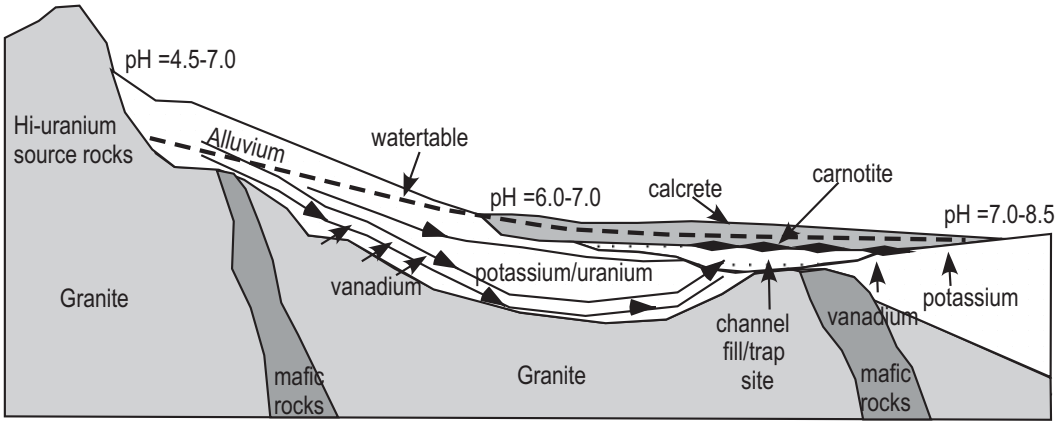

Fig. 10-6. Idealized model of calcrete-hosted deposit, such as Yeelirrie and others in arid climates in Western Australia. In the Langer Heinrich deposit in Namibia, the source of the V is black shale (Hartleb 1988). After Mann & Deutscher (1978) and Arakel (1988).

is later dissected, and then remobilized. In Western Australia, pre-existing laterite soil profiles may have served as a sink for U (Otto 1984).

For many arid land and wetland deposits, physical barriers to groundwater flow or changes in slope may initiate ore deposition (Batulin 1980). In non-pedogenic calcrete-hosted U deposits along valleys, basement highs in the alluvium near the deposit may have been barriers to flow (Fig. 10-7). These barriers direct groundwater toward the surface, where evaporation increases, CO_2 is exsolved, and the groundwater can mix with more oxygenated waters or with waters containing different solutes. In cool, wet climates, organic matter can accumulate where drainage impediments or changes in slope along valleys cause the water table to be high, promoting plant growth and inhibiting decay. Flow velocities are reduced, increasing the time of interaction between organic-rich sediments and passing uraniferous solutions (Otto 1984).

Various fixation mechanisms for U in surficial deposits have been proposed (Otto 1984) including:

1. Dissociation of soluble complexes; *e.g.*, uranyl carbonate species through loss of CO_2 to the atmosphere or precipitation of a carbonate mineral.
2. Evaporative concentration of solute species in near-surface groundwaters.
3. Change in valence state of V or U which decreases the solubility of the ore mineral. For example, carnotite may form, in part, by the oxidation of V^{4+} to V^{5+} where sufficient U^{6+} is available.
4. Mixing of waters creating local supersaturation with respect to U minerals.
5. Sorption by organic matter followed by reduction of the U by reduced sulfur species or organic matter.
6. Sorption by silica, iron hydroxides or oxyhydroxides, and clay.

The Archean Yilgarn Block in Western Australia hosts in its northern part surficial-type U occurrences of small size and low grade, except at Yeelirrie, which has reserves of 50,000 tonnes U at a grade of 0.13% U. The deposits are associated with non-pedogenic calcrete or dolocrete within intracratonic Tertiary to Quaternary drainage systems. The shallow, dry lakes and valleys are incised into Archean granite and greenstone belts, and filled with clastic material from the basement and evaporites (Fig. 10-6). Waters associated with the Yeelirrie deposit contain significant quantities of Zn, Sr, and F; the host rocks there and at other

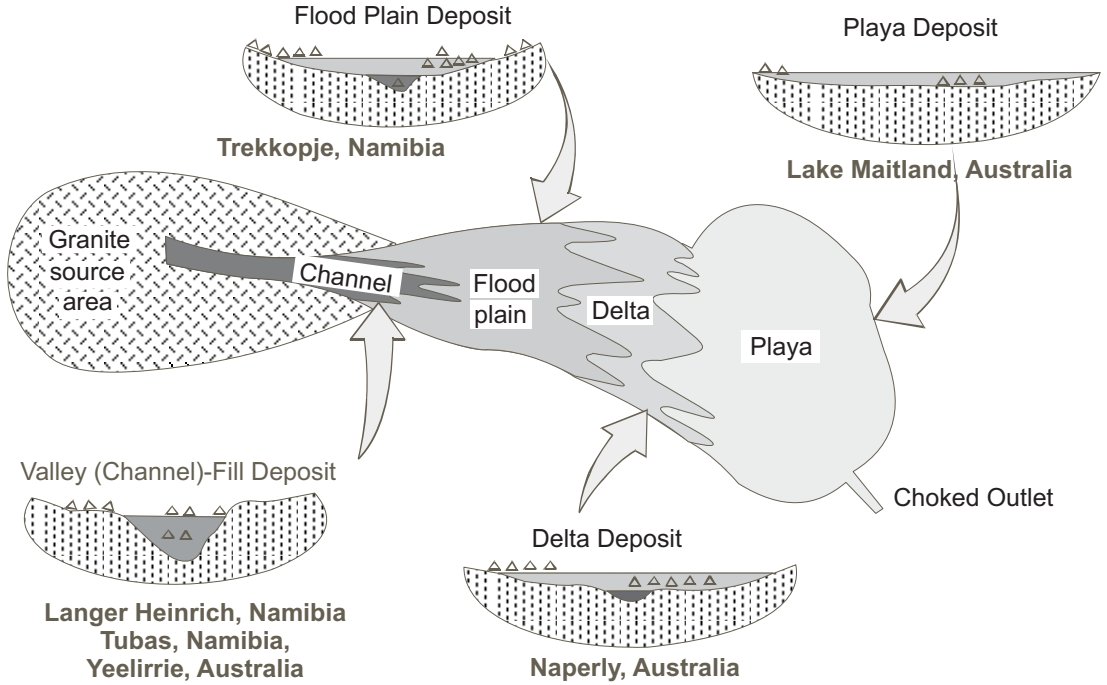

Fig. 10-7. Location of various types of surficial calcrete-hosted deposits in an outwash environment showing source of the U from U-rich granite, and deposition in channel facies, flood plain, delta and playa during mixing with fluids and evaporation. Modified from Butt *et al.* (1984) and Dahlkamp (1993).

deposits contain minor amounts of celestite, fluorite, and barite (Briot 1983).

Principal alteration of the host rocks at Yeelirrie is related to hydrology, resulting in Ca-, Mg-, Si-, and CO_2-metasomatism as cements, and leading selectively to the formation of calcrete, dolocrete, and other duricrust facies by gradual replacement of clay–sand material within the upper 10 m of the alluvial host sediments (Batulin 1980). Valley sediments consist of varying amounts of quartz and kaolinite, with minor illite, montmorillonite and feldspar. Calcrete and dolocrete formation resulted from the partial to complete replacement of kaolinite and quartz by dolomite and calcite. Gypsum and celestite may occur locally in larger amounts. The replacement processes were associated with an increase in rock volume provoking small-scale folds, faults, ubiquitous slickensides and, locally, diapiric structures or mounds bounded by faults.

The principal U mineral is carnotite that fills small fissures and voids, replaces the argillaceous matrix of the host rock, and coats calcite, dolomite, silica and sepiolite pore spaces in porcellaneous calcrete and sand. Playa deposits are hosted by near surface, thin calcrete horizons and alluvial and evaporitic sediments. Valleys are up to some hundred metres wide, several kilometres long and 1 to 15 m thick. Grades are a few hundred ppm U, up to 0.13% U in Yeelirrie, and the highest formed along the water table in calcrete which constitutes the principal aquifer.

Granitic rocks, anomalous in U content, served as the source for U (Fig. 10-6), and V is probably derived from mafic minerals in the granitic rocks or greenstone (Butt *et al.* 1984). The basin that hosts the deposits had low relief, low drainage gradient, large catchment area including deeply weathered granitic rocks (Fig. 10-7). Distribution of calcrete/dolocrete is mainly in axial segments of large channels becoming less well developed at playa margins.

Isotopic disequilibrium is the expected condition for most surficial U deposits, with the Western Australian deposits showing significant variations from equilibrium. Isotopic disequilibrium and ore textures in the deposit at Yeelirrie suggest that U continually dissolved and reprecipitated during an extended period in the late Pleistocene and Holocene. The age of mineralization is not known for the Yeelirrie deposit or for any other nearby deposits. Isotopic disequilibrium can be explained by several different models for U emplacement and movement. The most geologically reasonable models suggest that the U was deposited from 0.1 to 0.75 Ma ago. The age of Namibian deposits has been estimated from the regional geologic setting to be at least 0.5 Ma, but the deposits probably formed during a period of several tens to several hundreds of thousands of years. Most wetland U deposits are younger than 12,000 years, the maximum age for the host sediment, and probably continue to form today.

A general model for calcrete-hosted U deposits involves locations upstream with respect to local barriers formed by uplifted basement blocks or by local constrictions of the channel (Fig. 10-7). These constrictions allow development of upstream depressions which are temporarily flooded, conducive to formation of sedimentary calcrete, and diminishing phreatic water circulation. The stabilized phreatic lens promotes dolomitization of the original calcrete and concentration of U and V, which precipitate as carnotite during evaporation in arid to semi-arid climates (Batulin, 1980).

Wetland deposits

In wetland deposits, U is the only metal present in significant quantities, although Mo has been detected in some deposits. The deposits usually are in reducing environments that may range in organic matter content from a few percent to almost 100%. No U minerals have yet been recognized in these deposits. Uranium deposits in lateritic profiles are geochemically and mineralogically variable and complex. In addition to abundant Fe and Mn hydroxides and oxyhydroxides, the deposits generally contain Ti hydroxides, kaolinite and gibbsite. Ni, V, Cu, Mo, Zn, Co, As, Se, and S can be present in significant amounts, depending on the substrate.

Sedimentary hosts in which U is deposited tend to form in regions that are being denuded, so that these are not commonly preserved in the geologic record. Wetland surficial U deposits range in size from less than a hundred kilograms of contained U in thin, organic-rich soil near a uraniferous spring to about 500 tonnes along extensively mineralized valley-fill sediments. The grade of these deposits ranges from slight enrichments (a few tens of parts per million) to about 30% (dry basis) in uraniferous peat in Sweden (Otto 1984).

Wetlands in montane and subalpine settings can contain significant concentrations of U. Sorption by organic material, complexing of uranyl,

UO_2^{2+}, with humic and fulvic acids, and bacterial action can produce geochemical enrichment factors of 10,000 to 1 or greater between peat and U-bearing waters. The only wetland U deposit in the United States that has been mined is the Flodelle Creek deposit in Stevens County, Washington, which contains 450 tU (Owen 1990).

Phosphate and shale deposits

Unconventional resources are defined by OECD (2008) as resources from which U is recoverable as a minor by-product, such as U associated with phosphate rocks, non-ferrous ores, carbonatite, black shale and lignite. Most of the unconventional U resources are associated with U in phosphate rocks, although black shale is also a significant resource.

The world average U content in phosphate rock is estimated at 50–200 ppm, although marine phosphorite averages 6–120 ppm, and organic phosphorite deposits are up to 600 ppm. Marine phosphorite deposits form from upwelling of nutrient-rich marine waters onto a shallow continental shelf with restricted circulation (Chernoff & Orris 2002). Although the grades can reach 0.065% U and the resource is substantial, the U is also associated with other undesirable elements such as Se and As.

Currently no phosphates are mined for U, but U is recovered unofficially from phosphates used for the production of fertilizers by several countries and most countries do not report U from phosphorite as a resource. Processing of Moroccan phosphates produced 690 tU between 1975 and 1999 and about 17,150 tU were recovered in the United States from Florida phosphate rocks between 1954 and 1962. As much as 40,000 tU was also recovered from processing marine organic deposits in Kazakhstan (Orris & Chernoff 2002).

Reserves of U from phosphorite deposits are dominated by those from Morocco (Table 10-1). Estimates of reserves are extremely variable, with the latest estimates suggesting 22 million tU globally (OECD 2008). Notwithstanding the problems associated with extracting the U and other elements from phosphorites, these deposits represent a significant reservoir of U that may be more strategic in the near future.

Black shale also represents a significant reserve of U, although economic extraction of U is a challenge. Uranium in shale resides with organic matter. The U contents of black shale are variable but can reach 400 ppm, such as in the Ranstad deposit in Sweden. Exploration for black shale deposits is currently in progress in several countries, with consideration for a mix of metals in addition to U. Large U resources are associated with the Chattanooga (United States) and Ronneburg (Germany) black shales, which combined total 4.2 million tU (OECD 2008).

TABLE 10-1. ESTIMATED RESERVES FOR U IN PHOSPHATE DEPOSITS (OCED 2001).

Uranium inventories for phosphate deposits	
Country	**million tU**
Marine phosphorite	
Morocco	6.9
USA	1.2
Mexico	0.15
Jordan	0.1
Others	0.65
Subtotal	*9*
Organic phosphorite	
Kazakhstan	0.12
Russia	
Subtotal	*0.12*
Total	9.12

REFERENCES

ÄIKÄS, O. & SARIKKOLA, R. (1987): Uranium in Lower Proterozoic conglomerates of the Koli Area, Eastern Finland. *Uranium deposits in quartz-pebble conglomerates*, **IAEA-TECDOC-427**, 189-234.

ALLSOPP, H.L. & WELKE, H.J. (1986): Age limits to the Witwatersrand Supergroup. In: Anhaeusser CR Maske S, Mineral Deposits of southern Africa, *Geol. Soc. S Afr.* **1**, 495-496.

ANDERSON, J.R., GOODKNIGHT, C.S., SEWELL, J.M. & RILEY, J.K. (1987): Favorability of Precambrian quartz-pebble conglomerates in the United States as uranium hosts. *Uranium deposits in quartz-pebble conglomerates* **IAEA-TECDOC-427**, 7-40.

ARAKEL, A. V. (1988): Carnotite mineralization in inland drainage areas of Australia. *Ore Geol. Rev.* **3,** 289-311.

BATULIN, S.G. (1980): Regional factors of formation of uranium deposits in calcretes. *Lithology and Mineral Resources* **15**, 437-442.

BRIOT, P. (1983) : L'environnement hydrogeochimique du calcrete uranifere de Yeelirrie (Australie Occidentale). Hydrogeochemical

environment of uraniferous calcrete of Yeelirrie, Western Australia. *Mineral. Dep.* **18,** 191-206.

BRYNARD, H.L. & ANDREOLI, M.A.G. (1988): The overview of the regional geological and structural setting of the uraniferous granites of the Damara Orogen, Namibia. In: *Recognition of uranium uranium provinces*, IAEA, Vienna, 195-212.

BUTT, C.R.M., MANN, A.W. & HORWITZ, R.C. (1984): Regional setting, distribution and genesis of surficial uranium deposits in calcretes and associated sediments in Western Australia, In: *Surficial uranium deposits* **TECDOC-322**, IAEA, Vienna, 121-127.

CHERNOFF, C.B. & ORRIS, G.J. (2002): Data set of world phosphate mines, deposits, and occurrences—Part A. Geologic Data. USGS *Open-File Report* **02–156–A**, 352 p.

DAHLKAMP, F.J. (1993): *Uranium ore deposits.* Springer-Verlag, Berlin, 460p.

FERRIS, C.S. & RUUD, C.O. (1971): Brannerite: Its occurrences and recognition by microprobe, *Colorado School Mines Quarterly,* **66**, 1-35.

FRIMMEL, H.E. & MINTER, W.E.L. (2002): Recent Developments Concerning the Geological History and Genesis of the Witwatersrand Gold Deposits, South Africa. *Soc. Econ. Geol. Sp. Publ.* **9**, 17–45.

GRANDSTAFF, D.E., EDELMANN, M.J., FOSTER, R.W., ZBINDEN, E. & KIMBERLEY, M.M. (1986): Chemistry and mineralogy of Precambrian paleosols at the base of the Dominion and Pongola Groups (Transvaal, South Africa), *Precamb. Res.* **32**, 97-131.

HARTLEB J.W.O. (1988): The Langer Heinrich uranium deposit; Southwest Africa/Namibia; Unconventional uranium deposits. *Ore Geol. Rev.* **3,** 277-287.

IAEA (1987): *Uranium deposits in quartz-pebble conglomerates* **IAEA-TECDOC-427**, 459 pp.

KIMBERLEY, M.M., GRANDSTAFF, D.E. & TANAKA, R.T. (1984): Topographic control on Precambrian weathering in the Elliot Lake Uranium District, Canada, *J. Geol. Soc.* **141**, 229-233.

KIRK, J., RUIZ, J., CHESLEY, J., TITLEY, S. & WALSHE, J. (2001): A detrital model for the origin of gold and sulfides in the Witwatersrand Basin based on Re-Os isotopes. *Geochim. Cosmochim. Acta* **65,** 2149-2159.

LAMBERT, I., MCKAY, A. & MIEZITIS, Y. (1996): Australia's Uranium Resources and Production in a World Context, ANA Conference October 2001.

LAW, J. & PHILLIPS, N. (2006): Witwatersrand gold-pyrite-uraninite deposits do not support a reducing Archean atmosphere; evolution of early earth's atmosphere, hydrosphere, and biosphere; constraints from ore deposits. *Geol. Soc. Amer. Memoir* **198**, 121-141.

MAIR, J.A., MAYNES, A.D., PATCHETT, J.E. & RUSSEL, R.D. (1960): Isotopic evidence on the origin and age of the Blind River uranium deposits, *J. Geophys. Research,* **65**, 341-348.

MANN, A. W. & DEUTSCHER, R. L. (1978): Genesis principles for the precipitation of carnotite in calcrete drainages in Western Australia; Uranium geology in resource evaluation and exploration. *Econ. Geol. Bull. Soc. Econ. Geol.* **73,** 1724-1737.

MEDDAUGH, W.S. & HOLLAND, H.D. (1981): Age and origin of uraninite in the Elliot Lake, Ontario, uranium deposits, *Geol. Soc. Amer,* Abstract with Program **13**, 509 pp.

MINTER, W.E.L. (1981): The distribution and sedimentary arrangement of carbon in South African Proterozoic placer deposits, In: Armstrong, C.F., ed., Genesis of uranium- and gold-bearing Precambrian quartz-pebble conglomerates, *U.S. Geol Surv Prof Paper* **1161-P,** P1-P4.

MOSSMAN, D. J. (1999): Carbonaceous substances in mineral deposits; implications for geochemical exploration; Geochemical exploration 1997; selected papers from the 18th international Geochemical exploration symposium. *J. Geochem. Explor.* **66,** 241-247.

MOSSMAN, D. J., GOODARZI, F. & GENTZIS, T. (1993): Characterization of insoluble organic matter from the lower Proterozoic Huronian Supergroup, Elliot Lake, Ontario; Metalliferous black shales and related ore deposits. *Precamb. Res.* **61,** 279-293.

OECD/NEA-IAEA (2001): *Uranium 2001: Resources, Production and Demand, 2001 Red Book*. OECD, Paris, France.

OECD/NEA-IAEA (2008): *Uranium 2007: Resources, Production and Demand, 2007 Red Book*. OECD, Paris, France.

ORRIS, G.J. & CHERNOFF, C.B (2002): Data set of world phosphate mines, deposits, and occurrences—Part B. Location and Mineral

Economic Data. USGS *Open-File Report* **02–156–A**, 328 p.

OTTO, J.K. (1984): Surficial uranium deposits: summary and conclusions. In: *Surficial Uranium Deposits*, IAEA, Vienna, IAEA-TECDOC-322, 252 p.

OWEN, D. E. (1990): Economic, environmental and health implications of uraniferous montane and subalpine wetlands; AAPG Rocky Mountain Section meeting. *AAPG Bull.* **74,** 1340.

RICHARDSON, K.A., KILLEN, P.G. & CHARBONNEAU, B.W. (1975): Results of a reconnaissance type airborne gamma-ray spectrometer survey of the Blind River-Elliot Lake area, *Geol Survey Can Paper* **75-1A**, 133-135.

ROBERTSON, J.A. (1989): The Blind River (Elliot Lake) uranium deposits, In: *Uranium resources and geology of North America,* **TECDOC-500**, IAEA, Vienna, 111-147.

ROBINSON, A. & SPOONER, T.C. (1984): Post-depositional modification of uraninite-bearing quartz-pebble conglomerates from the Quirke ore zone, Elliot Lake, Canada, *Econ. Geol.* **79**, 297-321.

ROSCOE, S.M. (1969): Huronian rocks and uraniferous conglomerates in the Canadian Shield, *Geol Survey Canada Paper,* **68-40**, 205 pp.

ROSCOE S.M. & MINTER W.E.L. (1993): Pyritic paleoplacer gold and uranium deposits; Mineral deposit modeling. *Spec. Pap. Geol. Assoc. Can.* **40,** 103-124.

RUZICKA, V. & STEACY, H.R. (1976): Some sedimentary features of conglomeratic uranium ore from Elliot Lake, *Ontario, Geol. Survey of Canada Paper* **76-1A**, 343-346.

THEIS, N.J. (1979): Uranium-bearing and asssociated minerals in their geochemical and sedimentological context, Elliot Lake, *Ontario, Geol Surv Can Bull* ***304***, 50 pp.

THIEL, K., SAAGER, R. & MUFF, R. (1979): Distribution of uranium in early Precambrian gold-bearing conglomerates of the Kaapvaal Craton, South Africa: A review of a case study for the application of fission track micromapping of uranium, *Min Sci Eng* **11,** 225-245.

YAMAGUCHI, K.E. & OHMOTO, H. (2006): Evidence from sulfur isotope and trace elements in pyrites for their multiple post-depositional processes in uranium ores at the Stanleigh Mine, Elliot Lake, Ontario, Canada; Evolution of early Earth's atmosphere, hydrosphere, and biosphere; constraints from ore deposits. *Geol. Soc. Amer. Memoir* **198,** 143-156.

CHAPTER 11: IMPLICATIONS FOR EXPLORATION STRATEGIES

Kurt Kyser
Department of Geological Sciences and Geological Engineering,
Queen's University,
Kingston, Ontario, K7L 3N6, Canada
kyser@geol.queensu.ca

and

Michel Cuney
G2R, Nancy-Université, CNRS, CREGU,
B.P. 239,
F-54506 Vandoeuvre lés Nancy, France
michel.cuney@g2r.uhp-nancy.fr

COMMON DENOMINATORS

Exploration strategies for various types of U deposits vary depending on which type of deposit is being sought. Despite the diversity of deposit types, and therefore the diversity of exploration strategies, there are some general considerations that apply to exploration for all types of U deposits. The most important include the following:

1) Timing is everything. Without an idea of both the relative and absolute age of the deposit and the host, exploration strategies cannot evolve beyond prospector-driven. Effective exploration in any deposit requires detailed knowledge of the time-space relationships. For example, magmatic-related deposits form after advanced differentiation of peralkaline, post-orogenic parent magmas to allow extreme U enrichment in the latest magma intrusions and related magmatic fluids. At Rössing, the alaskite bodies were the last granite units to be emplaced in the succession of intrusive events of the Damara orogen. In collision zones, U deposits related to peraluminous leucogranite require melting of the crust, which is facilitated by crustal thickening at an appropriate time during convergence. Metasomatic U deposits are associated with metamorphism during uplift of an orogen, almost exclusively during the Proterozoic. Unconformity-related deposits, also exclusively Proterozoic, appear to require 75-100 m.y. after the basins form to allow the fluids the appropriate evolution in their chemistry and temperature to be able to leach and mobilize U. Uranium-bearing silicate phases are refractory to hydrothermal leaching by common geologic fluids but are easily leachable when they become metamict after several hundred million years of auto-irradiation of the mineral structure.

Although determining the age of U deposits is not straightforward, recent advances in ICP-MS and microsampling technologies, use of multiple decay systems such as both U-Pb and Sm-Nd, precise dating of associated gangue minerals of specific paragenesis and integration of age data with other geologic factors render geochronologic data easier to obtain and interpret and to do so more meaningfully for exploration. The timing of the mineralizing process is required in exploration so that the geologic, chemical and physical environment conducive to the mineralizing process at a critical time in the evolution of an environment can be realized.

Along with the actual age of the ores and, therefore, the critical time in earth history that an effective mineralizing environment was present, the timing of events that have subsequently affected the ores can reveal when elements such as radiogenic Pb have been mobilized from the deposits and moved into the surrounding environment. These elements would elevate element concentrations in the surrounding environment, with gradients in concentrations as vectors to the deposits (Holk *et al.* 2003, Kister *et al*. 2004).

2) Knowledge of the nature of the fluids involved in the ore generation process and manifestation of these fluids in appropriate environments are absolutely critical for refining exploration strategies. The critical factors involved in identifying the fluids include their temperature, pressure, oxygen fugacity and chemical composition. Without knowledge of the critical chemistry, temperature and pressure required for generation of the ores, it is difficult to identify the correct environment in which to explore. For example, most highly evolved alkaline intrusive

Short course co-sponsored by the the SGA and MAC, Québec City, May 2008, p. 243-257

bodies do not host U deposits because they do not evolve to concentrate U in the last fluids. Most areas of albitization do not host deposits presumably because the fluids were not carrying U or there was no trap. The discovery of the relation between diagenetic brines and the genesis of unconformity-related U deposits has led companies to explore deeper levels in the basement below the Athabasca Basin 20 years after the discovery of the outcropping Rabbit Lake and Cluff Lake deposits. However, there are areas in the Athabasca Basin with the appropriate geology, structure and alteration conducive to the ore-forming process, yet they are apparently devoid of any significant U unconformity-related mineralization. Most sandstone-hosted deposits occur in meanders of paleostreams where organic detritus could accumulate, but most such areas do not host ore. Understanding why barren areas that should have ore do not requires knowledge of the physical, chemical and temporal characteristics of the fluids required to form various types of U deposits.

3) Gradients in redox environments are a necessity for the generation of many types of U deposits that form in both low to high temperature environments. For example, roll-front deposits best exemplify the gradients that occur in U mobilization and fixation. Deposits in the Franceville Basin have characteristics very similar to unconformity-related deposits, but they occur at a redox boundary between oxidized sandstone and reduced shale within the basin. Unconformity-related deposits are normally associated with graphite or a reducing fluid from the basement. For high temperature environments the Rössing deposit shows the importance of redox boundaries represented by the Rössing graphite-sulfide-rich metasedimentary rocks. Evidence of redox gradients through changes in the oxidation state of Fe or C are definitive, although not unique, indicators of ore-forming environments.

4) The source of the uranium is often overlooked by many explorationists, but should be a factor in evaluating areas for potential mineralization. For many deposits, the source of the U is in units that have aberrantly high U contents, such as in volcanic glass in the case of tabular deposits or in alkaline intrusions in the case of some magmatic-type deposits. Enrichment of U in the source region of basin-hosted deposits certainly increases the probability that a deposit could form (*e.g.*, McNeal *et al.* 1981). Another critical aspect is the availability of U in the source region. Uraninite represents the most easily leachable U source by oxidized fluids. In certain refractory minerals, U is unlikely to be released unless those minerals become metamict. In sandstone-hosted deposits, unstable volcanic glass with high U contents, mainly of peralkaline composition, makes an ideal source because the U can be effectively mobilized. In the case of unconformity related deposits, hot and high saline Cl brines are able to dissolve U even from the most refractory minerals such as monazite (Hecht & Cuney 2000).

5) Carbon, particularly in the form of organic matter, is an effective reductant for fixing U. Relations between U deposition and organic matter are observed in many deposit types, from low temperature environments, in roll front-type deposits to very high temperature environments as at Rössing. Exactly why C is such an effective reductant is unclear, especially given that there are alternatives such as sulfides and ferrous iron. Although the latter have been shown to be the likely reductants in the formation of some deposits, these deposits tend not to be as large or as high grade relative to those where C is the reductant. In the case of calcrete-type deposits, redox plays a minimal role, except as a moderator of pH. For these deposits it is the solubility that is most important.

6) Uranium deposits are geochemical anomalies and as such, are best discovered using strategies that integrate geochemistry as a significant part of the exploration repertoire. For example, in certain leucogranitic massifs in France and Spain, anomalies of U concentrations proximal to deposits can extend for kilometres and have been used to direct reconnaissance surveys that led to the discovery of blind deposits (Leymarie 1989). An indirect guide to U mineralization is reflected by elevated concentrations of other mobile elements such as Ba or Sr and the iron oxidation ratio.

7) Although specific tectonic environments, structural settings and lithologies are required for all U deposit types, none of these are definitive indicators of mineralization because most of these settings, structures and lithologies do not host deposits. Thus, they are required for the deposits to form, but are not definitive indicators of mineralization. In effect, the only definitive

indicators are geochemical, both in terms of U concentration and in the associated elements.

8) Exploration for U deposits, as with any type of deposit, requires the integration of geology, geophysics and geochemistry and must embrace new technologies and research results to be effective and competitive. Although "luck" and "serendipity" will always be factors, exploration must be more purposeful, especially as the need to find deposits under cover becomes more urgent. In formulating exploration strategies, an analogy might be someone looking for a treasure hidden in a desk drawer in a house in some unfamiliar city, geology can get you in the right city and neighborhood, geophysics can get you in the right house, and geochemistry can get you in the right room in that house. However, you still need to find the exact drawer.

EXPLORATION STRATEGIES

Examples of exploration strategies for U do not abound in the literature. Below are examples of what has, or is being, used as components of exploration for various U deposits.

Geology

Using Rössing and Bokan Mountain intrusive-related deposits as end-member models, Ragland & Rogers (1980) used their tectonic environments to suggest that Pan-African belts, which they considered as a U province, have some similarities to the southern Appalachians. Some granitic rocks in certain tectonic belts of the southern Appalachians, particularly the peralkaline and peraluminous granitic rocks of the Raleigh-Kiokee, Inner Piedmont, and eastern Blue Ridge belts, in addition to those in the Grandfather Mountain Window, provide the most promising tectonic environments in which granitic U deposits can occur.

Exploration for unconformity-related deposits is based firstly on Proterozoic red-bed basins overlying basement complexes and source regions characterized by high U contents. There are nearly 200 basins that would qualify. Graphitic metasedimentary units within the basement complex are desirable, but certainly not necessary, as exemplified by the Nabarlek deposit in Northern Territory, Australia, but repeated brittle reactivations of ductile structures that may offset the basal unconformity and were foci for fluid flow and ore deposition are required.

Uranium ore deposits in the Grants Mineral Belt, New Mexico, occur in fluvial sandstone in the Jurassic Morrison Formation where U is concentrated by dark gray to black humate derived from decaying vegetation. The ores vary greatly in size and shape, generally occur in clusters, and often are difficult targets for drilling. Exploration was done primarily by drilling, delineating favorable ground on a wide spacing and then using closely spaced drilling in mineralized areas. Criteria for favorable areas includes the presence of a host sandstone, anomalous U contents, dark color of host rock, presence of carbonaceous matter, and position of an area with respect to mineralized trends (Fitch 1979).

Geophysics

The mainstay of exploration geophysics for U deposits is gamma ray spectroscopy used in airborne regional and local surveys, down-hole logging and on outcrops using hand-held units. The former is normally collected as part of airborne magnetic surveys with magnetics used to reveal the general geology. Airborne gamma-ray spectrometry directly measures U, K, and Th in surficial material.

Zones of alteration minerals can be mapped with remote sensing that can detect in the visible and the mid infrared sections of the electromagnetic spectrum the spectral response of minerals typical of alteration. For example, the two oxidation states of U and Fe have been proposed to map bleached alteration zones associated with U mineralization using multispectral sensors like Landsat ETM+ (Rajesh 2008).

Improved magnetotelluric methods have detected deep conductors and shallow alteration zones in the search for deep unconformity-related deposits in the Athabasca Basin (Farquharson & Craven 2008). Clay-rich, quartz-corroded quartz arenite has relatively low resistivity, whereas quartz-rich silicified zones are characterized by high resistivity. Although expensive, 3D seismic has been used to image details of basement topology, thereby locating more favorable areas for deep drilling.

Geochemistry

Geochemical detection of U deposits in sandstone-type deposits depends on the geochemical behavior of U and path-finder elements (Rose & Wright 1980). Uranium is dispersed under oxidizing conditions but is immobile under reducing conditions. Adsorption on freshly precipitated Fe-oxides and certain types of organic matter also limits dispersion unless high

concentrations of CO_3^{2-} or other complexers are present. Thorium accompanies U in most plutonic processes, but the two elements are separated under oxidizing conditions. Possible pathfinder elements associated with U in sandstone-type deposits include S, V, Mo, Se, As and at some deposits Cu, Ag, Cr, Pb, Zn, Ni, Co, Re, Be, P, Mn and rare earth elementss, plus He, Rn and other radioactive decay products.

Concentrations of U in stream water are dependent on climate and only locally on geology, showing association with the elements typical for felsic and alkaline rocks. U contents in stream water are opposite to those in stream sediments. U contents in floodplain sediment reflect the geology of the provenence, and high values occur in areas with felsic intrusive units, which are hosts for U mineralization, and areas with black shale and phosphorite deposits.

Most U deposits in sedimentary rocks are associated with geochemical provinces enriched in U and Th or with U-rich intrusive or volcanic rocks, although the deposits may be separated by tens of kilometres from these U-rich source rocks. Weak regional U and Th anomalies in sediments containing U deposits may be present. Anomalies in U, Se, Mo, V, As, He, Rn, and other path-finder elements in rock and in ground and surface waters can furnish geochemical guides to ore, as can thermoluminescence (Hochman & Ypma 1984), Pb (Holk *et al.* 2003), S and C isotopes, and textures of Fe and Ti oxides.

Lithogeochemical and mineralogical haloes around unconformity-type U deposits in northern Saskatchewan can expand the size of drill targets up to fifteen times in the sandstone units but are more restricted in the basement rocks. The ratio K_2O/Al_2O_3 proved useful in delineating illite distribution in the sandstone. For example, the Midwest deposit is characterized by a 500 m large bell-shaped zone with $K_2O/Al_2O_3 > 0.18$. Anomalously high B haloes, corresponding to dravite alteration are also characteristic of these deposits. Ni, As and Co are generally of more limited use because their haloes are restricted to a few tens of metres. Uranium (> 3 ppm) may form more than 200 m large anomalies around some deposits. The complexity of the basement lithology inhibits the use of individual elements as alteration guides other than in the intensely altered zone (Sopuck *et al.* 1983).

Lake water and sediment geochemistry and radiometric prospecting are significant tools in early regional exploration for U deposits in Canada (Cameron 1980). This is because of the superior mobility of U in surface waters, which allows the element to disperse widely from its source. The effectiveness of these methods for U in organic-rich terrain, such as the southern Canadian Shield, has been puzzling, but may reflect stable, soluble organic-uranium "complexes" that allow the metal to pass through organic-rich traps.

Two sampling media in the drainage basins of lakes include organic-rich, centre-lake sediments and surface waters. Waters have certain advantages over centre-lake sediments, such as lower sampling and preparation costs. The pH of lakewater has minimal effect on the partitioning of U between organic-rich sediment and water over the pH range 5.0-7.4, but above pH 7.4 there is a marked increase in the median U content of lake waters relative to the median U content of organic sediments (Cameron 1980). In glaciated terrain, such as the Canadian Shield, the development of anomalies in lakes is a two-stage process wherein U-rich detritus is transported down-ice from the mineralized source and then the metal is dispersed in solution from this detritus into the lakes. As a consequence, lake anomalies are most effectively followed up by boulder tracing.

Groundwater samples collected from boreholes tens of metres from unconformity-related U mineralization have high levels of U, Ra, Rn and He (Earle & Drever 1983). However, Rn and He distributions can be greatly affected by variations in permeability of the rocks and are frequently ineffective tools to detect buried mineralization (Butt & Gole 1985). Anomalous He concentrations can arise by accumulation over long times and by leakage from deep sources (Gingrich 1984).

Biogeochemistry has been developed for U exploration during the 1980s (Dunn 2007). For example, spruce twigs indicate that tree roots can extract anomalous U from groundwater that reflects deposits at 300 m depth in the Eastern Athabasca.

Analysis of groundwater can be a useful strategy for regional exploration for U in the reduced sediments in paleochannels, although multi-element data are required. Lead isotopes can be used to confirm the groundwater interpretations. Paleochannels containing U deposits in South Australia have neutral, moderately saline groundwaters whereas others are often saline and acidic waters that preferentially mobilize Ra, thereby negating the use of Rn or down-hole gamma logging (Dickson & Giblin 2007). If

reduction of U by bacteria is an effective mechanism for formation of U deposits in paleochannels, then microbially induced geochemical signals such as C isotopes or enhanced mobile metals should indicate favorable areas.

Fluids that produce many types of U deposits can produce significant alteration zones around the U mineralization. Clay minerals are ubiquitous up to hundreds of metres from hydrothermal U mineralization, and often there is zoning in the type of alteration minerals involved. The presence of reductants such as graphite or organic matter with, the alteration zones are among the major indicators of an environment conducive to U enrichment. Exploration techniques that exploit these features include airborne and ground geophysics, surface geochemistry and clay typology, the latter analyzed in the field by portable short-wave infrared (SWIR) spectrometers.

Exploration for U deposits will likely witness many more bust and boom periods. The last boom period was witness to limited success and in predominately brownfield areas. We should prepare ourselves for the next boom, and hopefully some of the facts and ideas in this volume will help.

REFERENCES

BUTT, R.M. & GOLE, M.J. (1985): Helium in soil and overburden gas as an exploration pathfinder – an assessment. *J. Geochem Explor*, **24**, 141-173.

CAMERON, E.M. (1980): Geochemical exploration for uranium in northern lakes; geochemical exploration for uranium. *J Geochem Explor* **13**, 221-250.

DICKSON, B.L. & GIBLIN, A.M. (2007): Effective exploration for uranium in South Australian palaeochannels; Geology of uranium deposits. *Trans.Inst. Mining & Metallurgy. Section B: Applied Earth Science* **116,** 50-54.

DUNN C.E. (2007): Biogeochemistry in Mineral Exploration. *Handbook of Exploration and Environmental Geochemistry* **9**, 1-460

EARLE, S.A.M. & DREVER, G.L. (1983): Hydrogeochemical exploration for uranium within the Athabasca Basin, northern Saskatchewan. *J. Geochem. Explor.* **19**, 57-73.

FARQUHARSON, C.G. & CRAVEN, J.A. (2008): Three-dimensional inversion of magnetotelluric data for mineral exploration: An example from the McArthur River uranium deposit, Saskatchewan, Canada. *J. Applied Geophysics*, in press.

FITCH, D.C. (1979): Exploration for uranium deposits in grants mineral belt, New Mexico. *AAPG Bull* **63**, 688.

GINGRICH, J.E. (1984): Radon as a geochemical exploration tool. *J. Geochem. Explor.* **21**, 19-39.

HECHT L. & CUNEY M. (2000): Hydrothermal alteration of monazite in the Precambrian basement of the Athabasca basin: implications for the genesis of unconformity related deposits. *Mineral. Dep.* **35**, 791-795

HOCHMAN, M.B.M. & YPMA P.J.M. (1984): Thermoluminescence as a tool in uranium exploration. *J. Geochem. Explor.* **22**, 315-331

HOLK, G.J., KYSER, T.K. DON CHIPLEY, HIATT, E.E. & MARLATT, J. (2003): Mobile Pb-isotopes in Proterozoic sedimentary basins as guides for exploration of uranium deposits. *J. Geochem. Explor.* **80**, 297-32

KISTER P., CUNEY M., GOLUBEV V.N., ROYER J.J., LE CARLIER DE VESLUD C., RIPPERT J.C. 2004. Radiogenic lead mobility in the Shea Creek unconformity-related uranium deposit (Saskatchewan, Canada): migration pathways and Pb loss quantification. *Comptes Rendus Geosciences*, **336**, 205-215.

LEYMARIE, P. (1989): Lithogeochemical exploration for uranium in leucogranites. *J. Geochem. Explor.* **34**, 147-156.

MCNEAL, J.M., LEE, D.E. & MILLARD, JR. H.T. (1981): The distribution of uranium and thorium in granitic rocks of the basin and range province, Western United States. *J. Geochem. Explor.* **14**, 25-40.

RAGLAND, P.C. & ROGERS, J.J.W. (1980): Favorable tectonic belts for granitic uranium deposits: Pan-Africa and the southern Appalachians. *J. Geochem. Explor.* **13**, 181-199.

RAJESH, H.M. (2008): Mapping Proterozoic unconformity-related uranium deposits in the Rockhole area, Northern Territory, Australia using landsat ETM+. *Ore Geol. Rev.* **33**, 382-396

ROSE, A.W. & WRIGHT, R.J. (1980): Geochemical exploration models for sedimentary uranium deposits; geochemical exploration for uranium. *J. Geochem. Explor.* **13**, 153-179.

SOPUCK, V.J., CARLA, A. DE, WRAY, E.M. & COOPER, B. (1983): The application of lithogeochemistry in the search for unconformity-type uranium deposits, Northern Saskatchewan, Canada. *J. Geochem. Explor.* **19**, 77-99